Oguz Okay   *Editor*

Polymeric Cryogels

Macroporous Gels with Remarkable Properties

Springer

263
Advances in Polymer Science

Aims and Scope

The series Advances in Polymer Science presents critical reviews of the present and future trends in polymer and biopolymer science. It covers all areas of research in polymer and biopolymer science including chemistry, physical chemistry, physics, material science.

The thematic volumes are addressed to scientists, whether at universities or in industry, who wish to keep abreast of the important advances in the covered topics.

Advances in Polymer Science enjoys a longstanding tradition and good reputation in its community. Each volume is dedicated to a current topic, and each review critically surveys one aspect of that topic, to place it within the context of the volume. The volumes typically summarize the significant developments of the last 5 to 10 years and discuss them critically, presenting selected examples, explaining and illustrating the important principles, and bringing together many important references of primary literature. On that basis, future research directions in the area can be discussed. Advances in Polymer Science volumes thus are important references for every polymer scientist, as well as for other scientists interested in polymer science - as an introduction to a neighboring field, or as a compilation of detailed information for the specialist.

Review articles for the individual volumes are invited by the volume editors. Single contributions can be specially commissioned.

Readership: Polymer scientists, or scientists in related fields interested in polymer and biopolymer science, at universities or in industry, graduate students.

Special offer:

For all clients with a standing order we offer the electronic form of Advances in Polymer Science free of charge.

Oguz Okay
Editor

Polymeric Cryogels

Macroporous Gels with Remarkable
Properties

With contributions by

F. Auriemma · A.D. Bannerman · C. De Rosa ·
R. Di Girolamo · V.I. Lozinsky · H. Mak · B. Mattiasson ·
O. Okay · P.D. Petrov · O.A. Shlyakhtin · C.B. Tsvetanov ·
W. Wan · L. Yang

Editor
Oguz Okay
Department of Chemistry
Istanbul Technical University
Istanbul, Turkey

Printed on acid-free paper

Preface

Cryogelation is a simple strategy that allows the preparation of macroporous gels, so-called cryogels, of high toughness and superfast responsivity. The term "cryogel" was mentioned in the literature for the first time in 1984 by Vladimir I. Lozinsky to designate polymeric gels formed in frozen media. Cryogels have attracted intense attention in the last 10 years due to their extraordinary properties, which have resulted in numerous biotechnological and biomedical applications. The present volume entitled *Polymeric Cryogels: Macroporous Gels with Remarkable Properties* is intended to review the principles of cryotropic gelation processes as well as the advances made during the past two decades in the preparation and application of cryogels based on both synthetic and natural polymers. It is my great pleasure to have Vladimir I. Lozinsky as one of the authors of this volume. I very much enjoyed discussing many aspects of cryogels and some secrets of cryogelation processes with him, both in Istanbul and at cryogenic temperatures in Moscow (Fig. 1).

The history of polymeric cryogels and mechanisms of their formation are reviewed in the first chapter. Chapters "Basic Principles of Cryotropic Gelation" and "Synthesis and Structure-Property Relationships of Cryogels" cover the basic principles of cryotropic gelation, the synthesis–structure–property relationships of cryogels, and some of their novel applications. Aqueous poly(vinyl alcohol) (PVA) solutions form physical gels by cryogenic treatments, which are of great interest due to their outstanding properties. Formation of PVA cryogels under various conditions is discussed in detail in chapters "A Brief History of Polymeric Cryogels," "Basic Principles of Cryotropic Gelation," "Kinetic Analysis of Cryotropic Gelation of Poly(vinyl alcohol)/water solutions by Small-Angle Neutron Scattering," and "Poly (vinyl alcohol) Cryogels for Biomedical Applications." The structure of PVA cryogels and the principal processes taking place during their formation are discussed in chapter "Kinetic Analysis of Cryotropic Gelation of Poly(vinyl alcohol)/water solutions by Small-Angle Neutron Scattering". An effective method for the synthesis of polymer cryogels is the initiation of cryogelation reactions using UV irradiation, which is reviewed in chapter "Cryogels via UV Irradiation". Chapter "Inorganic Cryogels" covers recent advances in inorganic cryogels. I have to mention that, although the term "inorganic cryogel" has been used as the generic

Fig. 1 Low temperature is a prerequisite for obtaining cryogels. O. Okay (*left*) and V. I. Lozinsky (*right*) discussing the content of this volume at −23 °C in Moscow (1 February 2014)

name for freeze-dried products of inorganic gels, precipitates, and colloidal solutions, it is more correct to call such freeze-dried products "cryostructurates" or "cryotexturates" rather than cryogels. However, as the term "cryogel" is most commonly used for inorganic materials obtained by free-drying, it will also be used in chapter "Inorganic Cryogels" to be consistent with previous studies in this field.

The last two contributions in this volume provide an overview of the biotechnological and biomedical applications of cryogels. Cryogels with their large pores open up a range of applications, e.g., isolation of microbial cells, capturing of cancer cells, use as matrices for immobilized cell reactors, and environmental separation. These applications of cryogels are reviewed in chapter "Cryogels for Biotechnological Applications." The unique mechanical properties of PVA cryogels make them an attractive candidate for biomedical, and especially medical device applications. In chapter "Poly(Vinyl Alcohol) Cryogels for Biomedical Applications," the formation process and processing parameters of PVA cryogels and their application in orthopedic and cardiovascular devices are reviewed and discussed.

The editor believes that the present volume covering a broad range of topics in the field of cryogels will contribute to a better understanding of the developments achieved during the past two decades in the synthesis and applications of cryogels. I also hope that this work will promote research in this rapidly developing area. I would like to thank all the authors who have contributed to this exciting volume on polymeric cryogels.

Istanbul, Turkey   Oguz Okay

Contents

A Brief History of Polymeric Cryogels

Vladimir I. Lozinsky

Contents

Abstract Polymeric cryogels, the gels formed in moderately frozen gelling systems, have been empirically known for many decades, but systematic scientific research on various cryogels and the peculiarities of cryotropic gel formation only commenced at the beginning of the 1980s. This historical review briefly describes the principal stages of the studies on these very interesting gel materials. It also discusses some mechanisms of their formation, as well as summarizes published data on the main representatives of chemically crosslinked (covalent), ionically linked, and noncovalent (physical) cryogels.

Keywords Polymeric cryogels • Cryogel history • Moderately frozen gelling systems • Cryotropic gelation processes

V.I. Lozinsky (✉)
Laboratory for Cryochemistry of (Bio)Polymers, A. N. Nesmeyanov Institute of Organoelement Compounds, Russian Academy of Sciences, Vavilov Street 28, 119991 Moscow, Russian Federation
e-mail: loz@ineos.ac.ru

1   Introductory Remarks

Polymeric cryogels are the gel systems formed via the cryogenic treatment (moderate freezing—frozen storage—thawing) of solutions or colloidal dispersions of the appropriate precursors [1]. On a microscopic level, moderately frozen molecular or colloid solutions are heterophase systems containing both solids (i.e., the polycrystals of frozen solvent) and some unfrozen fraction called "unfrozen liquid microphase" [2], where the solutes are concentrated. Thus, gelation can only occur within the latter unfrozen regions of the system while the crystals of frozen solvent act as porogens. Such specific conditions of gel formation are the key factors in determining the rather unusual heterophase macroporous morphology of the resulting polymer materials, the whole set of their physicochemical characteristics and, as a consequence, their operational capabilities. The present volume deals with the diverse aspects of preparation, properties, structure, and practical implementation of various cryogels based on synthetic organic or inorganic polymers, as well as on natural biopolymers. Taking into account the fact that the number of the works published in this field has grown almost exponentially during recent years (Fig. 1a), it is reasonable to first give a brief historical overview of these gel systems, which are very interesting both from the fundamental and applied viewpoints. Moreover, the authors of some recent publications devoted mainly to the applied aspects often seem to be unaware of the pioneering studies and main scientific sources. It is hoped that this chapter will also contribute to a better understanding of the developments achieved in cryotropic gel formation over the past three decades.

In many cases, it is difficult to indicate which exactly was the very first communication on some experimentally observed phenomenon, especially if it was discovered many years ago in the pre-electronic era, and the report appeared in an issue hardly available now, or if it was patented locally in a language not commonly used. The present brief historical information certainly has no claim to be an exhaustive review of all the early pioneering publications on cryogenically produced gel matrices. Nevertheless, we can assert that the term "cryogel" was most probably applied for the first time in a paper published in 1984 to designate polymeric materials prepared via chemical crosslinking of macromolecular precursors in moderately frozen organic media [4]. The term was created by combining "cryo" (from the Greek *kryos*, meaning frost or ice) and "gel," thus highlighting the specific formation conditions for the gels of this family. Besides the mentioned article, different terms were used for gels formed in frozen systems (mainly, aqueous ones): cryocoacervates [5], cryocoagulates [6], cryo-concentrated gels [7, 8], anomalous gels [9], freeze–thaw gels [10], etc. However, since the end of the 1980s the term "cryogel" has become more and more popular (Fig. 1b).

It should also be noted that several other materials are currently called "cryogels." Specific examples are as follows:

Published Items in Each Year

Citations in Each Year
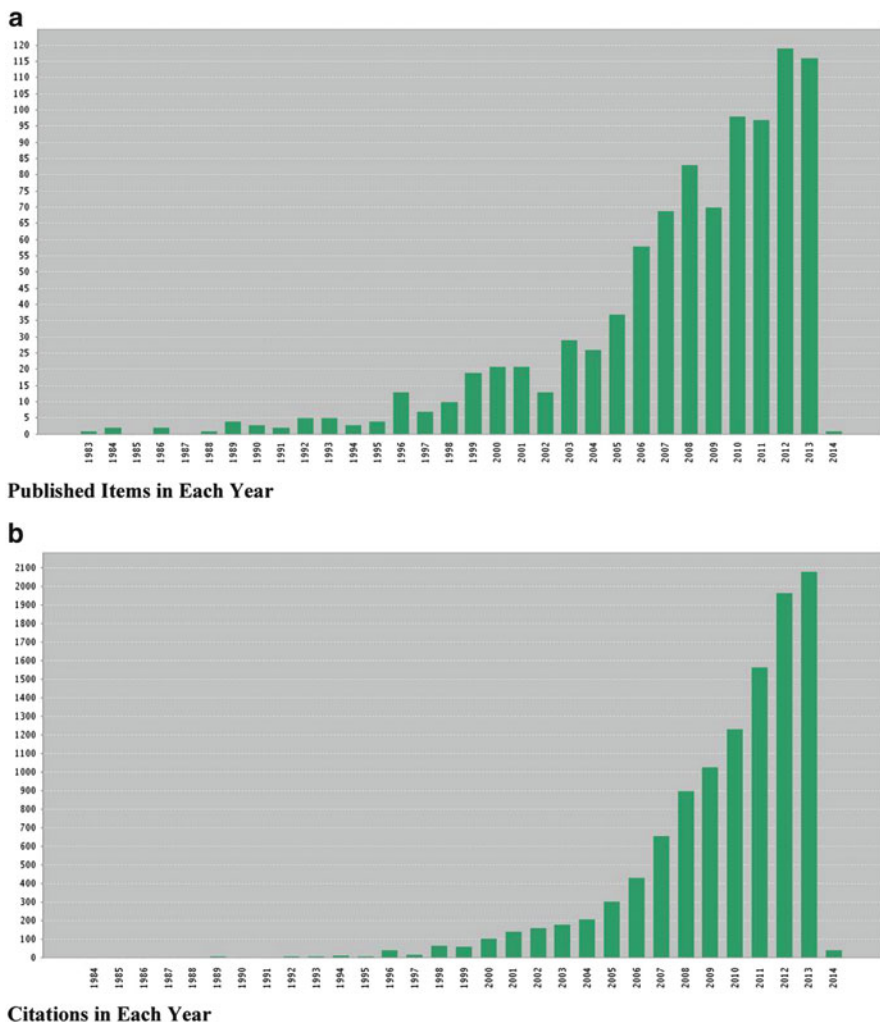
Fig. 1 The number of publications (**a**) and citations (**b**) with keywords "cryogel" or "cryogels" from 1980 to 1 November 2013 according to the ISI Web of Knowledge portal [3]

1. Commercially available jelly-like medical liniments causing a cooling-down effect when spread on the skin surface [11]. It is evident that this has no relation at all to gel formation under frozen conditions.
2. The proteinaceous water-swollen coagulates that are formed upon low-positive-temperature chilling of blood plasma taken from the patients with rheumatoid arthritis or some complex immune diseases [12, 13]. Since no freeze–thaw treatment is applied to the precursor liquid in order to induce the formation of such coagulates, the use of the term "cryogel" for this protein matter appears unjustified.

3. The so-called "carbon cryogels" prepared by swelling of certain crosslinked organic polymers, e.g., swelling of phenol–formaldehyde resins in crystallizable organic solvents such as benzene, followed by freezing of the swollen matter and finally freeze-drying to obtain a macroporous polymeric texturate, which is then subjected to high-temperature carbonization with the formation of activated carbon (charcoal) possessing specific macroporosity [14–16]. It is also obvious that such final materials (i.e., "carbon cryogels") are not gels at all, because gels are 3D networks constructed from organic or inorganic polymers and necessarily contain immobilized low molecular weight solvate liquid (i.e., water in the case of hydrogels).
4. Some authors have named the polymeric matrices fabricated via conventional freeze-drying by the term "cryogels." Certainly, freezing of polymeric solutions or colloidal dispersions causes solid–liquid phase separation, and the subsequent sublimation of the solidified solvent crystals "fixes" the system thus structured [17, 18], but no gelation occurs during these consecutive steps. Therefore, it is more correct to call such freeze-dried polymeric matrices "cryostructurates" or "cryotexturates" rather than "cryogels."

Taking into account the above considerations, one can conclude that the polymeric and biopolymeric materials mentioned above are not related directly to proper cryogels and that they are probably named by such a term rather accidentally.

2   Types of Initial Systems Capable of Being Precursors for the Preparation of Cryogels

Numerous studies on various aspects of cryotropic gelation phenomena have demonstrated that cryogels can be prepared, similarly to the traditional gels formed at positive temperatures, from precursor systems that fall into the following categories (see review articles [1, 18–29]):

- *Colloidal dispersions*: Freezing of colloid sols and the resulting cryo-concentration effects cause reinforcement of the interparticle interactions, leading to the formation of tight particle-to-particle contacts. These contacts are stabilized either by the cohesion forces or, if some reactive auxiliary substances are present, by the formation of chemical links between the grains of particulate matter. It seems likely that the freeze–thaw structuring and gelling of colloid systems is the oldest example of cryotropic gelation and has been known for many decades, especially by people who deal with the frozen storage of foodstuffs (some particular instances are given below).
- *Solutions of monomeric precursors*: Chemically or radiation-induced crosslinking polymerization or polycondensation in moderately frozen aqueous or organic media (depending on the chemical nature of the monomers) results in

covalently crosslinked gel materials that generally possess a wide-pore spongy morphology.

- *Solutions of high molecular weight precursors*: Covalent crosslinking, i.e., curing of macromolecules either with chemical agents or by irradiation (gamma-rays, electron beams, UV irradiation, photolysis in the presence of a suitable photoinitiator) in non-deeply frozen systems, results in chemically crosslinked highly porous matrices. The characteristics of the porosity of such gel materials (i.e., their macroporous or supermacroporous sponge-like texture) are governed by the freezing conditions, by the amount of freezable solvent, and by the size of porogen particles, namely, solvent polycrystals.
- *Solutions of so-called self-gelling polymers*: Such precursor systems are capable of forming physical (noncovalent) gels upon "worsening" of the thermodynamic quality of the solvent [1, 30] or by the addition of a solute that induces a change in the conformation of the macromolecular chains, e.g., a protein denaturant [31, 32].
- *Solutions of polyelectrolytes containing low molecular weight or polymeric crosslinking counterions*: These precursor systems are able to form sufficiently stable ionic bridges between the polyelectolyte chains. Such kind of gel formation is a relatively rare variant of the cryotropic gelation case, since the ion-exchange reactions are fast processes and, thus, it is technically difficult to freeze the precursor solution prior to its gelation. Therefore, some special methods must be implemented to overcome the mentioned impediments, that is, to shift the onset of gelation beyond the freezing of the reaction solution. For instance, an ionic crosslinker can be introduced in the feed solution in the form of a solid powdered salt having a negative temperature coefficient of solubility, i. e., its solubility rises with lowering of the temperature. In this way, the feed can first be frost-bound, and ionotropic gelling will then occur within the moderately frozen bulk system [33, 34].

The above classification of the precursor systems is also convenient for an overview of the "cryogel story," since different types of polymeric cryogels at the early stages of their history have been discovered virtually independently. This situation continued at least until the beginning of 1980s, when general approaches for the preparation of covalently crosslinked cryogels based on both monomeric and polymeric precursors were elaborated and patented [35]. The listed variants are considered here in the same sequence.

However, one important remark should be made first regarding the definitions of "positive" and "negative" temperatures. In the subsequent discussion, the freezing/melting point of the feed system is taken as "zero" in the temperature scale; therefore, the processes under the thermal conditions above this point occur at positive temperatures, while gel formation below this point occurs at negative temperatures. Further, in this context, we also use the terms "non-deeply frozen" or "moderately frozen" to designate frozen systems that are not completely solid at the corresponding negative temperature, and in which some fraction of unfrozen liquid microphase still exists. As a rule, such temperatures lie not lower than several tens of centigrade under the freezing/melting point of the corresponding feed solution [1, 2].

2.1 Polymeric/Biopolymeric Cryogels Formed by Freeze–Thaw Aging of Colloid Sols

Perhaps the earliest example of a technologically realized process in which freeze–thaw-induced gel formation was employed is the manufacture of the food product named "kori-tofu," which has been known for centuries and is still very popular in Japan [36]. The starting material for the fabrication of this soybean-protein food-stuff is the soya curd "tofu," a colloid-type dispersion of the salting-out coagulate of 11S globulins. Tofu is subjected to freezing, during which the SH groups of cysteine residues of the neighboring macromolecules are coupled into intermolecular disulfide bridges, thus resulting in the formation of a 3D supramolecular network of protein particles [37–40]. Another example of cryotropic gel formation of colloidal dispersions is the freeze–thaw-caused structuration of minced meat and pastes of myofibrillar protein isolates, e.g., those extracted from various kinds of fish, shrimp or Antarctic krill [41–48]. Since the major myofibrillar proteins, actin and myosin, are rich in cysteine, chemical crosslinking of proteinaceous colloid particles in non-deeply frozen systems is accompanied by the formation of interparticle covalent SS-bonds with the participation of air oxygen dissolved in the unfrozen liquid microphase. This gelation mechanism was elucidated using studies on the cryogel formation of model thiol-bearing polymers [49–52].

Cryotropic crosslinking of discrete particles of colloidal dispersions in the presence of a crosslinking agent to produce 3D macroporous polymeric materials has also been reported. The preparation of cryostructured collagen sponges [53–55] or the process of fabrication of leather-like materials from milled tanned leather wastes [56–58] are examples of such type of cryogel formation. In these cases, the respective dispersion was mixed with a crosslinking agent (e.g., glutaraldehyde) and then this heterophase reaction mass was frozen and kept in the frozen state for a necessary period of time and finally defrosted, resulting in spongy matter built of a supramolecular framework of chemically bound polymer particles. The same approach was also employed in subsequent years for the creation of macroporous materials based on covalently linked particulate matters like latexes [59, 60], microbial cells [27, 61], or small gel particles [27, 62, 63].

As well as covalent freeze–thaw gels derived from colloid dispersions, noncovalent cryogels with aligned macroporous morphology have also been prepared from particulate precursors. These include protein-containing systems [64–69], cryogels fabricated from the colloid solutions of gelatinized starch [5, 70–78], and cryostructured polymer matrices formed as a result of the freeze–thaw treatment of frost-sensitive latexes [79–84]. The nature of the interparticle links in the first case is a combination of hydrogen bonding, ionic interactions, and hydrophobic interactions. Multiple H-bonds are responsible for gelation of the starch-based systems, while the hydrophobic associations are the basis of particles "glueing" in the latex examples. The macroporous morphology of the resulting polymer materials and their physicochemical properties are determined by the initial

concentration of the dispersed particles; their size, shape, and chemical structure; and by the conditions of the freeze–thaw process. All these parameters must be taken into account in order either to prepare certain cryogels/cryostructurates or to prevent their formation when it is undesirable, as in the case of staving off the cryocoagulation phenomena in latex dispersions at negative temperatures [85].

2.2 Cryogels Prepared from Monomeric Precursors

The following three points are of principle significance for the preparation of cryogels from solutions of monomeric precursors:

1. The chosen solvent must crystallize rather than vitrify under the cryostructuring conditions; otherwise, if the solvent undergoes a glass transition, the unfrozen liquid microphase will not form and, hence, no cryo-concentrating effects will take place. This requirement is also valid for any other precursor system to be gelled cryogenically.
2. The solubility of the monomers should be high enough not only at positive temperatures, but also in the unfrozen liquid microphase. If the solubility of the monomer decreases drastically with decreasing temperature, the monomer concentration in the reaction medium becomes insufficient for the formation of a spatial network; that is, the critical concentration of gelation will not be reached. Various cryogels have been synthesized by using low molecular weight monomeric precursors, as in the majority of the reported cases, or macromonomers (macromers) such as the methacrylated derivatives of gelatine and chondroitin sulfate [86, 87], or poly(vinyl alcohol) [88, 89]. In the latter cases, the properties of the resulting gel matrices depend, along with common factors such as the monomer concentration or the freezing conditions, on the molecular weight of the macromonomer and on the amount of unsaturated groups in its molecule.
3. The crucial problem in the case of cryotropic gelation via free radical polymerization is the performance of the initiator system at negative temperatures. Chemical initiators such as peroxides that generate primary radicals owing to thermal decomposition are not suitable for cryopolymerization. Therefore, redox initiating systems capable of generating radicals at reduced temperatures are commonly employed [1, 26, 35, 90, 91]. Nonetheless, some rare cases are also known, where the "high-temperature" radical cryopolymerization of vinyl monomers has been carried out using thermally decomposed initiators. One such example is the 2,2′-azoisobutyronitrile-initiated copolymerization of styrene and divinylbenzene at 50 °C in the medium of crystallized naphthalene having a crystallization temperature of about 80 °C [35, 91, 92]. In the case of radiation-induced cryopolymerization, the above-discussed problem of the temperature-dependent activity of chemical initiators is virtually absent. The efficiency of radiation-induced processes is mainly a function of the applied radiation dose but not of the temperature, as demonstrated in the pioneering

studies conducted in Japan (see, e.g., [19, 93–100]). Yet another possibility for the preparation of cryogels of the polymerization type is the use of electron beams [101] or photoinitiation [102–104]. An essential point in this case is that the penetration capability of both these kinds of radiation is not very high, which limits the thickness of the samples. Therefore, the simplest approach, applicable in most laboratories, for the synthesis of polymerization-type cryogels is the use of a suitable chemical initiator system, where no specific radiation source is required and the amount of the added initiating substances can easily be controlled.

In the context of historical aspects of the development of polymerization-type cryogels, Table 1 summarizes the reaction components, e.g., the monomers, crosslinkers, initiator systems, solvents, and the temperature for cryogelation reactions starting from monomeric precursors. The data were taken from the pioneering reports on such gelation systems as well as from the most significant studies revealing the basic mechanisms of the key processes or ascertaining specific properties of the corresponding cryogels. Naturally, this selection is subjective, from the viewpoint of the author, and some works of good quality might have been missed.

Cryogels synthesized via polycondensation reactions are also known. These are mainly inorganic cryogels prepared by the sol–gel transformation in non-deeply frozen precursor systems, where the condensation of certain hydroxides accompanied by water liberation leads to the formation of polyoxides, as detailed in [173]. Polycondensation-type organic cryogels have also been reported in a few publications. Obviously, the first examples of such cryogels are those synthesized in frozen aqueous medium at $-15\ °C$ from the mixture of lysine (a trifunctional amino acid bearing two NH_2 groups and one COOH group) with water-soluble carbodiimide or from the mixture of lysyl-lysine (a dipeptide having three NH_2 groups) with glutaraldehyde [35]. In any case, the basic principle is that one of the precursors must be at least trifunctional or higher in order to ensure the branched 3D character of the forming polymer and its crosslinking. One recent example realizing this principle is the polycondensation-type cryogel prepared via the reaction of three-arm amino-terminated oligo(ethylene glycol) star polymers with dithio-bis (maleimido)ethane in the medium of non-deeply frozen dioxane at $-8\ °C$ [174]. Here, a 3D polymeric network forms as a result of the Michael addition of the primary amino groups to the double bonds of maleimide residues.

2.3 Preparation of Cryogels by Covalent Crosslinking of High Molecular Weight Precursors

As for the systems discussed in Sect. 2.2, the requirement of a good solubility of the high molecular weight precursors in the medium of the unfrozen liquid microphase is also important. If a decrease in the temperature and resulting freezing of the

Table 1 Examples of systems for the preparation and study of polymerization-type cryogels

Monomers and crosslinkers	Solvent[a]	Initiating system	Temperature of cryotropic gelation (°C)	What was done and reported	References
I. Chemical initiation					
Acrylamide + N,N'-methylene-bis-acrylamide	Water ($T_0 = 0$ °C)	APS + TMEDA	−10 to −30	Preparation of sponge-like poly(acrylamide) cryogels	[35, 90, 91]
				Study of the influence of cryostructuring conditions on the physicochemical and structural characteristics of resulting gel materials	[91, 105–114]
				Study of the gel formation dynamics	[108, 115, 116]
	Formamide ($T_0 = +2.9$ °C)		−8	Preparation of poly(acrylamide) cryogels in organic medium	[90, 91, 106]
	Water/dimethyl sulfoxide mixtures		−18	Preparation of poly(acrylamide) cryogels, study of their swelling behavior, mechanical properties, and porous structure	[117, 118]
Acrylamide + allyl glycidyl ether + N,N'-methylene-bis-acrylamide	Water	APS + TMEDA	−10 to −30	Preparation of epoxy-containing poly(acrylamide) cryogels, study of their properties and porous structure	[91, 119–125]
Acrylamide + 2-acrylamido-2-methylpropane sulfonic acid + N,N'-methylene-bis-acrylamide	Water-in-oil emulsion	APS + TMEDA	−4	Preparation and study of pH-responsive cryogel microbeads	[126]
Acrylamide + 2-acrylamido-2-methylpropane sulfonic acid + N,N'-methylene-bis-acrylamide	Water	APS + TMEDA	−18	Preparation of pH-responsive cryogels, study of their pH-dependent swelling behavior and wide pore morphology	[127]

(continued)

Table 1 (continued)

Monomers and crosslinkers	Solvent[a]	Initiating system	Temperature of cryotropic gelation (°C)	What was done and reported	References
N-Isopropylacrylamide + N,N'-methylene-bis-acrylamide	Water Dimethylsulfoxide ($T_0 = +18.4$ °C)	APS + TMEDA APS + TMEDA	−11 to −40 −20	Preparation of thermoresponsive poly(N-isopropylacrylamide) cryogels, study of their temperature-dependent swelling behavior, mechanical properties and porous structure	[128–132] [133, 134]
	Water or water/ dioxane mixtures	DDMBAPS + TMEDA	−8 to −12	Preparation of fast-thermoresponsive cryogels, study of their temperature-dependent swelling behavior and wide pore morphology	[135, 136]
N-Isopropylacrylamide + N,N-di-n-propylacrylamide + N,N'-methylene-bis-acrylamide	Water/dioxane (4:1)	APS + TMEDA	−28	Preparation of hydrophobically modified thermoresponsive poly(N-isopropropyla-crylamide)-based cryogels, study of their temperature-dependent swelling behavior and wide pore morphology	[137]
N-Isopropylacrylamide + acrylic acid + N,N-methylene-bis-acrylamide	Water	APS + TMEDA	−22	Preparation of thermo- and pH-responsive cryogels, study of their temperature- and pH-dependent swelling behavior, as well as of the wide pore morphology	[138, 139]
N-Isopropylacrylamide + itaconic acid + N,N-methylene-bis-acrylamide					[140]

Monomer	Solvent	Initiator	Temperature (°C)	Description	References
N-Isopropylacrylamide + N,N'-bis-(acryloyl)-cystamine	Water	APS + TMEDA	−15	Preparation of thermoresponsive cryogels with entrapped oily emulsions, study of the temperature-dependent swelling behavior and emulsion release	[141, 142]
N-Isopropylacrylamide + N-[3-(N,N'-dimethylamino)propyl]-acrylamide + N,N'-bis-(acryloyl)-cystamine	Water	APS + TMEDA	−10	Preparation of thermoresponsive cryogels molecularly imprinted by ibuprofen, study of the bonding/release thermodynamics	[143]
N,N-Diethylacrylamide + N,N'-methylene-bis-acrylamide	Water	APS + TMEDA	−10	Preparation of thermoresponsive poly(N,N-diethylacrylamide) cryogels and study of their temperature-dependent swelling behavior	[144]
2-Acrylamido-2-methylpropane sulfonic acid + N,N'-methylene-bis-acrylamide	Water	APS + TMEDA	−22	Preparation of pH-responsive cryogels, study of their pH-dependent swelling behavior and the wide pore morphology	[145, 146]
N,N-Dimethylacrylamide + oligoethylene glycol diacrylate	Water	APS + TMEDA	−12	Study of the gel formation dynamics	[147, 148]
N,N-Dimethylacrylamide and its mixtures with polar uncharged or ionic vinyl comonomers	Water	APS + TMEDA	−5 to −40	Preparation of cryogels exhibiting superabsorbent properties	[149]
N,N-Dimethylacrylamide + 2-(diethylamino)ethyl methacrylate + N,N'-methylene-bis-acrylamide	Water/ethanol (1:1)	APS + TMEDA	−26	Preparation of pH-responsive cryogels, study of their pH-dependent swelling behavior and the wide pore morphology	[150]

(continued)

Table 1 (continued)

Monomers and crosslinkers	Solvent[a]	Initiating system	Temperature of cryotropic gelation (°C)	What was done and reported	References
Methacrylic acid + oligoethylene glycol diacrylate	Water	APS + TMEDA	−20	Preparation of macroporous ion-exchange continuous chromatographic bed	[151]
2-Hydroxyethylmethacrylate + different crosslinking agents	Water or water/dioxane (2:1)	SPS + TMEDA	−8 to −13	Preparation of poly(2-hydroxy-ethylmethacrylate) cryogels and study of their properties	[152, 153]
2-Hydroxyethylmethacrylate + N,N-dimethylacrylamide + N,N'-methylene-bis-acrylamide	Water	APS + TMEDA	−12	Preparation of copolymeric cryogels, study of their swelling characteristics and the wide pore morphology	[154]
2-Hydroxyethylmethacrylate + N,N'-bis-(methacryloyl)-L-cystine	Water	APS + TMEDA	−12	Preparation of copolymeric cryogels, study of their swelling characteristics, wide pore morphology, and possibility to be dissolved upon action of added thiols	[155]
2-Hydroxyethylmethacrylate + N-vinyl imidazole + ethylene glycol dimethacrylate	Water	APS + TMEDA	−16	Preparation of imidazole-bearing cryogel, study of its physicochemical properties, porous structure, and metal-absorbing capacity	[156]
2-Hydroxyethylmethacrylate + N-methacryloyl-(L)-histidine methyl ester + N,N'-methylene-bis-acrylamide	Water	APS + TMEDA	−16	Preparation of the histidine-bearing bioaffinity matrix	[157]

Monomers	Solvent	Initiator	Temperature (°C)	Purpose	References
2-Hydroxyethylmethacrylate + vinyl-phenyl-boronic acid + oligoethylene glycol dimethacrylate	Water	APS + TMEDA	−12	Preparation of affinity matrix for the boronate affinity chromatography	[158]
N-Vinyl-caprolactam + oligoethylene glycol diacrylate	Water/dimethyl-sulfoxide mixtures	APS + TMEDA	−12	Preparation of temperature-responsive cryogels, study of their properties and the wide pore morphology	[159]
II. Initiation with radiation					
2-Hydroxyethylmethacrylate	Water	γ-rays	−24 to −196	Preparation of carriers for the immobilization of enzymes and cells, study of the properties and morphology of resulting cryogels as dependent on the cryopolymerization conditions	[93–98, 160, 161]
2-Hydroxyethylmethacrylate + acrolein	Water	γ-rays	−14 to −78	Preparation of aldehyde-bearing carriers for the immobilization of proteins	[99, 162]
2-Hydroxyethylmethacrylate + N-vinyl-pyrrolidone	Water	γ-rays	−78	Preparation of polymeric carriers for the immobilization of cells	[163]
2-Hydroxyethylmethacrylate + glycidyl methacrylate	Water	γ-rays	−78	Preparation of epoxide-bearing carriers for the immobilization of enzymes	[164]
Diacrylates or dimethacrylates of oligoethylene glycols	Water	γ-rays	−78	Preparation and study of physicochemical properties and macroporous morphology of respective cryogels	[95, 165]
Methoxyoligoethylene glycol methacrylates	Water	γ-rays	−78	Preparation of polymeric carriers for the immobilization of cells, study of properties and porosity of the resulting cryogels	[166, 167]

(continued)

Table 1 (continued)

Monomers and crosslinkers	Solvent[a]	Initiating system	Temperature of cryotropic gelation (°C)	What was done and reported	References
Acrylic acid + methylmethacrylate + oligoethylene glycol	Water-in-oil emulsion	γ-rays	No definite data	Preparation of polymeric carriers for the immobilization of enzymes	[168]
Olygoethylene glycol methacrylate + tetraethyleneglycol diacrylate	Water	β-beams	−5 to −30	Preparation and study of physicochemical properties and macroporous morphology of respective cryogels	[101]
III. Use of photoinitiation					
Acrylamide (or N-iso-propylacryamide, or 2-hydroxyethylmethacrylate) + oligoethylene glycol diacrylate	Water	H_2O_2 + UV irradiation	−20	Preparation and study of physicochemical properties and macroporous morphology of resultant cryogels	[102, 103]
Acrylamide + N,N'-methylene-bis-acrylamide	Water	1-[4-(2-hydroxyethyl)phenyl]-2-hydroxy-2-methyl-1-propane-1-one + UV irradiation	−13	Preparation of quickly swelling spongy poly(acrylamide) cryogels, study of their properties and wide pore morphology	[169]
		H_2O_2 + UV irradiation	−20	Synthesis and study of the poly (acrylamide) cryogel matrices for the immobilization of enzymes	[170]
N-Isopropylacrylamide or N,N-dimethylacrylamide + N,N'-methylene-bis-acrylamide + carbon nanotubes	Water	H_2O_2 + UV irradiation	−20	Preparation and study of cryogels with entrapped carbon nanotubes	[171]

Ethoxytriethylene glycol acrylate (or 2-hydroxy-ethylmethacrylate, or N,N'-methylene-bis-acrylamide)	Water	H_2O_2 + UV irradiation	−20	Synthesis and study of cryogel-based drug release matrices	[104]
Urethane diacrylate + poly(L-lactic acid)	Dioxane ($T_0 = +11.3\ °C$)	Diphenyl-(2,4,6-methyl-benzoyl)-phosphine oxide + UV irradiation	−25	Preparation of macroporous honeycomb cryogel and study of its properties and pore structure.	[172]

APS ammonium persulfate, *SPS* sodium persulfate, *TMEDA* N,N,N',N'-tetramethylethylenediamine, *DDMBAPS* dodecyl dimethyl benzyl ammonium persulfate

[a]T_0 is the freezing/melting temperature of the neat solvent

initial solution causes a loss of solubility and therefore precipitation/coagulation of the polymer, no crosslinked product can be obtained after thawing of the system, especially when the concentration of the crosslinking agent is relatively low. In addition, a rather important parameter is the molecular weight of the polymeric precursor, which determines both the initial viscosity of the feed solution prior to freezing and the viscosity in the reaction zone, i.e., within the volume of the unfrozen liquid microphase. Due to the generally high molecular weight of the polymeric precursors, very high viscosity of the reaction zone significantly reduces the segmental and translational mobilities of the polymer chains, thus preventing the occurrence of gelation reactions. Therefore, some preliminary experiments are often required to select the optimum molecular-weight characteristics of the corresponding polymeric precursor [1, 175, 176].

Cryogels prepared by chemical crosslinking of proteins were the first cases that exploited a scheme for producing immobilized biocatalysts. These were microbial or plant cells entrapped in a spongy carrier composed of serum albumin or gelatine cured with glutaraldehyde or formaldehyde, respectively [177–181]. In these early works, the factors influencing the gelation process and the properties of the final cryogels were not studied. Specific features inherent in this kind of cryotropic gelation and its mechanisms were basically established later using polymers chemically simpler than proteins, namely homopolymers or plain AB-copolymers, where the process of interest is not sophisticated by the numerous secondary interactions. Such a "modeling" approach found a series of significant effects that turned out to be characteristic for the formation of various cryogels. For instance, it was shown that cryogels in both aqueous [50, 182] and organic [4] media can be prepared at considerably lower initial concentration of precursors as compared to their gelation at positive temperatures. Thus, the effect of an apparent decrease in the critical concentration of gelation is inherent in the gel formation processes occurring in the non-deeply frozen reaction systems [1, 91]. The reason for such an effect is the cryo-concentrating phenomenon, which makes the concentration of the gelling agents considerably higher than that in the initial liquid feed. The same phenomenon generally causes the acceleration of cryochemical reactions in moderately frozen solutions over a certain range of negative temperatures [2, 183, 184] and is also observed during cryotropic gelation through covalent crosslinking of macromolecular precursors with suitable crosslinking agents, (see, e.g., [1, 91]). For instance, the oxidation of SH groups in thiol-containing poly(acrylamide) induced by water-dissolved air oxygen and leading to the formation of disulfide-crosslinked 3D polymeric network was at least five times faster in a frozen system at $-15\ ^{\circ}\text{C}$ than in a solution at $+15\ ^{\circ}\text{C}$. Moreover, the gel-point was reached about 1 h after freezing of the feed solution in the former case, whereas in the latter case the time was about 1 day [52].

Examples of the majority of the reported covalent cryogels prepared from macromolecular precursors are given in Table 2. These data show that such cryogels based on natural and synthetic polymers can be synthesized by chemical crosslinking or by irradiation techniques in frozen aqueous, organic, or mixed water–organic media. Thus, the chemical structure, physico-chemical properties,

Table 2 Examples of covalent cryogels prepared by crosslinking of macromolecular precursors in moderately frozen systems

High molecular weight precursors	Crosslinking agent	Solvent[a]	Temperature of cryotropic gelation (°C)	What was done and reported	References
I. Crosslinking with chemical agents					
Serum albumin	Glutaraldehyde	Water ($T_0 = 0$ °C)	−25	Preparation of macroporous carrier for the immobilization of thylakoids	[178]
			−20 to −25	Preparation of macroporous carrier for the immobilization of bacterial cells.	[179, 180]
			−20	Preparation of macroporous carrier for the immobilization of submembrane fraction of plant cells	[181]
Serum albumin	Cysteine	Water + urea	−3 to −78	Preparation of macroporous albumin cryogels	[31]
Gelatine	Formaldehyde	Water	−28	Preparation of macroporous carrier for the immobilization yeast cells	[177]
	Glutaraldehyde		−12	Preparation of macroporous scaffolds for tissue engineering	[185]
Gelatine + acrylonitrile	Glutaraldehyde, N,N'-methylene-bis-acrylamide	Water	−12	Preparation of composite cryogel via combination of polymer crosslinking and radical polymerization	[186]
Gelatine + fibrinogen	Glutaraldehyde	Water	−12	Preparation and study of covers on wounds	[187]
Gelatine + laminin	Glutaraldehyde	Water	−12	Preparation and study of macroporous scaffolds for tissue engineering	[188]
Collagen	Dialdehyde starch	Water	−15	Preparation and study of properties and macroporous morphology of resulting cryogels	[189]

(continued)

Table 2 (continued)

High molecular weight precursors	Crosslinking agent	Solvent[a]	Temperature of cryotropic gelation (°C)	What was done and reported	References
Collagen + hydroxyapatite	Water-soluble carbodiimide	Water	−18	Preparation and study of macroporous scaffolds for bone tissue engineering	[190]
Casein	Enzyme—transglutaminase	Water	−12	Preparation of macroporous scaffolds for tissue engineering	[185]
Thermo-coagulated soy protein isolate	Enzyme—transglutaminase	Water	−15	Preparation of macroporous protein scaffolds for tissue regeneration	[191]
Silk fibroin	Ethyleneglycol diglycidyl ether	Water	−5 to −22	Preparation and study of properties and macroporous morphology of resulting cryogels	[192]
SH-containing poly(acrylamide)	Water dissolved O_2	Water	−5 to −30	Study of the formation mechanisms of cryogels on the basis of thiol-containing polymers	[35, 49–52, 91]
Poly(β-D-glucose amine) (chitosan)	Glutaraldehyde	Aqueous acetic acid	−8 to −30	Preparation and study of physico-chemical properties and macroporous morphology of chitosan cryogels	[35, 50, 175, 182, 193, 194]
	Dialdehyde-dextran	Aqueous acetic acid	−32		[195]
Chitosan + gelatine	Dialdehyde-dextran	Aqueous acetic acid	−12		[196]
Poly(vinyl alcohol-*co*-vinyl acetate)	Epichlorohydrin	Water–NaOH solutions	−10	Preparation of macroporous polymeric cryogels	[35, 91]
Highly methoxylated pectin			−14		
Dextran			−9		
Cellulose	Epichlorohydrin	Water–NaOH–urea solutions	−20	Preparation and study of cryogels based on the cryogenically dissolved cellulose	[197]

Poly(vinyl alcohol-*co*-vinyl acetate)	Glutaraldehyde	Water–HCl solutions	−12 to −18	Preparation and study of physico-chemical properties and macroporous morphology of resulting cryogels	[91, 198]
Poly(vinyl alcohol-*co*-vinyl acetate) + particles of activated carbon	Glutaraldehyde		−12	Preparation and study of carbon-filled cryogels	[199, 200]
Poly(acrylamide)	Glutaraldehyde	Water–alkaline solutions	−5 to −20	Preparation and study of physico-chemical properties and macroporous morphology of resulting cryogels	[176, 201]
Chitosan + ovalbumin	Glutaraldehyde	Aqueous acetic acid	−18	Preparation of cryogel matrices for enzyme immobilization	[202]
Chitosan + gelatine	Glutaraldehyde	Aqueous acetic acid	−12	Preparation and study of physico-chemical properties of resulting cryogels	[203]
Chitosan + gelatine + hydroxyapatite			−20	Preparation and study of macroporous scaffolds for tissue engineering aims	[204]
Chitosan + agarose	Glutaraldehyde	Aqueous acetic acid	−20	Preparation of macroporous chromatographic matrices	[205]
Chitosan + gelatine + polypyrrole			−12	Synthesis and study of electroconducting cryogel matrices	[206]
Desoxyribonucleic acid	Ethylene glycol diglycidyl ether	Water–alkaline solution	−18	Preparation of DNA-cryogels, study of their properties, microstructure, and functional activities	[207–209]
Heparin + NH$_2$-end 4-arm star poly (ethylene glycol)	Water-soluble carbodiimide + N-hydroxysulfo-succineimide	Water	−20	Preparation and study of wide pore scaffolds for cell culture	[210]

(continued)

Table 2 (continued)

High molecular weight precursors	Crosslinking agent	Solvent[a]	Temperature of cryotropic gelation (°C)	What was done and reported	References
Poly(styrene-*co*-maleic anhydride)	Benzidine	Dimethylsulfoxide (T_0 = +18.4 °C)	+9	Preparation and study of physico-chemical properties of resulting cryogels	[35, 91]
Poly(*N*-vinyl-pyrrolidone-*co*-maleic anhydride)	4,4′-Diamino-diphenyloxide		+2 to −8		[4, 35, 50, 91]
Polystyrene	*p*-Xylylene-dichloride	Nitrobenzene (T_0 = +5.5 °C)	−4 to −27	Preparation and study of physico-chemical properties of resulting cryogels	[4, 35, 91]
Poly(iso-butylene)	Sulfur monochloride	Benzene (T_0 = +5.5 °C)	−18	Preparation of "single-hole" macroporous cryogel particles and study of their properties and microstructure	[211, 212]
Poly(iso-butylene) + silica nanoparticles			−5 to −15	Synthesis of butyl-rubber spongy composites and study of their properties	[213]
Poly(iso-butylene) + silica nanoparticles		Cyclohexane (T_0 = +6.5 °C)	−2; −18	Preparation of spongy composite butyl-rubber-cryogels and study of their physicochemical properties and porous morphology	[214]
II. Crosslinking by radiation					
Poly(vinyl alcohol) + poly(*N*-vinyl-pyrrolidone) + aloe vera	*γ*-rays	Water	−70	Preparation and study of hydrogels for wound dressing	[215]
III. Photo-induced crosslinking					
Poly(ethylene oxide)	UV irradiation + (4-ben-zoyl)benzyltri-methylammonium chloride	Water	−25	Preparation and study of physico-chemical properties of resulting cryogels	[216]
(Hydroxypropyl)methyl-cellulose or 2-hydroxyethyl-cellulose, or methyl-cellulose			−10 to −30		[217–219]

2-Hydroxy-ethylcellulose + poly (ethylene oxide)	−30	[220]
Poly(ethylene oxide) + sodium alginate + chitosan	−40	[221]
Poly(glycidol-*co*-ethyl glycidyl carbamate	−20	[222]

[a]T_0 is the freezing/melting temperature of a neat solvent

and porous morphology of cryogels discussed in this section can be varied over a very wide range, so that their potential applications are many. Judging from the published information, biomedical and biotechnological applications are the primary uses for the cryogels prepared from polymeric precursors. In addition, some other promising implementation fields also exist for such cryogels, including the employment of rubber-based "cryosponges" developed in Turkey as a reusable sorbent for the removal of oil spill from water surfaces [211, 212, 214, 223], crosslinked chitosan cryogels for the absorption of radionuclides from waste water [224, 225], crosslinked and partially saponificated poly(vinyl alcohol) cryogel composites containing activated carbon particles for the absorption of dyes [29, 199, 200], and so forth.

2.4 Physical (Noncovalent) Polymeric Cryogels

The publications on this group of cryogels are the most numerous and include several well-known and very informative reviews. The majority of these studies are related to poly(vinyl alcohol) (PVA) cryogels, which have been known since the 1970s [226–231]. The formation mechanisms of PVA cryogels [1, 29, 232–237] and their applications in various fields have been investigated extensively. These gel materials are used in medicine [1, 232, 235, 238–251], in biochemistry and biotechnology [1, 234, 252–262], in environmental protection [1, 263], in construction in the permafrost regions [1, 264, 265], etc. Such popularity of PVA cryogels is due to the combination of a set of remarkable features they possess, such as excellent physico-mechanical properties, a high thermal endurance compared with other physical hydrogels, a high resistance to abrasive erosion, a macroporosity that ensures good diffusion characteristics, the availability and relatively low cost of PVA itself, and a comparatively simple procedure for the preparation of such cryogels. In addition, PVA cryogels have a high biocompatibility and are nontoxic for biological objects.

Noncovalent cryogels based on other "self-gelling" synthetic and natural macromolecules have also been described for more than 40 years. In 1971, it was demonstrated that freezing of a 17 % solution of poly(acrylonitrile) in dimethylformamide/water (95–97:5–3, v/v) mixtures at $-78\ ^\circ$C leads to the formation of physical gels that are stable at room temperature [266]. Later, the freeze–thaw-induced formation of noncovalent cryogels was also reported for other polymeric systems. For instance, freezing of an aqueous solution of syndiotactic poly(methacrylic acid) and poly(ethylene oxide) mixture at $-78\ ^\circ$C, followed by its defrosting at room temperature, results in noncovalent cryogels [267]. Similarly, freezing of semidilute aqueous solutions of agar-agar or A-type gelatine at $-10\ ^\circ$C for 24 h followed by thawing at 25 $^\circ$C leads to the formation of biopolymer cryogels [30]. The cryogels thus obtained possess macroporous morphology, whose characteristics mainly depend on the type of polymeric precursor and its initial concentration in the feed. The cryogels formed from gelatinized starch [5, 70–78]

(mentioned in Sect. 2.1) as well as those based on starch-polysaccharides [268, 269] are also noncovalent cryogels that are stable at room temperature, but can be fused upon heating to 70–90 °C.

There is also a special case of the formation of physical cryogels where the self-gelation processes occur at a high rate even at positive temperatures. The aqueous solutions of >1 wt% agarose or >5–10 wt% gelatine belong to this category of gel-forming systems. When such solutions are being frozen at a moderate negative temperature, the ice is formed inside the already formed polymeric gel rather than in the liquid feed solution. As a consequence, the cryo-concentrating processes will not be realized to a significant extent, and the growing solvent polycrystals can even destroy the primary gel structure. The preparation of cryogels based on such quickly self-gelling precursors requires that freezing of the initial polymer solution should occur before the onset of the gelation. Principally, there are two possible ways to achieve this goal (1) freezing the initial hot solution very rapidly, e.g., in a liquid nitrogen bath, or (2) decreasing the self-gelation rate of the precursors by using specific additives capable of partially inhibiting the sol-to-gel transition. These two options were examined in detail in gelation systems containing agarose as a polymeric precursor [270, 271]. It was shown that the first option results in rather brittle gel materials with micrometer-sized pores. For the second approach, that is, to reduce the self-gelation rate of the precursor system, some solutes capable of partially interfering with H-bond formation between agarose chains were introduced into the initial feed solutions. This resulted in agarose cryogels with porosity and operational properties suitable for various applications, e.g., as wide-pore scaffolds for culturing of animal or human cells, including stem cells [271–277], and as supermacroporous continuous chromatographic beds for manipulation of particulate sorbates like viruses, cell organelles, and whole cells [272, 278]. It was found that the most convenient method of decelerating self-gelation in agarose solutions is to shift the pH so that some of the agarose hydroxyl groups are ionized, thus creating charges of the same sign along the chains, which causes certain repulsion between the chains [271].

Examples of various physical cryogels are summarized in Table 3, where the data are categorized according to the nature of the polymeric precursors, namely, polysaccharides, proteins, and synthetic polymers. The data for PVA cryogels are given separately due to the large number of papers published on these cryogels.

The history of PVA cryogels is also interesting because such gel systems have been discovered twice, as it were. First, there were mainly empiric recordings on the formation of these cryogels [230, 231] and the first patents were issued on the "virtual" applied possibilities of such materials [226–229]. Almost 10 years later, two approaches for increasing the strength of PVA cryogels were reported, namely, multiple freeze–thaw processing [299, 365–370] and the partial dehydration of frozen specimens *in vacuo* [9, 300, 301, 371]. These findings initiated numerous fundamental studies due to the amazing combination of cryogel properties and their macroporous structure. The investigations of frozen PVA solutions by nuclear magnetic resonance (NMR) and electron spin resonance (ESR) allowed better understanding of the fine details of the gelation processes inside frost-bound

Table 3 The examples of systems for the preparation of noncovalent (physical) cryogels

Polymeric precursor (its concentration in the feed)	Solvent	Conditions of cryotropic gel formation				What was done and reported	References
		Freezing temperature (°C)	Frozen storage duration (h)	Thawing rate (°C/min)	Number of freeze–thaw cycles		
I. Polysaccharides							
Agar-agar (0.25–1.0 wt%)	Water	−10	24	~0.2	1	Sponge-like cryogels with a rather brittle macropore walls were obtained	[30, 91]
Agarose (2–3 wt%)	Aqueous solutions of different pH values	−5 to −30	23	~0.3	1	Preparation of agarose-based cryogels, study of their physicochemical properties and peculiarities of the wide pore structure	[270–272]
Amylopectin	Water or 0.35 M NaCl solution	−6 to −24	18	3.00;	1	Preparation of polysaccharide cryogels, study of the influence of cryogenic process regimes on the properties of final cryogels, demonstration of synergism of the amylopectin and amylose interactions upon the gel formation	[268]
Amylopectin + amylose (0.5–2 g/dL)			18	0.30; 0.03			[74]
Carboxy-methylated curdlan (0.5–3 wt%)	Acidified water (pH 0.76–2.40)	−18	24–48	–	1–5	Preparation of the CM-curdlan-based cryogels, study of their swelling behavior and of the nature of interchain linking	[279]

	Solvent	Freezing temperature	Time			Description	References
Cress seed gum (1–7 wt%)	Water	−18; −30	24; 15	—	1	Preparation of the gum-based cryogels and evaluation of their rheological characteristics	[280]
β-Glucans from cereal sources (1–3 wt%)	Water	−18	24	—	1–12	Preparation of the β-glucan-based cryogels, study of their physicomechanical and thermal properties as depended on the source of polysaccharide isolation, molecular-weight parameters of gelling polymer, its initial concentration and conditions of cryogenic processing	[281, 282]
(3 wt%)	Aqueous solutions of glucose, fructose, sucrose, xylose or sorbitol	−15	24		14–22	Study of the influence of polyols on the physicochemical properties and macroporous morphology of resulting cryogels	[283]
Locust bean gum (0.5–5.1 wt%)	Water	−15	18–24	—	1–5	Preparation of the gum-based cryogels, study of the influence of freezing rate and freeze/thaw cycles number on the physicochemical properties of resulting cryogels	[284–287]

(continued)

Table 3 (continued)

Polymeric precursor (its concentration in the feed)	Solvent	Conditions of cryotropic gel formation				What was done and reported	References
		Freezing temperature (°C)	Frozen storage duration (h)	Thawing rate (°C/min)	Number of freeze–thaw cycles		
Locust bean gum (0.5–3 g/dL)	Water; aqueous solutions of urea, NaCl, Na$_2$SO$_4$	−10 to −30	18	3.00; 0.30; 0.03	1	Study of the nature of interchain links in the junction knots of 3D polymeric network; revealing the influence of the cryogenic process conditions on the physicochemical properties of final cryogels	[288]
(2 wt%)	Water	−20 to −60	1.5	1; 3; 7; 10	1	Study of the freezing and thawing rates influence on the mechanical properties of the gum-based cryogels	[289]
(1 wt%)	Aqueous solutions of glucose, fructose, sucrose or sorbitol	−20	24	–	1	Study of carbohydrates influence on the rheological properties of the gum-based cryogels, evaluation of the gum molecular weight influence on the physicochemical characteristics of resulting cryogels	[290]

Hyaluronic acid (1 wt%)	Aqueous HNO$_3$ solution (pH 1.5)	−20	15–72	—	1	Preparation of the hyaluronate-based matrices, study of their physicochemical and biomedical properties	[291–293]
Maltodextrin (0.1–15 g/dL)	Water	−6 to −24	18	3.00; 0.30; 0.03	1	Preparation of the maltodextrin-based cryogels and study of their physicochemical properties as dependent on the cryotropic gelation conditions	[269]
Xanthan (0.2–2 wt%)	Water	−20; −80	24	—	1–2	Preparation of xanthan cryogels and study of their rheological and thermal properties	[294, 295]
II. Proteins and peptides							
Gelatine, A-type (0.5–1.5 wt%)	Water	−10	24	~0.2	1	Sponge-like cryogels were prepared; the fragility of macropore walls increased with the growth of initial polymer concentration	[30, 91]
Gelatine B-type (0.2–2 g/dL)	Water	−30	24	0.5	1–4	Preparation of gelatine-based cryogels and study of their rheological properties as dependent on the cryogenic processing conditions	[87]
Gelatine, B-type (10 g/dL) + montmorillonite	Water-formamide mixture	−20	24	—	1	Preparation of composite cryogels and study of their properties and microstructure, revealing the effects of montmorillonite exfoliation	[296]

(continued)

Table 3 (continued)

Polymeric precursor (its concentration in the feed)	Conditions of cryotropic gel formation					What was done and reported	References
	Solvent	Freezing temperature (°C)	Frozen storage duration (h)	Thawing rate (°C/min)	Number of freeze–thaw cycles		
Ovalbumin (0.25–5.0 wt%)	Water + urea (0.125–5.0 mol/L)	−8 to −32	24	~0.3	1	Preparation of soft spongy cryogels, whose wide pore structure was governed by the freezing temperature, the thermal pre-history upon freezing, and the protein and urea concentration in the initial solutions	[31, 32, 185]
Dipeptide Fmoc-Phe-Phe (2–20 mmol/L) + glucono-lactone	Water or 0.1 M K_2SO_4 solution	−12	72	–	1	Preparation of cryogels based on the self-assembled dipeptide molecules, study of rheological properties and macroporous morphology of resulting cryogels	[297]
III. Synthetic polymers							
Poly(acrylo-nitrile) (~17 wt%)	Dimethylformamide/water (97–95/3–5, v/v)	−78	24	–	1	The gel's strength markedly grew with increase in water fraction in the composition of initial mixed solvent	[266]

Poly(methacrylic acid) + poly(ethylene oxide)	Water	−78	—	1	The polymeric phase of final heterogeneous material was composed from the interpolymer complexes; the phase had fibrillar structure, and the thickness of the fibrils depended on the poly(ethylene oxide) molecular weight	[267]
Poly(p-phenylene-vinylene) or poly(p-phenylene-ethynylene) (9.1 wt%)	Naphthalene ($T_0 = +80.4$ °C)	−78; +10; +45	6	1	Preparation of wide pore π-conjugated polyphenylene matrices, study of their properties and porous structure	[298]
IV. PVA cryogels[a]						
80/98 (3–9 g/dL)	Water	−75 to −80	2 min	1–6	Apparently the first report on the empiric observation of the fact of PVA cryogel formation	[230]
88.8/99.3 (2.5–15 wt%)		−20	45–150 min	—	The study of the temperature-dependent turbidity of water–PVA systems, the registration of the freeze–thaw-caused gel formation	[231]
105.6/99.6 (15 wt%)		−15	24–120	Multiple	Preparation of PVA cryogels and evaluation of their rigidity as	[299]

(continued)

Table 3 (continued)

Polymeric precursor (its concentration in the feed)	Solvent	Conditions of cryotropic gel formation				What was done and reported	References
		Freezing temperature (°C)	Frozen storage duration (h)	Thawing rate (°C/min)	Number of freeze–thaw cycles		
						depended on the number of freeze–thaw cycles	
105.6/99.6 (10–15 wt%)		−20 to −40 and partial lyophylization	12–24	–	1	Preparation of PVA cryogels via polymer solution freezing with the additional partial lyophilization; evaluation of mechanical strength of final gel species	[9, 300, 301]
66/99 (10–16 wt%)	DMSO ($T_0 = +18.4\ °C$)	−10	20	–	1	Apparently the first report on the possibility of PVA cryotropic gelation in frozen organic medium	[30]
69/99 (10 wt%)	Water	−15	12	–	1	Evidence of the noncovalent nature of intermolecular links in PVA cryogels	[302]
90/98 (8 wt%)		−10	24				
110/97.5 (6 wt%)		−20	18; 240				
95.6–110 or 98–99 (0.003 g/dL)		−25; −196	24		1–9		[303, 304]
iPVA: 660/99.9 (9 wt%)	Water	−20	20	–	1–4	Evidence of the key role of H-bonding for	[305–307]

aPVA: 74.8/99.9 (9 wt%)							
sPVA: 66/99.9							
aPVA: 74.8/99.9 (3 wt%)	D$_2$O or DMSO-d_6	−50	—		1	[308]	intermolecular linking in PVA cryogels via the interactions of OH groups of neighboring chains
iPVA:49.7/100 or 400/100 (3 wt%)							
37/98 (2.5 wt%); 69/99 (2.5 wt%)	Water	−20	25	—	1	[309]	
160/98 (0.001–8 g/dL)	Water	−25	24	—	1	[310]	Finding the critical concentration of gelation for the PVA cryogels case
138/100 (0.1–1.0 g/dL)		−10; −20; −30		3.00; 0.30; 0.03	1	[311]	
154/99.8 (15 wt%)	Water	−15	23	—	1–14	[312]	Experimental proving (using various methods of physicochemical analysis) that junction knots in PVA cryogels are microcrystallites
88/– (3–9 wt%)		200 K (ca. −73)	—	5 or 10 K/min	1	[313]	
18.5 to 78.8/99.8 (2–35 wt%)		−20	12	—	1	[314]	
35.7/99; 64/99; 88.9/99.8 (7–15 wt%)		−20	8	—	3–7	[315]	
89–98/99 (10–35 wt%)		−20	21	—	1–10	[316]	
61.6/98.7 (9–29 wt%)		−15	12	—	1	[317]	
115/98–99 (11 wt%)	D$_2$O	−22	4–20	—	1–10	[318–323]	
115/98–99 (5 and 10 wt%)		−13	0–6.5	—	1	[324]	
115/98–99 (5.03; 10.11; 14.22 wt%)			0–2	—	1	[325]	

Table 3 (continued)

Polymeric precursor (its concentration in the feed)	Solvent	Conditions of cryotropic gel formation				What was done and reported	References
		Freezing temperature (°C)	Frozen storage duration (h)	Thawing rate (°C/min)	Number of freeze–thaw cycles		
69/99 (7–14 wt%)	Water	−1 to −30	24	1.00; 0.20; 0.02	1	Revealing the significance of the defrosting rate for the formation of PVA cryogels, in general, and for the properties of the gels when those are formed.	[326, 327]
PVA 138/100 (0.1–1.0 g/dL)		−10, −20, −30		3.00; 0.30; 0.03			[311, 328]
81.7/98.5 (10 g/dL)		−18	18	0.20; 0.02			[329]
69/99; 86/100; 115/100 (8–12 g/dL)		−10; −20; −30; −40	24	0.30; 0.03; 0.003			[330, 331]
81.7/98 (10 wt%)	Water	−1 to −10	0–0.5	1.0	1	Studies on frozen PVA solutions	[332]
69/99 (14 wt%)	H_2O–D_2O mixtures	−10 to −30	1–10				[333, 334]
90/98 (10 wt%)	D_2O or DMSO-d_6	0 to −66	1	—			[335]
aPVA: 74.8/99.9 (3 wt%)		−50		—			[336]
iPVA: 400/100 (3 wt%) −/98.5 (20, 30, or 50 wt%)	H_2O or D_2O	0.25–2		—			[337]
69/99 (7–14 wt%)	Water	−1 to −30	24	1.00; 0.20; 0.02	1	Studies on the microstructure and porosity	[326, 333]

PVA	Solvent	Temperature (°C)	Time (h)	Conc.	Cycles	Notes	References
69/99; 86/100; 115/100 (8–12 g/dL)		−10; −20; −30; −40	24–240	0.30; 0.03; 0.003		characteristics of PVA cryogels.	[330, 331]
69/99 (10, 14, or 16 wt%)		−10; −20		–			[338]
77/99.5 (10, 20, or 30 wt%)		−20	24	–			[339]
160/99.3 (4, 8, or 12 wt%)	DMSO or DMSO–water mixtures	−20; −60	15	–			[340, 341]
82/98 (10 wt%)	Water	−20	24	0.2			[342]
145/99.4 (19 wt%)		−20	0.5	5.0	1–24		[343]
69/99 (12 g/dL)		−20	18	0.30; 0.03	1		[344]
72/97.5–99.5 (10–12 wt%)		−25	10	0.5	1–14		[345]
69/99 (8, 10, or 12 g/dL)	Water	−20	19	0.3	1–5	Studies on microstructure and porosity characteristics of PVA cryogels	[346]
88/98 (10 wt%)		−10	20	–	2		[347]
146–186/99 (10 wt%)	D₂O	−20	1	0.1	1–6		[348–350]
94/99 (10–20 wt%)		−32	1–12	–	1–16		[351]
22/98.5; 44/98.5; 74.8/98.5; 105.6/98.5; 74.8/96; 74.6/97.5; 74.8/99.9 (all 15 wt%)	Water	−60	6	0.389	1–20	Preparation of PVA cryogels and study of their properties as dependent on the cryotropic gelation conditions	[352]
74.8/98.5 (7.5–20 wt%)		−20	23	–	1		[353]
80/98 (15 wt%)		−25	16	–	1–4		[354]
35.4/99.6; 72.2/99.6 (both 10 or 15 wt%)		−20	1–24	–	1–9		[355, 356]
48/99; 103/99 (15 or 20 wt%)	Water	−20	6 or 12	–	2–5	Preparation of PVA cryogels and study of their properties as	[310]
108/99.7 (5 or 10 wt%)		−15	24		1–13		[357]

(continued)

Table 3 (continued)

Polymeric precursor (its concentration in the feed)	Solvent	Conditions of cryotropic gel formation				What was done and reported	References
		Freezing temperature (°C)	Frozen storage duration (h)	Thawing rate (°C/min)	Number of freeze–thaw cycles		
PVA 81.7/98 (10 wt%); 110/99.5 (9.4 g/dL)		−80	3	0.083; 0.11-1; 0.333	4	dependent on the cryotropic gelation conditions	[358]
83/100(−)		−16; −20	–	–	1		[359]
31–50/98–99 (5 or 10 wt%)		−18	12	1.7	1		[360]
aPVA: 84/99.9 or 342/99.9; sPVA:74.4/99.9 or 353/99.9 (2–8.8 g/dL)		−38	72	–	1		[361]
88/99 or 94/99 (20 wt%)	Water	−20	12	–	3		[362]
Mixtures of aPVA: 84/98 and sPVA: 35.2/99.8; 48.4/99.8; 193/98 (5 wt%)		−30	10	–	3	Preparation of PVA cryogels and study of their properties as dependent on the cryotropic gelation conditions	[363]
130/– (15 or 20 wt%)		−20	12	–	1		[364]

In the above boxes related to PVA cryogels, see the data of [30, 328, 330–333, 338, 346] that also contain information on the influence of the cryotropic gelation conditions on the properties of resulting PVA cryogels

Dash means no data; *aPVA* atactic polymer; *iPVA* PVA rich in isotactic fragments; *sPVA* syndiotactic-rich polymer

[a]For PVA cryogels the values of the polymer molecular weight (in kDa) and the deacylation degree (in %) are given in Column 1 as a vulgar fraction, when the data are available from the relevant publications

heterophase PVA–solvent systems [308, 332–337]. Features of the microstructure of PVA cryogels were ascertained using various microscopy techniques [330, 331, 333, 338–346] and other physicochemical analysis methods [237, 326, 347–351].

In these studies, the following five principal facts were established:

1. The nodes in the 3D supramolecular network of PVA cryogels have a noncovalent nature. Therefore, such cryogels can be fused upon heating above the gel melting temperature with the formation of a polymer solution without any change in the characteristics of PVA molecular weight compared to that before freezing [30, 302–304]. This feature is observed provided that the used polymer is pure, i.e., it contains no reactive admixtures, frequently present in industrial PVA specimens.
2. Intermolecular H-bonding via the interactions of OH groups of the neighboring PVA chains plays a key role in the formation of PVA cryogels [305–309].
3. The junction knots in these cryogels were experimentally proven to be PVA microcrystallites [312–317]. A series of works conducted by a team of Italian researchers on this topic [318–325] is very impressive; the same can be said about the precision study by a Japanese team who found that each junction knot in PVA cryogels includes, depending on the gel formation conditions, about 2–3 chains with around 24–120 segments [314].
4. The defrosting rate of frozen PVA solutions plays a significant role in the formation and properties of PVA cryogels [234, 311, 326–331].
5. The molecular weight of PVA, chain tacticity, amount of residual O-acyl groups, and PVA concentration, as well as the conditions of freezing, frozen storage, and thawing have a significant effect on the properties and macroporosity of PVA cryogels [1, 9, 10, 23, 29, 30, 232–236, 254, 258, 299–301, 310–316, 326–331, 333, 338, 346, 352–364, 366–372].

Because the number of publications dealing with the relationships between the preparation conditions of PVA cryogels and their properties is large, Table 3 summarizes only the most important of them, from the viewpoint of the author of this review. Apart from PVA cryogels formed from simple two-component feeds (e.g., from systems composed of PVA dissolved in a neat solvent), a large amount of data is also available in the literature on PVA cryogels that contain soluble foreign additives, both of low and high molecular weights. In the former case, the corresponding cryogels can be classified as those prepared from PVA dissolved in a mixed solvent, whereas in the latter case a more suitable term is "complex PVA cryogels." It should also be noted that there are also extensive studies on "composite PVA cryogels" that contain various discrete fillers. Different soluble and insoluble additives have been introduced in the initial PVA solutions to obtain complex and filled PVA cryogels, respectively. It was shown that the type of additives can affect, more or less, the properties and the microstructure of the resulting cryogels. Since the character of such an influence is very diverse and the observed effects can be multidirectional, such examples are not cited in Table 3. However, readers interested in the principal studies in these fields can find the corresponding references in the following reviews and recent experimental articles:

PVA formed in mixed solvents [1, 20, 23, 234, 264, 373], complex PVA cryogels [1, 234, 239, 374], and composite PVA cryogels [1, 20, 23, 29, 234, 236, 237, 252, 254, 265, 375–377].

2.5 Ionic (Ionotropic) Cryogels

As pointed out above, the accomplishment of gel formation through crosslinking of polyelectrolyte chains with suitable counterions within the space of the unfrozen liquid microphase is a difficult task because of the high rate of the ionic processes. As a rule, conventional ionotropic gelation occurs before freezing of the gelling system. This is the reason why there is only a limited number of successful examples of preparation of ionically crosslinked cryogels by this "direct" route (e.g., [33, 34]). However, the cryogenically structured macroporous gel-like matrices can be fabricated by using roundabout pathways.

One way is the freezing of the partially (incompletely) formed gel, followed by its frozen storage in order to complete the ionic crosslinking, and then sublimation of the frozen solvent crystals. Such a sequence of operations results in macroporous dry cryostructurates that are transformed upon swelling in macroporous gels. This approach was used, for instance, for the preparation of Ca-alginate-based wound/burn dressings [34], or wide-pore scaffolds for tissue engineering [378–380].

Another method includes freezing the polyelectrolyte solution, followed by the removal of frozen solvent crystals without their thawing. The latter can be done either via freeze-drying, or via cryoextraction, i.e., by rinsing the frozen sample at a negative temperature with a liquid that acts as a solvent for the crystalline phase but a nonsolvent for the polyelectrolyte. The resulting macroporous cryostructurate is then treated with an agent capable of either ionically crosslinking the polymeric chains, or recharging their ionogenic groups. This stage is also carried out in a nonsolvent for the macromolecular material. A macroporous gel is obtained upon subsequent swelling of the resulting material in the respective solvating liquids. This approach was employed for the fabrication of wide-pore cryostructured matrices based on both polyacids and polybases [1]. For example, in order to prepare Ca-alginate sponges, the initial aqueous sodium alginate solution was frozen, and ice polycrystals were then removed via vacuum sublimation or via cryoextraction with cold ethanol. The resultant cryogenically structured polymer was then immersed in an ethanolic solution of calcium salt for ionic crosslinking leading to water-insoluble sponge-like Ca-alginate cryogel [381]. Such sponges possessing a system of interconnected gross pores of capillary size are of interest as cell culture scaffolds in biotechnological systems [382–384]. The preparation of cryostuctured polyelectolytes through recharging of their ionic groups can be exemplified by chitosan-based sponges. Here, after removal of ice crystals from the frozen chitosan–aqueous acetic acid system, the resulting cryostructurate was treated with alkaline acetone, thus causing formation of water-insoluble unprotonated

chitosan base [385]. Wide-pore sponges of this material were also used as scaffolds for the 3D culturing of animal cells [386].

Thus, there are wide opportunities for the creation of diverse polyelectrolyte-based cryostructured gel-like matrices, whose properties and porous morphology can be varied in desired directions by an appropriate choice of the polymeric precursor and the respective counterions, their concentrations, by the freezing conditions, and by the procedure for the removal of frozen solvent.

3 Concluding Remarks

Fundamental studies and applied research on cryotropic gelation and various polymeric cryogels have been in progress for more than 40 years. As a result, numerous interesting observations have been made, mechanisms of the processes contributing to the formation of cryogels have been established, a series of cryogels possessing remarkable properties have been developed, and diverse practical applications have been realized (see reviews [1, 18–29, 184, 232–265, 387–404]).

It is evident that this part of polymer science did not start from a "clean slate." First of all, there were different empiric observations on the freeze–thaw-caused gelation in systems like the above mentioned kori-tofu case. Second, it is necessary to emphasize the key role of the knowledge accumulated on the specific features of various chemical reactions in non-deeply frozen multicomponent solutions. In this respect, the pioneering studies that revealed the occurrence per se of such reactions in the moderately frozen systems were of great significance (see, e.g., [405–408]). These studies identified the existence of an unfrozen liquid microphase, and gave quantitative descriptions of the kinetic peculiarities of the relevant cryochemical reactions [2, 409–412]. Third, another important basis for the development of research on cryotropic gel formation was information on routes for the preparation of conventional covalent and noncovalent gels, their properties, and the factors that influence them. Moreover, a series of studies on frozen polymer–solvent systems should also be noted (e.g., [413–417]). The results of these studies allow a deeper understanding of the important fact that, in moderately frozen macromolecular solutions and even in frozen gels, the chain segments do not lose a certain degree of mobility and, hence, interaction of such segments can cause further transformations within the system up to the formation of a spatial polymeric network. Therefore, all the listed sources can be considered as the roots that supplied the "tree of polymeric cryogels" with the necessary primary "nutrients" available at the time when intense studies on cryotropic gel formation began. The subsequent growth and branching of this tree produced fine fruits, these being both new fundamental knowledge and the development of such wonderful gel materials as polymeric cryogels with their multitudinous practical applications, which are discussed in some of the subsequent chapters of this volume.

References

1. Lozinsky VI (2002) Russ Chem Rev 71:489
2. Sergeev GB, Batyuk VA (1976) Russ Chem Rev 45:391
3. Thomson Reuters (2013) Web of science http://apps.webofknowledge.com/summary.do?SID=S2oiGehEbAGc9ng8Jb1&product=WOS&qid=1&search_mode=GeneralSearch
4. Lozinsky VI, Vainerman ES, Korotaeva GF, Rogozhin SV (1984) Colloid Polym Sci 262:617
5. Schulze WE, Yu DT, MacMasters MM (1964) Stärke 16:41
6. Vol'khin VV, Ponomarev EI, Zolotavin VL (1973) Kolloidn zhurn 35:144 (in Russian)
7. Tolstoguzov VB, Braudo EE (1983) J Texture Stud 14:183
8. Lawrence R, Consolacion F, Jelen P (1986) Food Technol 40:77
9. Watase M, Nishinari K, Nambu M (1983) Polym Commun 24:52
10. Nagura N, Nagura M, Ishikawa H (1984) Polym Commun 25:313
11. Cryogel (2007) Ice ball thermal storage. http://www.cryogel.com
12. Katsume C, Abe Y, Horiuchi T, Matsubara S, Ueno M, Matsugane T, Blasutig E, Smith JW, Malchesky PS, Nose Y (1983) Trans Am Soc Artif Inter Organs 29:463
13. Miyamoto K, Tokita K, Miyashita K, Sakashita E (2001) Int J Biol Macromol 28:183
14. Tamon H, Ishizaka H, Yamamoto T, Suzuki T (1999) Carbon 37:2049
15. Tamon H, Ishizaka H, Yamamoto T, Suzuki T (2001) Dry Technol 19:313
16. Job N, Thery A, Pirard R, Marien J, Kocon L, Rouzaud JN, Beguin F, Pirard JP (2005) Carbon 43:2481
17. Zhang H, Cooper AI (2007) Adv Mater 19:1529
18. Gutiérrez MC, Ferrer ML, del Monte F (2008) Chem Mater 20:634
19. Kaetsu I (1993) Adv Polym Sci 105:81
20. Lozinsky VI, Plieva FM, Galaev IY, Mattiasson B (2001) Bioseparation 10:163
21. Lozinsky VI, Galaev IY, Plieva FM, Savina IN, Jungvid H, Mattiasson B (2003) Trends Biotechnol 21:445
22. Dainiak MB, Galaev IY, Kumar A, Plieva FM, Mattiasson B (2007) Adv Biochem Eng Biotechnol 106:101
23. Lozinsky VI (2008) Russ Chem Bull 57:1015
24. Plieva FM, Galaev IY, Noppe W, Mattiasson B (2008) Trends Microbiol 16:543
25. Kumar A, Mishra R, Reinwald Y, Bhat S (2010) Mater Today 13:42
26. Plieva FM, Galaev IY, Mattiasson B (2010) Production and properties of cryogels by radical polymerization. In: Mattiasson B, Kumar A, Galaev I (eds) Macroporous polymers: production, properties and biological/biomedical applications. CRC, Boca Raton, p 23
27. Kirsebom H, Mattiasson B (2011) Polym Chem 2:1059
28. Plieva FM, Kirsebom H, Mattiasson B (2011) J Sep Sci 34:2164
29. Gun'ko VM, Savina IN, Mikhalovsky SV (2013) Adv Colloid Interface Sci 186–187:1
30. Rogozhin SV, Lozinsky VI, Vainerman ES, Domotenko LV, Mamtsis AM, Ivanova SA, Shtil'man MI, Korshak VV (1984) Doklady Akademii nauk SSSR 278:129–133 (in Russian)
31. Lozinsky VI, Konstantinova NR, Solov'eva NI (1994) Russian Patent 2,058,083
32. Konstantinova NR, Lozinsky VI (1997) Food Hydrocolloids 11:113
33. Vainerman ES, Lozinsky VI, Rogozhin SV, Raskina LP, Shapiro LA, Yakubovich VS, Bronshtein VY (1983) SU Patent 1,171,474

34. Vainerman ES, Lozinsky VI, Rogozhin SV, Raskina LP, Shapiro LA, Yakubovich VS, Shenker MB, Komissarova AL, Potapov VD, Gudochkova VM, Atyasova NM, Ivanova GA (1983) SU Patent 1,171,476
35. Lozinsky VI, Vainerman ES, Rogozhin SV (1982) SU Patent 1,008,214
36. Fukushima D (1981) J Am Oil Chem Soc 58:346
37. Watanabe T, Nakayama O, Iwasaki N (1963) Nippon Shokuhin Kogyo Gakkaishi 10:163 (in Japanese)
38. Hashizume K, Kakiuchi K, Koyama K, Watanabe T (1971) Agric Biol Chem 35:449
39. Watanabe T (1974) J Am Oil Chem Soc 51:111A
40. Shimoyama M, Tomadsu K, Oku S, Watanabe K (2000) J Agric Food Chem 48:2775
41. Buttkus H (1971) Can J Biochem 49:97
42. Buttkus H (1974) J Food Sci 39:484
43. Rogožin SV, Slonimskij GL, Rogovina LZ, Vajerman ES, Pivovarov PP (1981) Die Nahrung 25:391
44. Rogozhin SV, Belavtseva EM, Vainerman ES, Radchenko LG, Pivovarov PP, Golvina TO, Pertsevoy FV (1984) Die Nahrung 28:165
45. Jiang ST, Hwang BS, Tsao CY (1987) J Agric Food Chem 35:22
46. Jiang ST, Hwang BS, Tsao CY (1987) J Food Sci 52:117
47. Bhattacharya M, Hanna MA, Mandigo RW (1988) J Food Sci 53:696
48. Stoyachenko IA, Vainerman ES, Rogozhin SV (1988) Appl Biochem Microbiol 24:712
49. Vainerman ES, Lozinsky VI, Rogozhin SV (1981) Colloid Polym Sci 259:1198–1201
50. Rogozhin SV, Vainerman ES, Lozinsky VI (1982) Doklady Akademii nauk SSSR 263:115 (in Russian)
51. Lozinsky VI, Golovina TO, Vainerman ES, Rogozhin SV (1989) Polym Sci USSR 31A:367
52. Lozinsky VI, Golovina TO, Gusev DG (2000) Polymer 41:35
53. Rogozhin SV, Vainerman ES, Pichugin NM, Kirilenko YK, Lozinsky VI, Kosolapov AM, Gnezdilova TV, Chumakov SD, Aboyants RK, Istranov LP (1988) SU Patent 1,603,723
54. Lozinsky VI, Gnezdilova TV (1992) Russian Patent 2,053,796
55. Podorozhko EA, Kulakova EA, Kurskaya EA, Lozinsky VI (1995) Russian Patent 2,116,801
56. Rogozhin SV, Pichugin NM, Vainerman ES, Gnezdilova TV, Kirilenko YK, Chumakov SD, Lozinsky VI (1988) SU Patent 1,653,318
57. Mikhalev OI, Petrov AN, Genzdilova TV, Lozinsky VI, Alfimov MV (1992) Russian Patent 2,008,362
58. Kalinina EV, Semenova NN, Rogozhin SV, Lozinsky VI (1995) Russian Patent 2,116,350
59. Vainerman ES, Portnaya IB (1992) Russian Patent 2,108,350
60. Vainerman ES, Portnaya IB (1996) US Patent 5,494,939
61. Kirsebom H, Mattiasson B, Galaev IY (2009) Langmuir 25:8462
62. Kirsebom H, Mattiasson B, Galaev IY (2010) Macromol Rapid Commun 31:1095
63. Hajizadeh S, Xu C, Kirsebom H, Ye L, Mattiasson B (2013) J Chromatogr 1274A:6
64. Connell JJ (1959) Nature 183:664
65. Connell JJ, Howgate PF (1964) J Food Sci 29:717
66. Arai S, Watanabe M (1986) Agric Biol Chem 50:169
67. Podorozhko EA, Portnaya IB, Kulakova VK, Kurskaya EA (1995) Russian Patent 2,115,668
68. Podorozhko EA, Andreeva LM, Kurskaya EA, Lozinsky VI (1997) Russian Patent 2,118,495
69. Podorozhko EA, Kurskaya EA, Kulakova VK, Lozinsky VI (2000) Food Hydrocolloids 14:111
70. Schierbaum F, Richter M (1964) Die Nahrung 8:487
71. Chan WS, Toledo TR (1976) J Food Sci 4:301
72. Von Eberstein K, Hopcke R, Konieczny-Janda G, Stute R (1980) Stärke 32:397
73. Ferrero C, Martino MN, Zaritzky NE (1993) Int J Food Sci Technol 17:191
74. Lozinsky VI, Damshkaln LG, Brown R, Norton IT (2000) J Appl Polym Sci 78:371
75. Guraya HS, James C, Champague ET (2001) Starch/Stärke 53:64
76. Chung HJ, Jeong HY, Lim ST (2003) Carbohydr Polym 54:449

77. Wasserman LA, Vasil'ev VG, Motyakin MV, Blaszchak W, Fornal J, Damshkaln LG, Lozinsky VI, Yuryev VP (2009) Starch/Stärke 61:377
78. Qian D, Chang PR, Ma X (2011) Carbohydr Polym 86:1181
79. Blažek L, Dvoržak E, Myšik S (1964) Koll Zhurn 26:657 (in Russian)
80. Myšik S, Blažek L, Dvoržak E (1965) Koll Zhurn 27:563 (in Russian)
81. Kiseleva OG, Tikhonova TS, Khryukina NM, Neiman RE (1975) Koll Zhurn 37:783 (in Russian)
82. Nakamura A, Osada R (1977) Colloid Polym Sci 255:362
83. Vainerman ES, Podorozhko EA, Portnaya IB (1992) Russian Patent 2,062,227
84. Collard CAL, Cave RA, Grossiord N, Covington JA, Bon SAF (2009) Adv Mater 21:2894
85. Neiman RE (1967) Coagulation of synthetic latexes. Voronezh State University, Voronezh, pp 148–159 (in Russian)
86. Van Vlierberghe S, Dubruel P, Lippens E, Masschaele B, Van Hoorebeke L, Cornelisson M, Unger R, Kirkpatrick CJ, Schacht E (2008) J Mater Sci Mater Med 19:1459
87. Van Vlierberghe S, Dubruel P, Schacht E (2010) J Bioact Compat Polym 25:498
88. Artyukov AA, Shtilman MI, Kuskov AN, Pashkova LI, Tsatsakis AM, Rizos AK (2011) J Non-Cryst Solids 357:700
89. Artyukov AA, Shtilman MI, Kuskov AN, Fomina AP, Lisovyy DE, Golunova AS, Tsatsakis AM (2011) J Polym Res 18:667
90. Lozinsky VI, Korneeva MN, Vainerman ES, Rogozhin SV (1983) Doklady Akademii nauk SSSR 270:101 (in Russian)
91. Lozinsky VI (1994) Doctoral Science Thesis. Institute of Organoelement Compounds, Russian Academy of Sciences, Moscow (in Russian)
92. Rogozhin SV, Lozinsky VI, Vainerman ES, Korshak VV (1983) Doklady Akademii nauk SSSR 273:1140 (in Russian)
93. Yoshida M, Kumakura M, Kaetsu I (1979) Polymer 20:3
94. Yoshida M, Kumakura M, Kaetsu I (1979) Polymer 20:9
95. Kumakura M, Kaetsu I (1983) Makromol Chem 184:1831
96. Kaetsu I, Kumakura M, Yoshida M (1979) Biotechnol Bioeng 21:847
97. Kumakura M, Kaetsu I (1983) J Polym Sci Polym Lett 21:609
98. Kumakura M, Kaetsu I (1984) Polymer J 16:113
99. Kumakura M, Kaetsu I (1984) Colloid Polym Sci 262:450
100. Kumakura M (2001) Polym Adv Technol 12:415
101. Reichelt S, Abe C, Hainich S, Knolle W, Decker U, Prager A, Konieczny R (2013) Soft Matter 9:2484
102. Petrov P, Petrova E, Tsvetanov CB (2009) Polymer 50:1118
103. Petrov P, Pavlova S, Tsvetanov CB, Topalova Y, Dimkov R (2011) J Appl Polym Sci 122:1742
104. Kostova B, Momekova D, Petrov P, Momekov G, Toncheva-Moncheva N, Tsvetanov CB, Lambov N (2011) Polymer 52:1217
105. Lozinsky VI, Vainerman ES, Titova EF, Belavtseva EM, Rogozhin SV (1984) Colloid Polym Sci 262:769
106. Belavtseva EM, Titova EF, Lozinsky VI, Vainerman ES, Rogozhin SV (1984) Colloid Polym Sci 262:775–779
107. Lozinsky VI, Vainerman ES, Ivanova SA, Titova EF, Shtil'man MI, Belavtseva EM, Rogozhin SV (1986) Acta Polym 37:142
108. Lozinsky VI, Morozova SA, Vainerman ES, Titova EF, Shtil'man MI, Belavtseva EM, Rogozhin SV (1989) Acta Polym 40:8
109. Plieva FM, Savina IN, Deraz S, Andersson J, Galaev IY, Mattiasson B (2004) J Chromatogr 807B:129
110. Persson P, Baybak O, Plieva F, Galaev I, Mattiasson B, Nilsson B, Axelsson A (2004) Biotechnol Bioeng 88:224
111. Plieva FM, Andersson J, Galaev IY, Mattiasson B (2004) J Sep Sci 27:828

112. Plieva FM, Karlsson M, Aguilar MR, Gomez D, Mikhalovsky, Galaev IY (2005) Soft Matter 1:303
113. Plieva F, Huiting X, Galaev I, Bergenstähl B, Mattiasson B (2006) J Mater Chem 16:4065
114. Dinu MV, Ozmen MM, Dragan E, Okay O (2007) Polymer 48:195
115. Gusev DG, Lozinsky VI, Bakhmutov VI (1993) Eur Polym J 29:49
116. Kirsebom H, Rata G, Topgaard D, Mattiasson B, Galaev IY (2009) Macromolecules 42:5208
117. Ozmen MM, Okay O (2008) React Funct Polym 68:1467
118. Ozmen MM, Dinu MV, Okay O (2008) Polym Bull 60:169
119. Shtil'man MI, Denisova LA, Ostaeva GY, Donetsky IA, Kondaryuk VV, Pchelintseva OA, Lozinsky VI, Vainerman ES, Rogozhin SV (1987) SU Patent 1,531,440
120. Mattiasson B, Galaev I, Lozinsky V, Plieva F (2003) WO 2003/041830
121. Arvidsson P, Plieva FM, Savina IN, Lozinsky VI, Fexby S, Bulow L, Galaev IY, Mattiasson B (2002) J Chromatogr 977A:27
122. Arvidsson P, Plieva FM, Lozinsky VI, Galaev IY, Mattiasson B (2003) J Chromatogr 986A:275
123. Yao K, Shen S, Yun J, Wang L, He X, Yu X (2006) Chem Eng Sci 61:6701
124. Demiryas N, Tüzmen N, Galaev IY, Pişkin E, Denizli A (2007) J Appl Polym Sci 105:1808
125. He X, Yao K, Shen S, Yun J (2007) Chem Eng Sci 62:1334
126. Topus F, Okay O (2009) React Funct Polym 69:273
127. Ceylan D, Ozmen MM, Okay O (2006) J Appl Polym Sci 99:319
128. Zhang XZ, Zhuo RX (1999) Macromol Rap Commun 20:229
129. Zhang XZ, Zhuo RX (1999) Macromol Chem Phys 200:2602
130. Srivastava A, Jain E, Kumar A (2007) Mater Sci Eng 464:93
131. Chalal M, Ehrburger-Dolle F, Morfin I, Vial JC, de Armas MRA, Roman JS, Bülgen N, Pişkin E, Ziane O, Caslegno R (2009) Macromolecules 42:2749
132. Liu H, Liu M, Bai L, Sun S, Liu Y, Yang G (2011) Talanta 85:1193
133. Zhang XZ, Chu CC (2003) Chem Commun 2003(12):1446
134. Zhang XZ, Chu CC (2003) J Mater Chem 13:2457
135. Zhao Q, Sun J, Zhou Q (2007) J Appl Polym Sci 104:4080
136. Zhao Q, Sun J, Ling Q, Zhou Q (2008) J Polym Sci Polym Chem 19:6594
137. Xue W, Hampley IW, Huglin MB (2002) Polymer 43:5181
138. Xue W, Champ S, Huglin MB, Jones TGJ (2004) Eur Polym J 40:468
139. Akkaya B, Akkaya R (2012) J Macromol Sci Pure Appl Chem 49:736
140. Vakifli A, Demirel G, Caykara T (2010) J Appl Polym Sci 117:817
141. Komarova GA, Starodubtsev SG, Lozinsky VI, Kalinina EV, Landfester K, Khokhlov AR (2008) Langmuir 24:4467
142. Komarova GA, Starodubtsev SG, Lozinsky VI, Nasimova IR, Khokhlov AR (2013) J Appl Polym Sci 127:2703
143. Burova TV, Grinberg NV, Kalinina EV, Ivanov RV, Lozinsky VI, Alvarez-Lorenzo C, Grinberg VY (2011) Macromol Chem Phys 212:72
144. Lozinsky VI, Kalinina EV, Grinberg VY, Grinberg NV, Chupov VA, Platé NA (1997) Polym Sci 39A:1300
145. Ozmen MM, Okay O (2005) Polymer 46:8119
146. Ozmen MM, Okay O (2006) J Macromol Sci Pure Appl Chem 43:1215
147. Kirsebom H, Rata G, Topgaard D, Mattiasson B, Galaev IY (2008) Polymer 49:3855
148. Kirsebom H, Rata G, Topgaard D, Mattiasson B, Galaev IY (2009) Macromolecules 42:2009
149. Lozinsky VI, Zaborina OE (2011) Russian Patent 2,467,017
150. Caykara T, Küçüktepe S, Turan E (2006) Macromol Mater Eng 291:1278
151. Chen Z, Xu L, Liang Y, Wang J, Zhao M, Li Y (2008) J Chromatogr 1182A:128
152. Pavlova LA, Kostel'yanos-Dominges OM (1996) Zhurn Prikl Khim 69:829 (in Russian)
153. Pavlova LA, Kostel'yanos-Dominges OM (1996) Zhurn Prikl Khim 69:1558 (in Russian)
154. Savina IN, Cnudde V, D'Hollander S, Van Hoorebeke L, Mattiasson B, Galaev IY, Du Prez F (2007) Soft Matter 3:1176

155. Andac M, Plieva FM, Denizli A, Galaev IY, Mattiasson B (2008) Macromol Chem Phys 209:577
156. Tekin K, Uzun L, Sahin CA, Bektas S, Denizli A (2011) React Funct Polym 71:985
157. Bereli N, Erturk G, Denizli A (2012) Sep Sci Technol 47:1813
158. Srivastava A, Shakya AK, Kumar A (2012) Enzyme Microb Technol 51:373
159. Srivastava A, Kumar A (2010) J Mater Sci Mater Med 21:2937
160. Tamada M, Kasai N, Kaetsu I (1988) Biotechnol Bioeng 32:386
161. Higa OZ, Kumakura M (1977) Biomaterials 18:697
162. Kumakura M, Kaetsu I (1984) React Polym 2:243
163. Kumakura M, Kaetsu I (1984) J Chem Technol Biotechnol 34B:39
164. Di Nino G, Turrachio M, D'Archivio AA, Lora S, Corain B, Antonini G (2004) React Funct Polym 61:411
165. Kumakura M, Kaetsu I (1984) J Mol Catal 23:1
166. Yoshi F, Kaetsu I (1983) Appl Biochem Biotechnol 8:115
167. Fujimura N, Kaetsu I (1987) Biotechnol Bioeng 29:171
168. Piskin K, Arca E, Piskin E (1984) Appl Biochem Biotechnol 10:73
169. Kahveci MU, Beyazkilic Z, Yaggi Y (2010) J Polym Sci Polym Chem 48:4989
170. Christova N, Petrov P, Kabainova L (2013) Z Naturforsch 68c:47
171. Petrov PD, Geoigiev GL (2012) Eur Polym J 48:1366
172. Okaji R, Taki K, Nagamine S, Ohshima M (2012) J Appl Polym Sci 125:2874
173. Shlyakhtin O (2014) Inorganic cryogels. In: Okay O (ed) Polymeric cryogels: macroporous gels with remarkable properties, vol 263, Advances in polymer science. Springer, Heidelberg
174. Dispinar T, Van Camp W, De Cock LJ, De Geest BG, Du Prez PE (2012) Macromol Biosci 12:383
175. Nikonorov VV, Ivanov RV, Kil'deeva NR, Lozinsky VI (2011) Polym Sci 53A:1150
176. Ivanov RV, Lozinsky VI, Noh SK, Lee YR, Han SS, Lyoo WS (2008) J Appl Polym Sci 107:382
177. Cocquemcot MF, Thomas D, Champigny ML, Moyse A (1979) Eur J Appl Microbiol Biotechnol 8:37
178. Dhulster P, Parascandola P, Scardi V (1983) Enzyme Microb Technol 5:65
179. Estival F, Burstein C (1985) Enzyme Microb Technol 7:29
180. Papageorgiou GC, Lagoyanni T (1986) Appl Microbiol Biotechnol 23:417
181. Carpenter R, Lemieux S (1987) Appl Biochem Biotechnol 15:107
182. Lozinsky VI, Vainerman ES, Rogozhin SV (1982) Colloid Polym Sci 260:776
183. Pincock RE (1969) Acc Chem Res 2:97
184. Hansler M, Jakubke HD (1996) J Pept Sci 2:279
185. Elowsson L, Kirsebom H, Carmignac V, Durbeej M, Mattiasson B (2012) J Mater Sci Mater Med 23:2489
186. Jain E, Srivastava A, Kumar A (2009) J Mater Sci Mater Med 20:S173
187. Dainiak MB, Allan IU, Savina IN, Cornelio L, James ES, James SL, Mikhalovsky SV, Jungvid H, Galaev IY (2010) Biomaterials 31:67
188. Jurga M, Dainiak MB, Sarnowska A, Jablonska A, Tripathi A, Plieva FM, Savina IN, Strojek L, Jungvid H, Kumar A, Lukomska B, Domanska-Janik K, Fooraz N, McGuckin CP (2011) Biomaterials 32:3423
189. Mu C, Liu F, Cheng Q, Li H, Wu B, Zhang G (2010) Macromol Chem Eng 295:100
190. Rodrigues SC, Salgado CL, Sahu A, Garcia MP, Fernandes MH, Monteiro FJ (2013) J Biomed Mater Res 101A:1080
191. Chien KB, Shah RN (2012) Acta Biomater 8:694
192. Ak F, Oztoprak Z, Karakutuk I, Okay O (2013) Biomacromolecules 14:719
193. Kirsebom H, Aguilar MR, San Roman J, Fernandez M, Prieto MA, Bondar B (2007) J Bioact Compat Polym 22:2007
194. Nikonorov VV, Ivanov RV, Kil'deeva NR, Bulatnikova LN, Lozinsky VI (2010) Polym Sci 52A:828

195. Hoffmann B, Seitz D, Mencke A, Kokott A, Ziegler G (2009) J Mater Sci Mater Med 20:1497
196. Berillo D, Elowsson L, Kirsebom H (2012) Macromol Biosci 12:1090
197. Chang C, Zhang L, Zhou J, Zhang L, Kennedy JF (2010) Carbohydr Polym 82:122
198. Plieva FM, Karlsson M, Aguilar MR, Gomez D, Mikhalovsky S, Galaev IY, Mattiasson B (2006) J Appl Polym Sci 100:1057
199. Ivanov AE, Kozynchenko OP, Mikhalovska LI, Tennison SR, Jungvid H, Gun'ko VM, Mikhalovsky SV (2012) Phys Chem Chem Phys 14:16267
200. Zheng Y, Gun'ko VM, Howell CA, Sandeman SR, Phillips GJ, Kozynchenko OP, Tennison SR, Ivanov AE, Mikhalovsky SV (2012) ACS Appl Mater Interface 4:5936
201. Ivanov RV, Lozinsky VI, Noh SK, Han SS, Lyoo WS (2007) J Appl Polym Sci 106:1470
202. Hedström M, Plieva F, Galaev I, Mattiasson B (2008) Anal Bioanal Chem 390:907
203. Kathuria N, Triparthi A, Kar KK, Kumar A (2009) Acta Biomater 5:406
204. Peter M, Ganesh N, Selvamurugan N, Nair SV, Furuike T, Tamura H, Jayakumar R (2010) Carbohydr Polym 80:687
205. Sun S, Tang Y, Fu Q, Liu X, Guo L, Zhao Y, Chang C (2012) Int J Biol Macromol 50:1002
206. Vishnoi T, Kumar A (2013) J Mater Sci Mater Med 24:447
207. Orakdogen N, Karacan P, Okay O (2011) React Funct Polym 71:782
208. Okay O (2011) J Polym Sci Polym Phys 49:551
209. Karacan P, Okay O (2013) React Funct Polym 73:442
210. Welzel PB, Grimmer M, Renneberg C, Naujox L, Zschoche S, Freudenberg U, Werner C (2012) Biomacromolecules 13:2349
211. Tuncaboylu DC, Okay O (2009) Eur Polym J 45:2033
212. Karakutuk I, Okay O (2010) React Funct Polym 70:585
213. Liu X, Hu Y, Zou J, Chai, Li B (2013) Appl Mech Mater 295–298:1368
214. Tuncaboylu DC, Okay O (2010) Langmuir 26:7574
215. Park KR, Nho YC (2003) J Appl Polym Sci 90:1477
216. Doycheva M, Petrova E, Stamenova R, Tsvetanov C, Reiss G (2004) Macromol Mater Eng 289:676
217. Petrov P, Petrova E, Stamenova R, Tsvetanov C, Reiss G (2006) Polymer 47:6481
218. Petrov P, Petrova E, Tchorbanov B, Tsvetanov CB, Reiss G (2007) Polymer 48:4943
219. Velickova E, Winkelbausen E, Kuzmanova S, Cvetkovska M, Tsvetanov C (2009) React Funct Polym 69:688
220. Velickova E, Petrov P, Tsvetanov C, Kuzmanova S, Cvetkovska M, Winkelhausen E (2010) React Funct Polym 70:908
221. Jovanovic-Malinovska R, Cvetkovska M, Kuzmanova S, Tsvetanov C, Winkelhausen E (2010) Macedon J Chem Chem Eng 29:169
222. Petrov P, Utrata-Wesolek A, Trzebicka B, Tsvetanov CB, Dworak A, Aniol J, Sieron A (2011) Eur Polym J 47:981
223. Ceylan D, Dogu S, Karacik B, Yakan SD, Okay OS, Okay O (2009) Environ Sci Technol 43:3846
224. Veleshko IE, Nikonorov VV, Veleshko AN, Rumyantseva EV, Mikhailov SN, Lozinsky VI, Ivanov RV, Gal'braikh LS, Kil'deeva NR (2011) Fibre Chem 42:364
225. Kil'deeva NR, Veleshko IE, Vladimirov LV, Nikonorov VV, Lozinsky VI, Ivanov RV, Perminov PA, Mikhailov SN (2012) Fibre Chem 43:426
226. Inoue T (1972) Japanese Patent 47-012854
227. Inoue T (1973) Japanese Patent 48-030462
228. Inoue T (1972) Japanese Patent 48-030463
229. Inoue T (1972) US Patent 3,875,302
230. Kukharchik MM, Baramboim NK (1972) Vysokomolekul soed 14B:843 (in Russian)
231. Peppas NA (1975) Makromol Chem 176:3433
232. Nambu M (1990) Kobunshi Ronbunshu 47:695 (in Japanese)
233. Peppas NA, Stauffer SR (1991) J Control Release 16:305
234. Lozinsky VI (1998) Russ Chem Rev 67:573

235. Hassan CM, Peppas NA (2000) Adv Polym Sci 153:37
236. Gutiérrez MC, Aranaz I, Ferrer ML, del Monto F (2010) Production and properties of poly
     (vinyl alcohol) cryogels: recent developments. In: Mattiasson B, Kumar A, Galaev I (eds)
     Macroporous polymers: production, properties and biological/biomedical applications. CRC,
     Boca Raton, p 83
237. Shapiro YE (2011) Progr Polym Sci 36:1184
238. Suzuki M, Hirasa O (1993) Adv Polym Sci 10:241
239. Lazzeri L (1996) Trends Polym Sci 4:249
240. Chu KC, Rutt BK (1997) Magn Reson Med 37:314
241. Langer R, Peppas NA (2003) AIChE J 49:2990
242. Surry KJM, Austin HJB, Fenster A, Peters TM (2004) Phys Med Biol 49:5529
243. Fromageau J, Genninsson JL, Schmitt C, Maurice RL, Mongrain R, Cloutier G (2007) IEEE
     Trans Ultrason Ferroelectr Freq Control 54:498
244. Hoskins PR (2008) Ultrasound Med Biol 34:693
245. Ghanbari H, Viatge H, Kidane AG, Buriesci G, Tavakoli M, Seifalian AM (2009) Trends
     Biotech 27:359
246. Wang BH, Campbell G (2009) Spine 34:2745
247. Alves MH, Jensen BEB, Smith AAA, Zelikin AN (2011) Macromol Biosci 11:1293
248. Gajra B, Pandya SS, Vidyasagar G, Rabari H, Dedania RR, Rao S (2012) Int J Pharm Res
     4:20
249. Baker MI, Walsh SP, Schwartz Z, Boyan BD (2012) J Biomed Mater Res 100B:1451
250. Lamouche G, Kennedy BF, Kennedy KM, Bisaillon CE, Curatolo A, Campbell G, Pazos V,
     Sampson DD (2012) Biomed Optics Expr 3:1381
251. Iatridis JC, Nicoll SB, Michalek AJ, Walter BA, Gupta MS (2013) Spine J 13:243
252. Lozinsky VI, Vakula AV, Zubov AL (1992) Soviet Biotechnol #4:1
253. Varfolomeev SD, Rainina EI, Lozinsky VI (1992) Pure Appl Chem 64:1193
254. Lozinsky VI, Plieva FM (1998) Enzyme Microb Technol 23:227
255. Varfolomeev SD, Rainina EI, Lozinsky VI, Kalyuzhnyi SB, Sinitsyn AP, Makhlis TA,
     Bachurina GP, Bokova IG, Sklyankina OA, Agafonov EV (1990) In: de Bont JAM,
     Visser J, Mattiasson B, Tramper J. (eds) Physiology of immobilized cells: proceedings of
     an international symposium, Wageningen, The Netherlands, 10–13 Dec 1989. Elsevier,
     Amsterdam, p 325
256. Filippova IY, Bacheva AV, Baibak OV, Plieva FM, Lysogorskaya EN, Oksenoit ES,
     Lozinsky VI (2001) Russ Chem Bull 50:1896
257. Lozinsky VI, Galaev IY, Plieva FM, Savina IN, Jungvid H, Mattiasson B (2003) Trends
     Biotechnol 21:445
258. Lozinsky VI (2004) Chem Ind (Belgrade) 58:111
259. Sheldon RA (2007) Adv Synth Catal 349:1289
260. Kumar A, Srivastava A, Galaev IY, Mattiasson B (2007) Progr Polym Sci 32:1205
261. Plieva FM, Galaev IY, Noppe W, Mattiasson B (2008) Trends Microbiol 16:543
262. Stolarzewicz I, Bialecka-Florjańczyk E, Majewska E, Krzyczkowska J (2011) Chem
     Biochem Eng 25Q:135
263. Cunningham CJ, Ivshina IB, Lozinsky VI, Kuyukina MS, Philp JC (2004) Int Biodeterior
     Biodegr 54:167
264. Altunina LK, Kuvshinov VA, Dolgikh SN (2006) NATO Sci Ser IV Earth Environ Sci 65:103
265. Vasiliev NK, Ivanov AA, Sokurov VV, Shatalina IN, Vasilyev KN (2012) Cold Reg Sci
     Techn 70:94
266. Labudzińska A, Ziabicki A (1971) Koll Z u Z Polym 243:21
267. Kim HJ, Sakamoto M, Tanami H (1983) Kobunshi Ronbunshu 40:579 (in Japanese)
268. Lozinsky VI, Damshkaln LG, Brown CRT, Norton IT (2000) J Appl Polym Sci 75:1740
269. Lozinsky VI, Damshkaln LG, Brown CRT, Norton IT (2002) J Appl Polym Sci 83:1658
270. Lozinsky VI, Damshkaln LG, Plieva FM, Galaev IY, Mattiasson B (2001) Russian Patent
     2,220,987

271. Lozinsky VI, Damshkaln LG, Bloch KO, Vardi P, Grinberg NV, Burova TV, Grinberg VY (2008) J Appl Polym Sci 108:3046
272. Plieva FM, Galaev IY, Mattiasson B (2010) Macroporous polysaccharide gels. In: Mattiasson B, Kumar A, Galaev I (eds) Macroporous polymers: production, properties and biological/biomedical applications. CRC, Boca Raton, p 131
273. Bloch K, Lozinsky VI, Galaev IY, Yavriyanz K, Vorobeychik M, Azarov D, Damshkaln LG, Mattiasson D, Vardi P (2005) J Biomed Mater Res 75A:802
274. Petrenko YA, Petrenko AY, Lozinsky VI, Gurin IV, Gorokhova NA, Volkova NA, Sandomirskii BP (2007) Transplantologiya (Kyev) 9:221 (in Russian)
275. Petrenko YA, Petrenko AY, Damshkaln LG, Volkova NA, Lozinsky VI (2008) Bull Exp Biol Med 146:129
276. Petrenko YA, Volkova NA, Zhulikova EP, Damshkaln LG, Lozinsky VI, Petrenko AY (2008) Biopolym Cell 24:399
277. Bloch K, Vanichkin A, Damshkaln LG, Lozinsky VI (2010) Acta Biomater 6:1200
278. Mattiasson B, Galaev I, Lozinsky V, Plieva F (2003) WO 2003/031014
279. Wu J, Zhang H (2010) In: Williams OA, Phillips GO (eds) Gums and stabilizers for the food industry, vol 15. Royal Society of Chemistry, Cambridge, p 420
280. Najii S, Razavi SMA, Karazhiyan H (2013) Food Bioprocess Techn 6:1302
281. Lazaridou A, Biliaderis CG (2004) Food Hydrocolloids 18:933
282. Vaikousi H, Biliarderis CG (2005) Food Chem 91:505
283. Lazaridou A, Vaikousi H, Biliaderis CG (2008) Food Hydrocolloids 22:263
284. Dea ICM, Morris ER, Rees DA, Welsh J, Barnes HA, Price J (1977) Carbohydr Res 57:249
285. Bringham JE, Gidley MJ, Hoffmann RA, Smith CG (1994) Food Hydrocolloids 8:331
286. Tanaka R, Hatakeyama T, Hatakeyama H (1998) Polym Int 45:118
287. Hatakeyama T, Naoi S, Iljima M, Hatakeyama H (2005) Macromol Symp 224:253
288. Lozinsky VI, Damshkaln IG, Brown R, Norton IT (2000) Polym Int 49:1434
289. Zeira A, Nussinovich A (2004) J Texture Stud 34:561
290. Doyle JP, Giannouli P, Martin EJ, Brooks M, Morris ER (2006) Carbohydr Polym 64:391
291. Himeda Y, Yanagi S, Kakema T, Fujita F, Umeda T, Miyoshi T (2003) J Int Med Res 31:509
292. Himeda Y, Umeda T, Miyata Y, Miyoshi T (2004) J Genecol Surg 20:39
293. Himeda Y, Kaneko H, Umeda T, Miyata Y, Miyoshi T (2005) J Genecol Surg 21:55
294. Giannouli P, Morris ER (2003) Food Hydrocolloids 17:495
295. Najii S, Razavi SMA, Karazhiyan H (2013) Food Bioprocess Technol 6:1302
296. Mu C, Li X, Zhao Y, Zhang H, Wang L, Li D (2013) J Appl Polym Sci 128:3141
297. Berillo D, Mattiasson B, Galaev IY, Kirsebom H (2012) J Colloid Interface Sci 368:226
298. Zuo Z, Guo Y, Li Y, Lv J, Liu H, Li Y (2009) Macromol Rap Commun 30:1940
299. Watase M, Nishinari K, Nambu M (1983) Cryo-Lett 4:197
300. Watase M, Nishinari K (1983) Polym Commun 24:270
301. Watase M, Nishinari K, Ogino K, Nambu M (1983) Polym Commun 24:345
302. Lozinsky VI, Domotenko LV, Vainerman ES, Mamtsis AM, Rogozhin SV (1986) Polym Bull 15:333
303. Liu M, Cheng R, Wu C, Qian R (1997) J Polym Sci Polym Phys 35:2421
304. Liu M, Cheng R, Wu C (1999) Eur Polym J 35:1907
305. Kobayashi M, Ando I, Ishii T, Amiya S (1995) Macromolecules 28:6677
306. Kobayashi M, Ando I, Ishii T, Amiya S (1998) J Mol Struct 440:155
307. Kanekiyo M, Kobayashi M, Ando I, Kurosu H, Ishii T, Amiya S (1998) J Mol Struct 447:49
308. Masuda K, Horii F (1998) Macromolecules 31:5810
309. Lai S, Casu M, Saba G, Lai A, Husu I, Masci G, Crescenzi V (2002) Solid State Nucl Magn Reson 21:187
310. Peppas NA, Mongia NK (1997) Eur J Pharm Biopharm 43:51
311. Damshkaln LG, Simenel IA, Lozinsky VI (1999) J Appl Polym Sci 74:1978
312. Yakoyama F, Masada I, Shimamura K, Ikawa T, Monobe K (1986) Colloid Polym Sci 264:595

313. Hatakeyama T, Yamauchi A, Hatakeyama H (1987) Eur Polym J 23:361
314. Nishinari K, Watase M, Tanaka F (1996) J Chim Phys 93:880
315. Hassan CM, Peppas NA (2000) Macromolecules 33:2472
316. Holloway JL, Lowman AM, Palmese GR (2013) Soft Matter 9:826
317. Tretinnikov ON, Sushko NI, Zagorodskaya SA (2013) Polym Sci 55A:91
318. Ricciardi R, Gaillet C, Ducouret G, Lafuma F, Lauprêtre F (2003) Polymer 44:3375
319. Ricciardi R, Auriemma F, De Rosa C, Lauprêtre F (2004) Macromolecules 37:1921
320. Ricciardi R, Auriemma F, Gaillet C, De Rosa C, Lauprêtre F (2004) Macromolecules 37:9510
321. Ricciardi R, D'Errico G, Auriemma F, Ducouret G, Tedeschi AM, Gaillet C, De Rosa C, Lauprêtre F, Lafuma F (2005) Macromolecules 38:6629
322. Ricciardi R, Mangiapia G, Celso FL, Paduano L, Triolo R, Auriemma F, De Rosa C, Lauprêtre F (2005) Chem Mater 17:1183
323. Ricciardi R, Auriemma F, De Rosa C (2005) Macromol Symp 222:49
324. Auriemma F, De Rosa C, Triolo R (2006) Macromolecules 39:9429
325. Auriemma F, De Rosa C, Ricciardi R, Celso FL, Triolo R, Pipich V (2008) J Phys Chem 112B:816
326. Domotenko LV, Lozinsky VI, Vainerman ES, Rogozhin SV (1988) Polym Sci USSR 30A:1758
327. Lozinsky VI, Domotenko LV, Vainerman ES, Rogozhin SV (1989) Polym Sci USSR 31A:1983
328. Lozinsky VI, Damshkaln LG (2000) J Appl Polym Sci 77:2017
329. Lozinsky VI, Zubov AL, Savina IN, Plieva FM (2000) J Appl Polym Sci 77:1822
330. Lozinsky VI, Damshkaln LG, Shaskol'skii BL, Babushkina TA, Kurochkin IN, Kurochkin II (2007) Colloid J 69:747
331. Lozinsky VI, Damshkaln LG, Kurochkin IN, Kurochkin II (2012) Colloid J 74:319
332. Mikhalev OI, Yakovleva IV, Trofimov VI, Shapiro AB (1985) Cryo-Lett 6:245
333. Lozinsky VI, Vainerman ES, Domotenko LV, Blumenfel'd AL, Rogov VV, Barkovskaya EN, Fedin EI, Rogozhin SV (1989) Colloid J USSR 51:592
334. Mikhalev OI, Serpinski M, Lozinsky VI, Kapanin PV, Chkeidze II, Alfimov MV (1991) Cryo-Lett 12:197
335. Gusev DG, Lozinsky VI, Vainerman ES, Bakhmutov VI (1990) Magn Res Chem 28:651
336. Horii F, Masuda K, Kaji H (1997) Macromolecules 30:2519
337. Nakano T, Nakaoki T (2011) Polym J 43:875
338. Lozinsky VI, Vainerman ES, Domotenko LV, Mamtsis AM, Titova EF, Belavtseva EM, Rogozhin SV (1986) Colloid Polym Sci 264:19
339. Hyon SH, Cha WI, Ikada Y (1989) Kobunshi Ronbunshu 46:673 (in Japanese)
340. Trieu HH, Qutubuddin S (1994) Colloid Polym Sci 272:301
341. Trieu HH, Qutubuddin S (1995) Polymer 36:2531
342. Lozinsky VI, Zubov AL, Titova EF (1996) Enzyme Microb Technol 18:561
343. Willcox PJ, Howie DW, Schmidt-Rohr K, Hoagland DA, Gido S, Pudjijanto S, Kleiner LW, Venkatraman S (1999) J Polym Sci Polym Phys 37:3438
344. Lozinsky VI, Damshkaln LG (2001) J Appl Polym Sci 82:1609
345. Szczesna M, Galas E, Bielecki S (2001) J Mol Catal 11B:761
346. Lozinsky VI, Damshkaln LG, Kurochkin IN, Kurochkin II (2008) Colloid J 70:189
347. Nakaoki T, Yamashita H (2008) J Mol Struct 875:282
348. Millon LE, Mohammadi H, Wan WK (2006) J Biomed Mater Res 79B:305
349. Millon LE, Nieh MP, Hutter JL, Wan W (2007) Macromolecules 40:3655
350. Hudson SD, Hutter JL, Nieh MP, Pencer J, Millon LE, Wan W (2009) J Chem Phys 130: #034903
351. Valentin JL, López D, Hernández R, Mijangos C, Saalwächter K (2009) Macromolecules 42:263
352. Watase M, Nishinari K (1988) Makromol Chem 189:871
353. Hirai T, Asada Y, Suzuki T, Hayashi S, Nambu M (1989) J Appl Polym Sci 38:491

354. Urushizaki F, Yamaguchi H, Nakamura K, Namajiri S, Sugibayashi K, Morimoto Y (1990) Int J Pharm 58:135
355. Stauffer SR, Peppas NA (1992) Polymer 33:3932
356. Hickey AS, Peppas NA (1995) J Membr Sci 107:229
357. Hatakeyama T, Uno J, Yamada C, Kishi A, Hatakeyama H (2005) Thermochim Acta 431:144
358. Mori Y, Tokura H, Yoshikawa M (1997) J Mater Sci 32:491
359. Pazos V, Mongrain R, Tardif JC (2009) J Mech Behav Biomed Mater 2:542
360. Gonzalez JG, Alvarez VA (2011) Thermochim Acta 521:184
361. Fukae R, Yoshimura M, Yamamoto T, Nishinari K (2011) J Appl Polym Sci 120:573
362. Londoňo ME, Jaramillo JM (2011) DYNa-Colombia 78:132 (in Spanish)
363. Huang M, Cai D, Liu Y, Sun J, Wang J, Qin C, Dai L, Yamaura K (2012) Fiber Polym 13:955
364. Stasco J, Berzina-Cimdina L, Kalnins M (2012) Proc Eston Acad Sci 61:228
365. Numbu M, Motomachi H, Tatsuo K, Watase M (1982) Japanese Patent 57-164,870
366. Watase M (1983) Nippon Kagaku Kaisi #7:973 (in Japanese)
367. Watase M (1983) Nippon Kagaku Kaisi #9:1254 (in Japanese)
368. Nagura M, Nagura M, Ishikawa H (1984) Polym Commun 25:313
369. Watase M, Nishinari K (1985) Makromol Chem 186:1081
370. Watase M, Nishinari K (1985) J Polym Sci Polym Phys 23:1803
371. Numbu M (1981) Japanese Patent 56-045,439
372. Bercea M, Morariu S, Rusu D (2013) Soft Matter 9:1244
373. Lozinsky VI, Sakhno NG, Damshkaln LG, Bakeeva IV, Zubov VP, Kurochkin IN, Kurochkin II (2011) Colloid J 73:234
374. Lozinsky VI, Damshkaln LG, Ezernitskaya MG, Glotova YK, Antonov YA (2012) Soft Matter 8:8493
375. Podorozhko EA, Korlyukov AA, Lozinsky VI (2010) J Appl Polym Sci 117:1332
376. Podorozhko EA, Vorontsova TV, Lozinsky VI (2012) Colloid J 74:110
377. Podorozhko EA, D'yakonova EA, Kolosova OY, Klabukova LF, Lozinsky VI (2012) Colloid J 74:711
378. Shapiro L, Cohen S (1997) Biomaterials 18:583
379. Glicklis R, Shapiro L, Agbaria R, Merchuk JC, Cohen S (2000) Biotechnol Bioeng 67:344
380. Zmora S, Glicklis R, Cohen S (2002) Biomaterials 23:4087
381. Lozinsky VI, Simenel IA, Chebyshev AV (1994) Russian Patent 2,035,476
382. Shmarov MM, Tutykhina IL, Logunov DY, Tokarskaya EA, Naroditsky BS, Damshkaln LG, Ivanov RV, Lozinsky VI (2008) Russian Patent 2,381,272
383. Petrenko YA, Ivanov RV, Lozinsky VI, Petrenko AY (2011) Bull Exp Biol Med 150:543
384. Petrenko YA, Ivanov RV, Petrenko AY, Lozinsky VI (2011) J Mater Sci Mater Med 22:1529
385. Lozinsky VI, Zubov AL (1994) Russian Patent 2,078,099
386. Ho MH, Kuo PY, Hsieh HJ, Hsien TY, Hou LT, Lai JY, Wang DM (2004) Biomaterials 25:129
387. Mallik R, Hage DS (2006) J Sep Sci 29:1686
388. Plieva FM, Galaev IY, Mattiasson B (2007) J Sep Sci 30:1657
389. Jungbauer A, Hahn R (2008) J Chromatogr 1184A:62
390. Kumar A, Bhardwaj A (2008) Biomed Mater 3:#034008
391. Nordborg A, Hilder EF (2009) Anal Bioanal Chem 394:71
392. Bolto B, Tran T, Hoang M, Xie Z (2009) Progr Polym Sci 34:969
393. Svec F (2010) J Chromatogr 1217A:902
394. Tetala KKR, van Beek TA (2010) J Sep Sci 33:422
395. Kumar A, Srivastava A (2010) Nat Protocols 5:1737
396. Kirsebom H, Galaev IY, Mattiasson B (2011) J Polym Sci Polym Phys 49:173
397. Spross J, Sinz A (2011) J Sep Sci 34:1958
398. Arrua RD, Igarzabal CIA (2011) J Sep Sci 34:1974
399. Van Vlierberghe S, Dubruel P, Schacht E (2011) Biomacromolecules 12:1387
400. Gunasena DN, Rassi ZE (2012) Electrophoresis 33:251

401. Podgornik A, Krajnc NL (2012) J Sep Sci 35:3059
402. Pfaunmiller EL, Paulemond ML, Dupper C, Hage DS (2013) Anal Bioanal Chem 405:2133
403. Henderson TMA, Ladewig K, Haylock DN, McLean KM, O'Connor AJ (2013) J Mater Chem 21B:2682
404. Zhang H, Zhang F, Wu J (2013) React Funct Polym 73:923
405. Grant NC, Clark DE, Alburn HE (1961) J Am Chem Soc 83:4476
406. Batler AR, Bruice TC (1964) J Am Chem Soc 86:313
407. Pincock RE, Kiovsky TE (1965) J Am Chem Soc 87:2072
408. Pincock RE (1969) Acc Chem Res 2:97
409. Grinberg OY, Nikitaev AT, Zamaraev KI, Lebedev YS (1969) Zhurn Strukt Khim 10:230 (in Russian)
410. Sergeev GB, Batyuk VA, Stepanov MB, Sergeev BM (1973) Doklady Akademii nauk SSSR 213:891 (in Russian)
411. Kvlividze VI, Pylova MB (1977) Koll Zhurn 39:1167 (in Russian)
412. Sergeev GB, Sergeev BM, Kalnina IA (1984) Zhurn Fiz Khim 58:2431 (in Russian)
413. Kawai T (1958) J Polym Sci 32:425
414. Solms DJ, Rijke AM (1971) J Phys Chem 75:2623
415. Meryman HT (1971) Cryobiology 8:173
416. Smith P, Pennings AJ (1974) Polymer 15:413
417. Bhat S, Tripathi A, Kumar A (2011) J R Soc Interface 8:540

Basic Principles of Cryotropic Gelation

Vladimir I. Lozinsky and Oguz Okay

Contents

Abstract Polymeric cryogels are the gel systems formed in moderately frozen solutions or colloidal dispersions of precursors potentially capable of gelling. Polymeric cryogels are of growing practical interest in various applied areas. The fabrication of any cryogel includes the following necessary stages: preparation of the feed system, its freezing, incubation of the gelation system in a frozen state, and

V.I. Lozinsky (✉)
Laboratory for Cryochemistry of (Bio)Polymers, A.N. Nesmeyanov Institute of
Organoelement Compounds, Russian Academy of Sciences, Vavilov Street 28, 119991
Moscow, Russian Federation
e-mail: loz@ineos.ac.ru

O. Okay
Department of Chemistry, Istanbul Technical University, Maslak, 34469 Istanbul, Turkey
e-mail: okayo@itu.edu.tr

thawing of the frozen sample. The nature of gel precursors, their concentration in the initial feed, and the conditions of each of the stages affect the physicochemical properties and porous morphology of the resulting cryogels. Certain specific effects are inherent in the processes of cryotropic gel formation, namely, apparent decrease in the critical concentration of gelation, acceleration of gel formation over a certain range of negative temperatures, a bell-shaped temperature dependence of the cryotropic gelation efficiency, and generation of the specific porosity peculiar to cryogels. This chapter presents the basic principles of cryotropic gelation processes and also discusses the factors influencing the properties of various types of cryogels.

Keywords Cryotropic gelation • Unfrozen liquid microphase • Freezing • Frozen storage • Defrosting

Abbreviations

CCG	Critical concentration of gelation
CTAB	Cetyltrimethylammonium bromide
DMSO	Dimethylsulfoxide
GuAr	Gum arabic
LCST	Lower critical solution temperature
NMR	Nuclear magnetic resonance
PVA	Poly(vinyl alcohol)
SEM	Scanning electron microscopy
UCST	Upper critical solution temperature
UFLMP	Unfrozen liquid microphase
VA	Vinyl alcohol
VAc	Vinyl acetate

1   Introduction

As described in the previous chapter of this volume [1], studies on the gel formation processes in moderately frozen solutions or colloidal dispersions containing the necessary precursors started at the beginning of 1970s, although empirical observations of freeze–thaw-caused gelation were made long before. The experimental data obtained during the past four decades in this field have resulted in a sum of knowledge on the general aspects of cryotropic gelation, which is the subject of the present chapter. Before starting the discussion, the terminology will be defined in order to clarify what each specialized term means.

1.1 "Gels" in General, and "Cryogels" in Particular

There are many definitions of what the gels are [2–6], and some of these definitions are rather complicated because they include numerous significant properties of the polymeric systems classified as gels. However, at a qualitative level one can say that gels are systems consisting of polymer and immobilized solvent in which macromolecular chains are connected to each other via chemical or physical bonds, forming a 3D network. The definition can be made simpler still: gels are swollen spatial polymeric networks. If the immobilized solvent is water, then we deal with hydrogels; if the solvent is an organic liquid, then organogels are considered. Certainly, various intermediate variants are also possible when the solvents are water–organic mixtures. Depending on the nature of the interchain bonds in the nodes of the polymeric 3D network, gels are commonly classified as follows: covalent (i.e., chemically crosslinked) gels; ionically or ion-chelately crosslinked gels; and noncovalent or physical gels. "Mixed" variants also exist. The gel's bulk morphology (homophase or heterophase) is determined by the chemical structure of the constituent polymers and by the method of gel preparation. In this context, cryogels are gel systems whose formation occurs in moderately frozen solutions or colloidal dispersions of precursors potentially capable of gelling [7, 8]. Therefore, the occurrence of gel formation in the frozen precursor-containing system is the necessary specific feature that distinguishes cryotropic gelation from gel formation at temperatures above the freezing point of the feed [9].

1.2 "Cryotropic Gelation"

The word combination "cryotropic gelation" connects directly with the proper processes resulting in the formation of diverse cryogels. The term's construction is similar to that of the terms "chemotropic" (caused by chemical reactions), "ionotropic" (caused by ionic bonding), and thermotropic gel formation (caused by heating, as in the gelation of aqueous solutions of methylcellulose upon warming above the lower critical solution temperature, LCST). Hence, cryotropic gelation, derived from the Greek *kryos* (frost) and *tropos* (cause), is gel formation caused by the cryogenic treatment (freezing–frozen storage–thawing) of the precursor system. The solvent crystallization in this process acts as a trigger enabling the subsequent gelation phenomena.

1.3 "Positive" and "Negative" Temperature

These terms are defined as, respectively, the temperatures above and below the freezing/melting point of the initially liquid system (see [1]). In addition, in the course of further discussions on nonaqueous systems we will also operate, when

needed, with the relative temperature ΔT, defined as $\Delta T = T_i - T_0$, where T_0 is the freezing point of the solvent used and T_i is the gelation temperature. Thus, if gelation occurs in the medium of formamide ($T_0 = +2.9$ °C), $\Delta T = -20$ and $+20$ °C correspond to gelation temperatures T_i of -17.1 and $+22.9$ °C, respectively. Similarly, for gelation in cycloheptane with $T_0 = -12$ °C, $\Delta T = -20$ and $+20$ °C correspond to $T_i = -32$ and $+8$ °C, respectively.

1.4 "Gel-Fraction" and "Gel-Fraction Yield"

It is rather hard to measure experimentally with high precision the real content of the gel phase, that is, the amount of the separate system composed of the crosslinked polymer and immobilized solvent within the whole sample volume. This is particularly so for heterophase cryogels because the value measured will strongly depend on the swelling extent of the sample under a single set of examination conditions. That is why the notions "gel-fraction" and "gel-fraction yield" imply, although being insufficiently strict terminologically, the content or the yield of the dry crosslinked polymer relative to the dry weight of the respective precursors. Such a fraction is easily determined gravimetrically and does not depend on the swelling extent of the particular gel or cryogel samples. Besides, if the tightly bound solvate liquid is difficult to remove from the sample upon drying (as is frequently the case for hydrogels), the residual moisture amount can be quantified by auxiliary independent methods like Karl Fischer titration (e.g., see [10] for chitosan-based cryogels).

The goal of this chapter is to describe and discuss general aspects of cryotropic gelation with emphasis on its basic principles. The key factors affecting different stages of cryotropic gelation processes and, thus, influencing the properties and the structure of the resulting polymeric cryogels will also be considered. In addition, when the current knowledge level is sufficient, explanation will be given for the specific effects peculiar to this kind of gel formation.

2 Main Stages of the Cryotropic Gelation Processes

Similarly to the formation of conventional covalent gels, covalent cryogels are prepared either through the crosslinking polymerization or polycondensation of monomeric precursors, or by crosslinking (chemically or with radiation) of high molecular weight compounds, the latter being either in molecular-dissolved or in colloidal-dispersed forms [7, 8, 11]. In the case of noncovalent (physical) cryogels, the initial substances are usually polymers capable of self-gelling upon cooling of their solutions like water/gelatine [12] and poly(acrylonitrile)/N,N-dimethyl-formamide systems [13], or their colloidal dispersions like the gelatinized starch pastes [14, 15], or "cryosensitive" latexes [16, 17]. Ionic cryogels can, in principle,

be created from the solutions of polyelectrolytes by their crosslinking using counterions capable of forming low-dissociating ionic bonds between the charged groups of such macromolecular precursors [7, 8]. In all these cases, the procedure of cryogel preparation includes the following basic stages:

1. Preparation of the feed system
2. Freezing of the feed
3. Incubation of the system in a frozen state
4. Thawing of the frozen system

The conditions of each stage, including the properties of the particular precursors, affect more or less significantly the efficiency of cryotropic gel formation and, thus, the properties and structure of the resulting cryogel materials. So, it seems reasonable to discuss step-by-step the factors that are of importance for such freeze–thaw gelling systems.

2.1 Preparation of the Feed System

At first sight, preparation of the initial feed containing the precursors of the future cryogel is a rather simple and routine procedure. This is a necessary step for the preparation of any gel material both at positive and negative temperatures. However, definite peculiarities of the cryotropic gel formation generally dictate certain requirements for the preparation of the initial system. For instance, one should minimize the conversion of the precursor to the gel before freezing the feed. Otherwise, if the gel-point is attained prior to the start of solvent crystallization, the destruction of the primary 3D network thus formed may occur by the creation of a polycrystalline phase. Such a process is especially detrimental in quickly forming chemotropic gels because their covalently linked nodes do not allow the polymeric chains to be slid apart easily by the growing solvent crystals. These effects, in turn, can even result in splitting of the weakest covalent bonds in the structure of the spatial polymeric network, especially, as shown by Jellinek and Fox [18], when the crystallization fronts are moving rapidly.

There are two ways to "outrun" gelation of the still-unfrozen feed system. The first method is to freeze the feed as quickly as possible where the gelation reactions have already begun. The other method is to reduce the initial rate of such reactions, e.g., by chilling the feed to just above its freezing point before adding the initiator (the case of polymerization-type cryogels) or the crosslinking agent (the case of covalent cryogels formed via crosslinking of macromolecular precursors). The former way, such as the flash-freezing technique using liquid nitrogen, has two significant drawbacks. First, the initial solution may undergo a glass-transition instead of the required solvent crystallization so that no cryo-concentration effect can be generated. Second, when the solvent crystallization does occur, the size of the very quickly formed crystals is small, and so is the cross-section of the pores in the resulting cryogel. Therefore, the latter approach, i.e., decreasing the rate of the

corresponding reactions prior to freezing of the feed, looks more promising. As a rule, for fast-reacting systems this goal is reached simply by chilling the initial feed. Some examples of the procedures employed for the preparation of polymerization-type cryogels and cryogels via chemical crosslinking of the polymeric precursors can be found in [19–25] and [10, 26–32], respectively.

The above considerations are mainly related to the preparation of covalent cryogels, where chilling the initial solution prior to the addition of either initiator or crosslinking agent does not lead to the gelation per se. However, when dealing with the preparation of physical cryogels, especially with systems undergoing a fast sol-to-gel transition at positive temperatures (such as aqueous agarose solutions), the situation is complicated. In such physically gelling systems one must decrease the self-gelation rate of the precursors to shift the gel-point to longer reaction times so that the gel will form within the volume of the unfrozen liquid microphase. As discussed in Sect. 2.4 of [1], the preferable way is to use specific solutes capable of slowing down gelation, e.g., alkaline additives for the preparation of wide-pore agarose cryogels [33, 34].

Moreover, the feed compositions capable of producing ionically crosslinked cryogels are even more sophisticated due to the very high rates of ionic reactions. Besides, such reactions are only slightly sensitive to the temperature. Therefore, cooling the initial feed containing dissolved polyelectolytes and necessary crosslinking counterions cannot sufficiently decelerate ionotropic gel formation prior to freezing of the system. Possible ways for bypassing such difficulties are also discussed in Sect. 2.5 of [1]. In short, in terms of the composition of the precursor solution, only two variants are relevant. The first method is to use a crosslinking agent with a negative temperature coefficient of solubility, e.g., solid salts exhibiting increased water solubility as the temperature is decreased [7, 8]. The second method, namely the so-called internal gelation approach, is to induce gelation via auxiliary agents capable of gradual solubilization of the dispersed salt particles containing crosslinking counterions [35, 36]. Whereas the former variant has already been realized in the preparation of Ca-alginate-based cryogels [37, 38], no cases of the implementation of the latter variant are known so far to the authors of this chapter.

2.2 Freezing of the Feed

Freezing of the initial precursor-containing system is the crucial step for both the subsequent cryotropic gel formation per se and the properties of the resulting cryogels. This is due to several simultaneous processes that are launched during the transformation of the feed liquid into a frost-bound solid. These processes strongly alter the concentration and thermal mobility of the dissolved/dispersed gelation components, the volume of the unfrozen liquid fraction, its viscosity, and its polarity. Moreover, depending on the freezing conditions, they also influence the size and shape of the growing solvent polycrystals, thus biasing the macroporous

morphology of the resulting cryogels. In other words, freezing of the initial molecular or colloidal solution of the precursors affects not only the gelation efficiency, but also the structural characteristics of the final cryogel.

The key parameters of the freezing process are temperature, cooling rate, spontaneous or, if special procedures are employed, directed heat sink [39, 40], the ability of the initial liquid system to be supercooled, the presence of specially added or accidental (e.g., specks of dust) germs of crystallization, the thermal conductivity of the material, and the properties of the inner surface of the vessel containing the feed to be frozen. In this respect, it is also necessary to define the notions cooling/chilling rate and freezing rate as these two parameters are not identical, especially when the ambient temperature is not too low. The cooling/ chilling rate can be controlled rather strictly, for instance, by using precision programmable cryostats, whereas the freezing rate corresponding to the rate of solvent crystallization depends on many factors, particularly on the supercooling depth. For instance, in the case of slow chilling of dust-free feed solutions containing dissolved polymeric precursors, the supercooling effect can be very pronounced [8, 41]. This effect then results in an initial high rate of crystallization, and at high crystallization rates the size of the forming solvent crystals is small. If there is no supercooling, then the lower the freezing temperature, the smaller the size of solvent crystals [42, 43] and, hence, the smaller the cross-section of macropores in the resulting cryogels (see [8, 22, 23, 29, 34, 44–46] and also Sect. 4.1 in [47] of this volume). However, supercooling leads to a deviation from the above-indicated regularity. One such example is given in Fig. 1, which shows the micrographs of chitosan cryogels prepared in frozen aqueous systems at -10, -15, and $-30\ °C$ [10]. The quantitative data obtained from the images, namely the number and weight averages of the pore diameters and the coefficient of polydispersity of the pores, are listed in Table 1. The results show that the average diameter of large pores in the cryogel formed at $-10\ °C$ is smaller than in cryogel prepared at $-15\ °C$ (compare Fig. 1a with b). The reason for such an effect is exactly the supercooling phenomenon.

In some cases, a spatial polymer network may form while the gelling system is in the supercooled state. Such a nonequilibrium state was reported both during chemical gelation processes like crosslinking polymerization as well as during chilling-induced noncovalent gelation. The primary ordinary gel thus formed in the supercooled state of the gelation system will be subjected to physical stresses upon the start of the freezing process due to the movement of the crystallization fronts. Such an effect has been registered upon very slow chilling (0.003 °C/min) of 100 g/L poly(vinyl alcohol) (PVA) aqueous solutions [48]. It was shown that a low-melting physical gel with a fusion temperature of ~21.5 °C forms before freezing of the system. In contrast, the equiconcentrated cryogels formed via conventional freezing, i.e., without a significant supercooling effect, had fusion temperatures of the order of 70–75 °C.

Several approaches have been proposed in order to exclude the influence of supercooling on the formation of different cryogels. These approaches include either special freezing profiles or the use of crystallization initiators. The former
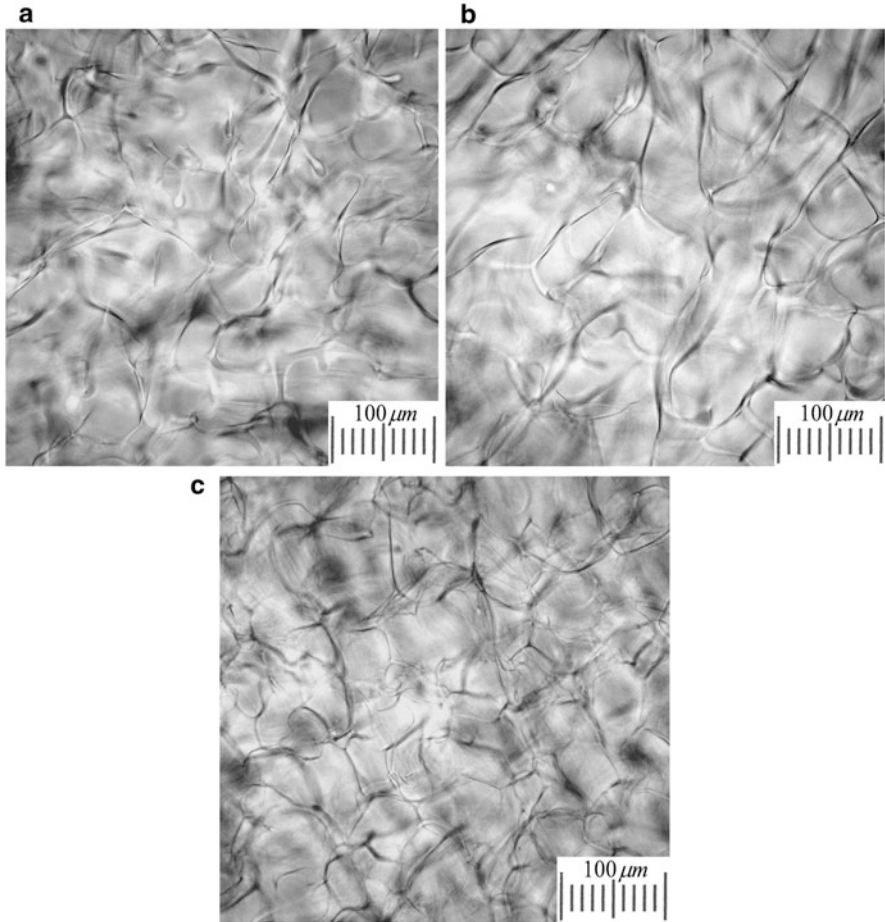
Fig. 1 (**a–c**) Optical micrographs of 2-mm-thick disks of chitosan cryogels formed in moderately frozen aqueous solutions using glutaraldehyde as a crosslinker at -10 (**a**), -15 (**b**), and -30°C (**c**). (From [10] with permission from Springer)

Table 1 Data on the quantitative analysis of microscopic images for the crosslinked chitosan cryogels formed at different negative temperatures

Temperature of cryogel synthesis ($^{\circ}$C)	D_n (μm)[a]	D_w (μm)[b]	k[c]
-10	57.4	70.1	1.22
-15	72.3	87.0	1.20
-30	44.3	56.0	1.26

From [10] with permission from Springer
[a]Number-average pore diameter: $D_n = (\sum(N_i \cdots D_i^3) : \sum N_i)^{1/3}$; the overall number of test objects in the micrograph is $\sum N_i$
[b]Weight-average pore diameter: $D_w = \{\sum(N_i \cdots D_i^6) : \sum (N_i \cdots D_i^3)\}^{1/3}$
[c]Coefficient of polydispersity: $k = D_w : D_n$
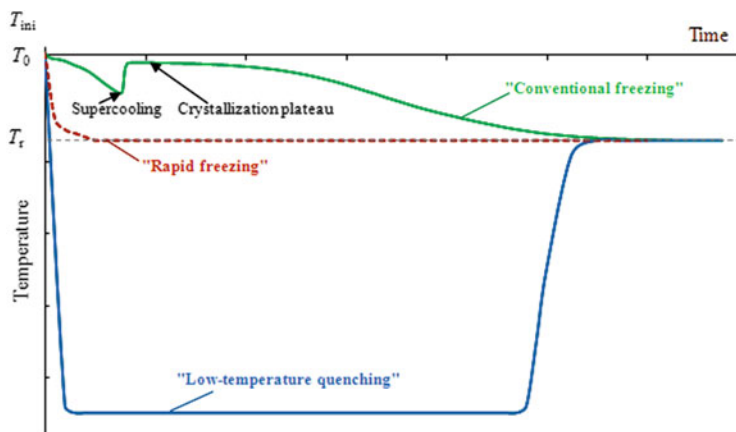
Fig. 2 Freezing profiles of the reaction system according to the conventional, rapid, and low-temperature quenching procedures. T_{ini} initial temperature of the system before the start of freezing; T_0 freezing point of the neat solvent; T_r reaction temperature. (From [49] with permission from Springer)

variant can be subdivided into two techniques utilizing different freezing profiles, namely the rapid freezing and low-temperature quenching techniques. The character of these freezing profiles is shown schematically in Fig. 2. The rapid freezing procedure includes placing the feed system, immediately after commencing of the gel formation process, into a low-temperature bath (e.g., liquid nitrogen) for a short time, usually less than 1 min, to ensure fast solvent crystallization. This is followed by transfer of the feed into a cryostat for frozen storage at the desired subzero temperature T_r. The second procedure, namely low-temperature quenching, also uses liquid nitrogen for fast freezing of the system of interest, but for a longer time (0.5–1 h) in order to make the reaction system completely solid. Then, the feed is placed into a cryostat at a preset negative temperature T_r (Fig. 2). Although both of these freezing procedures minimize the time period in the unfrozen state, they influence the dynamics of cryotropic gelation as well as the porous morphology of the resulting cryogels. In other words, the thermal prehistory of the feed during its freezing influences both the course of the cryotropic gelation and the gel properties. Such an influence was observed in the formation of poly(acrylamide) cryogels [23, 50] and in the linear cryopolymerization of acrylamide [49].

In this context, the use of "artificial" germs of crystallization looks rather attractive. For instance, crystals of silver iodide (AgI) are known to cause efficient ice formation in aqueous systems, thus preventing their supercooling [51, 52]. However, because of the polyvalent nature of both Ag and I atoms, this salt can act as a scavenger for free radicals and ion-radicals. Therefore, introduction of AgI powder into the solution of monomers will affect the course of cryogel formation via the radical reactions. This necessitates certain preliminary tests in order to make sure that such an additive has no undesired influence on cryotropic gelation. In this regard, ultrasound treatment of the initial feed as it is cooled below the freezing

point can be a better way to suppress supercooling. Such a physical impact on the liquid system causes cavitation of gas microbubbles within the whole volume of the sample, thus resulting in uniform nucleation of the solvent crystallization [53]. However, no practical examples of implementing this approach for the preparation of polymeric cryogels are known so far to the authors of this review. This is probably due to the absence of laboratory-scale ultrasound equipment suitable for cryotropic gelation procedures.

2.3 Incubation of the Gelation System in a Frozen State

Keeping the gelation system in a frozen state at a moderate negative temperature is the main stage in the synthesis of covalent cryogels, since the chemical reactions leading to gelation mainly occur during this time period [8]. In the case of physical cryogels, the pattern is not so straightforward and will be discussed later. Nonetheless, in both cases, polymeric cryogels form within the volume of the unfrozen liquid microphase (UFLMP, also called the "nonfrozen liquid microphase") where the precursors are concentrated as the solvent starts to crystallize [8]. Therefore, the concept of UFLMP will be discussed in more detail.

The term "unfrozen liquid microphase" was proposed by Sergeev and co-authors in 1973 for designating the liquid fraction at a particular negative temperature in a macroscopically frozen system [54]. This concept was developed in the course of exploration of various chemical reactions occurring in the non-deeply frozen multicomponent solutions of low molecular weight reactants. These studies, beginning from the initially empiric observations [55–61], then generalized by Pincock [62], and leading to a rather harmonious kinetic theory elaborated by Sergeev and Batyuk with coworkers [54, 63, 64], revealed the following three fundamental features of such processes and their mechanisms:

1. When the initial molecular or colloidal solution is non-deeply frozen, although the system looks like a completely solid matter, it is heterophase at a microscopic level and contains, along with the solvent polycrystals, a certain unfrozen fraction, UFLMP. Thus, the moderately or non-deeply frozen systems are those where UFLMP is still present. The existence of UFLMP at temperatures both above and below the eutectic point of the particular system is confirmed by different physicochemical methods, e.g., by the narrow NMR signals of the solutes [8, 41, 50, 52, 63–72] and by the shape of ESR spectra characteristic of the liquid microenvironment of spin probes [8, 63, 73–76]. The temperature boundary of the existence of UFLMP is stipulated by several factors such as the nature of the solvent, the amount of solutes, their physicochemical properties (e.g., molecular weight [77]), the flexibility of the chains in the case of polymeric precursors, thermal prehistory of the system during its freezing if the phase equilibrium is not yet attained, etc.

2. The concentration of solutes or dispersed colloid-size particles is increased because of their expulsion into the volume of UFLMP as the solvent is crystallized. This cryo-concentration effect is one of the major factors responsible for the increase in the rate of the chemical reactions and intensification of intermolecular interactions inside the unfrozen inclusions, which act as microreactors. Provided the reactants are easily soluble compounds and are completely concentrated within the UFLMP, the concentrating extent β at a certain negative temperature T can be estimated using the following formula [54]:

$$\beta = \frac{T_0 - T}{\Delta \sum C_i} \tag{1}$$

where T_0 is the crystallization point of the solvent, Δ is its cryoscopic constant, and C_i is the initial concentration of the solute i. Note that the concentrating extent β is the ratio of the total concentration of solutes within the UFLMP to that in the initial solution. It is also possible to measure the β values experimentally from the NMR spectra of such frozen systems, provided that their compositions are not too complex and the solvent is suitable for use in the NMR technique.

3. Owing to the competition of several oppositely directed factors, the temperature dependence of the efficiency of the process in terms of the reaction rate or the yield of the final products is, as a rule, bell-shaped. According to the structure–kinetic model developed by Sergeev-Batyuk [63, 64], the temperature of the maximum reaction rate ($T_{\max,r}$) of cryochemical reactions between low molecular weight substances with an order higher than 1 is given by the following equation:

$$T_{\max, r} = \left(\frac{E^2}{4R^2 \left[\left(\sum_j n_j \right) - 1 \right]^2} + \frac{ET_0}{R \left[\left(\sum_j n_j \right) - 1 \right]} \right)^{0.5} - \frac{E}{2 \left[\left(\sum_j n_j \right) - 1 \right]} \tag{2}$$

where E is the activation energy of the reaction, R is the universal gas constant, and n_j is the reaction order with respect to the jth component.

Most of these features of cryochemical reactions are also of great significance for cryotropic gelation processes [8]. Moreover, if the system contains polymeric solutes, the still-liquid fraction can exist even at rather low temperatures and such

systems are very sensitive to the thermal prehistory, i.e., the temperature profile used to reach the preset temperature point. For instance, upon freezing of concentrated aqueous PVA solutions, the presence of mobile water molecules was detected by NMR even at –50 °C [78]. In addition, since the relaxation processes in viscous liquids are very slow, the characteristics of UFLMP (such as its volume during freezing and defrosting stages) differ significantly, leading to hysteresis phenomena [76, 79]. Similarly to cryochemical reactions, the gelation rate and the gel-fraction yield of cryotropic gelation processes, as well as the mechanical characteristics of the final cryogels, are strongly dependent on the frozen storage temperature and are also bell-shaped. Such a character of temperature dependences was observed during the formation of covalent cryogels from monomeric [7, 8, 22, 23, 80–85] and macromolecular precursors [7, 8, 10, 27–29, 32, 45, 46, 86–88], for some physical cryogels [7, 8, 34, 44, 48, 89–103] as well as during linear cryopolymerization processes [49, 72, 104–106].

Based on the concept of UFLMP, the scheme of cryotropic gelation processes can be depicted by the simple diagram in Fig. 3, which reflects all the essential features of the systems [107]. When the initial feed containing the monomeric or polymeric precursors freezes at a moderate negative temperature (Fig. 3a), the frozen system consists of at least two phases, namely the solvent polycrystals and the UFLMP where the solutes are concentrated (Fig. 3b). Due to the considerable increase in the concentration of solutes in these liquid-like inclusions, the gelation can intensify and result in the formation of a 3D polymeric network within the volume of this phase. Thus, a cryogel is formed in a solution of the precursors that is much more concentrated than the initial solution. After thawing of the frozen system, numerous macropores arise in place of the melted solvent crystals (Fig. 3c). Hence, the crystals act as a pore template or porogen, whereas the structure of gel phase (the pore walls) is determined by the initial concentration of gelling agents and by the number of crosslinks of the respective spatial networks.

2.4 Thawing of the Frozen System

Thawing of the gelation system after incubation in a frozen state for a necessary time period is the last basic stage of the cryotropic gelation processes. The least energy-consuming procedure is a simple spontaneous thawing of the frozen system at an appropriate positive temperature. The conditions of thawing are generally unimportant as long as the formation of a particular covalent cryogel is mainly completed before this stage, i.e., if the reactions are virtually stopped and the gel-fraction yield reaches the maximum possible value. However, it is sometimes necessary to stop the gelation prior to its completion, e.g., for studying the variation in gel-fraction yield with reaction time [7, 8, 22, 23, 27, 28, 32, 86]. In this case, fast defrosting techniques should be employed in order to thaw the reacting system as quickly as possible, but without overheating. The reactions may also be stopped either by intense dilution or by addition of a relevant chemical inhibitor, e.g., free

a Initial system

1 →
2 →
3 →

Freezing →

b Frozen system

4 →
5

Thawing →

c Thawed cryogel

→ 6
→ 7
8

1 – High-molecular gel precursors
2 – Solvent
3 – Low-molecular gel precursors or solutes
4 – Polycrystals of frozen solvent
5 – Unfrozen liquid microphase
6 – Polymeric framework of a cryogel (gel walls of macropores)
7 – Macropores
8 – Solvent
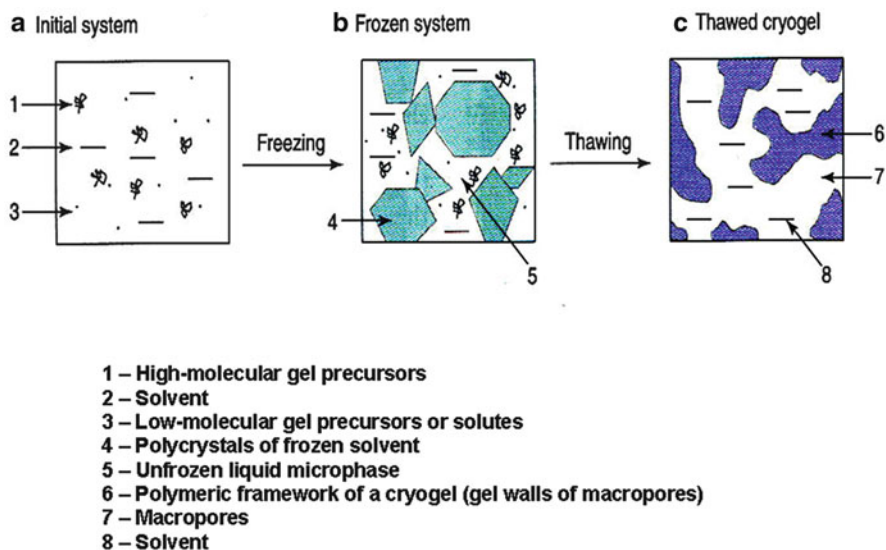
Fig. 3 (**a–c**) Conceptual diagram of the formation of polymeric cryogels. (From [107] with permission from Elsevier)

radical scavengers in radical-type reactions. Sometimes, a short-term microwave exposure can be used for fast defrosting [10, 65], or rapid heating of the frozen system with a programmed rate.

Similarly to the non-equivalence of the chilling and freezing rates of the initial feed, the rates of heating and defrosting (i.e., melting of the solvent crystals) should also be distinguished. Whereas the heating rate is easy to govern using programmable cryostats, the defrosting rate corresponding to the melting of solvent crystals is subject to multiple factors and is difficult to control.

The conditions of the thawing stage are often much more important in the preparation of physical cryogels than for covalent gels. If the physical cryogels are formed rapidly upon freezing of the feed containing certain precursors such as starch polysaccharides [14, 15, 98, 108, 109] or agarose [33, 34], the contribution of the thawing conditions to the final result is not very substantial. However, for slow gelation systems like the solutions of PVA [7, 8, 44, 48, 93–95, 97, 99, 110–114] or locust bean gum [100, 102, 115], the thawing conditions become significant. The plots in Fig. 4 illustrate the influence of the thawing rate on the shear modulus and the fusion temperature of physical PVA cryogels [44]. The cryogels were prepared by freezing of PVA solutions at $-20\,°C$ for 18 h followed by thawing at different rates. The different curves in Fig. 4 correspond to initial PVA concentrations of 120, 100, and 80 g/L. Both the shear modulus and the fusion temperature of the cryogels gradually increase as the thawing rate is decreased. For instance, at a PVA concentration of 80 g/L (curve 3), decreasing the thawing rate from 0.3 to 0.003 °C/min increases the modulus, i.e., the rigidity of the cryogels from 2 to 13 kPa. This effect is even more pronounced in more concentrated samples. Thus, for the system
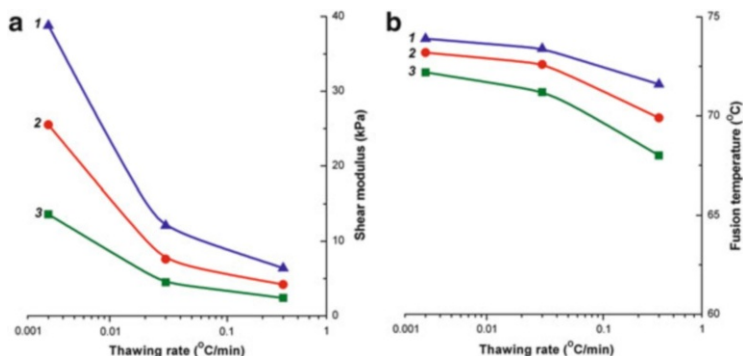
Fig. 4 Effect of the thawing rate on (**a**) the shear modulus and (**b**) the fusion temperature of PVA cryogels prepared by freezing of aqueous polymer solutions at $-20\,^\circ$C for 18 h. PVA concentrations were 120 (*1*), 100 (*2*), and 80 g/L (*3*). (Plotted based on data from [44])

containing 120 g/L PVA (curve 1), the modulus increases by factors of 1.77 and 5.64 as the heating rate is increased from 0.3 to 0.03 and 0.003 $^\circ$C/min, respectively. The slow-thawed samples are also more thermoresistant, as evidenced from the fusion temperatures (Fig. 4b), and the enthalpy of their fusion is also considerably greater than that of fast-thawed samples. Note that when the moderately frozen PVA solutions were heated with a high rate such as 15 $^\circ$C/min, no cryogels were obtained at all. Thawing of the samples at such a high rate led to the formation of viscous and turbid (heterogeneous) fluid instead of a rubber-elastic gel [44, 93, 95], whereas the efficiency of PVA cryotropic gelation (such as the yield of gel-fraction) increases when defrosting is slowed down [113]. The results thus show that the slower the thawing rate, the larger the modulus (i.e., strength of the resulting cryogels) and the heat endurance. The reason is the fact that, since gel formation proceeds slowly in highly viscous UFLMP medium, the sol–gel transition in such systems requires a long time to occur so the PVA microcrystallites in the nodes of spatial network become more perfect at slow thawing rates.

Studies on the fine details of the processes taking place at the thawing stage have shown that the formation of a supramolecular 3D physical network of PVA cryogels proceeds most intensively within the subzero temperature range between 4 and 1 $^\circ$C below the melting point of the system [44, 93, 99]. In NMR experiments, the well-resolved ^{13}C NMR signals of frozen samples in this temperature range indicate segmental mobility in PVA chains [78], which is a necessary factor for effective interchain interactions. Hence, the longer the system stays within this temperature range during defrosting, the higher is the gel formation efficiency. For instance, at a heating rate of 3 $^\circ$C/min, the temperature increases from –4 to –1 $^\circ$C within 1 min, while at a rate of 0.003 $^\circ$C/min, it takes about 17 h [111]. Thus, slow-enough defrosting ensures a prolonged passage time across the temperature diapason, which favors the formation of stronger PVA cryogels. At low heating rates, the system has sufficient time for slow PVA microcrystallization, which promotes the extent of intermolecular contacts. This leads to an increased degree of hydrogen-

binding cooperativity rather than to an increase in the number of microcrystallites. The former is manifested in a substantial increase in the fusion enthalpy, whereas the latter leads to a moderate increase in the fusion temperature of cryogels, i.e., to a small change in the entropy factor. At a qualitative level, there is an analogy with the crystallization of low molecular weight substances upon cooling of their hot saturated solutions; when the system is cooled slower, less crystals are formed, but their sizes are larger and the crystalline lattice becomes more perfect [116].

The regime of the thawing stage also influences markedly the macroporous structure of such noncovalent cryogels. During sufficiently slow heating of frozen samples, the gel formation occurs at subzero temperatures and, simultaneously, the re-crystallization of the frozen solvent is intensified, which has an impact on the porous morphology of the resulting cryogels. This influence is demonstrated by the micrographs in Fig. 5, which show thin sections of PVA cryogels formed at different heating rates. The cryogels were prepared from aqueous PVA solutions frozen under identical thermal conditions but defrosted at heating rates of 0.3 (Fig. 5a), 0.03 (Fig. 5b), and 0.003 °C/min (Fig. 5c). Because slowing of defrosting of the frozen system results in an increase in the rigidity of the corresponding cryogels (Fig. 4a), it can be suggested that such changes in their mechanical parameters are caused not only by the strengthening of the gel phase of heterogeneous material, but also by a decrease in the inhomogeneity of its structure, where the macropores act as defects. This was indeed observed. As seen in Fig. 5, the slower the thawing of the frozen system, the less pronounced is the orientation of the texture elements. Most likely, this effect is associated with the re-crystallization of ice at slow heating of the frozen samples when the system has enough time to balance the temperature fields, and the processes of mass transfer participating in re-crystallization become equiprobable in all directions. In this regard, the texture of the sample shown in Fig. 5b seems to be transient between the clearly unidirectional texture of the rapidly thawed sample (Fig. 5a) and the texture of a very slowly defrosted sample pierced with intersecting pores (Fig. 5c). In addition, slowing down of the heating rate at the thawing stage leads to a decrease in the total porosity of PVA cryogels and in a slight diminution in the average cross-section of the macropores (see caption to Fig. 5).

Another freeze–thaw procedure having a strong impact on the properties and porous morphology of noncovalent cryogels such as PVA-based cryogels is the use of multiple or iterative "freezing–frozen storage–defrosting" cycles. This variant of cryogenic treatment results in the growth of the crystallinity degree of PVA cryogels [117–120]. Such thermal cycling is able to increase considerably the strength of physical cryogels and their heat endurance [111, 121–133]. One of the reasons for this effect is the fact that the gelation system passes across the above-indicated subzero temperature zone several times, which is very favorable for such cryotropic gel formation. Thus, the durations of the several traversals at the subzero temperature range are virtually summed. Such a "temperature saw" also affects the pore morphology of the resulting cryogels. This is illustrated by the micrographs in Fig. 6, which show the effect of the number of cycles on the pore morphology of PVA cryogels. The second freeze–thaw cycle results in a significant increase both
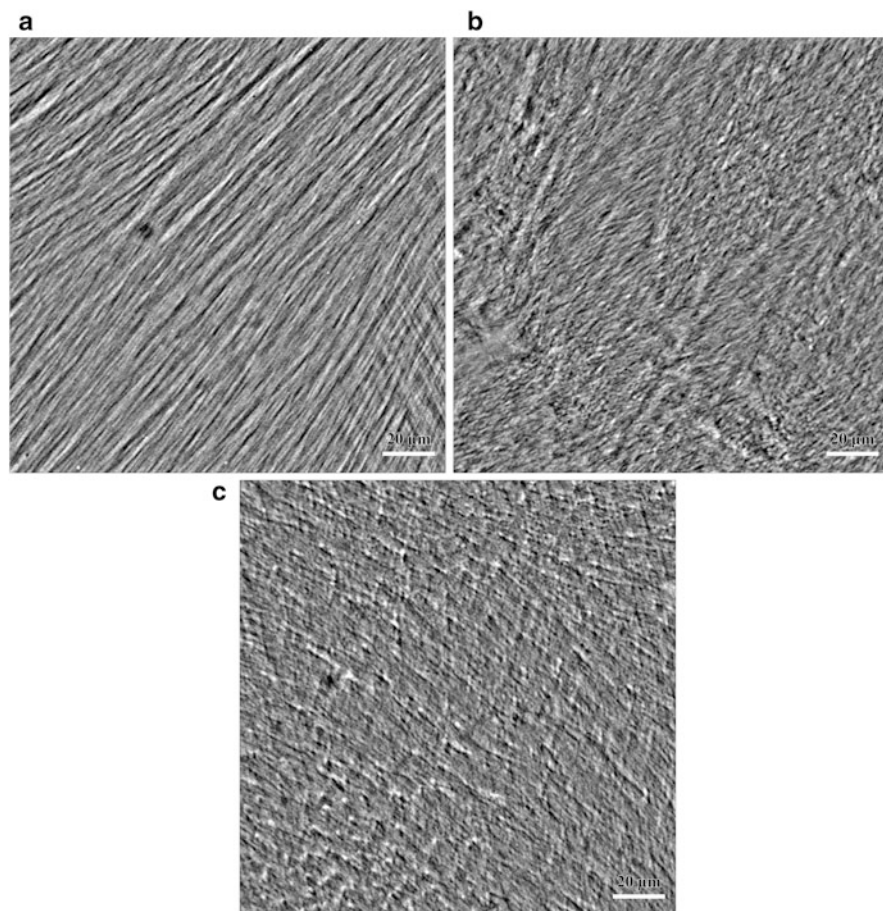
Fig. 5 (**a**–**c**) Optical micrographs of thin sections of PVA cryogels prepared by freezing of aqueous polymer solutions (100 g/L) at −20 °C for 18 h and then thawed at a rate of 0.3 (**a**), 0.03 (**b**), and 0.003 °C/min (**c**). The average size of macropores was 2.8 (**a**), 2.7 (**b**), and 2.5 μm (**c**). The fraction of macropores was 61.3 (**a**), 53.1 (**b**), and 49.6 % (**c**). *Scale bars*: 20 μm. (From [44] with permission from Springer)

in the average size of macropores (by a factor of 2–3) and in the total (macro) porosity (by ~30 %), whereas the subsequent cycles cause only a slight increase in these characteristics. At the same time, both the rigidity and the fusion temperature of the cryogels continue to increase with every following cycle. These experimental results demonstrate that the pore space of PVA cryogels is mainly expanded during the second freezing step when the ice crystals grow inside the micrometer-sized pores formed after the first freeze–thaw cycle, whereas the gel formation processes in the gel phase continue to occur at every subsequent thawing stage.
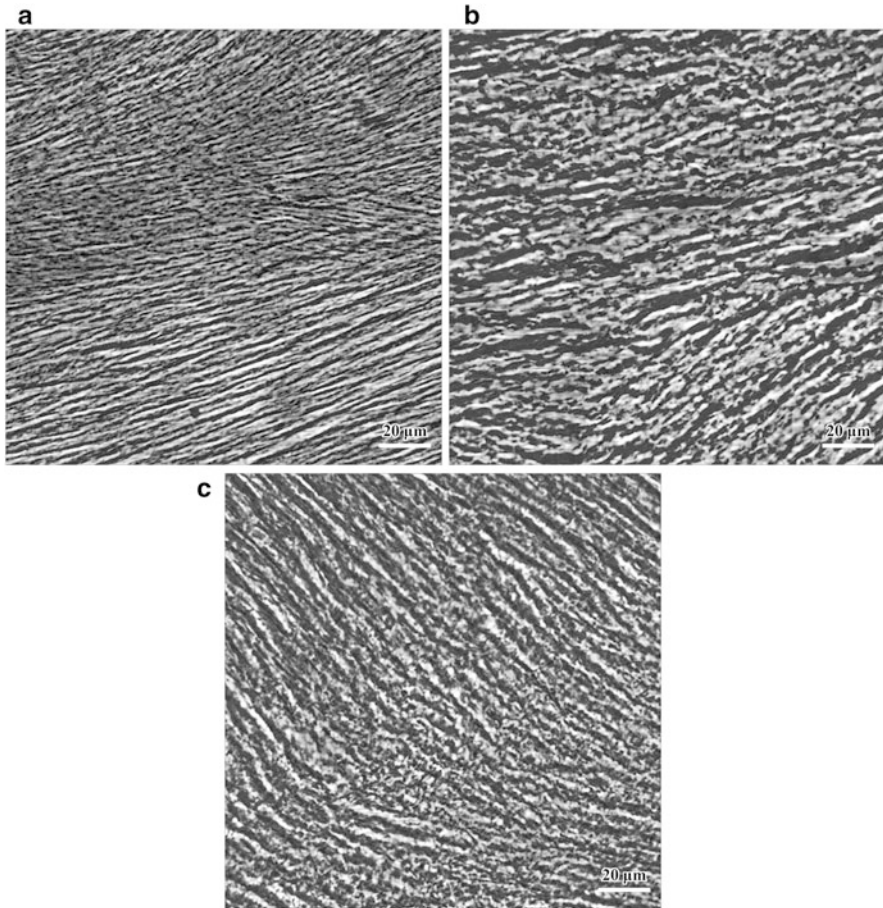
Fig. 6 (**a–c**) Optical micrographs of thin sections of PVA cryogels prepared by iterative freezing of aqueous polymer solutions (100 g/L) at $-20\,^{\circ}$C for 18 h and then thawed at a rate of $0.3\,^{\circ}$C/min. The number of freeze–thaw cycles was 1 (**a**), 2 (**b**), and 5 (**c**). The average size of macropores was 2.8 (**a**), 6.1 (**b**), and 6.5 μm (**c**). The fraction of macropores was 61.3 (**a**), 80.8 (**b**), and 79.8 % (**c**). *Scale bars*: 20 μm. (From [129] with permission from Springer)

In summary, we can conclude that the conditions of each step in the preparation of cryogels affect the course of gelation and, hence, the properties and structure of the resulting gel materials. The extent of the influence of the processing conditions is different and depends on the chemical nature of the cryogel precursors, their initial concentrations, and on the temperature regimes of the cryogenic stages, i.e., on the parameters of freezing, frozen storage, and defrosting. Therefore, there is no general procedure for the preparation of any cryogel; for each specific case a preliminary search for the most suitable conditions is required to obtain the materials with desired characteristics. Such a search can sometimes involve a lot of effort; however, it gives useful information regarding the factors that are important for each kind of cryotropic gelation process as well as the fine details of the corresponding mechanisms.

3 Specific Effects of Gel Formation in Moderately Frozen Systems

3.1 Apparent Decrease in the Critical Concentration of Gelation

One of the principal conditions for conventional gelation at positive temperatures is that the concentration of the precursors in the feed has to exceed a certain boundary value, called the critical concentration of gelation (CCG) [2]. The same is also true for cryotropic gel formation. In the early systematic studies on the main factors influencing the properties of freeze–thaw gels, it was found that cryogels can be obtained at initial precursor concentrations considerably lower than the critical values needed for gel formation at positive temperatures. Such a decrease in CCG is inherent in the formation of both chemically crosslinked cryogels [19, 20, 26, 27] and noncovalent gels [12]. This effect has been observed for cryostructuring in moderately frozen aqueous systems [20, 26, 27] as well as in organic systems [27]. Figures 7 and 8 represent typical examples of such an effect. These data concern covalent-type gelation in "solvent–polymeric precursor–crosslinking-agent" systems, namely crosslinked chitosan gels in an aqueous medium (Fig. 7) and crosslinked poly(styrene) gels in nitrobenzene medium (Fig. 8). Figure 7a shows the scheme of the crosslinking reaction of chitosan using glutaraldehyde as a crosslinker. In Fig. 7b, c, the gel-fraction yield is plotted against the initial chitosan concentration and the initial molar ratio of aldehyde to amine groups, respectively. The two curves represent data for chitosan gels formed at −8 and 24 °C. It is seen that the crosslinking of chitosan with glutaraldehyde at −8 °C results in the formation of cryogels at about one third of the initial polymer concentration compared with the formation of conventional gels at 24 °C. More-over, there is also an approximately threefold difference in the critical crosslinking agent concentration in terms of the molar ratio of aldehyde to amine groups (Fig. 7c). The reason for this phenomenon is the cryo-concentration effect (Fig. 3), since the gel phase of cryogels forms within the UFLMP, which is more concentrated than the initial solution. Therefore, the decrease in CCG in cryotropic gel formation is an apparent decrease due to the confinement of the reacting species to the microreactor UFLMP [8]. Qualitatively, the same trend was observed during the synthesis of covalent cryogels in organic media, which is exemplified by the crosslinking of poly(styrene) using 4,4′-xylylene-dichloride via the Friedel–Crafts reaction (Fig. 8a). Such cryogels possess a wide-pore spongy texture and can be obtained in moderately frozen nitrobenzene ($T_0 = +5.5$ °C). In Fig. 8b, the gel-fraction yield is plotted against the polymer concentration for gels prepared at relative temperatures ΔT of −19 °C and +28 °C. The critical polymer concentration at $\Delta T = -19$ °C is six times lower than that at 28 °C. Thus, the data in Figs. 7 and 8 demonstrate the universal character of the effect under discussion in both aqueous and organic media.
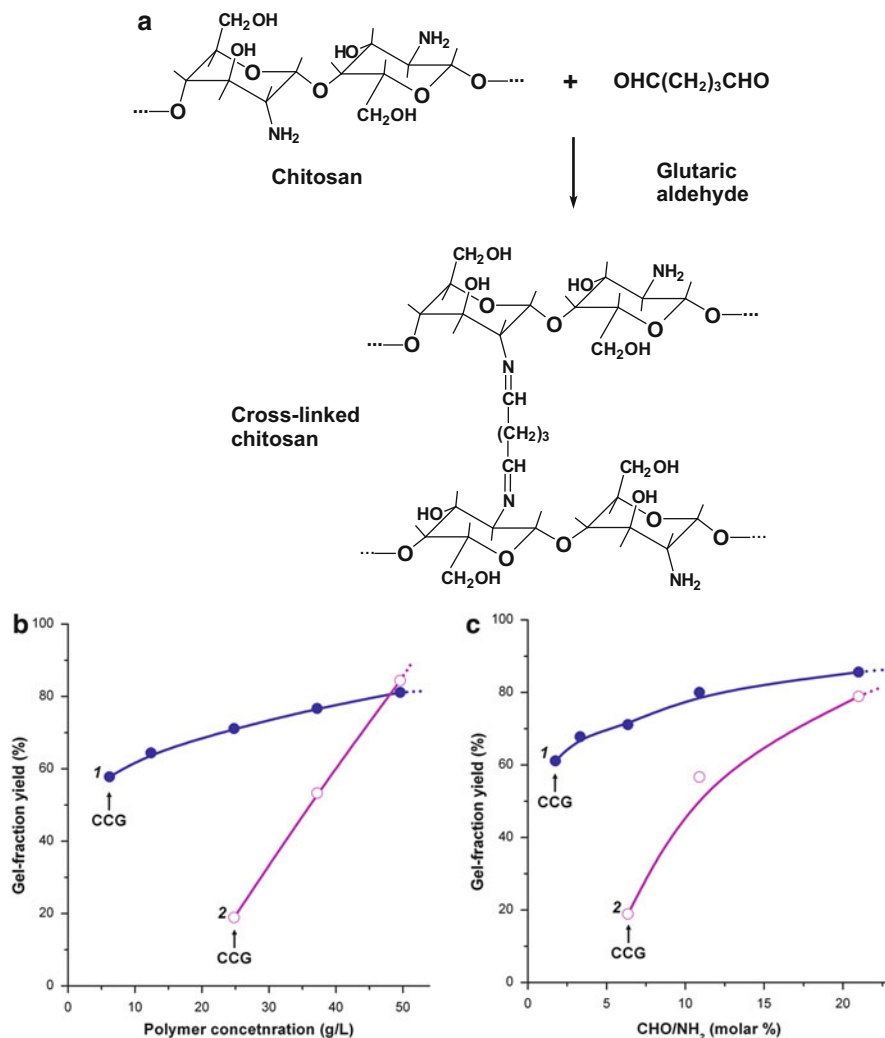
Fig. 7 (**a**) Crosslinking reaction of chitosan using glutaraldehyde as a crosslinker in aqueous acetic acid solutions. (**b**, **c**) Gel-fraction yield plotted against the initial chitosan concentration (**b**) and the initial molar ratio of aldehyde to amine groups (**c**). Gelation temperature was $-8^{\circ}C$ (*curve 1*) and 24° (*curve 2*). *CCG* critical concentration of gelation (Plotted based on the data from [26])

Another interesting example illustrating the cryo-concentration effect is the shift of pH during the acetalation reactions between the OH groups of poly(vinylalcohol-*co*-vinylacetate) (80:20 by mole) and CHO groups of glutaraldehyde (Fig. 9a). The mechanism of this reaction in acidic media includes the initial protonation of the carbonyl of aldehyde [134]. Thus, at low concentrations of hydroxonium ions, the reaction rate is slow and, therefore, the gels are usually synthesized at pH ≤ 1.5–1 in order to ensure high-enough yield of the gel-fraction [135, 136]. In Fig. 9b, c, the
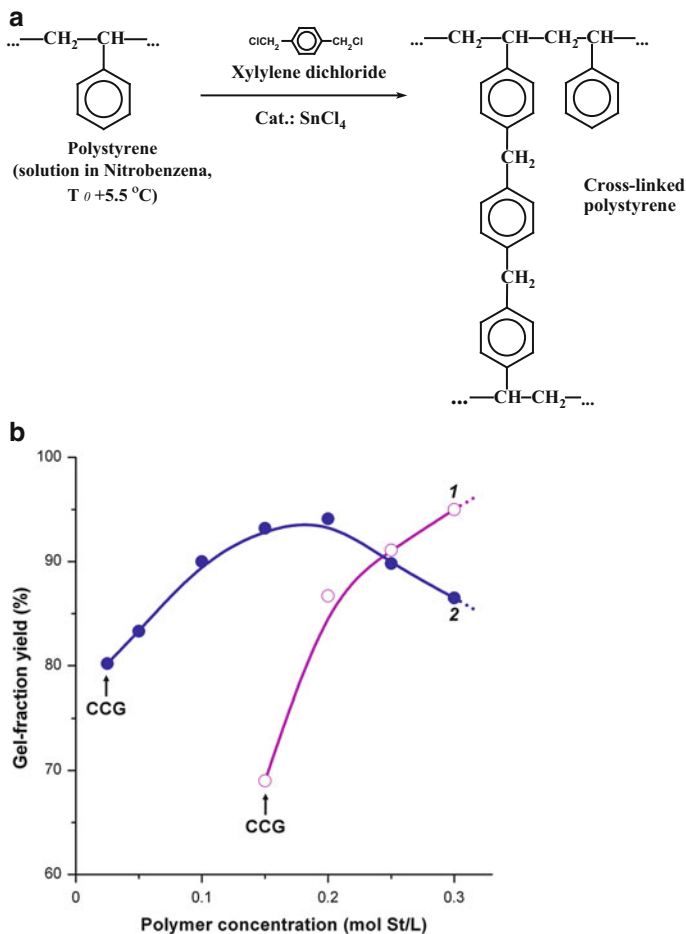
Fig. 8 (**a**) Crosslinking reaction of polystyrene using xylylene dichloride as a crosslinker in nitrobenzene. (**b**) Gel-fraction yield plotted against the initial polymer concentration expressed in molarity of styrene (*St*) units. Relative temperature (ΔT) was $-19\,°C$ (*curve 2*) and $28°C$ (*curve 1*). (Plotted based on the data from [26])

gel-fraction yield is plotted against the initial pH of the polymer solution for gelation at $24\,°C$ and for cryogelation at $-12\,°C$, respectively. The boundary pH value of the feed at which cryogels can be generated (Fig. 9c) has shifted by about 0.5 units toward less the acidic zone as compared to the case of conventional gels (Fig. 9b). Such a difference in pH corresponds to about a threefold difference in the concentration of H^+ ions. Thus, the apparent decrease in CCG due to the cryo-concentrating effect is reflected in this example with an increase in medium acidity rather than in the gel precursor concentration [7]. It is also interesting to compare the osmotic characteristics, e.g., the equilibrium swelling capacities of such gels and cryogels. Figure 9d, e shows the equilibrium swelling degrees of the gels and

a

$$...- (CH_2-CH-CH_2-CH)_m - (CH_2-CH)_n-...$$

$$\begin{array}{ccc} | & | & | \\ OH & OH & OCOCH_3 \end{array}$$

Poly(VA-*co*-VAc)

$$OHC- (CH_2)_3-CHO \quad [H^+]$$

Glutaraldehyde

$$...- (CH_2-CH-CH_2-CH)_{m'} - (CH_2-CH)_n-...$$

$$\begin{array}{ccc} | & | & | \\ O & O & OCOCH_3 \end{array}$$

$$\begin{array}{c} \backslash \quad / \\ CH \\ | \\ (CH_2)_3 \\ | \\ CH \\ / \quad \backslash \end{array}$$

Cross-linked
polymer

$$\begin{array}{cc} O & O \\ | & | \end{array}$$

$$...- (CH_2-CH-CH_2-CH)_{m'} - (CH_2-CH)_n-...$$

$$| $$

$$OCOCH_3$$
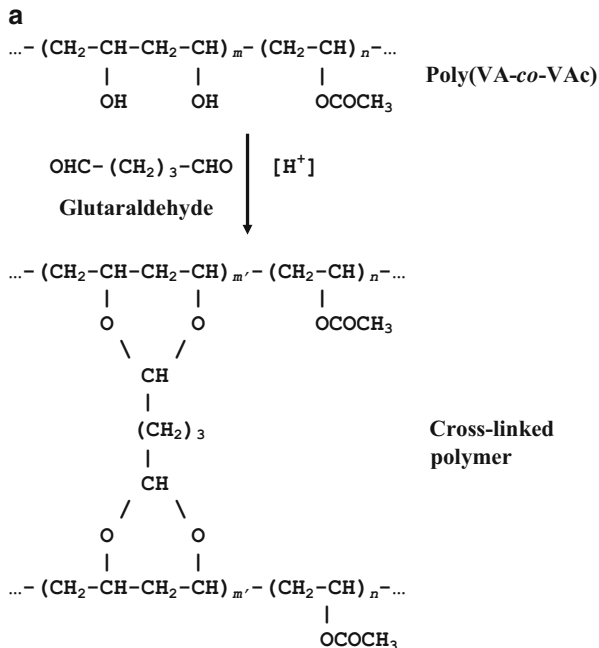
Fig. 9 (continued)

cryogels in water, plotted against the pH of the initial feed solution. The homophase chemically crosslinked PVA gels swell strongly in water (Fig. 9d), and their swelling degree increases considerably (from tens of grams to more than 100 g water per gram of dry polymer) as the pH of the feed rises from 1 to 3 due to the decreasing crosslinking efficiency. However, the heterophase sponge-like cryogels are not only formed under apparently less acidic initial conditions, but also their gel phase swells significantly less than the corresponding homophase gels (from several to 20–30 g water per gram of dry polymer). This indicates a higher crosslinking extent of the 3D networks in the cryogel samples as compared to the conventional gels synthesized under identical crosslinking agent content and pH. The reason for the different swelling behavior of PVA gels and cryogels is because the cryo-concentration processes in UFLMP give rise to an increase in the concentrations of both the gel precursors and H^+ ions. This facilitates the formation of a more concentrated, highly crosslinked gel matrix forming the pore walls in such cryogels.

In this connection, we should note that for such wide-pore gel matrices, the swelling capacity of the gel phase is an essential indicator of the polymer content in this phase and of the crosslinking extent. By contrast, the total volume occupied by such swollen gel materials is a less informative indicator for the properties of the polymeric network. This is due to the fact that the volume occupied by free solvent inside the capillary-sized pores accounts for the greater part of the liquid absorbed by these wide-pore sponges. In turn, the fraction of tightly bound solvate liquid
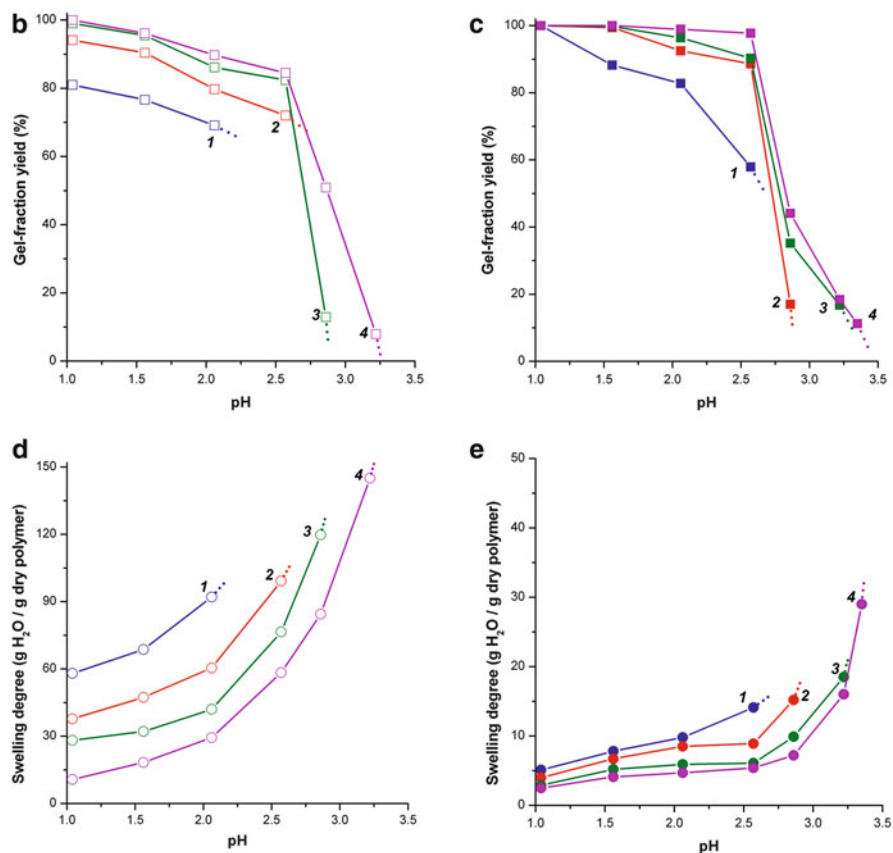
Fig. 9 (**a**) Crosslinking reaction of poly(VA-*co*-VAc) (80:20 by mole) using glutaraldehyde as a crosslinker in aqueous acid solution. (**b–e**) The gel-fraction yield (**b**, **c**) and the swelling degree of the gels in water (**d**, **e**) plotted against the initial pH of the feed solution. Gelation temperature was 24 °C (**b**, **d**) and −12 °C (**c**, **e**). Polymer concentration was 50 g/L. Glutaraldehyde molar ratio with respect to OH groups in the polymer was 5.6 (*curve 1*), 11.2 (*curve 2*), 16.8 (*curve 3*), and 22.4 mol % (*curve 4*). (Plotted based on the data from [8])

inside the pore walls is only a small share of the whole volume of liquid soaked up by such polymer materials. The net amount of the free liquid is determined by the inner volume of the large pores, which depends on the total mass of solvent crystals formed in the system during the cryotropic gelation process and, to a certain extent, on the size of these crystals. The liquid from the capillaries of the sponge-like cryogels can be squeezed off by mechanical compression, sometimes almost completely [46], whereas the solvate fraction can only be removed from the polymer matrix by intense drying, i.e., by heating under reduced pressure. Thus, the total volumetric swelling degree does not characterize the osmotic properties of the gel pore walls in the wide-pore cryogels. However, in some cases, comparison

of the swelling behavior of cryogel matrices in different solvents can be an indicator of the affinity of the capillary system of cryogels with respect to the tested liquids.

The apparent decrease in CCG is also characteristic during the formation of polymerization-type cryogels. This phenomenon was first observed upon comparison of the critical concentrations of vinyl and divinyl comonomers, namely acrylamide and N,N'-methylene(bis)acrylamide, for the formation of poly(acrylamide) gels and cryogels [7, 8, 19–23]. At room temperature, the CCG for this gelation system lies in the vicinity of 2 wt% and also varies depending on the ratio of vinyl and divinyl components [137–139]. However, when the polymerization occurs in a moderately frozen medium, wide-pore sponge-like poly(acrylamide) cryogels can be prepared using at least half the concentration of the comonomers [7, 19]. The physicochemical features of such gelation systems are considered in more detail in [47]. Here, it is reasonable to emphasize only that the effect of an apparent decrease in CCG is common for the formation of any type of chemically crosslinked cryogels, and this effect is mainly determined by the increase of precursor concentration in the volume of UFLMP as the solvent freezes out.

The question is whether the same decrease in CCG is also inherent in the formation of physical cryogels. The answer in most cases is obviously, yes. For instance, the gelation process of aqueous solutions of locust bean gum was investigated both at positive and negative temperatures. Locust bean gum is a polygalactomannan gum consisting of poly(1,4-β-D-mannose) main chain and 1,6-α-D-galactose pendant chains with a mannose to galactose ratio of 1:4 [140]. Solutions (1–4 wt%) of locust bean gum remain fluid during prolonged storage at positive temperatures and they transform into very weak gels only after 2–3 months [141]. However, cryogenic treatment of the same feed systems produces cryogels within a short period of time [100, 102, 115, 142–144]. Thus, the effect of CCG decrease was clearly demonstrated for such cryogels. They are thermoreversible, i.e., the cryogels can be melted by heating and they form again after a new freeze–thaw cycle. The morphology of the cryogels based on locust bean gum is heterogeneous; they resemble soft sponges as long as the initial polysaccharide concentration is lower than 2.0–2.5 wt%. Such sponge-like cryogels exclude free liquid under a slight compression. Although cryogenic treatment of more concentrated locust bean gum solutions also yields gel materials, they do not exclude free liquid under a moderate pressing. However, the latter gels are similar to the physical PVA cryogels in that they are also macroporous because, during cryotropic gel formation, ice polycrystals act as porogens and macropores of various sizes and architecture remain in the cryogel body after thawing.

There are also other examples of the manifestation of a CCG decrease during the formation of noncovalent cryogels. The precursors (i.e., polysaccharides, proteins, synthetic polymers) together with the conditions of gel formation processes and the appearance of the final material are listed in Table 2. These data demonstrate the universal character of the CCG decrease in both aqueous and organic media during cryotropic gelation as compared to conventional gelation. The best studied among the processes of the formation of noncovalent cryogels is the cryotropic gelation of PVA solutions. The reason for this is twofold: First, the final "products", i.e., the

Table 2 Influence of the freeze–thaw treatment on the solutions of polymeric precursors capable of forming physically crosslinked gels

Precursor	Precursor concentration in the feed (wt%)	Solvent	Temperature of the gelation process (°C)	Appearance of the samples after the gel formation process	References
Agar-agar	0.5	Water	+20	Rather weak gel	[12]
			−10	Sponge-like cryogel	
	1.0		+20	Weak gel	
			−10	Sponge-like cryogel	
Agarose (low-gelling-g-tempera-ture brand)	0.5	Water	+20	Jelly-like system	[7]
			−20	Weak sponge-like cryogel	
Amylopectin	1.0	Water	+18	Thin precipitate	[98]
			−18	Non-spongy cryogel	
	5.0		+18	Very viscous paste	
			−18	Non-spongy rigid cryogel	
Gelatin (A-type)	0.5	Water	+20	Liquid	[12]
			−10	Sponge-like cryogel	
	1.0		+20	Liquid	
			−10	Sponge-like cryogel	
	1.5		+20	Very weak gel	
			−10	Sponge-like cryogel	
Locust-bean gum	0.3	Water	+18	Turbid liquid	[100, 115]
			−30	Spongy cryogel	
	3.0		+18	Viscous opaque paste	
			−30	Non-spongy cryogel	
Maltodextrin[a]	12.5	Water	+18	Opalescent liquid	[101]
			−24	Spongy weak cryogel	
Oat β-glucan	3.0	Water	+22	No gel formation	[145, 146]
			−18	Spongy cryogel	
Potato starch	2.5	Water	+18	Rather weak starch gel	[147]
			−18	Sponge-like cryogel	
PVA[b]	15.0	Water	+25	Mechanically weak gel	[13]
PVA[c]	10.0	Water	+20	Liquid	[12, 92]
			−10	Non-spongy cryogel	
			−20	Rather rigid cryogel	
	16.0		+20	Liquid	
			+2	Very weak gel	
			−10	Rigid cryogel	
			−20	Rigid cryogel	
	13.0	DMSO	$\Delta T = +1.6$	Liquid	[12]
			$\Delta T = -28.4$	Rather rigid cryogel	

[a]Molecular weight 8 kDa
[b]Duration of the incubation at gelation temperature 12 days
[c]Molecular weight 69 kDa

noncovalent PVA cryogels, possess outstanding mechanical and thermophysical properties. Second, owing to the very simple structure of the polymer itself, they are very convenient model systems for studying the fine mechanisms of cryotropic noncovalent gelation [8, 111, 112, 127, 129, 130, 148–152]. The shift in CCG upon the formation of PVA cryogels is also very remarkable. Even concentrated (10–16 wt%) aqueous and DMSO solutions of PVA (the latter must be highly deacylated PVA) do not transform to gels at room temperature for many days, whereas the freeze–thaw cycle produces viscoelastic cryogels that can be fused only when heated up to 60–80 °C. Similarly to the formation of chemically crosslinked cryogels, the main reason for such a decrease in CCG is the cryo-concentration of the gel precursors, strengthening the polymer–polymer interactions owing to higher overlapping of the polymer coils in the more concentrated medium of UFLMP.

3.2 Acceleration of Gel Formation Over a Certain Range of Negative Temperatures

One of the important consequences of the cryo-concentration effect is an acceleration of cryotropic gel formation processes within a certain range of negative temperatures as compared with conventional gelation [8]. Since the rate of the second or higher order reactions is proportional to a positive power of the concentration of the reactants, a freezing-induced increase in the precursor concentration within the UFLMP accelerates cryogelation reactions [54, 62–64]. The reaction scheme in Fig. 10a illustrates the oxidative gelation of a thiol-derivative of poly (acrylamide) in the presence of water-dissolved air oxygen acting as a crosslinking agent [28, 153, 154]. Since the number of free SH groups decreases during the course of interchain coupling through the formation of disulfide crosslinks, the evolution of SH group concentration with time reflects the process dynamics. Figure 10b shows the variation in the amount of residual SH groups in 2 wt% aqueous polymer solutions at positive (15 and 25 °C) and negative (−15 and −25 °C) temperatures. Two arrows (Fig. 10b) indicate the vicinity of the gel points for the unfrozen and frozen gelation systems. The rate of the decrease in thiol group content (i.e., the crosslinking rate) increases and the gel point shifts to shorter times in the moderately frozen polymer solutions as compared to unfrozen solutions. Remarkable is the shortening of the gelation time, which differs by a factor of about 22 in favor of cryotropic gel formation.

The thermal prehistory of such cryogenically gelling systems also influences the process dynamics. The kinetic data in Fig. 10b were obtained by conventional freezing of the feeds, i.e., without low-temperature quenching, as mentioned in Sect. 2.2. When the same reaction solutions are subjected to the low-temperature quenching technique to freeze the feeds quickly, one obtains the plots illustrated in Fig.10c. Here, the decrease in the thiol group content of the polymer is shown during the course of the first 2 h of the reaction. Note that the zero time in these plots
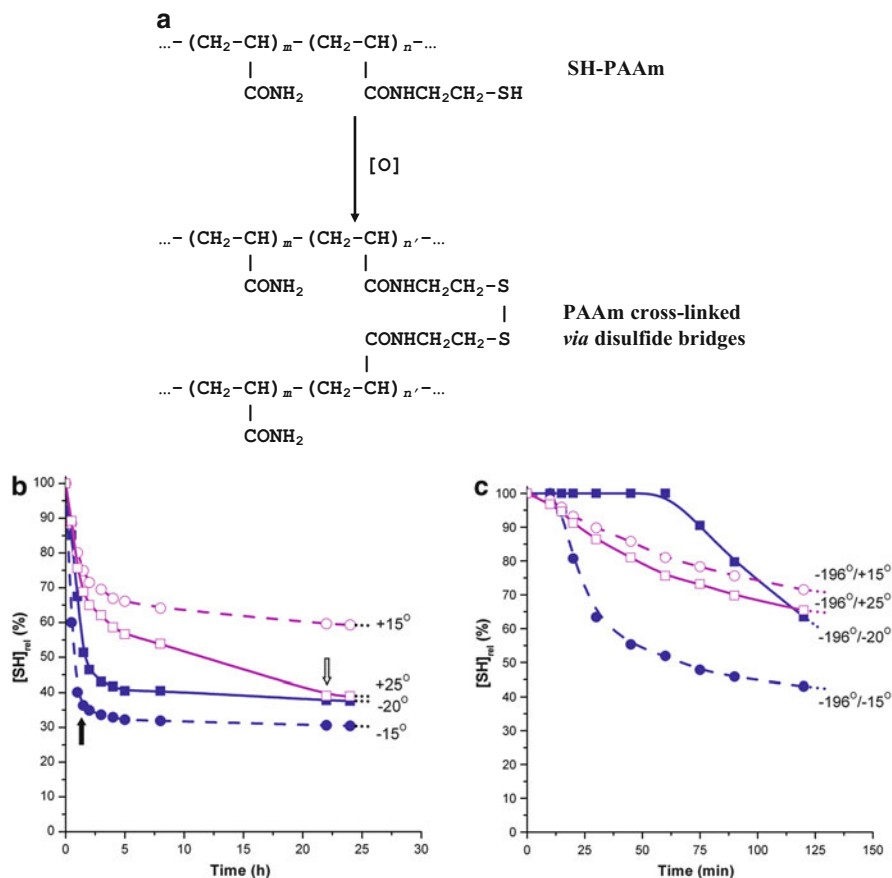
Fig. 10 (**a**) Crosslinking reaction of thiol-containing poly(acrylamide) in aqueous acid solutions. (**b, c**) Variation in the percentage of residual thiol groups on the polymer chains with reaction time. The freezing technique was conventional (**b**) or low-temperature quenching (**c**). Gelation temperatures are indicated. *White* and *black arrows* in **b** indicate the vicinity of the gel points in unfrozen and frozen gelation systems, respectively. Plotted from the data of [28]

corresponds to the moment of transfer of the reaction solutions from liquid nitrogen into the cryostat/thermostat chamber with a pre-set temperature. A certain delay (i.e., lag period) is observable at the start of the reactions at negative temperatures, followed by a quick decline of the SH content of polymer chains. For the gelation reactions conducted at positive temperatures, the reaction rates with and without low-temperature quenching are identical. However, at negative temperatures, low-temperature quenching further accelerates the gelation reactions. Moreover, except for the lag phase, the slope of the kinetic curves obtained both at −15 and −20 °C is much higher than that obtained at positive temperatures. Thus, independent of the thermal history, the rate of the crosslinking reactions is much faster in frozen solutions than in unfrozen solutions due to the existence of UFLMP.

The volume and concentration of solutes in UFLMP depend on the cryoscopic properties of the solvent, the freezing temperature, concentration of the precursors in the feed, their solubility, and their dimensions, i.e., molecular weights. In this connection, it is of interest to demonstrate how the presence of an inert additive (e.g., an inert polymer) can affect the reaction kinetics in such non-deeply frozen systems. This effect was investigated in cysteine–cystine conversion by oxygen [28]. Figure 11a shows the scheme of the oxidation of cysteine, a thiol-containing amino acid, to the respective disulfide by water-dissolved air oxygen. Figure 11b presents the kinetic curves of this reaction as the dependence of the thiol group content of cysteine on the reaction time [28]. When the reactions are conducted at room temperature or at $-15\,°C$ (represented by the curves 1 and 3, respectively, in Fig. 11b), the concentration of SH groups slowly diminishes with time due to this oxidation, i.e., the reactions proceed slowly. When the initial cysteine solution also contains about 1 wt% poly(acrylamide) as an inert polymeric additive, no marked effect was observed at room temperature (curve 2 in Fig. 11b). Thus, the polymer

does not have any chemical impact on the process of interest. However, a significant acceleration of cysteine oxidation occurs in the presence of polymer when the temperature is decreased to $-15\,^{\circ}\text{C}$ (curve 4 in Fig. 11b). Since the water solubility of cysteine is low, the slow rate of the reactions in the frozen solution at $-15\,^{\circ}\text{C}$ is due to the fact that the system is in the post-eutectic state and the amount of cysteine dissolved in UFLMP is very small. However, the presence of a hydrophilic unreactive polymer carrying bound water molecules increases the solubility of both cysteine and oxygen so that their concentrations in UFLMP increase and, hence, the reaction rate increases. This example also demonstrates one of the possible approaches for performing the reactions with thermally instable and insufficiently soluble low molecular weight substances. The presence of an inert polymeric additive during cryogelation protects the precursors from thermal decomposition and accelerates the reactions due to the cryo-concentration effect.

The acceleration of gel formation and the non-equivalence of its dynamics, depending on the thermal prehistory of moderately frozen reaction systems, were also observed during the synthesis of polymerization-type cryogels. One typical example is the formation of poly(acrylamide) gels starting from acrylamide monomer and N,N'-methylene(bis)acrylamide crosslinker in aqueous solutions with using of redox initiator systems (Fig. 12a). In Fig. 12b, c, gel fraction versus reaction time plots at various gelation temperatures are shown for reaction solutions frozen by conventional and low-temperature quenching procedures, respectively [23]. At positive temperatures, lowering the reaction temperature from 25 to $13\,^{\circ}\text{C}$ causes a decrease in the rate of ordinary gel formation, and thus results in a lower gel-fraction yield. This is expected. However, performing the reactions in a moderately frozen system leads to a faster gelation as well as to a higher yield (Fig. 12b). The freezing mode, i.e., the thermal history of bringing the system to the reaction temperature, also affects the course of cryotropic gel formation (cf. Fig. 12b, c), thus pointing to the non-equivalence of the phase states in such differently frozen polymerizing systems. Similar trends were also observed by use of NMR during the formation of poly(acrylamide) cryogels [50], as well as during the linear cryopolymerization of acrylamide in moderately frozen aqueous media, where different freezing procedures (conventional freezing, flash freezing, and low-temperature quenching) were employed [65].

The acceleration of gelation over a certain range of negative temperatures is also inherent during the formation of physical cryogels. This fact was already partially touched upon in the discussion of the data in Table 2, for instance, regarding the gelation time of aqueous solutions of locust bean gum or PVA. The same effect was also observed in maltodextrin- and β-glucan-containing systems [101, 145, 146], i.e., in systems where the noncovalent self-gelation at positive temperatures proceeds at a rather slow rate. Probably, somewhat similar events do take place in fast-gelling systems such as aqueous solutions of agarose, amylopectin, amylopectin–amylose mixtures, or concentrated solutions of gelatin. However, because of their rapid self-gelation before freezing, the additional acceleration due to the presence of UFLMP can hardly be detected.

a

$m\,(CH_2=CH)$ $+$ $n\,(CH_2=CH)$
           | |
        $CONH_2$ $CONH$
                                      |
                                 CH_2
                                      |
                               $CONH$
                                      |
                             $CH_2=CH$

   Acrylamide   **N,N'-methylene-**
                          -bis-acrylamide

$R\bullet\;\downarrow$

$\ldots-(CH_2-CH)_m-(CH_2-CH)_n-\ldots$
            | |
       $CONH_2$ $CONH$
                                   |
                               CH_2
                                 |
                             $CONH$
                               |
                    $\ldots-CH_2-CH-\ldots$

      Cross-linked
      poly(acrylamide)
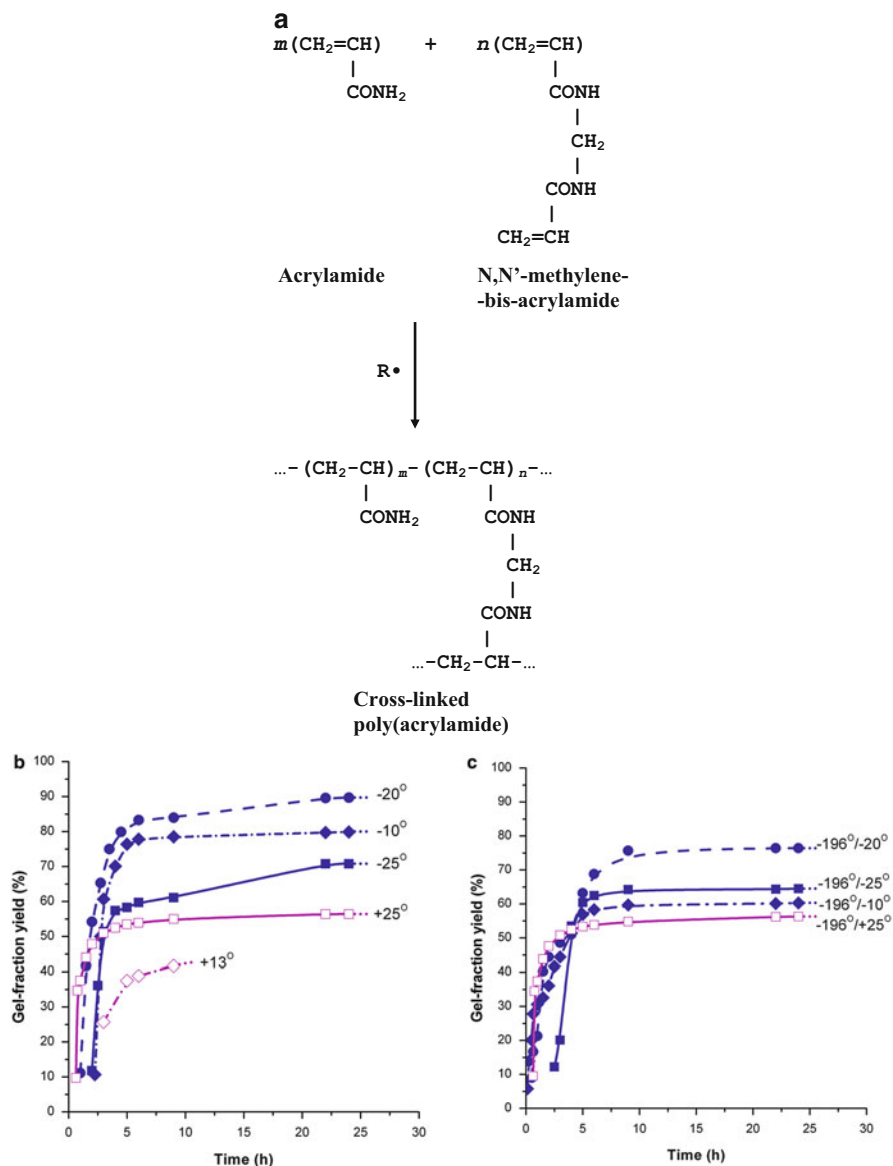
Fig. 12 (**a**) Free-radical crosslinking copolymerization of acrylamide and N,N'-methylene(bis) acrylamide. (**b**, **c**) Gel-fraction yield plotted against reaction time for the case of conventional freezing (**b**) and low-temperature quenching (**c**). Gelation temperatures are indicated. (Plotted based on the data from [23])

3.3 Bell-Shaped Temperature Dependence of Cryotropic Gelation Efficiency

In early studies on the kinetic features of simple model reactions in moderately frozen systems, it was found that the temperature dependence of the reaction rates is bell-shaped [62, 63]. This type of temperature dependence is a consequence of competition between the acceleration effect because of the cryo-concentration and the deceleration effect due to the decreasing thermal mobility of the reactants and increasing viscosity in the medium of UFLMP at negative temperatures [54, 63]. The temperature dependence of cryotropic gelation efficiency is, as a rule, also bell-shaped during the formation of both covalent and noncovalent cryogels [8]. In the following, such effects are demonstrated for cryogels produced via chemical crosslinking of macromolecular precursors as well as for the polymerization-type and noncovalent cryogels.

Figure 13 shows the temperature dependence of the gel-fraction yield during the formation of chitosan-based cryogels, when this polyaminosaccharide was crosslinked with various amounts of glutaraldehyde (for the reaction scheme see Fig. 7a). The results reveal that, in the moderately frozen aqueous medium, the highest performance of the crosslinking process was achieved in the vicinity of -25 °C, whereas above and below this temperature the gel-fraction yield was lower [10].

Because the freezing procedure employed (i.e., the thermal history of the system) influences the cryotropic gelation dynamics, it is reasonable to anticipate that it can also affect the temperature dependence of the gel formation efficiency. Indeed, this assumption was confirmed experimentally. Figure 14 is a relevant example showing the temperature dependence of the initial rate (v_0) of SH group decline in the course of oxidative gelation of thiol-bearing poly(acrylamide) [28]. Curves 1 and 2 correspond to the reaction systems subjected to conventional freezing and low-temperature quenching procedures, respectively. The distinctions are obvious: when the reaction solution is subjected to the low-temperature quenching procedure, the initial rates become slower over the whole range of reaction temperatures studied, and the position of the maximum shifts towards a lower temperature. These results testify once again that the reaction conditions in moderately frozen systems, especially at the initial stages, differ significantly depending on the thermal prehistory, i.e., on the freezing procedure employed. Most probably, one of the main reasons for this effect is the nonequivalence of the phase states in such differently frozen gelling systems. Nonetheless, the bell-like character of curves 1 and 2 in Fig. 14 is very similar, thus showing the generality of the tendencies described by such temperature dependences, irrespective of the thermal history. At the same time, no differences were observed in v_0 values for the gelation in solutions without any freezing (solid line in Fig. 14) and initially frozen in a liquid nitrogen followed by placing in a thermostat with pre-set positive temperature (dashed line in Fig. 14).

Fig. 13 Gel-fraction yield plotted against temperature for chitosan cryogels crosslinked using glutaraldehyde. Polymer concentration in the initial solution was 1.6 wt%. NH_2-to-CHO molar ratio was 2.5:1 (*curve 1*), 15:1 (*curve 2*) and 25:1 (*curve 3*). (From [10] with permission from Springer)
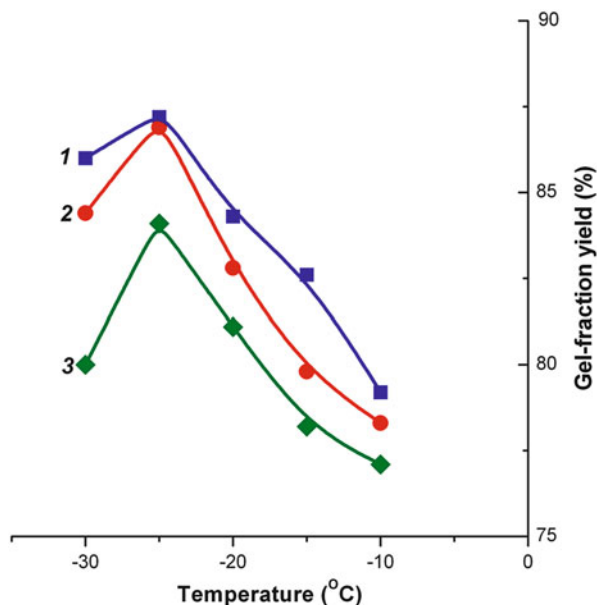
The bell-shaped temperature dependence of the gelation rates is, as mentioned already, due to the competition between the favorable and adverse factors. The favorable factors are as follows:

1. The cryo-concentration effect leads to increased concentrations of solutes within the UFLMP, facilitating the reaction efficiency.
2. The effect of the so-called thermodynamic selection of the reactions [63] that are characterized by the lowest values of the activation energy.
3. The heat sink from the reaction system is useful for the exothermic processes so that it is also one of the favorable factors, provided that the heat is released during the gelation, as it usually is for free-radical polymerization.
4. Since the dielectric conductivity ε increases as the temperature decreases, the polarity of the solvent in UFLMP is higher than its polarity at positive temperatures, which is an additional favorable factor. For example, during the heterolytic reactions where the separation of charges is of significance, e.g., coupling of polymeric precursors through the formation of aldimine (Fig. 7a), alkyl-aryl (Fig. 8a), or acetal (Fig. 9a) crosslinks, increasing the polarity of the reaction medium also increases the efficiency of the respective reactions.
5. During the formation of noncovalent cryogels from the polymeric precursors exhibiting an upper-critical-solution-temperature (UCST) behavior, cooling down the reaction solution also facilitates the sol-to-gel transition.

There are also several factors acting adversely on gel formation in moderately frozen systems as follows:

Fig. 14 Initial rate ν_o of the decrease of thiol groups in aqueous solutions of thiol-containing poly (acrylamide) plotted against temperature. Freezing procedures were conventional (*curve 1*) and low-temperature quenching (*curve 2*). Polymer concentration in the initial solution was 2 g/L. (From [28] with permission from Elsevier)
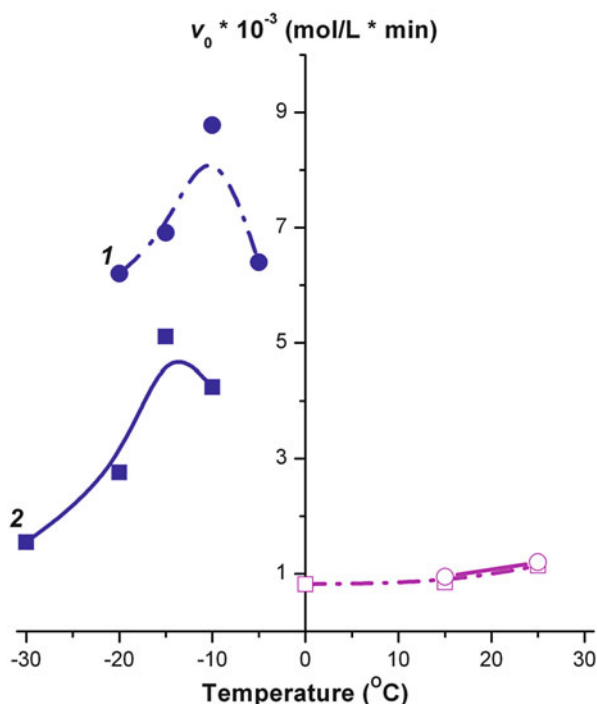
1. According to the Arrhenius principle, a decrease in temperature lowers the thermal mobility of the solutes and thus, decelerates the reactions. This is the most significant unfavorable factor affecting the cryogelation process.
2. The high viscosity of UFLMP is the second unfavorable factor for cryotropic gel formation. This factor is significant for cryogelation reactions starting from polymeric precursors. Since the lower the temperature of a moderately frozen system, the larger the amount of frozen solvent and, thus, the higher the polymer concentration in UFLMP, the resulting high viscosity strongly hinders the translational and segmental mobilities of the polymeric precursors and interferes with their interactions. The molecular weight of the polymeric precursors also affects the course of gel formation. The higher the molecular weight of the polymeric solute, the higher is the extent of coil overlap and, hence, the higher is the probability of intermolecular interactions. On the other hand, the higher the chain length of the polymers, the higher is the viscosity of the equiconcentrated polymer solutions. Thus, these two trends act oppositely and compete against each other in the course of gel formation. This is also the reason why a bell-like dependence of the gelation efficiency on the molecular weight of the polymeric precursors is often observed. For particular examples, see [32, 44, 155] dealing with the synthesis of chitosan and poly(acrylamide) cryogels via crosslinking by glutaraldehyde, and with the noncovalent cryotropic gelation of aqueous

Fig. 15 Temperature dependence of the gel-fraction yield during the preparation of poly(styrene) gels (*circles*) and cryogels (*squares*) in nitrobenzene using 4,4′-xylylene dichloride as a crosslinker. The temperature scale is the relative temperature ΔT (as explained in Sect. 1). Polymer and crosslinker concentrations in the initial nitrobenzene solution were 0.3 M and 9.1 mol%, respectively (both with respect to the styrene units). (Plotted based on the data from [27])
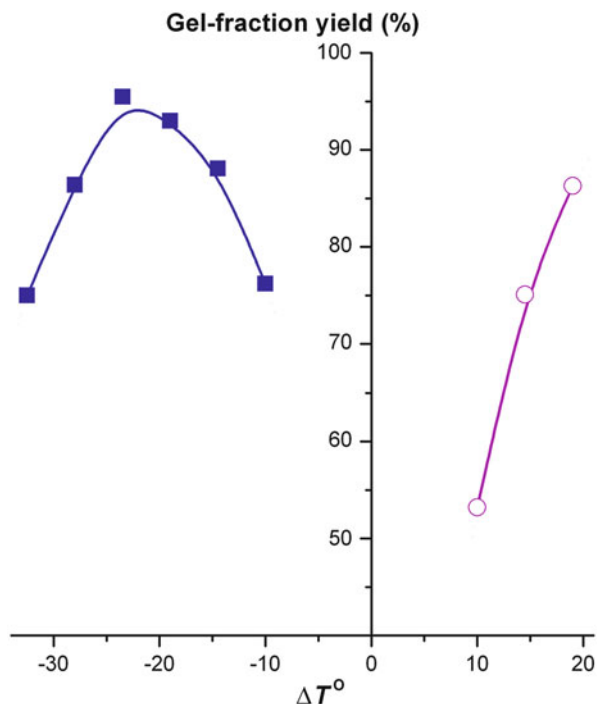
solutions of PVA of various molecular weights. Therefore, it is desirable to perform some preliminary experiments with polymeric precursors of different molecular weights in order to search for an optimum value of this parameter.

3. The formation rate of crosslinks between the polymer chains is also a factor capable of hindering the gelation processes inside the UFLMP. When the reactions proceed slowly, the crosslinks are generated rather uniformly throughout the UFLMP. However, for the fast reactions, the polymer chains are rapidly bridged by the introduction of the first crosslinks, once the primary network is formed, the subsequent crosslinks in highly viscous UFLMP are strongly hampered. This effect can result in a pronounced inhomogeneity in the crosslink density distribution within the network. To minimize this effect and, thus, to prepare cryogels with reproducible properties and porous morphology, one can reduce the reaction rates and the initial concentration of the precursors.

All these favorable and unfavorable factors and mechanisms are effective to a different extent during cryotropic gelation in both aqueous and organic media. For instance, Fig. 15 shows the bell-like temperature dependence of the gel-fraction yield when poly(styrene) was crosslinked with 4,4′-xylylene dichloride in nitrobenzene (see Fig. 8a for the reaction scheme). At temperatures 30–40 °C lower than room temperature, the efficiency of polymer crosslinking is higher than in unfrozen solutions (curve with open circles in Fig. 15) [27]. Thus, close similarity in the character of such temperature dependences for the processes in frozen aqueous and

Fig. 16 Time for the onset of gelation t_{g-p} plotted against the temperature during the crosslinking copolymerization of acrylamide and N,N'-methylene(bis) acrylamide. Freezing modes were conventional freezing (*curve 1*) and low-temperature quenching (*curve 2*). Initial monomer concentration was 3 wt%. Molar ratio of vinyl to divinyl monomers in the feed was 30:1. (From [23] with permission from Wiley)
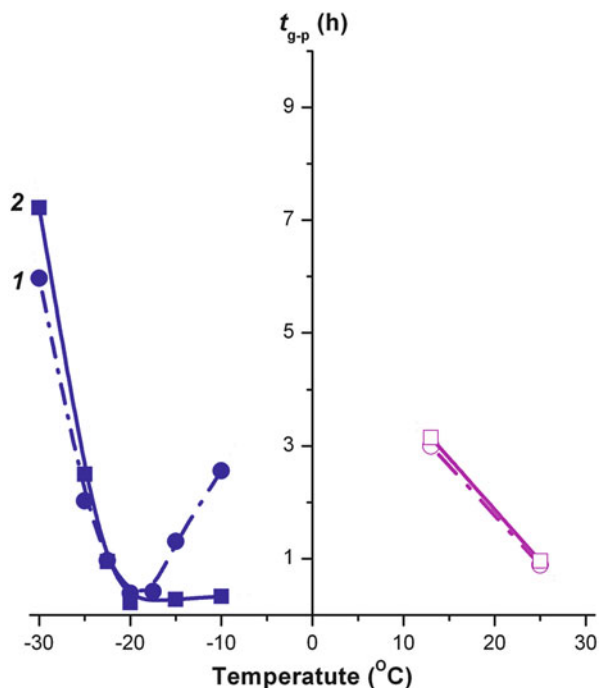
organic media obviously proves that the same factors are responsible for the efficiency of cryotropic gel formation in solvent–polymeric precursor–crosslinking agent systems, irrespective of the type of crystallizing solvent.

Temperature dependences of the rate of cryogelation reactions and the cryogel properties were also investigated in reaction systems leading to the formation of polymerization-type cryogels, i.e., in solvent–monomers–initiator systems. Figure 16 shows the reaction time for the onset of gelation (i.e., the gel-point time, t_{g-p}) during the redox-initiated copolymerization of acrylamide and N,N''-methylene(bis)acrylamide in aqueous solutions plotted against the reaction temperature. The curves 1 and 2 in Fig. 16 represent the trend of data obtained from the reaction solutions subjected to conventional freezing and low-temperature quenching procedures, respectively [23]. The shortest time to reach the gel point at −20 °C was 15 and 14 min for the conventional freezing and low-temperature quenching, respectively. At room temperature, this time is about four times longer (~1 h). This feature was already touched on in the discussion on the acceleration effect inherent in cryotropic gelation as compared with gel formation at positive temperatures. Moreover, an interesting point can also be gained by comparing curves 1 and 2 in Fig. 16 within the temperature interval from −20 to −10 °C. For the reaction solution subjected to the conventional freezing procedure (curve 1), i.e., when the solution just after initiator addition is placed into the cryostat chamber with the required preset temperature, a concave upward bell-like dependence of t_{g-p} on the reaction temperature was observed. In contrast, application of the
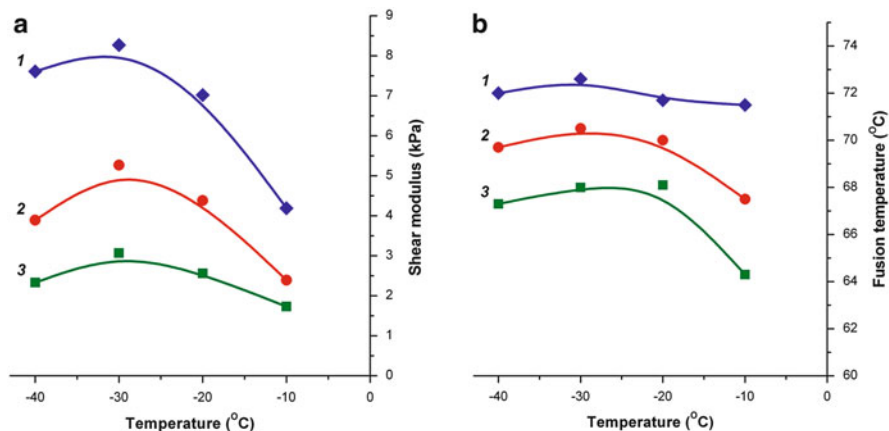
Fig. 17 Influence of the freezing/frozen storage temperature on (**a**) the shear modulus and (**b**) the fusion temperature of PVA cryogels. Initial polymer concentrations were 120 (*curve 1*), 100 (*curve 2*), and 80 g/L (*curve 3*). (Plotted based on the data from [44])

low-temperature quenching procedure using liquid nitrogen markedly alters the temperature dependence between −10 and −20 °C. This result most probably indicates that, when a deeply frozen system is heated to the subzero level, the concentration of the reactants in the resulting UFLMP at the early stages of gel formation is higher than that in the UFLMP formed as a result of a conventional mode of freezing. The reason for such an effect is obviously a low rate of solid-to-liquid phase transition of solvent crystals after the low-temperature quenching [23, 50, 65]. This phenomenon in its nature resembles prolonged (days) thawing of snow and ice in spring when the environmental temperature is already considerably higher than the ice melting point.

The last example in this section concerns the temperature dependence of the efficiency of the noncovalent cryotropic gel formation. This is illustrated in Fig. 17 for PVA cryogels, where their shear moduli (Fig. 17a) and the fusion temperatures (Fig. 17b) are plotted as a function of the freezing temperature. The cryogels were prepared by freezing aqueous solutions of PVA (80–120 g/L) for a fixed time at various negative temperatures followed by defrosting at the same rate [44]. The modulus and the fusion temperature of the cryogels represent their rigidity and heat endurance, respectively, and are indicators of the gelation performance. It can be seen that both of these parameters also have bell-shaped dependences on the process temperature. This also indicates the competition of the facilitating and inhibiting mechanisms participating in the formation of such gel matrices. Thus, lowering the storage temperature of the frozen solution results in the formation of a larger mass of solvent crystals and, hence, increases the polymer concentration in UFLMP so that PVA gelation becomes more efficient, as in the case of systems having a higher initial PVA concentration in the feed. On the other hand, the drastic increase in viscosity within UFLMP hinders efficient intermolecular interactions

and, thus, formation of PVA microcrystallites, the nodes in the final cryogel. As a result, the temperature dependences of the respective parameters pass through the maxima, a common trend for the formation of physical cryogels in general.

Summing up the discussion on the influence of favorable and detrimental factors on cryotropic gel formation, one can see that their competition is the main reason for the bell-like temperature dependence of the gelation efficiency. This effect is manifested both for chemically crosslinked cryogels and noncovalent gels, when either monomeric or polymeric precursors are used, and both in aqueous and organic media. So, such bell-shaped dependences are a characteristic feature of cryotropic gel formation. However, the exact position of the corresponding maxima or minima on the temperature axis depends on the particular cryogelation system. Therefore, the necessity of preliminary search for the "optimal" temperature conditions for freezing and for frozen storage is evident. Although such preliminary studies can require time and effort, only this path will result in cryogels with the best possible properties and structure.

3.4 Generation of Specific Porosity Peculiar to Cryogels

The scheme in Fig. 3 visually demonstrates formation of macroporosity in cryogels due to the presence of polycrystals of frozen solvent acting as porogens. Depending on the nature of the cryogel precursors, their initial concentrations, the type of the solvent used, and the cryogenic processing conditions, it is possible to obtain cryogels with pores having a cross-section from the submicron range up to several micrometers (Figs. 5 and 6), or supermacroporous (wide pore) gel matrices similar to the sponge-like chitosan-based cryogels (Fig. 1) where the cross-section of large pores ranges from tens to hundreds of micrometers. Certainly, some "intermediate" variants are also possible. The main characteristics of the porosity of cryogels have been described in several review papers [8, 9, 107, 111, 114, 130, 148–150, 152, 156–164], and are also considered in [47]. However, certain aspects of macroporosity generation in the course of freeze–thaw gelation will be discussed in this section.

We will first consider the reason why the size of pores in the cryogels varies by two orders of magnitude depending on the synthesis conditions. This is mainly due to the different size of the pore template (i.e., the frozen solvent polycrystals), which depends on the amount of freezable solvent under the freezing conditions employed. For instance, when the initial concentration of the monomeric precursors is not too high, i.e., less than 10 wt%, the fraction of free solvent freezable at moderate negative temperatures is large, and the viscosity of the feed solution is not so high as to markedly inhibit crystal growth. This effect leads to the formation of large polycrystals and, hence, large pores. On the other hand, when the initial concentration of the polymeric precursors is high, a greater part of the solvent is bound to the dissolved macromolecules so that the volume of the freezable liquid is considerably less than in the previous case, leading to a high solution viscosity that

hinders the growth of solvent crystals. As a result, only relatively small porogen particles can be formed, thus generating relatively small pores in the resulting cryogels.

In this connection, PVA solutions subjected to multiple freeze–thaw cycles represent a specific case where the porosity characteristics are governed not only by the conditions of the first cryogenic cycle, but also by the following cycles [111, 126–130, 133, 149, 165, 166]. As illustrated in Fig. 6, the most significant step-like changes in the size and shape of the macropores occur during the second cycle. During this cycle, the free solvent crystallizes mainly within the space of the already formed "primary" macropores, where the liquid contains only a small amount of sol-fraction [113]. Therefore, the viscosity within this space is considerably lower than that of the initial PVA solution, and larger ice particles are formed. In addition to widening of the primary pores by these growing crystals, a certain compression of the pore walls owing to the physical stresses caused by the ice crystallization also occurs, thus facilitating compaction of the proper gel phase in the heterophase material. As a consequence, after the second freeze–thaw cycle, the cross-section of the macropores increases by a factor of 2–3, whereas further cryogenic cycles have an insignificant influence on the size and shape of these pores [133].

The cryogenic processing conditions of PVA solutions also affect significantly the porous structure of PVA cryogels. To demonstrate this effect, noncovalent PVA cryogels were prepared starting from aqueous solutions of PVA (100 g/L) according to two different freezing and frozen-storage procedures [44]:

(a) PVA solution was frozen at $-20\,°C$ for 24 h
(b) PVA solution was first frozen at $-20\,°C$ for 1 h, then incubated at a fixed negative temperature between -5 and $-1.1\,°C$ for 23 h

The micrographs in Fig. 18a, b represent thin sections of PVA cryogels formed by the two procedures, respectively, where the latter was incubated at $-2\,°C$. The morphology of the cryogel formed by a single-temperature freezing differs markedly from the two-temperature freezing procedure. As pointed out in Sect. 2.4, at a storage temperature of $-2\,°C$, cryotropic gelation of PVA occurs with the highest efficiency. Moreover, ice re-crystallization phenomena are also very intensive at this temperature [167–169]. Since the prolonged incubation of the frozen sample at $-2\,°C$ equalizes the temperature fields in all directions, the branched crystals are formed as a result of the re-crystallization. After defrosting, such secondary crystals leave a net-like system of intersecting macropores in the body of the PVA cryogel.

The next key feature of the textural morphology of freeze–thaw gels is the interconnected character of their macropores. The main reason for such a porous character is the 3D growth of porogen particles (i.e., solvent crystals) during freezing of the feed system, whereby the growth stops for a particular facet of a crystal when it comes into tight contact with some facet of a neighboring growing crystal [8]. During subsequent thawing of the frozen sample, these contact areas are transformed into the connections between macropores. When the unidirectional freezing technique is employed, the propagation rates of different facets are
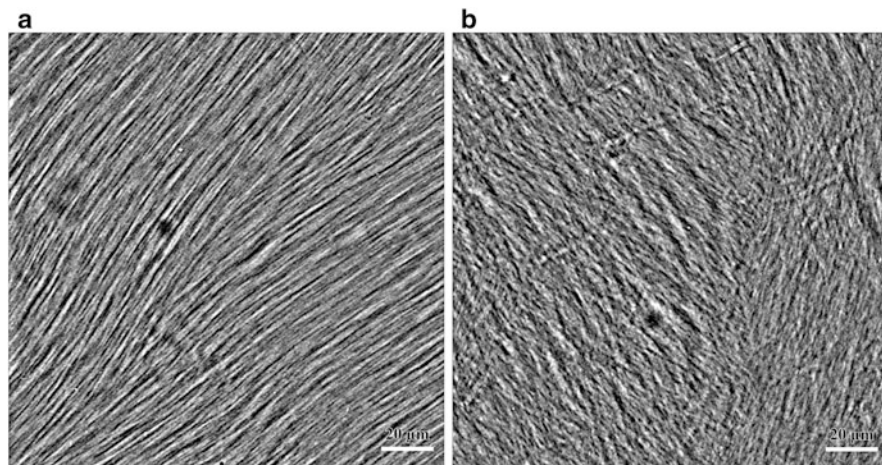
Fig. 18 Micrographs of thin sections of PVA cryogels prepared from aqueous solutions of PVA (100 g/L) using (**a**) single-temperature and (**b**) two-temperature procedures. The freezing/storage-frozen regimes were −20 °C for 24 h (**a**) and −20 °C for 1 h and then −2 °C for 23 h (**b**). The average size of macropores was 2.8 (**a**) and 2.4 μm (**b**). The fraction of macropores was 61.3 (**a**) and 52.5 % (**b**). *Scale bars*: 20 μm. (From [44] with permission from Springer)

strongly unequal, and crystal growth dominates in the direction that follows the vector of temperature gradient. Nonetheless, other facets are also enlarged and have the possibility to come into contact with their neighbors, thus forming future connections between the unidirected macropores in the defrosted cryogel.

The interconnected character of the pores in stimuli-responsive cryogels is also responsible for their fast response rate to a change in the external conditions. As is well known [170, 171], hydrogels may exhibit drastic volume changes in response to specific external stimuli, such as temperature, solvent quality, pH, electric field, etc. However, such stimuli-responsive hydrogels prepared by conventional techniques exhibit a slow rate of response to external stimuli. For instance, the kinetics of the collapse of temperature-sensitive swollen hydrogels is controlled by heat transfer into the gel and by diffusion of the solvent out of the gel, where both of these processes depend on the size of the gel sample. The larger the gel size, the lower is its response rate. The presence of interconnected pores of capillary size in cryogels, as well as the high polymer content of their pore walls, ensure their very fast volumetric response to external stimuli. Thermoresponsive poly(*N*,*N*-diethyla-crylamide) and poly(*N*-isopropylacrylamide) cryogels are typical examples of stimuli-responsive cryogels [172, 173]. As the temperature passes across the critical (LCST) point, the gel phase (pore walls) deswells so that the inner water is rapidly squeezed out of the cryogel through the system of interconnected capillaries. In such spongy gel matrices, absorption or desorption of water occurs through the macropores by convection, which is much faster than the diffusion process that dominates inside the conventional hydrogels. Figure 19 shows a typical example of the dynamics of heating-induced collapse of poly(*N*,*N*-diethylacrylamide) gels,
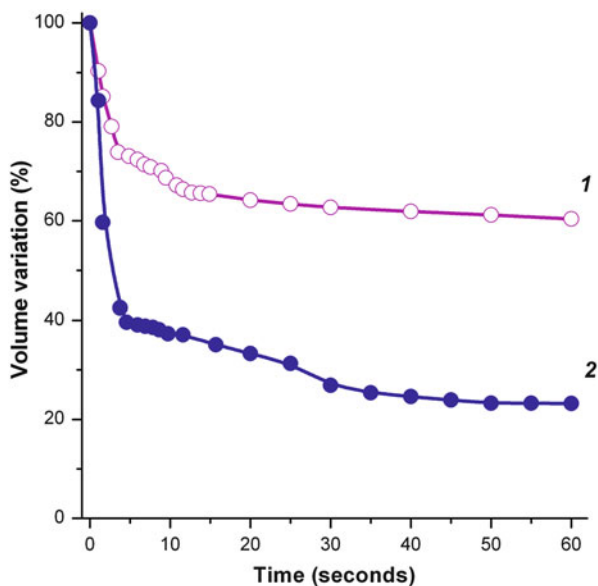
Fig. 19 Thermally induced collapse of poly(*N,N*-diethylacrylamide) hydrogel (*curve 1*) and cryogel samples (*curve 2*) upon increasing the temperature from room temperature to 60 °C. The variation in the volume of the gel samples is shown as a function of the deswelling time. Synthesis conditions: initial monomer concentration 5.66 wt%; molar ratio of vinyl to divinyl monomers 200:1; gelation temperature +20 °C (*curve 1*) and −10°C (*curve 2*). (From [172] with permission from Springer)

where the variation in gel volume is plotted against the deswelling time. Here, the gel samples swollen to equilibrium in water at room temperature were immersed in water at 60 °C, and the volume change was recorded as a function of time. Data obtained from hydrogels and cryogels are shown in curves 1 and 2 of Fig. 19, respectively. Compared to the conventional gel, the rate of deswelling is much faster and the extent of volume variation is much larger for the cryogel sample due to its 3D pore structure.

Another aspect related to the formation of macroporous structure in polymeric cryogels is the implementation of auxiliary porogens in addition to the solvent crystals. Combination of various pore-forming agents allows one to vary the macroporous morphology of the cryogel-type materials over a very wide range. Such auxiliary agents can be divided into two groups: first, the pore-formers that can be later extracted from the gels, such as silica particles, salts, or oil droplets; and second, those that cannot, such as gas bubbles. In the first case, the corresponding porogens can be either temporarily insoluble or even soluble in the feed, while the second group includes permanently insoluble disperse matter playing the role of pores.

One of the simplest examples of a temporarily insoluble porogen is chalk or silica powder, whose particles are initially dispersed in the feed to be cryogenically

treated. Such feed systems result in the formation of composite cryogels with incorporated fillers, which are then dissolved by rinsing the composite with aqueous acid or alkali. The pores formed with the aid of such additives are isolated from each other and have a size close to that of the filler grains, whereas the system of interconnected macropores is ensured by cryotropic gel formation. Hydrophobic oil can also be used as an insoluble porogen in the preparation of hydrophilic thermo- or pH-responsive poly(N-isopropylacrylamide)-based copolymer cryogels [174–176]. After preparation of such wide-pore spongy gel composites, they contain entrapped microdroplets of hydrophobic liquid. These droplets can be removed upon the stimulus-induced collapse of the cryogel, i.e., by heating or by changing pH. Since the collapse is reversible, when the collapsed cryogel is placed in oil-free water, it swells again so that additional "non-cryotropic" spherical pores filled with water instead of oil microdroplets can be obtained. By iterative collapse–swelling cycles it is possible to remove completely such hydrophobic auxiliary porogens.

The soluble auxiliary pore-forming agents are compounds dissolved in the common solvent together with the gel precursors. The porogenic properties of these agents may affect the crystallization of the liquid medium so that they are also called modifiers of solvent crystals. This effect is illustrated by the micrographs in Fig. 20, which show the images of thin sections of PVA cryogels prepared in the presence of various low molecular weight salts at two different concentrations. All the samples were cryostructured under identical freeze–thaw conditions, and Table 3 summarizes their porosity parameters [177]. The porous morphology of PVA cryogels is affected by both the nature and the concentration of low molecular weight electrolyte additives. The size of the macropores decreases as the salt concentration is increased, in accord with the well-known influence of salts on the spatial geometry and size of ice crystals [167, 178, 179]. Moreover, the influence of other processes like the salting-out effect, which leads to an increase in the ionic strength of UFLMP, cannot be excluded. As a result, certain integral changes in the macroporous morphology of cryogels can be registered at the resolution provided by an optical microscope. In other words, such low molecular weight salt additives act as powerful pore modifiers for the resulting cryogels, and their impact is achieved via their influence on the course of solvent crystallization.

Certain soluble auxiliary pore forming agents may induce a liquid–liquid phase separation. Spongy PVA-based cryogels prepared from "water–PVA–gum arabic" feeds are a good example of the influence of such phenomenon on the formation of additional pores in cryogels [180]. Aqueous feed systems containing a gel-forming agent (PVA) and a polymeric additive (gum arabic) unable to form noncovalent cryogels are interesting because they demonstrate the effect of thermodynamic incompatibility of the polymeric components on the texture of the resulting cryogels. Several types of PVA cryogels prepared from such multicomponent feeds have been described, where the auxiliary pore-forming agents were both synthetic polymers and natural biopolymers such as polysaccharides, proteins, and nucleic acids. All of these additives affect the properties and the porous structure of the formed PVA cryogels [181–187]. There are potentially two extreme variants of PVA-based feed systems capable of liquid-phase de-mixing. First, the
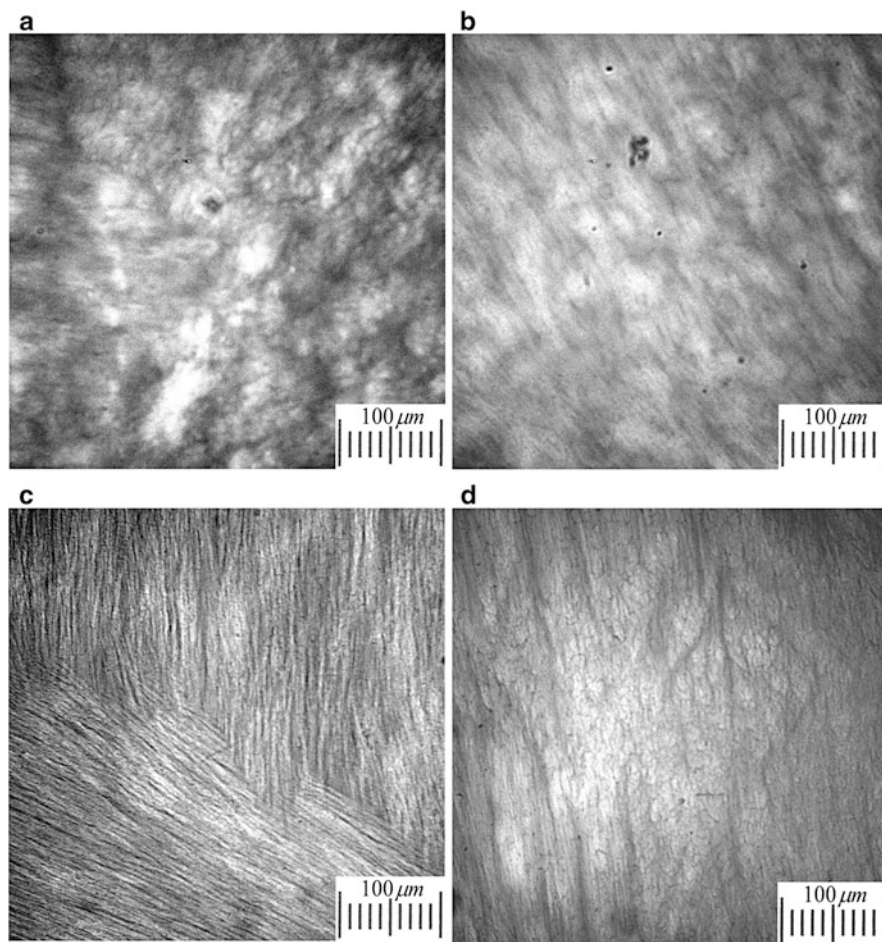
Fig. 20 (continued)

solution of PVA and the polymer additive can be frozen while in a homophase liquid state. As the pure ice is initially crystallized, both polymeric components are concentrated in the UFLMP. This cryo-concentration process causes liquid–liquid phase separation within the volume of the unfrozen inclusions. In the second case, the initial common solution of PVA and the polymeric additive can undergo liquid–liquid separation prior to the cryogenic treatment, a behavior inherent in the well-known Albertsson's liquid two-phase polymeric systems [188], so that the already formed two coexisting liquids are frozen. Certainly, there can be some intermediate variants because the phase segregation in viscous polymer solutions occurs rather slowly, i.e., the process is kinetically controlled.

An example of the first case is the preparation of macroporous PVA cryogels in aqueous solutions of PVA in the presence of poly(ethylene glycol) of molecular
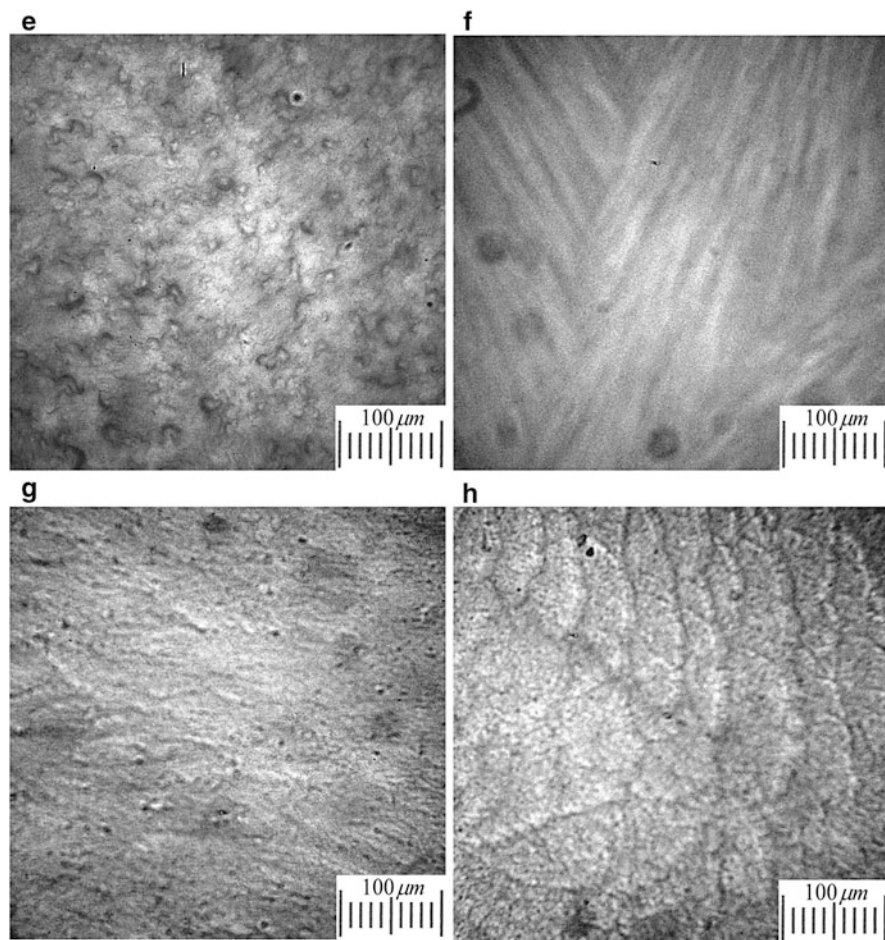
Fig. 20 (**a–h**) Micrographs of thin sections of PVA cryogels formed in the presence of alkali metal chloride additives at a concentration of 0.6 (**a**, **b**, **c**, **d**) and 1.2 M (**e**, **f**, **g**, **h**). Salt additives: LiCl (**a**, **e**), NaCl (**b**, **f**), KCl (**c**, **g**), and CsCl (**d**, **h**). Initial polymer concentration was 100 g/L. Conditions of cryotropic gelation were freezing at −20°C for 24 h and defrosting with a rate of 0.03 °C/min. (From [177] with permission from Springer)

weight 1,000 g/mol (PEG-1000) acting as an auxiliary porogen [182]. At PEG-1000 concentrations below 10 wt%, although the initial solution is homophase, two liquid phases appear within the UFLMP during the course of the freezing/frozen-storage stage due to the freeze-induced concentrating effect. NMR studies show that these are PVA-rich and PEG-rich phases [151, 189]. Cryotropic gelation of the PVA-rich phase fixes the morphology of the complex system containing segregated phases. Thus, the PEG-rich phase acts as the auxiliary porogen causing the forma-tion of so-called "compartments" [189], i.e., the large pores in addition to the ice-templated pores.

Table 3 Data from morphometric analysis of images of thin sections of PVA cryogels formed without and with salt additives

Alkali metal chloride	Salt concentration in the initial solution (M)	Morphometric data	
		Fraction of macropores (%)	Average size of macropores (μm)
–	0	57.7	5.62
LiCl	0.3	61.6	4.73
	0.6	63.8	3.02
	0.9	53.8	2.74
	1.2	46.9	2.51
NaCl	0.3	42.0	2.40
	0.6	55.4	2.32
	0.9	76.6	2.14
	1.2	48.6	2.11
KCl	0.3	50.1	2.77
	0.6	57.6	3.03
	0.9	64.4	2.62
	1.2	52.7	2.58
CsCl	0.3	47.0	2.29
	0.6	54.4	2.79
	0.9	52.1	2.77
	1.2	55.1	2.81

From [177] with permission from Springer

Another type of auxiliary extractable porogen is gum arabic (GuAr), which was used for the preparation of PVA cryogels from the above-mentioned two-phase ternary system, namely from the "water–PVA–GuAr" system. This system contains the gel-forming PVA and the water-soluble GuAr, whose aqueous solutions per se are not transformed into cryogels after freezing–frozen storage–thawing stages. The cryotropic gelation of such feeds at various PVA/GuAr ratios and concentrations, as well as the properties of the resulting gel matrices were explored in detail in the study [180]. The micrographs in Fig. 21 demonstrate the hierarchy of the macropores in such cryogels. Here, the morphology of the cryogel samples is given at four different magnifications. The dark areas in the pictures are the PVA-based gel phase stained with Congo Red, while the clear areas are the pores of various shape and size. The gross through-hole pores with a cross-section of the order of 1 mm can be observed, even in the survey photograph of a whole 2-mm-thick disc (Fig. 21a). These capillary-sized pores are also seen in an optical microscope at a low magnification (Fig. 21b). At a fivefold higher resolution (Fig. 21c), one can distinguish a high porous morphology of the gel matter, which is the continuous phase in this spongy heterogeneous material, where the roundish pores are also observed. The micrograph in Fig. 21d of the thin section illustrates the structure of space between the gross pores. Here, at least two kinds of pores are distinguished within these gel matrices, namely the "larger" roundish pores of 10–70 μm in diameter (some of which are somewhat deformed) and the "smaller" pores, also rounded, of ~1–5 μm in diameter. Hence, these micrographs
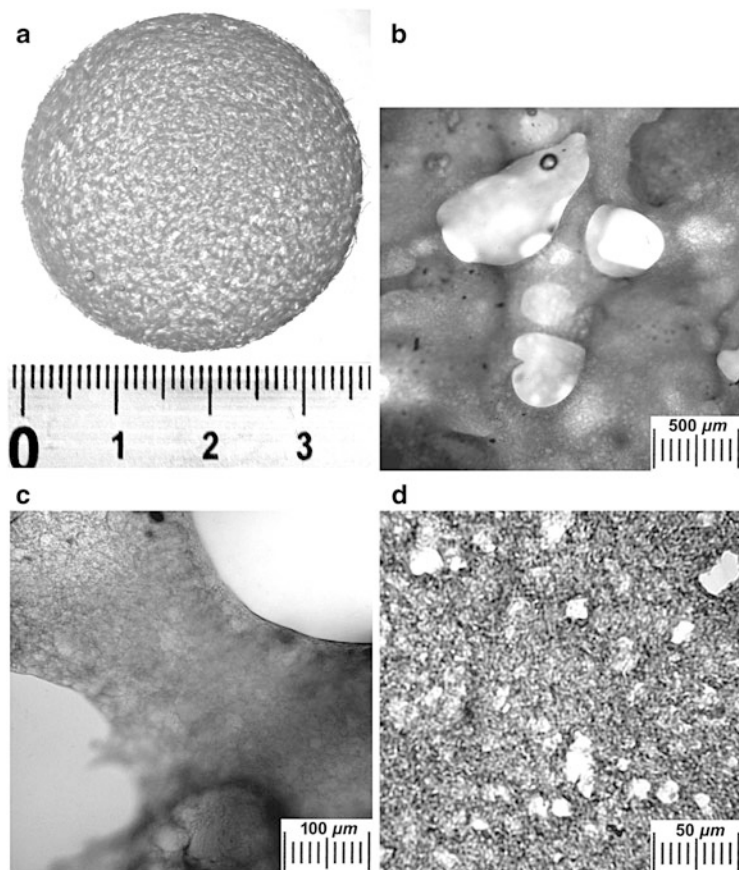
Fig. 21 Porous morphology of wide-pore PVA cryogels prepared using the feed system water–PVA–GuAr. (**a**) Photograph of 2-mm-thick disc stained with Congo Red. (**b**, **c**) Survey micrographs of the same disc obtained with an optical microscope at two different magnifications. (**d**) The image of a thin section of the disc. (From [180] with permission from RCS)

testify to the definite hierarchy in the porous morphology of such polymeric gels prepared by combining the processes of liquid–liquid phase separation and cryotropic gelation.

Note that the fine microstructure of such gel systems is provided by the light microscopy of their thin sections, a technique successfully employed for the analysis of various PVA cryogels, including conventional, complex, and composite gels [44, 48, 133, 150, 177, 190]. This technique is important because it allows visualization of the intact morphology of water-swollen PVA cryogels, whereas, for instance, SEM analysis allows the observation of either dried or frozen (cryo-SEM) samples that are not intact.

The hierarchical pore system of the cryogels under discussion is manifested in the presence of several kinds of macropores that differ significantly in their size.

Whereas the largest capillary pores are interconnected and, therefore, liquids can easily leak through blocks of such wide-pore cryogels (Fig. 21a, b), the rounded pores of other kinds are closed (Fig. 21c, d). The former are replicas of the continuous GuAr-rich phase in the two-phase system formed as a result of liquid–liquid separation. The heterogeneous morphology of such a system is fixed by the cryotropic gelation of the PVA-rich phase. Since the cross-section of pores in conventional PVA cryogels generated by the ice polycrystals does not usually exceed 1–3 μm [92, 95, 126, 150, 165, 166, 177, 191], it is evident that the 10–70-μm pores (Fig. 21b, d) are also replicas of the non-gelling GuAr-rich phase, but in this case dispersed as liquid droplets in the bulk PVA-rich phase. Moreover, the smallest pores visible in the light microscopy image of Fig. 21d are, most probably, left in the gel matter by the ice particles after thawing. The pores of the latter type have a rounded shape, whereas those observed in the "conventional" PVA cryogels prepared under the same conditions but without foreign polymeric additives are usually anisodiametric (prolate) in their shape (see Figs. 5, 6, and 18). We have to mention that the round-shaped ice-derived pores in PVA cryogels are also inherent in the gel matrices prepared with the addition of surfactants as pore modifiers, which are capable of influencing the shape of the ice crystals by decreasing the surface tension at the solid–liquid interface during crystal growth [192]. Thus, such "rounding" of the pores inside the gel phase of wide-pore cryogels fabricated from the water–PVA–GuAr feeds are probably due to the surfactant properties of GuAr macromolecules present in a small amount in the initial PVA-rich phase.

The last type of auxiliary pore-forming agents that will be considered here are the gaseous porogens. These agents are constantly being entrapped in the cryogel matrix and perform as the pores per se. Examples of such porogens are small gas bubbles, and the resulting gas-filled cryogels can be termed "foamed cryogels." Inside the foamed freeze–thaw gels, two sorts of macropores can be distinguished: the cryogenically induced macropores, i.e., those derived from the thawed solvent polycrystals, and the closed microbubbles remaining entrapped in the cryogel after defrosting of the frozen foam. Such gas-filled gel materials, PVA-based gels in particular, have been prepared, studied, and some promising instances of their practical application have been reported [192–197]. In these works, the gaseous porogen was generated either using physical methods, e.g., whipping, barbotage, microfluidic foaming techniques [192–194, 197], or via the chemical liberation of gas products, e.g., by the reaction of ammonium chloride with sodium nitrite ($NH_4Cl + NaNO_2 \rightarrow NaCl + 2H_2O + N_2\uparrow$), that were introduced into the feed prior to its freezing [196].

For instance, foamed cryogels were fabricated by mechanical whipping of aqueous PVA solutions followed by freezing of the resulting foams, storing the samples frozen, and then slowly defrosting [193]. The peculiarities of the porous morphology of such gel foamed matrices are illustrated by the microphotographs in Fig. 22a, b, which show thin sections of the samples prepared by cryostructuring of the PVA-based liquid foam. These foamed cryogels possess two sorts of pores distinguishable by optical light microscopy. The first type are the gross round pores of ~50 to ~250 μm in diameter formed by the auxiliary pore-forming agent, i.e., by
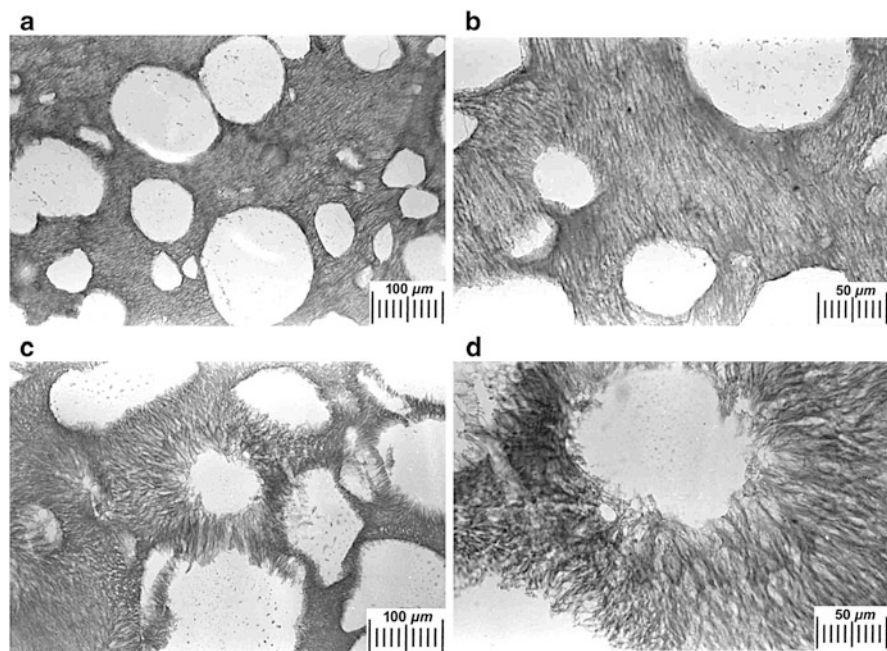
Fig. 22 Optical micrographs at two different magnifications of thin sections of foamed PVA cryogels prepared from the fluid foam produced by whipping of aqueous polymer solutions in the (**a**, **b**) absence and (**c**, **d**) presence of the surfactant CTAB at a concentration of 0.415 mM. Initial polymer concentration was 120 g/L. Cryotropic gelation conditions: freezing temperature −20 °C; freezing duration 18 h, thawing rate 0.03 °C/min. (From [192] with permission from Springer)

the air bubbles. The second type are smaller prolate pores with a cross-section of around 1–3 μm within the gel phase in the space between the bubbles. The pores of the latter type are typical of cryogenically induced pores in conventional PVA cryogels (e.g., see Figs. 5 and 6), and these pores are filled with water rather than gas. The microbubble-type pores generated by simple whipping or by the barbotage of a gas through a porous filter to the initial polymer solution have a wide size distribution. In this respect, a recently developed microfluidic foaming technique is attractive because it allows a rather narrow, practically monodisperse distribution of pore dimensions [197]. The air bubbles entrapped in the PVA cryogel matrix decrease its density down to values smaller than that of water, thus imparting buoyancy to such cryogels, i.e., foamed cryogels can float in water for a long time and do not sink [193].

The impact of surfactant additives on the porous structure of foamed cryogels is of special interest. Fig. 22c, d shows the micrographs, at two different magnifications, of thin sections of foamed PVA cryogels stained with Congo Red. The gel samples were prepared by whipping of an aqueous PVA solution having the same initial polymer concentration as the sample shown in Fig. 22a, b, but it additionally contained dissolved surfactant, cetyltrimethylammonium bromide (CTAB). Even

at a small concentration of CTAB (e.g., 0.415 mM), the microstructure of the cryogel undergoes very significant changes [192]. The cross-section of the ice-templated pores is enlarged from 1–3 µm (Fig. 22b) to 4–5 µm (Fig. 22d) due to the presence of the ionic surfactant. Simultaneously, the morphology of the gel–gas interfaces also changes drastically. Although the surface of these interfaces in surfactant-free foamed cryogel is almost smooth (Fig. 22a, b), the presence of CTAB causes pronounced ulceration of the surface (Fig. 22c, d). A similar effect was also observed using sodium dodecyl sulfate as an anionic surfactant additive [192]. Thus, the presence of surfactants significantly affects the shape of the gaseous macropores. It is evident that bubbles with such a pitted surface cannot exist in the initial liquid foam, since such foam would be absolutely unstable. Therefore, this unusual morphology of the gas–gel interfaces appears to be due to the decreased surface tension between the liquid–gas interfaces and the growing facets of ice crystals, which can evidently pierce the air bubbles. However, the freezing solidification of the foam and consequent formation of cryogel in the bubble walls prevent the complete destruction of the bubbles, thus "imprinting" a certain intermediate structure of the boundary layers. Hence, surfactants similar to CTAB in terms of their influence on the foams can be considered as auxiliary modifiers of the architecture of gaseous pores within the foamed cryogels.

The results presented here thus show that there are very broad possibilities for affecting the macroporosity parameters in diverse cryogels and to govern, within certain limits, the architecture and size of the pores templated by the solvent crystals. In addition, there are many possibilities for creating multifarious additional macropores in these gel matrices by using auxiliary porogens. In each particular case, the approach employed depends on the purpose of the produced cryogel and on the set of material properties required for its efficient application.

4 Conclusions

Finalizing the overview of the literature related to the general aspects of cryotropic gelation processes, the following basic conclusions can be drawn [7–9, 105, 107, 111, 114, 148]:

1. Cryotropic gel formation is a liquid-phase process occurring in the unfrozen liquid microphase of a macroscopically frozen system.
2. The final products of such cryostructuring are macroporous, sometimes wide-pore sponge-like, gel matrices, i.e., cryogels.
3. Due to concentrating of solutes in the unfrozen liquid microphase, an apparent decrease in the critical concentration of gelation is observed in cryotropic gel formation as compared to gelation at positive temperatures
4. Acceleration of the gel formation is usually observed in the moderately frozen systems over a definite range of negative temperatures. The key reason for such

an acceleration is also the increased concentration of gel precursors in the unfrozen liquid microphase compared with their concentration in the initial feed.

5. A bell-like dependence of the gelation efficiency on the process temperature is inherent in cryotropic gel formation.

6. The properties and macroporous morphology of cryogels are controlled by the gelation temperature, solvent used, concentration of the gelling compounds, the presence of other solutes, freezing and thawing rates, freezing mode, duration of the frozen storage, and some other factors.

Finally, polymeric cryogels have a wide range of applications; this statement is confirmed by the majority of recent experimental papers and reviews relating to the implementation of cryogel-type materials in various applied areas (e.g., see reviews [152, 163, 164, 198–203] published in 2013). Certain important aspects related to the application of various cryogels are also considered in the subsequent chapters of the present volume.

References

1. Lozinsky VI (2014) A brief history of polymeric cryogels. In: Okay O (ed) Polymeric cryogels: macroporous gels with remarkable properties. Advances in Polymer Science, vol 263. Springer, Heidelberg
2. Papkov SP (1974) Gel-like state of polymers. Khimiya, Moscow, in Russian
3. Kudela V (1987) Encyclopedia of polymer science and engineering, vol. 7. Wiley, New York, p 783
4. Tanaka T (1987) In: Nicolini C (ed) Structure and dynamics of biopolymers. Dordrecht: M. Nijhoff, p 237
5. Rogovina LZ, Vasil'ev VG, Braudo EE (2008) Polym Sci 50C:85
6. Nishinari K (2009) Prog Colloid Polym Sci 136:87
7. Lozinsky VI (1994) DSc Thesis, Institute of Organoelement Compounds, Russian Academy of Sciences. Moscow, in Russian
8. Lozinsky VI (2002) Russ Chem Revs 71:489
9. Lozinsky VI, Plieva FM, Galaev IY, Mattiasson B (2001) Bioseparation 10:163
10. Nikonorov VV, Ivanov RV, Kil'deeva NR, Bulatnikova LN, Lozinsky VI (2010) Polym Sci 52A:828
11. Lozinsky VI, Vainerman ES, Rogozhin SV (1982) SU Patent 1,008,214
12. Rogozhin SV, Lozinsky VI, Vainerman ES, Domotenko LV, Mamtsis AM, Ivanova SA, Shtil'man MI, Korshak VV (1984) Doklady Akademii nauk SSSR 278:129–133, in Russian
13. Labudzińska A, Ziabicki A (1971) Koll Z u Z Polym 243:21
14. Schulze WE, Yu DT, MacMaters MM (1964) Stärke 16:41
15. Schierbaum F, Richter M (1964) Nahrung 8:487, in German
16. Blažek L, Dvoržak E, Myšik S (1964) Koll Zhurn 26:657, in Russian
17. Neiman RE (1967) Coagulation of synthetic latexes. Voronezh State University, Voronezh, pp 148–159, in Russian

18. Jellinek HHG, Fok SY (1967) Makromol Chem 104:18
19. Lozinsky VI, Korneeva MN, Vainerman ES, Rogozhin SV (1983) Doklady Akademii nauk SSSR 270:101, in Russian
20. Lozinsky VI, Vainerman ES, Titova EF, Belavtseva EM, Rogozhin SV (1984) Colloid Polym Sci 262:769
21. Belavtseva EM, Titova EF, Lozinsky VI, Vainerman ES, Rogozhin SV (1984) Colloid Polym Sci 262:775–779
22. Lozinsky VI, Vainerman ES, Ivanova SA, Titova EF, Shtil'man MI, Belavtseva EM, Rogozhin SV (1986) Acta Polym 37:142
23. Lozinsky VI, Morozova SA, Vainerman ES, Titova EF, Shtil'man MI, Belavtseva EM, Rogozhin SV (1989) Acta Polym 40:8
24. Ozmen MM, Okay O (2008) React Funct Polym 68:1467
25. Ozmen MM, Dinu MV, Okay O (2008) Polym Bull 60:169
26. Lozinsky VI, Vainerman ES, Rogozhin SV (1982) Colloid Polym Sci 260:776
27. Lozinsky VI, Vainerman ES, Korotaeva GF, Rogozhin SV (1984) Colloid Polym Sci 262:617
28. Lozinsky VI, Golovina TO, Gusev DG (2000) Polymer 41:35
29. Ivanov RV, Lozinsky VI, Noh SK, Han SS, Lyoo WS (2007) J Appl Polym Sci 106:1470
30. Tuncaboylu DC, Okay O (2009) Eur Polym J 45:2033
31. Orakdogen N, Karacan P, Okay O (2011) React Funct Polym 71:782
32. Nikonorov VV, Ivanov RV, Kil'deeva NR, Lozinsky VI (2011) Polym Sci 53A:1150
33. Bloch K, Lozinsky VI, Galaev IY, Yavriyanz K, Vorobeychik M, Azarov D, Damshkaln LG, Mattiasson D, Vardi P (2005) J Biomed Mater Res 75A:802
34. Lozinsky VI, Damshkaln LG, Bloch KO, Vardi P, Grinberg NV, Burova TV, Grinberg VY (2008) J Appl Polym Sci 108:3046
35. Flink JM, Johansen A (1985) Biotechnol Lett 7(10):765
36. Johansen A, Flink JM (1986) Biotechnol Lett 8(2):121
37. Vainerman ES, Lozinsky VI, Rogozhin SV, Raskina LP, Shapiro LA, Yakubovich VS, Bronshtein VY (1983) SU Patent 1:171,474
38. Vainerman ES, Lozinsky VI, Rogozhin SV, Raskina LP, Shapiro LA, Yakubovich VS, Shenker MB, Komissarova AL, Potapov VD, Gudochkova VM, Atyasova NM, Ivanova GA (1983) SU Patent 1,171,476
39. Zhang H, Cooper AI (2007) Adv Mater 19:1529
40. Gutiérrez MC, Ferrer ML, del Monte F (2008) Chem Mater 20:634
41. Franks F (1981) In: Morris GJ, Clarke A (eds) Effects of low temperatures on biological membranes. Academic, New York 3
42. Luyet BJ (1966) In: Meryman HT (ed) Cryobiology. Academic, New York, 115
43. Libbrecht KG (2005) Rep Prog Phys 68:855
44. Lozinsky VI, Damshkaln LG, Shaskol'skii BL, Babushkina TA, Kurochkin IN, Kurochkin II (2007) Colloid J 69:747
45. Tuncaboylu DC, Okay O (2010) Langmuir 26:7574
46. Ak F, Oztoprak Z, Karakutuk I, Okay O (2013) Biomacromolecules 14:719
47. Okay O, Lozinsky VI (2014) Synthesis and structure–property relationships of cryogels. In: Okay O (ed) Polymeric cryogels: macroporous gels with remarkable properties. Advances in polymer science, vol 263. Springer, Heidelberg
48. Lozinsky VI, Damshkaln LG, Kurochkin IN, Kurochkin II (2012) Colloid J 74:319
49. Ivanov RV, Lozinsky VI (2006) Polym Sci 48A:1232
50. Gusev DG, Lozinsky VI, Bakhmutov VI (1993) Eur Polym J 29:49
51. Vonnegut B, Chessin H (1971) Science 174:945
52. Kirsebom H, Rata G, Topgaard D, Mattiasson B, Galaev IY (2008) Polymer 49:3855
53. Zheng L, Sun DW (2006) Trends Food Sci Technol 17:16
54. Sergeev GB, Batyuk VA, Stepanov MB, Sergeev BM (1973) Doklady Akademii nauk SSSR 213:891, in Russian
55. Grant NH, Clark DE, Alburn HE (1961) J Am Chem Soc 83:4476

56. Grant NH, Clark DE, Alburn HE (1962) J Am Chem Soc 84:876
57. Butler AR, Bruice TC (1964) J Am Chem Soc 86:313
58. Bruice TC, Butler AR (1964) J Am Chem Soc 86:4104
59. Pincock RE, Kiovsky TE (1965) J Am Chem Soc 87:2072
60. Grant NH, Clark DE, Alburn HE (1966) J Am Chem Soc 88:4071
61. Pincock RE, Kiovsky TE (1966) J Chem Educ 43:358
62. Pincock RE (1969) Acc Chem Res 2:97
63. Sergeev GB, Batyuk VA (1976) Russ Chem Rev 45:391
64. Batyuk VA (1987) The chemistry of low temperatures and cryochemical technology. Moscow State University, Moscow, p 163, in Russian
65. Ivanov RV, Babushkina TA, Lozinsky VI (2005) Polymer Sci 47A:791
66. Kuntz ID (1971) J Am Chem Soc 93:514
67. Kvlividze VI, Pylova MB (1977) Kolloidn zhurn 39:1167, in Russian
68. Katayama S, Fujiwara S (1980) J Phys Chem 84:2320
69. Suzuki E, Nagashima N (1982) Bull Chem Soc Jpn 55:2730
70. Ogino K, Sato H (1995) J Polym Sci Polym Phys 33:445
71. Masuda K, Horii F (1998) Macromolecules 31:5810
72. Martin DR, Ablett S, Darke A, Sutton RL, Sahagian M (1999) J Food Sci 64:46
73. Mil' EM, Kovarskii AL, Vasserman AM (1973) Izv AN SSSR Ser khim 10:2211, in Russian
74. Mikhalev OI, Yakovleva IV, Trofimov VI, Shapiro AB (1985) Cryo Lett 6:245
75. Mikhalev OI, Karpov IN, Kazarova EB, Alfimov MV (1989) Chem Phys Lett 164:96
76. Mikhalev OI, Serpinski M, Lozinsky VI, Kapanin PV, Chkeidze II, Alfimov MV (1991) Cryo Lett 12:197
77. Smith P, Pennings AJ (1974) Polymer 15:413
78. Gusev DG, Lozinsky VI, Vainerman ES, Bakhmutov VI (1990) Magn Reson Chem 28:651
79. Ricciardi R, Auriemma F, Gaillet C, De Rosa C, Lauprêtre F (2004) Macromolecules 37:9510
80. Kaetsu I (1993) Adv Polym Sci 105:81
81. Zhang XZ, Zhuo RX (1999) Macromol Rapid Commun 20:229
82. Kumakura M (2001) Polym Adv Technol 12:415
83. Yao K, Shen S, Yun J, Wang L, He X, Yu X (2006) Chem Eng Sci 61:6701
84. Plieva FM, Galaev IY, Mattiasson B (2007) J Sep Sci 30:1657
85. Reichelt S, Abe C, Hainich S, Knolle W, Decker U, Prager A, Konieczny R (2013) Soft Matter 9:2484
86. Lozinsky VI, Golovina TO, Vainerman ES, Rogozhin SV (1989) Polym Sci USSR 31A:367
87. Petrov P, Petrova E, Tchorbanov B, Tsvetanov CB, Reiss G (2007) Polymer 48:4943
88. Liu X, Hu Y, Zou J, Chai, Li B (2013) Appl Mech Mater 295–298:1368
89. Watase M, Nishinari K, Nambu M (1983) Polym Commun 24:52
90. Watase M, Nishinari K (1983) Polym Commun 24:270
91. Watase M, Nishinari K, Ogino K, Nambu M (1983) Polym Commun 24:345
92. Lozinsky VI, Vainerman ES, Domotenko LV, Mamtsis AM, Titova EF, Belavtseva EM, Rogozhin SV (1986) Colloid Polym Sci 264:19
93. Domotenko LV, Lozinsky VI, Vainerman ES, Rogozhin SV (1988) Polym Sci USSR 30A:1758
94. Lozinsky VI, Domotenko LV, Vainerman ES, Rogozhin SV (1989) Polym Sci USSR 31A:1983
95. Lozinsky VI, Vainerman ES, Domotenko LV, Blumenfel'd AL, Rogov VV, Barkovskaya EN, Fedin EI, Rogozhin SV (1989) Colloid J USSR 51:592
96. Konstantinova NR, Lozinsky VI (1997) Food Hydrocolloids 11:113
97. Damshkaln LG, Simenel IA, Lozinsky VI (1999) J Appl Polym Sci 74:1978
98. Lozinsky VI, Damshkaln LG, Brown CRT, Norton IT (2000) J Appl Polym Sci 75:1740
99. Lozinsky VI, Damshkaln LG (2000) J Appl Polym Sci 77:2017
100. Lozinsky VI, Damshkaln IG, Brown R, Norton IT (2000) Polym Int 49:1434
101. Lozinsky VI, Damshkaln LG, Brown CRT, Norton IT (2002) J Appl Polym Sci 83:1658

102. Zeira A, Nussinovich A (2004) J Texture Stud 34:561
103. Elowsson L, Kirsebom H, Carmignac V, Durbeej M, Mattiasson B (2012) J Mater Sci Mater Med 23:2489
104. Lozinsky VI, Ivanov RV, Kalinina EV, Timofeeva GI, Khokhlov AR (2001) Macromol Rapid Commun 22:1441
105. Lozinsky VI, Ivanov RV (2003) In: Monakov YB (ed) Synthesis and modification of polymers. Khimiya, Moscow, p 68, in Russian
106. Zaborina OE, Buzin MI, Lozinsky VI (2012) Polym Sci 54B:354
107. Lozinsky VI, Galaev IY, Plieva FM, Savina IN, Jungvid H, Mattiasson B (2003) Trends Biotechnol 21:445
108. Ferrero C, Martino MN, Zaritzky NE (1993) Int J Food Sci Technol 17:191
109. Lozinsky VI, Damshkaln LG, Brown R, Norton IT (2000) J Appl Polym Sci 78:371
110. Hyon SH, Cha WI, Ikada Y (1989) Kobunshi Ronbunshu 46:673, in Japanese
111. Lozinsky VI (1998) Russ Chem Rev 67:573
112. Lozinsky VI, Plieva FM (1998) Enzyme Microb Technol 23:227
113. Lozinsky VI, Zubov AL, Savina IN, Plieva FM (2000) J Appl Polym Sci 77:1822
114. Lozinsky VI (2008) Russ Chem Bull 57:1015
115. Tanaka R, Hatakeyama T, Hatakeyama H (1998) Polym Int 45:118
116. Matusevich LN (1968) Crystallization from solutions in chemical industry. Khimiya, Moscow, p 304, in Russian
117. Hassan CM, Ward JH, Peppas NA (2000) Polymer 41:6729
118. Ricciardi R, Gaillet C, Ducouret G, Lafuma F, Laupretre F (2003) Polymer 44:3375
119. Ricciardi R, Auriemma F, Rosa CD, Laupretre F (2004) Macromolecules 37:1921
120. Valentín JL, López D, Hernández R, Mijangos C, Saalwächter K (2009) Macromolecules 42:263
121. Watase M, Nishinari K, Nambu M (1983) Cryo Lett 4:197
122. Watase M (1983) Nippon Kagaku Kaisi 7:973, in Japanese
123. Nagura M, Nagura M, Ishikawa H (1984) Polym Commun 25:313
124. Watase M, Nishinari K (1985) Makromol Chem 186:1081
125. Watase M, Nishinari K (1985) J Polym Sci Polym Phys 23:1803
126. Yokoyama F, Masada I, Shimamura K, Ikawa T, Monobe K (1986) Colloid Polym Sci 264:595
127. Nambu M (1990) Kobunshi Ronbunshu 47:695, in Japanese
128. Urushizaki F, Yamaguchi H, Nakamura K, Namajiri S, Sugibayashi K, Morimoto Y (1990) Int J Pharm 58:135
129. Peppas NA, Stauffer SR (1991) J Control Release 16:305
130. Hassan CM, Peppas NA (2000) Adv Polym Sci 153:37
131. Wan WK, Campbell G, Zhang ZF, Hui AJ, Boughner DR (2002) J Biomed Mater Res 63:854
132. Sweeszkowski W, Ku DN, Bersee HEN, Kurzcydlowski KJ (2006) Biomaterials 27:1536
133. Lozinsky VI, Damshkaln LG, Kurochkin IN, Kurochkin II (2008) Colloid J 70:189
134. Roberts JD, Caserio MC (1977) Basic principles of organic chemistry, 2nd edn. W.A. Benjamin, Menlo Park
135. Horkay F, Nagy M (1981) Acta Chim Acad Sci Hung 107:321
136. Peppas NA (1987) In: Peppas NA (ed) Hydrogels in biology and medicine II. CRC, Boca Raton, p 1
137. Davis BJ (1964) Ann NY Acad Sci 121:404
138. Sun K, Sehon AH (1965) Can J Chem 43:969
139. Righetti PG, Brost BSW, Snyder RS (1981) J Biochem Biophys Methods 4:347
140. Maier H, Anderson M, Karl C, Magnuson K, Whistler RL (1993) In: Whistler RL, BeMiller JN (eds) Industrial gums. Academic, San Diego, p 181
141. Richardson PH, Clark AH, Russell AL, Aymard P, Norton IT (1999) Macromolecules 32:1519
142. Dea ICM, Morris ER, Rees DA, Welsh J, Barnes HA, Price J (1977) Carbohydr Res 57:249

143. Dea ICM (1987) In: Yalpani M (ed) Industrial polysaccharides: genetic engineering, structure/property relations and applications. Elsevier, Amsterdam, p 207
144. Bringham JE, Gidley MJ, Hoffmann RA, Smith CG (1994) Food Hydrocolloid 8:331
145. Lazaridou A, Biliaderis CG, Izydorczyk MS (2003) Food Hydrocolloid 17:693
146. Lazaridou A, Biliaderis CG (2004) Food Hydrocolloid 18:933
147. Richter M, Augustat S, Schierbaum F (1969) Ausgewahlte Metoden Der Starkechemie. VEB Fachbuchverlag, Leipzig, in German
148. Lozinsky VI, Vakula AV, Zubov AL (1992) Soviet Biotechnol #4:1
149. Gutiérrez MC, Aranaz I, Ferrer ML, del Monto F (2010) Production and properties of poly (vinyl alcohol) cryogels: recent developments. In: Mattiasson B, Kumar A, Galaev I (eds) Macroporous polymers: production, properties and biological/biomedical applications. CRC, Boca Raton, p 83
150. Alves MH, Jensen BEB, Smith AAA, Zelikin AN (2011) Macromol Biosci 11:1293
151. Shapiro YE (2011) Prog Polym Sci 36:1184
152. Gun'ko VM, Savina IN, Mikhalovsky SV (2013) Adv Colloid Interface Sci 186/187:1
153. Vainerman ES, Lozinsky VI, Rogozhin SV (1981) Colloid Polym Sci 259:1198–1201
154. Lozinsky VI, Golovina TO, Vainerman ES, Rogozin SV (1989) Polym Sci USSR 31A:367
155. Ivanov RV, Lozinsky VI, Noh SK, Lee YR, Han SS, Lyoo WS (2008) J Appl Polym Sci 107:382
156. Dainiak MB, Galaev IY, Kumar A, Plieva FM, Mattiasson B (2007) Adv Biochem Eng Biotechnol 106:101
157. Plieva FM, Galaev IY, Noppe W, Mattiasson B (2008) Trends Microbiol 16:543
158. Kumar A, Mishra R, Reinwald Y, Bhat S (2010) Mater Today 13:42
159. Okay O (2010) Production of macroporous polymeric materials by phase separation polymerization. In: Mattiasson B, Kumar A, Galaev I (eds) Macroporous polymers: production, properties and biological/biomedical applications. CRC, Boca Raton, p 3
160. Plieva FM, Galaev IY, Mattiasson B (2010) Production and properties of cryogels by radical polymerization. In: Mattiasson B, Kumar A, Galaev I (eds) Macroporous polymers: production, properties and biological/biomedical applications. CRC, Boca Raton, p 23
161. Kirsebom H, Mattiasson B (2011) Polym Chem 2:1059
162. Plieva FM, Kirsebom H, Mattiasson B (2011) J Sep Sci 34:2164
163. Henderson TMA, Ladewig K, Haylock DN, McLean KM, O'Connor AJ (2013) J Mater Chem B 1:2682
164. Zhang H, Zhang F, Wu J (2013) React Funct Polym 73:923
165. Trieu HH, Qutubuddin S (1995) Polymer 36:2531
166. Willcox PJ, Howie DW, Schmidt-Rohr K, Hoagland DA, Gido S, Pudjijanto S, Kleiner LW, Venkatraman S (1999) J Polym Sci Polym Phys 37:3438
167. Franks F (ed) (1982) Water and aqueous solutions at subzero temperatures. New York, Plenum
168. Regand A, Goff HD (2003) Food Hydrocolloid 17:95
169. Libbrecht KG (2005) Reports Prog Phys 68:855
170. Ward MA, Georgiu TK (2011) Polymers 3:1215
171. Doring A, Birnbaum W, Kuckling D (2013) Chem Soc Rev 42:7391
172. Lozinsky VI, Kalinina EV, Grinberg VY, Grinberg NV, Chupov VA, Platé NA (1997) Polym Sci 39A:1300
173. Zhang XZ, Zhuo RX (1999) Macromol Chem Phys 200:2602
174. Komarova GA, Starodubtsev SG, Lozinsky VI, Kalinina EV, Landfester K, Khokhlov AR (2008) Langmuir 24:4467
175. Komarova GA, Starodubtsev SG, Lozinsky VI, Nasimova IR, Khokhlov AR (2013) J Appl Polym Sci 127:2703
176. Komarova GA, Starodubtsev SG, Khokhlov AR (2013) Polym Sci 55A:415
177. Lozinsky VI, Sakhno NG, Damshkaln LG, Bakeeva IV, Zubov VP, Kurochkin IN, Kurochkin II (2011) Colloid J 73:234

178. Finnegan WG, Pitter RL (1997) J Colloid Interface Sci 189:322
179. Wang S, Amornwittawat N, Banatlao J, Chung M, Kao Y, Wen X (2009) J Phys Chem 113B:13891
180. Lozinsky VI, Damshkaln LG, Ezernitskaya MG, Glotova YK, Antonov YA (2012) Soft Matter 8:8493
181. Suzuki M, Hirasa O (1993) Adv Polym Sci 110:241
182. Lozinsky VI, Solodova EV, Zubov AL, Simenel IA (1995) J Appl Polym Sci 58:171
183. Cascone MG, Maltini S, Barbani, Laus M (1999) J Mater Sci Mater Med 10:431
184. Cascone MG, Barbani N, Maltini S, Lazzeri L (2001) Polym Int 50:1241
185. Bajpai A, Saini R (2005) Polym Int 54:796
186. Mathews DT, Birney YA, Cahill PA, McGuinness CB (2008) J Appl Polym Sci 109:1129
187. Bajpai A, Saini R (2009) J Mater Sci Mater Med 20:2063
188. Albertsson PA (1971) Partition of cell particles and macromolecules, 2nd edn. Wiley-Interscience, New York
189. Shapiro YE, Shapiro TI (1999) J Colloid Interface Sci 217:322
190. Savina IN, Lozinsky VI (2004) Colloid J 66:343
191. Trieu HH, Qutubuddin S (1964) Colloid Polym Sci 272:301
192. Lozinsky VI, Damshkaln LG, Kurochkin IN, Kurochkin II (2005) Colloid J 67:589
193. Lozinsky VI, Damshkaln LG (2001) J Appl Polym Sci 82:1609
194. Altunina LK, Manzhai BN, Fufaeva MS (2006) Russ J Appl Chem 79:1669
195. Altunina LK, Kuvshinov VA, Dolgikh SN (2006) In: Lombardi S, Altunina LK, Beaubien SE (eds) Advances in the geological storage of carbon dioxide. NATO Science Series IV: earth and environmental sciences, vol. 65. Springer, Netherlands, p.103
196. Altunina LK, Manzhai BN, Stas'eva LA, Fufaeva MS (2007) Russ J Appl Chem 80:1647
197. Colosi C, Costantini M, Barbetta A, Pecci R, Bedini R, Dentini M (2013) Langmuir 29:82
198. Iatridis JC, Nicoll SB, Michalek AJ, Walter BA, Gupta MS (2013) Spine J 13:243
199. Barroso T, Hussain A, Roque ACA, Aguiar-Ricardo A (2013) Biotechnol J 8:671
200. Pfaunmiller EL, Paulemond ML, Dupper CM, Hage DS (2013) Anal Bioanal Chem 405:2133
201. Sheldon RA, van Pelt S (2013) Chem Soc Rev 42:6223
202. Kharkar PM, Kiick KL, Kloxin AM (2013) Chem Soc Rev 42:7335
203. Tanthapanichakoon W, Tamon H, Nakasawa K, Charinpanitkul T (2013) Eng J 17:1

Synthesis and Structure–Property Relationships of Cryogels

Oguz Okay and Vladimir I. Lozinsky

Contents

O. Okay (✉)
Department of Chemistry, Istanbul Technical University, 34469 Istanbul, Turkey
e-mail: okayo@itu.edu.tr

V.I. Lozinsky
Laboratory for Cryochemistry of (Bio)Polymers, A.N. Nesmeyanov Institute of
Organoelement Compounds, Russian Academy of Sciences, Vavilov Street 28, 119991
Moscow, Russian Federation
e-mail: loz@ineos.ac.ru

Abstract Polymeric gels belong to the most important class of functional polymers in modern biotechnology. They are useful materials for drug delivery systems, artificial organs, separation operations in biotechnology, processing of agricultural products, on–off switches, sensors, and actuators. Despite this fact and considerable research in this field, the design and control of gel-based devices still present some problems due to the their poor mechanical performance and slow rate of response to external stimuli. Cryogelation techniques discovered more than 30 years ago overcome these limitations by producing macroporous gels with high toughness and superfast responsivity. This chapter discusses how and why the properties of gels significantly alter upon transition from homogeneous gelation to a cryogelation regime. The formation and structure–property relationships of cryogels starting from monovinyl–divinyl monomers, as well as from linear polymer chains, are reviewed using examples from the recent literature. Some novel cryogels with a wide range of tunable properties and their applications are also presented in detail. These include DNA cryogels for the removal of carcinogens from aqueous environments, silk fibroin cryogels as mechanically strong scaffolds for bone tissue engineering applications, poly(acrylic acid) cryogels as self-oscillation systems, and rubber cryogels as reusable oil sorbent for the removal of oil spill from seawater.

Keywords Cryogels • Porosity formation • Gelation • Elasticity • Swelling

Abbreviations

α	Dissociation degree
χ	Polymer–solvent interaction parameter
λ	Deformation ratio
ν_e	Effective crosslink density
σ	Nominal stress
σ_{comp}	Compressive stress
σ_p	Critical stress corresponding to the plateau regime
AAc	Acrylic acid
AAm	Acrylamide
AMPS	2-Acrylamido-2-methylpropane sulfonic acid sodium salt
APS	Ammonium persulfate
BAAm	*N,N*-methylene(bis)acrylamide
BDDE	1,4-Butanediol diglycidyl ether
C	Monomer concentration in the unfrozen zones
CBR	*cis*-Polybutadiene
C_o	Initial concentration of the monomeric or the polymeric precursors
C_R	Rubber concentration
C_{SF}	Fibroin concentration
DMA	*N,N*-Dimethylacrylamide

DMSO   Dimethyl sulfoxide
DNA   Deoxyribonucleic acid
E Young's modulus
EGDE   Ethylene glycol diglycidyl ether
EtBr   Ethidium bromide
f Effective charge density
G Shear modulus
HEMA   2-Hydroxyethyl methacrylate
k Reduced flow rate
m_{rel} Normalized gel mass with respect to its equilibrium swollen mass
NIPA N-Isopropylacrylamide
P Total porosity or the volume fraction of frozen solvent in the reaction
          system
PAAc   Poly(acrylic acid)
PAAm   Polyacrylamide
PAMPS   Poly(AMPS)
PDMA   Poly(DMA)
PIB   Butyl rubber, a linear polyisobutylene containing small amounts of
          internal unsaturated groups (isoprene units)
PMAAc   Poly(methacrylic acid)
PNIPA   Poly(NIPA)
P_s Swollen state porosity
PSA   Poly(SA)
PVA   Poly(vinyl alcohol)
q_v Equilibrium volume swelling ratio (with respect to dry state)
q_w Equilibrium weight swelling ratio (with respect to dry state)
SA   Sodium acrylate
SBR   Styrene-butadiene rubber
SEM   Scanning electron microscopy
TEMED N,N,N',N'-Tetramethylethylenediamine
T_{prep} Cryogelation temperature
V_1 Molar volume of solvent
V_{eq} Volume swelling ratio with respect to the after preparation state of gels
V_p Total volume of open pores

1   Introduction

Polymeric gels are crosslinked polymers swollen in a liquid. The polymer serves as
a matrix to hold the liquid together, while the liquid inside the gel allows free
diffusion of some solute molecules. Polymeric gels can be prepared from either
monomeric or polymeric precursors dissolved in a solvent. However, the most
commonly used method is the free-radical crosslinking copolymerization of a
monovinyl monomer with a divinyl monomer (crosslinker) in solution. In the

case of hydrophilic gels, called hydrogels, an ionic comonomer is also included in the monomer mixture to increase the swelling capacity in aqueous environment. The desired property of gels, such as the swelling capacity, the modulus of elasticity, and the degree of heterogeneity, is obtained by adjusting the concentration as well as the composition of the reaction constituents [1]. Ionic hydrogels swell up to 1,000 times their dry volume when in contact with water. They also exhibit drastic volume changes in response to specific external stimuli such as temperature, solvent quality, pH, electric field, etc [2]. Depending on the design of the hydrogel matrices, this volume change may occur continuously over a range of stimulus level, or discontinuously at a critical stimulus level. These properties of hydrogels and their similarities to biological systems have received considerable interest over the last three decades. Today, these soft and smart materials belong to the most important class of functional polymers in modern biotechnology [3]. They are useful materials for drug delivery systems, artificial organs, separation operations in biotechnology, processing of agricultural products, on–off switches, sensors, and actuators [1, 4].

Despite this fact and considerable research in this field, the design and control of gel-based devices still present some problems because a number of network properties are inversely coupled. For example, decreasing the degree of crosslinking of gels in order to increase their mesh size results in their accelerated degradation. Further, loosely crosslinked gels are fragile materials when handled in the swollen state; typically, they rupture at very low strains due to the lack of an efficient energy dissipation mechanism in the gel network. Moreover, the response rate of gels to external stimuli is not as fast as required in many application areas. This is due to the fact that the kinetics of the gel volume change involves absorbing or desorbing solvent by the polymer network, which is a diffusive process. This process is slow, and even slower near the critical point [5]. Hence, design of gels with a good mechanical performance together with a fast response rate is crucially important in many existing and potential application areas of soft materials.

A number of techniques for toughening of gels have recently been proposed, including double network gels [6], topological gels [7], gels formed by hydrophobic associations [8], gels made by mobile crosslinkers such as clay nanoparticles (nanocomposite hydrogels) [9], and microsphere composite hydrogels [10]. Although these techniques create energy dissipation mechanisms to slow crack propagation and, thus, improve the mechanical properties of gels, they exhibit a slow response rate to external stimuli. In order to achieve rapid changes in the gel volume, a common strategy is to create an interconnected pore structure inside the gel network [11]. For a polymer network having an interconnected pore structure, absorption or desorption of solvent occurs through the pores by convection, which is much faster than the diffusion process that dominates the nonporous polymer networks.[1] The basic technique for obtaining polymer gels with a macroporous

---

[1] In the early works, the space between the network chains in a swollen homogeneous gel was defined as "porosity" or "molecular porosity." However, this term is clearly misleading because
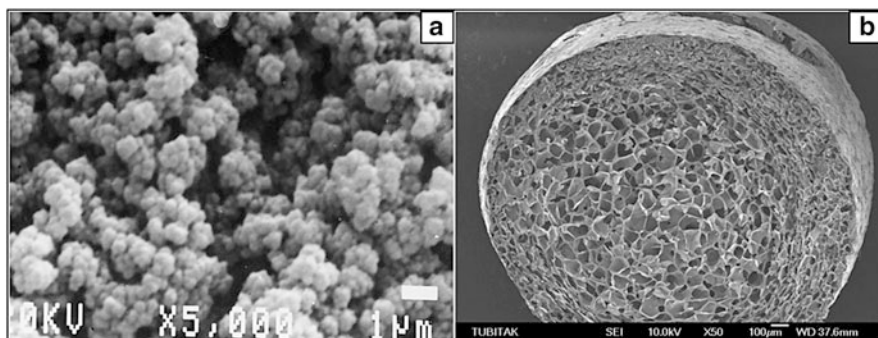
Fig. 1 SEM images of macroporous networks formed by (**a**) phase separation and (**b**) cryogelation techniques. (**a**) PNIPA network: C_o= 20 % (w/v); BAAm = 30 wt% (with respect to NIPA); T_{prep}=22.5 °C; diluent, water. (Reprinted from [14] with permission from Elsevier). (**b**) PAAm network: $T_{prep} = -18$ °C; C_o= 3 % (w/v); crosslinker ratio (molar ratio of BAAm to AAm) = 1:80. (From [23] with permission of Taylor & Francis Group, LLC). *Scale bars*: 1 μm (**b**), 100 μm (**b**)

structure was discovered at the end of the 1950s [11–13]. This technique involves the free-radical crosslinking copolymerization of the monomer–crosslinker mixture in the presence of an inert substance (the diluent or porogen), which is soluble in the monomer mixture. In order to obtain macroporous structures, a phase separation must occur during the course of the network formation process so that the two-phase structure formed is fixed by the formation of additional crosslinks [12]. After the polymerization, the diluent is removed from the network, leaving a porous structure within the highly crosslinked polymer network. This mechanism of porosity formation known as "reaction-induced phase separation" leads to the formation of macroporous gels consisting of agglomerates of polymer particles of various sizes that look like cauliflowers. Figure 1a shows a typical scanning electron microscopy (SEM) image of a poly(N-isopropylacrylamide) (PNIPA) gel network formed by the phase separation technique [14]. Although macroporous gels formed by phase separation exhibit a fast response rate to external stimuli [14], their aggregate-like morphology (consisting of rather weakly joined microgel particles) inevitably causes a significant reduction in their mechanical properties. Moreover, since a large amount of crosslinker has to be used to induce a phase separation during gelation, the network chains do not behave like flexible polymer chains sensitive to external stimuli.

Cryogelation is a simple strategy that allows the preparation of macroporous gels with high toughness and superfast responsivity. Although discovered over 30 years

---

the distance between the chains varies between zero and several nanometers depending on the external conditions. Further, removing the solvent from a homogeneous gel results in a polymer network that is nonporous. Thus, "porous gels" refers to materials having a dry state porosity, characterized by a lower density of the network due to the voids as compared to the density of the matrix polymer (see [11] for a detailed discussion).

ago [15–19], cryogels have attracted intense attention only in the last 10 years due to their extraordinary properties [20–22]. For instance, they do not display undesirable properties such as brittleness, which is commonly observed for macroporous gels formed by phase separation polymerization. Cryogels are very tough and can withstand high levels of deformation, such as elongation and torsion; they can also be squeezed almost completely without any crack propagation. The cryogelation technique is based on the natural principle that sea ice is less salty than sea water, i.e., the rejection of brine from freezing salt solutions. This principle is a consequence of the insolubility of the salts in ice compared to their excellent solubility in water. In cryogelation reactions, the reaction solution, generally containing the monomers and the initiator, is cooled below the freezing point of the system; since the monomers and the initiator will be enriched in the unfrozen microzones surrounded by solvent crystals, the polymerization reactions only proceed in these unfrozen regions containing a high concentration of monomer. The increased monomer concentration in the unfrozen reaction zones (i.e., cryo-concentration) is the main characteristic of the cryogelation reactions and is responsible for the extraordinary properties of cryogels. A macroporous structure in the final material appears due to the existence of solvent crystals acting as a template (or porogen) for the formation of the pores. The removal of template (e.g., ice) is achieved by simply holding the cryogel at temperatures above the solvent freezing point. This is another advantage of the cryogelation technique over the phase separation technique, where the latter requires extensive extraction of the gel to remove the porogen. In contrast to the cauliflower-like microstructure of macroporous gels formed by phase separation, cryogels exhibit a regular assembly of large pores of 10^0–10^1 μm in size separated by dense pore walls of several micrometers in thickness (Fig. 1b) [23].

This chapter discusses the conditions for formation of macroporous gels by the cryogelation technique. It also discusses how and why the properties of gels significantly alter upon transition from conventional gelation to the cryogelation regime. The formation and structure–property relationships of cryogels starting from monovinyl–divinyl monomers, as well as from linear polymer chains, are reviewed using examples from the recent literature. Some novel cryogels based on DNA, silk fibroin, poly(acrylic acid), and several types of rubbers with a wide range of tunable properties are also presented in details together with their applications.

2   Preparation and Characterization of Cryogels

Cryogels are mainly prepared by crosslinking polymerization of monomers or by crosslinking of linear polymers in frozen solutions. The most commonly used monomeric and polymeric precursors, the crosslinkers, the general preparation conditions, and characterization techniques are summarized in this section.

2.1 Monomeric and Polymeric Precursors, Crosslinkers

Several monovinyl–divinyl comonomer pairs have been used for the preparation of cryogels by free-radical crosslinking copolymerization. Mainly, water-soluble monomers have been used in the synthesis of cryogels, such as acrylamide (AAm) [16, 24–26], *N*,*N*-diethylacrylamide [27], *N*,*N*-dimethylacrylamide (DMA) [28–30], acrylic acid (AAc) [31], *N*-isopropylacrylamide (NIPA) [32–34], 2-hydroxyethyl methacrylate (HEMA) [35], and 2-acrylamido-2-methylpropane sulfonic acid sodium salt (AMPS) [36], in combination with *N*,*N*-methylene(bis) acrylamide (BAAm), poly(ethylene glycol diacrylate), or biodegradable crosslinkers [33, 35]. Nanosized clay particles (Laponite) can also be used as a multifunctional crosslinker in the preparation of cryogels exhibiting very high extensibility [34]. An ammonium persulfate (APS) and *N*,*N*,*N'*,*N'*-tetramethylethylenediamine (TEMED) redox initiator system is generally used to initiate the polymerization reactions. Since the decomposition of the radical initiators is temperature dependent, the reaction solutions should be cooled before addition of the initiator. Otherwise, gelation will start before freezing of the reaction system, resulting in the formation of conventional gels. Alternatively, polymerization inhibitors such as hydroquinone can be included in the reaction system to shift the onset of the reactions beyond freezing of the solution [23]. Cryogelation reactions can also be initiated by ultraviolet (UV) or electron-beam radiations so that the freezing time before the initiation step can be controlled [37–39]. Controlled radical polymerization techniques such as reversible addition-fragmentation chain transfer (RAFT) reactions have also been utilized for the preparation of cryogels both in aqueous and organic media [30, 40]. Inspired by the double-network (DN) technology developed by Gong and coworkers [6], DN cryogels with dual sensitivity have also been prepared by conducting the cryogelation reactions within the macropores of the single-network cryogels [41].

Cryogels can also be prepared starting from linear polymers in the presence of a chemical crosslinker in aqueous or organic solutions. Several natural and synthetic polymers have been used for the preparation of cryogels. The most popular crosslinker for proteins is glutaraldehyde, which is highly active towards the amine groups of a peptide chain in aqueous solutions. Proteins (e.g., gelatin, fibrinogen, collagen, and bovine serum albumin), polysaccharides (e.g., chitosan, hyaluronic acid), and synthetic polymers such as polyacrylamide (PAAm) and poly (vinyl alcohol) (PVA) can be crosslinked using glutaraldehyde in their frozen solutions [17, 42–44]. Cryogels were also prepared via crosslinking of amino end-functionalized star-shaped poly(ethylene glycol) with heparin in aqueous solutions [45]. However, it is not always necessary to use a crosslinker in the preparation of cryogels from polymeric precursors. For example, the hydrogen bonds formed between PVA chains in the unfrozen reaction phase lead to microcrystalline domains that act as crosslinkers in PVA cryogels [44, 46].

Di-epoxides such as ethylene glycol diglycidyl ether (EGDE) and 1,4-butanediol diglycidyl ether (BDDE) in the presence of TEMED catalyst have been used as
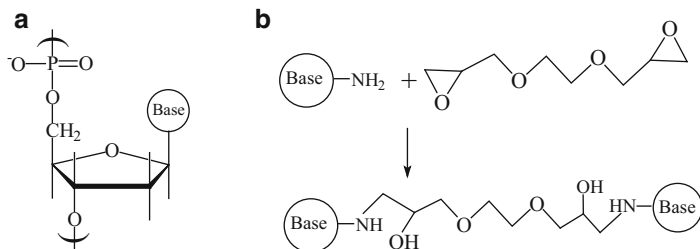
Scheme 1 (**a**) Nucleotide repeat unit of DNA and (**b**) the crosslinking reaction of the amino groups on the nucleotide bases with EGDE, leading to DNA cryogels

crosslinkers in the preparation of DNA and fibroin cryogels [47–50]. EGDE and BDDE contain epoxide groups on both ends that can react with nucleophiles such as amino groups, sulfhydryls, and hydroxyls. Because the amino groups on the nucleotide bases of DNA react with EGDE, heat-resistant interstrand crosslinks form during the cryogelation reactions, leading to the formation of DNA cryogels (Scheme 1) [48]. Silk fibroin cryogels can also be prepared using EGDE as a crosslinker. Here, EGDE crosslinks between the NH_2 groups of arginine and the lysine residues of fibroin molecules trigger the conformational transition of fibroin from the random coil to β-sheet structure and, hence, cryogel formation [49, 50]. Thus, fibroin cryogels contain both chemical crosslinks and β-sheet structures acting as physical crosslinks.

Rubber cryogels can be prepared using sulfur monochloride (S_2Cl_2) as a crosslinker [51–57]. Sulfur monochloride, a liquid at room temperature and soluble in organic solvents, is an effective crosslinker for the crosslinking processes of several types of rubbers, such as natural rubber, butyl rubber (PIB), *cis*-polybutadiene (CBR), and styrene-butadiene rubber (SBR) in organic media such as benzene, cyclohexane, and toluene [52, 53, 55]. The crosslinking reactions between the internal unsaturated groups of the rubbers via sulfur monochloride proceed in steps, as in the reaction between ethylene and sulfur monochloride (Scheme 2) [55]. Attack of sulfur dichloride on the internal vinyl group of the polymer leads to the formation of pendant sulfur chloride groups on the chains acting as potential crosslink points. Reaction of these groups with the internal vinyl groups on other chains is responsible for the formation of effective crosslinks.

Instead of linear polymers, micrometer-sized gel particles can also be used for the preparation of cryogels [58]. Such cryogels, with pore walls composed of close-packed particles, have been obtained by crosslinking of frozen aqueous suspensions of PNIPA gel particles or spherical and rod-shaped bacterial cells using glutaraldehyde as a crosslinker [58].

$$S_2Cl_2 \rightleftharpoons SCl_2 + S$$
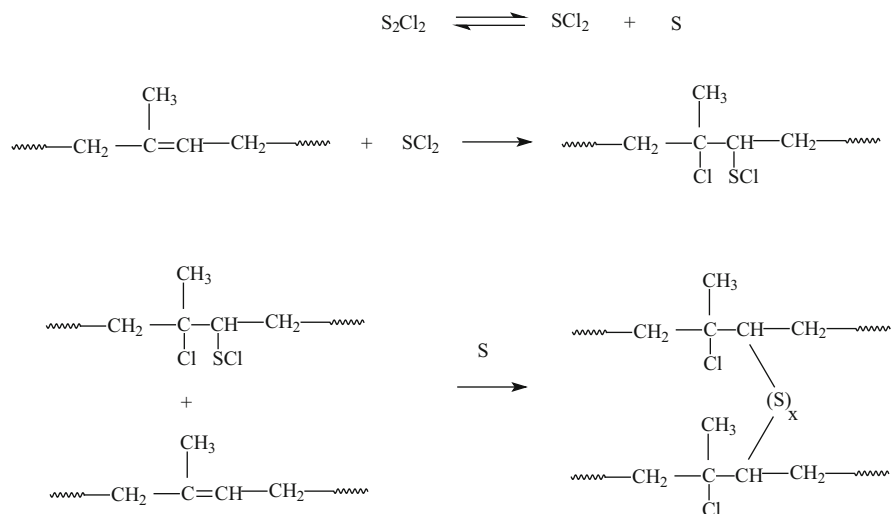
Scheme 2 Crosslinking reactions between the internal unsaturated groups of PIB via sulfur monochloride

2.2 Solvents and the Cryogelation Temperature

Water is cheap and benign to biological systems and, therefore, it is the most commonly used solvent in cryogelation reactions. Organic solvents such as dimethyl sulfoxide (DMSO) [32, 59], dioxane [24, 33, 40], formamide [24], nitrobenzene [60], benzene [52], and cyclohexane [53] with relatively high freezing points can also be used for the preparation of hydrophobic cryogels. Since the cryo-concentration of the reaction constituents in the unfrozen domains is a requirement for the formation of cryogels, the gelation temperature T_{prep} is the most important experimental parameter [61]. A so-called moderate temperature is commonly used for cryogelation reactions [62], which means a sufficiently low temperature, e.g., several degrees lower than the freezing point of the system. T_{prep} is usually set to 2–20 °C below the bulk freezing temperature of the solvent. In addition, the type of cooling of the reaction solution to T_{prep} also affects the cryogel properties. For example, liquid cooling provides much faster freezing of the reaction solution than air cooling, leading to the generation of smaller pores [52].

2.3 Monomer or Polymer Concentration

The initial concentration C_o of the monomeric or the polymeric precursors is another important parameter in cryogel preparation. Due to the effect of cryo-concentration, cryogels can be prepared at much lower concentrations compared

to the conventional gels [42]. For example, in the free-radical crosslinking copolymerization of AMPS and BAAm (17 mol % of the comonomer mixture) at T_{prep} = −22 °C, crosslinked polymer starts to form at C_o = 0.1 %, as compared to 5 % when conducted at T_{prep} = 25 °C [63]. In the preparation of PIB cryogels in benzene using S_2Cl_2 crosslinker (6 % v/w with respect to PIB), critical PIB concentration for gelation is 0.08 ± 0.02 % at −18 °C, compared to 4 % at T_{prep} = 20 °C [52]. Therefore, cryogels can be prepared over a wider concentration range compared to the conventional gels; however, since the cryogels formed at very low C_o are mechanically weak, the usual concentration range is between 2 and 20 % (w/v). Because increasing C_o or decreasing T_{prep} decreases the pore size of the cryogels and simultaneously increases their mechanical strength, these synthesis parameters can be used to tune the properties of cryogels.

2.4   Geometry of Cryogels

Cryogels can be prepared in various shapes such as blocks, sheets, discs, and beads [64]. Cryogels as continuous-bed columns (monoliths) for chromatographic separation of biomolecules have been prepared by filling the gelation solution in plastic syringes with a closed outlet at the bottom and then immersing the syringes in a cryostat at T_{prep} [29, 65–67]. To ensure the reproducibility of the freezing patterns, reaction mixtures of the same volume, and syringes of the same dimensions, should be used for every synthesis [68]. After completion of the cryogelation reaction, the cryogel blocks are thawed at room temperature and then thoroughly washed with a good solvent to remove unreacted species. Cryogels can also be prepared in the form of membranes by injecting the reaction solution between two glass plates separated by a spacer.

In contrast to blocks consisting of a single piece of macroporous material, cryogels in the form of beads are suitable for packing in columns with different scales. However, due to a number of preparation difficulties, there are only a few publications on the preparation of cryogel beads. For instance, if the cryogelation reactions are carried out under the conditions of the usual suspension polymerization technique, odd-shaped gel particles with a broad size distribution are obtained, due to collisions between the frozen droplets [69]. It was shown that cryogel particles can be prepared inside the wall of a hollow plastic carrier to make them resistant to intensive stirring [70]. Yun et al. utilized a microfluidic flow focusing technique to generate a suspension of aqueous gelation solution in a water-immiscible organic phase [71, 72]. After keeping the droplets at subzero temperatures, PAAm-based cryogel beads of 1 mm in diameter were produced. Alginate-agarose, PAAm, and DNA-based cryogel beads have been prepared recently by dropwise addition of the aqueous reaction solution into the paraffin oil as the continuous phase at temperatures between −15 and −20 °C [47, 64, 73]. The diameter of the cryogel beads could be adjusted by changing the tip diameter of
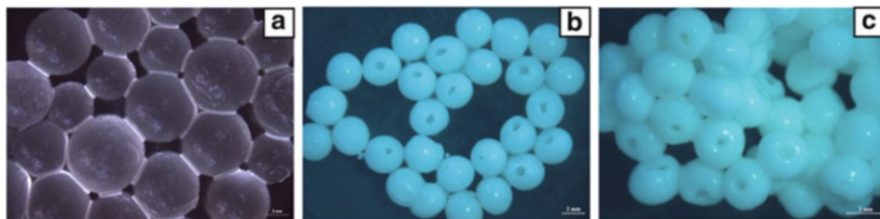
Fig. 2 Optical microscopy images of cryogel beads. (**a**) Ionic PAAc cryogel beads formed at −18 °C. (From [73] with permission from Elsevier). (**b**) Frozen PIB solution droplets in liquid nitrogen, and (**c**) crosslinked PIB beads just after preparation. S_2Cl_2 = 20 % (v/w); PIB concentration = 10 % (w/v). (From [69] with permission from Elsevier). *Scale bars*: 2 mm

the pipettes from which the aqueous phase was added into the oil phase. Figure 2a shows images of ionic PAAm cryogel beads prepared at −18 °C [73].

Preparation of hydrophobic cryogel beads have also been reported recently [69]. Cryogelation reactions were carried out within the droplets of frozen benzene solutions containing PIB and sulfur monochloride as a crosslinker. Spherical millimeter-sized PIB cryogel beads with a polydispersity of less than 10 % were obtained by use of two techniques. First, the reaction solution is dropped into liquid nitrogen to create small frozen organic droplets at −196 °C. Then, the frozen droplets are transferred into ethanol at −18 °C as the continuous phase, and the cryogelation reactions are carried out without stirring. Images in Fig. 2b show frozen solution droplets in liquid nitrogen, and Fig. 2c shows PIB beads just after preparation [69]. Freezing of PIB solution in liquid nitrogen results in the formation of uniform frozen solution droplets with an opening in their shells. The spherical shape and the morphology of the frozen droplets remain unchanged after the crosslinking reactions as well as after swelling of the crosslinked particles in toluene. The second technique involves dropwise addition of the organic solution into a continuous phase at −18 °C without stirring [69]. Here, the density of the continuous phase was so adjusted that the droplets slowly fall through the solution. An ethylene glycol–ethanol mixture (1:4 by volume) having a density close to that of the organic droplets was used as the continuous phase of the reaction. Similarly to the first technique, the resultant PIB beads have openings on their surfaces. Although the formation mechanism of a single large hole in the surface of the particle is still unclear, polymer/solvent phase separation during freezing and subsequent interfacial free energy minimization may be responsible for this process [74].

2.5 Morphological and Mechanical Characterization

Study of the macroporous structure of gels is a challenging task since there is no standard method for the pore-structure determination of such soft materials.

Although techniques such as optical microscopy, environmental scanning electron microscopy (ESEM), and confocal laser scanning microscopy (CLSM) can be used for the morphological characterization of cryogels in their swollen states, they do not lead to sufficient resolution to reveal the fine structure of cryogels. Due to the compressibility of gels under high pressure, other techniques such as mercury intrusion porosimetry and gas adsorption/desorption are not suitable for pore-structure characterization and can only be applied to dry materials. SEM is a suitable technique for characterizing the fine structure of cryogels; however, it also requires drying of the gel samples, which might result in structural changes. Nevertheless, it is assumed that freeze-drying and the sample preparation do not result in alteration of the pore structures due to the formation of dense pore walls during cryo-concentration. Therefore, SEM has been generally used to visualize the morphology and calculate the average pore size of cryogels. Moreover, the flow-through characteristics of cryogels in the form of blocks or beads can also be used to estimate their pore sizes and morphologies. More details about other characterization techniques used for cryogels can be found in recent reviews by Gun'ko and Savina [75, 76].

The total volume of open pores V_p of the cryogels can easily be estimated through uptake of a poor solvent, such as acetone for PAAm or methanol for PIB cryogels. Since a poor solvent for polymer can only enter into the pores of polymer networks, V_p (milliliters of pores in 1 g of dry polymer network) can be calculated as:

$$V_p = \frac{(m_{NS} - m_{dry})}{m_{dry} d_1} \tag{1}$$

where m_{NS} and m_{dry} are the weight of the cryogel in the poor solvent and its dry weight, respectively, and d_1 is the solvent density. The total porosity P of dried cryogels (milliliters of pores in 1 mL of dry polymer network) can be estimated from their densities as:

$$P = 1 - \frac{d_0}{d_2} \tag{2}$$

where d_o is the apparent density(i.e., density of the porous network) and d_2 is the (nonporous) polymer density. The relative values of the equilibrium volume (q_v) and the equilibrium weight swelling capacities (q_w) of the cryogels also provide information about their internal structure in the swollen state. These swelling ratios are calculated as:

$$q_v = (D/D_{dry})^3 \tag{3a}$$

$$q_w = (m/m_{dry}) \tag{3b}$$

where D and D_{dry} are the gel diameters in equilibrium swollen and dry states, respectively, and m is the weight of equilibrium swollen gel. During the cryogel swelling process, the pores inside the cryogel network are rapidly filled with the solvent; at the same time, the network region making up the pore walls of the cryogel takes up solvent from the environment by diffusion process. Therefore, the swelling of cryogels is governed by two separate processes: (1) solvation (swelling) of the pore walls and (2) filling of the pores by the solvent.

The equilibrium weight swelling ratio q_w includes the amount of solvent taken up by both of these processes. By contrast, if we assume isotropic swelling (i.e., the volume of the pores remains constant upon swelling), the volume swelling ratio q_v of cryogels is caused by solvation of the pore walls, i.e., by the first process. Thus, q_v only includes the amount of solvent taken up by the gel portion of the cryogel network. Accordingly, the higher the difference between q_w and q_v, the higher is the volume of the pores in swollen cryogels. The swollen state porosity P_s of the cryogels can be estimated from their volume and the weight swelling ratios using the equation [11]:

$$P_s = 1 - \frac{q_v}{1 + (q_w - 1)\, d_2/d_1} \tag{4}$$

Several techniques are available for the mechanical characterization of cryogels in swollen and dried states. Uniaxial compression tests are conducted on cylindrical cryogel samples to determine the Young's modulus E or shear modulus G from the slope of stress–strain curves at low compressions, while the stress at 3 or 5 % compression is reported as the compressive stress σ_{comp}. For uniaxial compression of a cylindrical gel sample, the statistical theories of rubber elasticity yield for Gaussian chains an equation of the form [77, 78]:

$$\sigma = G\left(\lambda - \lambda^{-2}\right) \tag{5a}$$

where σ is the nominal stress and λ is the corresponding deformation ratio (deformed length/initial length). In contrast to a cylindrical cryogel sample, the interpretation of the compression test data of a spherical cryogel particle is complicated. This is due to significant variation in the contact area between the wall and the originally spherical gel during deformation. For a sphere with a constant volume during deformation, the Hertz equation can be used to estimate the modulus of cryogel beads [79–84]:

$$F = \frac{4}{3} G D_1^{0.5} \Delta D^{1.5} \tag{5b}$$

Here, F is the force and ΔD is the deformation, $\Delta D = D_1 - D_2$, where D_1 and D_2 are the initial undeformed and deformed diameters of the sample, respectively. According to (5b), a linear relation is expected if $(3/4)F D_1^{-0.5}$ is plotted against $\Delta D^{1.5}$ with a slope equal to the modulus G of the beads. Indeed, linear plots were
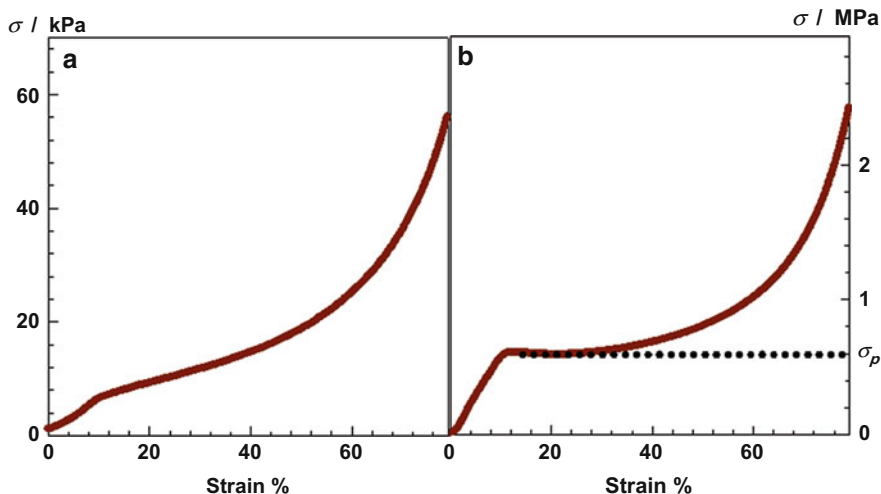
Fig. 3 Stress–strain curves of a fibroin cryogel in (**a**) swollen and (**b**) dry states are shown as the dependence of the nominal stress σ on the degree of compression; $T_{\text{prep}} = -18\,°C$; $C_{\text{SF}} = 4.2\,\%$; EGDE = 20 mmol/g epoxide; TEMED = 0.07 %

obtained for both hydrophilic and hydrophobic cryogel beads [47, 69, 73]. It was shown that the modulus (i.e., the effective crosslink density of the cryogel beads) decreases with decreasing bead diameter [73]. This size-dependent crosslink density of the beads is attributed to the fact that the gelation reactions at the surface layer of the droplets slow down due to the contact of this region with the continuous phase. This will reduce the crosslink density of the surface layer of the resulting gel beads. Since decreasing the size of the droplets increases the surface-to-volume ratio of the final beads, the smaller the bead diameter, the smaller its average crosslink density.

The large strain properties of some spongy cryogels can also be investigated by uniaxial compression tests up to complete compression. Typical stress–strain curves of cryogels in swollen and dry states are shown in Fig. 3a, b as the dependence of nominal stress σ on percentage compression [50]. During compression of the swollen cryogel, the curve is quite linear up to a critical strain, indicating that the pores filled with solvent remain mechanically stable. As the cryogel is further squeezed under the piston, the pores gradually release solvent due to buckling of the pore walls so that it can easily be compressed. Similarly, the stress–strain curve of the dried cryogel is first linear, indicating that the macroporous structure remains mechanically stable in this range of strain. This linear elastic regime is followed by a near-plateau regime, indicating that the network easily deforms due to the collapse of its pores under the pressure. The critical stress corresponding to the plateau regime, denoted by σ_p in Fig. 3b, is a measure of the mechanical stability of the porous structure of cryogels. Finally, the steep increase of the curve in the third regime corresponds to the compression of the

nearly nonporous polymer network. Although freeze-dried hydrogels are also porous, no distinct plateau is observed in stress–strain curves [50], which is attributed to the weak network structure due to the absence of cryo-concentration.

Squeezability of the cryogels and their reusability, as well as the continuous extraction capacity for the removal of pollutants, are determined by subjecting the cryogel samples to successive sorption–squeezing cycles under identical conditions. In a typical procedure [54], the cryogel sample is first immersed in the test solution for 1 min and then it is left to drip for 30 s. The cryogel is weighed and put into a Büchner funnel and squeezed for 30 s under 50 mm vacuum. Then, it is weighed again to calculate the amount of solution taken up by one gram of cryogel. This sorption–squeezing cycle is repeated many times to obtain the recycling efficiency and continuous extraction capacity of the cryogels.

3 Transition from Gelation to Cryogelation: Gels Versus Cryogels

Since cryo-concentration is a characteristic phenomenon of cryogelation, it is necessary first to discuss how increased monomer concentration at gelation affects the properties of conventional gels. Several studies show that the gel structure and, thus, the gel properties strongly depend on the initial monomer concentration [11, 13, 85–89]. No continuous network is formed below a critical concentration of monomer. Increasing the amount of monomer at polymerization causes the polymer chains to entangle so that the network formed in a semidilute solution can swell poorly, even when exposed to a good solvent. This increase in the monomer concentration also decreases the probability of cyclization reactions, so that a large fraction of the crosslinker is consumed in effective crosslinks [85]. In accord with the experiments, the statistical model proposed by Bromberg et al. predicts that the effective crosslink density of gels scales with the second power of the monomer concentration [89, 90]. As a consequence, the network structure formed becomes increasingly tight as the monomer concentration increases.

Let us now consider what will happen to the monomer concentration when the polymerization temperature is decreased below the freezing point of the reaction system. During freezing, the monomers and the initiator are expelled from the forming solvent crystals and become entrapped within channels between the crystals. As a consequence, the polymerization reactions can only take place in spatially restricted reaction fields, which are the unfrozen microchannels of the apparently frozen system. The reason why solvent does not freeze below the bulk freezing temperature is attributed to the freezing point depression of the solvent due to the solutes, e.g., monomers and polymers [91–93]. For instance, about 6 % of the water in swollen PAAm hydrogels remains unfrozen, even at $-24\,^\circ\text{C}$ [26]. Kirsebom used ^{1}H NMR to estimate the monomer concentration in the unfrozen microchannels [28]. The reaction system studied was the crosslinking copolymerization of DMA
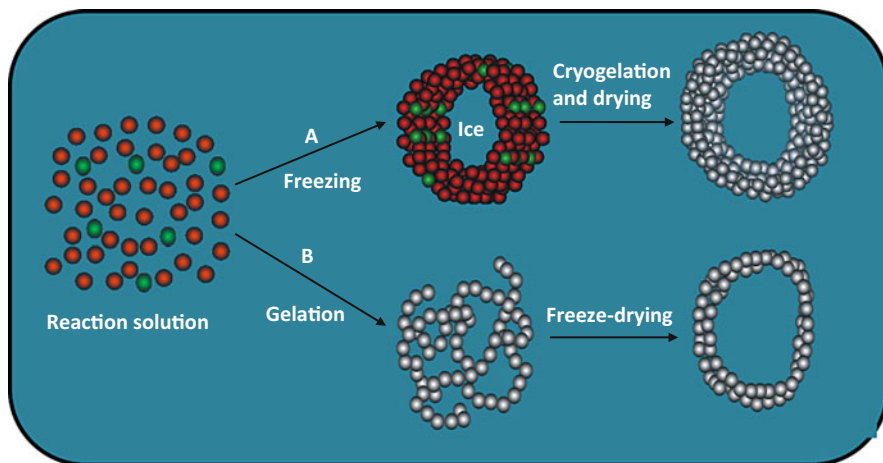
Fig. 4 Formation process of a pore by cryogelation (**a**) and by freeze-drying (**b**). *Red*, *green*, and *gray* circles represent monovinyl monomers, divinyl monomers, and polymer repeat units, respectively

and poly(ethylene glycol) diacrylate in aqueous solutions. It was found that the local concentration of the monomers in the unfrozen zones was 32.6 and 45.5 wt% at $T_{prep} = -10$ and -20 °C, respectively, as compared to the initial (nominal) monomer concentration of 6 wt% [28]. Thus, the actual concentration of the monomer in the microchannels is about sixfold larger than its nominal concentration. As a consequence, the critical monomer concentration for the onset of gelation is much lower in cryogelation compared to the conventional gelation systems. This cryo-concentration effect is also responsible for the fact that a high polymer content of the gel phase produces thick and dense pore walls in the resulting cryogels.

The transition from conventional gelation to the cryogelation regime requires that the cryo-concentration of reaction constituents occurs before onset of the gelation reactions. For instance, freeze-drying of an already formed gel does not lead to materials with cryogel properties due to the formation of ice crystals in a gel rather than in a solution. This is illustrated schematically in Fig. 4, which compares the formation process of a pore by cryogelation and by freeze-drying. The pore wall produced by cryogelation is a dense polymeric gel because of the cryo-concentrated solution of the monomers around the ice crystals. In contrast, the pore wall formed after freeze-drying of a conventional gel is a loosely crosslinked gel due to the absence of cryo-concentration. As a consequence, the porous structures produced during cryogelation are mechanically stable, even under large strain conditions. Typical images of swollen and freeze-dried hydrogel and cryogel samples formed from aqueous silk fibroin solutions are shown in Fig. 5 [50]. The gels were prepared under identical conditions except that the gel preparation temperature, T_{prep}, was -18°C for the cryogel and 50 °C for the hydrogel [50]. After freeze-drying, the

Fig. 5 Images of the cryogel (*top row*) and hydrogel samples (*bottom row*) formed at −18 and 50 °C, respectively, in swollen and dry states. $C_{SF} = 4.2$ wt% EGDE = 20 mmol/g; TEMED = 0.10 %. *Scale bars*: 1 mm (SEM images on *far right*), 20 μm (*inset*). (From [50] with permission from the American Chemical Society)

scaffold derived from the cryogel retains its original shape, whereas a lateral distortion in the cylindrical shape of the hydrogel scaffold is observed. SEM images of these samples (Fig. 5) also show that the cylindrical shape of the hydrogel scaffold is partially destroyed due to the weak network structure. In contrast, cryogel scaffold is mechanically stable and consists of regular, interconnected pores of diameters from 5 to 10 μm that are separated by thick pore walls.

How does the local concentration of the monomer in the unfrozen reaction zones vary depending on the cryogelation conditions? What is the volume fraction of frozen solvent in the reaction system? A simple thermodynamic model was recently developed to answer these questions [36]. The model considers a polymeric gel in equilibrium with a solvent at a given temperature. As the temperature is decreased below the freezing temperature of the solvent, solvent freezes out of the gel phase so that a two-phase system forms that consists of pure solvent crystals and an unfrozen gel. The equilibrium condition between these two phases at a given temperature T_{prep} is such that the chemical potentials of solvent crystals (μ_1^{cry}) and of liquid solvent in the gel (μ_1^{gel}) must be equal. μ_1^{gel} in the gel phase is $\mu_1^{gel} = \mu_1^{o} + RT_{prep} \, ln \, a_1$, where μ_1^{o} is the chemical potential of pure liquid solvent and a_1 is the activity of solvent in the gel. Equating μ_1^{cry} and μ_1^{gel} at T_{prep} and, since $\mu_1^{o} - \mu_1^{cry}$ equals the molar Gibbs free energy change for melting of solvent crystals, one obtains:

$$\ln a_1 \;=\; \frac{\Delta H_m}{R}\left(\frac{1}{T_f^0} - \frac{1}{T_{\text{prep}}}\right) \tag{6}$$

where ΔH_{m} and T_{f}^0 are the molar enthalpy of fusion and the normal freezing point of pure solvent, respectively, and R is the gas constant.[2] The Flory–Rehner theory including the ideal Donnan equilibria gives the following relation between the activity of a swelling agent (solvent) in the gel and the gel parameters [77]:

$$\ln a_1 \;=\; \ln(1 - \nu_2) \;+\; \nu_2 \;+\; \chi\nu_2^2 \;+\; \nu_e V_1\left[\nu_2^{1/3}\left(\nu_2^0\right)^{2/3} - 0.5\nu_2\right] \;-f\nu_2 \tag{7}$$

where ν_2 and ν_2^0 are the volume fractions of crosslinked polymer in the equilibrium swollen gel and after gel preparation, respectively, χ is the polymer–solvent interaction parameter, ν_{e} is the effective crosslink density of the network, V_1 is the molar volume of solvent, and f is the effective charge density, i.e., the fraction of charged units in the network chains that are effective in gel swelling. Since $\nu_2 = \nu_2^0$ after cryogel preparation, substituting (7) into (6) yields [36]:

$$\frac{1}{T_{\text{prep}}} \;=\; \frac{1}{T_{\text{f}}^0} \;-\; \frac{R}{\Delta H_{\text{m}}}\left[\ln\left(1 - \nu_2^0\right) \;+\; \nu_2^0 + \chi\left(\nu_2^0\right)^2 + \; 0.5\nu_e V_1\nu_2^0 - f\nu_2^0\right] \tag{8}$$

Using (8), one may estimate the polymer concentration ν_2^0 in the unfrozen gel phase at a given temperature T_{prep} ($T_{\text{prep}} < T_{\text{f}}^0$). To apply (8) to the cryogelation systems, we assume that the monomers completely accumulate in the unfrozen reaction phase before the onset of gelation. We also assume that, after cryogelation, the conversion of monomer to crosslinked polymer is complete. Thus, the monomer concentration C in the unfrozen zones (in % w/v) can be estimated from ν_2^0 as:

$$C = \left(\nu_2^0 d_2\right)10^2 \tag{9}$$

The volume fraction of frozen solvent in the reaction system, P, can also be estimated as:

$$P \;=\; 1 \;-\; \frac{C_{\text{o}}}{C} \tag{10}$$

where C_{o} is the nominal monomer concentration. Since the frozen solvent acts as a template in the cryogels, P also corresponds to their porosities (volume of pores/

---

[2] Assuming ideally dilute solutions, (6) leads to the well-known equation $T_{\text{prep}} - T_f^0 = - K_f m_2$, where K_{f} is the freezing-point-depression constant, and m_2 is the solute molality. However, this equation cannot be used for the cryogelation system due to the high concentration of solutes in the unfrozen domains.
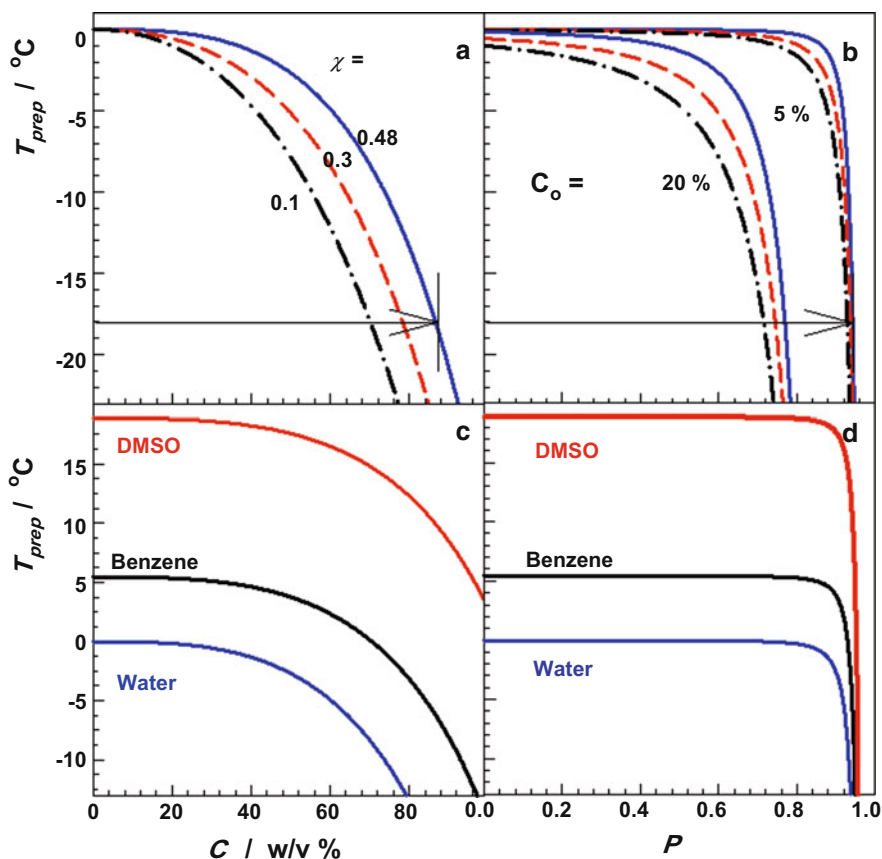
Fig. 6 (**a, c**) Monomer concentration C in the unfrozen gel phase and (**b, d**) volume fraction of frozen solvent in the cryogels P shown as a function of the temperature T_{prep}. (**a, b**) The solvent was water. Calculations are for various χ parameters indicated. P was calculated for $C_o = 5$ and 20 %. (**c, d**) $\chi = 0.48$; $C_o = 5$ %. Calculations are for the various solvents indicated: $\nu_e = 20$ mol/m^3; $\Delta H_m (V_1, T_f^o) = 6.01$ kJ/mol (18 mL/mol, 0 °C), 9.9 kJ/mol (89 mL/mol, 5.4 °C), and 14.4 kJ/mol (71.03 mL/mol, 19 °C) for water, benzene, and DMSO, respectively. The *arrows* in **b** and **c** illustrate the increase in monomer concentration in the unfrozen phase and the volume of frozen solvent at $T_{prep} = -18$ °C

cryogel volume). According to (8), the nominal monomer concentration C_o does not influence the monomer concentration C in the unfrozen phase; however, decreasing C_o, i.e., increasing water content, increases the porosity of cryogels at a given temperature T_{prep}.

Calculations using (8) show that the temperature T_{prep} significantly affects the monomer concentration in the unfrozen phase. Figure 6a, b shows how the monomer concentration C in the unfrozen domains and the volume fraction of frozen solvent in the resulting cryogel P vary with the temperature T_{prep}. Calculations were for water as the solvent and for various polymer–solvent interaction parameters χ

indicated in the figure (χ is assumed to be independent of temperature). Let us first consider the solid curve in Fig. 6a, which was calculated for $\chi = 0.48$, corresponding to polyacrylamide–water system [94]. At $T_{prep} = -18\ °C$, as indicated by the arrow, C is predicted to be 86 %. This means that, as the solvent crystallizes at $-18\ °C$, the monomer concentration in the unfrozen phase rises continuously until attaining its equilibrium value of 86 %. For an initial monomer concentration (C_o) of 5 %, P becomes 0.94 (Fig. 6b), indicating that 94 % of the reaction system consists of solvent crystals acting as template for pore formation. Increasing the initial monomer concentration from 5 to 20 % decreases the volume fraction of frozen solvent, i.e., porosity from 94 to 77 %. Figure 6a, b also shows that the lower the T_{prep}, the higher the monomer concentration in the reaction zones and the larger the porosity.

Moreover, decreasing the χ parameter at a given T_{prep} (i.e., increasing the solvating power of the solvent) also decreases the monomer concentration in the unfrozen zones and, thus, the total volume of the pores in the final cryogels. This is attributed to the increasing amount of uncrystallizable solvent bound to polymer chains as the quality of the diluent is increased. Figure 6c, d presents the results of calculations for three different solvents. As the temperature drops below the freezing temperature of the pure solvent, which is 0, 5.4, and 19 $°C$ for water, benzene, and DMSO, respectively, the monomer concentration in the unfrozen zones rapidly increases. Cryogels with 95 % porosities could be obtained at $T_{prep} = -3, +3,$ and $+17\ °C$ using water, benzene, and DMSO as the polymerization solvent, respectively. Thus, the cryogelation temperature can be adjusted by selecting a suitable solvent. As will be seen in the following sections, the prediction of simulation results is in qualitative agreement with the experimental findings.

The theoretical results in Fig. 6 also show that cryo-concentration and the resulting transition from gelation to the cryogelation regime occurs at temperatures close to the freezing point of the pure solvent. As a result, a drastic change in the gel properties has to be expected at these temperatures. For instance, increased monomer concentration due to cryo-concentration would lead to a significant increase in the elastic modulus and a decrease in the swelling capacity of the gels.

This was indeed observed experimentally, but at lower temperatures. The results of such measurements are shown in Fig. 7a–c for PAAm hydrogels, where the elastic modulus G, the equilibrium weight q_w, volume swelling ratio q_v of the gels, and their dry and swollen state porosities, P and P_s, respectively, are plotted against T_{prep} [26]. The gels were prepared by free-radical crosslinking copolymerization of AAm with BAAm in aqueous solution at various T_{prep} between $-25\ °C$ and $+25\ °C$ [26]. The dotted rectangular area in Fig. 7a–c indicates the transition between homogeneous gelation and cryogelation regimes occurring between -6 and $-10\ °C$. Depending on T_{prep}, two types of gels can be obtained:

1. At $T_{prep} \geq -6\ °C$: The gels exhibit a relatively low modulus of elasticity around 1.5 kPa. Both the weight q_w and the volume swelling ratios q_v of gels are equal to ~20, and they are independent of T_{prep}.
2. At $T_{prep} \leq -10\ °C$: Decreasing T_{prep} below –6 $°C$ results in a fourfold increase in the elastic modulus of gels. Moreover, the weight swelling ratio q_w remains
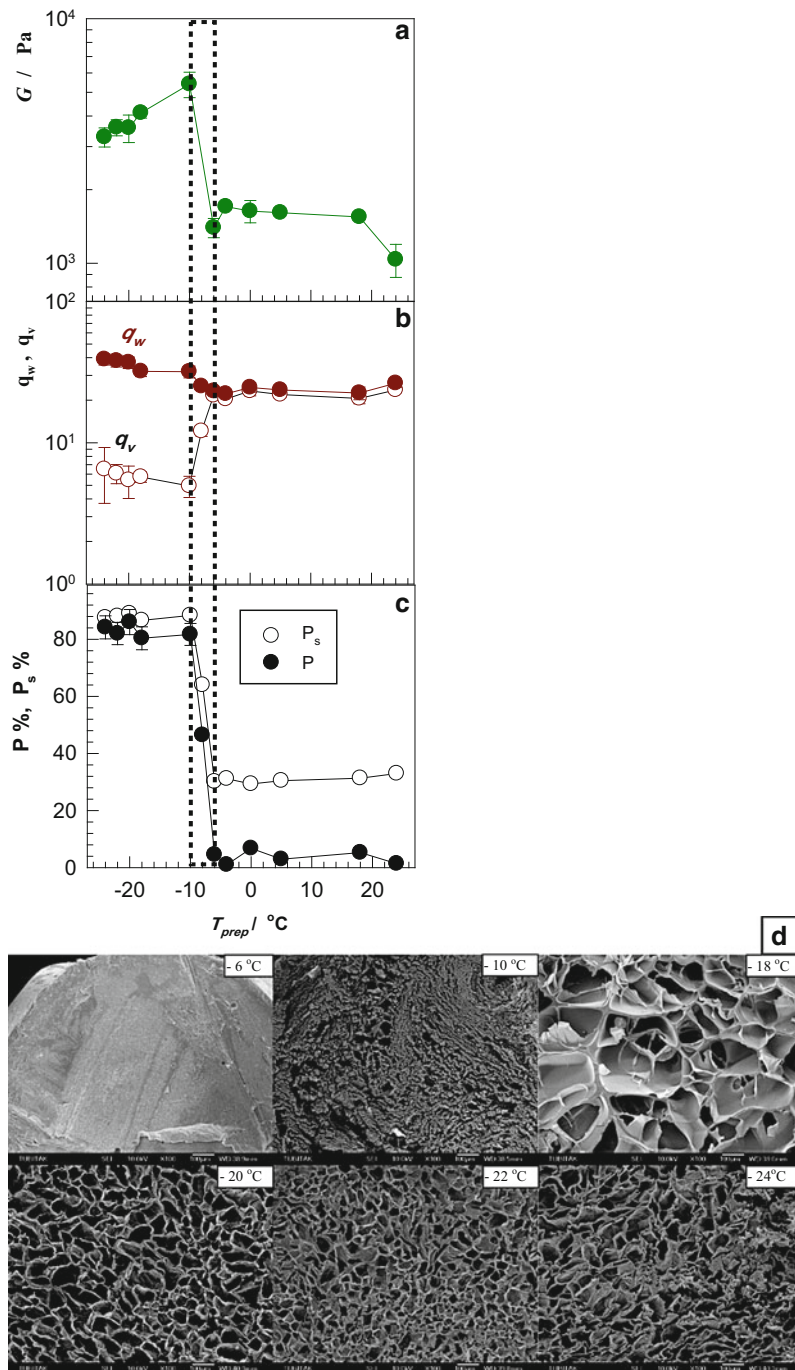
Fig. 7 (**a**) The elastic modulus G, (**b**) the equilibrium weight q_w and volume swelling ratios q_v, and (**c**) the swollen state porosity P_s and the dry state porosity P of PAAm gels shown as functions of the cryogelation temperature T_{prep}. (**d**) SEM images of PAAm networks formed at the various

almost unchanged as T_{prep} is decreased below $-6\,°C$ while the volume swelling ratio q_v rapidly decreases. At $T_{prep} \leq -10\,°C$, the gels swell about sixfold more by weight than by volume. According to (4), these results suggest the appearance of pores in the gel matrices prepared at $T_{prep} \leq -10\,°C$.

Indeed, the gels formed at $T_{prep} \geq -6\,°C$ were transparent, whereas those formed below $-6\,°C$ were opaque and exhibited 85 % porosities [26]. The total volume of pores, V_p, of the hydrogels estimated from the uptake of a poor solvent (cyclohexane) was in the range of 3–6 mL/g for the gels prepared below $-6\,°C$, whereas those formed at higher temperatures exhibited negligible pore volumes. The SEM images in Fig. 7d illustrate the microstructure of the networks formed at various T_{prep}. All the polymer samples formed below $-6\,°C$ have a porous structure with pore diameters of 10–70 μm, whereas those formed at or above $-6\,°C$ exhibit a continuous morphology. At $-10\,°C$, the pore walls seem to be too weak, so that they are more or less fused together to form large aggregates. Thus, the drastic change in the network microstructure induced by lowering T_{prep} from -6 to $-10\,°C$ is reflected by the swelling and elasticity tests, with decreasing volume swelling ratio and increasing modulus of elasticity of gels.

Similar results were also reported for polyelectrolyte hydrogels prepared from AMPS or sodium acrylate (SA) monomers with BAAm crosslinker in aqueous solutions [36, 95]. At $T_{prep} \geq -8\,°C$, ionic hydrogels derived from AMPS exhibit relatively high volume swelling ratios V_{eq} of the order of 10^1 and low moduli of elasticity G in the range of 10^2–$10^3\,Pa$ [36]. Decrease of T_{prep} below $-8\,°C$ results in a tenfold decrease in the swelling ratio and about tenfold increase in the elastic modulus of gels. Moreover, the gels formed at or above $-8\,°C$ were transparent, whereas those formed at lower temperatures were opaque, indicating that these gels have separate domains in a spatial scale of submicrometer to micrometer [36]. Thus, the transition from homogeneous gelation to the cryogelation regime and the drastic change in the properties of poly(AMPS) (PAMPS) hydrogels appear if T_{prep} is decreased below $-8\,°C$. In poly(sodium acrylate) (PSA) cryogels, this transition was observed at T_{prep} between -6 and $-9\,°C$ [95].

Experiments were also carried out to investigate the transition to the cryogelation regime in organic media. For this purpose, solution crosslinking of PIB was carried out using sulfur monochloride as a crosslinker in cyclohexane (freezing point $= 6.5\,°C$) at various temperatures T_{prep} between -22 and $20\,°C$ [53]. The organogels formed at $T_{prep} > -2\,°C$ were nonporous, whereas those formed at lower temperature were porous and exhibited typical cryogel morphologies with a total volume of pores of about 2.5 mL/g [53]. Thus, the transition to the cryogelation regime occurs at around $-1\,°C$, i.e., about $8\,°C$ below the freezing point of cyclohexane.

Figure 8 compares the response rate of PIB gels formed at temperatures both below and above the transition temperature [53]. Here, the normalized gel mass m_{rel}

Fig. 7 (continued) T_{prep} indicated. $C_o = 5$ % (w/v), $X = 1/80$. *Scale bars*: 100 μm. Magnification 100×. (Reprinted from [26] with permission from Elsevier)
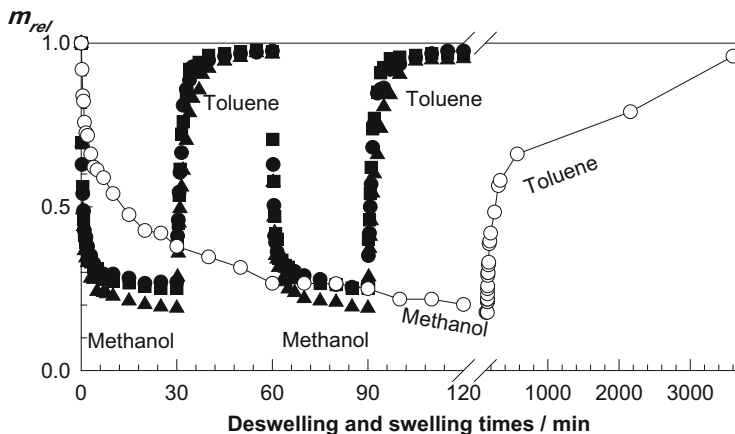
Fig. 8 The normalized mass m_{rel} of PIB gels shown as a function of the time of deswelling in methanol and re-swelling in toluene. $S_2Cl_2 = 5.7$ %; reaction time = 3 days. $T_{prep} = -2$ (*filled triangle*), -10 (*filled circle*), -18 (*filled square*), and 17 °C (*open circle*). (Reprinted from [53] with permission from Elsevier)

(mass of gel at time t/equilibrium swollen mass in toluene) is plotted against the time t of deswelling in methanol and re-swelling in toluene. Both the swelling and deswelling rates of the gel prepared at subzero temperatures are much faster than those prepared at 17 °C; the low-temperature gels undergo two successive deswelling–swelling cycles before the room-temperature gel assumes its equilibrium collapsed conformation in methanol. They also exhibit reversible swelling–deswelling cycles, i.e., the gels return to their original shape and original mass after a short reswelling period. The collapsed gel formed at 17 °C reswells again within 3 days, compared to 10 min for gels formed at subzero temperatures. Similar results were reported for several cryogels formed below the transition temperature [26, 36, 63, 96]. For example, strong polyelectrolyte PAMPS cryogels prepared below –8 °C exhibit completely reversible swelling and deswelling cycles in water and acetone, respectively [36]. Those formed at higher temperatures were too soft in their swollen states in water; during the first deswelling process in acetone, they were broken into several pieces so that a cycle could not be completed. We have to note that cryogels starting from their dry states swell much faster than their collapsed states in equilibrium with a poor solvent. For example, PAAm cryogel, when collapsed in acetone, swells within 1 min to attain its equilibrium swollen state in water, whereas swelling takes only 4 s starting from its dry state [26]. The relatively slower rate of swelling of collapsed cryogels compared to dry gels is related to the nonsolvent molecules on the surface of the collapsed gel samples, which decrease the solvating power of the liquid around the gel sample and slow down the swelling process.

The mechanical properties of gels also change significantly below the transition temperature due to the cryo-concentration phenomenon. This is illustrated in
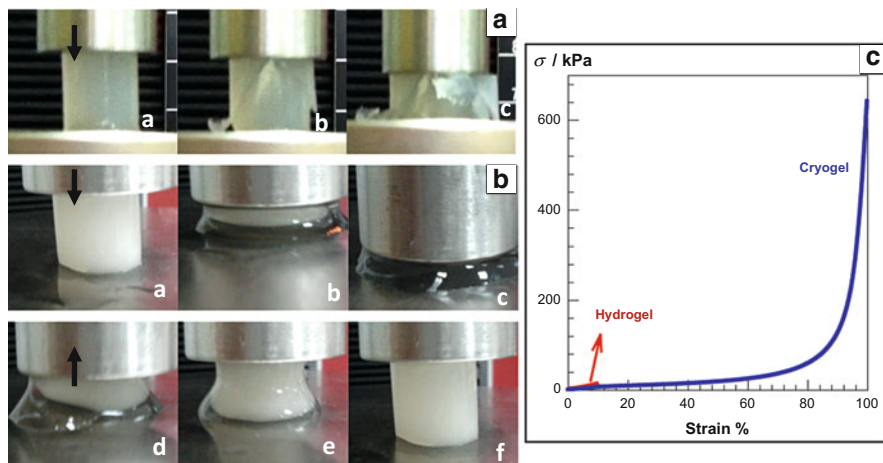
Fig. 9 Photographs of (**a**) fibroin hydrogels and (**b**) cryogels formed at $T_{prep} = 50$ and $-18\ °C$, respectively, during the compression tests. $C_{SF} = 4.2\ \%$; EGDE = 20 mmol/g; TEMED = 0.10 %. A*rrows* indicate the direction of piston movement. (**c**) Stress–strain curves of these gel samples are shown as the dependence of the nominal stress σ on the degree of compression. (From [50] with permission from the American Chemical Society)

Fig. 9a, b, which shows images of fibroin gels formed above and below the transition temperature, respectively [50]. The fibroin hydrogel formed at 50 °C ruptures under low deformation, indicating that the mechanical stress applied is localized without effective dissipation. However, fibroin cryogel formed at $-18\ °C$ remains mechanically stable up to almost complete compression. An important point is that, as the cryogel is squeezed under the piston or via manual hand compression, the gel releases all its water from within the pores so that it can be compressed up to 99.8 % compression ratio. Although no energy dissipation mechanism was introduced in the cryogels, release of water from the pores under stress seems to prevent crack formation at large deformation ratios. After release of the load, the gel sample immediately recovers its original shape by absorbing the released water. Figure 9c shows the stress–strain curves of these gel samples under compression. The hydrogel ruptures at about 10 % compression and at a compressive nominal stress of 15 kPa, whereas the cryogel sustains 99.8 % compression at 640 kPa stress. Successive compression tests conducted on the same gel sample between 0 and 99.8 % strain show reversibility of the stress–strain curves of the cryogels and reveal that no cracking occurs during the experiments [50]. The improved mechanical properties of cryogels originate from the high polymer content of the unfrozen liquid channels of the reaction system. Thus, after cryogelation, the gel channels with high polymer content are perfect materials for building the pore walls.

The experimental results thus indicate that the formation of cryogels requires a temperature T_{prep} of at least 8 °C below the bulk freezing temperature of solvent. In contrast, however, the theoretical results given in Fig. 6 predict that this transition
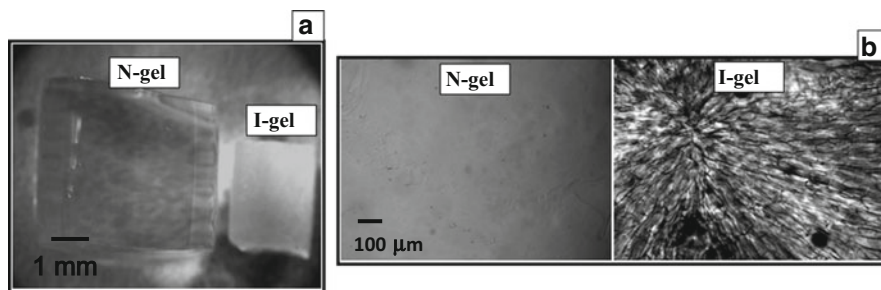
Fig. 10 (**a**, **b**) Different magnification images of swollen PAMPS gel samples taken using the optical microscope. The gels were prepared without (N-gel) and with precooling of the reaction solution (I-gel). $T_{prep} = -2\,^\circ C$, $X = 1/6$. The initial diameters of the gel samples were 4.3 mm. In their swollen states, the diameters became 9.80 mm (N-gel) and 4.65 mm (I-gel). *Scale bars*: 1 mm (**a**) and 100 μm (**b**). (From [23] with permission from Taylor & Francis Group, LLC)

should occur at temperatures close to the solvent freezing temperature. This discrepancy may partially be attributed to the nonequilibrium effects during freezing [91]. The concentrated unfrozen polymer solutions at low temperatures have high viscosities that may slow down the equilibration of solvent and the growth of solvent crystals to an extent that stops freezing. Moreover, the initial non-isothermal reaction period may also be responsible for the observed deviation from theory. We have to mention that T_{prep} is the temperature of the thermostated bath in which the gelation reactions are carried out. Since the polymerization initiator (or crosslinker) should be added into the monomer (or polymer) solution before freezing of the reaction system, the polymerization and crosslinking reactions proceed non-isothermally from the moment of initiator addition to the moment when the temperature of the reaction system reaches T_{prep}. Therefore, the time needed for bulk freezing of the reaction system strongly depends on T_{prep}. For example, aqueous reaction mixtures containing AMPS and BAAm at $T_{prep} = -22\,^\circ C$ became frozen within 4–5 min, whereas those at $-5\,^\circ C$ required more than 1 h for freezing [36]. Compared to these freezing times, the gelation time recorded using the falling-ball technique was 5 min at $0\,^\circ C$ [36]. Thus, gelation and gel growth reactions at $T_{prep} = -5\,^\circ C$ mainly proceed before the onset of bulk freezing of the system, whereas the reactions at $-22\,^\circ C$ occur in the unfrozen microzones. Therefore, variation in the cooling rate depending on T_{prep} may also be responsible for the appearance of porous structures at temperatures much below the bulk freezing point of the reaction system. This also suggests that isothermal gelation could provide formation of cryogels at a temperature close to the freezing point of the solvent.

To check this point, experiments were designed to control the freezing of the reaction solutions [23]. Figure 10a shows the images of two equilibrium swollen PAMPS gel samples prepared at $T_{prep} = -2\,^\circ C$. Both the gel samples were prepared under identical conditions except for the initial temperature of the gelation system. In the case of the isothermal gel (I-gel), after addition of the initiator into
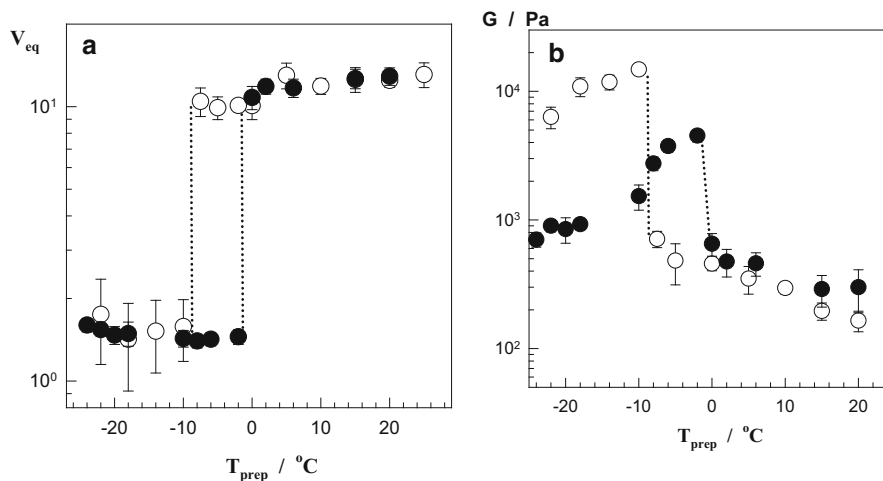
Fig. 11 The equilibrium volume swelling ratio V_{rel} (*left*) and the elastic modulus G of equilibrium swollen PAMPS hydrogels (*right*) shown as a function of T_{prep}. *Filled* and *open symbols* represent data obtained from I- and N-gels, respectively. $X = 1/6$. The *dotted lines* represent the transition temperature. (From [23] with permission of Taylor & Francis Group, LLC)

the reaction solution, the system was immediately cooled down to $-196\ ^\circ$C using liquid nitrogen and, then, the system was immersed into a thermostat at $T_{prep} = -2\ ^\circ$C. The reactions before reaching $-2\ ^\circ$C were very slow such that a near isothermal condition was provided. No such precooling step was applied for the preparation of the usual gel sample (N-gel). Although the initial diameters of both gel samples after their preparation were the same (4.3 mm), the swollen volume of N-gel was about tenfold larger than the volume of I-gel. Further, the N-gel was transparent while the I-gel was opaque, both after preparation and after equilibrium swelling in water. The magnified images of the equilibrium swollen gel samples taken with an optical microscope also illustrate the structural differences between the two gel samples (Fig. 10b). Whereas the N-gel was homogeneous in the swollen state, the I-gel exhibited a discontinuous morphology consisting of solvent and gel domains. This means that N- and I-gels prepared at the same T_{prep} are formed in homogeneous gelation and cryogelation regimes, respectively.

In Fig. 11, the equilibrium volume swelling ratio V_{eq} and the modulus of elasticity G of swollen PAMPS gels are shown as a function of T_{prep} [23]. Filled and open symbols represent data points obtained from I- and N-gels, respectively. It is seen that, providing isothermal gelation conditions, the transition temperature shifts from $-8\ ^\circ$C to a temperature close to the solvent freezing point ($-1 \pm 1\ ^\circ$C), as predicted by the simulation results (Fig. 6). Another point shown in Fig. 11 is that the elastic modulus of I-gels prepared below $-10\ ^\circ$C is much lower than that of N-gels. This is an indication of the reduced rate of the crosslinking reactions during the formation of I-gels. Thus, the network build-up process seems to take place mainly during the non-isothermal period between $0\ ^\circ$C and T_{prep} so that the I-gels prepared with precooling exhibit a lower modulus of elasticity than the N-gels.

4 Effect of Synthesis Parameters

The properties of cryogels depend on many parameters, including the cryogelation conditions and the composition of the reaction constituents. As the challenge is to control the porous structure and, thus, the cryogel properties, this section focuses on the effect of the synthesis parameters on the morphology of cryogels, with examples selected from the literature.

4.1 Temperature and Freezing Rate

It is known that the size of ice crystals can be controlled by varying the freezing temperature and the freezing rate. For example, to produce large ice crystals, the freezing temperature should be as high as possible and the time for crystallization should be extended. To produce small crystals, freezing should be at a very low temperature and the freezing rate should be high in order to reduce the time available for ice crystals to grow. Because solvent crystals in the cryogelation systems act as templates for the formation of pores, the same relationship usually exists between the pore size of cryogels and the gelation temperature T_{prep} [25, 39, 68]. Because the lower the T_{prep}, the faster the cooling rate of the gelation solution and, thus, the shorter the time period until the freezing temperature of the reaction solution is reached, the T_{prep} and the rate of cooling(or combination of both) do affect the properties of cryogels.

Ivanov et al. investigated the temperature-dependent variation of pore diameter in PAAm cryogels [43]. Cryogels were prepared by crosslinking of linear PAAm chains in aqueous solutions using glutaraldehyde as a crosslinker. It was shown that the pore diameter decreases from 30–60 μm to 10–20 μm as T_{prep} is decreased from −5 to −20 °C [43]. In PAAm cryogels prepared from AAm and BAAm monomers, the largest pore size was obtained at $T_{prep} = -18$ °C and decreased as T_{prep} was further reduced down to −24 °C (Fig. 7d) [26]. The average pore diameters were 60, 32, and 22 μm for $T_{prep} = -18, -20,$ and −22 °C, respectively. Similar results were also reported for cryogels derived from aqueous solutions of fibroin chains or DMA monomer (Fig. 12) [28, 50]. In PSA cryogels, the pore diameter decreases from 25 to 11 μm as T_{prep} is decreased from −9 to −20 °C [95]. Since lower T_{prep} means faster freezing of the reaction solution, decreasing pore size with decreasing T_{prep} is consistent with the fact that a larger number of small solvent crystals form as the freezing rate is increased. Additionally, since solvent in large voids is preferentially frozen relative to that in small capillaries due to a smaller freezing-point depression, it is thought that, at T_{prep} close to the solvent freezing point, only solvent in large voids freezes during gelation, leading to large pores. We have to note that there are also conflicting data regarding the temperature dependence of pore size, especially at very low temperatures. This is attributed to the weakness of the cryogel matrices formed at low T_{prep}, which leads to collapse of the porous structure upon drying.
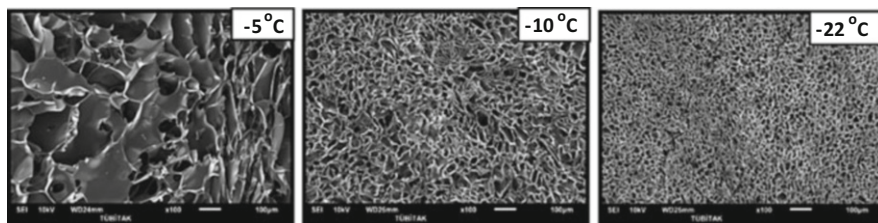
Fig. 12 SEM images of fibroin cryogel networks formed at the various temperatures (T_{prep}) indicated. S*cale bars*: 100 μm. (From [50] with permission from the American Chemical Society)

The formation of polyhedral pores in hydrophilic cryogels may be explained as follows [97, 98]: Water molecules in crosslinked hydrophilic polymers are known to exist in three states: (1) free water in the middle of the mesh of the network, (2) bound water adjacent to the network chains, and (3) film water adsorbed on the bound water layer. Freezing of free water and the growth of ice crystals thus formed may lead to deformation of the polymer network by stretching the hydrated network chains around the ice crystals. Although the polymer elasticity allows easy deformation of the network chains, the high viscosity of the system may slow down growth of the crystals. As a consequence, one may expect formation of ice crystals in the mesh of polymer network separated by swollen polymer chains. Moreover, the total surface energy of ice crystals is minimized by the crystals coming together, forming four ice crystals in contact, with angles of 120° where the forces of interfacial tension balance.

Experiments were also designed to study the effects of freezing rate on the morphology of the cryogels. For this purpose, one part of the reaction solution was slowly frozen in a freezer in contact with air, while the other part was fast frozen in a cryostat in contact with a liquid. The initial cooling rate decreased from 54 to 4 °C/min as the cooling liquid was replaced with cooling air at −18 °C [53]. Figure 13 shows SEM images of the PIB gel network prepared in cyclohexane at $T_{prep} = -10\,^{\circ}C$ under fast and slow freezing conditions [53]. It is seen that the size of the pores increases as the freezing rate decreases. Increasing the freezing rate of the reaction solution necessarily reduces the time available for solvent crystals to grow, which would inhibit the formation of large crystals. Thus, small solvent crystals form under fast freezing conditions, which leads to small pores after thawing. Further, increasing the freezing rate shortens the duration of the initial non-isothermal period of the reactions so that the crosslinking mainly occurs in the unfrozen microzones of the apparently frozen reaction system. This may also decrease the size of the pores.

A similar effect of the freezing rate of the gelation solution can be observed by changing the initiator concentration. During the preparation of PSA cryogels in aqueous solutions and using a APS/TEMED redox initiator system, increasing the APS concentration from 1.75 to 3.5 mm decreased the average pore size of the cryogels [95]. This is due to the faster rate of polymerization, which leads to smaller ice crystals. However, further increase in APS concentration decreases the porosity
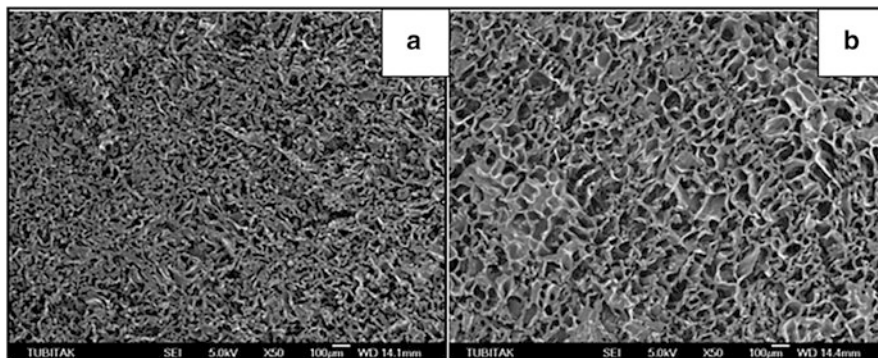
Fig. 13 SEM of PIB networks formed at $T_{prep} = -10\ °C$ under (**a**) fast and (**b**) slow freezing conditions. Reaction time = 3 days; S_2Cl_2 = 5.7 %. *Scale bars*: 100 μm. Magnification 50×. (Reprinted from [53] with permission from Elsevier)

of the cryogels due to the very fast polymerization that occurs before the freezing of the reaction solution. A similar effect of the initiator was also observed in the preparation of PAAm cryogels [25].

The preparation of aligned porous materials with micrometer-sized pores is of particular importance for applications such as tissue engineering, microfluidics, and organic electronics [99, 100]. It was shown that cryogels with an aligned pore structure could be prepared at low freezing rates (i.e., at temperatures close to the transition temperature to the cryogelation regime) or at low polymerization rates (i.e., at a low monomer concentration) [53, 101]. Another requirement is that the solvent used in the reactions should be a solvating diluent for the polymer so that no phase separation takes place during cooling of the gelation solution. For example, during the solution crosslinking of 5 % PIB in cyclohexane, cryogels start to form at or above $-2\ °C$ [53]. Moreover, the cyclohexane–PIB system did not show significant temperature effect and, thus, any liquid–liquid phase separation could be prevented during the cryogelation reactions of PIB. SEM images of dried cryogels formed at temperatures T_{prep} close to this upper temperature limit showed an oriented porous structure of the materials [53]. The micrographs in Fig. 14a,b show the alignment of the pores in the gel network formed at $T_{prep} = -2\ °C$. The structure consists of brick-shaped pores of about 100 μm in length and 50 μm in width, separated by pore walls of 10–20 μm in thickness. The aligned porous structure of the sample indicates directional freezing of the solvent crystals in the direction from the surface to the interior, i.e., in the direction of the temperature gradient. Note that experiments carried out by decreasing the reactor diameter from 16.4 to 3.7 mm partially destroyed the regularity of the pore structure, probably due to the increasing rate of freezing of the reaction solution. Decreasing the temperature or increasing the cooling rate also destroyed the regularity of the porous structure of the network. The pores of 10–100 μm in size formed at $-2\ °C$ became increasingly irregular as T_{prep} decreased [53].
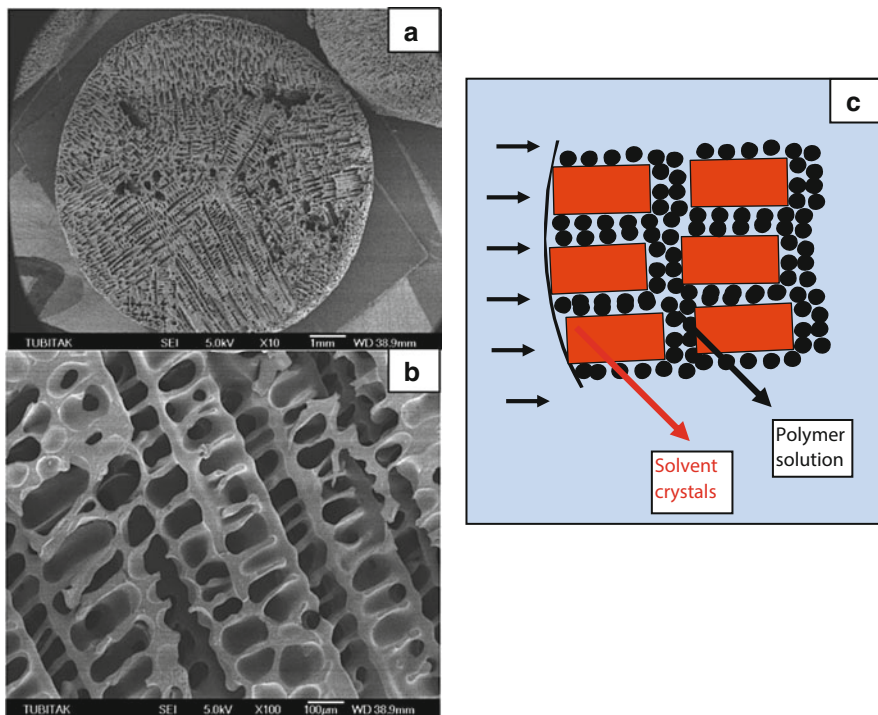
Fig. 14 (**a, b**) SEM of PIB network formed in cyclohexane at $T_{\text{prep}} = -2\ °C$. Reaction time = 24 h; $S_2Cl_2 = 5.7\ \%$.(**c**) Scheme showing the directional freezing of PIB solution from the surface to the interior at low cooling rates, i.e., at high T_{prep}. S*cale bars*: 1 mm (**a**), 100 μm (**b**). (Reprinted from [53] with permission from Elsevier)

Because of the poor thermal conductivity of the reaction solution, a temperature gradient is formed in the radial direction and freezing of the solvent cyclohexane starts from the surface of the cylindrical reactor, which is in contact with the cooling liquid at $-2\ °C$. As the solvent freezes, both the PIB chains and the crosslinker S_2Cl_2 are excluded from the solvent crystals due to cryo-concentration and aggregate around the growing crystals to form an unfrozen part of the system. This is illustrated schematically in Fig. 14c. As the freezing progresses, a polymer concentration gradient, as well as a temperature gradient, is established across the moving freezing front. This leads to macroscopic instabilities, due to which the moving freezing front collapses, leaving behind pockets of unfrozen concentrated polymer solution [99, 100]. Further, due to the relatively high T_{prep}, the freezing rate is slow so that the growing solvent crystals can be encapsulated in the concentrated solution and cannot grow further. Thus, directional freezing under a temperature gradient causes crystallization of many isolated solvent crystal phases, leaving an unfrozen gel phase with high polymer content. After the crosslinking reactions, the polymer phase becomes insoluble and, after thawing, preserves the structure that had been conferred to it by the surrounding solvent crystals.
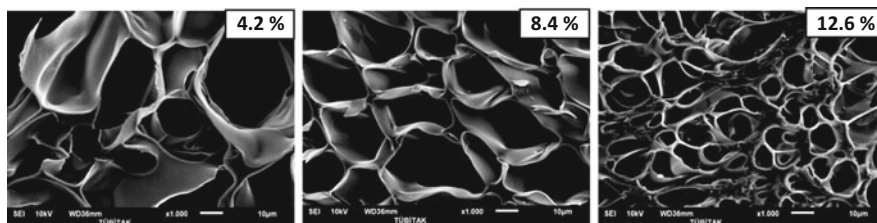
Fig. 15 SEM images of cryogel networks formed at the various fibroin concentrations indicated. S*cale bars*: 10 μm. (From [50] with permission from the American Chemical Society)

4.2 Monomer or Polymer Concentration

It was observed that the architecture or morphology of the cryogel network essentially does not depend on monomer concentration, whereas the size of the structure responds sensitively. In PAAm cryogels, the average pore diameter was found to decrease from 55 to 10 μm with increasing monomer concentration from 3 to 30 % [26]. At the same time, the average thickness of the pore walls increased from 3 to 15 μm. In PAAm cryogels with functional epoxy groups, Plieva et al. also reported decreasing pore size but increasing thickness of pore walls with increasing monomer concentration from 6 to 22 % at $T_{prep} = -12\,°C$ [24]. Kirsebom et al. also showed that larger pores and thinner pore walls in poly(DMA) (PDMA) cryogels can be produced from 3 wt% monomer concentration as compared to 12 wt% [28]. In contrast, however, an increasing pore size with increasing concentration was reported for PAMPS hydrogels obtained at $T_{prep} = -22\,°C$ [63]. This finding is attributed to collapse of the large pores in such polyelectrolyte gels formed at low monomer concentrations. In cryogelation reactions starting from polymer precursors, increasing the polymer concentration also leads to cryogels with thicker pore walls but a smaller pore size. For instance, at $T_{prep} = -18\,°C$, the pore diameter of fibroin cryogels decreased from 33 ± 10 to 10 ± 3 μm as the fibroin concentration increased from 4.2 to 12.6 % (Fig. 15) [50]. Thus, the higher the monomer (or polymer) concentration, the smaller the pore diameters and the thicker the pore walls [39]. The inverse relation between the precursor concentration and the pore size is related to the higher amount of unfrozen microdomains during gelation as the amount of solute is increased.

4.3 Charge Density

The pore diameters of nonionic PAAm and ionic PAMPS cryogels formed under identical conditions at $-22\,°C$ were reported as 100–150 and 30–50 μm, respectively [36]. Thus, the pore size decreases with increasing charge density of the network chains. Calculation results using (8) also predict that an increase in the

charge density f of the network chains would decrease the volume fraction of ice in the reaction system so that the pores in the final gels would be smaller [36].

4.4 Crosslinker Concentration

In PAAm and PSA cryogels formed using BAAm crosslinker, no appreciable change in the size of the pores was reported with changes in the crosslinker level [26, 95]. However, in fibroin cryogels formed at $T_{prep} = -18\ ^\circ C$ and in the presence of EGDE as a crosslinker, the average pore diameter decreased from 55 ± 10 to 23 ± 7 μm and the pore-size distribution became narrower as the amount of EGDE increased from 10 to 30 mmol/g [50]. Similar results were reported for rubber cryogels formed using S_2Cl_2 crosslinker. As S_2Cl_2 concentration is increased, both the polydispersity and the average diameter of the pores decrease [52]. This could be due to the increased rigidity of the gel in the unfrozen domains as the amount of crosslinker is increased.

4.5 Additives and Solvent

The presence of low molecular weight salts significantly affects the microstructure of the cryogels formed in aqueous solutions. For instance, addition of NaCl or $CaCl_2$ in aqueous cryogelation solutions results in materials with thicker pore walls and smaller pores [102]. As the NaCl content in the reaction mixture is increased from 0 to 10 % (w/w), the pore size of PAMPS cryogels decreases from 30–50 to 10–20 μm [36]. This is due to the fact that the addition of salts into the reaction system decreases the bulk freezing temperature so that the volume of the nonfrozen solution increases. This leads to the formation of gels with smaller pores. Indeed, as the NaCl content in the reaction mixture is increased from 0 to 10 %(w/v), the bulk freezing times of AMPS-BAAm reaction mixtures at $T_{prep} = -22\ ^\circ C$ increased from 5 to 35 min, whereas their gelation times at $0\ ^\circ C$ remained constant (5 ± 1 min) [36]. Moreover, addition of a polymerization inhibitor such as hydroquinone into the reaction solution produces more monodisperse and smaller pores in PAAm cryogels [23]. Hydroquinone provides homogeneous nucleation of ice crystals due to the shift of the gel point beyond freezing of the reaction solution, so that the number of crystals increases while their size decreases, leading to the formation of small pores in PAAm cryogels.

The addition of micro- or nanoparticles in the cryogelation system produces hybrid cryogels with increased modulus of elasticity [56, 103–106]. For instance, such cryogels were prepared by the addition of tetramethoxysilane in aqueous solutions of PVA before its freeze–thaw treatment [104]. They can also be prepared by crosslinking of PIB in cyclohexane containing silica nanoparticles and using S_2Cl_2 as a crosslinking agent [56]. The microstructure of the hybrid PIB cryogels

consists of two types of pores: 10^1 μm large pores due to the cyclohexane crystals acting as a template during gelation and 10^{-1}–10^0 μm small pores between the aggregates of the nanoparticles. The nanoparticles in hybrid cryogels accumulate within the large pores where cyclohexane crystals originally resided. The cryogels exhibit a 300-fold larger modulus of elasticity than those prepared in the absence of nanoparticles [56]. It was shown that these hybrid cryogels can be converted into organic cryogels by dissolving the silica component in aqueous hydrofluoric acid, whereas removing the polymer component by calcination results in porous silica networks with 10^{-1}-μm-sized pores [56].

The internal morphology of cryogels is also dependent on the type of solvent used in cryogelation reactions. This effect arises due to the different shape of solvent crystals as well as due to the temperature-dependent variations of the interactions between the polymer and solvent. For instance, PAAm cryogels prepared in formamide at −20 °C have an oriented porous structure with long pores as a result of the formation of needle-like formamide crystals [25]. Moreover, in contrast to the interconnected 3D pore structure of PNIPA cryogels formed in water, those formed in dioxane/water medium have a closed pore structure with thick (10–40 μm) pore walls [33]. The effect of polymer–solvent interactions on the morphology of cryogels can be illustrated using PIB cryogels formed in cyclohexane and in benzene under identical conditions. Besides their molecular sizes, benzene and cyclohexane have similar freezing and melting properties; they both form high temperature orientationally disordered crystals and their melting temperatures in the bulk are close (5.5 versus 6.5 °C for benzene and cyclohexane, respectively) [107]. However, since the chemical structure of cyclohexane is close to that of the repeating unit of polyisobutylene, it is a good solvent for PIB. In contrast to cyclohexane, benzene is a poor solvent for PIB and becomes poorer as the temperature decreases [53]. SEM images of PIB networks formed in benzene and in cyclohexane show different morphologies. In contrast to the regular morphology of the cryogels prepared in cyclohexane, those formed in benzene exhibit a broad size distribution of pores from micrometer to millimeter sizes [52]. Further, the total volume of pores V_p in PIB gels formed in benzene was found to increase from 6 to 9 mL/g as T_{prep} is decreased from −2 to −18 °C, in contrast to the value of about 2.5 mL/g for all low-temperature gels formed in cyclohexane [52, 53]. The differences observed in the morphology of the gels are due to the cooling-induced phase separation of the PIB chains in benzene [52]. Thus, the gel cannot absorb all the available solvent during gelation so that a macrophase separation should occur during the initial non-isothermal period of the reactions.

If the cryogelation reactions are conducted in a good solvent/poor solvent mixture, the mechanism of pore structure formation by cryogelation can be combined with the reaction-induced phase separation. For instance, PAAm cryogels formed at −12 °C in acetone–water mixtures exhibit two types of pores [102]. The 10–80 μm large pores are due to the ice crystals acting as a template during gelation while the submicrometer-sized pores in the pore walls are due to the χ-induced phase separation in the unfrozen phase enriched with acetone (a poor solvent for PAAm) and the monomers [102]. Another interesting example is PAAm cryogels

prepared at -18 °C in aqueous DMSO solutions of various compositions [59]. DMSO–water mixtures exhibit a marked freezing point depression and the reaction system will freeze at -18 °C if the DMSO content is less than about 30 % (v/v). Indeed, the hydrogels formed in the solvent mixture with less than 30 % DMSO by volume have irregular large pores of about 10^1 μm in diameter, typical for macroporous networks created by the cryogelation technique. Nonporous hydrogels were obtained in solutions containing 25 % DMSO, while at larger DMSO contents the structure of the hydrogel networks consists of aggregates of microspheres that look like cauliflowers, as typical for a macroporous network formed by a reaction-induced phase separation mechanism [59]. The results were interpreted as a transition from cryogelation to phase separation copolymerization due to the marked freezing point depression of the solvent mixture, as well as due to the action of the mixed solvent as a poor solvating diluent at -18 °C [59].

5 Novel Cryogels and Their Applications

In this section, some novel cryogel materials based on DNA, silk fibroin, poly (acrylic acid), and several types of rubber are presented, and their applications in various fields are summarized.

5.1 DNA Cryogels for Removal of Carcinogenic Agents

Deoxyribonucleic acid (DNA) serves as the carrier of genetic information in living organisms and is composed of building blocks called nucleotides, which consist of deoxyribose sugar, a phosphate group, and four bases (adenine, thymine, guanine, and cytosine). DNA has a double-helical (ds) conformation in its native state, which is stabilized by hydrogen bonds between the bases attached to the two strands [108]. When a DNA solution is subjected to high temperatures, the hydrogen bonds holding the two strands together break and the double helix dissociates into two single strands (ss) having a random coil conformation [109]. Due to its unique ds-structure, DNA has highly specific functions, such as intercalation, groove-binding interactions, and electrostatic interactions. These functions are specific for DNA molecules and are difficult to reproduce in synthetic polymers. Although films and fibers can be prepared from DNA, such materials are water soluble, biochemically unstable, and mechanically weak.

A DNA hydrogel is a network of chemically crosslinked DNA strands swollen in aqueous solutions [110–112]. Such soft materials are good candidates for making use of characteristics of DNA such as coil–globule transition, biocompatibility, selective binding, and molecular recognition [113, 114]. DNA hydrogels can be prepared by crosslinking of DNA in aqueous solutions at 50 °C using diepoxides such as EGDE or BDDE as chemical crosslinking agents [112, 115]. The reaction

between epoxides and DNA is of nucleophilic substitution type (S_N2 reaction) and occurs at the nucleophilic sites in DNA, mainly at the N7 position of guanine. DNA hydrogels are responsive systems that exhibit drastic volume changes in response to external stimuli, such as acetone [115], poly(ethylene glycol) [112], inorganic salts [116, 117], polyamines [117], cationic macromolecules [118], or surfactants [117]. Responsive DNA hydrogels with a wide range of tunable properties, such as the conformation of the network strands, viscoelasticity, and nonlinear elasticity (strain hardening), have been prepared in the past few years [111, 112, 119].

Recently, DNA cryogels with excellent mechanical properties have been obtained by conducting gelation reactions at subzero temperatures [47, 48]. DNA cryogels were prepared at $T_{prep} = -18$ °C from frozen aqueous solutions of ds-DNA (about 2,000 base pairs long) containing BDDE crosslinker and TEMED catalyst. Infrared (IR) and fluorescence measurements show the predominantly ds-DNA conformation of the network chains of DNA cryogels. An almost complete conversion of soluble to crosslinked DNA required 3 % DNA and 0.39 % BDDE, corresponding to the presence of an equimolar ratio of epoxy to DNA base pair in the gelation solutions [48]. DNA cryogels exhibited weight swelling ratios (q_w) between 40 and 130, indicating that they are in a highly swollen state with 98–99 % water in the cryogel structure. However, their volume swelling ratios q_v are about one order of magnitude smaller than their weight swelling ratios q_w. The total porosity P_s of the cryogels estimated from their q_w and q_v values using (4) is 93–99 % for all the cryogels. The total volume of the pores V_p in the cryogels, estimated from the uptake of methanol, is between 3 and 20 mL/g, indicating that the total pore volume of the cryogel samples is much larger than the bulk gel volume. This suggests that most of the water in swollen cryogels is within the pores, while the crosslinked DNA forming the pore walls is less swollen. Mechanical tests show that the cryogels formed at 5 % DNA are very tough and can be compressed up to about 80 % strain without any crack development [48]. They also exhibit completely reversible swelling–deswelling cycles in response to solvent changes.

Carcinogenic agents having planar aromatic groups can intercalate into DNA double helices, which means that DNA can be used to prepare selective and efficient adsorbents of such specific toxic agents. It was shown that DNA cryogels can be used for the removal of such toxic agents from aqueous solutions [47, 48]. This is exampled by use of the classical intercalator ethidium bromide (EtBr), which is a four-ringed aromatic molecule with three of the rings conjugated. The nature of the interaction of EtBr with DNA has been examined by a variety of techniques over the past 50 years [120–123]. It is generally recognized that the strong mode of binding of EtBr to ds-DNA results in the intercalation of the planar phenanthridium ring between adjacent base pairs on the double helix. The intercalation of EtBr both increases the distance between base pairs by 0.3 nm and unwinds the double helix by 26°, which causes an increase in length of the DNA [124, 125]. Moreover, at high concentrations, EtBr also interacts with DNA by electrostatic interactions.

Figure 16a shows the EtBr concentration in the external solution ($C_{f, t}$) plotted against the contact time t with DNA cryogels [48]. For comparison, the behavior of
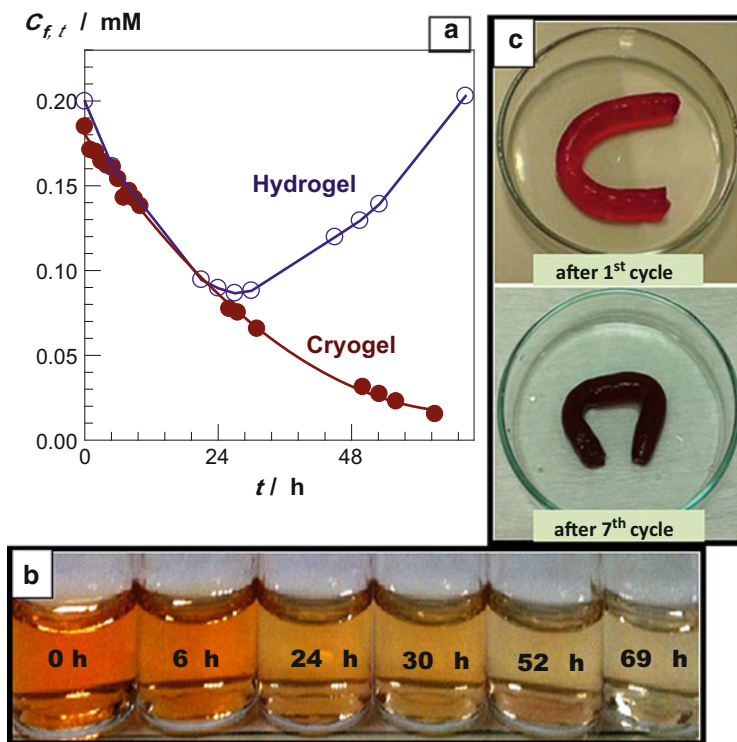
Fig. 16 (**a**) EtBr concentration ($C_{f,t}$) in the external solution plotted against the contact time t with the cryogel and hydrogel of DNA. (**b**) Images of the external EtBr solution at various times during the first absorption cycle using DNA cryogel. (**c**) Images of DNA cryogel after the first and seventh absorption cycles. (From [48] with permission from Elsevier)

DNA hydrogels prepared by usual gelation process is also shown. The initial EtBr concentration in the solution is 0.2 mM. During the first 24 h, $C_{f,\,t}$ decreases with almost the same rate, and both gel samples bind 0.10–0.15 mol EtBr per mole of nucleotide. At longer times, the hydrogel sample starts to disintegrate, as can be seen in Fig. 16 from the increase in EtBr concentration. After about 3 days, DNA hydrogel completely dissolved in EtBr solution (see below for explanation). In contrast, the DNA cryogel remained stable over the whole time period while continuously absorbing EtBr, during which time the color of the solution changed from red to clear (Fig. 16b). This highlights the stability of DNA strands in the cryogels and, thus, demonstrates that DNA cryogels are effective sorbents as compared to DNA hydrogels. The cryogel samples subjected to nine successive sorption cycles in 0.2 mM EtBr solutions also remained stable in aqueous solutions. As can be seen in Fig. 16c, the color of the cryogel changes from clear to red during the first cycle and becomes dark red after seven cycles, revealing an increasing amount of bound EtBr in the cryogel.
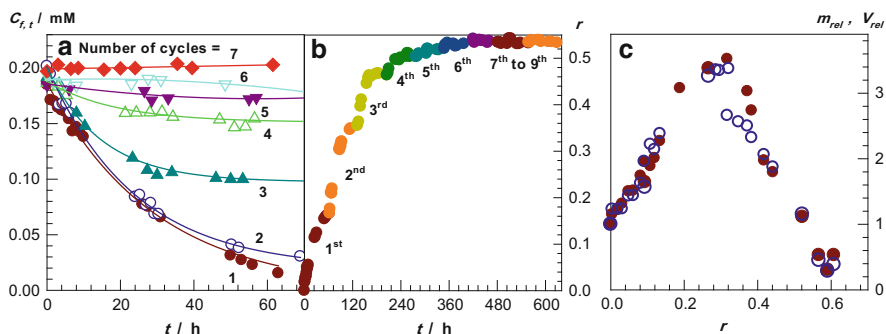
Fig. 17 (**a**) EtBr concentration ($C_{f, t}$) plotted against the contact time t for DNA cryogels. The results of seven successive sorption cycles are shown. (**b**) EtBr bound per nucleotide r plotted against the cumulative contact time t of nine successive cycles. (**c**) Relative gel mass m_{rel} (*filled symbols*) and volume V_{rel} (*open symbols*) of DNA cryogels shown as a function of r. (From [48] with permission from Elsevier)

The results of seven successive sorption cycles are shown in Fig. 17a, where $C_{f, t}$ is plotted against the contact time with the DNA cryogel. During the first two cycles, EtBr concentration decreases from 0.2 mM to about 0.02 mM, i.e., 90 % of the EtBr in the solution is absorbed by the cryogel. The sorption capacity decreases in the following cycles and the cryogel saturates after six cycles. In Fig. 17b, the number of EtBr molecules bound per nucleotide (denoted by r) is plotted against cumulative contact time of successive cycles. A rapid sorption of EtBr by the cryogel up to $r =0.45$, followed by a slow sorption process, can be seen from the figure. Repeated tests showed that the total capacity of the cryogels is 0.6 ± 0.1 EtBr molecules per nucleotide. Since the maximum amount of EtBr that can bind to DNA is one molecule per base pair, the results show that this value can be achieved using cryogels without disturbing the integrity of the gel structure.

The swelling behavior of the cryogels depending on the amount of bound EtBr per nucleotide is illustrated in Fig. 17c [48]. Here, the normalized cryogel mass m_{rel} and volume V_{rel} with respect to those in pure water are shown as a function of r. At low ratios of bound EtBr to DNA ($r < 0.3$), the gel swells with increasing amount of bound EtBr. After a 3.5-fold increase in the volume and mass of the gel at $r = 0.3$, it starts to deswell again and finally attains a compact mass at $r = 0.6$. The equality of mass and volume changes of the cryogels demonstrates that this unusual swelling behavior is related to the gel structure, but not the porosity changes depending on EtBr binding.

To understand the unique swelling behavior of DNA cryogels in EtBr solutions, one has to consider the nature of interactions of EtBr with nucleic acids in aqueous solutions. Previous studies indicate the existence of two main types of EtBr binding to DNA [121, 122]. At low values of r, EtBr binds strongly to DNA sites by intercalation, which appears to be saturated when one EtBr molecule is bound for every 2.1 ± 0.2 base pairs, i.e., $r = 0.24 \pm 0.02$. This is the accepted maximum

value for intercalation based on the neighbor exclusion model. Sorption of EtBr by the cryogels with 90 % efficiency, observed at $r < 0.25$, is thus attributed to the intercalation of EtBr within the double helical DNA strands. Moreover, the intercalation of EtBr into DNA changes the rotation angle between adjacent base pairs and unwinds the helix, resulting in lengthening of the DNA strand [124, 125]. This process also increases the viscosity of DNA solutions due to the increasing hydrodynamic size of DNA strands [126]. The extent of the increase in viscosity depends on the number of EtBr molecules bound per nucleotide; this behavior is also a characteristic of all DNA intercalators. Thus, the initial swelling of DNA gels at $r < 0.3$ may originate from the increasing length of DNA network chains, which decreases the elastically effective crosslink density of the cryogels. We should mention that the disintegration of DNA hydrogels at $r = 0.10–0.15$ could also be related to this phenomenon (Fig. 16a). Lengthening and stiffening of the helix due to intercalated DNA decreases the crosslink density of the hydrogels [48], leading to their dissolution in EtBr solutions. In contrast, cryogels are stable in EtBr solutions due to the dense pore walls formed during cryo-concentration.

The swelling response of DNA cryogels to changes in EtBr concentration between 3 and 300 μM also suggests that they can be used to detect DNA-binding substrates in aqueous solutions. On the other hand, it was reported that at high r ratios ($r > 0.25$), after the primary sites of DNA have been filled, a secondary binding process occurs arising from electrostatic interactions between phosphate residues and EtBr molecules attached outside the helix. As a consequence, in this range of r, the cryogel deswells with increasing concentration of EtBr, which is similar to the behavior of polyelectrolyte hydrogels immersed in aqueous solutions of increasing salt concentration. The results thus show that DNA cryogels can be used as a specific sorbents to remove carcinogenic agents from aqueous solutions. Moreover, the response of DNA cryogels to changes in EtBr concentration between 3 and 300 μM also suggests that they can be used to detect DNA-binding substrates in aqueous solutions.

5.2 Fibroin Cryogels as Mechanically Strong Scaffolds

Silk fibroin derived from *Bombyx mori* is a fibrous protein exhibiting extraordinary material properties such as good biocompatibility, biodegradability, high strength and toughness, and ease of processability [127–129]. Silk fibroin has been used for cell culture, wound dressing, drug delivery, enzyme immobilization, and as a scaffold for bone tissue engineering [130, 131]. Silk fibroin has a blocky structure consisting of less-ordered hydrophilic blocks and crystallizable hydrophobic blocks [132–135]. Hydrophilic blocks provide solubility in water and are responsible for fibroin elasticity and toughness, whereas hydrophobic blocks form intermolecular β-sheet structures leading to the insolubility and high strength of fibroin. Several techniques have been developed to produce porous fibroin scaffolds such as freeze–thawing, porogen leaching, gas foaming, electrospinning, and freeze-drying

[136–146]. The principle of the porogen leaching and gas foaming techniques is the use of porogens, such as sodium chloride and ammonium percarbonate acting as a template and gas-forming agent, respectively. After treatment of fibroin/porogen composites with alcohols to induce β-sheet formation, the porogen is leached out with water to form the pores of the scaffolds. To produce fibroin scaffolds by freeze-drying, aqueous fibroin solutions are mixed with alcohol to obtain a gel precipitate following freezing at a low temperature, and are finally freeze-dried [137]. It was shown that the porogen leaching and gas foaming techniques produce scaffolds having larger pores (100–200 μm) than the scaffolds formed by freeze-drying (10–50 μm). The compressive moduli of the scaffolds vary, depending on the preparation conditions between 10 kPa and 3 MPa.

An alternative simple route for the production of 3D highly porous fibroin networks is the cryogelation technique. Silk fibroin cryogels with remarkable properties were recently obtained from frozen fibroin solutions (4.2–12.6 %) at subzero temperatures between −5 and −22 °C [50]. This was achieved by the addition of EGDE to the cryogelation system. It was shown that the cryogelation reactions conducted in the absence of EGDE did not lead to gel formation after 1 day of reaction time, indicating that cryo-concentration alone does not induce fibroin gelation. Experiments indicate that the presence of EGDE triggers the conformational transition of fibroin from random coil to β-sheet structure and, hence, fibroin gelation [49, 50]. Figure 18a shows the amide I band region of ATR-FTIR spectra, presenting the carbonyl stretching vibration of amide groups on silk fibroin. The spectrum of fibroin before gelation (dotted curve in Fig. 18a) is characterized by a peak at 1,640 cm^{-1}, which indicates the presence of primarily random coil and/or β-helix conformations [147, 148]. After cryogelation, all samples display a main peak at 1,620 cm^{-1}, which was assigned to the β-sheet conformation [148]. In addition to the main peak, shoulders at 1,660 and 1,698 cm^{-1} are seen, which can be assigned to α-helix and β-turn conformations, respectively. This indicates the occurrence of a conformational transition from random coil to β-sheet structure in frozen fibroin solutions. Further evidence for the β-sheet formation comes from the X-ray profiles of freeze-dried cryogels (Fig. 18b). Silk fibroin before gelation (dotted curve in Fig. 18b) exhibits a broad peak at around 22°, indicating an amorphous structure [149]. After gelation, all the cryogels show a distinct peak at 20.9° and two minor peaks at 9.8 and 24.5°. These are the characteristic peaks of the β-sheet crystalline structure of silk fibroin, corresponding to β-crystalline spacing distances of 4.3, 9.0, and 3.6 A°, respectively [149, 150]. The results of β-sheet content analysis show that fibroin chains before gelation have 12 ± 2 % β-sheet structures, while their contribution increases to 33 ± 2 % [50].

One of the unique features of fibroin cryogels is their elasticity, which allows them to resist compression without any crack development. All the cryogel samples were very tough and could be compressed up to about 99.8 % strain without any crack development; during compression, water inside the cryogel was removed (Fig. 9). Upon unloading, the compressed cryogel immediately swelled to recover its original shape.
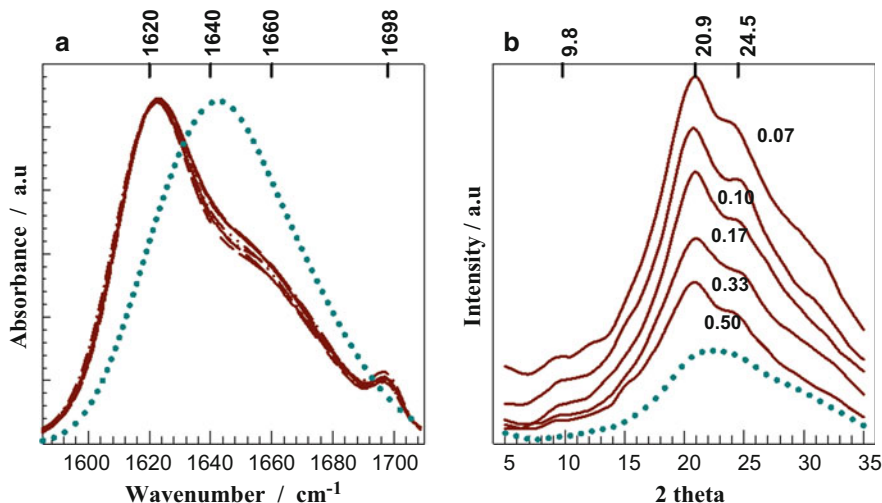
Fig. 18 Amide I region of (**a**) FTIR spectra and (**b**) X-ray diffraction profile of freeze-dried fibroin cryogels. Data obtained by freeze-drying of silk fibroin solutions before gelation are also shown (*dotted curves*).(**a**) TEMED content (%): 0.07 (*solid curve*), 0.10 (*long dash*), 0.13 (*short dash*), 0.17 (*short-long*), 0.25 (*dash-dot-dot*), 0.33 (*short-long-short*), and 0.50 % (*dash-dot*). (**b**) TEMED content (%) is indicated on the curves. $T_{prep} = -18$ °C; $C_{SF} = 4.2$ wt%; EGDE = 20 mmol/g. (From [50] with permission from the American Chemical Society)

It was shown that the critical stress σ_p corresponding to the plateau regime in the stress–strain curves of cryogel scaffolds increases with decreasing pore diameter, that is, with decreasing gelation temperature T_{prep} or with increasing fibroin or EGDE concentrations [50]. Figure 19a shows the stress–strain curves of cryogel scaffolds formed at $T_{prep} = -18$ °C and at three different fibroin concentrations C_{SF}. Inspection of the curves reveals that the critical stress σ_p increases from 0.6 to 4.4 MPa with increasing fibroin concentration C_{SF} from 4.2 to 12.6 %, i.e., with decreasing pore diameter from 33 to 10 μm (Fig. 15). The results suggest an increasing mechanical stability of the porous structure of fibroin scaffolds with decreasing size of the pores. Indeed, the compressive modulus and the compressive stress measurements of the scaffolds support this finding. The cryogel scaffolds formed at $T_{prep} = -18$ °C and $C_{SF} = 4.2$ % exhibit a compressive modulus E of 8 ± 1 MPa, with a compressive nominal stress σ_{comp} of 0.22 ± 0.04 MPa. These values are about one order of magnitude higher than those of the hydrogel scaffolds formed at $T_{prep} = 50$ °C. As illustrated in Fig. 19b, the modulus E and the compressive stress σ_{comp} further increase to 48 and 1 MPa, respectively, as C_{SF} is increased from 4.2 to 12.6 %.

We have to mention that fibroin scaffolds formed by freeze-drying of fibroin solutions pretreated with alcohols exhibit compression moduli of 10–100 kPa, whereas the salt leaching method generates scaffolds with a modulus of 0.5 MPa [137]. The largest compressive modulus and compressive strength reported so far
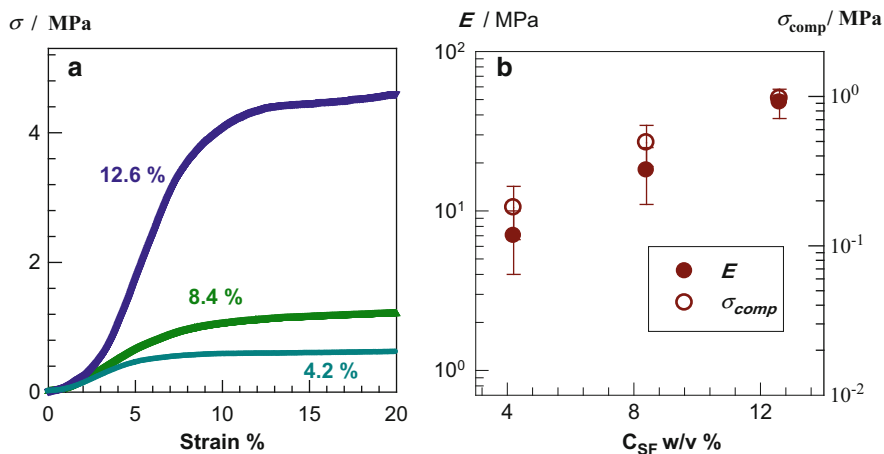
Fig. 19 (a) Stress–strain curves of fibroin scaffolds formed at various C_{SF}, shown as the dependence of the nominal stress σ on the degree of compression. C_{SF} as indicated in the figure; $T_{prep} = -18\ °C$; EGDE = 20 mmol/g; TEMED = 0.25 %. (b) The compressive modulus E and compressive stress σ_{comp} of fibroin scaffolds are shown as a function of fibroin concentration C_{SF} in the feed. $T_{prep} = -18\ °C$; EGDE = 20 mmol/g; TEMED = 0.25 %. (From [50] with permission from the American Chemical Society)

for fibroin scaffolds are 3 MPa and 60 kPa, respectively, which were for gels produced by the gas foaming technique [137]. Thus, as compared to other techniques, cryogelation conducted at $T_{prep} = -18\ °C$ and using 12.6 % fibroin in the feed leads to fibroin scaffolds exhibiting 16-fold larger modulus and strength (48 ± 10 MPa and 970 ± 50 kPa, respectively). The extraordinary strength of the cryogel scaffolds originates from the high fibroin concentration of the pore walls; gelation in frozen solutions confines the fibroin in a small region of the reaction volume, forming the pore walls of the final material. This also provides a high degree of toughness to cryogels in their swollen states.

5.3 Poly(Acrylic Acid) Cryogels as Self-Oscillating Systems

Conventional responsive hydrogels either swell or deswell in contact with external stimuli, that is, they make only a single action in response to external variables. In contrast, however, the so-called self-oscillating hydrogels exhibit swelling–deswelling cycles in contact with a solution [151]. Thus, self-oscillating hydrogels create dynamic rhythms and may open new application areas such as self-walking microactuators or micropumps with peristaltic motion, pacemakers, timers, and oscillatory drug release systems [151].

Self-oscillating hydrogel systems can be designed by coupling a responsive hydrogel sample with oscillating chemical reactions. For example, the Belousov–Zhabotinsky (BZ) reaction is a well-known oscillating system and the overall process of the reaction is the oxidation of a substrate such as malonic acid in the presence of oxidizing agent (bromate) and metal catalyst in an acidic solution [152, 153]. Yoshida and coworkers used poly(N-isopropyl acrylamide) gel in a BZ reaction to produce a self-oscillating gel system [151, 154]. Crook et al. used poly(methacrylic acid) (PMAAc) gel in a Landolt oscillating reaction system consisting of bromate, sulfite, and ferrocyanide ions [155, 156]. Although the actual mechanism of this bromated oscillation system is complicated, the overall reaction consists of two main steps: (1) the oxidation of sulfite by bromate and (2) the oxidation of ferrocyanide by bromate, i.e., [155]:

$$BrO_3^- + 3HSO_3^- + H^+Br^- + 3SO_4^{2-} + 4H^+ \tag{11a}$$

$$BrO_3^- + 6Fe(CN)_6^{4-} + 6H^+Br^- + 6Fe(CN)_6^{3-} + 3H_2O \tag{11b}$$
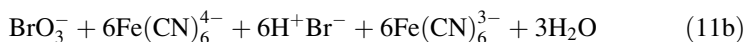
Thus, the first reaction produces H^+ ions so that pH of the reaction solution decreases, while the second reaction consumes H^+ ions so that the pH again increases. In response to the oscillatory pH changes in solution, a weak polyelectrolyte gel such as PMAAc oscillates between swollen and collapsed states.

However, all of the self-oscillating conventional hydrogels are limited in their size to microscopic dimensions, due to their slow rate of response to external stimuli. Recently, it was shown that centimeter-sized poly(acrylic acid) (PAAc) cryogels can be used as a pH oscillator in oscillatory bromate–sulfite–ferrocyanide reactions [31]. The cryogels were prepared at $-18\,°C$ from frozen aqueous solutions of acrylic acid (AAc) monomer and BAAm crosslinker. Fast responsive macroporous PAAc cryogels could be obtained at an initial monomer concentration C_o of $\leq 4\%$ (w/v). In Fig. 20, the diameter D of PAAc cryogels formed at $C_o = 2\%$ is shown as a function of time during three successive deswelling–reswelling cycles in methanol and water, respectively. The gel diameter D varies between 8 and 2 mm, i.e., the gel exhibits completely reversible cycles. This 64-fold change in the gel volume during the swelling–deswelling cycles does not induce any crack formation, and the network structure remains stable. The results thus suggest that such gel samples are useful materials in oscillating reaction systems.

Indeed, PAAc cryogels coupled with a bromate oscillator oscillated between swollen and collapsed states [31]. The reactions of bromate, sulfite, and ferrocyanide ions were conducted in an open continuously stirred tank reactor. Four feed solutions (potassium bromate, sodium sulfite, potassium ferrocyanide, and sulfuric acid) were supplied continuously to the reactor, during which the pH of the reaction solution was monitored as a function of time. The flow rate of the feed solutions is an important parameter in determining the extent of pH oscillations. In Fig. 21, pH versus time plots are shown for four different reduced flow rates k, defined as the flow rate of the feed solutions divided by the reaction volume. It is seen that the pH of the solution oscillates between 6.2–6.9 and 3.2–3.8. The dissociation degree α of a weak electrolyte relates to pH by:
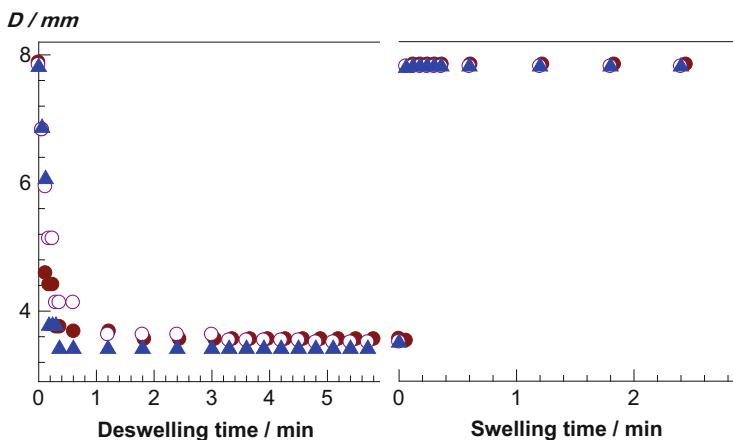
Fig. 20 Deswelling–reswelling kinetics of PAAc cryogels formed at 2 % initial monomer concentration are shown as the variation in gel diameter D with time. The data points are results of the measurements during the first (*filled circle*), second (*open circle*), and third (*filled triangle*) deswelling–reswelling cycles. (From [31] with permission from John Wiley & Sons)

$$\text{pH} \; = \; pK_a \; + \; \log\left(\frac{\alpha}{1-\alpha}\right) \tag{12}$$

Using $pK_a = 4.25$, as reported for PAAc gels [157], one may calculate the dissociation degree α as 0.15 and 0.99 for pH values of 3.5 and 6.5, respectively. Thus, if PAAc gel is immersed into this solution, the concentration of the mobile ions (Na^+) inside the gel will change sevenfold during these pH oscillations. Figure 21 also shows that the larger the flow rate k, the larger the extent of oscillation. Furthermore, increasing flow rate also increases the time period at high and low pH values. For example, at $k = 1\times10^{-4}$ and 1×10^{-3} s^{-1}, the pH of the solution remains above pH 6 for 25 and 75 min in each cycle, respectively. The results in Fig. 21 also demonstrate that the oscillation proceeds monotonically with fixed values of the maximum and minimum pH.

Figure 22 demonstrates the behavior of PAAc cryogels in this pH oscillating system. Here, the pH and the gel diameter D are plotted as a function of time at a flow rate $k = 5\times10^{-4}$ s^{-1}. Gel samples of 5 mm in diameter and about 1 cm in length (approximately 1 cm^3) were used in the experiments. Images of the gel samples were taken every minute using an image analyzing system, while the pH of the solution was also monitored by PC. The images in Fig. 22 were taken from the gel sample in swollen and collapsed states. It is seen that, depending on the pH oscillations, the diameter of the gel sample periodically varies between 7 and 5 mm, indicating a threefold change in the gel volume.

At high pH, the concentration of the mobile ions inside the PAAc cryogel increases (12) so that the difference between the mobile ion concentration inside
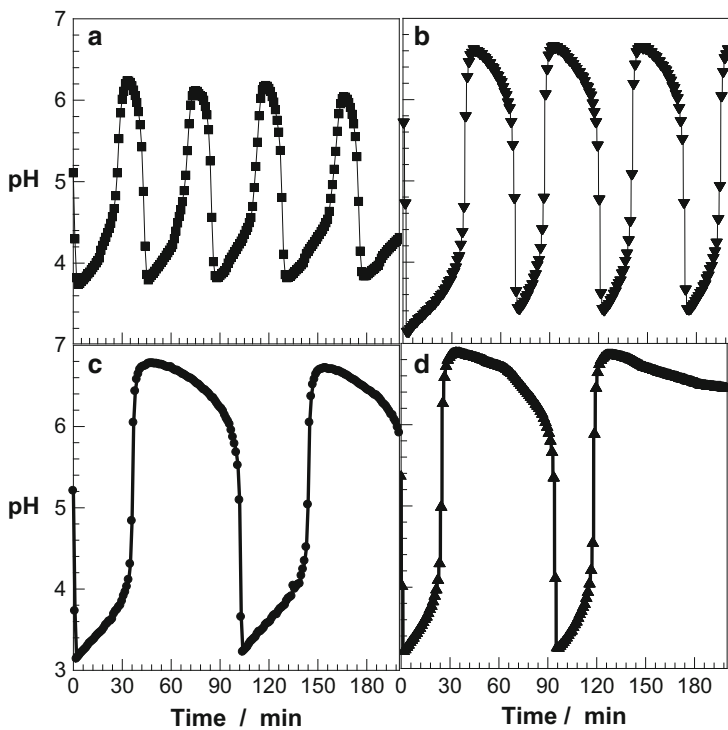
Fig. 21 (**a–d**) pH of the reaction solution shown as a function of time. Flow rate $k = 1 \times 10^{-4}$ (**a**), 2×10^{-4} (**b**), 3.5×10^{-4} (**c**), and 10×10^{-4} s^{-1} (**d**). (From [31] with permission from John Wiley & Sons)

and outside the gel rises, which creates additional osmotic pressure that expands the gel. The opposite behavior occurs at low pH, which induces deswelling of the gel sample. However, the extent of volume change in the pH oscillating reaction is much smaller than that observed in swelling–deswelling experiments, as shown in Fig. 20. This is due to the high salt concentration in oscillating reaction systems, which partially screens the charge interactions within the cryogel.

The results thus show that PAAc cryogels produce periodic swelling–deswelling oscillations in the bromate oscillation system. As the response rate of cryogels does not depend on their size, much larger cryogel samples can also be used in self-oscillating systems. This suggests that, like the back-and-forth motion of a piston of a heat engine, a pH-responsive cryogel could be used as a working substance to convert random molecular energy into macroscopic mechanical energy of lower entropy.
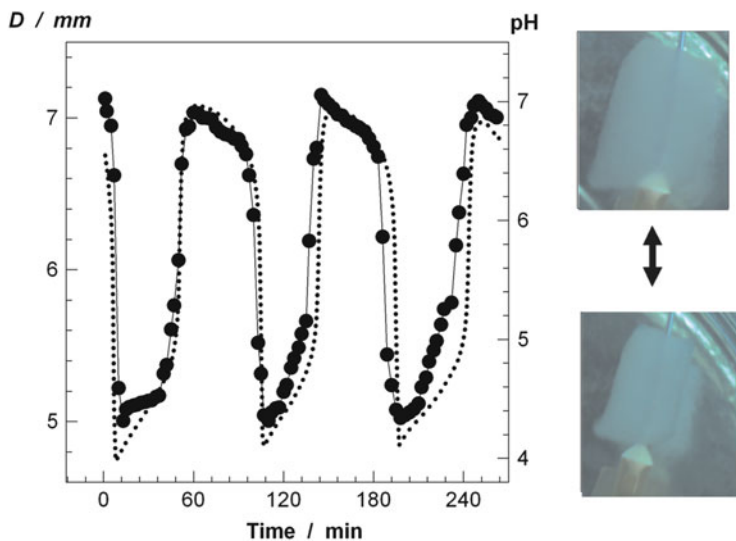
Fig. 22 Variations in pH (*dotted curves*) and gel diameter D (*symbols*) as a function of time. Flow rate $k = 5 \times 10^{-4} \, \text{s}^{-1}$. The pictures on the *right* show the gel samples at high and low pH. (From [31] with permission from John Wiley & Sons)

5.4 Rubber Cryogels as Reusable Oil Sorbents

Accidents involving oil tankers can result in the release of large volumes of crude oil, and this risk significantly increases along narrow seaways with heavy maritime traffic. Removal of crude oil and petroleum products that are spilled at sea has been a serious problem in recent decades [158]. Among existing techniques for the removal of oil, the use of sorbents is generally considered to be one of the most efficient techniques [159, 160]. The properties of an ideal sorbent material for oil spill cleanup include hydrophobicity, high uptake capacity and high rate of uptake, buoyancy, reusability or biodegradability, and recoverability of oil. Although several materials have been proposed as sorbents for oil removal, polymeric materials based on nonwoven polypropylene are the most commonly used commercial sorbents in oil spill cleanup [161–165]. However, commercial oil sorbents are not reusable, meaning that they form a solid waste after the cleanup procedures.

The reusability of the sorbents and the recoverability of the crude oil are important aspects of oil spill cleanup procedures. Because cryogels are squeezable gels and the liquid in the cryogels can simply be recovered via manual hand compression, hydrophobic cryogels are good candidates as oil sorbents for oil spill removal. The most suitable polymeric precursor for the preparation of cryogels as sorbent for crude oil can be estimated using the solubility parameters. According to the Hildebrand theory [166], the solvating (swelling) power of a polymer–solvent medium can be estimated from $(\delta_1 - \delta_2)^2$, where δ_1 and δ_2 are the solubility

parameters for the solvent and the polymer, respectively. The solubility of a polymer in a solvent is favored when $(\delta_1 - \delta_2)^2$ is minimized, i.e., when the solubility parameters of the two components are most closely matched. The value of δ_1 for aliphatic and some aromatic hydrocarbons, as a model for crude oil, is close to the δ_2 of rubbers such as PIB, CBR, and SBR (16.5–16.8, 18.0, and 18.1 MPa$^{1/2}$, respectively) [51, 167, 168]. As a consequence, crude oil is a good solvent for these rubbers and can be used for the production of cryogels for use as oil sorbents.

As detailed in Sect. 2.1, the dilute solutions of rubbers such as PIB, SBR, and CBR can be crosslinked using sulfur monochloride (S_2Cl_2) as a crosslinking agent. Experiments show that S_2Cl_2 is an efficient crosslinking agent in organic solutions such as benzene or cyclohexane, even at very low reaction temperatures down to -22 °C and at crosslinker ratios down to about 0.9 mol S_2Cl_2/mol internal vinyl group on the rubber [52, 53, 55]. The reaction between S_2Cl_2 and the unsaturated groups of the rubbers PIB, CBR, and SBR in frozen organic solutions is due to the effect of cryo-concentration below the freezing point of the solvent. For instance, when a 5 % (w/v) PIB solution in benzene is frozen at -18 °C, 14 % of the benzene remains unfrozen in the apparently frozen system, making the PIB concentration in the unfrozen regions about 36 %, which is high enough to conduct the crosslinking reactions even at -18 °C [52].

Figure 23 shows SEM images of CBR, SBR, and PIB cryogels formed in benzene at $T_{prep} = -18$ °C and at a rubber concentration C_R of 5 % (w/v) [55]. The crosslinker (S_2Cl_2) concentration is 6 and 12 % in the upper and lower panels, respectively. The cryogels derived from CBR and SBR exhibit an aligned porous structure consisting of regular pores with sizes 10^1–10^2 μm, separated by pore walls of 10–20 μm in thickness. Decreasing the concentration of CBR or SBR in the feed further increased the regularity of the porous structure [55]. As indicated in Sect. 4.1, the regularity of the pore structure increases with decreasing freezing rate of the reaction solution, or by conducting the cryogelation reactions under isothermal conditions. The latter facilitates homogeneous nucleation of solvent crystals so that the polymer network formed will exhibit monodisperse pores. In the present case, gelation occurs non-isothermally during the initial cooling period of the reaction solution from 20 °C to -18 °C, which takes place in about 5 min [55]. Since decreasing the polymer concentration C_R also decreases the rate of the crosslinking reactions, the gel point is shifted towards longer reaction times as C_R is decreased, so that gelation occurs isothermally in the apparently frozen system, leading to the formation of more regular pores. In contrast, gel networks formed from PIB exhibit a broad size distribution of irregular pores from micrometer to millimeter sizes. Thus, the use of PIB in the gel preparation destroys the regularity of the porous structure in the organogels.

The variation in the morphologies of the cryogels depends on the type of rubber and originates from the different solvating power of benzene for different types of rubber. For instance, Fig. 24a shows the normalized weight swelling ratio m_{rel} of conventional gels based on PIB, CBR, and SBR in benzene plotted against the swelling temperature [55]. Both CBR and SBR gels exhibit temperature-independent swelling behavior and, thus, benzene is a good solvent for these
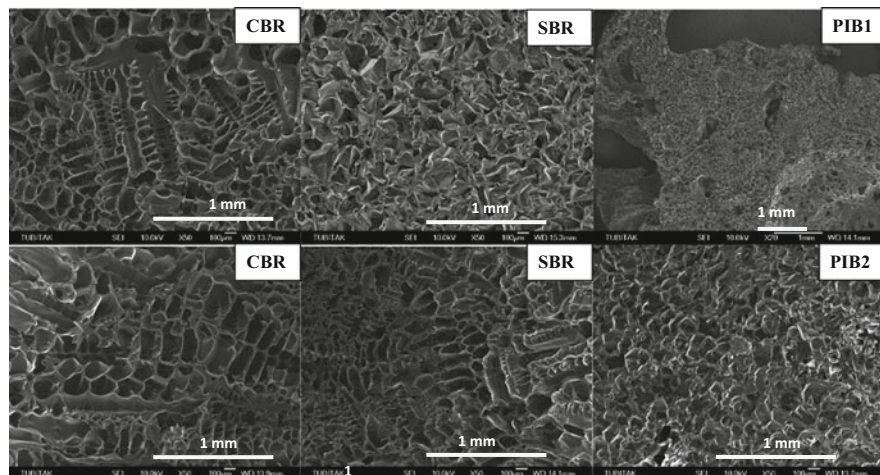
Fig. 23 SEM of the gel networks formed from the various rubbers indicated. $C_R = 5$ %; $S_2Cl_2 = 6$ % (*upper row*) and 12 % (*bottom row*). The degree of unsaturation of PIB was 1.1 % (PIB1) and 2.3 % (PIB2). (From [55] with permission from Elsevier)
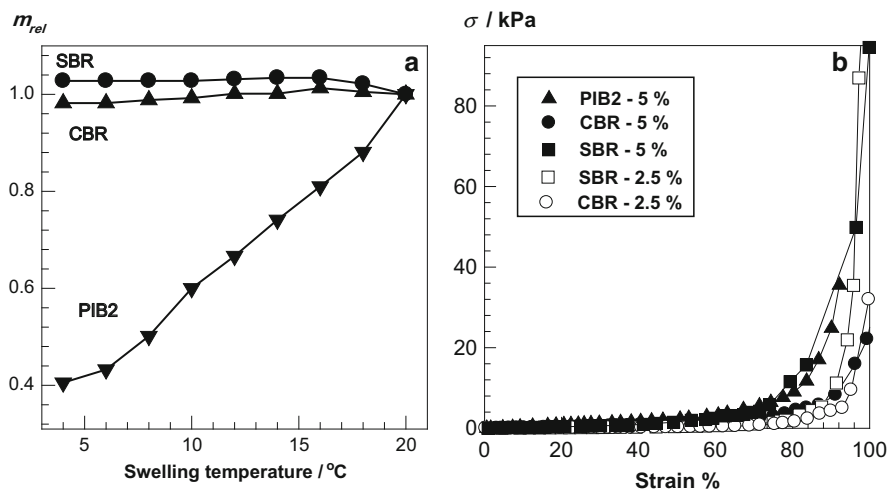
Fig. 24 (a) Normalized weight swelling ratio m_{rel} of conventional gels based on SBR, CBR, and PIB2 in benzene shown as a function of the swelling temperature. The gels were prepared at 20 °C in the presence of 12 % S_2Cl_2. (b) Typical stress–strain data of rubber cryogels. Types of rubber and the rubber concentration at gel preparation are indicated. (From [55] with permission from Elsevier)

polymers over the whole range of temperatures investigated. This indicates that CBR and SBR remain in the solution during the initial cooling period of the gelation reactions so that only the cryogelation mechanism is responsible for formation of the pores in these networks. However, the swelling capacity of PIB gel strongly depends on the temperature (Fig. 24a); the gel continuously deswells as the temperature is decreased and benzene becomes a poor solvent at low temperatures. Thus, PIB chains are not only expelled from the solution due to cryoconcentration but they also undergo a cooling-induced phase separation to form agglomerates of various sizes. Accordingly, both cryogelation and cooling-induced phase separation mechanisms govern the process of formation of the pores in PIB networks. The formation of millimeter-sized large pores also supports the idea that two mechanisms are operative in the formation of the porous structure in PIB networks.

The total pore volume V_p of the cryogels formed at $C_R = 5$ % (w/v) was 7 ± 0.5 mL/g, independent of the type of rubber and the crosslinker concentration. The value of V_p further increased with decreasing the rubber concentration C_R to 2.5 % (w/v) [55]. Typical stress–strain data of the cryogels derived from PIB, CBR, and SBR are shown in Fig. 24b. None of the rubber cryogels broke, even at a strain of 99.9 %. Sorption tests show that the cryogels are effective sorbents for various pollutants, e.g., crude oil, gasoline, diesel, and olive oil [54, 55, 69]. The sorption rate of all cryogels is very rapid due to their interconnected pore structure and they absorb the pollutants in less than 10–20 min to attain thermodynamic equilibrium. Moreover, PIB gels exhibit the fastest uptake rate for the pollutants, probably due to their large pores formed by phase separation. In Fig. 25a, the maximum sorption capacities of CBR, SBR, and PIB cryogels are compared for various pollutants. SBR or CBR cryogels sorb 35–38 g crude oil or 23–26 g olive oil per gram, as compared to 23 g/g and 9 g/g, respectively, using the PIB gel. We should mention that the widely used oil sorbents based on polypropylene have sorption capacities for both crude oil and olive oil of about 15 g/g [54]. Thus, SBR and CBR gels have sorption capacities about twice that of the commercial oil sorbents. Another point shown in Fig. 25a is that the sorption capacity of the cryogels is highest for crude oil, i.e., for the pollutant with highest viscosity. This implies that, although increased viscosity of the pollutant decreases the rate of sorption, favorable hydrophobic interactions between the crude oil and the hydrophobic polymer dominate the sorption process so that more oil is retained within the rubber gels.

The reusability of rubber cryogels and their continuous sorption capacities were also demonstrated by conducting sorption–squeezing cycles [54, 55]. The cycles were repeated 20 times to obtain the recycling efficiency and continuous extraction capacity of the cryogels. The results are shown in Fig. 26, where the uptake capacity of the gels in each cycle for various pollutants is plotted against the number of sorption–squeezing cycles. The amount of pollutant sorbed in each cycle is almost
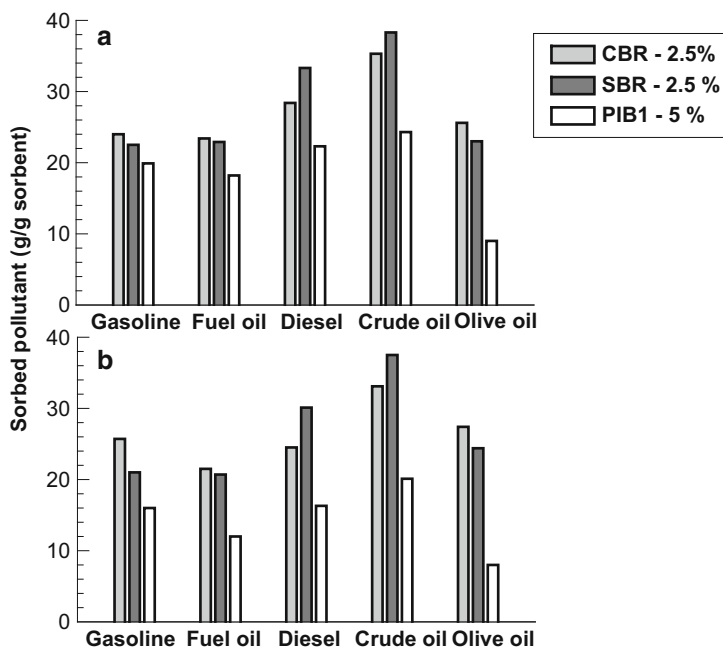
Fig. 25 (**a**) Maximum and (**b**) continuous sorption capacities of the cryogels for various pollutants. Types of rubber and the rubber concentration at gel preparation are indicated. $S_2Cl_2 = 6$ %. (From [55] with permission from Elsevier)

constant for the number of cycles larger than six; for example, it is equal to 37.5 ± 0.1 g crude oil/g and 24.4 ± 0.1 g olive oil/g for SBR gels formed at $C_R = 2.5$ %. The average of the sorption capacities (i.e., the continuous extraction capacities) of the best sorbents are collected in Fig. 25b. The results clearly demonstrate that the continuous capacity is close to the maximum capacity of gels, indicating high reusability of all cryogels and recoverability of crude oil, petroleum products, and olive oil. Sorption tests conducted using pollutants that spread on the water surface gave similar results as those in Fig. 26 [55]. The fact that 37.5 g crude oil can be recovered by 1 g of SBR gel in one cycle means that about one ton of crude oil can be separated from surface waters by use of 1 kg SBR gel within 25 cycles. Due to the fast responsivity of the cryogel, when put onto sea water, it immediately absorbs crude oil on the water surface. Successive sorption–squeezing cycles can continuously remove crude oil from water and, at the same time, crude oil is recovered.
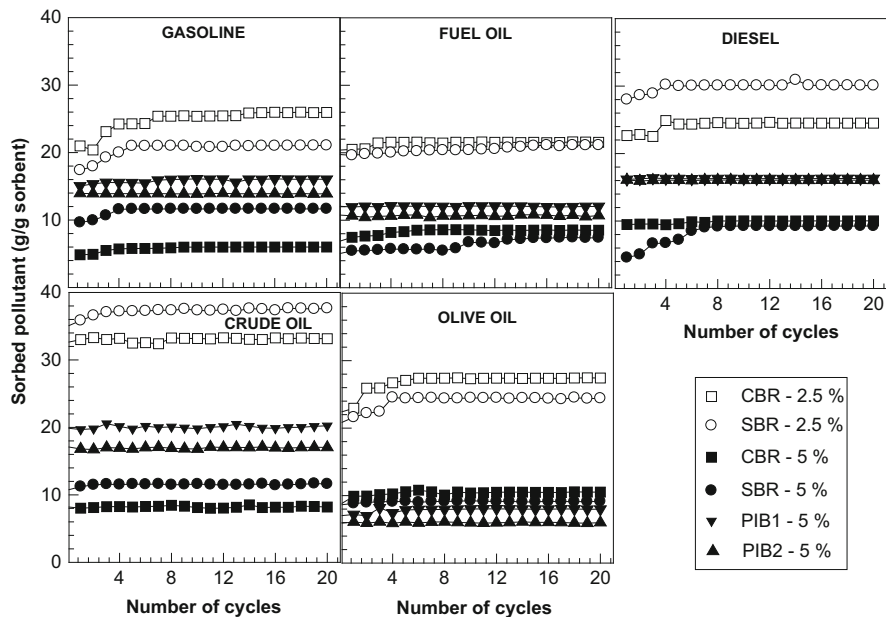
Fig. 26 Continuous extraction capacities of the cryogels for various pollutants as a function of the number of cycles. $S_2Cl_2 = 6$ %. $C_R = 5$ %: PIB1 (*inverted triangle*), PIB2 (*filled triangle*), CBR (*filled square*), SBR (*open circle*). $C_R = 2.5$ %: CBR (*open square*) and SBR (*open circle*). (From [55] with permission from Elsevier)

6   Concluding Remarks

In recent years, strategies for the synthesis of macroporous gels have been continually optimized and the concept of cryogelation has become increasingly important for the synthesis of such smart materials. Cryogelation is a simple strategy that allows the preparation of macroporous gels with high toughness and superfast responsivity. Although discovered over 30 years ago, cryogels have attracted intense attention only in the last 10 years due to their extraordinary properties. Cryogels are very tough gels that can withstandhigh levels of deformation, such as elongation and torsion, and can be squeezed almost completely without any crack propagation. The cryogelation temperature, the freezing rate of the reaction solutions, the type and concentration of the gel precursors, and the solvent are the main synthesis parameters determining the properties of the resultant cryogel. Some novel cryogels presented in this chapter (including DNA, silk fibroin, PAAc, and rubber cryogels) show that cryogelation technology opens new application areas for macroporous materials. Current research in the field of macroporous gels is focused on tailor-made design of the pore structure. The polymerization and/or crosslinking reactions at subzero temperatures that lead to cryogels are multicomponent systems composed of a polymer network, soluble polymers, and low molecular weight

compounds (monomers and solvent) in equilibrium with solvent crystals. All concentrations and properties of the system components change continuously during the cryogelation process. A more complete understanding of this complicated gel formation system is needed in order to improve the structuring of cryogels overall length scales from nanometer to micrometer. Moreover, because the volume swelling ratio of the cryogels and their porosity are inversely coupled, new synthetic approaches are also needed for the preparation of cryogels exhibiting drastic volume changes in response to external stimuli.

References

1. Gerlach G, Arndt KF (2009) Hydrogel sensors and actuators. In: Urban G (ed) Springer series on chemical sensors and biosensors, vol 6. Springer, Berlin
2. Shibayama M, Tanaka T (1993) Adv Polym Sci 109:1
3. Galaev I, Mattiasson B (2008) Smart polymers. Applications in biotechnology and biomedicine, 2nd edn. CRC Press, NY
4. Suzuki M, Hirasa O (1993) Adv Polym Sci 110:241
5. Tanaka T, Fillmore DJ (1979) J Chem Phys 70:1214
6. Gong JP, Katsuyama Y, Kurokawa T, Osada Y (2003) Adv Mater 15:1155
7. Okumura Y, Ito K (2001) Adv Mater 13:485
8. Tuncaboylu DC, Sari M, Oppermann W, Okay O (2011) Macromolecules 44:4997
9. Haraguchi K, Takehisa T (2002) Adv Mater 14:1120
10. Huang T, Xu H, Jiao K, Zhu L, Brown HR, Wang H (2007) Adv Mater 19:1622
11. Okay O (2000) Prog Polym Sci 25:711
12. Seidl J, Malinsky J, Dusek K, Heitz W (1967) Adv Polym Sci 5:113
13. Dusek K (1982) In: Haward RN (ed) Developments in polymerization, vol 3, Applied Science, London, p 143
14. Sayil C, Okay O (2001) Polymer 42:7639
15. Vainerman ES, Lozinsky VI, Rogozhin SV (1981) Colloid Polym Sci 259:1198
16. Lozinsky VI, Vainerman ES, Titova EF, Belavtseva EM, Rogozhin SV (1984) Colloid Polym Sci 262:769
17. Lozinsky VI (2002) Russ Chem Rev 71:489
18. Lozinsky VI, Plieva FM, Galaev IY, Mattiasson B (2002) Bioseparation 10:163
19. Lozinsky VI, Galaev IY, Plieva FM, Savina IN, Jungvid H, Mattiasson B (2003) Trends Biotechnol 21:445
20. Mattiasson B, Kumar A, Galaev IY (2010) Macroporous polymers. Production, properties, and biotechnological/biomedical applications. CRC Press, New York
21. Henderson TMA, Ladewig K, Haylock DN, McLean KM, O'Connor AJ (2013) J Mater Chem B 1:2682
22. Kirsebom H, Mattiasson B (2011) Polym Chem 2:1059
23. Ozmen MM, Dinu MV, Dragan ES, Okay O (2007) J Macromol Sci Part A 44:1195
24. Plieva FM, Karlsson M, Aguilar MR, Gomez D, Mikhalovsky S, Galaev IY (2005) Soft Matter 1:303
25. Plieva F, Huiting X, Galaev IY, Bergenstahl B, Mattiasson B (2006) J Mater Chem 16:4065
26. Dinu MV, Ozmen MM, Dragan ES, Okay O (2007) Polymer 48:195

27. Lozinsky VI, Kalinina EV, Grinberg VY, Grinberg NV, Chupov VV, Plate NA (1997) Polym Sci Ser A 39:1300
28. Kirsebom H, Rata G, Topgaard D, Mattiasson B, Galaev IY (2009) Macromolecules 42:5208
29. Kumar A, Plieva FM, Galaev IY, Mattiasson B (2003) J Immunol Methods 283:185
30. Sun X-L, He W-D, Li J, Li L-Y, Zhang B-Y, Pan T-T (2009) J Polym Sci Part A Polym Chem 47:6863
31. Bilici C, Karayel S, Demir TT, Okay O (2010) J Appl Polym Sci 118:2981
32. Zhang X-Z, Chu C-C (2003) Chem Commun 12:1446
33. Perez P, Plieva F, Gallardo A, Roman JS, Aguilar MR, Morfin I, Ehrburger-Dolle F, Bley F, Mikhalovsky S, Galaev IY, Mattiasson B (2008) Biomacromolecules 9:66
34. Zheng S, Wang T, Liu D, Liu X, Wang C, Tong Z (2013) Polymer 54:1846
35. Andac M, Plieva FM, Denizli A, Galaev IY, Mattiasson B (2008) Macromol Chem Phys 209:577
36. Ozmen MM, Okay O (2005) Polymer 46:8119
37. Petrov P, Petrova E, Tsvetanov CB (2009) Polymer 50:1118
38. Kahveci MU, Beyazkilic Z, Yagci Y (2010) J Polym Sci Part A Polym Chem 48:4989
39. Reichelt S, Abe C, Hainich S, Knolle W, Decker U, Prager A, Konieczny R (2013) Soft Matter 9:2484
40. Sun X-L, He W-D, Pan T-T, Ding Z-L, Zhang Y-J (2010) Polymer 51:110
41. Zhao Q, Sun J, Wu X, Lin Y (2011) Soft Matter 7:4284
42. Lozinsky VI, Vainerman ES, Rogozhin SV (1982) Colloid Polym Sci 260:776
43. Ivanov RV, Lozinsky VI, Noh SK, Han SS, Lyoo WS (2007) J Appl Polym Sci 106:1470
44. Lozinsky VI, Plieva FM (1998) Enzyme Microb Technol 23:227
45. Welzel PB, Grimmer M, Renneberg C, Naujox L, Zschoche S, Freudenberg U, Werner C (2012) Biomacromolecules 13:2349
46. Auriemma F, DeRosa C, Ricciardi R, Lo Celso F, Triolo R, Pipich V (2008) J Phys Chem B 112:816
47. Orakdogen N, Karacan P, Okay O (2011) React Funct Polym 71:782
48. Karacan P, Okay O (2013) React Funct Polym 73:442
49. Karakutuk I, Ak F, Okay O (2012) Biomacromolecules 13:1122
50. Ak F, Oztoprak Z, Karakutuk I, Okay O (2013) Biomacromolecules 14:719
51. Okay O, Durmaz S, Erman B (2000) Macromolecules 33:4822
52. Ceylan D, Okay O (2007) Macromolecules 40:8742
53. Dogu S, Okay O (2008) Polymer 49:4626
54. Ceylan D, Dogu S, Karacik B, Yakan S, Okay OS, Okay O (2009) Environ Sci Technol 43:3846
55. Karakutuk I, Okay O (2010) React Funct Polym 70:585
56. Tuncaboylu DC, Okay O (2010) Langmuir 26:7574
57. Pojanavaraphan T, Liu L, Ceylan D, Okay O, Magaraphan R, Schiraldi DA (2011) Macromolecules 44:923
58. Kirsebom H, Mattiasson B, Galaev IY (2009) Langmuir 25:8462
59. Ozmen MM, Okay O (2008) React Funct Polym 68:1467
60. Lozinsky VI, Vainerman ES, Korotaeva GF, Rogozhin SV (1984) Colloid Polym Sci 262:617
61. Lozinsky VI, Morozova SA, Vainerman ES, Titova EF, Shtil'man MI, Belavtseva EM, Rogozhin SV (1989) Acta Polym 40:8
62. Ivanov RV, Babushkina TA, Lozinsky VI (2005) Polym Sci Ser A 47:791
63. Ozmen MM, Okay O (2006) J Macromol Sci Part A 43:1215
64. Tripathi A, Kumar A (2011) Macromol Biosci 11:22
65. Arvidsson P, Plieva FM, Savina IN, Lozinsky VI, Fexby S, Bulow L, Galaev IY, Mattiasson B (2002) J Chromatogr A 977:27
66. Arvidsson P, Plieva FM, Lozinsky VI, Galaev IY, Mattiasson B (2003) J Chromatogr A 986:275
67. Plieva FM, Andersson J, Galaev IY, Mattiasson B (2004) J Sep Sci 27:828

68. Plieva FM, Savina IN, Deraz S, Andersson J, Galaev IY, Mattiasson B (2004) J Chromatogr B 807:129
69. Tuncaboylu DC, Okay O (2009) Eur Polym J 45:2033
70. Plieva FM, Mattiasson B (2008) Ind Eng Chem Res 47:4131
71. Yun J, Tu C, Lin D-Q, Xu L, Guo Y, Shen S, Zhang S, Yao K, Guan Y-X, Yao S-J (2012) J Chromatogr A 1247:81
72. Yun J, Dafoe JT, Peterson E, Xu L, Yao S-J (2013) J Chromatogr A 1284:148
73. Topuz F, Okay O (2009) React Funct Polym 69:273
74. Yin W, Yates MZ (2008) Langmuir 24:701
75. Gun'ko VM, Savina IN, Mikhalovsky SV (2013) Adv Colloid Int Sci 187–188:1
76. Savina IN, Tomlins PE, Mikhalovsky SV, Galaev IY (2010) Characterization of macroporous gels. In: Mattiasson B, Kumar A, Galaev IY (eds) Macroporous polymers. Production, properties, and biotechnological/biomedical applications. CRC Press, New York, p 211
77. Flory PJ (1953) Principles of polymer chemistry. NY, Cornell University Press, Ithaca
78. Treloar LRG (1975) The physics of rubber elasticity. University Press, Oxford
79. Hertz H (1881) Über die Berührung Fester Elastischer Körper (on the Contact of Elastic Solids). J. Reine und Angewandte Mathematik 92:156. In: Jones DE, Schott GA (eds) (1896) Miscellaneous papers b H. Hertz. Macmillan, London
80. Knaebel A, Rebre SR, Lequeux F (1997) Polym Gels Networks 5:107
81. Briscoe BJ, Liu KK, Williams DR (1998) J Colloid Int Sci 200:256
82. Barquins M, Shanahan MER (1997) Int J Adhes Adhes 17:313
83. Lozinsky VI, Zubov AL, Titova EF (1996) Enzyme Microb Technol 18:561
84. Lu W-M, Tung K-L, Hung S-M, Shiau J-S, Hwang K-J (2001) Powder Techn 116:1
85. Funke W, Okay O, Joos-Muller B (1998) Adv Polym Sci 36:139
86. Oppermann W, Rose S, Rehage G (1985) Br Polym J 17:175
87. Baker JP, Hong LH, Blanch HW, Prausnitz JM (1994) Macromolecules 27:1446
88. Naghash HJ, Okay O (1996) J Appl Polym Sci 60:971
89. Gundogan N, Okay O, Oppermann W (2004) Macromol Chem Phys 205:814
90. Bromberg L, Grosberg AY, Matsuo ES, Suzuki Y, Tanaka T (1997) J Chem Phys 106:2906
91. Wolfe J, Bryant G, Koster KL (2002) Cryo-Lett 23:157
92. Franks F (1986) Cryo-Lett 7:207
93. Watanabe K, Mizoguchi M (2002) Cold Reg Sci Technol 34:103
94. Okay O, Durmaz S (2002) Polymer 43:1215
95. Loo S-L, Krantz WB, Lim T-T, Fane AG, Hu X (2013) Soft Matter 9:224
96. Ceylan D, Ozmen MM, Okay O (2006) J Appl Polym Sci 99:319
97. Okoroafor EU, Newborough M, Highgate D, Augood P (1998) J Phys D Appl Phys 31:3120
98. Patil RD, Mark JE, Apostolov A, Vassileva E, Fakirov S (2000) Eur Polym J 36:1055
99. Zhang H, Cooper AI (2007) Adv Mater 19:1529
100. Zhang H, Edgar D, Murray P, Rak-Raszewska A, Glennon-Alty L, Cooper AI (2008) Adv Funct Mater 18:222
101. Zhang X-Z, Chu C-C (2003) J Mater Chem 13:2457
102. Kirsebom H, Topgaard D, Galaev IY, Mattiasson B (2010) Langmuir 26:16129
103. Lozinsky VI, Zubov AL, Kulakova VK, Titova EF, Rogozhin SV (1992) J Appl Polym 44:1423
104. Lozinsky VI, Bakeeva IV, Presnyak EP, Damshkaln LG, Zubov VP (2007) J Appl Polym Sci 105:2689
105. Lozinsky VI, Savina IN (2002) Colloid J 64:336
106. Podorozhko EA, D'yakonova EA, Kolosova O, Klabukova LF, Lozinsky VI (2012) Colloid J 74:708
107. Dosseh G, Xia Y, Alba-Simionesco C (2003) J Phys Chem B 107:6445
108. Xu J, LaBean TH, Craig SL (2004) In: Ciferri A (ed) Supramolecular polymers, CRC Press, New York, Chapter 12, p 445

109. Bloomfield VA, Crothers DM, Tinoco I (2000) Nucleic acids: structures, properties, and functions. University Science, Sausalito
110. Okay O (2011) J Polym Sci B Polym Phys 49:551
111. Topuz F, Okay O (2008) Macromolecules 41:8847
112. Topuz F, Okay O (2009) Biomacromolecules 10:2652
113. Murakami Y, Maeda M (2005) Biomacromolecules 6:2927
114. Ishizuka N, Hashimoto Y, Matsuo Y, Ijiro K (2006) Colloids Surf A 284–285:440
115. Amiya T, Tanaka T (1987) Macromolecules 20:1162
116. Horkay F, Basser PJ (2004) Biomacromolecules 5:232
117. Costa D, Miguel MG, Lindman B (2007) J Phys Chem B 111:8444
118. Costa D, Miguel MG, Lindman B (2010) Adv Coll Int Sci 158:21
119. Orakdogen N, Erman B, Okay O (2010) Macromolecules 43:1530
120. LePecq J-B, Yot P, Paoletti C (1964) C R Acad Sci 259:1786
121. Waring MJ (1965) J Mol Biol 13:269
122. Pohl FM, Jouin TM, Baehr W, Holbrook JJ (1972) Proc Natl Acad Sci USA 69:3805
123. Celedon A, Wirtz D, Sun S (2010) J Phys Chem B 114:16929
124. Sobell HM, Tsai CC, Jain SC, Gilbert SG (1977) J Mol Biol 114:333
125. Berman HM, Young PR (1981) Annu Rev Biophys Bioeng 10:87
126. Faulhaber K, Granzhan A, Ihmels H, Otto D, Thomas L, Wells S (2011) Photobiol Sci 10:1535
127. Vepari C, Kaplan DL (2007) Prog Polym Sci 32:991
128. Vollrath F, Porter D (2009) Polymer 50:5623
129. Hardy JG, Romer LM, Scheibel TR (2008) Polymer 49:4309
130. Murphy AR, Kaplan DL (2009) J Mater Chem 19:6443
131. Vlierberghe SV, Dubruel P, Schacht E (2011) Biomacromolecules 12:1387
132. Zhou CZ, Confalonieri F, Medina N, Zivanovic Y, Esnault C, Yang T, Jacquet M, Janin J, Duguet M, Perasso R, Li ZG (2000) Nucleic Acids Res 28:2413
133. Sofia S, McCarthy MB, Gronowicz G, Kaplan DL (2001) J Biomed Mater Res 54:139
134. Jin HJ, Fridrikh SV, Rutledge GC, Kaplan DL (2002) Biomacromolecules 3:1233
135. Jin HJ, Kaplan DL (2003) Nature 424:1057
136. Karageorgiou V, Kaplan D (2005) Biomaterials 26:5474
137. Nazarov R, Jin HJ, Kaplan DL (2004) Biomacromolecules 5:718
138. Ki CS, Park SY, Kim HJ, Jung HM, Woo KM, Lee JW, Park YH (2008) Biotechnol Lett 30:405
139. Hutmacher DW (2000) Biomaterials 21:2529
140. Li MZ, Lu SZ, Wu ZY, Yan HJ (2001) J Appl Polym Sci 79:2185
141. Li MZ, Wu ZY, Zhang CS, Lu SZ, Yan HJ, Huang D, Ye HL (2001) J Appl Polym Sci 79:2192
142. Lv Q, Feng QL (2006) J Mater Sci Mater Med 17:1349
143. Liu X, Ma PX (2004) Ann Biomed Eng 32:477
144. Zhang Q, Yan S, Li M (2009) Materials 2:2276
145. Kim UJ, Park J, Kim HJ, Wada M, Kaplan DL (2005) Biomaterials 26:2775
146. Min S, Gao X, Liu L, Tian L, Zhu L, Zhang H, Yao JJ (2009) Biomater Sci 20:1961
147. Chen X, Knight DP, Shao ZZ, Vollrath F (2002) Biochemistry 41:14944
148. Mo C, Holland C, Porter D, Shao Z, Vollrath F (2009) Biomacromolecules 10:2724
149. Kim UJ, Park J, Li C, Jin HJ, Valluzzi R, Kaplan DL (2004) Biomacromolecules 5:786
150. Ayub ZH, Arai M, Hirabayashi K (1993) Biosci Biotech Biochem 57:1910
151. Yoshida R, Takahashi T, Yamaguchi T, Ichijo H (1997) Adv Mater 9:175
152. Luo Y, Epstein IR (1991) J Am Chem Soc 113:1518
153. Rabai G, Orban M, Epstein IR (1990) Acc Chem Res 23:258
154. Yoshida R, Ichijo H, Hakuta T, Yamaguchi T (1995) Macromol Rapid Commun 16:305
155. Crook CJ, Smith A, Jones RAL, Ryan AJ (2002) Phys Chem Chem Phys 4:1367
156. Edblom EC, Luo Y, Orban M, Kustin K, Epstein IR (1989) J Phys Chem 93:2722

157. Ende MTA, Peppas NA (1996) J Appl Polym Sci 59:673
158. National Research Council (2003) Oil in the sea III: inputs, fates, and effects. National Academies Press, Washington, DC
159. Adebajo MO, Frost RL, Kloprogge JT, Carmody O, Kokot S (2003) J Porous Mat 10:159
160. Valderrama C, Gamisans X, Heras FX, Cortina JL, Farran A (2007) React Funct Polym 67:1515
161. Sun X-F, Sun R, Sun J-X (2002) J Agric Food Chem 50:6428
162. Deschamps G, Caruel H, Borredon M-E, Bonnin C, Vignoles C (2003) Environ Sci Technol 37:1013
163. Radetic MM, Jocic DM, Jovancic PM, Petrovic ZL, Thomas HF (2003) Environ Sci Technol 37:1008
164. Wei QF, Mather RR, Fotheringham AF (2005) Bioresour Technol 96:331
165. Carmody O, Frost R, Xi Y, Kokot S (2007) Surf Sci 601:2066
166. Gardon JL (1965) In: Mark HF, Gaylord NG, Bikales NM (eds) Encyclopedia of polymer science and technology. Interscience, New Yok, vol 3, p 833
167. Barton AFM (1991) CRC handbook of solubility parameters and other cohesion parameters, second edition. CRC Press, New York
168. Stirna U, Cabulis U, Beverte I (2008) J Cell Plastics 44:139

Kinetic Analysis of Cryotropic Gelation of Poly(Vinyl Alcohol)/Water Solutions by Small-Angle Neutron Scattering

Claudio De Rosa, Finizia Auriemma, and Rocco Di Girolamo

Contents

Abstract Aqueous poly(vinyl alcohol) (PVA) solutions subjected to cryogenic treatment form strong physical gels. The cryogenic treatment basically consists of freezing an initially homogeneous polymer solution at low temperatures, storing in the frozen state for a definite time, and defrosting. These gels are of great interest for biotechnology, medicine, the food industry, and many other applications. The outstanding properties of these systems depend on a complex macroporous architecture, whereby PVA chains and water molecules are organized over different hierarchical length scales. The structure and the principal processes subtending the formation of these systems are discussed in the framework of our current understanding of polymer gels. These processes involve formation of ice crystals, PVA

C. De Rosa • F. Auriemma (✉) • R. Di Girolamo
Dipartimento di Scienze Chimiche, Università di Napoli Federico II, Complesso Monte Sant' Angelo, via Cintia, 80126 Napoli, Italy
e-mail: finizia.auriemma@unina.it

crystallization, liquid–liquid phase separation, hydrogen bonding, and entanglements. Small angle neutron scattering is used to follow the cryotropic gelation of PVA/water solutions and detailed information is extracted concerning the gelation mechanism and kinetic parameters related to the formation of these complex systems.

Abbreviations

a-PS	Atactic polystyrene
BP	Berghmans point
CLSM	Confocal laser scanning microscopy
C_p	Polymer concentration
$d\sigma/d\Omega$	Scattering cross-section
d_s	Surface fractal dimension
DSC	Differential scanning calorimetry
F	Free energy
$\langle \Phi \rangle$	Order parameter
$f_c(DSC)$	Fractions of crystalline phase from DSC analysis
$f_c(NMR)$	Fraction of rigid protons from NMR measurements
$f_c(XR)$	Crystallinity index from WAXS analysis
LL	Liquid–liquid phase separation
NMR	Nuclear magnetic resonance
PEG	Poly(ethylene glycol)
PVA	Poly(vinyl alcohol)
q	Scattering vector
SANS	Small angle neutron scattering
SEM	Scanning electronic microscopy
TEM	Transmission electron microscopy
T_g	Glass transition temperature
T_m	Melting temperature
TR-SANS	Time resolving-SANS
UCST	Upper critical solution temperature
WAXS	Wide angle X-ray scattering

1   Introduction

In this chapter, we deal with kinetic and mechanistic aspects associated with the complex cryotropic gelation of semidilute aqueous solutions of poly(vinyl alcohol) (PVA). The possibility of obtaining strong physical gels by cryogenic treatments of PVA/water solutions has been well known since the 1970s [1–6]. The cryogenic treatment basically consists of freezing an initially homogeneous polymer solution at low temperatures, storing in the frozen state for a definite time, and defrosting. Freezing is generally performed at high cooling rates and, in order to improve the strength of the gels, freezing and thawing are repeated a number of times. The strength of PVA cryogels prepared by means of freeze–thaw cycles depends on the initial polymer concentration in the solution to be frozen, the thawing rate, the permanence time of the solution at low temperatures, and the number of imposed freeze–thaw cycles. Cryogel strength is virtually independent of the temperature of freezing and the cooling rate of the initial solution to that temperature [4, 5, 7]. Strong physical gels can be obtained even by imposing a single freeze–thaw cycle, either with use of slow thawing rates or by the prolonged storage of the samples at subzero temperatures [3].

The large interest in PVA cryotropic hydrogels is due to a number of unique properties, including high dimensional stability, large deformability, maintenance of high conservative elastic modulus even after immersion in water for a long time [8, 9], and self-healing performance [10]. In addition, the well-tested biocompatibility of freeze–thaw PVA hydrogels and their ability to incorporate and release large amounts of host molecules of different size in their structure make these systems particularly attractive for biomedical and biotechnological applications [1, 5, 11].

The outstanding physical properties of freeze–thaw PVA hydrogels derive from their complex structure, whereby PVA chains and solvent molecules are organized at different hierarchical length scales. These gels exhibit a structure that includes an interconnected network of micro- and macropores filled by a polymer-poor phase. The network scaffolding is ensured by interconnected regions of a polymer-rich phase [1]. The latter phase is itself organized and consists of small fringed micelle-like crystalline aggregates of PVA chains and amorphous domains. The PVA chains in the amorphous domains are swollen by the solvent and act as tie chains that connect the PVA crystallites.

Section 2 is aimed at recalling the general aspects of polymer gels. These concepts turn out to be useful in Sect. 3 for understanding the mechanism of formation, the structure, and the properties of PVA hydrogels generated by physical crosslinking processes, first in general terms, then focusing on freeze–thaw PVA hydrogels in particular. The structure of freeze–thaw PVA hydrogels is discussed in detail and possible mechanisms leading to their formations are illustrated, emphasizing some aspects that have been investigated using time-resolving analysis with small angle neutron scattering (TR-SANS). TR-SANS is used to follow the structural transformations occurring during consecutive freeze–thaw cycles, with the

aim of extracting appropriate descriptors of the structural transformations occurring at the relevant length scale and the kinetic parameters. Chemical hydrogels of PVA are not included in the present context, in spite of their importance and interesting properties in several applications. Some excellent reviews on this subject may be found in the literature [1, 12, 13]. The last section is devoted to the conclusions and outlook.

It is worth noting that understanding the factors that govern the cryogelation mechanism of homogeneous polymer solutions is useful both in fundamental studies of the phenomena subtending the formation of macroporous gels in PVA and polymers in general and from an applicative standpoint. Such knowledge can enable control of the final architecture of cryogels by simply tuning the conditions of preparation, with the aim of obtaining materials with enhanced properties for tailored applications.

2 General Considerations

Polymer gels are mesoscopic systems that include a liquid phase (solvent) and a crosslinked three-dimensional (3D) polymer network intimately swollen by the solvent (solvate) [14–16]. The two phases cannot be distinguished at macroscopic level, meaning that the gels at macroscale are homogeneous systems.

Gels, are generally formed starting from a solution of a low or high molecular mass precursor (sol) as a result of a crosslinking process that is able to create a macroscopic 3D network (gel). Because the presence of crosslinks reduces the mobility of the molecular species that have reacted to become part of the network, the solvent may end up entrapped within the network-gel in high amounts instead of being rejected. It is worth noting that, although the solvent may largely exceed the polymeric component by weight, gels do not behave as viscous polymer solutions, but rather behave as elastic solids or semisolids able to withstand their own weight, even over long time scales.

The liquid component of a gel may either be a pure solvent of the initial precursor or a polymer-poor liquid phase. The mobility of the solute and solvent molecules in these liquid domains is high, as in a solution. Consequently, gels combine the properties of a solid network structure and a liquid solution at the mesoscale level, giving rise to materials with unique properties that are useful for a variety of applications.

In particular, polymer gels (depending on the chemical constitution of the components, processing conditions, and phase composition) may feature a gamut of properties that range from those of hard and tough materials to those of elastomers, that is, they are able to undergo large deformation upon application of pressure and to quickly recover the initial shape and dimensions when the external stress is removed [12–18]. In all cases, the high dimensional stability of gels is ensured by the presence of a network, which can be built by either physical or chemical crosslinks, giving rise to either physical or chemical gels.

Examples of physical crosslinks are microcrystalline aggregates, entangled chains, ionic interactions between charged atoms or groups of atoms, and hydrogen bonds. Physical gels are also reversible because the physical crosslinks can be created and removed by appropriate physical stimuli (e.g., pH, contact with a nonsolvent, etc.), and, typically, temperature. For this reason, they are often named "thermoreversible."

In chemical gels, the crosslinks are covalent bonds connecting the arms of the 3D network. As a result of covalent bonding, chemical gels are irreversible.

Whereas chemical gels are generally strong, physical gels may be strong or weak, depending on the strength of the interactions involved in the crosslinks. Strong physical gels have strong physical crosslinks between polymer chains that are effectively permanent for a given set of experimental conditions [15–17, 19]. As an example, strong physical junctions may consist of glassy or microcrystalline nodules, triple helices, or coiled-coils as, for instance, in the case of hydrogels formed from fibrous proteins or biomacromolecules.

Weak physical gels have reversible links formed from temporary weak interactions between chains, of the order of kT. These associations have finite lifetimes, breaking and reforming continuously. Examples of weak physical bonds are hydrogen bonds, ionic associations, and micellar aggregates of block copolymers.

The outstanding physical properties of gels associated with their fast stimuli response have noticeably stimulated research for a long time. Polymeric gels have been developed that are "smart," i.e., able to quickly respond to different external stimuli [15, 20]. For instance, Tanaka's gels have valuable applications because they can expand and contract up to 1,000 times their original volume in response to external stimuli. These gels could be used as artificial muscles, set in motion by a specific electric pulse [21]. More importantly, the polymers in the gels can capture or expel specific substances as they grow or shrink, so that the gels could be used, for example, as super-sponges to absorb and immobilize toxic waste, or as molecular filters of various sorts [18, 20–23]. Among the smart gels, there are materials that imitate proteins by recognizing conditions and responding to their environment. For example, smart gels can be fine-tuned to draw humidity from the air when it is over a certain level at a given temperature. Other gels can release insulin when the glucose level in the water-rich phase drops below a given point [15, 18]. Moreover, it is worth remembering that gels represent an important intermediate step in polymer processing for obtaining highly oriented fibers showing high strength and high modulus (e.g., ultrahigh-strength polyethylene fibers Dyneema and Spectra) [17].

The outstanding properties of gels are directly related to the chemical nature of their constituents, their reciprocal arrangement and interactions, and their mobility in the space. Structure and mobility in a gel, in turn, are fixed by the preparative conditions and processing. Although a gel may be assimilated to a single giant branched macromolecule, the structure of its parts covers different orders of hierarchical organization on different length scales. Roughly, the hierarchical apparatus of gels ranges from a few nanometers for the size of knots; to hundreds of nanometers for the organization of matter between first neighboring knots; to

microns for the relative organization of clusters of knots; and so on. Gels may include macro- and/or microscale heterogeneities such as macro- and micropores inside their structure. The length scales and the kind and degree of heterogeneities in a gel have a strong influence on its final properties. Therefore, the design of preparation/processing methods for achieving gels with tailored morphology able to ensure prefixed properties is a research area of great applicative interest.

From a fundamental point of view, the achievement of this goal needs the establishment of precise relationships between the functionality of the gel and its fundamental constituents, their chemical nature, their geometric arrangement, and their mobility. Of primary interest in basic research in the field of polymer gels are (1) definition of the structural organization of gel components on different length scales and (2) the structural and morphological transformations of a gel in the initial state (preparative ensemble), during its performance under application of external stimuli on the proper time scale (applicative ensemble), and in the final state (end use ensemble) [24]. In the present context we focus on gels in the preparative ensemble.

2.1   Physical Gels in the Preparative Ensemble: Main Processes Creating Networks

Physical gels may originate from a large number of processes able to create junctions (Fig. 1). Each one of these processes may act alone or in synergy with the other processes to induce the sol–gel transitions (gelations). Gelation is not a first-order phase transition and does not lead to a state of thermodynamic equilibrium [16]. Instead, the kinetics of the process and the way a crosslinking process is activated play key roles in the transition [17, 25].

As shown in Fig. 1, sol–gel transitions may be easily driven by the entanglements established among the polymer chains in a semidilute or concentrated homogeneous solution , i.e., at concentrations higher than that occupied by each polymer coil within its own pervaded volume, corresponding to the overlap concentration [19]. This means that polymer random coils should overlap in order to establish an entangled network [24] and, hence, to form a gel.

Besides entanglements, a second kind of crosslinking process leading to gelation involves physical associations such as polar–polar interactions, ionic forces, colloid interactions, hydrogen bonding, or complex associations such as formation of multiple helices and/or coiled-coils in biopolymers, self-assembly with formation of micellar aggregates in amphiphilic block copolymers, and so on.

As shown in Fig. 1, gelation may be also driven by phase transitions as for instance crystallization. Under specific conditions, formation of crystals from a homogeneous solution can give rise to junctions and then to a gel. This happens, for example, with poly(vinyl chloride) [15], isotactic polystyrene, polyethylene [15, 26–31], and many other polymers [32]. In these gels, the junctions are constituted
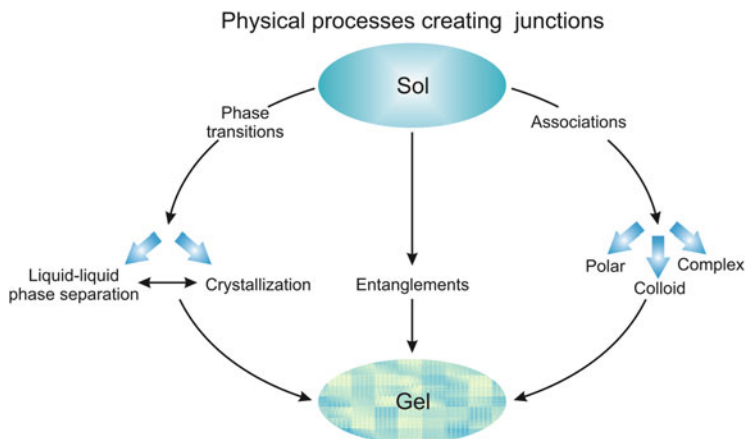
Fig. 1 Different processes able to produce a network and therefore a physical gel, and their possible correlations [17]

by small fringed micelle-like crystals or chain-folded lamellae, while the connectivity is ensured by portions of chains connecting the crystallites throughout the macroscopic samples, swollen by the solvent.

Finally, gels may be also generated through a liquid–liquid (LL) phase separation, or a combination of LL phase separation and crystallization, as we shall see in Sect. 2.2 [17, 25].

Regardless of the kind of process, gelation involves complex mechanisms and the gradual formation of junctions [16, 19]. As long as these junctions form aggregates of small dimensions, the system is still a sol (Fig. 2a). Gel is formed when the concentration of junctions reaches a threshold value, so that at least a single aggregate having infinite size is created, that is, aggregates having the same size as the macroscopic sample (Fig. 2b). Above this threshold value some sol (aggregates of finite size, indicated with an arrow in Fig. 2b) may still survive, and these aggregates end up connected to the gel only in the later stages of the process. This is in essence the (site) percolation model [16, 19].

2.2 Metastability and Sol–Gel Transitions

In order to better understand the mechanism of formation of a 3D network, and then a gel, via a gradual crosslinking (both physical and chemical) process according to the percolative scheme shown in Fig. 2, we need to emphasize that, regardless of the processes involved in the creation of junctions, these processes compete with gelation [16, 17, 25]. As a result of this competition, the process is arrested at an intermediate level instead of proceeding to completion, so that the system does not attain the ultimate thermodynamically stable state, but reaches a state far from
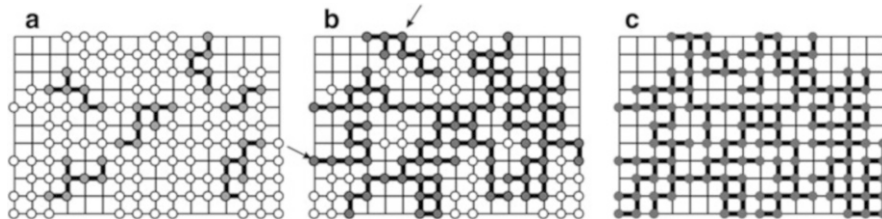
Fig. 2 Scheme of percolation in a two-dimensional network [16, 19]. Only ≈72 % of the sites are occupied by "particles" able to form a junction. Each particle may form 1–4 junctions with a first neighboring particle. *Empty balls* correspond to unbound particles, *filled balls* are the particles connected with at least one first neighbor. (**a**) Sol: The fraction of particles that have created a junction is below a threshold value. (**b**) Immediately above this threshold, we have an aggregate of infinite dimensions (i.e., the aggregate is of the same size as the macroscopic sample) swollen by the solvent, unreacted particles, and aggregates of finite dimensions (indicated by an *arrow*). (**c**) Gelation progresses to include all particles

equilibrium [17, 25]. This means that, although gels are often quite long-living with respect to the lifetime of an experiment, they are usually in a metastable state [17, 25]. For instance, in the framework of the percolation model shown in Fig. 2, for crystallization-driven gels, when the number density of crystallites that gradually form in a solution achieves a threshold value, they give rise to a percolative network extending all over the macroscopic sample, with consequent formation of a gel. Simultaneously, the crystallization process is arrested at an intermediate state far from equilibrium, namely, corresponding to a metastable state. This mechanism is valid for any process able to form junctions [17, 25].

The formation of a gel and the concept of a gel as a metastable state of matter fits quite well with the Ostwald "stage rule" [33]. This rule was formulated at the end of the nineteenth century and states that "a phase transformation from one stable state to another proceeds via metastable states, whenever such states exist, in stages of increasing stability." Although this rule does not explain why phase transitions evolve in this way, it is considered an intrinsic property of matter.

A metastable state of matter is a state that can exist on the basis of the laws of thermodynamics and is stable with respect to infinitesimal fluctuations, yet it does not represent the state of ultimate stability. In Fig. 3, the free energy, F, is reported as a function of an "order parameter" $\langle \Phi \rangle$. It is apparent that both metastable (M) and ultimate stable (E) states are such that the first derivative of F with respect to $\langle \Phi \rangle$, $dF/d\langle \Phi \rangle$, is equal to zero, and the second derivative ($d^2F/d\langle \Phi \rangle^2$) is positive. Evolution from the metastable state M to the equilibrium state E needs activation, ΔF. Although a metastable state will evolve to an equilibrium state sooner or later, its lifetime may be longer than the timescale of the experiment [17, 25].

At this point, it is important to introduce two different classes of metastability: classical metastability and circumstantial metastability [25].

A kind of classical metastability occurs in the case of thermodynamic phase transitions, as for instance in the case of an LL phase separation. Here, the order parameter $\langle \Phi \rangle$ may be identified with the polymer concentration. Fig. 3 states that at

Fig. 3 Scheme of a metastable state (*M*) in a plot of the free energy *F* as a function of the order parameter $\langle \Phi \rangle$. ΔF represents an activation barrier bringing the system from the metastable state *M* to the equilibrium state *E* [33]
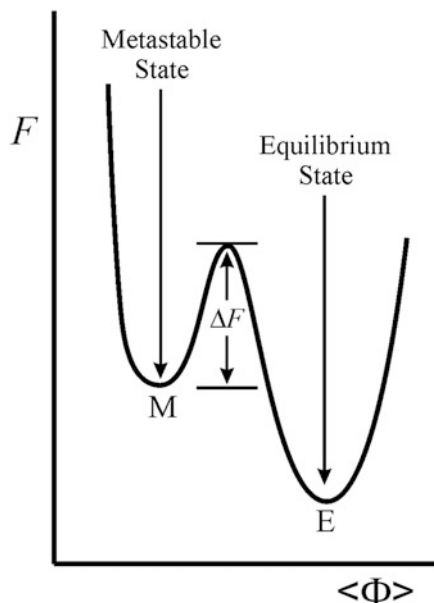
a given concentration (and temperature) a solution in a state of metastability *M* may reach the equilibrium state *E* corresponding to phase separation, only by crossing a barrier ΔF able to create nuclei of the two phases. The nuclei, once formed, grow, thus decreasing the free energy and the system reaches the ultimate state of thermodynamic equilibrium at its own pace.

The concept of circumstantial metastability [25] comes into play in the case of gels. Here, the order parameter $\langle \Phi \rangle$ may be identified with the gel fraction, i.e., the fraction of "particles" (i.e., molecules, bonds, chains, portion of chains, etc.) in Fig. 2 attached to a macroscopic aggregate during its development. If we assume that all particles have a functionality of 4 in the square lattice of Fig. 2, each particle is expected to form a connection with all particles located in the first neighboring sites in the final state. However, in the configuration of Fig. 2c it is evident that some particles are connected with only two or a maximum of three of the available first neighboring particles. Therefore, the system in Fig. 2c is far from equilibrium; it is in a metastable state, and can attain a state of lower free energy only by crossing a thermodynamic barrier. The reason why it may assume a frozen-in configuration such as that in Fig. 2c can be explained by kinetics. Some agency able to create metastability comes into play [25], reducing the "reactivity" of the particles and freezing the gel in that configuration. The nature of the agency able to create a metastable state in a sol–gel transition could be the presence of impurities blocking the functionality of some particles, the high viscosity achieved by the system at onset of gelation, the temperature, and many other factors.

2.3   Role of Phase Separations in Gel Formation

The arguments of Sect. 2.2 mean that two specific conditions must be fulfilled in order for a phase transformation to lead to a macroscopic network of junctions and thus to a gel [17]: first, the phase transformation must be incomplete and, second, it must stop wherever connectivity has been established throughout the whole macroscopic sample.

The first condition is driven by thermodynamics, but it is always controlled by the kinetics of the process through some kind of agency able to create metastability [25]. Because of this agency, the system fails to attain its ultimate stability (corresponding to completion of the process) and is arrested in one of the multiple minima of the free energy profile with respect to the order parameter $\langle \Phi \rangle$ (Fig. 3).

The second condition is a geometric factor and it is not related to the process, but represents the *condicio sine qua non* for obtaining a gel. It is worth noting that the connectivity can be established either by individual chain molecules or by a continuity of microphase separated domains, or by a combination of both kinds of associations [25]. As a consequence, a large variety of morphologies may be obtained, depending on the chemical nature of the polymer, the kind of solvent, the initial polymer concentration, the gelation temperature, the rate of cooling/heating to this temperature, and so on.

Although application of the above general concepts to understand physical gelation is, at least on a qualitative ground, straightforward in the case of crystallization, it is more tricky in the case of LL phase separations.

LL phase separation may play a key role in the gelation of some noncrystalline polymers such as atactic polystyrene (a-PS) [34–36]. For a-PS, the physical junctions are not crystals and there are no specific interchain interactions, yet a-PS can form gels. Arnauts and Berghmans were the first to explain the gelation of a-PS in terms of LL phase separation combined with vitrification [36]. In this case, vitrification acts as the agency responsible for arrest of the LL phase separation, and locks the system in a metastable state.

This mechanism is illustrated in Fig. 4a, where the phase behavior of a polymer solution featuring an upper critical solution temperature (UCST) behavior at T_c is shown as an example, with T_c being the critical temperature. Curve b in Fig. 4 is the binodal, i.e., the curve delineating the concentration of the polymer-rich and polymer-poor phases in equilibrium at each temperature. The LL phase separation occurs at temperatures below the binodal, in any case at temperatures below the T_c. In Fig. 4, the curve s represents the spinodal, which is the ultimate thermodynamic limit of stability for homogeneous solutions. Below this curve, homogeneous solutions are unstable and undergo phase separation due to the effect of infinitesimally small fluctuations in composition and density (spinodal decomposition). For concentrations that fall in the region between the spinodal and binodal, homogeneous solutions are in a (classical) metastable state, that is, they are stable with respect to concentration and density fluctuations, and undergo phase separation by a free-energy-activated process involving nucleation and growth. Finally, curve g in
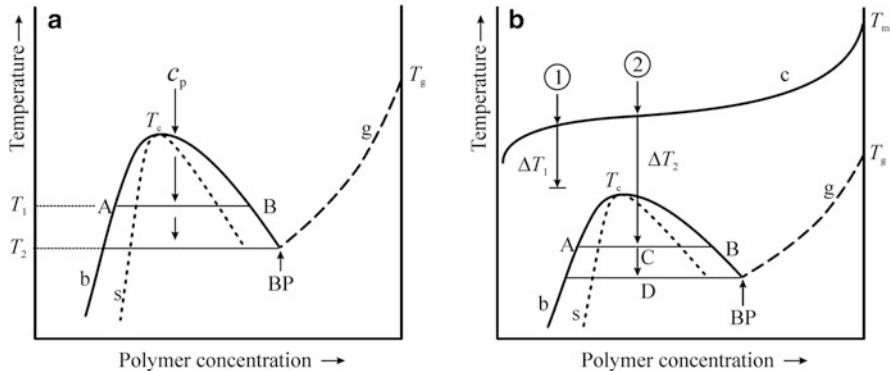
Fig. 4 Schematic phase diagrams of a polymer solution showing LL phase separation with UCST behavior. *Curve s* is the spinodal, *curve b* is the binodal, and *curve g* is the glass transition temperature as a function of polymer concentration. *BP* indicates the Berghmans point. (**a**) LL phase separation is the only thermodynamic transformation of the system [17, 25, 36]. (**b**) *Curve c* shows the crystallization temperature of a polymer fully miscible in a solvent as a function of concentration in the solution [17, 25]. The LL phase coexistence curve (combined with vitrification) is a (classical) metastable process that lies beneath the crystallization curve *c*. In route *1*, a polymer solution is supercooled at ΔT_1, and the only active process is polymer crystallization. In route *2*, the initially homogeneous solution is supercooled to a larger undercooling than ΔT_1, namely ΔT_2. Crystallization may compete either with LL phase separation when reaching point *C*, or LL phase separation coupled with vitrification when reaching point *D*. At *C*, crystallization may take place in the polymer-rich phase. At *D*, both LL phase separation and crystallization may become arrested by vitrification

Fig. 4 represents the dependence of the glass transition temperature T_g, on the polymer concentration. Because T_g of the pure polymer decreases by addition of the solvent, curve g intersects the binodal at the point BP, named Berghmans point after Hugo Berghmans [36].

Starting from a homogeneous polymer solution with concentration C_p, the LL phase separation sets in by decreasing the temperature below T_c, for instance, at temperature T_1. The tie line (isotherm) intersects the binodal at points A and B (see Fig. 4), and these points define the concentrations of the polymer-poor and polymer-rich phases in equilibrium at T_1, originating from the LL phase separation.

We recall that, regardless of the exact mechanism leading to phase separation (spinodal decomposition or nucleation and growth), the ultimate stable morphology obtained upon de-mixing should correspond to a two-layered liquid in order to minimize the specific interfacial area [37]. Spinodal decomposition is driven by spontaneous barrier-free composition fluctuations, so that, since the beginning and during the transient stages of the transformation, the morphology is characterized by a kind of a bi-continuous network of the two phases. By contrast, in the case of nucleation and growth, droplets of one phase are formed in the continuous matrix of the other phases before reaching macroscopic segregation. Therefore, during the de-mixing process a gamut of morphologies develops, gradually leading to the coalescence of the small domains of the two phases into increasingly bigger

domains, up to the ultimate layered morphology. The transient morphologies depend not only on the initial concentration and temperature, which in turn define the relative amount of the two phases in equilibrium based on the lever rule [19], but also on the degree of evolution of the phase separation and, hence, on the time of observation [25].

At temperatures lower than T_1, the intersection point B shifts towards higher concentrations up to reach the Berghmans point BP at T_2 (see Fig. 4). At this point, the polymer-rich phase vitrifies, blocking the progress of the phase separation. A first direct consequence of vitrification is that at and below the temperature corresponding to BP, the system ends up in a metastable state characterized by the same phase morphology prevailing at the stage of vitrification, instead of attaining the ultimate thermodynamically stable state characterized by the segregation of the two phases in layers [17, 25].

A second consequence of vitrification is that morphological development is arrested and all further compositional changes cease, and the glass transition becomes invariant with composition. If, at the moment of the arrest of LL phase separation, the vitrified phase has become connected throughout the macroscopic sample volume, the solution converts into a gel [17, 25]. Possible limiting morphologies of these gels are illustrated as an example in Fig. 5.

Gels may also arise from a combination of LL phase separation coupled with crystallization [17, 25]. This is a more complex situation and occurs when one or more metastable states lie "buried" beneath the state of ultimate stability in the phase diagram [17, 25]. A hierarchy of metastability arises in this case due to the possibility of several metastable phases. These metastable phases, once formed, can evolve faster than the transition leading to the ultimate stable phase and can dominate the whole transformation process.

As an example, Fig. 4b illustrates the case of a fully miscible polymer solution, in which polymer crystallization takes place at equilibrium values of temperatures delineated by the curve c. Hence, for this system, at temperatures below the curve c, the crystalline state corresponds to the state of ultimate stability. However, the system in Fig. 4b also displays a metastable LL phase separation, as indicated by curve b, lying below the crystallization curve c. Also shown is the glass transition temperature T_g of the polymer as a function of polymer concentration intersecting the binodal at the Berghmans point BP. A first set of metastable states may arise because of the high undercooling ΔT that is generally required for crystallization to take place at practical rates. Besides crystallization, other sets of metastable states may also arise for this system, depending on the undercooling, according to a hierarchy. Such scheme fits quite well what occurs in the case of poly(phenylene ether) in cyclohexanol, as an example [38]. In Fig. 4b, route 1 shows that, starting from an initially homogeneous solution, crystallization takes place at low undercooling ΔT_1 if sufficient time is allowed. At low undercooling, only crystallization takes place. In route 2, the undercooling ΔT_2 is larger than ΔT_1 and crosses the binodal. Depending on the magnitude of the undercooling, either de-mixing occurs first and crystals are formed in the polymer-rich phase (point C) or the polymer-rich phase vitrifies at and below the Berghmans point (point D), and both
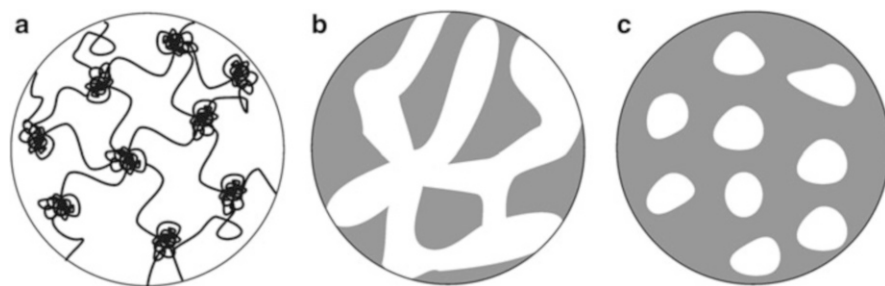
Fig. 5 Three typical frozen-in morphologies of gels obtainable by LL phase separation interrupted by vitrification: (**a**) Molecularly connected morphology comprising glassy spheres of the polymer-rich phase connected by isolated solvated chains. (**b**) Bi-continuous two-phase morphology. (**c**) Continuous glassy phase including droplets of the polymer-poor phase. The polymer-rich phase is *gray*, the solvent-rich phase is *white*. In **b**, the connectivity of the two phases could only be represented in two dimensions. For crystallizable polymers, the physical crosslinks in **a–c** may also be small crystallites, either in the shape of chain-folded lamellae or fringed micelle-like aggregates

de-mixing and crystallization processes are arrested by vitrification. In both cases, gels may be formed only if the degree of connectivity in the polymer-rich phase achieves a threshold value. Furthermore, regardless of undercooling depth, the above hierarchy of metastability may become accessible only if the initial homogeneous solution is cooled to the target temperature at high rates. For low cooling rates, crystallization is likely to occur during the cooling process before the attainment of binodal and/or vitrification. In route 1 of Fig. 4b, homogeneous gelation may take place if small crystallites are formed that are well interconnected all over the macroscopic sample by well solvated tie chains (as shown in Fig. 5a), the difference being that the amorphous nodules are replaced by chain-folded lamellae or fringed micelle-like crystals. By contrast, the structures of gels that are likely to result from route 2 of Fig. 4b are porous and heterogeneous (as shown in Fig. 5b, c). They consist of two bi-continuous phases meandering around each other, namely a polymer-rich and a polymer-poor phase. In these gels, the regions of the polymer-poor phase act as pores and allow small and large molecules to diffuse, whereas the polymer-rich regions are heterogeneous and include an amorphous phase swollen by the solvent and small crystals or glassy nodules of the polymer. The chains in the amorphous phase connect the crystallites and/or the glassy nodules constituting the physical crosslinks of the 3D macroscopic network of the gels.

3 Poly(Vinyl Alcohol) Hydrogels

PVA is one of the most studied gel-forming polymers and is able to give rise to a large variety of gels of widespread interest, using several kinds of solvents and under a large variety of preparation/processing conditions [1]. Confining our attention to PVA hydrogels, it has been shown that aqueous solutions of PVA can form gels under several conditions and that the properties of the resultant systems are largely dependent on the structure fixed by the preparative route.

In this section, after a brief discussion of the principal categories of PVA physical hydrogels in general, the PVA hydrogels obtained by cryogenic treatments are treated in detail.

3.1 Crystal Structure of PVA

PVA is an atactic polymer obtained by free radical polymerization of vinyl acetate and successive hydrolysis. The hydrolysis of poly(vinyl acetate) (PVAc) does not convert all the acetate groups into hydroxyl groups, but gives rise to PVA polymers with a partial degree of hydrolysis that depends on the extent of the reaction.

The properties of PVA are strongly influenced by the degree of hydrolysis [39]. For instance, the water solubility of PVA depends on the degree of hydrolysis and the molecular weight [12]. The higher the degree of hydrolysis of PVA grades, the lower the corresponding PVA solubility. Residual acetate groups in partially hydrolyzed PVA improve water solubility by disrupting polymer–polymer inter- and intrachain hydrogen bonding between hydroxyl groups and, consequently, promote polymer–solvent interactions [12]. In highly hydrolyzed PVA grades, the water solubility decreases due to unhindered formation of polymer–polymer interchain and intrachain hydrogen bonds between the pendant hydroxyl groups, so that establishment of effective interactions of PVA chains with the solvent are prevented.

In spite of the lack of stereoregularity, atactic PVA is a semicrystalline polymer [40, 41]. The crystal structure of PVA was resolved in 1948 by Bunn [41]. It is characterized by chains in a *trans*-planar conformation, packed in a monoclinic unit cell with $a = 7.81$ Å, $b = 2.52$ Å (chain axis), $c = 5.51$ Å, and $\beta = 91.7°$ (see Fig. 6).

The arrangement of chains inside the crystals can be described as consisting of double layers of chains running parallel to the *bc*-plane, and stacked along the *a*-axis. These double layers are defined by the hydrogen bonds established between the hydroxyl groups belonging to first adjacent chains facing along *a*. Consecutive double layers establish only weak van der Waals interactions. The degree of stereoregularity of PVA significantly affects the crystallizability, and atactic PVA is more easily crystallized than the isotactic and syndiotactic counterparts [1, 12].
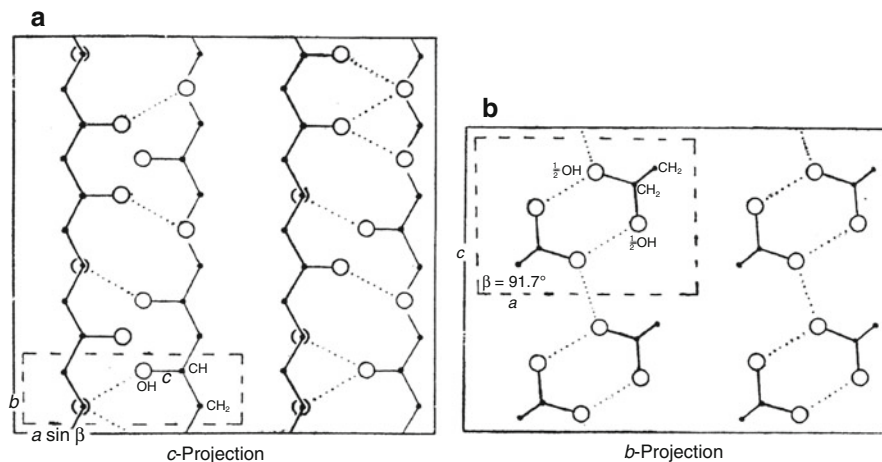
Fig. 6 (**a**, **b**) Model of the crystal structure of atactic PVA, proposed by Bunn [41] in the c-axis (**a**) and b-axis (**b**) projections. *Dotted lines* represent hydrogen bonds established between the hydroxyl groups belonging to adjacent chains along the a-axis within a double layer. The unit cell is indicated by *dashed lines*. Since PVA is atactic, the occupation factors of –OH groups is ½
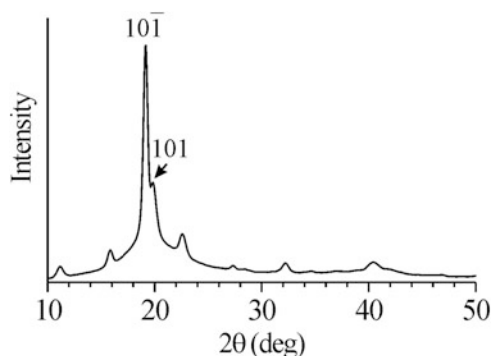
Fig. 7 X-ray powder diffraction profile of crystalline PVA. The $10\bar{1}$ and 101 reflections at $2\theta = 19.4°$ and $20°$, respectively, are indicated [42]. (Reproduced with permission from [42]. Copyright 2004 by American Chemical Society)

The melting temperature of PVA ranges between 220 and 240 °C. The glass transition temperature is 85 °C in dried PVA samples [1], and decreases with the amount of water adsorbed by PVA due to plasticization effects. For instance, the glass transition temperature of PVA containing 10 wt% of water is $\approx$37 °C.

The wide angle X-ray (WAXS) powder diffraction profile of crystalline PVA is reported in Fig. 7 [42]. A strong peak at $d = 4.68$ Å ($2\theta = 19.4°$) and a shoulder at $d = 4.43$ Å ($2\theta = 20°$) are present, corresponding to the $10\bar{1}$ and 101 reflections, respectively, of the monoclinic unit cell [41].

3.2 PVA Physical Hydrogels

The formation of physical gels from water solutions of PVA has been widely studied. In fact, it is well known that aqueous PVA solutions undergo gelation upon cooling. In these gels, the physical cross-links are generally fringed micelle-like PVA crystallites. In particular, Komatsu et al. [43] found that the phase diagram of this system shows an upper critical solution temperature (UCST), and that the spinodal curve crosses the sol–gel transition curve. This phase diagram is redrawn in Fig. 8.

It is apparent that gelation takes place both below and above the spinodal curve, indicating that gels may be formed either accompanied by spinodal decomposition or without liquid–liquid phase separation, respectively [43]. In both cases, crystalline gels are formed where small crystals of PVA in the monoclinic form [40, 41] act as junctions [43, 44]. Statistical gels having a homogeneous structure are formed in the temperature–concentration region above the spinodal; however, the supramolecular structure of the hydrogels that develop in the temperature–concentration region below the spinodal is considerably different and more heterogeneous than the structure of the statistical gels [17, 24, 25, 43]. As discussed in Sect. 2, the development of an interconnected structure in the polymer-rich phase formed by spinodal decomposition is not necessarily the origin of gelation [17, 25]. In fact, in order to have a gel some agency should come into play to arrest PVA crystallization and/or LL phase separation at an intermediate stage, creating circumstantial metastability [25]. In the case of PVA, the network structure may be easily created by occurrence of LL phase separation, which arrests crystallization, and/or vitrification that arrests both crystallization and LL phase separation (Fig. 5b). Since the glass transition of dry PVA is equal to $\approx 85\,^\circ$C and is lowered to $\approx 37\,^\circ$C by the presence of ≈ 10 wt% water, LL phase separation of aqueous solutions of PVA are likely to occur below the Berghmans point [17, 25]. This means that PVA hydrogels formed below the spinodal may correspond to metastable frozen-in configurations affected by vitrification. Whatever the exact mechanism of gelation of PVA, the physical junctions of the macroscopic network are not only PVA crystallites, but also entanglements and hydrogen bonds.

Formation of physical gels from aqueous PVA solutions may also occur by impairing the thermodynamic quality of the solvent as a result of the introduction of nonsolvent additives [4, 5, 45]. However, in all cases, the so-obtained thermoreversible PVA gels possess low melting temperatures ($T_m < 30$–$40\,^\circ$C), low mechanical strength, and they are not able to retain their size and dimensions for a long time.

Attempts to make stronger physical hydrogels of PVA include induction of crystallization through dehydration at a slow drying rate [1, 46] and/or fast drying rate procedures such as annealing, under different conditions [1, 47]. The presence of crystals in physical hydrogels of PVA generally results in better mechanical properties than in PVA gels prepared through chemical or radiation-induced techniques.

Fig. 8 Sol–gel transition
curve, spinodal, and binodal
of water/PVA binary system
(redrawn from [43]). The
left arrow indicates the
glass transition temperature
of 37 °C relative to a PVA
sample that had not been
dried before DSC
measurement and contained
≈10 wt% water.
(Reproduced with
permission from
[43]. Copyright 1986 by
Wiley)
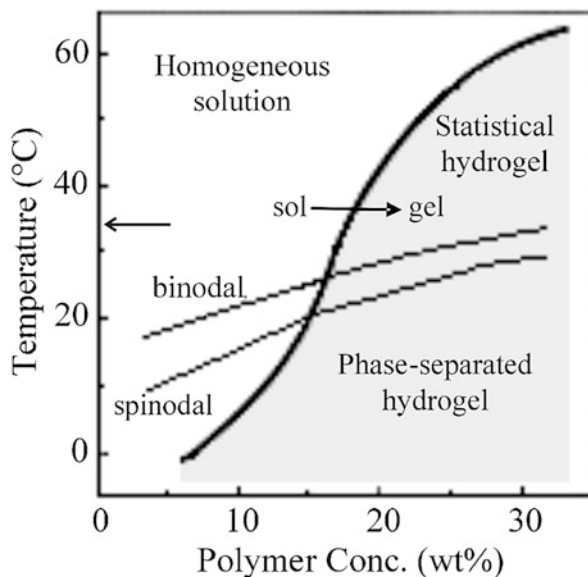
3.3 PVA Cryogels

In water/PVA systems, gelation may also be induced by cryogenic treatments, i.e.,
at temperatures where the formation of ice crystals takes place [1–7]. Cryogelation
was introduced at the beginning of the 1970s as a new technique for the preparation
of PVA physical hydrogels having improved mechanical properties [2, 48] with
respect to those obtained using more conventional methods. As already stated in the
"Introduction," this cryogenic process consists in submitting a PVA aqueous
solution to repeated cycles of freezing at subzero temperature ($T < -4$ °C) and
thawing to room temperature. In PVA hydrogels prepared by the freeze–thaw
technique and having a rather high PVA content, the junctions in the stable
supramolecular network are crystallites [1, 49].

Peppas made the first attempts to understand the freeze–thaw process of PVA
solutions to form hydrogels by performing turbidimetric measurements [1,
2]. Peppas studied the gelation mechanism on water solutions with PVA content
in the range 2.5–15 wt%, frozen at −20 °C for 45–150 min, and then thawed at
23 °C for long periods of time (up to 12 h). He explained the appearance of turbidity
after freezing in terms of a partial crystallization of chain segments into microcrys-
talline aggregates. Moreover, Peppas demonstrated that crystallinity increases with
increasing freezing time as well as with increasing PVA concentration [2].

Yokoyama and coworkers [49] performed X-ray diffraction experiments on
PVA hydrogels. The X-ray diffraction patterns of these gels showed the presence
of crystalline reflections. However, a deeper analysis of diffraction data was not

carried out because of the very low crystallinity in these systems and the presence of a broadly diffuse scattering due to the water [1, 49].

Watase and Nishinari [8] examined PVA hydrogels obtained by freeze–thaw cycles (−20 °C for 11 h, followed by 15 °C for 7 h), starting from an aqueous 15 wt% PVA solution. PVA specimens used were of five different degrees of hydrolysis, ranging from 96.0 up to 99.9 mol% hydrolyzed acetate groups. In this study, the PVA gel samples were immersed in water for 4 days before the analysis. The authors [8] reported X-ray diffraction patterns for PVA gels in the stretched and unstretched states. The X-ray diffraction profiles exhibited a halo characteristic of amorphous materials at $2\theta = 26$–$27°$ and a weak crystalline peak at about $2\theta = 19.5°$, corresponding to a d spacing of 4.53 Å. This characteristic crystalline peak was not observed for gels with a rather low degree of hydrolysis of PVA (96.0 mol%) stretched at low deformation, but it appeared at draw ratios higher than five times the initial length. The differential scanning calorimetry (DSC) thermograms of the PVA hydrogels showed an endothermic peak at about 60 °C, attributed to the disentanglements of flexible molecular chains. Another endothermic peak at higher temperature was found for all samples except for the sample prepared with PVA at the lowest degree of hydrolysis. This second peak was considered to be due to the melting of crystalline regions. The authors concluded that repeated freeze–thaw cycles as well as stretching increase the degree of crystallinity and that the elasticity is strongly affected by the latter parameter [8]. In a following study on PVA hydrogels obtained by freeze–thaw cycles, the same authors [50] pointed out by rheology, DSC, and X-ray analysis how slight differences in the degree of hydrolysis may significantly change the gel structure. They showed that the presence of bulky acetate groups can inhibit the formation of PVA gels [50].

The structure and dynamics of PVA hydrogels obtained by freeze–thaw cycles have been studied by ^{13}C NMR and ^{1}H pulse NMR methods [51–54]. Kobayashi et al. [51, 52] used high-resolution solid-state ^{13}C NMR experiments to show the role of intermolecular hydrogen bonds in the formation of PVA hydrogels through the formation of interchains crosslinks. The hydrogen bonds can be studied by observing the methine carbon lines in the immobile regions of gels; the lines can be assigned to carbons involved in two, one, and no hydrogen bonds [55]. The hydrogen bonds in the crosslinked region in PVA gels have the same NMR characteristics as those observed in the solid neat PVA. From such evidence, it was concluded that microcrystallites are formed in PVA gels.

As an example, the X-ray powder diffraction profiles of freeze–thaw PVA hydrogel samples are reported in Fig. 9 after subtraction of a straight baseline, approximating the background contribution. These gels were obtained by subjecting a 11 wt% aqueous solution of PVA to a different number of consecutive cycles consisting of a freezing step (20 h at −22 °C) followed by a thawing step (4 h at 25 °C) [42]. The as-formed PVA hydrogels obtained by one to nine freeze–thaw cycles are denoted as GEL-1 to GEL-9 samples. For comparison, the diffraction profile of pure water is also shown in Fig. 9.
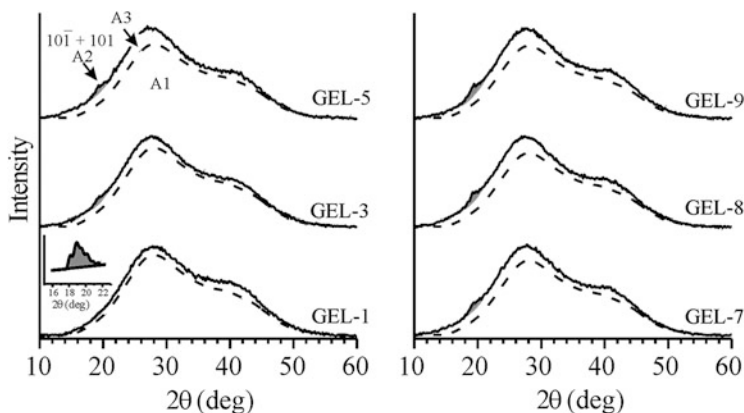
Fig. 9 X-ray powder diffraction profiles of freshly prepared PVA cryogels (samples GEL-*n*) obtained by different numbers *n* of freeze–thaw cycles (*solid lines*). The X-ray diffraction profile of liquid water is also shown (*dashed lines*). The $10\bar{1}$ and 101 reflections of PVA crystals in the monoclinic form, in the 2θ range 18–21°, are shown in *gray*. In the case of GEL-1, the crystalline reflections are evidenced in the *inset* at an enlarged scale. (Reproduced with permission from [42]. Copyright 2004 by the American Chemical Society)

The diffraction profiles of these gels may be considered as arising from the sum of three contributions: a large contribution (region A1) derived from the pure water or a polymer-poor phase (dashed line), a small diffraction component in the range 18–21° derived from crystalline aggregates of PVA (region A2), and a third contribution (region A3) derived from the amorphous PVA phase swollen by the solvent (see Fig. 9). Therefore, at least three phases coexist in these gels: a polymer-poor phase consisting of almost pure solvent, PVA crystallites, and swollen amorphous PVA. It is apparent that the largest contribution to the X-ray diffraction scattering is due to water, whose relative amount is $\approx 88\%$ in the case of GEL-1 and gradually decreases with increasing number of freeze–thaw cycles, reaching the value of $\approx 85\%$ in the case of GEL-9 [42]. However, in all cases, the presence of $10\bar{1}$ and 101 Bragg reflections of PVA crystals in the monoclinic form, in the 2θ range 18–21°, is the hallmark that PVA cryogels are crystalline.

The presence of crystals in PVA cryogels has been confirmed by numerous techniques, including ^{1}H NMR free induction decay experiments, and DSC analysis [56, 57].

In Fig. 10, the fractions of crystalline PVA with respect to the total amount of PVA in the crystalline and swollen amorphous phases, obtained by X-ray powder diffraction analysis, $f_c(XR)$ [57], are reported as a function of the number of freeze–thaw cycles for the as-formed PVA hydrogels. They are compared with the fractions of crystalline PVA with respect to the total amount of PVA in hydrogels, as determined by DSC, $f_c(DSC)$ [42, 57], and the fractions of rigid protons calculated from ^{1}H free induction decay experiments, $f_c(NMR)$ [56, 57]. In all cases, the
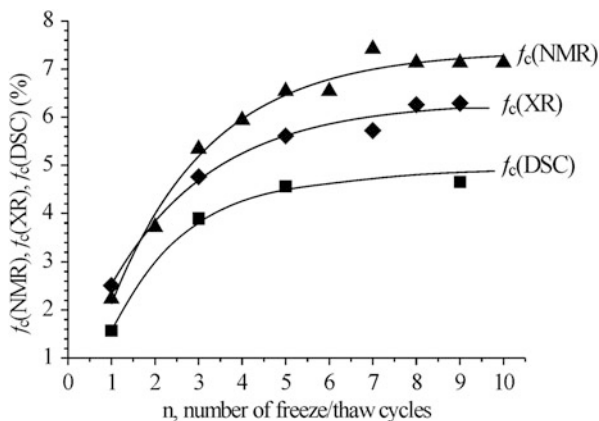
Fig. 10 Fraction (%) of crystalline PVA with respect to the total amount of PVA in the crystalline and swollen amorphous phases, obtained by X-ray powder diffraction analysis, $fc(XR)$ *(diamonds)* [42]; fraction of crystalline PVA with respect to the total amount of PVA in hydrogels, determined by DSC, $fc(DSC)$ *(squares)* [57]; and fraction of rigid protons, calculated from ^1H free induction decay experiments, $fc(NMR)$ *(triangles)* [56, 57], as a function of the number of freeze–thaw cycles (n) for the as-formed PVA hydrogels. (Reproduced with permission from [57]. Copyright 2004 by the American Chemical Society)

cryogels were obtained using the same protocol, starting from a D_2O solution of 11 wt% PVA. It is apparent that the percentage of rigid PVA protons $f_c(NMR)$ and the values of $f_c(XR)$ are in good agreement. They both increase with increasing number of freeze–thaw cycles, from a value of 2.5 % up to a nearly plateau value after about five cycles. In particular, for GEL-9 the degree of crystallinity is around 6–7 %. The values of $f_c(DSC)$ show the same plateau behavior after five freeze–thaw cycles, even though they are systematically lower than the values of $f_c(XR)$ and $f_c(NMR)$. This is due to the fact that, as a result of the small size of crystallites in PVA hydrogels and the presence of large amounts of water, in the DSC heating curves of these gels there is a strong overlap between the endothermic transition due to the melting of PVA crystals and exothermic phenomena due to PVA solubilization and solvation (or even recrystallization) [57].

More sophisticated NMR techniques have been also applied to measure the crystallinity in PVA cryogels [58]. For instance, pulsed mixed magic-sandwich echo sequences have been applied in a low-field NMR spectrometer [58]. This kind of pulse sequence provides near-quantitative refocusing of the rigid contribution to the initial part of proton free induction decay [58], allowing for a more quantitative determination of crystallinity in these gels. The results so obtained essentially confirm those shown in Fig. 10.

3.4 Structure of PVA Cryogels at Different Length Scales

The three-phase model adopted to describe the fraction of crystalline PVA in freeze–thaw hydrogels from X-ray diffraction analysis is in agreement with numerous studies.

For instance, in 1986, Yokoyama et al. investigated the morphology and structure of PVA freeze–thaw hydrogels (5–15 wt% of PVA), using a variety of techniques including X-ray diffraction, scanning electronic microscopy (SEM), and light optical microscopy [49]. They showed, by SEM analysis, that these gels have a porous structure, where the pore size increases from approximately 1 to 10 μm as the polymer concentration decreases from 15 to 5 wt%. They proposed a three-phase model to describe the porous structure of these gels (Fig. 11). The model consists of a water phase with a very low PVA concentration, an amorphous phase in which each PVA chain is swollen by water, and a PVA crystalline phase that partially prevents the motions of the amorphous chains. According to this model, the pores are mainly occupied by a polymer-poor phase that forms an interconnected continuous network, meandering through polymer-rich regions. The ice crystals are accommodated in the polymer-poor phase during the freezing step. The polymer-rich regions, in turn, are interconnected and build up the 3D network scaffold of the gels delimiting the pores. These regions consist of a swollen amorphous phase and PVA crystallites where the amorphous portions of chains connect the crystalline domains acting as junctions. Formation of the crystalline crosslinks ensures high dimensional stability and gives elastic properties to these gels.

The porous structure of PVA hydrogels is already imprinted in the first freeze–thaw cycle. This was shown by Fergg et al., using confocal laser scanning microscopy (CLSM) in the fluorescent mode [59], in the case of PVA hydrogels obtained by imposing a single freeze–thaw cycle (−15 °C for 24 h, then room temperature for 3 h). The advantage of using CLSM is that water does not need to be removed from hydrogels prior to examination. In the case of SEM analysis, dehydration procedures are always required before performing the observations, with the consequent drawback that the native morphology of gels might be significantly altered. Selected CLSM micrographs (extracted from [59]) of PVA hydrogels are shown in Fig. 12.

The pore or mesh size in these cryogels increases from ≈2 to 7 μm with decreasing PVA concentration. The CLSM analysis also indicates a tight interconnection of the pores all over the macroscopic samples, a uniform size of pores in the bulk, and no preferential structural orientation [59].

The complex architecture of PVA hydrogels, which includes a polymer-poor phase filling the pores and interconnected polymer-rich regions building the 3D network, made up by crystalline crosslinks connected by PVA chains belonging to the swollen amorphous regions (Fig. 11), has also been confirmed by small angle neutron scattering (SANS) measurements. Typical SANS profiles from as-formed PVA hydrogels obtained by subjecting a deuterated water solution of 11 wt% PVA
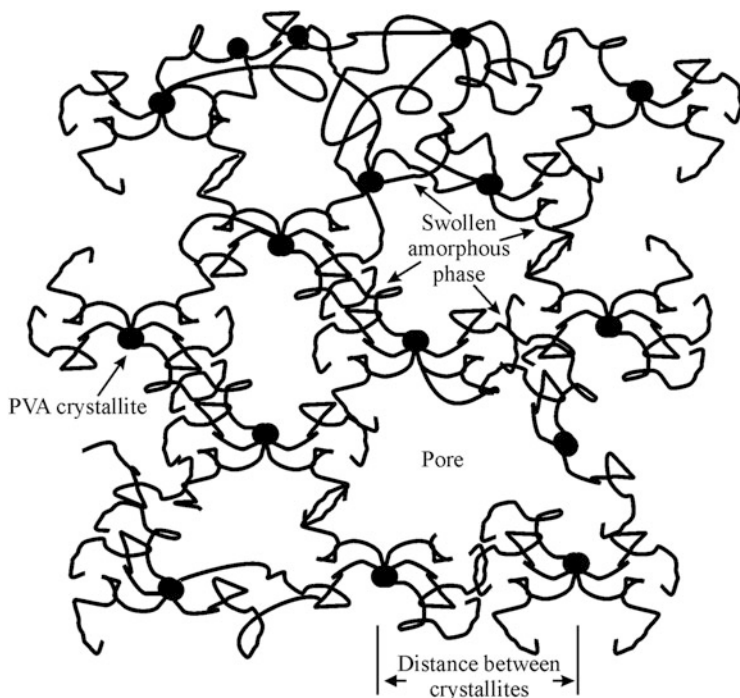
Fig. 11 Structural model of the porous structure for PVA hydrogels prepared by repeated freezing and thawing cycles [49]

to one (GEL-1) and nine (GEL-9) consecutive freeze–thaw cycles (20 h at $-22\,^{\circ}$C, then 4 h at 25 $^{\circ}$C) are shown in Fig. 13 [60]. The SANS profile of the initial homogeneous solution is also shown in Fig. 13a.

It is apparent that the scattering cross-section profile $(d\sigma/d\Omega)$ from the homogeneous PVA solution denotes the presence of small scattering objects, essentially corresponding to individual chains of PVA with a Gaussian coil conformation (Fig. 13a). This curve is different from those of PVA GEL-n samples, indicating that PVA chains and solvent molecules are highly organized in these gels. In the SANS profiles of the gels, three different regions can be distinguished:

1. A region at low q values ($q < 0.09\,\mathrm{nm}^{-1}$), where $q = 4\pi/(\lambda\sin\theta)$. In this region, the scattering cross-section exhibits an upturn, which is not present in the SANS curve of the initial homogeneous solution. In this zone, the data reflect a supramolecular organization, which has been associated with the presence of two separated phases constituted of polymer-rich and polymer-poor regions.
2. A region at intermediate q values ($0.09 < q < 0.35\,\mathrm{nm}^{-1}$). In this region, an inflexion point is present at q^*, which gives the average distance L between the scattering crystallites, where $L \approx 2\pi/q^*$. In all gel samples, this inflexion point
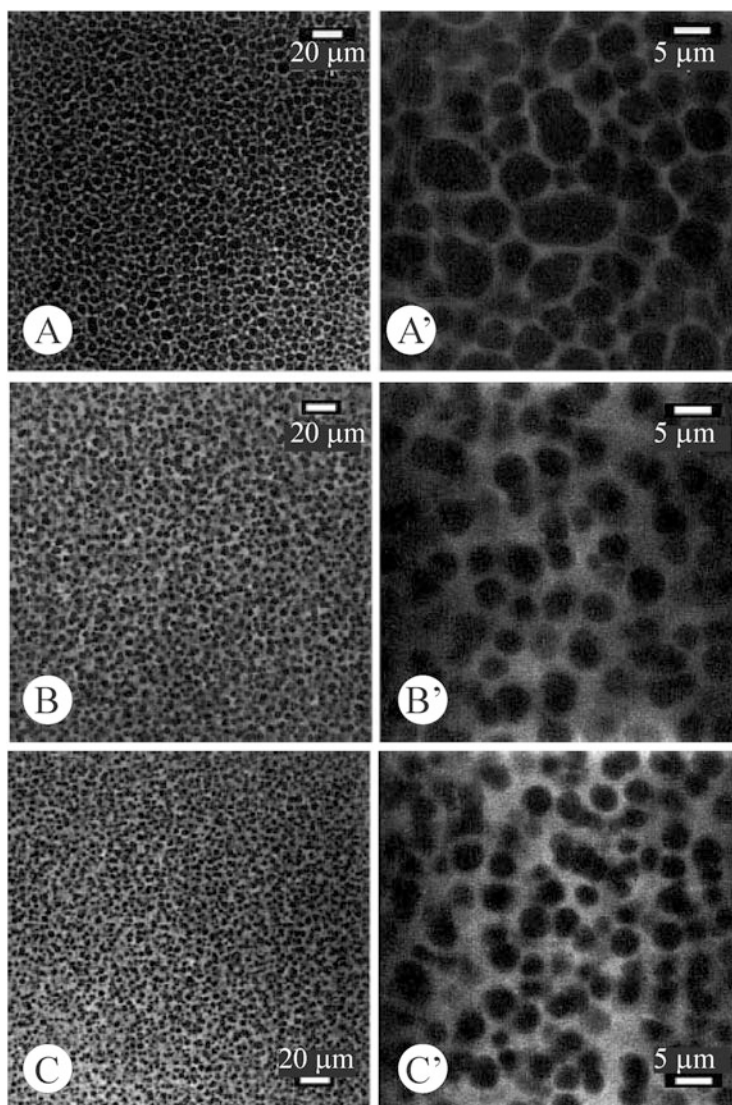
Fig. 12 (**a–c′**) Confocal laser scanning microscopy (CLSM) images of PVA hydrogels obtained by imposing a single freeze–thaw cycle on initial water solutions of PVA containing poly(ethylene glycol) PEG-600 of weight composition PVA/PEG/water 8/10/90 (**a, a′**), 12/10/90 (**b, b′**), and 16/10/90 (**c, c′**). All samples were examined after washing out PEG-600 and after addition of 5-dichlorotriazine fluorescein as fluorochrome. Images of bulk structures were taken at 10 μm (**a, a′**) and 15 μm under the surface (**b, b′, c, c′**) at two different magnifications as indicated [59]. (Reproduced with permission from [59]. Copyright 2001 by Springer)
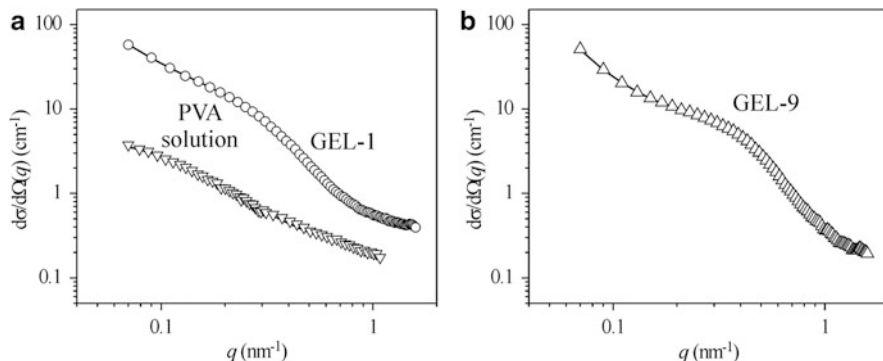
Fig. 13 SANS data from freshly prepared PVA cryogels (samples GEL-n) obtained by subjecting a deuterated water solution of 11 wt% PVA to (**a**) one (GEL-1) and (**b**) nine (GEL-9) consecutive freeze–thaw cycles (20 h at $-22\ ^\circ$C, followed by 4 h at 25 $^\circ$C). Data from the initial PVA solution (∇) used for gel preparation are included in **a**. $d\sigma/d\Omega$ is the scattering cross-section and q is the scattering vector, where $q = 4\pi/(\lambda\ \sin\theta)$, with θ being one half of the scattering angle. (Reproduced with permission from [60]. Copyright 2002 by the American Chemical Society)

occurs at $q^* \approx 0.03$ nm^{-1}, indicating a distance between crystallites of the order of 20 nm.

3. A region where $0.35 < q < 0.8$ nm^{-1}. In this zone, the scattering cross-sections decrease with a power law $d\sigma/d\Omega \propto q^{-D}$, where the value of D depends on the number of cycles. More precisely, $D \approx 2$ for GEL-1 and $D \approx 3$ for GEL-9. Provided we are looking in this region at the boundary structure between two phases, possibly the crystallites and the swollen amorphous phase, we may apply the surface fractal concept to the function $d\sigma/d\Omega$. According to this concept, the exponent D is related to the surface fractal dimension d_s in a d-dimensional space, through $D = 2d - d_s$. For example, in 3D space, d_s ranges from 2 to 3, corresponding to a range of D from 4 to 3. If the boundary were smooth, Porod's law $\left(d\sigma/d\Omega \propto q^{-4}\right)$ would be observed. For our PVA gels, values of D less than 4 suggest that the boundary is not smooth, due to some degree of interpenetration between the amorphous and crystalline phases at the interface.

From the analysis of SANS data [60], an average size of PVA crystallites equal to about 3 nm could be established, in good agreement with the coherence length of crystallites determined from the width at mid-height of $10\overline{1}$ reflection in the X-ray diffraction profiles of these gels (Fig. 9) by applying the Scherrer formula [42].

The hierarchical structural model emerging from microscopic, WAXS, and SANS investigations of PVA cryogels is shown in Fig. 14.

According to this model, PVA chains and solvent molecules in these gels are organized over different hierarchical length scales. At the micrometer length scale, two bi-continuous phases meandering around each other co-exist, consisting of

Fig. 14 The bi-continuous structure of PVA hydrogels obtained by freeze–thaw cycles with a PVA-rich phase and a PVA-poor phase. The fine structure of the polymer-rich region, including PVA crystallites and a swollen phase, is also indicated
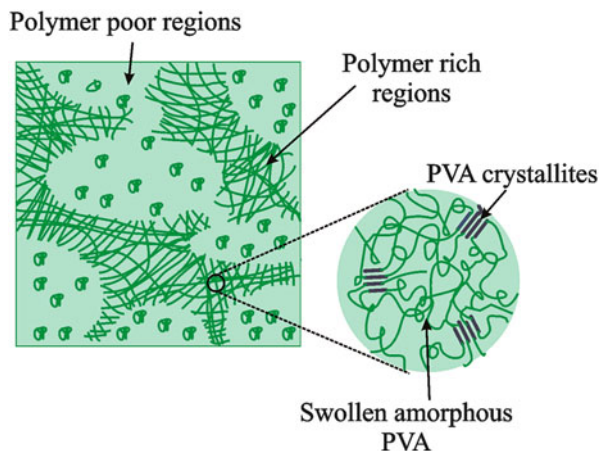
polymer-rich and polymer-poor regions [4–6, 60, 61]. The polymer-rich regions (of average dimensions on the order of micrometers) [60] include crystallites of PVA of size equal to 3–4 nm [42, 60] and a swollen amorphous phase. The average distance between crystallites is on the order of 10–20 nm [60]. The polymer-poor regions, in turn, constitute the macropores and have sizes on the order of 1–10 μm [1, 4–6, 62, 63]. The physical crosslinks of the macroscopic network are essentially PVA crystallites connected by portions of chains swollen by the solvent [42, 57, 61].

3.5 Influence of Addition of Other Solvents

The influence of additional solvents to PVA/water solutions in the preparation of PVA gels by the freeze–thaw technique has been studied by numerous authors.

As an example, Hyon and Ikada prepared transparent hydrogels from PVA solutions in mixed solvents of water and water-miscible organic compounds [1, 64] such as dimethyl sulfoxide, glycerine, ethylene glycol, propylene glycol, and ethyl alcohol. Upon cooling these solutions to subzero temperatures, the presence of the organic solvent mixed with water prevents the PVA solution from freezing. At these temperatures PVA crystallization takes place, giving rise to formation of gels. The successive extraction of the organic solvent from the gels by exchange with water provides fully hydrated gels of PVA with high tensile strength, high water uptake, and high light transmittance. The last property is very important, especially for contact lenses applications [65]. The mechanism of gelation and formation of gels with increased light transmittance was explained as follows [64]: As the homogeneous solution is cooled, molecular motions are constrained. The consequence is that the interchain interactions of PVA, probably due to hydrogen

bonds, are promoted to yield small crystalline nuclei. Crystallization can proceed further as the solution remains at low temperatures for longer times. The crystallites serve as crosslinks to hold the 3D network structure. By addition of organic solvent, the PVA solution is prevented from freezing, even at temperatures below 0 °C. This permits PVA crystallization to proceed without a significant volume expansion. Therefore, the resulting gel contains pores smaller than 3 μm, giving rise to a transparent gel [1, 64].

In the case of PVA gels prepared by freezing and thawing techniques in the presence of ethylene glycol, Berghmans et al. suggested a two-step mechanism [66] involving a liquid–liquid phase separation in the first step (evidenced from the fact that the gel becomes opaque) followed by PVA crystallization in the polymer-rich phase in the second step.

Extensive studies have also been performed on PVA gels using mixtures of dimethyl sulfoxide and water as solvent (60/40 v/v) [67–73]. It was shown that gels prepared by freezing below –20 °C are transparent. Their properties depend on the ratio of dimethyl sulfoxide to water. It was also noted that gelation occurs below –20 °C without phase separation. However, above this temperature, LL phase separation plays an important role for the gelation process, giving rise to opaque gels.

Kanaya et al. used wide and small angle neutron scattering and light scattering experiments to provide extensive information concerning the structural organization of PVA gels formed in mixtures of DMSO and water at various length scales [67–73]. The presence of small PVA crystallites acting as crosslinks for the 3D network of these gels was confirmed. The crystallites have a sharp surface, presenting an average size of ≈7 nm and average distance of about 15–20 nm.

Trieu and Qutubuddin also investigated the structure of freeze–thaw PVA gels obtained from aqueous DMSO solutions [74, 75]. The authors characterized the gels by using freeze-etching and critical point drying SEM techniques. A higher porosity was observed at the surface than in the bulk of the gel.

It is worth noting that, regardless of the kind of solvent (pure water and/or water mixtures with other solvents), features common to PVA gels obtained by cryotropic treatments are the presence of a complex porous architecture that includes macropores filled with a polymer-poor phase and meandering polymer-rich regions. The tight interconnection of these pores allows for almost unhindered diffusion of large and small molecules [1, 4–6, 62, 63]. The polymer-rich regions are interconnected and constitute a biphasic 3D network consisting of a swollen amorphous PVA phase and PVA crystallites (Fig. 14). In all cases, although hydrogen bond interactions play a key role in creating the physical junctions of the network, the high dimensional stability and mechanical strength achieved by these gels is due to the presence of crystalline crosslinks. In particular, the size and amount of PVA crystalline aggregates in freeze–thaw PVA hydrogels play important roles in gel performance because the dimensional stability, toughness, strength to external stresses, and thermal stability of PVA cryogels are critically dependent on these parameters.

3.6   Mechanism of Formation of PVA Cryogels

The mechanism of formation of the hierarchical structure of PVA cryogels featuring an open porous structure is the result of the occurrence of at least three concomitant and, at the same time, conflicting processes: crystallization of the solvent, LL phase separation, and crystallization of PVA. At subzero temperatures, solutions having the typical concentrations used for preparation of PVA cryogels are below the spinodal curve shown in Fig. 8 [4–6, 43]. Therefore, during freezing and successive permanence of the solution at subzero temperatures, a LL phase separation may occur in addition to the crystallization of solvent and PVA. The exact mechanism of formation of the macroporous structure (i.e., water crystallization at subzero temperatures or LL phase separation, or the concomitant effect of both transitions) depends on a number of factors such as the cooling rate at subzero temperatures, the use of other solvents mixed with water, the presence of additives, and the PVA concentration [4–6].

Applying the arguments given in Sect. 2, the formation mechanism of PVA cryogels represents a paradigmatic example of the Ostwald "stage rule" [17, 25, 33]. This means that, upon formation of these gels, a hierarchy of metastability may arise due to the possible occurrence of several metastable phases via different processes [17, 25]. Therefore, when a given process is arrested by an agency before completion, the system is frozen in a phase of circumstantial metastability that, once formed, has the potential to evolve faster than the transition leading to the ultimate stable phase and may dominate the whole transformation process [17, 25].

Lozinsky and coworkers [4–6] suggested a general mechanism for cryotropic gelation, which is illustrated in Fig. 15.

In this model, the initial solution (Fig. 15a), is frozen at temperatures slightly below the solvent crystallization point, giving rise to an inhomogeneous system that includes an unfrozen liquid microphase along with crystals of the frozen solvent (Fig. 15b). Since the polymer (and any other additive) are generally rejected in the unfrozen liquid microphase, the solute concentration in the unfrozen liquid microphase is higher than in the initial solution. At this stage, a crosslinking process (chemical or physical) may easily take place in the unfrozen liquid microphase, leading to the formation of microgel fractions. If the regions occupied by the microgel fraction achieve an interconnected structure, a macroscopic gel is obtained upon defrosting. Thus, Lozinsky considered that cryogels are formed inside these unfrozen microregions of the frozen system [4–6]. During freezing, the crystals of frozen solvent act as a porogen and grow until they meet the facets of other solvent crystals. Upon thawing, the system transforms into a macroporous cryogel containing large interconnected pores with variable size and geometry (Fig. 15c). The dimensions and shape of the pores are related to the volume of the unfrozen liquid microphase, which depends on numerous factors such as the nature of solvent, initial polymer concentration, the molecular weight of solutes, the system temperature, and the presence of soluble or insoluble admixtures [4–6].
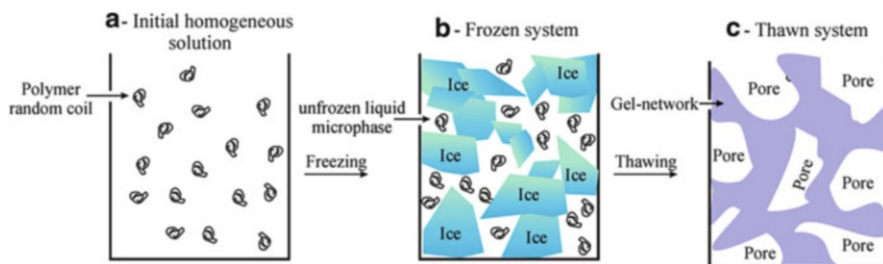
Fig. 15 Mechanism for cryotropic gelation according to the model suggested by Lozinsky [4–6]. During (**a**) freezing of an initially homogeneous solution, incomplete solvent crystallization occurs, leading to (**b**) the formation of an unfrozen liquid microphase. Gelation takes place in these unfrozen regions, forming a microgel fraction. (**c**) Upon defrosting, the regions occupied by solvent crystals give rise to the pores, whereas the regions occupied by the microgel fraction may achieve an interconnected structure that gives rise to the macroscopic 3D network of the gels

Based on data obtained by cryogenic transmission electron microscopy (cryo-TEM), solid-state NMR, X-ray scattering, and DSC, Willcox et al. [61] proposed a model for PVA cryogels similar to that proposed by Yokoyama (Fig. 11) [49]. In particular, they showed that during the first freeze–thaw cycle a few small crystallites are formed (with size of about 3–8 nm), which are connected in an irregular porous network by amorphous chains highly swollen by the solvent. They found that the average crystal–crystal distance (mesh size) is ≈30 nm. Upon aging these gels, or by subjecting them to a second freeze–thaw cycle, the level of crystallinity increases, whereas the crystallite size and the mesh size remain nearly constant. This suggests that the formation of secondary crystallites does not affect the network connectivity. Cryo-TEM observation of these gels essentially confirmed the presence of pores located at the same mesh distance as crystallites [61]. Therefore, Willcox and colleagues [61] point out the existence of pores sized one order of magnitude lower than the macropores visualized in other investigations [49, 59] (Fig. 12). We infer that these pores are formed inside the polymer-rich regions and coexist with the macropores. The possible mechanism of formation of these gels, involving dendritic ice crystallization and possibly spinodal decomposition, are also discussed [61].

Our group has used TR-SANS to perform extensive investigations on the cryotropic gelation of PVA/D$_2$O solutions during consecutive freeze–thaw cycles [76, 77]. Measurements have been performed on solutions of 5.03, 10.11, and 14.22 wt% PVA, corresponding to PVA volume fractions Φ of 0.042, 0.086, and 0.12, respectively. In Fig. 16a, the SANS data collected during the freezing (at –13 °C) and thawing (at 20 °C) steps are shown for a solution with PVA volume fraction $\Phi = 0.086$ [76, 77] as an example.

The scattering cross-section increases during freezing (Fig. 16a). This increase is essentially due to structural changes associated with the crystallization of the water in the solution. Nearly constant values are achieved for the frozen solution after 30 min at –13 °C (curve d in Fig. 16a). The presence of a knee at
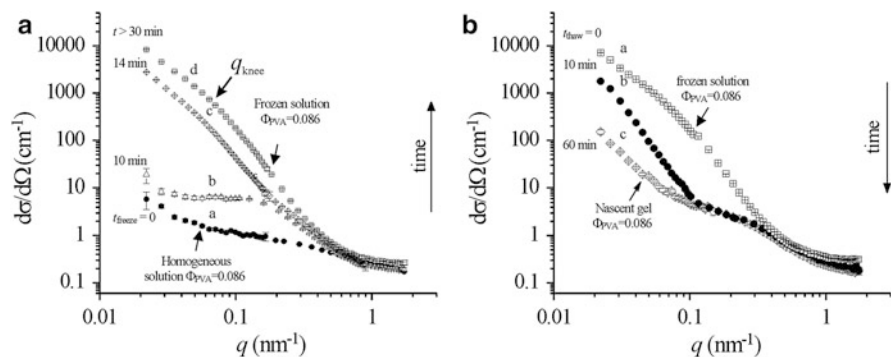
Fig. 16 Change in the scattering cross-section as a function of the scattering vector q: (**a**) from an initial solution with $\Phi_{PVA} = 0.086$, collected at room temperature ($t_{freeze} = 0$) (*a*) and after successive freezing and permanence of the solution at $-13\ ^\circ C$ for 10 min (*b*), 14 min (*c*), and 30 min (*d*); and (**b**) from the frozen solution after 390 min at $-13\ ^\circ C$ ($t_{thaw} = 0$) (*a*) and after successive thawing and permanence at 20 $^\circ C$ for 10 min (*b*) and 60 min (*c*). (Reproduced with permission from [77]. Copyright 2008 by the American Chemical Society)

$q_{knee} \approx 0.07\ nm^{-1}$, with a power law dependence of the scattering cross-section as $d\sigma/d\Omega \approx q^{-2.2}$ for $q < q_{knee}$ and as $d\sigma/d\Omega \approx q^{-3.7}$ for $q > q_{knee}$ (curve d in Fig. 16a), indicates that the frozen system includes heterogeneities within the ice matrix, corresponding to the unfrozen liquid microphase [76, 77] of characteristic size $L = 2\pi/q_{knee} \approx 75$–80 nm. The above analysis also indicates that the unfrozen liquid microphase is organized to form fractal aggregates of dimensions above 300 nm within the ice matrix. This scenario is in agreement with the mechanism for cryotropic gelation suggested by Lozinsky [4–6] (Fig. 15).

The solutions with PVA content $\Phi = 0.086$, and 0.12 form a gel upon defrosting after 390 min at $-13\ ^\circ C$ (curve c of Fig. 16b). However, the solution with $\Phi = 0.042$ is unable to jellify upon the same cryotropic treatment [77]. This indicates that for polymer concentrations below a critical value, the total volume of the unfrozen liquid microphase is too low to form cluster aggregates [77]. The clustering process, in turn, plays a key role in formation of the gel.

It is worth noting that the analysis of SANS data in Fig. 16a, related to the early stages of cryogelation from PVA homogeneous solutions, does not provide any evidence of LL phase separation during the prolonged treatment at subzero temperatures, as expected from the phase diagram of Komatsu et al. [43] (Fig. 8). In fact, the fastest process that could be detected in our approach is crystallization of the solvent [76, 77]. Using the concept of hierarchical metastability [17, 25], this occurs because the spinodal decomposition is buried by the crystallization of water. In this hypothesis and in agreement with the cryogelation mechanism proposed by Lozinsky [4–6] (Fig. 15), the formation of macropores in these gels is due to crystallization of the solvent, which acts as a porogen. However, the lack of evidence of LL phase separation may also be due to the fact that in the early stages of spinodal decomposition, concentration fluctuation corresponds to wavelengths

higher than $2\pi/q_{min}$ ($\approx$300 nm) [24, 37, 78], with $q_{min} = 0.02$ nm^{-1} being the lowest value of the scattering vector q that was achieved in the experimental set-up. In this second hypothesis, the scattering intensity is expected to show a peak at $q < q_{min}$, but this low q region was not sampled [24, 37].

During thawing, the scattering cross-section decreases (Fig. 16b). This indicates that, upon defrosting, the frozen solution evolves towards a system characterized by alternation of dense and diluted regions that have origin in the regions occupied at subzero temperatures by ice and the unfrozen liquid microphase, respectively [77]. For PVA concentrations higher than a critical value, dense and diluted regions are likely to form an interpenetrated network of two co-continuous phases, resulting in a transparent gel in the nascent state (curve c of Fig. 16b) where the characteristic size of the phase-separated domains is of the order of few tens of nanometers [77].

The nascent gels become opaque upon aging at room temperature for few hours due to the increase in size of the regions that are alternatively dense and diluted [77]. The coarsening of the heterogeneous structure imprinted by the cryotropic treatment is driven by the tendency of the dense and dilute regions to minimize their surface of contact, and is the hallmark that these gels are in a state far from equilibrium. In fact, the fast cryogenic treatment causes the formation of transparent gels having the same composition as the initial homogeneous solution. On the basis of the phase diagram by Komatsu et al. [43] (Fig. 8), solutions containing 10–12 wt% PVA (corresponding to PVA volume fraction Φ in the range 0.086–0.12) are in the one-phase region and should not give rise to a gel at room temperature. However, the nascent gels obtained from these solutions by cryotropic treatment at -13 °C do not transform back into the initial homogeneous solution once they are brought back to room temperature because a strong network scaffolding has already been formed due to the presence of PVA crystallites. These gels are stable up to 50–60 °C [57] and can be aged for long time in sealed vials, maintaining their properties. Moreover, the nascent gels obtained after a single freeze–thaw cycle are already too strong to evolve towards complete elimination of the solvent [24]. Nascent gels, instead, react via microsyneresis and the size of the dense and diluted regions increases [24]. The coarsening of the heterogeneous structure of the nascent and transparent gels, up to becoming opaque, also suggests that spinodal decomposition occurs [79, 80]. This phenomenon has indeed been observed for other gels [79, 80]. It generally occurs when a swollen gel is suddenly brought into another state that may be located either in the two-phase or one-phase region of its phase diagram [80]. Regardless of the region of the phase diagram in which the new state is located, it has been shown that the system becomes opaque without any appreciable volume change, suggesting occurrence of spinodal decomposition in both cases. However, in contrast to the usual fluids, the domain growth is slow because the elastic force of the gel suppresses the surface tension force, which is the driving force of domain growth [79, 80].

3.7 Kinetic Analysis of SANS Data

A more in-depth analysis of TR-SANS data collected during the first freezing step (Fig. 16a) indicates that the structural changes that occur at correlation distances between 60–300 nm and 7–60 nm are different and involve different characteristic times [77]. Therefore, the scattering data collected in the relevant q ranges were analyzed separately by evaluating the Lorentz-corrected integral Ψ of the scattering cross-section in the q range between $q_1 = 0.022$ and $q_2 = 0.108$ nm^{-1} for $\Psi_{low}(t)$ and between $q_1 = 0.108$ and $q_2 = 0.881$ nm^{-1} for $\Psi_{high}(t)$ as a function of time. This kind of integral corresponds to the scattering invariant when the integration limits in q are extended from zero to infinite. For this reason, the function Ψ corresponds to a sort of "reduced scattering invariant." A working hypothesis is that, in the early stages of gelation, the SANS patterns contain additive contributions from the aggregated and non-aggregated phases and that the interaction between these two phases may be neglected. Thus, changes in the reduced scattering invariant $\Psi_{low}(t)$ probe structural changes occurring in the initially homogeneous solution during permanence at subzero temperatures at length scales of the order of hundreds of nanometers, essentially due to water crystallization [77]. By contrast, changes in the reduced scattering invariant $\Psi_{high}(t)$ probe structural changes occurring at length scales of the order of nanometers, essentially due to PVA crystallization inside the unfrozen liquid microphase [77].

The values of the reduced scattering invariant calculated from the SANS data collected during the first freezing step of PVA/D$_2$O solutions are reported in Fig. 17 as a function of the permanence time of the solutions at $-13\,°C$. In Fig. 17a′ (inset), the values of $\Psi_{low}(t)$ of pure D$_2$O are also shown for comparison.

The sigma shape of the curves describing the structural changes occurring at a length scale of hundreds of nanometers (Fig. 17a) reflects the formation of ice crystals of pure water (Fig. 17a′), which takes about 10–15 min regardless of PVA concentration [77].

By contrast, the values of the reduced scattering invariant calculated in the high q region $\Psi_{high}(t)$ increase with the permanence time of the PVA solutions at subzero temperature according to a smoothed sigma shape (Fig. 17b), and reflect structural changes at length scales of tens of nanometers due to the crystallization of PVA in the unfrozen liquid microphase. It is apparent that the values of $\Psi_{high}(t)$, regardless of PVA concentration, increase smoothly in the first 30 min, present an upturn at around 30–40 min, and increase smoothly again in the successive 120–330 min of freezing, without reaching any plateau value, even for prolonged times of permanence at $-13\,°C$. This suggests that after completion of the crystallization of the solvent (which takes about 10–15 min), the PVA chains, which are mostly segregated in the unfrozen liquid microphase, tend to form precrystalline or crystalline aggregates, probably because the concentration of the liquid microphase reaches the eutectic composition [77]. However, although the temperature of the system ($-13\,°C$) is probably below the eutectic temperature, the full crystallization of PVA may not be achieved and is slowed down due to the fact that the unfrozen liquid
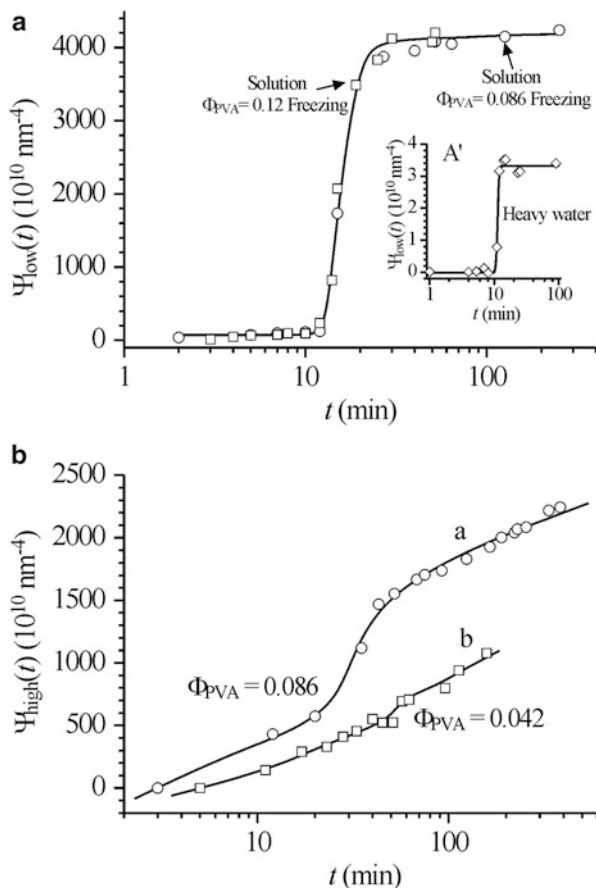
Fig. 17 (**a, a′**) Reduced scattering invariant, Ψ_{low} (t), as a function of time during treatment at –13 °C from a D_2O solution with $\Phi_{PVA} = 0.086$ (*circles*) and 0.12 (*squares*) PVA volume fraction (**a**) and from pure D_2O (**a′**, *inset*). The *curves* reflect structural changes occurring at length scales of the order of hundreds of nanometers, essentially due to water crystallization. (**b**) Reduced scattering invariant, Ψ_{high} (t), as a function of time during the treatment at –13 °C from a D_2O solution with 0.086 (*curve a*) and 0.042 (*curve b*) PVA volume fraction. The *curves* reflect structural changes occurring at length scales of the order of nanometers, essentially due to PVA crystallization inside the unfrozen liquid microphase. (Reproduced with permission from [77]. Copyright 2008 by the American Chemical Society)

microphase jellifies, preventing attainment of thermodynamic equilibrium [77]. The formation of the gel microphase may be determined by aggregation of PVA chains in a confined environment, which is driven by hydrogen bonding, consequent formation of crystallites, and vitrification of the swollen amorphous phase at a temperature that is probably below the glass transition [4–6]. This scenario holds both for solutions with PVA volume fraction $\Phi \geq 0.086$ and for
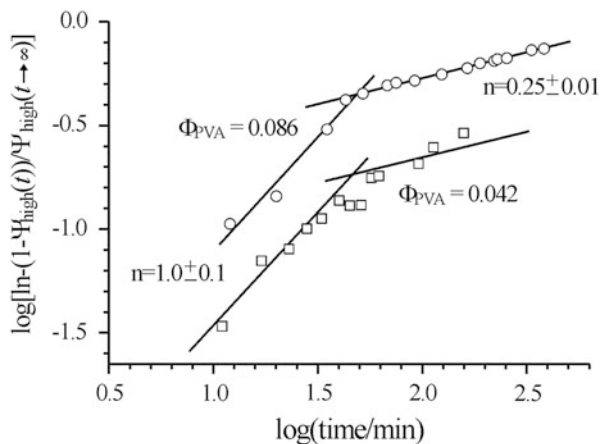
Fig. 18 Avrami plot of the reduced scattering invariant $\Psi_{\text{high}}(t)$ normalized to the extrapolated value of the scattering invariant at infinite time $\Psi_{\text{high}}(t \to \infty)$ for solutions with PVA volume fraction Φ_{PVA} of 0.086 (*circles*) and 0.042 (*squares*). The Avrami exponents n are indicated. (Reproduced with permission from [77]. Copyright 2008 by the American Chemical Society)

more dilute PVA solutions with $\Phi = 0.042$ (curve b of Fig. 17b). In fact, the SANS data in Fig. 17b indicate that in dilute PVA solution ($\Phi = 0.042$), crystallization of PVA probably also takes place, even though a macroscopic gel is not formed upon defrosting because the relative amount of the gel microphase is too low to give rise to an interconnected macroscopic gel network at subzero temperatures [77].

The data in Fig. 17b may be used to extrapolate the value of the reduced scattering invariant $\Psi_{\text{high}}(t)$ at infinite time $\Psi_{\text{high}}(t \to \infty)$ [77]. The ratio of $\Psi_{\text{high}}(t)$ to $\Psi_{\text{high}}(t \to \infty)$ is proportional to the extent of PVA crystallization in the unfrozen liquid microphase. This parameter is used in the Avrami plot shown in Fig. 18 [77]. Avrami analysis of the confined crystallization in these gels indicates that the confined crystallization of PVA follows first-order kinetics ($n = 1$) during the first 40 min, and becomes slower in the later stages with an apparent exponent $n < 1$ [77]. For the frozen solution, an exponent of $n \approx 1$ is consistent with a one-dimensional (fibrillar) growth mechanism controlled by heterogeneous (athermal) nucleation [81], triggered by the active surface of ice at the interface with the unfrozen liquid microphase. The low Avrami exponent of 0.25 is rather uncommon [82, 83]. A possible reason for a value of n lower than 1 in the later stages of crystallization kinetics of PVA in the frozen solution may be the restriction of crystal growth because previously formed PVA crystals reduce the mobility of PVA chains dissolved in the unfrozen liquid microphase. This reduced mobility, in turn, results in jellification of the unfrozen microphase [77].

4   Concluding Remarks and Outlook

Poly(vinyl alcohol) cryogels are strong physical gels that form as a result of different crosslinking processes that occur simultaneously in synergy or in competition. We demonstrate here that the concept of circumstantial metastability and the hierarchy of metastable states may turn out to be useful in unraveling the complex mechanisms subtending their formation. In particular, we have shown that kinetic analysis of the cryotropic gelation from PVA solutions using time-resolving SANS has allowed an unprecedented level of comprehension of this process. At least three elementary steps have been identified:

- Incomplete solvent crystallization occurring at subzero temperatures, with consequent formation of an unfrozen liquid microphase of eutectic composition
- Incomplete PVA crystallization in the unfrozen liquid microphase, with consequent formation of a microgel fraction
- Coarsening of the dense and diluted regions imprinted by the cryogenic treatment, occurring at room temperature

A wealth of applications have been proposed for these gels in many different fields, including biomedicine and diagnostics. Applications include the building of artificial muscles [84, 85] or phantom organs for NMR imaging and mammography [86, 87], controlled drug release [11, 88–90], and biotechnology in which these gels act as carriers of immobilized bioaffinity ligands, enzymes, and cells [4–6, 91].

More recently, it has been pointed out that aged gels possess self-healing properties at room temperature, without the need for any stimulus or healing agent [10]. Welding occurs spontaneously via chain diffusion across the interface provided that a sufficient number of PVA free hydroxyl groups survive at the contact between the two cut surfaces [10].

A further interesting property of PVA cryogels is that, whereas a long aging in sealed vials at room temperature induces large variations in their structure and properties, the porous structure imprinted by cryotropic treatment is not greatly altered upon drying and during the successive rehydration step. Rehydrated gels almost completely recover the volume, shape, and physical properties of the as-formed freeze–thaw PVA hydrogels [42, 57, 62, 63]. It has been shown that the outstanding physical and mechanical properties of freeze–thaw PVA hydrogels in the as-prepared state can be preserved, even for a long time, by drying the samples immediately after preparation and then restoring when needed by rehydration of the dried samples [42, 57, 63].

Finally, it is worth mentioning that PVA cryogels are able to incorporate different soluble and insoluble additives inside the pores to obtain composite materials of both scientific and applied interest [4–6]. In particular, PVA-based cryogels have been obtained that include inside the porous structure nanoparticles of solid crystalline compounds, co-elastic gels, microorganisms, gas bubbles, or microdroplets of liquids immiscible with PVA solutions [4–6, 92–98].

There are still several basic issues regarding PVA cryogels that deserve further investigation, especially related to the complex dynamics of water molecules and polymer chains. The identification of smart processing routes to obtain systems with tailored pore size and pore size distribution, and with well-defined viscoelastic properties, is critically dependent on fundamental study of the dynamics of these systems, coupled with modeling.

References

1. Hassan CM, Peppas NA (2000) Structure and applications of poly(vinyl alcohol) hydrogels produced by conventional crosslinking or by freezing/thawing methods. Adv Polym Sci 153:37
2. Peppas NM (1975) Turbidimetric studies of aqueous poly(vinyl alcohol) solutions. Makromol Chem 176:3433
3. Stauffer S, Peppas NA (1992) Poly(vinyl alcohol) hydrogels prepared by freezing-thawing cyclic processing. Polymer 33:3932
4. Lozinsky VI (1998) Cryotropic gelation of poly(vinyl alcohol) solutions. Russ Chem Rev 67:573
5. Lozinsky VI (2002) Cryogels on the basis of natural and synthetic polymers: preparation, properties and application. Russ Chem Rev 71:489
6. Lozinsky VI, Galaev IY, Plieva FM, Savina IN, Jungvid H, Mattiasson B (2003) Polymeric cryogels as promising materials of biotechnological interest. Trends Biotechnol 21:445
7. Lozinsky VI, Damshkaln LG (2000) Study of cryostructuration of polymer systems. XVII. Poly(vinyl alcohol) cryogels: dynamics of the cryotropic gel formation. J Appl Polym Sci 77:2017
8. Watase M, Nishinari K (1985) Reological and DSC changes in poly(vinyl alcohol) gels induced by immersion in water. J Polym Sci Part B: Polym Phys Ed 23:1803
9. Nishinari K, Watase M, Tanaka F (1996) Structure of junction zones in poly(vinyl alcohol) gels by rheological and thermal studies. J Chim Phys Phys Chim Biol 93:880
10. Zhang H, Xia H, Zhao Y (2012) Poly(vinyl alcohol) hydrogel can autonomously self-heal. ACS Macro Lett 1:1233
11. Peppas NA, Mongia NK (1997) Ultrapure poly(vinyl alcohol) hydrogels with mucoadhesive drug delivery characteristics. Eur J Pharm Biopharm 43:51
12. Finch CA (1992) Polyvinyl alcohol – developments. Wiley, London
13. Bolto B, Tran T, Hoang M, Xie Z (2009) Crosslinked poly(vinyl alcohol) membranes. Prog Polym Sci 34:969
14. Cohen Addad JP (1996) Physical properties of polymeric gels. Wiley, London
15. Loh XJ, Scherman OA (2013) Polymeric and self-assembled hydrogels. The Royal Society of Chemistry, Cambridge
16. Papon P, Leblond J, Meijer PHE (2002) The physics of phase transitions: concepts and applications. Springer, Berlin
17. Keller A (1995) Aspects of polymer gels. Faraday Discuss 101:1
18. Shibayama M, Tanaka T (1993) Volume phase transition and related phenomena of polymer gels. Adv Polym Sci 109:1
19. Rubinstein M, Colby RH (2003) Polymer physics. Oxford University Press, New York
20. Tanaka T (1981) Gels Sci Am 244:124
21. Tanaka T, Sun ST, Hirokawa Y, Katayama S, Kucera J, Hirose Y, Amiya T (1987) Mechanical instability of gels at the phase transition. Nature 325:796

22. Durmaz-Hilmioglu N, Yildirim AE, Sakaoglu AS, Tulbentci S (2001) Acetic acid dehydration by pervaporation. Chem Eng Proc 40:263
23. Benzekri K, Essamri A, Toreis N, Souissi A, Maarouf T, Mas A (2001) Membranes d'alcool polyvinylique traitées par plasma d'acide acrylique. Application à la déshydratation des mélanges eau–éthanol par pervaporation. Eur Polym J 37:1607
24. deGennes P-G (1979) Scaling concepts in polymer physics. Cornell University Press, Ithaca
25. Keller A, Cheng SZD (1998) The role of metastability in polymer phase transitions. Polymer 39:4461
26. Atkins EDT, Isaac DH, Keller A, Miyasaka K (1977) Analysis of anomalous X-ray diffraction effects of isotactic polystyrene gels and its implications for chain conformation and isomeric homogeneity. J Polym Sci Polym Phys Ed 15:211
27. Atkins EDT, Isaac DH, Keller A (1980) Conformation of polystyrene with special emphasis to the near all-trans extended-chain model relevant in polystyrene gel. J Polym Sci Polym Phys Ed 18:71
28. Atkins EDT, Keller A, Shapiro JS, Lemstra PJ (1981) Extended-chain structure for isotactic polystyrene: additional X-ray diffraction and calorimetric results. Polymer 22:1161
29. Girolamo M, Keller A, Miyasaka M, Overbergh N (1976) Gelation-crystallization in isotactic polystyrene solutions and its implications to crystal morphology, to the origin and structure of gels, and to the chemical homogeneity of polyolefins. J Polym Sci Polym Phys Ed 14:39
30. Chatani Y, Nakamura N (1993) Coiled-coil molecular model for isotactic polystyrene gels. Polymer 34:1644
31. Auriemma F, De Rosa C, Corradini P (2004) Non-helical chain conformations of isotactic polymers in the crystalline state. Macromol Chem Phys 205:390
32. Guenet J-M (1992) Thermoreversible gelation of polymers and biopolymers. Academic, London, 1992
33. Ostwald W (1897) Studies on the formation and inversion of solids. First paper: supersaturation and supercooling. Z Phys Chem 22:289
34. Hikmet RM, Callister S, Keller A (1988) Thermoreversible gelation of atactic polystyrene: phase transformation and morphology. Polymer 29:1378
35. Wellinghoff ST, Shaw J, Baer E (1979) Polymeric materials from the gel state. The development of fringed micelle structure in a glass. Macromolecules 12:932
36. Arnauts J, Berghmans H (1987) Amorphous thermoreversible gels of atactic polystyrene. Polym Commun 28:66
37. Strobl GR (2007) The physics of polymers. Springer, Berlin
38. Berghmans S, Mewis J, Berghmans H, Meijer H (1995) Phase behavior and structure formation in solutions of poly(2,6-dimethyl-1,4-phenylene ether). Polymer 36:3085
39. Tubbs RK (1966) Sequence distribution of partially hydrolyzed poly(vinyl acetate). J Polym Sci A1 4:623
40. Bunn CW, Peiser HS (1947) Mixed crystal formation in high polymers. Nature 159:161
41. Bunn CW (1948) Crystal structure of polyvinyl alcohol. Nature 161:929
42. Ricciardi R, Auriemma F, De Rosa C, Lauprêtre F (2004) X-ray diffraction analysis of poly (vinyl alcohol) hydrogels obtained by freezing and thawing techniques. Macromolecules 37:1921
43. Komatsu M, Inoue T, Miyasaka K (1986) Light-scattering studies on the sol–gel transition in aqueous solutions of poly(vinyl alcohol). J Polym Sci: Polym Phys Ed 24:303
44. Kawanishi K, Komatsu M, Inoue T (1987) Thermodynamic consideration of the sol-gel transition in polymer solutions. Polymer 28:980
45. Pines E, Prins W (1973) Structure-property relations of thermoreversible macromolecular hydrogels. Macromolecules 6:888
46. Peppas NA (1976) Crystallization of polyvinyl alcohol-water films by slow dehydration. Eur Polym J 12:495
47. Mallapragada SK, Peppas NA (1996) Dissolution mechanism of semicrystalline poly(vinyl alcohol) in water. J Polym Sci Part B: Polym Phys 34:1339

48. Kukharchik MM, Baramboim NK (1972) Change in the properties of aqueous solutions of poly (vinyl alcohol) during cryolytic action. Vysokomol Soedin 14B:843
49. Yokoyama F, Masada I, Shimamura K, Ikawa T, Monobe K (1986) Morphology and structure of highly elastic poly(vinyl alcohol) hydrogel prepared by repeated freezing-and-melting. Colloid Polym Sci 264:595
50. Watase M, Nishinari K (1989) Effect of the degree of saponification on the rheological and thermal properties of poly(vinyl alcohol) gels. Makromol Chem 190:155
51. Kobayashi M, Ando I, Ishii T, Amiya S (1995) Structural study of poly(vinyl alcohol) in the gel state by high-resolution solid-state ^{13}C NMR spectroscopy. Macromolecules 28:6677
52. Kobayashi M, Ando I, Ishii T, Amiya S (1998) Structural and dynamical studies of poly(vinyl alcohol) gels by high-resolution solid-state ^{13}C NMR spectroscopy. J Mol Struct 440:155
53. Kobayashi M, Kanekiyo M, Ando I (1998) A study of molecular motion of PVA/water system by high-pressure ^{1}H pulse-NMR method. Polym Gels Netw 6:347
54. Kanekiyo M, Kobayashi M, Ando I, Kurosu H, Ishii T, Amiya S (1998) A structural and dynamic study of poly(vinyl alcohol) in the gel state by solid-state ^{13}C NMR and ^{1}H pulse NMR. J Mol Struct 447:49
55. Terao T, Maeda S, Saika A (1983) High-resolution solid-state carbon-13 NMR of poly(vinyl alcohol): enhancement of tacticity splitting by intramolecular hydrogen bonds. Macromolecules 16:1535
56. Ricciardi R, Gaillet C, Ducouret G, Lafuma F, Lauprêtre F (2003) Investigation of the relationships between the chain organization and rheological properties of atactic poly(vinyl alcohol) hydrogels. Polymer 44:3375
57. Ricciardi R, Auriemma F, Gaillet C, De Rosa C, Lauprêtre F (2004) Investigation of the crystallinity of freeze/thaw poly(vinyl alcohol) hydrogels by different techniques. Macromolecules 37:9510
58. Valentín JL, López D, Hernández R, Mijangos C, Saalwächter K (2009) Structure of poly (vinyl alcohol) cryo-hydrogels as studied by proton low-field NMR spectroscopy. Macromolecules 42:263
59. Fergg F, Keil FJ, Quader H (2001) Investigations of the microscopic structure of poly(vinyl alcohol) hydrogels by confocal laser scanning microscopy. Colloid Polym Sci 279:61
60. Ricciardi R, Mangiapia G, Lo Celso F, Paduano L, Triolo R, Auriemma F, De Rosa C, Lauprêtre F (2005) Structural organization of poly(vinyl alcohol) hydrogels obtained by freezing and thawing techniques: a SANS study. Chem Mater 17:1183
61. Willcox PJ, Howie DW Jr, Schimdt-Rohr K, Hoagland A, Gido SP, Pudjijanto S, Kleiner LW, Venkatraman S (1999) Microstructure of poly(vinyl alcohol) hydrogels produced by freeze/thaw cycling. J Polym Sci Part B: Polym Phys 37:3438
62. Ricciardi R, D'Errico G, Auriemma F, Ducouret G, Tedeschi AM, De Rosa C, Lauprêtre F, Lafuma F (2005) Short time dynamics of solvent molecules and supramolecular organization of poly (vinyl alcohol) hydrogels obtained by freeze/thaw techniques. Macromolecules 38:6629
63. Tedeschi A, Auriemma F, Ricciardi R, Mangiapia G, Trifuoggi M, Franco L, De Rosa C, Heenan RK, Paduano L, D'Errico G (2006) A study of the microstructural and diffusion properties of poly(vinyl alcohol) cryogels containing surfactant supramolecular aggregates. J Phys Chem B 110:23031
64. Hyon S-H, Ikada Y (1987) Porous and transparent poly(vinyl alcohol) gel and method of manufacturing the same. US Patent 4663358
65. Hyon S-H, Cha W-I, Ikada Y, Kita M, Ogura Y, Honda Y (1994) Poly(vinyl alcohol) hydrogels as soft contact lens material. J Biomater Sci Polym Ed 5:397
66. Berghmans H, Stoks W (1986) Thermoreversible gelation of vinylpolymers. In: Kleintjens LA, Lemstra PJ (eds) Integration of fundamental polymer science and technology. Springer, London
67. Kanaya T, Ohkura M, Kaji H, Furusaka M, Misawa M (1994) Structure of poly(viny1 alcohol) gels studied by wide- and small-angle neutron scattering. Macromolecules 27:5609

68. Kanaya T, Takeshita H, Nishikoji Y, Ohkura M, Nishida K, Kaji K (1998) Micro- and mesoscopic structure of poly(vinyl alcohol) gels determined by neutron and light scattering. Supramol Sci 5:215
69. Kanaya T, Ohkura M, Takeshita H, Kaji H, Furusaka M, Yamaoka H, Wignall GD (1995) Gelation process of poly(viny1 alcohol) as studied by small-angle neutron and light scattering. Macromolecules 28:3168
70. Takeshita H, Kanaya T, Nishida K, Kaji K (2002) Small-angle neutron scattering studies on network structure of transparent and opaque PVA gels. Physica B 311:78
71. Takeshita H, Kanaya T, Nishida K, Kaji K (1999) Gelation process and phase separation of PVA solutions as studied by a light scattering technique. Macromolecules 32:7815
72. Ohkura M, Kanaya T, Kaji K (1992) Gels of poly(vinyl alcohol) from dimethyl sulphoxide/water solutions. Polymer 33:3686–3690
73. Takeshita H, Kanaya T, Nishida K, Kaji K, Takahashi T, Hashimoto M (2000) Ultra-small-angle neutron scattering studies on phase separation of poly(vinyl alcohol) gels. Phys Rev E 61:2125
74. Trieu H, Qutubuddin S (1994) Polyvinyl alcohol hydrogels I: microscopic structure by freeze-etching and critical point drying techniques. Colloid Polym Sci 272:301
75. Trieu H, Qutubuddin S (1995) Poly(vinyl alcohol) hydrogels: 2. Effects of processing parameters on structure and properties. Polymer 36:2531
76. Auriemma F, De Rosa C, Triolo R (2006) Slow crystallization kinetics of poly(vinyl alcohol) in confined environment during cryotropic gelation of aqueous solutions. Macromolecules 39:9429
77. Auriemma F, De Rosa C, Ricciardi R, Lo Celso F, Triolo R, Pipich V (2008) Time-resolving analysis of cryotropic gelation of water/poly(vinyl alcohol) solutions via small-angle neutron scattering. J Phys Chem B 112:816
78. Cahn JW (1965) Phase separation by spinodal decomposition in isotropic systems. J Chem Phys 42:93
79. Hirotsu S, Kaneki A (1988) Dynamics of phase transition in polymer gels: studies of spinodal decomposition and pattern formation. In: Komura S, Furukawa H (eds) Dynamics of ordering process in condensed matter. Plenum, Kyoto, pp 481–486
80. Takeshita H, Kanaya T, Nishida K, Kaji K (2001) Spinodal decomposition and syneresis of PVA gel. Macromolecules 34:7894
81. Wunderlich B (1980) Macromolecular physics, crystal melting, vol 3. Academic, New York
82. Grebowicz J, Cheng SZD, Wunderlich B (1986) Kinetics of transitions involving condis crystals. J Polym Sci Part B Polym Phys 24:675
83. Cheng SZD (1988) Kinetics of mesophase transitions in thermotropic copolyesters. 1: calorimetric study. Macromolecules 21:2475
84. Bao QB, Higham PA (1991) Hydrogel intervertebral disc nucleus. US5047055
85. Hyon SH, Cha WI, Oka M, Ikada Y (1993) Shock absorbing ability of joint materials. III. Effect of molecular weight and saturated water content on the loss factor of PVA-hydrogels. Polym Prep Jpn (Eng Ed) 42:71
86. Mano I, Goshima H, Nambu M (1986) New polyvinyl alcohol gel materials for MRI phantoms. Magn Reson Med 3:921
87. Kharine A, Manohar S, Seeton R, Kolkman RGM, Bolt RA, Steenbergen W, de Mul FFM (2003) Poly(vinyl alcohol) gels for use as tissue phantoms in photoacoustic mammography. Phys Med Biol 48:357
88. Takamura A, Ishii T, Hidaka H (1992) Drug release from poly(vinyl alcohol) gel prepared by freeze-thaw procedure. J Control Release 20:21
89. Peppas NA, Scott JE (1992) Controlled release from poly(vinyl alcohol) gels prepared by freezing-thawing processes. J Control Release 18:95
90. Ficek BJ, Peppas NA (1993) Novel preparation of poly (vinyl alcohol) microparticles without crosslinking agent for controlled drug delivery of proteins. J Control Release 27:259
91. Gutiérrez MC, Aranaz I, Ferrer ML, del Monto F (2010) Productions and properties of poly (vinyl alcohol) hydrogels: recent developments. In: Mattiasson B, Kumar A, Galaev IY (eds)

Macroporous polymers: production, properties and biological/biomedical applications. CRC, Boca Raton, p 83

92. Podorozhko EA, D'yakonova EA, Kolosova OY, Klabukov LF, Lozinsky VI (2012) A study of cryostructuring of polymer systems. 34. Poly(vinyl alcohol) composite cryogels filled with microparticles of polymer dispersion. Colloid J 74:708

93. Podorozhko EA, Vorontsova TV, Lozinsky VI (2012) Study of cryostructuring of polymer systems. 32. Morphology and physicochemical properties of composite poly(vinyl alcohol) cryogels filled with hydrophobic liquid microdroplets. Colloid J 74:110

94. Lozinsky VI, Zubov AL, Titova EF (1997) Poly(vinyl alcohol) cryogels employed as matrices for cell immobilization. 2. Entrapped cells resemble porous fillers in their effects on the properties of PVA-cryogel carrier. Enzyme Microb Technol 20:182

95. Podorozhko EA, Korlyukov AA, Lozinsky VI (2010) Cryostructuring of polymer systems. XXX. Poly(vinyl alcohol)-based composite cryogels filled with small disperse oil droplets: a gel system capable of mechanically induced releasing of the lipophilic constituents. J Appl Polym Sci 117:1332.

96. Abitbol T, Johnstone T, Quinn TM, Gray DG (2011) Reinforcement with cellulose nanocrystals of poly(vinyl alcohol) hydrogels prepared by cyclic freezing and thawing. Soft Mater 7:2373

97. Pan Y, Xiong D, Chen X (2007) Mechanical properties of nanohydroxyapatite reinforced poly (vinyl alcohol) gel composites as biomaterial. J Mater Sci 42:5129

98. Lozinsky VI, Damshkaln LG (2001) Study of cryostructuration of polymer systems. XX. Foamed poly(vinyl alcohol) cryogels. J Appl Polym Sci 82:1609

Cryogels via UV Irradiation

Petar D. Petrov and Christo B. Tsvetanov

Contents

Abstract An effective and facile method for the synthesis of chemically crosslinked supermacroporous polymer cryogels based on UV irradiation is reviewed. The influence of key factors like the irradiation dose, temperature of freezing, concentration of polymer or monomer precursor, molar mass of polymer precursor, and the type and amount of the photoinitiator on crosslinking efficiency is discussed. The versatility of the method for preparation of a large number of biocompatible, biodegradable, and/or stimuli-responsive cryogels is demonstrated. Examples include some specific properties of well-investigated polyacrylamide (PAAm) and poly(N-isopropylacrylamide) (PNIPAAm) cryogels obtained by photocrosslinking as well as novel cryogels based on cellulose derivatives, hydrophobically modified polyglycidol (PGL), and ethoxytriethyleneglycol acrylate (ETEGA). Part of this review is focused on the applicability of supermacroporous cryogels as carriers of different species such as drugs, enzymes, nanoparticles, and cells immobilized in either cryogel walls (polymer matrix) or interconnected pores.

P.D. Petrov (✉) • C.B. Tsvetanov

Institute of Polymers, Bulgarian Academy of Sciences, Akad. G. Bonchev Str. 103 A, Sofia 1113, Bulgaria

e-mail: ppetrov@polymer.bas.bg

Abbreviations

AAm	Acrylamide
AgNPs	Silver nanoparticles
BBTMAC	(4-Benzoylbenzyl)trimethylammonium chloride
BisAAm	N,N'-methylenebisacrylamide
CNT	Carbon nanotube
DMAEMA	2-(Dimetylamino)ethyl methacrylate
DS	Degree of swelling
ETEGA	Ethoxytriethyleneglycol acrylate
GF	Gel fraction
HEC	2-Hydroxyethylcellulose
HEMA	2-Hydroxyethyl methacrylate
HPC	Hydroxypropylcellulose
HPMC	(Hydroxypropyl)methylcellulose
LCST	Lower critical solution temperature
MC	Methylcellulose
NIPAAm	N-Isopropylacrylamide
OEGMA	Oligo(ethyleneglycol) methacrylate
PAAm	Polyacrylamide
PEGDA	Poly(ethylene glycol) diacrylate
PEO	Poly(ethylene oxide)
PETEGA	Poly(ethoxytriethyleneglycol) acrylate
PGL	Polyglycidol
PHEMA	Poly(2-hydroxyethyl methacrylate)
PNIPAAm	Poly(N-isopropylacrylamide)
T_{VPT}	Temperature of volume phase transition
VCL	Vinyl caprolactam
UV	Ultraviolet

1   Introduction

Supermacroporous polymer cryogels are attractive materials due to their unique heterogeneous structure composed of large interconnected pores that are filled with solvent and surrounded by thin walls. Such a structure makes the diffusion of fluids and species within the volume of cryogel easy and, thereby, facilitates mass and heat transfer [1, 2]. Polymer cryogels are formed as a result of freezing of low or high molar mass precursors (dissolved most often in water), crosslinking, and subsequent thawing. A very important feature determining the success of

preparation of a heterogeneous open porous structure is that the solvent is frozen before the beginning of crosslinking reactions, i.e., the reaction system is cryostructured. In the case of chemical crosslinking by a redox system, which is one of the most frequently used approaches for synthesis of polymer cryogels, the polymerization rate has to be slow enough to prevent crosslinking of the system from the time of mixing of the reagents until the complete cryostructuration, i.e., any crosslinking in solution must be avoided [3]. Typically, when using a redox system, the time required for preparation of cryogels varies from 16 to 24 h [4–6].

From this point of view, the most efficient methods for regular cryostructuration of the system are those based on chemical crosslinking induced by high energy radiation (gamma-rays, electron beam) [7–9]. Here, the solution of reagents is first allowed to freeze, forming well-separated large interconnected ice crystals and nonfrozen liquid microphase. Then, the polymer network is formed. Usually, the irradiation procedure takes 60–180 min and saves time in the preparation of cryogels. However, the complex and expensive equipment needed in combination with the safety requirements seem to limit the wide use of these methods.

Ten years ago, the UV irradiation technique was successfully employed for the first time by our team for the synthesis of poly(ethylene oxide) (PEO) cryogels [10]. This method starts with freezing of the solvent and conducts the crosslinking reaction after the complete structuring of the system. Thus, together with full control over the formation of large-size crystals and nonfrozen liquid microphase, the method benefits from the facile procedure and easy access to a UV light source. By optimizing the experimental conditions, PEO cryogels of very high gel fraction (GF) yield (95 %) were obtained.

This review summarizes the recent achievements in preparation of various supermacroporous polymer cryogels via UV-induced crosslinking in partly frozen systems. The method is equally effective for the formation of cryogels from both water-soluble high molar mass linear polymers and vinyl monomers. Special attention is paid to some novel materials based on biodegradable and/or stimuli-responsive polymers and their application in some emerging fields, as well as the fabrication of nanocomposites with intriguing properties.

2 Cryogels from Water-Soluble High Molar Mass Polymers

Cryogels from high molar mass polymer precursors were obtained by a simple procedure involving preparation of semidilute/concentrated polymer solution (0.5–5 mass%) containing a photoinitiator, followed by freezing, UV-induced crosslinking, and thawing. Notably, the crosslinking reaction is very fast and formation of the polymer network can be completed within several minutes. The accepted mechanism of crosslinking of high molar mass linear polymers induced by UV light involves generation and subsequent recombination of macroradicals [10]
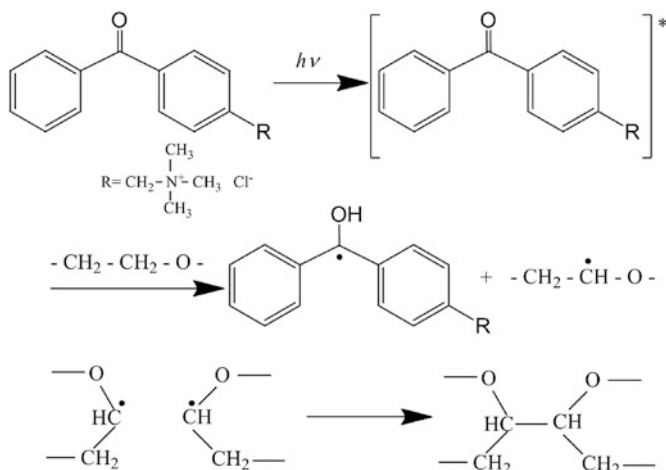
Fig. 1 Mechanism of photochemical crosslinking of PEO with photoinitiator (4-benzoylbenzyl) trimethylammonium chloride

with the aid of a photoinitiator. A substantial advantage of this method is the fact that no functional groups are required. Figure 1 shows one example of photocrosslinking of PEO in the presence of a water-soluble photoinitiator, (4-benzoylbenzyl)trimethylammonium chloride (BBTMAC). Upon UV irradiation, the benzophenone derivative undergoes several photophysical processes to afford an n,π^* triplet state, which then proceeds to reduction of BBTMAC and hydrogen atom abstraction from the PEO chain. Photocrosslinking occurs by a recombination reaction of two macroradicals to produce covalent bonds between two main chains.

One should point out that in the case of cryogels, the crosslinking reaction takes place in the nonfrozen liquid microphase, where the concentration of polymer is higher than in the initial solution due to the cryo-concentration phenomena. Therefore, under such conditions the probability for recombination of two macroradicals is increased. This fact explains why cellulose derivatives, which degrade in solution upon UV irradiation, were successfully crosslinked via cryogenic treatment [11, 12]. Figure 2 shows the storage (G') and loss (G'') moduli in the 0.1–10 Hz frequency range of 3 mass% aqueous 2-hydroxyethylcellulose (HEC) solutions irradiated with UV light in the frozen state ($-30\,°C$) and at room temperature.

The two samples exhibit quite different rheological behavior. For the HEC solution irradiated at room temperature, a strong dependence of G'' on the frequency (f) and a cross-over at ca. 0.2 Hz were registered. Moreover, it was established that the viscosity of the initial solution was higher than that of the solution after irradiation at room temperature, which is evidence for the degradation of HEC macromolecules. In contrast, the apparent values of G' and G'' of the sample obtained from the frozen aqueous systems exhibited little dependence on f, and $G' > G''$ over the entire f range explored. The observed results are consistent with the typical behavior of polymer gels and indicate that crosslinking reactions

occur predominantly under the chosen experimental conditions. It has been described that two processes, degradation and crosslinking, are in competition at high-energy irradiation of cellulose derivatives with either an electron beam or gamma-rays [13–15]. When exposed to ionizing radiation at ambient temperature in the solid state and in aqueous solutions, the cellulose derivatives undergo degradation, whereas the best results for crosslinking have been obtained at paste-like conditions (25–40 mass%, depending on the polymer). Based on the theory of cryotropic gelation, it is assumed that most of the solvent forms crystals during freezing of aqueous solutions of cellulose derivatives, whereas the polymer, the photoinitiator, and the water molecules connected to the polymer through hydrogen bonds (non-freezable solvent) form a nonfrozen liquid microphase. Obviously, the polymer concentration in the liquid microphase is very high (cryo-concentration effect) and the reaction conditions closely resemble the conditions of the paste-like state. Therefore, during UV irradiation in the frozen state, the rate of crosslinking is much higher than the rate of chain scission reactions and a cryogel is formed.

Indeed, nonionic HEC, (hydroxypropyl)methylcellulose (HPMC), methylcellulose (MC), and cationic 2-hydroxyethylcellulose can be crosslinked via UV irradiation assisted by the cryogenic treatment (Table 1).

All cryogels based on cellulose derivatives are opaque materials and a significant part of the water (>65 %) can be separated easily by compression at low mechanical loads. A scanning electron microscopy (SEM) image of a HEC cryogel (Fig. 3) illustrates the typical supermacroporous structure of the material, which consists of large interconnected pores (50–200 µm) surrounded by thin walls.

The main factors affecting the efficiency of crosslinking and the properties of the material are the type and molar mass of polymer, the concentration of initial solution, the type and amount of photoinitiator, the temperature of freezing, and the irradiation dose. As a rule, each parameter has to be optimized to reach the maximum GF yield for given polymer, as exemplified below for HEC.

Table 1 Cryogels obtained via UV irradiation of frozen systems based on aqueous solutions of nonionic and cationic cellulose derivatives

Cellulose derivative	Molar mass (g/mol)	Gel fraction yield[max] (%)	Degree of swelling
HEC[a]	1,300,000	95	13
HEC[a]	300,000	78	15
HEC[a]	90,000	51	22
Quaternized HEC[b]	900,000	75	12
HPMC[c]	120,000	50	22
MC[d]	88,000	46	25

Reproduced from [11] with permission from Elsevier

Experimental conditions: 2–5 mass% BBTMAC, irradiation time 2 min (irradiation dose 11.4 J/cm^{2}, input power 93 mW/cm^{2}, maximum wavelength at 365 nm)

HEC 2-hydroxyethylcellulose, *HPMC* (hydroxypropyl)methylcellulose, *MC* methylcellulose

[a]Degree of substitution (DS) 1.5; molar degree of substitution (MS) 2.5

[b]MS of quaternary ammonium moiety 0.4

[c]DS 1.1–1.6; MS 0.1–0.3

[d]DS 1.5–1.9

Fig. 3 SEM micrograph of HEC cryogel prepared at a freezing temperature of −20 °C, initial polymer concentration 1 mass%, polymer molar mass 1,300,000 g/mol, 2 mass% BBTMAC, irradiation time 2 min. Reprinted from [12] with permission from Elsevier
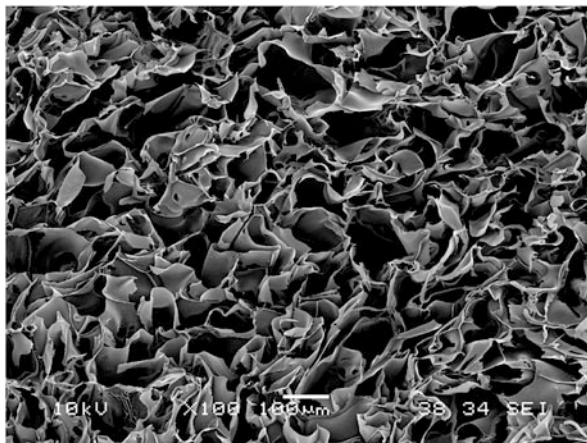
It was found that the GF yield of cryogels prepared by irradiation of frozen aqueous solutions of HEC (concentration 3 mass%, 5 mass% BBTMAC) with UV light at an irradiation dose rate of 5.7 J/cm^{2} min increases with the irradiation time in the first 2 min and then reaches a constant value. Consequently, 2 min of irradiation is adequate for crosslinking of HEC in a frozen aqueous system and results in cryogels of good quality (the material maintains its integrity and original shape in water). The extremely short time required for the formation of a polymer network avoids the side effects of excessive heating during irradiation.

The dependence of the GF yield of HEC cryogels, crosslinked at −20 °C, on the initial concentration of HEC solutions is shown in Fig. 4.

Cryogels are formed at substantially low polymer concentrations, which is attributed to the cryo-concentration phenomenon. The GF yield increases with

increasing concentration and reaches a maximum at a polymer concentration of 1 mass% for HECs with molar masses of 1,300,000 g/mol and 300,000 g/mol, and 2 mass% for HEC with molar mass of 90,000 g/mol, and decreases at higher concentrations. In addition, the higher the molar mass of polymers, the higher the GF yield of cryogels.

HEC cryogels of good quality and high GF yield can be prepared by freezing the initial solution at a temperature between -15 and $-30\ ^{\circ}C$ at a cooling rate of $1\ ^{\circ}C/min$ (Fig. 5). Note that the maximum value of GF yield is reached at $-20\ ^{\circ}C$.

The use of an aromatic photoinitiator for preparation of HEC cryogels is not always desirable, especially when the materials obtained are intended for application in medicine and pharmacy. Therefore, studies have focused on the formation of cryogels of cellulose derivatives using hydrogen peroxide as a photoinitiator (Fig. 6) [12, 16]. H_2O_2 generates hydroxyl radicals during its photo-homolysis [17]. These radicals react with the polymer chains, giving rise to macroradicals that form a polymer network by recombination. The by-product of this reaction is water and, consequently, the material obtained can be used without additional purification. The GF yield of HEC cryogels obtained with H_2O_2 is slightly lower compared to BBTMAC at the same concentration (Fig. 6); however, one can prepare monolithic material that maintains its original shape and can be handled.

It is well known that cellulose derivatives are biodegradable polymers that undergo degradation by cleavage of the glycosidic linkages through the action of enzymes or microorganisms [15]. The process of enzymatic degradation of HEC cryogels has a specific feature. SEM analysis (Fig. 7) at an intermediate stage of degradation (12 h, 62 % weight loss) illustrates that the cryogel walls appear thinner and partially destroyed. This means that the enzyme molecules do not only attack the HEC network at the gel surface (typical for hydrogels), but that they also penetrate into the macroscopic pores and digest the whole polymer structure.

Fig. 5 Gel fraction yield of HEC cryogels obtained at various negative temperatures. Cryogels were prepared at initial polymer concentration 1 mass%, polymer molar mass 1,300,000 g/mol, 2 mass% BBTMAC, irradiation time 2 min. Reprinted from [12] with permission from Elsevier
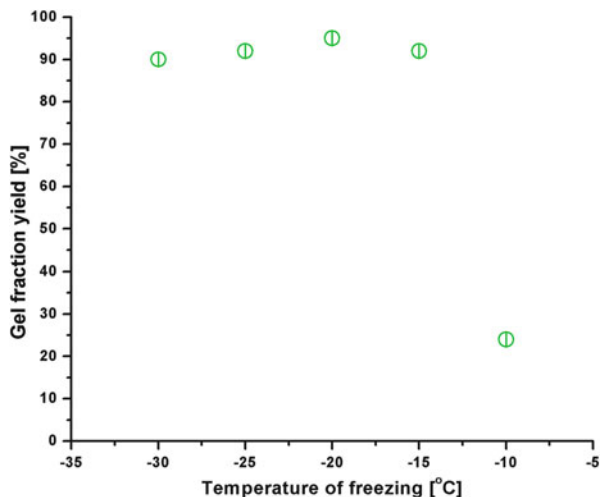
Fig. 6 Gel fraction yield of HEC cryogels prepared with different photoinitiators. Cryogels were prepared at a freezing temperature of −20 °C, initial polymer concentration 1 mass%, polymer molar mass 1,300,000 g/mol, 2 mass% initiator, irradiation time 2 min
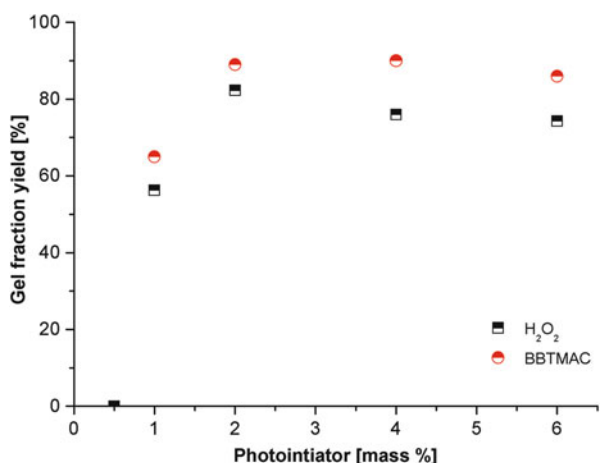
On the other hand, it was found that HEC cryogels degrade slower than conventional HEC hydrogels of similar GF yield.

An appropriate strategy for increasing the GF yield and enhancing the mechanical strength of cryogels based on cellulose derivatives is to incorporate suitable crosslinking agents into the polymer network [11]. For instance, the storage modulus of HPMC cryogel prepared in the presence of 3 mass% N,N'-methylenebisacrylamide (BisAAm) is an order of magnitude higher than that of HPMC cryogel obtained without crosslinking agent. More interesting, the formation of a polymer co-network between HEC and another polymer such as chitosan (CS) leads to a material with significantly increased storage modulus and

Fig. 7 SEM micrograph of HEC cryogel after 12 h action of the enzyme cellulase. Cryogel was prepared at a freezing temperature of $-20\,°C$, initial polymer concentration 1 mass%, polymer molar mass 1,300,000 g/mol, 2 mass% BBTMAC, irradiation time 2 min. Reprinted from [12] with permission from Elsevier
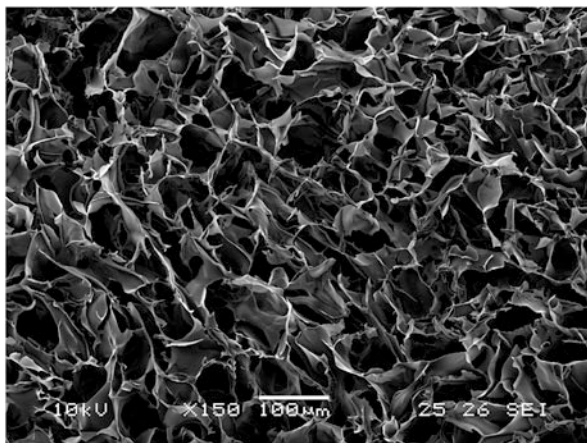
Fig. 8 Dependence of the elastic modulus G' of cryogels on the HEC-to-chitosan weight ratio. Cryogels were prepared at a freezing temperature of $-20\,°C$, 5 mass% H_2O_2, 30 mass% BisAAm, initial polymer concentration 1.5 mass%, irradiation time 2 min. Reprinted from [18] with permission from Elsevier
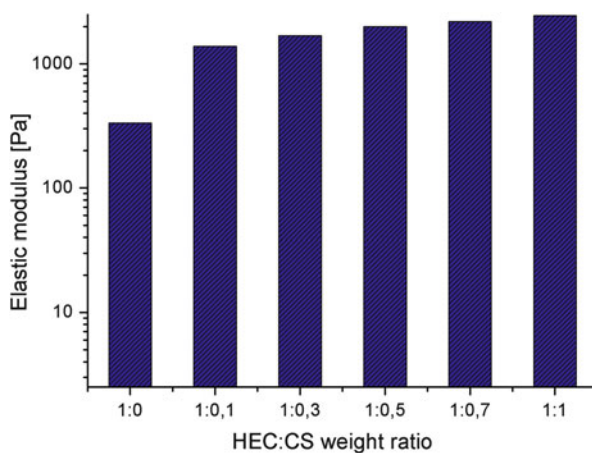
pH-responsive properties [18]. The increase in chitosan content in the polymer co-network increases the mechanical strength of cryogels (Fig. 8).

Similarly, the degree of swelling (DS) of HEC–chitosan cryogels increases proportionally with increasing chitosan content. In acidic conditions, amino groups in chitosan are protonated and chitosan segments swell more at pH 4 than in neutral water. Thus, the DS of HEC–chitosan cryogels at pH 4 is higher than at pH 7 for all compositions studied (Fig. 9). The pH-triggered volume phase transition (swelling/shrinking) is a fast and reproducible process, i.e., HEC–chitosan cryogels can reach many times the defined DS in acidic or neutral water within 15–20 s.

The UV irradiation technique has also been successfully employed in the preparation of novel macroporous cryogels based on hydrophobically modified high molar mass polyglycidol (Fig. 10) [19]. It is known that by varying the degree of modification of polymer, it is possible to obtain temperature-responsive materials with tunable properties [20]. For all copolymer compositions studied

Fig. 9 Degree of swelling (*ES*) of HEC–chitosan cryogels of different composition in acidic and neutral water. Cryogels were prepared at a freezing temperature of −20 °C, initial polymer concentration 1.5 mass%, 30 mass% BisAAm, irradiation time 2 min. Reprinted from [18] with permission from Elsevier
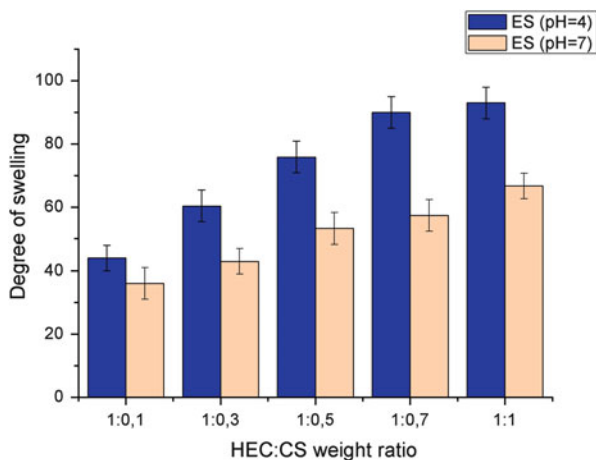
Fig. 10 Temperature-responsive poly(glycidol-*co*-ethyl glycidyl carbamate) (hydrophobically modified polyglycidol) precursor used for the synthesis of cryogels. Reprinted from [19] with permission from Elsevier
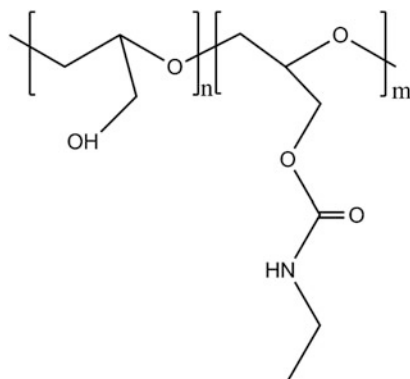
(copolymer molar mass 1,250,000 g/mol; molar degree of modification 32, 37, and 40 %), the maximum value of the GF yield was achieved at an initial copolymer concentration of 2 mass%, irradiation time 4 min (irradiation dose 22.8 J/cm^2), and 5 mass% BBTMAC.

Photochemical crosslinking of high molar mass polyacrylamide (PAAm) in a frozen aqueous system has been achieved as an alternative to the commonly used synthesis of PAAm cryogels from acrylamide. Advantageously, starting from a high molar mass precursor one may omit the use of crosslinking agent [16].

3 Cryogels from Water-Soluble Vinyl Monomers

It has been demonstrated by several teams that the UV irradiation technique can be used for the synthesis of polymer cryogels from different vinyl monomers (Table 2) in the presence of a photoinitiator and a crosslinking agent.
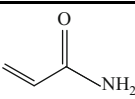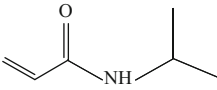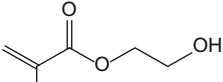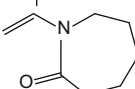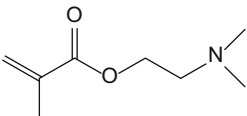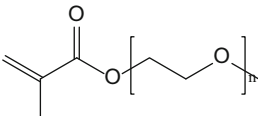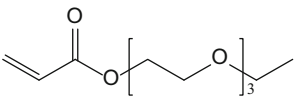
The polymer network is formed in the nonfrozen liquid microphase by a free radical photopolymerization/crosslinking reaction (Fig. 11) at defined negative temperature. The use of crosslinking agent provides the formation of a three-dimensional network instead of linear macrochains. Specifically, the concentration of reagents in the microphase is much higher than the concentration in the initial solution, due to the fact that a large amount of the solvent forms crystals.

The incorporation of crosslinks between the polymer chains also contributes to the mechanical strength of the material. A comparison between two polyacrylamide cryogels, synthesized from 5 mass% monomer solution containing crosslinking agent poly(ethylene glycol) diacrylate (PEGDA, 10 mass%) and 5 mass% polymer solutions without PEGDA, revealed that the latter cryogel has a storage modulus several times lower than the cryogel synthesized from monomer (Fig. 12). However, the addition of 10 mass% PEGDA to the polymer solution resulted in a cryogel with G' similar to that of AAm/PEGDA-based cryogels.

The choice of a powerful source of UV light seems to be the crucial factor for fast monomer conversion and formation of polymer network. The results from experiments carred out with a Dymax 5000-EC UV curing equipment with 400 W metal halide flood lamp emitting full spectrum UV–visible light at an irradiation dose rate of 5.7 J/cm^2 min (input power 93 mW/cm^2) showed that 5 min of irradiation is sufficient for preparation of disk-shaped cryogels of good quality [16, 21, 22]. Moreover, in the case of NIPAAm, ETEGA, and AAm, cryogels of extremely high GF yield (nearly quantitative monomer conversion) were obtained (Table 3). Thus, the as-synthesized materials do not contain undesirable monomer and crosslinking agent and can be directly used without any extraction procedure. The conversion of HEMA to a PHEMA network within the studied concentration range was also very high. Only vinyl caprolactam (VCL) cannot form cryogels of high GF yield, and the possible reason for the low crosslinking efficiency can be attributed to the poor solubility of VCL in water. The use of non-crystallizable co-solvent (ethanol; 10 vol%) seems to affect the regular cryostructuring and hinder the formation of polymer network.

In general, the time for preparation of polymer cryogels from vinyl monomers via UV irradiation is much shorter compared to the most often used technique, which is based on a redox system. Since the reagents can be dissolved quickly in the solvent and the reaction time is only 5 min, the freezing/cryostructuring of the system appears to be the longest stage in the preparation procedure. Usually, depending on the sample size and shape, the solvent can be frozen within several (up to 120) minutes, making completion of the entire process possible in less than 1 h. It should be noted that all the commercially available monomers listed in Table 3 can be used without any purification, which further facilitates the synthesis

Table 2 Monomer precursors used for the synthesis of polymer cryogels via the UV irradiation technique

Monomer	Structural formula	Solvent	References
Acrylamide (AAm)		Water	[16, 21]
N-Isopropylacrylamide (NIPAAm)		Water	[16]
2-Hydroxyethyl methacrylate (HEMA)		Water	[16]
N-Vinylcaprolactam (VCL)		Water/ ethanol	[16]
2-(Dimetylamino)ethyl methacrylate (DMAEMA)		1,4-Dioxane	[22]
Oligo(ethyleneglycol) methacrylate (OEGMA)		1,4-Dioxane	[22]
Ethoxytriethyleneglycol acrylate (ETEGA)		Water	[23, 24]
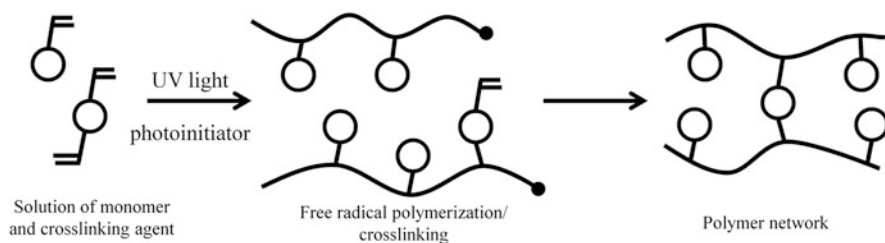
Fig. 11 Formation of polymer network from vinyl monomer and bifunctional crosslinking agent via UV irradiation

procedure. In addition, a very high crosslinking efficiency was reached without any purging of the reagent solution with an inert gas.

Certain limitations of the technique described in this review arise from the penetration depth of the irradiation. To fabricate material with identical behavior throughout the whole structure, it is recommended that the entire sample be
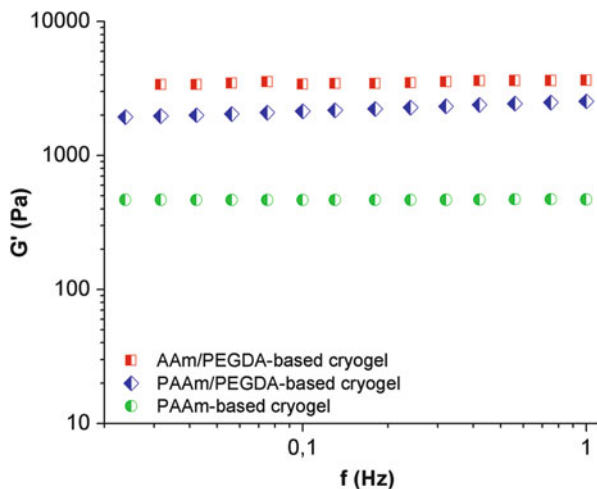
Fig. 12 Frequency dependence of the storage moduli G' of polyacrylamide cryogels prepared from 5 mass% monomeric (AAm) or polymeric precursors (PAAm) with and without PEGDA crosslinker. *AAm/PEGDA* AAm + 10 mass% PEGDA, *PAAm/PEGDA* PAAm + 10 mass% PEGDA, *PAAm* PAAm without PEGDA. Cryogels were formed at a freezing temperature of -20 °C, irradiation time 5 min, and 5 mass% H_2O_2. Reprinted from [16] with permission from Elsevier

irradiated simultaneously. Therefore, the UV irradiation technique is useful for preparation of flat (up to 10 mm), disk-shaped [10–12, 16, 18, 19, 21, 22], and cylindrical cryogels with diameters up to 32 mm [23].

Polymer cryogels obtained by photocrosslinking of frozen systems possess randomly distributed pores [24]. The diffusion of liquids in such cryogels is relatively isotropic (Fig. 13a). In the case of directionally frozen systems, the structure obtained is aligned and the diffusion of liquids through the cryogel follows a one-dimentional pathway, diffusing faster parallel to the direction of freezing (Fig. 13b).

Compression tests performed to determine the aligned cryogel strength revealed that the sample crushed parallel to the freezing direction has a Young's modulus of 10 kPa and the sample crushed in the perpendicular direction has a Young's modulus of 0.9 kPa.

4 Temperature-Responsive Polymer Cryogels

Temperature-responsive polymer cryogels are among the most intriguing representatives of the so-called "inteligent" hydrogels due to their numerous advantages. The hydration/dehydration behavior of cryogels is much more rapid compared to conventional hydrogels obtained from the same polymer [25]. This behavior has

Table 3 Formation of cryogels from monomers via UV irradiation

Monomer precursor	Monomer concentration (mass%)	Irradiation time (min)	Gel fraction yield (%)
NIPAAm	2	5	>99
	5	5	>99
	10	5	97
	15	5	87
AAm	2	5	>99
	5	5	>99
	10	5	96
	15	5	90
ETEGA	2	5	>99
	5	5	>99
	10	5	>99
HEMA	2	5	92
	5	5	92
	10	5	92
	15	5	87
VCL	2	10	–
	5	10	–
	10	10	25
	15	10	15

Reproduced from [16] with permission fromElsevier

Experimental conditions: temperature of freezing −20 °C, 5 mass% H_2O_2, 10 mass% PEGDA (molar mass 575 g/mol)

NIPAAm N-isopropylacrylamide, *AAm* acrylamide, *ETEGA* ethoxytriethyleneglycol acrylate, *HEMA* 2-hydroxyethyl methacrylate, *VCL* vinyl caprolactam
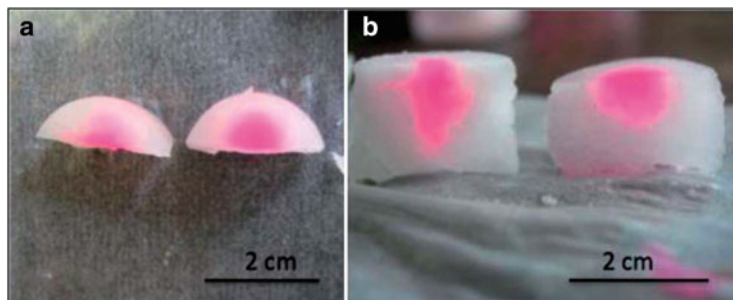
Fig. 13 Diffusion of Rhodamine B-stained water through aligned porous polyOEGMA hydrogel (*left*) and randomly macroporous polyOEGMA hydrogel (*right*) at room temperature: (**a**) birds-eye view, (**b**) cross-sectional view. Reprinted form [24] with permission from the Royal Society of Chemistry

been attributed to the spongy-like structure of the cryogel, which contains a large amount of free water. During hydration/dehydration of the cryogel, the interconnected pores, with their very smooth wall interfaces, dramatically facilitate the diffusion of water and heat exchange.
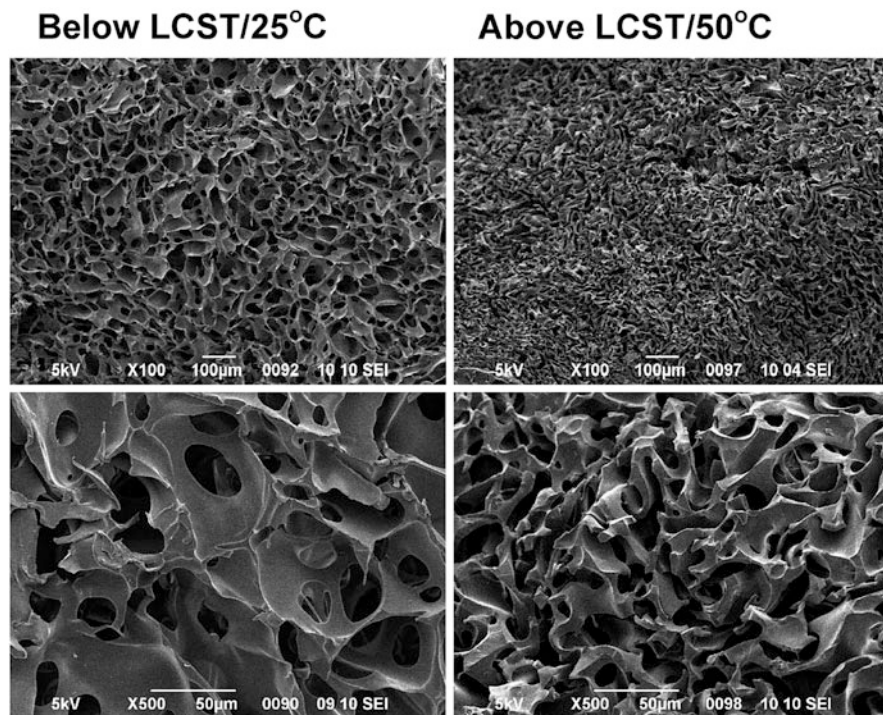
Fig. 14 SEM micrographs of PNIPAAm cryogel prepared from samples immersed in water at 25 °C (*left*) and 50 °C (*right*). Cryogel was synthesized from 5 mass% monomer solution, containing H_2O_2 (5 mass% to monomer) and PEGDA (10 mass%), frozen at -20 °C, and irradiated with UV light for 5 min. Reprinted from [16] with permission from Elsevier

The interior morphologies of PNIPAAm cryogel at temperatures below and above the temperature of volume phase transition (T_{VPT}) are shown in Fig. 14. At 25 °C, the PNIPAAm cryogel is swollen and has a supermacroporous structure with round-shaped interconnected pores (50–100 μm) surrounded by thin walls (ca. 1–2 μm). The phase transition of PNIPAAm caused a drastic decrease in the volume of cryogel, resulting in much smaller pores (Fig. 14, right). Notably, the cryogel does not lose its open porous structure in the deswollen state.

The extremely fast volume phase transition from hydrophilic to hydrophobic state of the polymer network is demonstrated in Fig. 15 for cryogels based on PNIPAAm and hydroxypropylcellulose (HPC). When the temperature changed from 20 to 60 °C, the gel collapsed and reached a near-equilibrium state within 10–12 s. This behavior is attributed to both the existence of a large amount of free water in the pores, which facilitates the heat transfer, and the thin compact cryogel walls, which tend to respond more quickly to temperature changes. The fact that the cryogels preserve their capillary structure above T_{VPT} plays an important role in the rapid transition from hydrophobic to hydrophilic state. As also seen from Fig. 15,

Fig. 15 Deswelling–
reswelling kinetics of HPC
and PNIPAAm cryogels
synthesized via UV
irradiation. Reprinted from
[16] with permission from
Elsevier
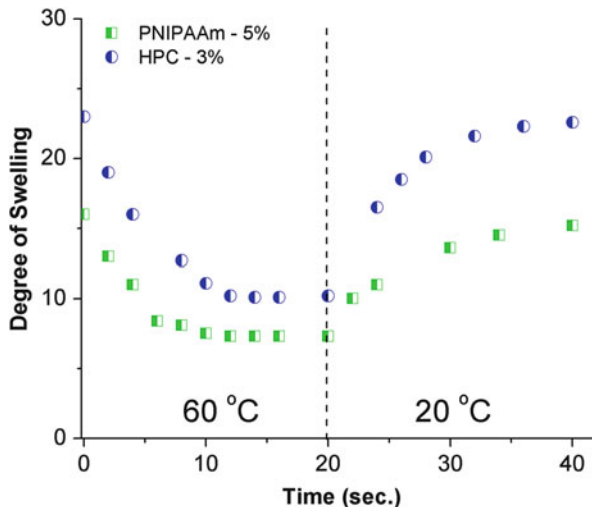
the cryogel reached 90 % of the equilibrium degree of swelling at 20 °C within 15–20 s.

The temperature of volume phase transition of each cryogel depends on the nature of the polymer network. The T_{VPT}, estimated as the maximum of the first derivative of the swelling versus temperature curve, of PNIPAAm, HPC, and PETEGA cryogels are 32, 48, and 33 °C, respectively. Most often, T_{VPT} is close to the lower critical solution temperature (LCST) of the linear polymer analog; however, unlike it, the transition is not so sharp.

The swelling versus temperature curves of hydrophobically modified PGL cryogels of different composition are shown in Fig. 16. As a rule, an increase in the degree of modification results in decreased T_{VPT}. Obviously, the gels containing lower amounts of hydrophilic groups need less energy to overcome contributions from the hydrogen bonds formed between the water molecules and polymer network, and the gels collapse at lower temperatures. Thus, one may design hydrophobically modified PGL cryogels with the desired T_{VPT} just by tuning the degree of modification of the precursor. It should be noted that changing the concentration of the copolymer solutions studied (1–5 mass%) did not cause any shift of T_{VPT}.

The ability of stimuli-responsive hydrogels to undergo a reversible volume phase transition in a defined and reproducible manner under given environmental parameters is a crucial precondition for their practical application. Multiple swelling–deswelling experiments conducted with PNIPAAm, PETEGA, and HPC cryogels at different temperatures revealed nearly equal degrees of swelling for each material at a defined temperature. This indicates that the cryogel is able to reproduce its former interior structure and volume after many cycles of volume phase transition without any mechanical destruction. An exception was observed only for hydrophobically modified PGL cryogels. A decrease in the degree of

Fig. 16 Temperature
dependence of the swelling
degree of different
hydrophobically modified
PGL cryogels (degree of
modification 32, 37, and
40 mol%) obtained at a
freezing temperature of
−20 °C, initial polymer
concentration 3 mass%,
5 mass% BBTMAC,
irradiation time 4 min.
Reprinted from [19] with
permission from Elsevier
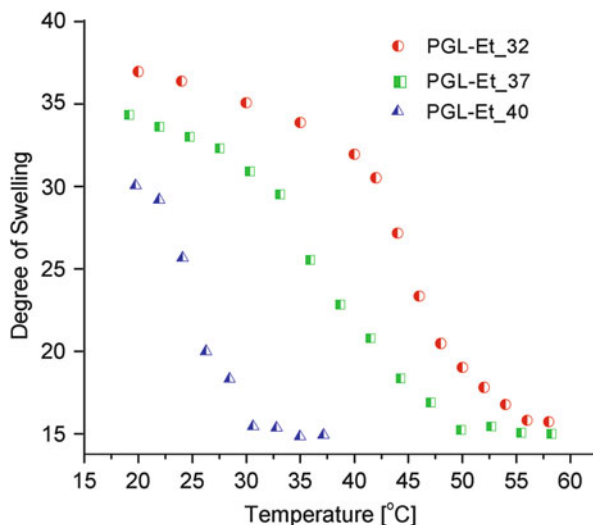
swelling was found after the fifth cycle of temperature changes and was caused by separation of small pieces from the edge of the cryogel. This destruction is attributed to the lower strength of ether bonds in the PGL network upon mechanical deformation accompanied by the temperature changes.

5   Nanocomposites Based on Polymer Cryogels

Fabrication of nanocomposite cryogels is a versatile platform for imparting specific properties to the material. Basically, the specific heterogeneous structure of the cryogel makes possible the incorporation of nanosized fillers via two different routes: into the cryogel walls and into the cryogel channels. This, however, may lead to nanocomposite cryogels with different behaviors and properties, even though they were prepared from the same initial components. For instance, two types of HPC cryogels containing silver nanoparticles (AgNPs), either entrapped into the gel walls (polymer matrix) or included into the pores, were synthesized via UV-induced crosslinking [16]. AgNPs were immobilized in the channels of the gel by immersing a pre-made freeze-dried HPC cryogel in an aqueous dispersion of AgNPs. The freeze-drying process preserves the spongy-like macroporous structure of materials and, thus, the dispersion can easily fill the channels (interconnected pores) of the dry cryogel in a few seconds. The second approach is based on mixing of AgNPs and polymer prior to freezing and crosslinking. Cryogenic treatment led to phase-separated ice crystals and nonfrozen liquid microphase containing AgNPs, reagents, and physically bound water. Because the reaction of crosslinking occurs only in the liquid microphase forming the gel walls, AgNPs were embedded into the crosslinked polymer matrix. It is noteworthy that both types of materials exhibited

completely different properties. The cryogels containing AgNPs only in the channels released them immediately when compressed (Fig. 17a) or, in the case of temperature-responsive polymers, by switching to temperatures above the corresponding T_{VPT} [16]. In addition, placed in a large excess of water, the cryogels released the particles within several hours without external stimuli. In contrast, the cryogels with AgNPs embedded in the walls did not release any nanoparticles (Fig. 17b) due to the dense polymer network. In the latter case, only a slow release of Ag^+ was registered.

Supermacroporous carbon nanotube (CNT)–polymer nanocomposites based on various polymer cryogels have been prepared via photocrosslinking of either polymer or monomer precursors [26, 27]. The two different strategies described above were exploited to fabricate foam-like materials (aerogels) with CNTs located either in the cryogel walls or on the cryogel inner surface (Fig. 18).

Intererestingly, the inclusion of a CNT dispersion into the pores of a pre-made cryogel and the subsequent freezing resulted in deposition of both single- and multiwalled CNTs onto the inner surface of the polymer matrix. It is assumed that during cryogenic treatment most of the water in the system forms ice crystals, whereas CNTs are accumulated on the surface of crystals and are gradually pushed to the cryogel walls. Based on this original technique, supermacroporous aerogels of high electrical conductivity at relatively low CNT content (0.12 mass%) were obtained. Specifically for the UV irradiation technique, when the nanotubes were added into the system before crosslinking, a decrease in the gel fraction yield was found. Such a result is attributed to the ability of CNTs to absorb UV light, which interferes with the regular crosslinking of polymer matrix, thus yielding cryogels with a lower mechanical strength than the pure cryogels from the same precursor.

6 Applications

One of the main applications of polymer cryogels is their use in biotechnology as carriers of cells, bacteria, and enzymes [1, 2]. The advantages of immobilized microorganisms over cultures in suspension include the easier collection and purification of bioproducts, better stability and performance under storage and operational conditions, tolerance against toxic compounds, etc.

Photocrosslinked HEC cryogels have been studied as matrices for immobilization of *Saccharomyces cerevisiae* cells [28, 29]. The systems obtained can be re-used many times for production of ethanol in a batch reactor. Even after 6 months of storage, *S. cerevisiae* cells were able to produce over 40 g ethanol in 1 L reactor volume. However, the larger pore size of cryogels as compared to the cell size allows unhindered difusion of the cells located at the periphery of the polymer matrix into the medium. Therefore, a mixed system is formed consisting of immobilized and free cells. The leakage of cells was significantly reduced by covering the HEC cryogel, containing *S. cerevisiae* cells, with an outer layer based on photocrosslinked poly(ethylene oxide) (PEO) hydrogel [30]. The PEO
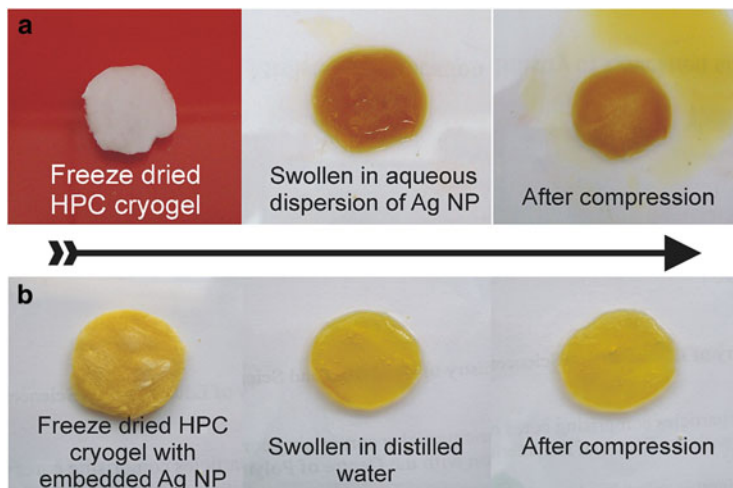
Fig. 17 Nanocomposite polymer cryogels based on HPC and silver nanoparticles immobilized into (**a**) the pores and (**b**) the walls of the cryogel. Reprinted from [16] with permission from Elsevier
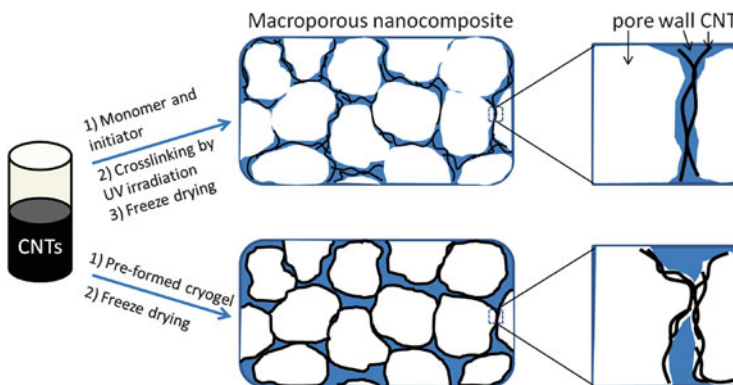
Fig. 18 Fabrication of CNT–cryogel composites with nanotubes embedded into the cryogel walls (*top*) and nanotubes deposited onto the inner surface of the cryogel (*bottom*). Reprinted from [27] with permission from Elsevier

layer did not hinder the diffusion of nutrient and fermentation products. In this case, ethanol production was up to 77 % of the theoretical yield.

Photocrosslinked PEO cryogel was investigated as carrier for different xenobiotic-degrading bacteria [31, 32]. The cryogel exhibited good mechanical strength, nontoxicity, and high biocompatibility with bacteria. It was found that the enzyme activity of immobilized bacteria is many times higher than that of the free culture.

Production of a rhamnolipid biosurfactant by cells of *Pseudomonas aeruginosa* strain BN10 immobilized into PEO and PAAm cryogels was investigated under semicontinuous shake flask conditions and compared to biosurfactant secretion by free cells [33]. The yield of rhamnolipids in the immobilized system exceeded that of the free bacterial cells, distinguishing an effective bioprocess. The polymer matrices possessed chemical and biological stability and very good physico-mechanical characteristics, which are prerequisites for a high life span of these materials for the production of rhamnolipids.

The temperature-responsive properties of poly(glycidol-*co*-ethyl glycidyl carbamate) cryogels were exploited for the growth of fibroblast cells on their surface [19]. It was shown that the nonionic hydrophilic surface hinders interactions with cells. When the environmental temperature is above T_{VPT} of the cryogel, the support became hydrophobic, allowing cell attachment and proliferation.

Supermacroporous PNIPAAm cryogels containing urease were prepared via the UV irradiation technique, with hydrogen peroxide as initiator [34]. Taking the advantage of cryostructuration phenomenon during the cryogenic treatment, most enzyme molecules were embedded into the cryogel walls. Although the enzyme was physically entrapped, the system exhibited remarkable resistance against leakage due to the dense polymer network formed in the cryogel walls. The immobilized urease can catalyze the hydrolysis of urea over a broad temperature range in both batch and flow regimes. The interconnected macropores assist unhindered diffusion of the substrate and reaction products through the gel, thus paving the way for consecutive re-use at a constant activity, in contrast to the conventional PNIPAAm hydrogel (Fig. 19). The relatively high flow rate through the cryogel matrix and the good activity of urease make it possible to directly remove urea from the feed solution in a continuous flow regime. Hence, this material might be attractive for treatment of contaminated water, blood detoxication, the dialysate regeneration system of artificial kidneys, removal of urea from beverages, etc.

Encapsulation of a high amount of enzyme, comparable to the weight of cryogel matrix, is only possible when the enzyme solution fills the large volume pores of a pre-made cryogel. In this case, the performance of the system depends strongly on the enzyme retention. It was demonstrated that the fabrication of an outer PEO layer onto a PHEMA cryogel containing urease in the pores (Fig. 20) is an effective strategy for preventing leakage of enzyme into the medium [35]. Moreover, one could expect that the urease molecules, simply located in the confined space of the macropores, are not restricted and behave like the free enzyme molecules. Due to the high sensitivity of urease, such a system is able to detect very low contamination of metal ions in water and, therefore, can find application as a biosensor.

One important issue in modern medicine is linked to the controlled release of active substances. It is assumed that a drug delivery system can supply a constant dose of the active substance over a period of several hours or days, depending on the particular disease. Thus, it has an advantage over the conventional system, characterized by a spontaneous release of the active substance immediately after administration (known as the "burst" effect) [36]. The potential of polymer cryogels for

Fig. 19 Effect of reaction time and number of cycles on the enzymatic activity of urease immobilized in PNIPAAm cryogel and PNIPAAm hydrogel, incubated in 10 mL urea solution (3.2 g/L) at 50 °C. Reprinted from [34] with permission from John Wiley & Sons
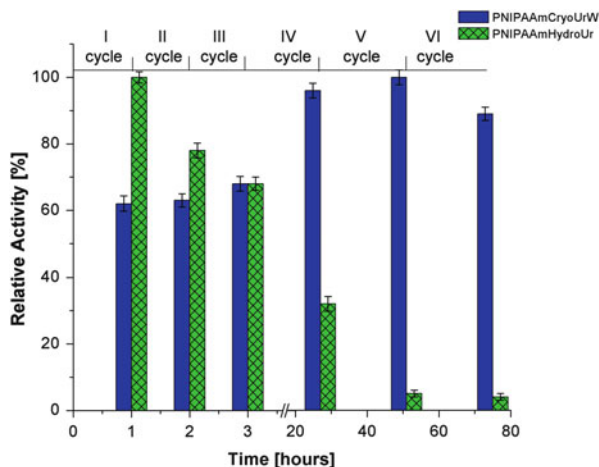
Fig. 20 Digital image of double-layered gel comprising a PHEMA core containing urease and a PEO outer layer. Reprinted from [35] with permission from John Wiley & Sons
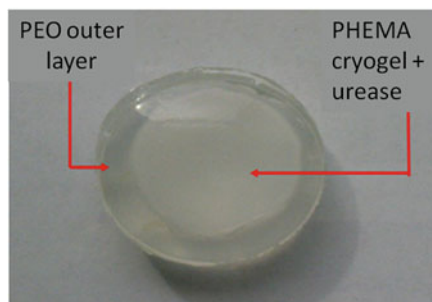
encapsulation and sustained release of hydrophilic drugs has been investigated [21, 22]. By design, the water-soluble drug verapamil hydrochloride was entrapped in the walls of different cryogels. In vitro experiments showed that the swelling behavior of polymer matrices at physiological temperature plays a key role in the drug release profile. For instance, the temperature-responsive PETEGA (Fig. 21) and PNIPAAm cryogels, which are in a hydrophobic state at 37 °C, released the drug over a period of more than 8 h. Following a slight initial burst effect, from the second hour post-incubation the drug release process is characterized by time-independent kinetics (zero-order kinetics with correlation coefficient $R = 0.998$). This sustained release is attributed to the hindered diffusion of drug molecules across the deswollen polymer network.

On the other hand, drug delivery systems based on hydrophilic PHEMA or HEC–chitosan cryogels exhibited prolonged drug release at 37 °C after incorporation of a high amount of crosslinking agent (30 mass%) into the polymer network [19, 22]. It is suggested that the high crosslink density of the polymer network is responsible for the reduced rate of diffusion of drug molecules.

Fig. 21 Release kinetics of
verapamil hydrochloride
from PETEGA cryogel at
37 °C. Reproduced from
[22] with permission from
Elsevier
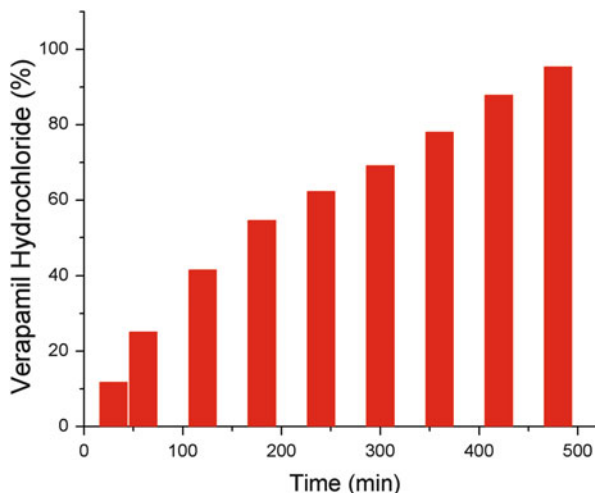
7   Conclusions

The combination of cryogenic treatment and UV irradiation is a facile method for
the synthesis of chemically crosslinked supermacroporous polymer cryogels from
both polymer and monomer precursors. Effective crosslinking and a high gel
fraction yield can be achieved by irradiation of partly frozen systems with a UV
curing equipment comprising a 400 W metal halide flood lamp emitting full-
spectrum UV–visible light at an irradiation dose rate of 5.7 J/cm^2 min (input
power 93 mW/cm^2) for 2–5 min. The cryogels obtained possess an open porous
structure, which imparts a very rapid water uptake and, in the case of stimuli-
responsive polymers, reversible ultrarapid volume phase transition.

Cryogels of cellulose derivatives were successfully synthesized by UV irradia-
tion of their partly frozen solutions. The use of H_2O_2 initiator for photocrosslinking
of biocompatible and biodegradable polymers allows preparation of "green" gel
materials that can be further exploited without any additional purification.

In general, different species such as water-soluble drugs, enzymes,
nanoparticles, and nanotubes can be immobilized either within the cryogel walls
or into the cryogel pores, depending on the experimental protocol. Hence, one can
fabricate materials with specific properties, for instance, drug carriers exhibiting
either fast or prolonged release profiles.

References

1. Lozinsky VI (2002) Cryogels on the basis of natural and synthetic polymers: preparation, properties and areas of implementation. Russ Chem Rev 71:489–511
2. Lozinsky VI, Galaev IY, Plieva FM, Savina IN, Jungvid H, Mattiasson B (2003) Polymeric cryogels as promising materials of biotechnological interest. Trends Biotechnol 21:445–451
3. Kirsebom H, Mattiasson B (2011) Cryostructuration as a tool for preparing highly porous polymer materials. Polym Chem 2:1059–1062
4. Ivanov RV, Lozinsky VI, Noh SK, Han SS, Lyoo WS (2007) Preparation and characterization of polyacrylamide cryogels produced from a high-molecular-weight precursor. I. Influence of the reaction temperature and concentration of the crosslinking agent. J Appl Polym Sci 106:470–475
5. Zhang X-Z, Zhuo R-X (1999) Preparation of fast responsive, temperature-sensitive poly (N-isopropylacrylamide) hydrogel. Macromol Chem Phys 200:2602–2605
6. Dinu MV, Ozmen MM, Dragan ES, Okay O (2007) Freezing as a path to build macroporous structures: superfast responsive polyacrylamide hydrogels. Polymer 48:195–204
7. Yoshida M, Kumakura M, Kaetsu I (1979) Immobilization of enzymes by radiation-induced polymerization of glass-forming monomers: 1. Immobilization of some enzymes by poly (2-hydroxyethyl methacrylate). Polymer 20:3–8
8. Yoshida M, Kumakura M, Kaetsu I (1979) Immobilization of enzymes by radiation-induced polymerization of glass-forming monomers: 2. Effects of cooling rate and solvent on porosity and activity of immobilized enzymes. Polymer 20:9–12
9. Kumakura M, Kaetsu I (1984) Immobilization of cellulase using porous polymer matrix. J Appl Polym Sci 29:2713–2718
10. Doycheva M, Petrova E, Stamenova R, Tsvetanov CB, Riess G (2004) UV induced cross-linking of poly(ethylene oxide) in aqueous solution. Macromol Mater Eng 289:676–680
11. Petrov P, Petrova E, Stamenova R, Tsvetanov CB, Riess G (2006) Cryogels of cellulose derivatives prepared via UV irradiation of moderately frozen systems. Polymer 47:6481–6484
12. Petrov P, Petrova E, Tchorbanov B, Tsvetanov CB (2007) Synthesis of biodegradable hydroxyethylcellulose cryogels by UV irradiation. Polymer 48:4943–4949
13. Wach RA, Mitomo H, Yoshii F, Kume T (2001) Hydrogel of biodegradable cellulose derivatives. ii. Effect of some factors on radiation-induced crosslinking of CMC. J Appl Polym Sci 81:3030–3037
14. Wach RA, Mitomo H, Yoshii F, Kume T (2002) Hydrogel of radiation-induced cross-linked hydroxypropylcellulose. Macromol Mater Eng 287:285–295
15. Wach RA, Mitomo H, Nagasawa N, Yoshii F (2003) Radiation crosslinking of methylcellulose and hydroxyethylcellulose in concentrated aqueous solutions. Nucl Instrum Methods Phys Res Sect B 211:533–544
16. Petrov P, Petrova E, Tsvetanov CB (2009) UV-assisted synthesis of supermacroporous polymer hydrogels. Polymer 50:1118–1123
17. Fechine GJM, Barros JAG, Catalani LH (2004) Poly(N-vinyl-2-pyrrolidone) hydrogel production by ultraviolet radiation: new methodologies to accelerate crosslinking. Polymer 45:4705–4709
18. Stoyneva V, Momekova D, Kostova B, Petrov P (2014) Stimuli sensitive super-macroporous cryogels based on photo-crosslinked 2-hydroxyethylcellulose and chitosan. Carbohydr Polym 99:825–830
19. Petrov P, Utrata-Wesołek A, Trzebicka B, Tsvetanov CB, Dworak A, Anioł J, Sieroń A (2011) Biocompatible cryogels of thermosensitive polyglycidol derivatives with ultra-rapid swelling properties. Eur Polym J 47:981–988
20. Jamróz-Piegza M, Utrata-Wesołek A, Trzebicka B, Dworak A (2006) Hydrophobic modification of high molar mass polyglycidol to thermosensitive polymers. Eur Polym J 42:2497–2506

21. Petrov P, Momekova D, Kostova B, Momekov G, Toncheva- Moncheva N, Tsvetanov CB, Lambov N (2010) Super-macroporous poly(ethoxytriethyleneglycol acrylate) hydrogels for sustained delivery of hydrophilic drugs. J Control Release 148:81–82
22. Kostova B, Momekova D, Petrov P, Momekov G, Toncheva-Moncheva N, Tsvetanov CB, Lambov N (2011) Poly(ethoxytriethylene glycol acrylate) cryogels as novel sustained drug release systems for oral application. Polymer 52:1217–1222
23. Kahveci MU, Beyazkilic Z, Yagci Y (2010) Polyacrylamide cryogels by photoinitiated free radical polymerization. J Polym Sci Polym Chem 48:4989–4994
24. Barrow M, Zhang H (2013) Aligned porous stimuli-responsive hydrogels via directional freezing and frozen UV initiated polymerization. Soft Matter 9:2723–2729
25. Zhang X-Z, Chu C-C (2003) Thermosensitive PNIPAAm cryogel with superfast and stable oscillatory properties. Chem Commun 2003(12):1446–1447
26. Petrov PD, Georgiev GL (2011) Ice-mediated coating of macroporous cryogels by carbon nanotubes: a concept towards electrically conducting nanocomposites. Chem Commun 47:5768–5770
27. Petrov PD, Georgiev GL (2012) Fabrication of super-macroporous nanocomposites by deposition of carbon nanotubes onto polymer cryogels. Eur Polym J 48:1366–1373
28. Velickova E, Winkelhausen E, Kuzmanova S, Cvetkovska M, Tsvetanov C (2009) Hydroxyethylcellulose cryogels used for entrapment of Saccharomyces cerevisiae cells. React Funct Polym 69:688–693
29. Winkelhausen E, Velickova E, Amartey SA, Kuzmanova S (2010) Ethanol production using immobilized saccharomyces cerevisiae in lyophilized cellulose gel. Appl Biochem Biotechnol 162:2214–2220
30. Velickova E, Petrov P, Tsvetanov C, Kuzmanova S, Cvetkovska M, Winkelhausen E (2010) Entrapment of Saccharomyces cerevisiae cells in u.v. crosslinked hydroxyethylcellulose/poly (ethylene oxide) double-layered gels. React Funct Polym 70:908–915
31. Satchanska G, Topalova Y, Dimkov R, Petrov P, Tsvetanov C, Selenska-Pobell S, Gorbovskaya A, Bogdanov V, Golovinsky E (2009) Phenol biodegradation by two xenobiotics-tolerant bacteria immobilized in poly(ethylene oxide) cryogels. Compt Rend Acad Bulg Sci 62:957–964
32. Topalova Y, Dimkov R, Todorova Y, Daskalova E, Petrov P (2011) Biodegradation of phenol by immobilized in PEO-cryogel Bacillus laterosporus bt-271 in sequencing bath biofilter. Biotechnol Biotech Equip 25:2613–2619
33. Christova N, Petrov P, Kabaivanova L (2013) Biosurfactant production by pseudomonas aeruginosa BN10 cells entrapped in cryogels. Z Naturforsch 68C(1–2):47–52
34. Petrov P, Pavlova S, Tsvetanov CB, Topalova Y, Dimkov R (2011) In situ entrapment of urease in cryogels of poly(N-isopropylacrylamide): an effective strategy for noncovalent immobilization of enzymes. J Appl Polym Sci 122:1742–1748
35. Petrov P, Jeleva D, Tsvetanov CB (2012) Encapsulation of urease in double-layered hydrogels of macroporous poly(2-hydroxyethyl methacrylate) core and poly(ethylene oxide) outer layer: fabrication and biosensing properties. Polym Int 61:235–239
36. Ravi Kumar MNV, Kumar N, Domb AJ, Arora MA (2002) Pharmaceutical polymeric controlled drug delivery systems. Adv Polym Sci 160:45–117

Inorganic Cryogels

Oleg A. Shlyakhtin

Contents

Abstract Recent advances in the application of cryogels in the synthesis and processing of inorganic as well as carbon-based materials are briefly summarized. Synthesis of complex oxides by using polymeric cryogels causes a substantial reduction in phase formation temperature and thus promotes a significant decrease in grain size. Freeze-drying of co-precipitated gels and residues prevents the agglomeration of nanocrystallites usually observed during atmospheric drying. This feature is also widely used for the isolation of nanoparticles prepared by various wet chemical methods. Ceramic materials with oriented tubular pores and mesoporous pore walls can be obtained by using directed crystallization of ice from ceramic slurries. Carbon cryogels with a specific surface area of up to 2,000 $m^2\,g^{-1}$ can be prepared by thermal processing of the corresponding polymeric precursors. Cryogel-derived composites of carbon nanotubes and graphene-based materials

O.A. Shlyakhtin (✉)
Inorganic Chemistry Division, Department of Chemistry, M.V. Lomonosov Moscow State University, 119991 Moscow, Russia
e-mail: oleg@inorg.chem.msu.ru

with various oxides demonstrate outstanding mechanical properties and enhanced electrical conductivity.

Keywords Freeze-drying synthesis • Co-precipitation • Nanoparticle isolation • Oriented porosity • Carbon cryogel

Abbreviations

CNT	Carbon nanotubes
FESEM	Field emission SEM
GO	Graphene oxide
HAP	Hydroxyapatite
RGO	Reduced graphene oxide
RF	Resorcinol-formaldehyde
SEM	Scanning electron microscopy
TEM	Transmission electron microscopy

1   Introduction

The term "cryogel" was first introduced into the field of inorganic materials by Klvana and Pajonk [1–3], who considered cryogels, together with xerogels and aerogels, as one of the possible drying products of $SiO_2.nH_2O$- and $Al_2O_3.nH_2O$-based hydrogels. In their experiments, freezing and freeze-drying of wet gels were used to avoid pore collapse due to the extreme surface tension effects of water removal during atmospheric drying and to retain most of the tiny morphological features of gels in the dried state. As the term "cryogel" is most commonly used in papers on inorganic materials obtained by freeze-drying [4–6], it will be used here to be consistent with previous studies in this field. Therefore, the first studies on the synthesis of inorganic cryogels go back to the early 1970s [7–9], soon after the discovery of the freeze-drying synthesis of inorganic materials from frozen aqueous solutions by Landsberg and Campbell [10].

This "extended" approach, whereby a cryogel is considered as the freeze-drying product of any frozen liquid–solid system composed of a freeze-driable solvent and at least one solid inorganic substance or carbon, is rather close to the concepts used in a number of recent papers on the synthesis and processing of inorganic materials. None of these products are true gels; indeed, some of them have never been gels. Nevertheless, most of these products have several common features that will be described in this brief review. Following the well-known approach "It doesn't matter whether a cat is white or black, as long as it catches mice" [11], the review will focus on the most interesting examples of cryogel applications in the synthesis and processing of inorganic materials during the last 6–7 years.

Many earlier studies on inorganic cryogels and the freeze-drying products of frozen solutions were summarized in our previous monograph and review papers [12–15]. A large number of papers on inorganic–polymer hybrids, composites, and their biomedical applications are reviewed in other chapters of this volume. The scope of this review is limited to cryogel-derived inorganic materials containing a minor amount of polymer, and to the contribution of polymer properties to the performance of the final composite or single phase material. Taking into account the growing number of applications of carbon-based materials and the similarity between the approaches to the synthesis of inorganic and carbon-based cryogels, this new and promising kind of material and its structure will also be briefly summarized.

2   Metal Oxide Cryogels

2.1   *Cryogenic Polymer-Gel Synthesis*

The only cryogel application in materials synthesis where true polymeric cryogels always form is the low temperature modification of the Pechini method [16]. The idea of various solution-based methods that aim to synthesize multicomponent materials is to retain the chemical homogeneity of the starting multicomponent aqueous solution during the process from solution to the final solid oxide material. Usually, these methods are applied in order to reduce the synthesis temperature and, hence, to reduce the grain size of as-obtained multicomponent oxide powders. In the case of the Pechini method, the formation of a gel due to the polycondensation of ethylene glycol and citric acid reduces the mobility of salt components and, hence, prevents their separate crystallization during solvent evaporation. In spite of the rather complex chemical processes occurring during the synthesis [17], the Pechini method is simple and useful for laboratory applications. Usually, citric acid and ethylene glycol are added to the aqueous solution of nitrates of the cations, taken in a ratio corresponding to their proportion in the final oxide material. Evaporation of the solvent by slow heating is accompanied by the formation of a wet gel. Thermal decomposition of this gel followed by heat treatment at an elevated temperature results in the formation of the final ultradisperse, often nanocrystalline, oxide powder. One of the main disadvantages of this method is the poor reproducibility of the ignition procedure, which often occurs non-uniformly in various parts of the gel-like precursors [18].

Another solution-based method for material synthesis is based on the freeze-drying of frozen aqueous solutions of components, followed by thermal decomposition of freeze-dried precursors [10]. The nitrates of a number of cations that are readily available and easily soluble in water are also used in this method. However, freezing of the nitrate solutions of transition metals and rare earth elements or their soluble complex compounds is accompanied by their vitrification [12]. Freeze-

drying of these species often occurs at temperatures exceeding their glass transition temperature, T_g, which results in their devitrification and the so-called collapse of drying products, leading to a sticky viscous mass that is not useful for further processing.

A combination of these two different approaches, namely the Pechini method and freeze-drying of aqueous solutions, results in the "cryogenic polymer-gel synthesis" method [18–26]. This method consists of three independent steps: (1) gel formation, (2) freezing and freeze-drying, and (3) heat treatment, i.e., calcination. The procedure for preparation of the starting solution in this technique resembles that of the Pechini method. Along with the traditional components such as nitrate salts, citric acid, and ethylene glycol [19, 20], acetates can also be used instead of nitrates [21, 22], and EDTA instead of citric acid as a complexing agent [18]. The most variable component reported in the literature is the gel-forming agent. In addition to the polycondensation products of ethylene glycol and citric acid, several other soluble or gel-forming polymers or components can also be used, such as the triblock copolymer P-123 [23], silane modified propylene glycol [21], agarose, gelatin, poly(vinyl alcohol) [22], and even soluble starch [24, 25].

According to the cryogenic polymer-gel synthesis method, the gels formed at the first stage are frozen and freeze-dried, during which the 3D network formed by the soluble polymers remains intact. As a consequence, glassy mixed solutions of metal complexes or salts are allocated within the mesh of the gel network so that they cannot join to each other, even during drying at $T > T_g$. The freeze-drying product remains solid, irrespective of salt compositions, thus making it more suitable for subsequent powder processing. The thermal decomposition of freeze-dried cryogels containing significant amounts of organics is accompanied by internal redox reactions and significant reduction of the formal phase formation temperature. This flash-like thermal decomposition is useful for the synthesis of kinetically complicated compounds like higher members of homological series. In this case, the easily formed binary intermediates and the first members of homological series do not lose their reactivity, as often occurs during the slow heating of precursors. In contrast to Pechini-like precursors, thermal decomposition of freeze-dried cryogels occurs more uniformly, thus promoting a better chemical and morphological homogeneity of thermolysis products. The large difference in the specific molar volumes of the precursor and decomposition product leads to a significant decrease in grain size during thermal decomposition, as grain growth is limited by a short time and reduced temperature of the heat treatment during thermolysis. Both these factors make this method rather attractive for the synthesis of ultrafine and nanocrystalline powders of individual oxides, their solid solutions, and complex oxide compounds.

As an example of this type of material synthesis, Fig. 1a shows a field emission SEM (FESEM) image of a Co_3O_4 cryogel, synthesized using citric acid and P-123 as complexing and gel-forming agents, respectively [23]. The macroporous structure of Co_3O_4 consists of interconnected spheres of around 200 nm in diameter, as also seen from the TEM image of the same sample in Fig. 1b. Each sphere forming the internal structure is an assembly of many nanocrystals with a diameter of around 10 nm, introducing a mesoporous structure within the macroporous Co_3O_4 [23].
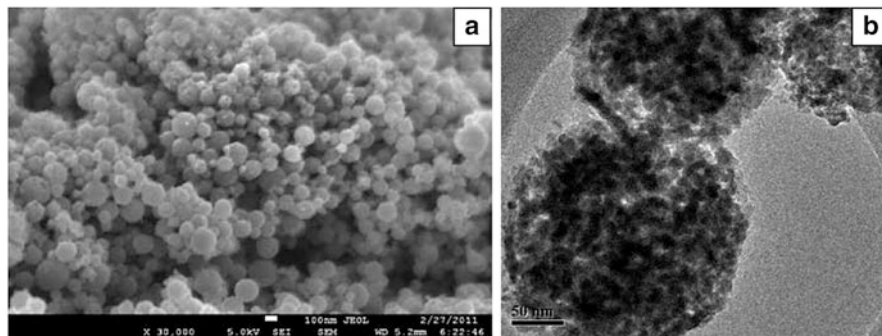
Fig. 1 (**a**) FESEM and (**b**) TEM images of sintered Co_3O_4 cryogel samples. Reprinted from [23] with permission from the American Chemical Society

2.2 *Precipitated and Co-precipitated Cryogels*

Another method for the preparation of multicomponent oxide materials via cryogels is the co-precipitation process. In this process, multicomponent aqueous solutions containing cations in the stoichiometric ratio required for the final material are mixed with a solution of precipitant. This results in intense simultaneous precipitation of the poorly soluble compounds, i.e., hydroxides, carbonates, or oxalates of target cations. Due to the small but different solubility of the precipitates formed by different cations, as well as due to the different rates of their precipitation from solution, the first and the last portions of the precipitate are enriched by different components. Although this nano-inhomogeneity was postulated a long time ago, modern experimental methods like high resolution electron microscopy have recently allowed the observation of this difference experimentally [26]. The products of co-precipitation are used mostly as precursors for the synthesis of complex oxides by means of thermal decomposition. According to numerous experimental results, the chemical inhomogeneity of the co-precipitation products at the nanolevel is almost negligible for solid state reactions at elevated temperatures. From a practical point of view, multicomponent cryogels are excellent precursors for the synthesis of multicomponent oxide compounds.

Another essential feature of cryogel precursors is their low level of particle agglomeration. Common atmospheric drying, especially at elevated temperatures, usually results in the formation of undesirable interparticle bridges and formation of dense and strong agglomerates that are retained in the course of further thermal processing. Capillary effects during the removal of liquid water at atmospheric pressure cause a substantial densification of the residue and a significant reduction in the mean distance between separate particles due to elimination of largest pores. Smaller distances between particles promote better grain growth during thermal processing of precursors and as-obtained oxide powders.

Both agglomeration and grain growth are undesirable for a number of applications of ultradisperse oxide powders obtained from co-precipitated precursors. These problems can be solved by freezing of as-obtained residues followed by freeze-drying. Removal of ice at low temperatures and reduced pressures hinders the interparticle bridging process almost completely. Taking into account that precipitation/co-precipitation results in the formation of nanosized residue particles able to retain their size during further processing, cryogel synthesis is a useful preparation method for multicomponent nanomaterials [26–63].

In the case of oxide solid solutions [28–31] or complex oxide formation [26, 32–39], a high chemical homogeneity of the precursor promotes fast and uniform formation of the target product during its thermal processing. However, even in the case of non-reacting components, it was shown that cryogel synthesis is useful for the synthesis of nanocomposites [27, 40–54]. It is also possible to synthesize core–shell oxide particles by this method when precipitation of the components is performed not simultaneously, but sequentially [55].

All these features are also attractive for the synthesis of solid-state catalysts for various reactions in the gas and liquid state. The low thermal stability of silver and noble metal oxides allows one to obtain the metal catalyst with oxide promoter and/or support in a single synthesis. In this case, the starting gel contains hydroxides of both components. Thermal processing of freeze-dried multicomponent cryogels at 600–1,300° C causes the decomposition of Al hydroxides to oxides, whereas the corresponding compounds of Ag [40–42], Pt, and Pd [43–45] are decomposed to metals. The introduction of a carbon support into the starting multicomponent solution, followed by liquid phase reduction by $NaBH_4$ or ethylene glycol and, finally, freezing and freeze-drying produces PtNi and PtRh catalysts without additional heat treatment (Fig. 2) [27, 46, 47]. Similar methods can be used for the preparation of free-standing PtAu nanoparticle catalyst [48] and well-dispersed water-soluble CdTe quantum dots in montmorillonite clay host media [54].

Variation of the thermal processing conditions allows modification of the micromorphology of the particles thus formed, and ensures the maximum sinterability of oxide powders in order to obtain dense functional ceramics at the lowest possible temperatures [56, 57]. The absence of hard agglomerates in the starting powder is crucial for the production of optically transparent, fully dense ceramics [33] that can be used as the active body of solid state lasers instead of single crystals [58–60]. The products of cryogel synthesis can also be used as templates in topochemical reactions with easy melting components. When the reaction of complex oxide formation is limited by diffusion of the mobile component into the precursor particles, the size and the shape of the complex oxide particles can be controlled by directed modification of the particles of cryogel precursor [61–63].

Similar approaches and methods have been applied to single component cryogels. As the chemical homogeneity of the cryogel is not critical in this case, the main reason to use cryogel precursors is to protect their unique micromorphology during drying. In most cases, the cryogel precursors are used to obtain various oxide nanoparticles, e.g., Co_3O_4 [23], CeO_2 [64], V_2O_5 [65], and ZrO_2 [66]. Cryogels of silica are widely used as sorbents or cryogenic thermal insulators
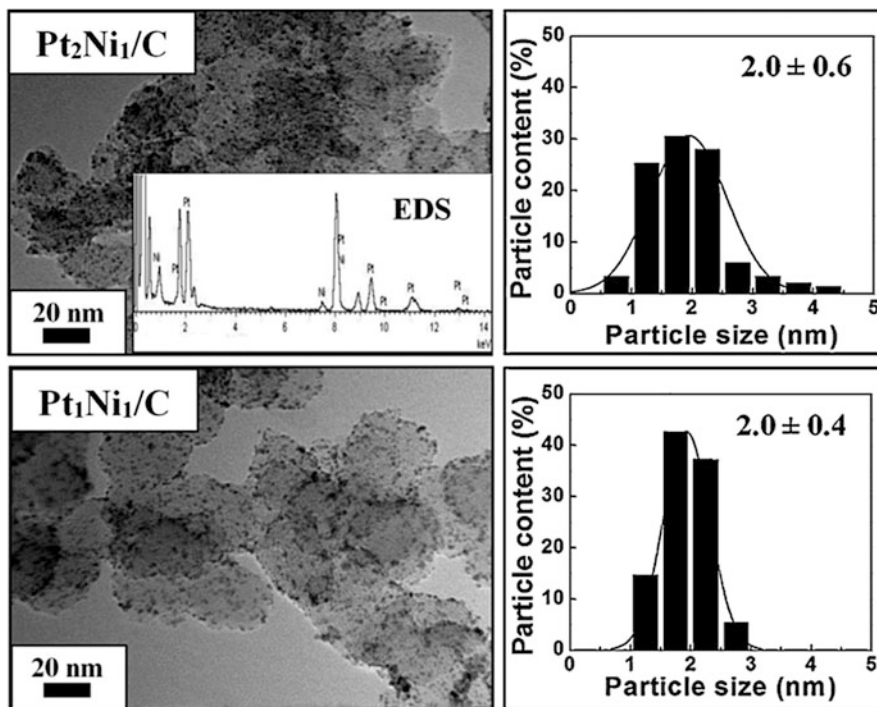
Fig. 2 TEM images of two carbon-supported PtNi catalysts with different Pt:Ni ratios (*left*) and particle-size distributions for the metal nanoparticles (*right*). *Inset* shows energy-dispersive X-ray spectroscopy (*EDS*) spectrum for the Pt_2Ni_1/C catalyst. (From [27] with permission from Elsevier)

thermal insulators [15, 67–77]. In this case, the most important morphological feature of silica gels protected during drying is their extended mesoporosity. Due to the enhanced thermal stability of their architecture, cryogel-derived Al_2O_3 nanopowders can be used as excellent catalyst supports for high temperature chemical reactions [75, 76].

The growing importance of photovoltaic applications has attracted attention to TiO_2 cryogels. Along with TiO_2 hydrogels prepared by the hydrolysis of $TiCl_4$, titanium butoxides, and propoxides [77, 78], titania nanoparticles can also be obtained by acid leaching of $BaTiO_3$ [79, 80]. Careful selection of leaching conditions allows preparation of TiO_2 anatase or rutile polymorphs. Moreover, the relatively high density of TiO_2 nanoparticles, which complicates their application in E-ink displays, can be reduced by the cryogel synthesis of hollow TiO_2 nanospheres [78]. For this purpose, hydrated TiO_2 is precipitated on the surface of poly(methyl methacrylate) or poly(butyl acrylate) spheres and, after freeze-drying, the polymer core is removed by firing. Figure 3 shows SEM images of such TiO_2 hollow spheres prepared by oven- and freeze-drying [78]. Many broken spheres appear after oven drying but the cryogel synthesis method significantly reduces the number of damaged spheres.
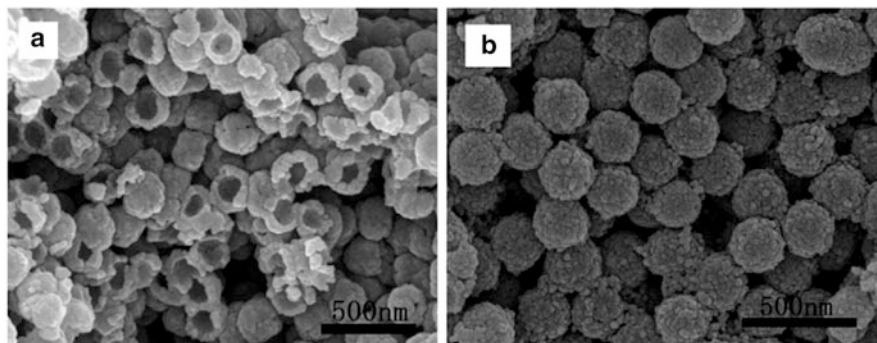
Fig. 3 SEM images of TiO$_2$ hollow spheres by (**a**) oven-drying and (**b**) freeze-drying. (From [78] with permission from Elsevier)

Due to the excellent biocompatibility of calcium phosphate, its application as a particulate cryogel has attracted interest for creating biocompatible substrates for drug delivery and encapsulation of biomolecules [81]. Hydroxyapatite is one of the best materials for the production of biocompatible ceramics. Prevention of hard agglomerate formation during drying significantly enhances its sinterability and, thus, the high morphological homogeneity of these powders permits reduction of the sintering temperature [82]. Cryogel-derived microspheres of YPO$_4$ after the conversion of stable [89]Y to β-emitter ^{90}Y by neutron irradiation become an efficient instrument of local intra-arterial radiotherapy [83].

Synthesis of gold cryogels is similar to the corresponding procedure for supported catalysts described above, and involves reduction of HAuCl$_4$ by NaBH$_4$ solution followed by separation and freeze-drying of the obtained gold particles. Despite significant catalytic activity of the nanocrystalline gold, recent studies on these cryogels also show their plasmonic properties. Here, an important option of the cryogel method is the possibility of functionalization of nanoparticles in the course of their synthesis. The dried gold particles demonstrate a good re-dispersibility and retain their plasmonic properties [84, 85]. The application of 2-[4-(2-hydroxyethyl)-1-piperazinyl]ethanesulfonic acid (HEPES) as both template and reducing agent instead of borohydride leads to branched gold nanocrystals [86].

2.3 Cryogels for Particle Isolation

One of the basic methods for investigation of chemical reactions is the analysis of reaction intermediates by various physico-chemical methods. The best method for such studies is analysis in situ, in real time, and in the real reaction environment. However, in many cases, analysis in situ is complicated by the limitations of analysis methods, e.g., the time of sample study may exceed the reaction time. In order to overcome these limitations, a series of reaction intermediates should be

isolated and preserved for further detailed study ex situ. In the case of solid state reactions, usually performed at elevated temperatures, the isolation of intermediates is mainly performed by quenching, i.e., fast cooling of the reaction mixture to the temperature of reaction termination. In the case of precipitation reactions in aqueous solutions, similar quenching can be performed by fast cooling of the reaction medium to liquid nitrogen temperature. Elimination of frozen solvent by freeze-drying thus allows further investigation of reaction intermediates by various solid state analysis methods. It was shown that this approach is useful in the study of the formation and transformation of nanoparticles in aqueous solutions, such as TiO_2 [87, 88], ZrO_2 [89], ZnO [90], and calcium phosphate and its derivatives [91, 92].

Hydrothermal processing of aqueous solutions is an efficient and widely used preparation method for nanocrystalline individual and complex oxides. An essential feature of this method is the high level of crystallographic ordering in the resulting nanopowders. Although the applications of oxide nanoparticles mainly demand crystallographically ordered species, many other chemical synthesis methods for such nanoparticles often result in amorphous or poorly crystalline products. Thermal processing of amorphous powders at elevated temperatures in order to enhance their crystallinity is usually accompanied by significant agglomeration and grain growth of nanocrystallites. Similar problems also exist in hydrothermal processing during isolation of the nanocrystalline reaction products from the liquid reaction medium. The high surface energy of these powders results in their significant aggregation and agglomeration. Therefore, freezing and subsequent freeze-drying are often applied as a final stage of the hydrothermal synthesis process to prevent aggregation and agglomeration [93–101].

Another important example of a successful application of cryogenic approaches to particle isolation concerns the separation of magnetic nanoparticles. Magnetic properties of ferri- and ferromagnetic particles in the nanosize range depend essentially on their size. The magnetization behavior of superparamagnetic, small single-domain, and multidomain particles is substantially different. However, the transition from superparamagnetic particle rotation to the domain wall movement mechanism can occur during grain growth within a 100 nm size range. This difference in magnetic behavior is essential for the biomedical applications of magnetic nanoparticles and, therefore, has attracted growing attention during the last few years. The influence of particle size on the magnetization behavior of nanoparticles has an important role in their agglomeration processes. Depending on the character and extent of the interparticle contact, the closely located magnetic particles could demonstrate individual, mutually independent, or cooperative magnetic behavior. These particles are often produced and stored in aqueous or nonaqueous suspensions but their detailed studies can only be carried out in the solid state. Taking into account these features, isolation of magnetic particles by freezing and freeze-drying of suspensions and magnetic liquids is widely used in sample preparation for magnetic studies of such particles [102–108], as well as for the investigation of other kinds of suspension-derived ultrafine solids [109, 110]. In the case of hydrophobic particles and, hence, nonaqueous suspension media, the continuous phase can be first substituted with another solvent having a moderate

freezing point and a reasonable vapor pressure at this temperature [111], and then frozen and freeze-dried [112].

Along with research-oriented isolation of nanoparticles, cryogel processing can be an efficient powder-processing method for industrial and other large-scale applications. The increasing use of nanopowders in industry creates growing problems, first of all due to the contamination of production facilities and the environment by the tiny, often harmful particles. This problem is especially important for the nuclear industry, with its traditionally severe demands for industrial safety. The processing risks of fine powders can be substantially reduced by their granulation. Formation of micro- or millimeter-sized granules by spraying binder-containing suspension into liquid nitrogen, freeze-drying, and thermal processing of the product allows substantial reduction of dust formation [113]. Another positive effect of granulation is the better flowability of granulated powders [114, 115]. Nanopowders usually exhibit enhanced adherence to the processing surfaces and poor flowability due to the large internal friction caused by the enhanced contact surface of nanopowders. The latter effect is especially important during the production of dense ceramics from nanopowders because the internal friction effects often cause significant internal stresses during the compaction of these powders before sintering. Application of freeze-granulation is an efficient method of solving this problem too [116, 117].

We have to note that the freeze-drying method may, in some cases, negatively affect the product properties. For instance, it was shown that nanocrystalline zeolite powder located in a mesoporous zeolite support by means of wet impregnation followed by atmospheric drying exhibits significant catalytic activity in the reaction of toluene dispropoportionation, whereas the activity of a similar composite obtained by freeze-drying of the same precursors was much lower [118]. This difference can be attributed to the additional mesoporosity created during atmospheric drying due to the aggregation and agglomeration of zeolite nanoparticles. As mentioned before, the cryogel method ensures the fixation and isolation of individual particles during the drying stage, thus excluding, in the present case, the positive effect of particle aggregation.

2.4   Cryogel-Derived Bulk Materials

One of the most efficient applications of cryogenic processing in the production of ceramic materials is the freeze casting process. Common industrial methods to ensure the uniform filling of the mold by ceramic powder during the production of complex-shaped ceramics are based on the preparation of aqueous slurry containing a large amount of polymeric additives. Elimination of these additives during the subsequent thermal processing causes significant internal stresses in the ceramic and promotes cracking. Application of polymeric cryogels provides a feasible alternative to this traditional method. Thus, low temperature sol–gel transition in the polymer solution during freezing of the mold, followed by thawing or freeze-

drying, produces raw ceramics of high mechanical strength using much lower amounts of polymeric additives [119–124].

Freeze casting can be performed with the application of natural polymeric components like starch or gelatin [119], whereas modern industrial production techniques mostly involve the use of aqueous solutions of polyvinyl alcohol or polyvinyl acetate [125]. Preservation of complex-shaped porous preforms by freeze-drying is used in advanced modern methods for forming complex 3D structures such as nanoimprint lithography [126] and computer-driven layer-by-layer casting (robocasting) [127]. In order to enhance the mechanical strength of the raw cast after thawing, a freeze-gelation can be combined with the photopolymerization of soluble monomers or oligomers introduced into the slurry instead of polymers [128]. Taking into account the large number of pores left after the removal of frozen ice and the significant mechanical strength of raw casts, the freeze casting method can be especially useful in the production of porous ceramics [129]. The micron-sized pores formed due to the ice template are useful for biomedical applications and for the production of biocompatible ceramic materials [130–135].

The number of inorganic systems where low temperature sol–gel transitions are also observed is rather limited. One such system is the aqueous silica sols forming dense cryogels. When $SiO_2.nH_2O$ is introduced into the composition of raw ceramic slurry, the amount of polymeric additives can be reduced significantly or even neglected [50, 89, 136–139]. Modification of the porous structure of SiO_2 cryogels allows the formation of porous materials with a density as low as 0.05 g cm^{-3} and with excellent thermal insulation properties at cryogenic temperatures [15]. The strengthening effect of hydrous alumina and zirconia cryogels is less pronounced. However, if the wall thickness of the ceramic detail is large enough and its shape is not too complex, it is possible to apply freeze casting even in the absence of polymer or hydrous silica. In this case, removal of ice from the frozen mold by sublimation becomes a necessary stage of the production technique [123, 129, 140–147].

Another method of cryogel application in the production of ceramics is generation of tubular aligned pores in raw casts by means of directed crystallization of ice followed by freeze-drying. It was found that freezing of ceramic slurry in a large temperature gradient causes the formation of columnar ice crystals with diameters of 2–3 to 70–80 μm and lengths up to several millimeters. Formation of these crystals causes expulsion of the solid particles of suspension or slurry and their accumulation in the interconnected space between the ice columns. Because the size of solid particles is usually smaller than the diameter of ice crystals, freeze-drying of such samples followed by soft sintering in order to ensure their mechanical strength results in the formation of ceramics with bimodal porosity. Along with large columnar pores in place of oriented ice crystallites, these materials also contain randomly distributed submicron-sized pores or mesopores left by the tiny ice crystals formed between ceramic particles in the column walls [148–151].

Studies on directed crystallization also show that the most important external factor determining the character of ice crystallization and ceramic particle

distribution is the displacement velocity of the interface between the frozen body and the liquid [152–156]. When this velocity is lower than a critical value, ice crystallization causes the expulsion of solid particles in front of ice crystallites. On the other hand, too high a displacement velocity causes the fragmentation of the crystallization interface, loss of the orientation of ice crystals, and disordered distribution of solid particles. The main factor determining this velocity is the temperature gradient. The thickness of the ceramic walls, along with the concentration of slurry, also correlate with the displacement velocity. In order to retain the order and the spatial orientation in this system, the size of ceramic particles should be considerably smaller than the diameter of ice crystals. The lower concentration limit of solid particles in suspension is determined by the demand for mechanical strength of the sample after freeze-drying and is close to 5 mass%. A concentration of solid particles above 55 % usually results in significant interactions between the particles in suspension, causing the formation of lateral bridges between nearest walls and closing the columnar pores.

Taking into account the fact that these features of crystallization process are very similar for different ceramic materials, a number of ceramics with oriented porosity have been obtained recently [146, 157–167]. The bimodal porosity with large longitudinal pores and numerous mesopores in the pore walls is very suitable for catalyst supports for gas phase reactions. Large oriented pores ensure rapid transport of gaseous reagents, while the mesopores in the pore walls are an ideal location for catalyst nanoparticles in order to ensure their maximum exposure to reagents [168–171]. Similarly to the cryogel synthesis of individual particles, the directed crystallization method also produces metal catalysts on oxide supports in the same synthesis run [172, 173].

The porosity features of ceramic materials prepared by directed ice crystallization are also useful for the development of biomaterials. Since the size of the pores can be varied by changing the crystallization conditions, the materials are suitable for the synthesis of ceramic scaffolds. The oriented character of the porosity leads to an anisotropy in the mechanical properties of such ceramics that is similar to the anisotropy of natural bones [132, 174–178]. The most significant progress in this direction was achieved by the development of hydroxyapatite (HAP) ceramics with a compression strength close to that of natural bone [179], and also by the development of tough Al_2O_3-PMMA layered nacre-like composites [180].

3   Carbon Cryogels and Related Materials

3.1   Polymer-Derived Cryogels

The most common synthesis technique for carbon cryogels from polymer precursors is based on their thermal processing in a non-oxidizing atmosphere, usually argon or nitrogen, at 800–1,000 °C. The polymer precursor is mainly synthesized by
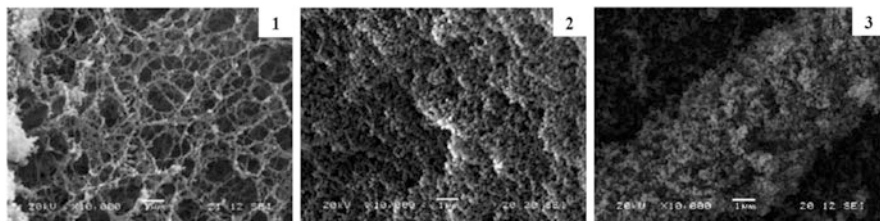
Fig. 4 SEM images of resorcinol-formaldehyde cryogel, aerogel, and xerogel obtained by (**a**) freeze-drying, (**b**) critical extraction with liquid carbon dioxide, and (**c**) heating in an inert atmosphere, respectively. (From [185] with permission from Elsevier)

the polycondensation of resorcinol and formaldehyde in aqueous solutions in the presence of a basic catalyst, usually Na_2CO_3. Further processing of as-obtained polymer hydrogel by freezing and freeze-drying results in the formation of a polymer precursor with micron-sized pores formed by ice crystallization. Thermal processing of the precursor at elevated temperatures results in, along with the carbonization of polymer, the formation of a number of mesopores in the walls of larger pores. The essentially bimodal character of the porosity makes this material similar to metal oxide cryogels [181–185].

It was shown that the method of drying of resorcinol-formaldehyde (RF) gels influences the morphology of the resulting networks as well as their carbonized derivatives [185]. Figure 4 shows SEM images of RF cryogel, aerogel, and xerogel obtained by freeze-drying, critical extraction with liquid carbon dioxide, and heating in an inert atmosphere, respectively. RF-derived carbon xerogel has the most compact structure with the lowest specific surface area (<900 m^2 g^{-1}). The corresponding carbon aerogel exhibits an intermediate value for the surface area (ca. 1,000 m^2 g^{-1}), while the carbon cryogel has the highest surface area ($>2,500$ m^2 g^{-1}) [185]. The micromorphology of carbon cryogels can be varied by changing the ratio of the components and by the conditions of polycondensation as well as by the freezing and thermal processing conditions. By careful selection of these parameters, one may obtain carbon cryogels with a specific surface area of up to 2,000 m^2 g^{-1} [186]. In recent years, considerable efforts have been made in the search for inexpensive and environmentally friendly precursors for the preparation of carbon cryogels, including natural substances like tannin [187–191].

Most of the applications of polymer-derived carbon cryogels are based on their high specific surface area. These materials can be used as an efficient catalyst support in a non-oxidizing environment [192–196] or as sorbent for a number of organic species [186, 197–199]. A combination of high specific surface area with good electronic conductivity makes carbon cryogels a promising electrode material for electric double-layer supercapacitors [200–206]. The application of furaldehyde instead of formaldehyde in the polycondensation reaction provides modification of the carbon surface by nitrogen-containing groups [203, 204]. This modification leads to a significant improvement in capacitance of the N-modified carbon electrode due to the better wetting of the carbon surface by electrolyte and additional electrochemical processes on the electrode surface.

Carbon cryogels exhibiting low density, good electronic conductivity, and significant flexibility are also very useful for the development of composite anodes for lithium-ion batteries, because the electrochemically active components of the batteries often suffer from significant volume expansion and related integrity loss during electrochemical cycling [207, 208]. The mechanical strength of carbon cryogels is often insufficient for a number of applications. This problem can be solved by the reinforcement of cryogels using ultradisperse particles and fibers of other substances that can be introduced at the early stages of polymer precursor synthesis [206, 209, 210]. A similar approach can be used for modification of the sorption properties of carbon cryogels by creating a composite with zeolites [211], while the electronic conductivity can be further enhanced by the introduction of graphene colloid into the starting mixture for RF polycondensation [212].

3.2 Carbon-Based Particulate Materials

Cryogenic processing of carbon-based nanomaterials appeared during the last two decades is similar to the processing of their oxide counterparts. The two main tasks solved by freezing and freeze-drying of carbon-containing suspensions are the isolation of nanoparticles from the dispersion medium and the directed formation of 2D and 3D structures from these particles. In the preparation of carbon-based nanomaterials, since supercritical drying is applied more frequently than freeze-drying, the products of freeze-drying are also often called "aerogels."

Taking into account the fact that, in many studies, single-layer graphene nanosheets have not been isolated and investigated, it is more reasonable to call them "graphene materials" [213]. Graphene-based cryogels have been prepared by the reduction of exfoliated graphite oxide [214–217] by templated chemical vapor deposition (CVD)-based synthesis from CH_4 on MgO catalyst [218], and by ultrasonic agitation of flake graphite in a specially selected nonpolar solvent [219]. It seems that the latter kind of cryogel is closest to graphene nanomaterials because true graphene consisting of carbon atoms should be hydrophobic [220]. Re-dispersibility of the other cryogel products in water could be realized by the oxidation of their surface. However, some of these cryogel-based materials demonstrate outstanding functional properties, such as a specific surface area of over 2,000 $m^2 \ g^{-1}$, high methane storage capacity [218], high electrochemical capacitance in aqueous alkaline electrolytes [214], and good electrochemical performance as anode material of Li-ion batteries [217].

Increasing application of graphene oxide as a precursor for graphene-based materials has revealed a number of interesting properties of the reduced graphene oxides and the poorly conducting but hydrophilic graphene oxide. First of all, the graphene oxide-based materials (GO) have enhanced sorption activities [221–223] and good catalytic properties [224, 225]. They are usually obtained by the oxidative exfoliation of graphite, while their subsequent reduction results in the synthesis of a number of reduced graphene oxides (RGO) of different C:O ratios. Both GO and

RGO form stable cryogels suitable for unidirectional ice crystallization [173, 221, 223]. As-obtained 3D porous monoliths are good supports for the nanocrystalline gold and silver catalysts [173].

Cryogenic processing is often applied to the preparation of carbon nanotubes (CNT) in their purification stage. These nanoparticles are usually obtained by means of catalytic decomposition of hydrocarbons. The application of CNTs requires separation of metal catalyst by acid dissolution, followed by careful washing of the reaction products. Separation of the different kinds of nanotubes that often grow simultaneously during CVD is also performed in the liquid phase. Air drying of as-obtained CNT suspensions results in significant aggregation of nanotubes, whereas freeze-drying yields re-dispersible, free flowing powders [226–229]. Due to the high mechanical strength of CNTs, the synthesis of solid CNT foams using the same approach results in the formation of stable porous frameworks with variable porosity, especially when a small amount of polymer binder is added [230–233]. Good electrical conductivity of these materials makes them suitable electrode material for proton-exchange membrane fuel cells [230, 233].

Both CNTs and graphene-based particulates are well-known as efficient conductive dopants. Cryogel synthesis of composite electrode materials with these nanocrystalline components causes considerable improvement in the electrochemical performance of Li-ion battery anode materials, which often suffer from insufficient electronic conductivity and the loss of electrical contact between particles [234–237]. Corresponding enhancement of the electrochemical capacitance and rate capability is also observed for supercapacitor electrodes made of "carbon–carbon" composite formed by CNTs and a small amount of reduced graphene oxide [238]. Along with a better electrical conductivity, the introduction of 1 vol% multiwalled CNTs could significantly enhance the fracture toughness of hot-pressed dense alumina ceramics [239]. It is essential in all these cases that the surface of CNTs should be first oxidized in order to ensure good contact with the oxide ceramic matrix. The Vickers microhardness and mechanical wear resistance of copper-based metal matrix composites obtained by spark plasma sintering can also be improved significantly by adding 4 % of double-wall CNTs [240], while the corresponding thermal conductivity values decrease compared with pure copper [241]. Along with doping of other components, the CNTs can also be doped by the cryogel method. In this case, CNTs have been filled with $CdCl_2$ solution under vacuum and carefully washed. Further processing of the freeze-drying product in H_2S environment results in the formation of nanocrystalline H_2S inside the nanotubes [242].

4 Conclusions

The different materials reviewed in this chapter demonstrate several synthetic strategies in which the cryogel method can be successfully applied. Two basic features of cryogel synthesis make this method useful in different situations: the

high chemical homogeneity of the multicomponent precursors, and the easy control of product porosity at macro- and meso-levels. Additional advantages of cryogenic methods in materials synthesis and processing include the availability of industrially produced freeze-drying equipment, which makes it simple and easy to scale up synthetic processes developed at the laboratory scale. In spite of 40 years of history of cryogel synthesis, it remains a modern, useful, and efficient tool for materials scientists and engineers.

References

1. Klvana D, Chaouki J, Repellin-Lacroix M, Pajonk GM (1989) Rev Phys Appl Colloid 4:C4–29
2. Pajonk GM (1989) Rev Phys Appl Colloid 4:C4–13
3. Pajonk GM, Repellin-Lacroix M, Abournadasse S, Chaouki J, Klvana D (1990) J Non-Cryst Solids 121:66
4. Scheurell K, Hoppe E, Brzezinka KW, Kemnitz E (2004) J Mater Chem 14:2560
5. Borlaf M, Poveda JM, Moreno R, Colomer MT (2012) J Sol-Gel Sci Technol 63:408
6. Shu K, Wang C, Wang M, Zhao C, Wallace GC (2014) J Mater Chem A 2:1325
7. Trambouze Y (1969) Ann Bull Inst Intern du Froid 9:13
8. Trambouze Y (1970) Chimie & Industrie Genie Chimique 103:2338
9. Roehrig FK, Wright TR (1972) J Am Ceram Soc 55:58
10. Landsberg A, Campbell TT (1965) J Metals 17:856
11. Wikipedia (2014) Deng_Xiaoping_theory. Wikipedia, The free encyclopedia. Available at http://en.wikipedia.org/wiki/Deng_Xiaoping_Theory
12. Tretyakov YD, Oleynikov NN, Shlyakhtin OA (1997) Cryochemical technology of advanced materials. Chapman Hall, London
13. Tretyakov YD, Shlyakhtin OA (1999) J Mater Chem 9:19
14. Shlyakhtin OA, Oleinikov NN, Tretyakov YD (2005) Cryochemical synthesis of materials. In: Komarneni S, Lee B (eds) Chemical processing of ceramics (2nd edn), vol 28, Materials engineering series. CRC, Boca Raton, p 77
15. Shlyakhtin OA, Oh YJ (2009) J Electroceramics 23:452
16. Rusnano (2011) Pechini method. In: Glossary of nanotechnology and related terms. Available at http://eng.thesaurus.rusnano.com/wiki/article2075
17. Petrykin V, Kakihana M (2005) Chemistry and applications of polymeric gel precursors. In: Sakka S, Kozuka H (eds) Handbook of sol-gel science and technology, vol 1. Kluwer, Dordrecht, p 77
18. Junliang L, Yanwei Z, Cuijing G, Wei Z, Xiaowei Y (2010) J Eur Ceram Soc 30:993
19. Jing Y, Patakangas J, Lund PD, Zhu B (2013) Int J Hydrogen Energy 38:16532
20. Fujioka Y, Frantti J, Asiri AM, Obaid AY, Jiang H, Nieminen RM (2012) J Phys Chem C 116:17029
21. Tezuka S, Sato Y, Komukai T, Takatsuka Y, Kato H, Kakihana M (2013) Appl Phys Express 6:072101
22. Iwamura M, Petrykin V, Kakihana M (2007) J Ceram Soc Japan 115:920
23. Wang X, Sumboja A, Khoo E, Yan C, Lee PS (2012) J Phys Chem C 116:4930
24. Xiao Q, Tang X, Liu Y, Zhong Y, Zhu W (2012) J Am Ceram Soc 95:1544
25. Xiao Q, Tang X, Liu Y, Zhong Y, Zhu W (2013) Front Chem Sci Eng 7:297

26. Wang R, Crozier PA, Sharma R, Adams JB (2006) J Phys Chem B 110:18278
27. Lee S, Kim HJ, Choi SM, Seo MH, Kim WB (2012) Appl Catal A 429–430:39
28. Panova TI, Glushkova VB, Lapshin AE (2008) Glass Phys Chem 34:206
29. Yang H, Nie S (2009) Mater Chem Phys 114:279
30. Kirit S, Dimple S (2012) J Cryst Growth 352:224
31. Vanea E, Simon V (2013) Appl Surf Sci 280:144
32. Naci Koc S, Oksuzomer F, Yasar E, Akturk S, Gurkaynak MA (2006) Mater Res Bull 41:2291
33. Chesnaud A, Bogicevic C, Karolak F, Estournes C, Dezanneau G (2007) Chem Commun 2007(15):1550
34. Mionic M, Alexander DTL, Forro L, Magrez A (2008) Phys Stat Sol 245:1915
35. Moriyama D, Hirata Y, Sameshima S, Matsunaga N, Doi T, Kashima N, Nagaya S (2009) J Ceram Soc Japan 117:635
36. Shiratani K, Hirata Y, Sameshima S, Matsunaga N, Nakahara S (2011) Ceram Intern 37:1525
37. Chao C, Ren Z, Liu Z, Xiao Z, Xu G, Li X, Wei X, Shen G, Han G (2011) Appl Surf Sci 257:9768
38. Shlyakhtin OA, Skundin AM, Yoon SJ, Oh YJ (2009) Mater Lett 63:109
39. Shlyakhtin OA, Mazo GN, Malyshev SA, Kolchina LN, Knot'ko AV, Loktev AS, Dedov AG (2013) Mater Res Bull 48:245
40. Harelind H, Gunnarsson F, Vaghefi SMS, Skoglundh M, Carlsson PA (2012) ACS Catal 2:1615
41. Kannisto H, Arve K, Pingel T, Hellman A, Harelind H, Eranen K, Olsson E, Skoglundh M, Murzin DY (2013) Catal Sci Technol 3:644
42. Gunnarsson F, Zheng JY, Kannisto H, Cid C, Lindholm A, Milh M, Skoglundh M, Harelind H (2013) Top Catal 56:416
43. Kirchhoff M, Specht U, Veser G (2005) Nanotechnology 16:S401
44. Osaki T, Shima S, Miki T, Tai Y (2012) Catal Lett 142:541
45. Osaki T, Yamada K, Watari K, Tajiri K, Shima S, Miki T, Tai Y (2012) Catal Lett 142:95
46. Kim HJ, Choi SM, Nam SH, Seo MH, Kim WB (2009) Catal Today 146:9
47. Kim HJ, Choi SM, Nam SH, Seo MH, Kim WB (2009) Appl Catal A 352:145
48. Choi JH, Park KW, Park IS, Kim K, Lee JS, Sung YE (2006) J Electrochem Soc 153:A1812
49. Jalota S, Bhaduri SB, Cuneyt Tas A (2007) J Biomed Mater Res B 80:304
50. Osaki T, Nagashima K, Watari K, Tajiri K (2007) J Non-Cryst Solids 353:2436
51. Wang X, Ma Y, Li S, Zhu B, Muhammed M (2012) Int J Hydrogen Energy 37:19380
52. Han C, Ma Y, Pei C (2013) J Non-Cryst Solids 369:5
53. Jimeno C, Miras J, Esquena J (2013) Catal Lett 143:616
54. Cao YC (2012) J Colloid Interface Sci 368:139
55. Ko HH, Chen HT, Yen FL, Lu WC, Kuo CW, Wang MC (2012) Int J Mol Sci 13:1658
56. Shlyakhtin OA, Oh YJ (2006) J Am Ceram Soc 89:3366
57. Shlyakhtin OA, Oh YJ (2009) Int J Appl Ceram Technol 6:312
58. Gong H, Tang DY, Huang H (2009) J Am Ceram Soc 92:812
59. Gong H, Zhang J, Tang DY, Xie GQ, Huang H, Ma J (2011) J Nanopart Res 13:3853
60. Suarez M, Fernandez A, Menendez JL, Nygren M, Torrecillas R, Zhao Z (2010) J Eur Ceram Soc 30:1489
61. Shlyakhtin OA, Yoon YS, Choi SH, Oh YJ (2004) Electrochim Acta 50:505
62. Shlyakhtin OA, Choi SH, Yoon YS, Oh YJ (2005) J Power Sources 141:122
63. Jain G, Yang J, Balasubramanian M, Xu JJ (2005) Chem Mater 17:3850
64. Qi L, Fresnais J, Muller P, Theodoly O, Berret JF, Chapel JP (2012) Langmuir 28:11448
65. Li Y, Yao J, Uchaker E, Yang J, Huang Y, Zhang M, Cao G (2013) Adv Energy Mater 3:1171
66. Bianchi CL, Ardizzone S, Cappelletti G (2004) Surf Interface Anal 36:745
67. Hessien M, Lerone P, Suchaud M, LeBeau B, Nouali H, Guari Y, Prouzet E (2012) Chem Commun 48:10022
68. Su LF, Miao L, Tanemura S, Xu G (2012) Sci Technol Adv Mater 13:035003

69. Prokopowicz M (2010) J Sol Gel Sci Technol 53:525
70. Lu P, Hsieh YL (2012) Powder Technol 225:149
71. Hashkovsky SV, Shilova OA, Kuznetsova LA (2005) Glass Phys Chem 31:352
72. Chen R, Luo Y, Sun J, Li G (2012) Propellants Explos Pyrotech 37:422
73. Kuechl DE, Benin AI, Knight LM, Abrevaya H, Wilson ST, Sinkler W, Mezza TM, Willis RR (2010) Micropor Mesopor Mater 127:104
74. Rahman IA, Vejayakumaran P, Sipaut CS, Ismail J, Chee CK (2008) Ceram Intern 34:2059
75. Sinko K (2013) Mater Lett 107:344
76. Osaki T, Yamada K, Watari K, Tajiri K, Shima S, Miki T, Tai Y (2012) J Sol Gel Sci Technol 61:268
77. Fazio S, Guzm'an J, Colomer MT, Salomoni A, Moreno R (2008) J Eur Ceram Soc 28:2171
78. Wang S, Mei Y, Li X, Tan T (2012) Mater Lett 74:1
79. Liu L, Isobe T, Ling H, Okada K, Nakajima A (2011) Mater Res Bull 46:175
80. Yamamoto N, Isobe T, Matsushita S, Nakajima A (2012) J Ceram Soc Japan 120:483
81. Jiang PJ, Wynn-Jones G, Grover LM (2010) J Mater Sci 45:5257
82. Girija EK, Suresh Kumar G, Thamizhavel A, Yokogawa Y, Narayana Kalkura S (2012) Powder Technol 225:190
83. Kawashita M, Matsui N, Li Z, Miyazaki T, Kanetaka H (2011) J Biomed Mater Res B 99:45
84. Khlebtsov BN, Khanadeev VA, Panfilova EV, Pylaev TE, Bibikova OA, Staroverov SA, Bogatyrev VA, Dykman LA, Khlebtsov NG (2013) Nanotech Russia 8:209
85. Khlebtsov BN, Panfilova EV, Terentyuk GS, Maksimova IL, Ivanov AV, Khlebtsov NG (2012) Langmuir 28:8994
86. Xie J, Lee JY, Wang DIC (2007) Chem Mater 19:2823
87. Jung HS, Shin H, Kim JR, Kim JY, Hong KS, Lee JK (2004) Langmuir 20:11732
88. Shin H, Jung HS, Hong KS, Lee JK (2005) J Solid State Chem 178:15
89. Chiavacci LA, Santilli CV, Pulcinelli SH, Bourgaux C, Briois V (2004) Chem Mater 16:3995
90. Kaluza S, Muhler M (2009) Catal Lett 129:287
91. Sanchez-Enriquez J, Reyes-Gasga J (2013) Ultrasonics Sonochem 20:1948
92. Kim S, Ryu HS, Shin H, Jung HS, Hong KS (2005) Mater Chem Phys 91:500
93. Millot N, Xin B, Pighini C, Aymes D (2005) J Eur Ceram Soc 25:2013
94. Kim SJ, Lee K, Kim JH, Lee NH, Kim SJ (2006) Mater Lett 60:364
95. Yang H, Ouyang J, Tang A (2007) J Phys Chem B 111:8006
96. Boldrin P, Hebb AK, Chaudhry AA, Otley L, Thiebaut B, Bishop P, Darr JA (2007) Ind Eng Chem Res 46:4830
97. Nalbandian L, Delimitis A, Zaspalis VT, Deliyanni EA, Bakoyannakis DN, Peleka EN (2008) Micropor Mesopor Mater 114:465
98. Zhang Z, Brown S, Goodall JBM, Weng X, Thompson K, Gonga K, Kellici S, Clark RJH, Evans JRG, Darr JA (2009) J Alloys Compd 476:451
99. Kim SJ, Yun YU, Oh HJ, Hong SH, Roberts CA, Routray K, Wachs IE (2010) J Phys Chem Lett 1:130
100. Szepesi CJ, Cantonnet J, Allen Kimel R, Adair JH (2011) J Am Ceram Soc 94:4200
101. Long Y, Hui J, Wang P, Hu S, Xu B, Xiang G, Zhuang J, Lu X, Wang X (2012) Chem Commun 48:5925
102. Gamarra LF, Brito GES, Pontuschka WM, Amaro E, Parma AHC, Goya GF (2005) J Magn Magn Mater 289:439
103. Frandsen C, Morup S (2006) J Phys Condens Matter 18:7079
104. Arelaro AD, Brandl AL, Lima E, Gamarra LF, Brito GES, Pontuschka WM, Goya GF (2006) J Appl Phys 97:10J316
105. Ludwig F, Heim E, Menzel D, Schilling M (2006) J Appl Phys 99:08P106
106. Ludwig F, Heim E, Schilling M (2007) J Appl Phys 101:113909
107. Ludwig F, Heim E, Schilling M (2009) J Magn Magn Mater 321:1644

108. Schmidl F, Weber P, Koettig T, Buttner M, Prass S, Becker C, Mans M, Heinrich J, Roder M, Wagner K, Berkov DV, Goernert P, Glockl G, Weitschies W, Seidel P (2007) J Magn Magn Mater 311:171

109. Candelario VM, Guiberteau F, Moreno R, Ortiz AL (2013) J Eur Ceram Soc 33:2473

110. Chubilleau C, Lenoir B, Masschelein P, Dauscher A, Candolfi C, Guilmeau E, Godart C (2013) J Mater Sci 48:2761

111. Teagarden DL, Baker DS (2002) Eur J Pharm Sci 15:115

112. Schaefer J, Rasmussen DH, Partch R (2013) Drying Technol 31:856

113. Deqiong Z, Shuming P, Xiaojun C, Xiaoling G, Tongzai Y (2010) J Nucl Mater 396:245

114. Jerndal E, Mattisson T, Lyngfelt A (2009) Energ Fuels 23:665

115. Garcia E, Mesquita-Guimaraes J, Miranzo P, Osendi MI (2011) Surf Coat Technol 205:4304

116. Vicent M, Sanchez E, Molina T, Nieto I, Moreno R (2012) J Eur Ceram Soc 32:1019

117. Olhero SM, Ganesh I, Torres PMC, Alves FJ, Ferreira JMF (2009) J Am Ceram Soc 92:9

118. Mavrodinova V, Popova M, Valchev V, Nickolov R, Minchev C (2005) J Colloid Interface Sci 286:268

119. Yao D, Xia Y, Zeng Y, Zuo K, Jiang D (2012) Mater Lett 68:75

120. Wu H, Li D, Tang Y, Sun B, Xu D (2009) J Mater Proc Technol 18–19:5886

121. Roy S, Wanner A (2008) Compos Sci Technol 68:1136

122. Tallon C, Jach D, Moreno R, Isabel Nieto M, Rokicki G, Szafran M (2009) J Eur Ceram Soc 29:875

123. Zuo KH, Zeng Y, Jiang D (2008) Int J Appl Ceram Technol 5:198

124. Zou J, Zhang Y, Li R (2011) Int J Appl Ceram Technol 8:482

125. Zuo KH, Zeng YP, Jiang D (2013) Adv Eng Mater 15:490

126. Grimm S, Lange A, Enke D, Steinhart M (2012) J Mater Chem 22:9490

127. Schlordt T, Schwanke S, Keppner F, Fey T, Travitzky N, Greil P (2013) J Eur Ceram Soc 33:3243

128. de Hazan Y (2012) J Am Ceram Soc 95:177

129. Ren L, Zeng Y, Jiang D (2009) Ceram Intern 35:1267

130. Depan D, Kumar AP, Singh RP (2009) Acta Biomat 5:93

131. Landi E, Valentini F, Tampieri A (2008) Acta Biomat 4:1620

132. Monmaturapoj N, Soodsawang W, Thepsuwan W (2012) J Porous Mater 19:441

133. Zuo KH, Zhang Y, Zeng YP, Jiang D (2011) Ceram Intern 37:407

134. Sinha A, Guha A (2009) Mater Sci Eng C 29:1330

135. Jiang L, Morelius E, Zhang J, Wolcott M, Holbery J (2008) J Compos Mater 42:2629

136. Jelic TA, Bronic J, Hadzija M, Subotic B, Maric I (2007) Micropor Mesopor Mater 105:65

137. Koch D, Andresen L, Schmedders T, Grathwohl G (2003) J Sol-Gel Sci Technol 26:149

138. Koch D, Soltmann C, Grathwohl G (2007) Key Eng Mater 336–338:1683

139. Ding S, Zeng YP, Jiang D (2007) J Am Ceram Soc 90:2276

140. Moritz T, Richter HJ (2006) J Am Ceram Soc 89:2394

141. Moritz T, Richter HJ (2007) J Eur Ceram Soc 27:4595

142. Lu K, Kessler CS, Davis RM (2006) J Am Ceram Soc 89:2459

143. Lu K (2007) J Am Ceram Soc 90:3753

144. Cho YK, Yang TY, Lee JM, Yoon SY, Stevens R, Park HC (2008) J Phys Chem Solids 69:1525

145. Gannon P, Sofie S, Deibert M, Smith R, Gorokhovsky V (2009) J Appl Electrochem 39:497

146. Zhang R, Fang D, Pei Y, Zhou L (2012) Ceram Intern 38:4373

147. Hu L, Zhang Y, Zhan S, Zhou Y (2012) Mater Lett 82:152

148. Mukai SR, Nishihara H, Tamon H (2003) Micropor Mesopor Mater 63:43

149. Mukai SR, Nishihara H, Tamon H (2004) Chem Commun 2004(7):874

150. Nishihara H, Mukai SR, Yamashita D, Tamon H (2005) Chem Mater 17:683

151. Zhang H, Cooper AI (2007) Adv Mater 19:1529

152. Deville S (2008) Adv Eng Mater 10:155

153. Deville S, Maire E, Bernard-Granger G, Lasalle A, Bogner A, Gauthier C, Leloup J, Guizard C (2009) Nat Mater 9:966
154. Munch E, Saiz E, Tomsia AP, Deville S (2009) J Am Ceram Soc 92:1534
155. Deville S, Maire E, Bernard-Granger G, Lasalle A, Bogner A, Gauthier C, Leloup J, Guizard C (2010) J Am Ceram Soc 93:2507
156. Lasalle A, Guizard C, Deville S, Rossignol F, Carles P (2011) J Am Ceram Soc 94:244
157. Olevsky EA, Wang X, Bruce E, Stern MB, Wildhack S, Aldinger F (2007) Scripta Mater 56:867
158. Lee SH, Jun SH, Kim HE, Koh YH (2008) J Am Ceram Soc 91:1912
159. Mukai SR, Nishihara H, Tamon H (2008) Micropor Mesopor Mater 116:166
160. Nishihara H, Iwamura S, Kyotani T (2008) J Mater Chem 18:3662
161. Chino Y, Dunand DC (2008) Acta Mater 56:105
162. Fukushima M, Nakata M, Zhou Y, Ohji T, Yoshizawa Y (2010) J Eur Ceram Soc 14:2889
163. Nishihara H, Mukai SR, Shichi S, Tamon H (2010) Mater Lett 64:959
164. Mukai SR, Onodera K, Yamada I (2011) Adsorption 17:49
165. Oh S, Chang S, Suk M (2012) Trans Nonferrous Met Soc China 22:s688
166. Fukushima M (2013) J Ceram Soc Japan 121:182
167. Tamon H, Akatsuka T, Mori H, Sano N (2013) Chem Eng Trans 32:2059
168. Khaleghi E, Olevsky E, Meyers M (2009) J Am Ceram Soc 92:1487
169. Yoon HJ, Kim UC, Kim JH, Koh YH (2010) J Am Ceram Soc 93:1580
170. Zheng J, Salamon D, Lefferts L, Wessling M, Winnubst L (2010) Micropor Mesopor Mater 134:216
171. Hu L, Wang C, Huang Y, Sun C, Lu S, Hu Z (2010) J Eur Ceram Soc 30:3389
172. Deng ZY, Fernandes HR, Ventura JM, Kannan S, Ferreira JMF (2007) J Am Ceram Soc 90:1265
173. He Y, Zhang N, Gong Q, Li Z, Gao J, Xiu H (2012) Mater Chem Phys 134:585
174. Fu Q, Rahaman MN, Dogan F, Sonny Bal B (2008) J Biomed Mater Res B 86:125
175. Fu Q, Rahaman MN, Dogan F, Sonny Bal B (2008) J Biomed Mater Res B 86:514
176. Fu Q, Rahaman MN, Dogan F, Sonny Bal B (2008) Biomed Mater 3:025005
177. Rahaman MN, Fu Q (2008) J Am Ceram Soc 91:4137
178. Zuo KH, Zeng Y, Jiang D (2010) Mater Design 31:3090
179. Deville S, Saiz E, Nalla RK, Tomsia AP (2006) Science 311:515
180. Munch E, Launey ME, Alsem DH, Saiz E, Tomsia AP, Ritchie RO (2008) Science 322:1516
181. Tamon H, Ishizaka H (1999) Drying Technol 17:1653
182. Tamon H, Ishizaka H, Yamamoto T, Suzuki T (1999) Carbon 37:2049
183. Tamon H, Ishizaka H, Yamamoto T, Suzuki T (2000) Carbon 38:1099
184. Szczurek A, Amaral-Labat G, Fierro V, Pizzi A, Celzard A (2011) Sci Technol Adv Mater 12:035001
185. Czakkel O, Marthi K, Geissler E, Laszlo K (2005) Micropor Mesopor Mater 86:124
186. Feaver A, Cao G (2006) Carbon 44:590
187. Alvares Rodrigues L, Parmentier J, Parra JB, Thim GP (2013) J Sol Gel Sci Technol 67:519
188. Kraiwattanawong K, Mukai SR, Tamon H, Lothongkum AW (2007) Micropor Mesopor Mater 98:258
189. Kraiwattanawong K, Mukai SR, Tamon H, Lothongkum AW (2008) J Porous Mater 15:695
190. Kraiwattanawong K, Mukai SR, Tamon H, Lothongkum AW (2008) Micropor Mesopor Mater 115:432
191. Amaral-Labat G, Szczurek A, Fierro V, Stein N, Boulanger C, Pizzi A, Celzard A (2012) Biomass Bioenerg 39:274
192. Arbizzani C, Beninati S, Manferrari E, Soavi F, Mastragostino M (2006) J Power Sources 161:826
193. Arbizzani C, Beninati S, Soavi F, Varzi A, Mastragostino M (2008) J Power Sources 185:615
194. Babic VM, Vracar LM, Radmilovic V, Krstajic NV (2006) Electrochim Acta 51:3820

195. Elezovic NR, Babic BM, Krstajic NV, Gajic-Krstajic LM, Vracar LM (2007) Int J Hydrogen Energ 32:1991
196. Babic VM, Kaluderovic BV, Vracar LM, Radmilovic V, Krstajic NV (2007) J Serb Chem Soc 72:773
197. Horikawa T, Sekida T, Hayashi J, Katoh M, Do DD (2011) Carbon 49:416
198. Yamamoto T, Kataoka S, Ohmori T (2010) J Hazard Mater 177:331
199. Kim SI, Yamamoto T, Endo A, Ohmori T, Nakaiwa M (2006) Micropor Mesopor Mater 96:191
200. Garcia BB, Feaver AM, Zhang Q, Champion RD, Cao G, Fister TT, Nagle KP, Seidler GT (2008) J Appl Phys 104:014305
201. Garcia BB, Candelaria SL, Liu D, Sepheri S, Cruz JA, Cao G (2011) Renew Energ 36:1788
202. Arbizzani C, Beninati S, Lazzari M, Soavi F, Mastragostino M (2007) J Power Sources 174:648
203. Candelaria SL, Garcia BB, Liu D, Cao G (2012) J Mater Chem 22:9884
204. Candelaria SL, Chen R, Jeong YH, Cao G (2012) Energy Environ Sci 5:5619
205. Song MS, Nahm S, Oh YJ (2008) J Kor Ceram Soc 45:662
206. Kraiwattanawong K, Sano N, Tamon H (2013) Micropor Mesopor Mater 165:228
207. Pan A, Liu D, Zhou X, Garcia BB, Liang S, Liu J, Cao G (2010) J Power Sources 195:3893
208. Zhang M, Li Y, Uchaker E, Candelaria S, Shen L, Wang T, Cao G (2013) Nano Energ 2:769
209. Kraiwattanawong K, Sano N, Tamon H (2011) Carbon 49:3404
210. Kraiwattanawong K, Sano N, Tamon H (2012) Micropor Mesopor Mater 153:47
211. Babic B, Kokunesoski M, Miljkovic M, Prekajski M, Matovic B, Gulicovski J, Bucevac D (2012) Ceram Int 38:4875
212. Markovic ZM, Babic BM, Dramicanin MD, Holclajtner Antunovic ID, Pavlovic VB, Perusko DB, Todorovic Markovic BM (2012) Synth Metals 162:743
213. Editorial (2013) Carbon 65:1
214. Zhang X, Sui Z, Xu B, Yue S, Luo Y, Zhan W, Liu B (2011) J Mater Chem 21:6494
215. Wu T, Chen M, Zhang L, Xu X, Liu Y, Yan J, Wang W, Gao J (2013) J Mater Chem A 1:7612
216. Cao Y, Feng J, Wu P (2010) Carbon 48:3834
217. Yang XW, He YS, Liao XZ, Ma ZF (2011) Acta Phys Chim Sinica 27:2583
218. Ning G, Xu C, Mu L, Chen G, Wang G, Gao J, Fan Z, Qian W, Wei F (2012) Chem Commun 48:6815
219. Oyer AJ, Carillo JMY, Hire CC, Schniepp HC, Asandei AD, Dobrynin AV, Adamson DH (2012) J Am Chem Soc 134:5018
220. Leenaerts O, Partoens E, Peeters FM (2009) Phys Rev B 79:235440
221. Mi X, Huang G, Xie W, Wang W, Liu Y, Gao J (2012) Carbon 50:4856
222. He Y, Zhang N, Wu F, Xu F, Liu Y, Gao J (2013) Mater Res Bull 48:3553
223. Ma J, Wang X, Liu Y, Wu T, Liu Y, Guo Y, Li R, Sun X, Wu F, Li C, Gao J (2013) J Mater Chem A 1:2192
224. Dhakshinamoorthy A, Alvaro M, Concepcion P, Fornes V, Garcia H (2012) Chem Commun 48:5443
225. He Y, Zhang N, Long Y, Sun H, Qiu H, Gao J (2012) Adv Mater Res 430–432:488
226. Maugey M, Neri W, Zakri C, Derre Penicaud A, Noe L, Chorro M, Launois P, Monthioux M, Poulin P (2007) J Nanosci Nanotechnol 7:2633
227. Kim TH, Doe C, Kline SR, Choi SM (2007) Adv Mater 19:929
228. Meng Z, Wu D, Wang L, Zhu H, Li Q (2012) Particuology 10:614
229. Taquahashi Y, Ogawa Y, Takagi A, Tsuji M, Morita K, Kanno J (2013) J Toxicol Sci 38:619
230. Yun YS, Bak H, Jin HJ (2010) Synth Metals 160:561
231. Nakagawa K, Thongprachan N, Charinpanitkul T, Tanthapanichakoon W (2010) Chem Eng Sci 65:1438
232. Nakagawa K, Yasumura Y, Thongprachan N, Noriaki Sano N (2011) Chem Eng Proc Proc Intens 50:22

233. Bryning MB, Milkie DE, Islam MF, Hough LA, Kikkawa JM, Yodh AG (2007) Adv Mater 19:661
234. Liang L, Liu H, Yang W (2013) J Alloys Compd 559:167
235. Zhou X, Yin YX, Wan LJ, Guo YG (2012) Chem Commun 48:2198
236. Xin X, Yao X, Zhang Y, Liu Z, Xu X (2012) J Solid State Electrochem 16:2733
237. Jiang X, Yang X, Zhu Y, Shen J, Fan K, Li C (2013) J Power Sources 237:178
238. You B, Wang L, Yao L, Yang J (2013) Chem Commun 49:5016
239. Michálek M, Sedláček J, Parchoviansky M, Michálková M, Galusek D (2014) Ceram Intern 40:1289
240. Guiderdoni C, Estournes C, Peigney A, Weibel A, Turq V, Laurent C (2011) Carbon 49:4535
241. Khaleghi E, Torikachvili M, Meyers MA, Olevsky EA (2012) Mater Lett 79:256
242. Capobianchi A, Foglia S, Imperatori P, Notargiacomo A, Giammatteo M, Del Buono T, Palange E (2007) Carbon 45:2205

Cryogels for Biotechnological Applications

Bo Mattiasson

Contents

B. Mattiasson (✉)
Department of Biotechnology, Lund University, Lund, Sweden

Indienz AB, c/o Department of Chemistry, Lund University, Lund, Sweden
e-mail: bogmattiasson@gmail.com

Abstract Cryogels are formed in a semifrozen state when the solvent is frozen, but solutes are still soluble. The ice crystals are porogens and, upon thawing the system, pores appear where the frozen solvent was found earlier. Such gels have large pores, are elastic, and offer interesting opportunities in biotechnology. Cryogels with their large pores can meet demands that traditional chromatographic media cannot. This also opens up opportunities for the separation of cells because upon passage through the gel cells may interact with specific groups on the pore walls, thereby becoming retarded and/or captured. A range of applications have been studied: isolation of microbial cells, capturing of cancer cells, and use of cryogels as matrices for immobilized cell reactors. Furthermore, the robustness of the gels allows new applications, for example in environmental separation.

Keywords Cell chromatography • Immobilized cells • Molecular imprinting • Cell bioreactors • Composite cryogels

Abbreviations

AAm	Acrylamide
BSA	Bovine serum albumin
ECS	Extra capillary space
HFR	Hollow fiber reactor
HMs	Heavy metal ions
HSA	Human serum albumin
ICS	Intra capillary space
IDA	Immuno-diacetic-acid
MIP	Molecularly imprinted polymer
MPG	Macroporous gel particle
NIP	Non-imprinted polymer
NIPA	N-Isopropyl acrylamide
PAAm	Polyacrylamide
PEG	Polyethylene glycol
PHEMA	Poly(2-hydroxyethyl methacrylate)
PVA	Polyvinyl alcohol
SEM	Scanning electron microscope

1 Introduction

Polymeric materials play essential roles in the life sciences. The supermacroporous cryogels were first used for immobilization of microbial cells [1], but later found many new and exciting applications [2]. Their high porosity combined with very good biocompatibility, mechanical strength, and ease of preparation are reasons

why cryogels are becoming popular in several sectors of life science research and development.

Use of chromatographic supports is frequent in many different subdisciplines of the life sciences. One may then ask, why should cryogels be used? There are several properties of these gels that make them well suited to meet some of the challenges that bioseparation and other aspects of life science are facing.

Cryogels are supermacroporous materials with a network of interconnected pores of diameters from a few micrometers up to 100 μm. This makes such structures attractive when dealing with particulate-containing fluids such as crude cell homogenates or even cell suspensions. Furthermore, it is possible to produce cryogels without use of toxic chemicals, and the gels may be produced from biocompatible polymers.

The high porosity may also be advantageous when cells are kept within such gels, since it gives good mass transport of substrates to the cells and waste products from the cells. This can apply to cell separation, cell adsorption, and even cell immobilization. A special aspect of the latter is cell culture for use in tissue engineering.

Cryogels may be produced as beads, but more frequently they are in the shape of monoliths or sheets. The gel structure is normally elastic and spongy, which makes it possible to use such monoliths in column operation without any leakage along the column walls. A column is used with a slightly smaller inner diameter than the outer diameter of the cryogel; the elasticity helps to tighten the column along the walls. The elasticity makes it possible to use cryogels for protein separation by letting the target protein bind to a cryogel in its "native" form, and then compressing the gel before elution. This leads to elution in a smaller volume and, thus, to an increased concentration of the recovered protein. A twofold increase in concentration has been obtained [3].

The large pores of cryogels contribute to a relatively small inner surface of such structures and, thus, a lower capacity than reported for conventional chromatographic materials.

It should be stressed that one can produce cryogels in many different shapes. There are, however, some limitations with regard to size. Since the production is based upon freezing and subsequent polymerization, it is problematic to generate homogeneous cryogels if larger dimensions are used. Up to 20–25 mm thickness is regarded as acceptable; above that, inhomogeneities will disturb the picture. If one wants to use wide columns, then the cryogel is produced as sheets that are stacked on top of each other. It has been demonstrated that scaling up from small column chromatography to a large column composed of stacked sheets is easy and that the performance is as predicted. Furthermore, no material is lost between the different sheets.

2   Materials Used for Formation of Cryogels

There are a range of different materials that can be used when cryogels are applied in biotechnology. Most commonly used are polymers based on acrylic building blocks that are polymerized in the semifrozen state. Cryogels formed from pre-made polymers are also described, e.g., polyvinyl alcohol (PVA), chitosan, and agarose. Biocompatibility, ease of biodegradation, mechanical robustness, and the ability to be chemically modified are some of the reasons governing the choice of such polymers for different applications.

2.1   Introduction of Functionality in the Cryogel

The polymer backbone is often rather inert. In order to make it useful for separation purposes one needs to introduce functionalities. This can be done by adding specific monomers to the mixture that is to be polymerized, or one can introduce functionality afterwards. A third variant is to add particles with functionality and they become incorporated into a composite cryogel.

When monomers with desired properties are available, it is a very convenient mode of operation to simply add such monomers to the reaction mixture. One can then also try to control the properties of the final product by varying the proportions of different monomers. Many examples in this chapter are based on this approach. Thus, ion-exchange cryogels can be produced, as well as cryogels with epoxy groups that later can be used for introducing ligands that may be too labile to withstand the polymerization procedure. Cryogels built from pre-made polymers, e.g., PVA and agarose, are most often modified after the gel has been formed.

3   Entrapment of Cells

An early development in the area of utilization of cryogels in biotechnology was immobilization of microbial cells in PVA gels that were produced via repeated freeze–thaw cycles [4]. The first reports indicated that high viability, good mass transfer, and mechanical stability were obtained. The gels were elastic and could therefore be used repeatedly. Table 1 lists some of the reports on cryogels with immobilized biocatalysts (microbial cells and/or enzymes).

When immobilizing microbial cells it is often advantageous to start with a spore suspension and then activate the dormant organism after immobilization. This has clearly been demonstrated for *Clostridium acetobutylicum* [39], but also with spores from *Rhizopus oryzae* [8, 9]. In this latter case, the fungus was cultivated within PVA cryobeads. The catalyst was used for production of L-(+) lactic acid, and it was reported that the immobilized cells had a higher resistance to high concentrations of lactic acid that otherwise would inhibit cell metabolism and

Table 1 Immobilized microorganisms and/or enzymes in cryogels, listed according to application

Cell	Product	Comment	References
Production of chemicals			
Kluyveromyces marxianus	Ethanol	PVA gels compared to alginate PVA-cryogels were superior in continuous or semicontinuous operation	[5]
Clostridium acetobutylicum	Acetone-butanol-ethanol (ABE)	Algal biomass was converted into biofuel. Different algal species gave different product profiles	[6]
Corynebacterium glutamicum	L-Lysine	PVA-cryogel	[7]
Rhizopus oryze	Lactic acid	–	[8, 9]
Humicola lutea	Acid proteinase	Entrapped spores were germinated. Entrapment in PVA together with N,N'-methylenebisacrylamide and PEG	[10]
Acidithiobacillus ferrooxidans	Oxidation of Fe^{3+}	PVA-cryogel	[11]
Bacillus agaradhaerens	β-Cyclodextrin	Integrated immobilized cell-reactor adsorption system	[12]
Aspergillus sp.	Extracellular enzymes	Repeated use of immobilized preparation showing high productivity	[13]
Bacillus pumilus	Prednisolon	Immobilized in PVA-cryogel produced by radiation polymerization	[14]
Bacillus subtilis	Proteinase	Repeated batch processes	[15]
Saccharomyces sp.	Beer	Cells immobilized in PVA-particles	[16]
Escherichia coli	Biodegradation of organophosphate neurotoxin	Recombinant cells in PVA-cryogel	[17]
Arthrobacter globiformis	Dehydrogenation of steroids	–	[18]
Aspergillus clavolans	Ribonuclease	Bubble column bioreactor	[19]
Champagne yeasts	Champagne	–	[20]
Enzymes			
Laccase	Treatment of apple juice	Improving juice quality by treatment with immobilized laccase	[21]
Proteases	Hydrolysis of proteins	Proteases immobilized in albumin/chitosan gel	[22]
Naranginase	Debittering of juice	Enzyme immobilized in PVA-cryogel	[23]
Acetylcholineesterase + PEG-modified choline oxidase	Analysis of acetylcholine	Co-immobilized enzymes	[24]

(continued)

Table 1 (continued)

Cell	Product	Comment	References
Chymotrypsin	Enantioselective hydrolysis	In water-poor media	[25]
PEG-modified glucose oxidase	Analysis of glucose	Entrapment of PEG–enzyme	[26]
Lipase (porcine)	Enantioselective hydrolysis	Enzyme covalently immobilized in PVA-cryogel	[27]
Lipase from *Mucor* sp.	Synthesis of esters, etc.	Enzyme in PVA	[28]
Environmental applications			
Rhodococcus sp	Petroleum remediation	Using fluidized bed reactor. For degradation of alkanes and 2–3-ringed polycyclic aromatic hydrocarbons	[29]
Mixed culture	Wastewater remediation	–	[30]
Rhodococcus sp.	Oxidation of hydrocarbons	Immobilization via adsorption on hydrophobized poly (acrylamide) cryogel	[31]
Rhodococcus sp.	Soil contaminated with crude oil	Improved survival rate with cryogel-immobilized cells	[32]
Mixed culture	Diesel-contaminated soil	PVA-cryogel	[33]
Basic study	Atrazine in water	PVA-cryogel	[34]
Analytical applications			
Glucose analysis	Glucose oxidase	Enzyme immobilized in albumin/chitosan gel	[22]
Pseudomonas putida	Detection of phenol	Clark electrode used for detection	[35]
Pseudomonas sp.	Detection of proline	Clark electrode	[36]
E. coli	Detection of organophosphorus neurotoxins	pH-glass electrode	[37]
Photobacterium fischeri	Toxicity assessment	Phenol-containing water	[38]

eventually turn off the process. This observation is important since many reports in the literature on lactic acid production clearly indicate that the inhibition from increasing concentrations of lactic acid is a major hurdle to overcome in development of an economically viable process [40].

Entrapment of spores were also used when *Humicola lutea* was immobilized in PVA crosslinked via *N,N'*-methylenebisacrylamide with or without added PEG. It
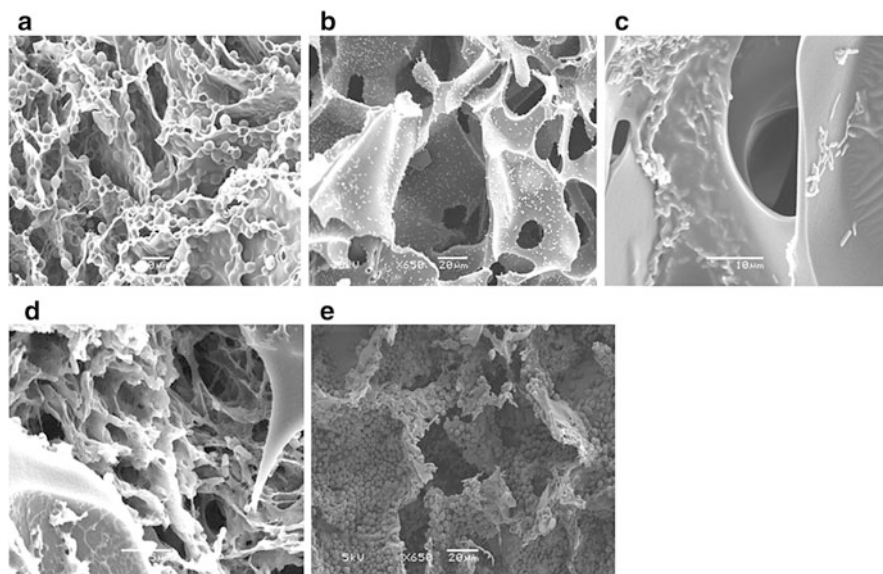
Fig. 1 Scanning electron micrograph (SEM) images of different immobilized cell preparations. (**a**) Yeast cells immobilized into pore walls of dextran cryogel and designed inside a protective plastic core (from [41] with permission). (**b**) *E. coli* cells attached onto the surface of ion-exchange PAAm cryogel column (from [42] with permission), (**c**) *E. coli* cells entrapped into agarose and introduced onto the surfaces of PAAm cryogel monolith through the "double-freezing" approach. (**d**) *E. coli* cells entrapped into PVA and formed inside the interconnected pores of PAAm cyogel monolith through the "double-freezing" approach (from [41] with permission). (**e**) Yeast cells on the surface of an ion-exchange PAAm cryogel monolith. (From [43] with permission)

was clearly shown that the entrapped preparation was more stable and produced acid proteinase during more cycles as compared to free cells. Furthermore, the presence of PEG increases both the productivity and stability of the process [10].

Microbial cells that are entrapped can be more stable to drying and storage. In a study using double polymer networks (see Sect. 8.3 for details on the technique), it was possible to retain a high percentage of activity, even for up to 7 months of storage at 22 °C (Fig. 1) [41].

Besides entrapment, cells may also be adsorbed or grow in an adhesive mode [31, 44]. This latter situation might be advantageous from the mass transfer point of view, but there is larger risk of leakage of cells from the preparation. The same rules are valid for immobilizing cells in cryogels as for situations when other matrices are used. The only feature that differs is that cryogels have very large pores and will thus allow loading of cells after the gel is formed. Table 1 lists some of the processes studied with cells immobilized in cryogels.

4   Cryogels Built from Crosslinked Cells

The formation of cryogels is based upon the fact that when an aqueous solution freezes, the solutes and suspended material will be expelled and concentrated in the interstitial space between the ice crystals (a process known as cryo-concentration). When particles are in the presence of a crosslinking agent it is possible to crosslink them, thereby creating the walls in a cryogel (Fig. 2) [45, 46]. This technique was used for making cryogels with a high density of cells in the solid phase and, at the same time, having good conditions for mass transfer of substrates and products to and from the cells. It was possible to obtain cryogels with good mechanical properties by the crosslinking. When glutaraldehyde was used as crosslinking agent, the cells lost their viability. These preparations were, however, suitable for bioconversion processes when only one or a few enzymes were involved. Cryostructured *Clostridium acetobutylicum* were produced with the idea of producing butanol. In order to obtain viable cells, new macromolecular crosslinkers had to be produced [47]. The cryogels made from viable cells were more efficient and reached higher product concentrations than a corresponding amount of cells in suspension [48]. Interestingly, it was possible to form a cryogel by crosslinking human red blood cells (Fig. 3). Such preparations might have applications as autologous scaffolds for tissue engineering [49].

5   Continuous Cell Seeding

When immobilized cells are growing and dividing, they will ultimately start to release free cells into the medium. This has often been regarded as a drawback, but it can also be utilized for continuous seeding with new cells.

6   Mammalian Cells in Cryogels as Bioreactors

Cultivation of mammalian cells is very much dependent on an efficient exchange of substrate and products to/from the cells. Therefore, open structures are attractive for cultivation of such cells. Much work has been done on cultivation in 2D format, but if the system is for efficient production of, e.g., biopharmaceuticals, then cultivation in 3D format is needed. Different types of microcarriers have been used successfully in gently stirred tanks. Initially, just the surface of the microcarrier was used, but developments on porous networks are now providing good 3D environments for mammalian cells to grow [50, 51].

It is attractive to use packed-bed bioreactors when utilizing mammalian cells growing in an adhesive manner. Cryogels seem appropriate for this due to their open structure, good flow properties, and possible surface chemistry. Small gel
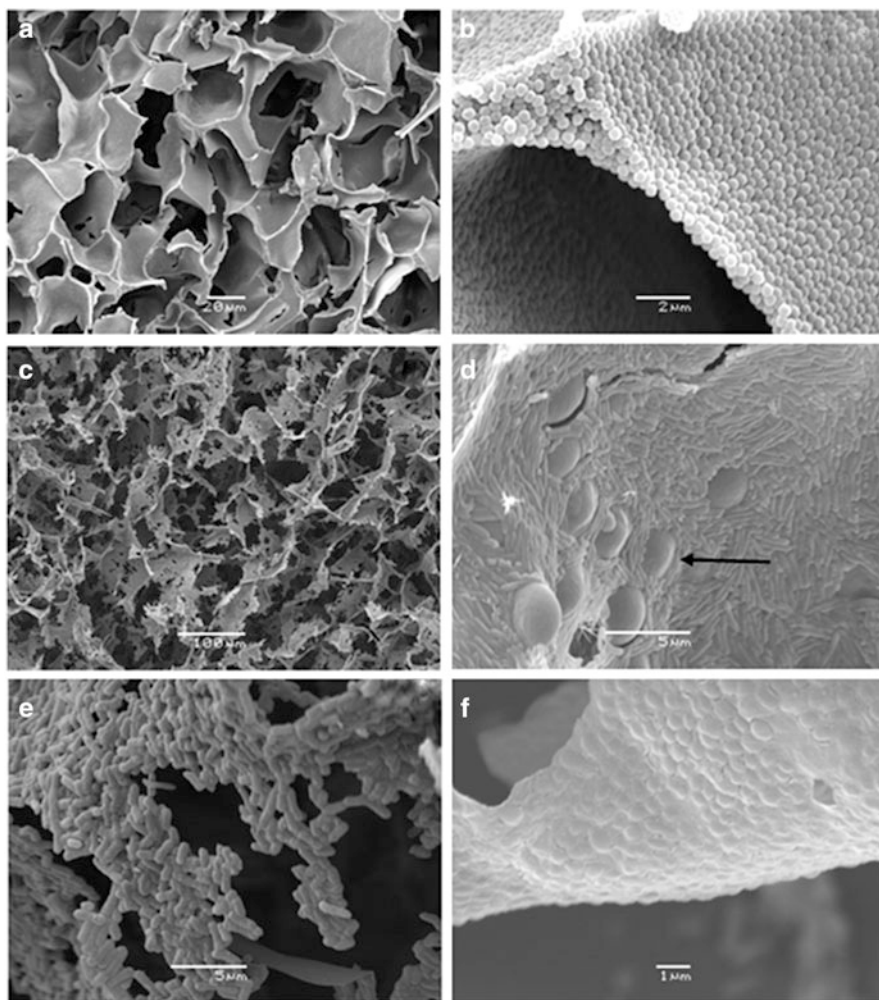
Fig. 2 SEM images of gels prepared from *N*-isopropyl acrylamide (NIPA) or bacterial suspensions. (**a, b**) Prepared gel of a 5 % (w/v) NIPA particle suspension at −12 °C that was crosslinked with 20 μL glutaraldehyde, shown at low and high magnification. (**c**) Prepared gel of a 10 % (wet weight/volume) *C. saccharolyticus* suspension at −12 °C that was crosslinked with 10 μL glutaraldehyde. (**d**) 15 % (wet weight/volume) *C. saccharolyticus* and *S. cerevisiae* suspension (ratio 10:1 w/w) crosslinked with 10 μL glutaraldehyde at –12 °C; *arrow* indicates *S. cerevisiae* incorporated into the structure. (**e**) 10 % (wet weight/volume) *E. coli* gel. (**f**) 15 % (wet weight/ volume) *Ralstonia eutropha* gel; both samples (**e**) and (**f**) were prepared by crosslinking with 10 μL of glutaraldehyde. All gels were prepared in 1 mL batches (From [45] with permission)

plugs with modified surfaces for use as efficient cell culture media have been used in continuous processing for production of urokinase (Figs. 4 and 5) [52] and monoclonal antibodies [43, 53]. In this latter study, cryogel that was surface modified (also within the pores) with gelatin was produced within plastic housings
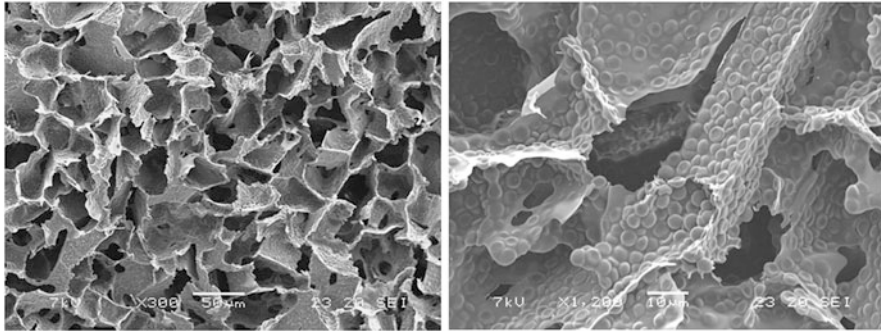
Fig. 3 SEM of cryogel prepared by crosslinking bovine blood diluted with phosphate-buffered saline, shown at low (*left*) and high (*right*) magnification. The pores are replicas of the ice crystals, and the individual blood cells are clearly seen in the walls. (From [49] with permission)
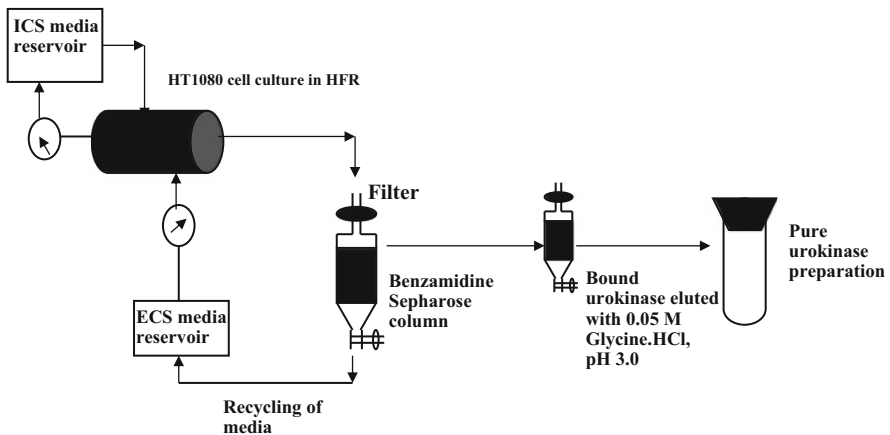
Fig. 4 In situ recovery of urokinase from HT1080 cells growing in a hollow fiber reactor (*HFR*). Benzamidine Sepharose column is used to capture urokinase from the media circulating through the extracapillary space (*ECS*). A separate media reservoir is used to circulate media through the intracapillary space (*ICS*)

(see Sect. 10 for more details). The dimensions of these housings were 9 mm in diameter and 7 mm long. By packing such particles into a column, seeding with hybridoma cells, and feeding medium continuously, it was possible to establish a continuous production of monoclonal antibodies. Crucial factors to keep under control are enrichment of ammonia and/or lactate in the medium. The cells are sensitive to increased concentrations of these metabolites. Therefore, it was also evaluated whether one could replace glutamine (a common component of cell culture media) with α-ketoglutarate, which does not have any nitrogen atoms but can be converted into glutamic acid via one enzymatic step, thereby capturing one ammonium ion; later it can be converted into glutamine by taking up one more
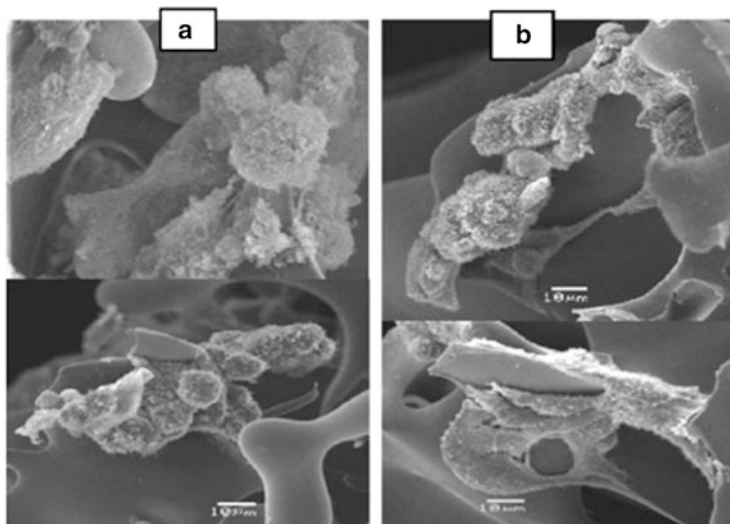
Fig. 5 SEM pictures of (**a**) human kidney cell line HT1080 and (**b**) HT116 human colon cancer cell line grown on gelatin-AAm cryogel scaffold for 18 and 15 days, respectively. The sections were taken at different places inside the gel

ammonium ion. The results were encouraging, with a high productivity of mono-clonal antibodies, almost equal to that of the best optimized medium. Most studies on culturing of mammalian cells are devoted towards tissue engineering, which is outside the scope of this review.

7 Chromatographic Separation of Particulate Matter

7.1 Cells

Compared to separation of soluble biomolecules, cell separation presents some additional challenges. Cells have surfaces where many points of possible interaction with an affinity matrix are present. This means that when a cell comes into contact with a solid support, several interactions may take place simultaneously, or within a very short time frame. That, in turn, leads to a much firmer binding than can be expected on the basis of the strength of the individual binding. The result of this is that cells get stuck on the column and are very difficult to elute out in viable shape. This has been the situation when columns packed with chromatographic beds have been used with the intention of separating cells.
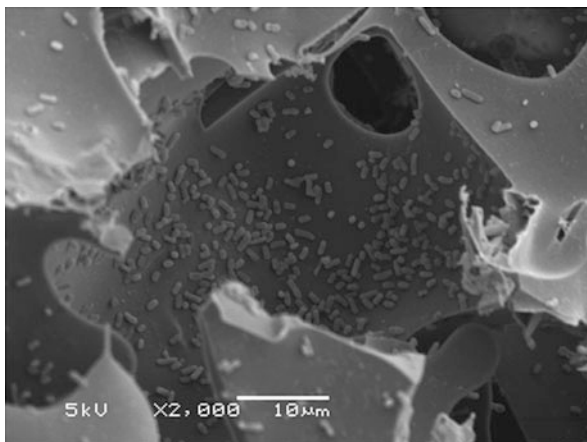
Fig. 6 SEM photograph of supermacroporous anion-exchange matrix with bound *E. coli* cells. The magnification is indicated by the *scale bar*. The sample was fixed in 2.5 % glutaraldehyde in 0.15 M sodium dodecylate buffer pH 7.2 overnight, postfixed in 1 % osmium tetroxide for 1 h, dehydrated in ethanol, and critical point dried. The sample was then coated with gold/palladium (40/60) and examined using a JEOL JSM-5600LV scanning electron microscope. (Reproduced from [54] with permission)

When using cryogels, a much more open structure is used, which reduces the risk that cells will be bound from different angles. However, in cryogels also, there is a risk for too-strong binding. One mode of operation would be to operate with very low substitution on the gel matrix. This is a sensitive issue since a too low a degree of derivatization would lead to no capturing of cells at all. Since the firmness of binding to some extent is a function of time, it is possible to modulate the time of contact and thereby facilitate release of bound cells. Another mode of operation is to work under conditions where binding is weakened, e.g., by modulating the pH or by adding a competing ligand in free solution that may interact with the cell surface, thereby blocking, or at least reducing, the possibilities for optimal binding to the support.

Cells have been separated on cryogels. The initial studies were carried out on bacterial cells because they are robust and easier to handle than mammalian cells. In this context, it needs to be stressed that the diffusion rate of cells is extremely low. In order to facilitate binding of cells to the adsorbent, the flow through the column was stopped for a short time before continuing the buffer flow.

In initial studies to demonstrate that it is possible to capture cells and then successfully harvest them, an anion-exchanger was used [54]. The monomers used for producing the cryogel were acrylamide, N,N'-methylenebisacrylamide, and the charged monomer 2-(dimethylamino)ethyl methacrylate. The concentration of charged groups in the final cryogel was approximately 1,000 μmol of tertiary amino groups per gram of dry gel. A gel matrix of 5 mL constituted one column, and initially a trial was made to verify that microbial cells could pass through the gel. The eluting medium was HEPES buffer, 20 mM pH 7.0 containing 1 M NaCl. The high concentration of salt was sufficient to suppress electrostatic interactions.

This led to a recovery of more than 95 % of the cells in the eluate from the column. The cells were eluted in a wide peak. To evaluate whether the broadness of the peak was due to heterogeneity among the cells, fractions were collected at the beginning of the peak and towards the end of the elution. Both fractions showed an identical elution pattern when re-chromatographed. This means that the peak broadening was not ascribed to a heterogeneous population of cells, but rather that cells were somewhat retarded during passage through the column.

However, when applying *Escherichia coli* cells at low ionic strength, the cells were captured and then eluted with 0.35–0.40 M NaCl. Recovery of 70–80 % was obtained. Viability tests showed full viability. The SEM photo in Fig. 6 shows that the cells were evenly distributed on the gel surface. It is interesting to observe that the cells are attracted to the plain surfaces and are not held by mechanical entrapment in "dead-flow" zones.

Studies were also carried out using immobilized metal affinity chromatography. A strain of *E. coli* with histidine on the surface was passed through iminodiacetic acid gel (IDA gel). Cells were captured and could not be eluted with high salt concentrations; up to 1.6 M NaCl was tested. However, imidazol or EDTA released the cells with a recovery yield of approximately 80 % [55].

Separation of different cells was carried out using an IDA gel. Two different organisms were used, *E. coli* and *Bacillus halodurans*. These two species were chosen since it is possible to detect one in the present of the other because *B. halodurans* grows at pH 10, which is not so for *E. coli*. Thus, by plate-counting on plates with different pH values, one could get a clear picture of the distribution of cells in the different fractions collected after chromatography [55]. The *B. halodurans* cells have increased amounts of acidic and hydrophobic amino acids on the surface, and therefore it was not expected that this cell type would bind well to the IDA column. The results confirmed this; most of the *B. halodurans* cells came in the flow-through peak whereas the *E. coli* cells were retarded on the gel and could be eluted afterwards. In all cases, good yields (80 % and upwards) and viability in the same range were observed.

If cells have relatively similar surface structures, then it may be advantageous to first specifically modify one group of cells that will be separated from the other. In the case of lymphocytes, B and T cells have many similarities, but differ in the fact that T cells have immunoglobulins on their surfaces, whereas B cells excrete immunoglobulins. By exposing the mixed cell population to a goat antibody directed against human IgG it was possible to add a separation handle on the B cells. When passing such a preparation through a cryogel with immobilized protein A, binding between protein A and the Fc-region of IgG took place and those cells with goat-anti-human-IgG on their surfaces were retarded, whereas the T cells passed through without being retarded. After proper washing, the captured cells were released by a pulse of dog IgG, with a yield of cells in the range of 80 % and a similar figure for viability (Fig. 7) [56].

The multipoint attachment of cells to the surface of the adsorbent is a real problem when developing chromatographic separation. After the cells have attached via a few interactions, more binding takes place that makes it difficult or even impossible to elute cells in a viable form. During elution, some interactions

Fig. 7 Fractionation of human peripheral blood lymphocytes before and after passage through the supermacroporous monolithic cryogel-Protein A column. Lymphocytes (1 mL, 3.0×10^7 cells/mL) were treated with goat anti-human IgG (H + L) and applied on a 2 mL cryogel-Protein A column. The cells bound on the column were released with 2 mL of dog IgG (30 mg/mL). (Reproduced from [56] with permission)

COLUMN PERFORMANCE
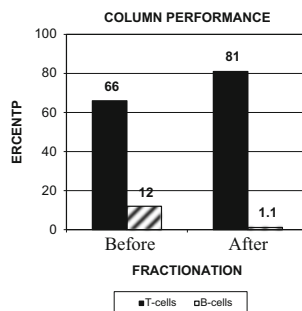
B-lymphocytes
Binding: 91%
Recovery: 70%
Viability: >80%

T-lymphocytes
Breakthrough: 81%
Viability: >90%

will break whereas others remain. Since it is a dynamic process, there may always be some interactions keeping the cells bound and thereby preventing successful elution. This is seen in many traditional chromatographic systems. An advantage with cryogels is their elasticity. This property was exploited when developing a chemo–mechanical elution procedure. In this method, the eluting medium is added to the chromatographic column to weaken the binding of the cells to the gel. The gel then is compressed. This mechanical force breaks many interactions and it is possible to elute cells with high yields and high viability [57, 58]. The principle is schematically illustrated in Fig. 8. In Figs. 9 and 10 some elution data for two different microbial cells are given.

7.2 Organelles and Other Subcellular Particles

There are also possibilities for using cryogels for isolation of other particulate structures, e.g., organelles. It has been clearly shown that it is possible to isolate "viable" mitochondria from a homogenate of mammalian tissue. The isolated mitochondria expressed their characteristic metabolic behavior [59].

During production of cloned proteins it often happens that inclusion bodies are formed. Such structures can be harvested using affinity-mediated separation in cryogels. After lysis of the cells, the inclusion bodies are labeled by antibodies against the protein that forms the inclusion bodies. Bypassing a homogenate (including inclusion bodies, cell debris, and soluble proteins) through a cryogel with immobilized protein A or the semispecific ligand sulfametazin, it is possible to capture the inclusion bodies selectively. IgG interaction with protein A usually requires harsher elution conditions, often low pH. After proper washing, one can then elute the inclusion bodies. With sulfametazin as capturing agent, it was sufficient to add 1 M NaCl. Yields in these processes were often in the range of
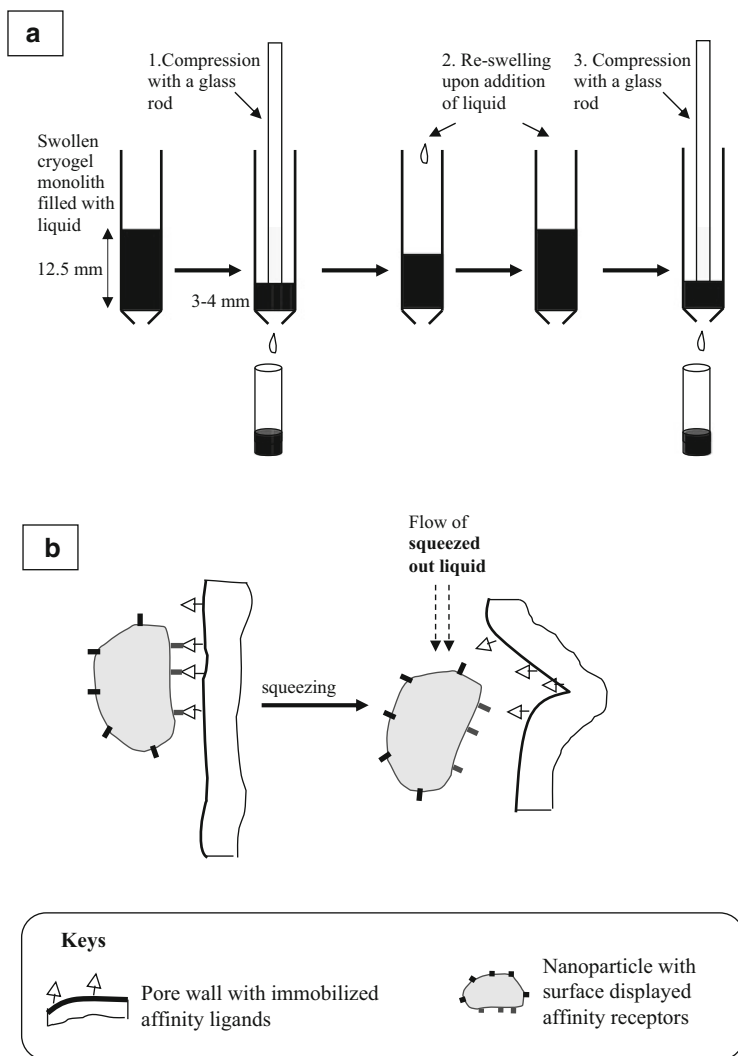
Fig. 8 (**a**) Procedure used for the release of captured bioparticles by mechanical compression of monolithic affinity cryogel. (**b**) Mechanism of detachment of bound cells induced by cryogel deformation. (Reproduced from [57] with permission)

50–70 % [60]. If longer columns are used, it might be possible to improve that figure.
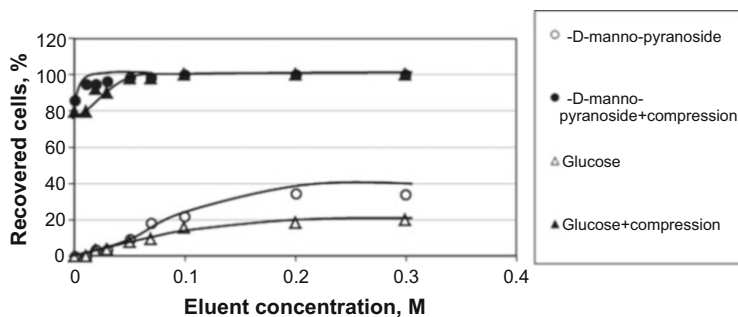
Fig. 9 Release of bound yeast cells by conventional elution and by compression of 5 % ConA-cryogel monoliths (12.5 × 7.1 mm) equilibrated with different concentrations of the eluent. The amount of bound cells was taken as 100 %. (Reproduced from [58] with permission)
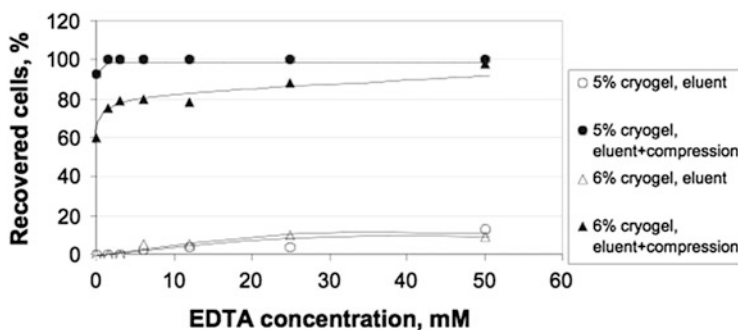
Fig. 10 Release of bound recombinant *E. coli* cells by conventional elution and by mechanical compression of Ni(II)-IDAcryogel monoliths equilibrated with different concentrations of EDTA. The amount of bound cells was assumed to be 100 %. (Reproduced from [57] with permission)

7.3 Viruses and Phages

Besides separation of cells, it is also possible to isolate biological particles such as organelles, viruses, and phages.

A library of affinity ligands that have great potential, but have not been utilized to their full potential, is the phage display library. Phages are filamentous particles of approximately 1 μm length and a diameter of about 6 nm. When dealing with cryogels, the pore dimensions allow one to operate with intact phages, even if they are 1 μm long. A library of M 13 phages was screened for binders that would capture lactoferrin. The selected phages were immobilized in a cryogel and the adsorbent was used for capturing lactoferrin from defatted milk. Bound lactoferrin was eluted with 1 M NaCl and a purity of 95 % was obtained. One should be aware that this type of gel has low capacity, but could be of interest in initial screening phases when one needs to obtain small amounts of relatively pure protein [61, 62].
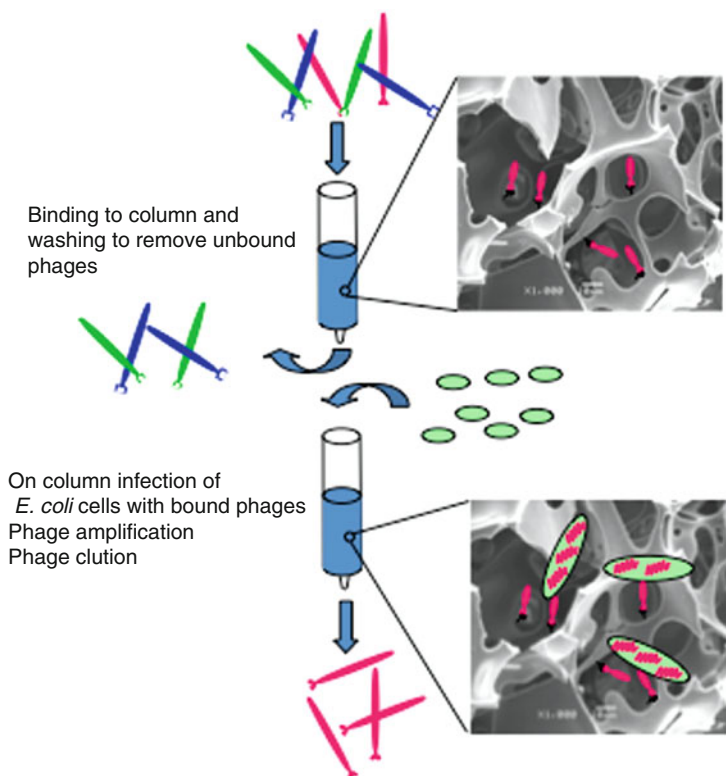
Fig. 11 Panning procedures:the chromatopanning protocol without (*top*) and with (*bottom*) on-column infection. (Reproduced from [63] with permission)

One can also turn the affinity interactions around in the sense that lactoferrin can be immobilized and then the phages can be captured and subsequently eluted after proper washing. By such an affinity step, one could pass a phage library through an affinity column, capture those phages with affinity for the affinity ligand, and wash out the rest. This could be regarded as an alternative to the conventional panning procedures that are labor- and time-demanding. However, it is also possible to take the technology one step further due to the large pores of the cryogel. After having captured phages on the immobilized ligand and washing away those that do not bind, it is possible to introduce *E. coli* cells into the pore system of the cryogel, stop the flow, and let the phages infect the bacterial cells for 0.5–1 h before the cells are washed out of the column. The experiment was very encouraging because a result was reached that was equal to that obtained after three rounds of traditional panning. The time for the complete cycle was approximately 23 h as compared to 152 h for the conventional procedure. This new technique was named "chromatopanning" (see Figs. 11 and 12) [63].
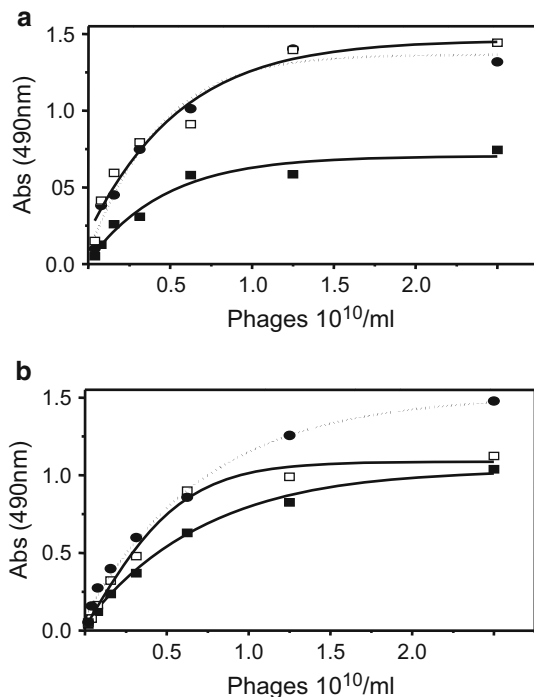
Fig. 12 (**a, b**) Efficiency of the panning procedures. Different phage libraries, C6 and L15, were used in both a tube biopanning and a chromatopanning procedure. In both procedures, three rounds were performed as described in [63]. The binding efficiency of the obtained phages was determined using phage ELISA (for experimental details see [63]). (**a**) Biopanning with a C6 library. (**b**) Biopanning with a L15 library. Tube panning: round 1 (*filled square*), round 3 (*open square*); column panning: round 1 (*filled circle*-dotted line). (Reproduced from [63] with permission)
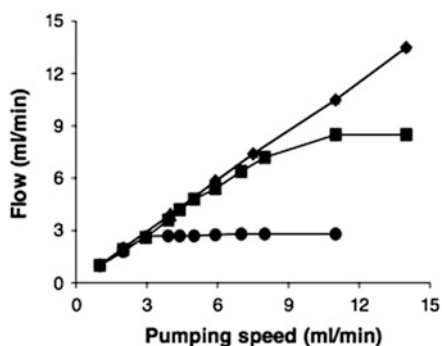
Fig. 13 Flow resistance of columns packed with Sephadex G-100 (*circles*), Sephacryl S-1000 SF (*squares*) and anion-exchange cryogels (*diamonds*). The results are presented as measured flow rate versus the set-up flow rate determined in a separate experiment when the pump settings were calibrated against flow rate with no column connected. Supermacroporous monolithic cryogels were prepared in a 5 mL syringe at −12 °C. (Reproduced from [65] with permission)

Based on the results above and experiences reported in literature on convective interaction media (CIM) discs, it is obvious that macroporous chromatographic materials have good potential for isolation of virus particles [64].

8   Chromatography of Biomolecules

Cryogels have an open structure and therefore produce low back-pressure when used in chromatographic applications (Fig. 13). This positive feature is counteracted by the fact that the large pores also result in a low capacity for adsorption of proteins. Thus, in many comparisons, gels like Sepharose may be at least ten times better with regard to capacity. The ability to operate with a high flow-rate favors use of the cryogels. Still, the low capacity is a problem when the gels are used for separation of proteins or other biomolecules. Much effort has gone into improving the capacity of the cryogels and some different strategies are presented next.

Means of increasing the binding capacity include: grafting, formation of composites, crosslinked nanoparticles with affinity, and double cryogel networks.

8.1   Grafting

It is possible to graft polymer chains to the pore walls of cryogels. This can be done either by having a pre-made polymer that is attached to the pore wall, or by initiating polymerization at the pore wall and then feeding monomers to build the polymer from the pore wall and out.

Savina et al. have mainly focused on building the polymer from the pore wall and out into the pore lumen. To achieve this, one needs to use an initiator that will start the polymerization. Savina et al. used diperiodatocuprate(III) complex as initiator. It was possible to first treat the pore wall with the initiator and then add the monomers after removing excess initiator [66–69]. It was possible to graft more than 100 % (w/w) of the weight of the polymer backbone. If the initiator was added concomitantly with the monomers, then a lot of soluble polymers were obtained. Therefore, a two-step procedure was utilized: first treating the polymer wall with initiator and then introducing the monomers.

Studies on the grafting of charged polymers made it clear that the density of polymers on the polymer backbone has a strong influence on the behavior of the ion-exchange adsorbent obtained [66–69]. With a large amount of initiator, a lot of short polymers were grafted, whereas when a lower amount of initiator was used, less but longer polymer chains were formed. When adsorbing small molecules (e.g., the dye Orange G) to an anion exchanger, there were no differences in the amount of small molecules bound if the amount of polymer was the same, even if there were differences with regard to polymer chain length. However, when it came to proteins (e.g., bovine serum albumin, BSA), it was found that the long polymer chains were

Table 2 Composite cryogels

Composite particle	Size	Functionality	Polymer backbone	References
Diatomite particle	2 μm	Metal chelate	PHEMA	[72]
Sporopollenin	–	Metal chelate	PHEMA	[73]
SiO$_2$ nanoparticle	–	Grafted cation exchanger	PAAm	[74]
Porous adsorbent bead	25 μm	Aminogroups	PVA	[75]
Iron nanoparticle	1–100 nm	–	–	[76]
Agarose bead	–	–	–	[77]
Activated carbon	–	Binding organic molecules	–	[78]
Entrapped emulsion	–	Hydrophobicity	Thermoresponsive	[79]
Oil droplet	–	Hydrophobicity	PVA	[80]

PHEMA poly(2-hydroxyethyl methacrylate), *PAAm* polyacrylamide

far more efficient at capturing BSA than short chains. The explanation for this behavior is that the small molecules penetrate and gain access to the charged groups where they bind, whereas proteins are excluded at tight polymers on the pore walls because of steric reasons, but are favored when long polymers are present because then multipoint attachment can take place.

That grafting contributes to improving the capacity was clearly shown. If no grafting was done, then 0.65 mg/mL was adsorbed, whereas with a grafting of 105 % (w/w) then 12 mg/mL was adsorbed. This represents an 18-fold increase in capacity, but is still far lower than that reached with the conventional tighter gels.

A cation-exchange cryogel was produced by in-situ graft-polymerization with sulfo groups to an acrylamide cryogel [70]. The grafting was performed using potassium diperiodocuprate in a similar mode to that used by Savina et al. [66]. The new ion-exchanger was evaluated using lysozyme as a target. The capacity was still low, even though it was increased as compared to non-grafted gels. However, it was argued that the possibility of operating at high flow velocities could partially compensate for the low capacity because each cycle can be run much faster.

One example where grafted cryogels were successfully applied is the capture of plasmid DNA from non-clarified bacterial lysate using a polycation-grafted monolith [71].

8.2 Composite Cryogels for Separation Purposes

Entrapment of adsorbent particles within a cryogel has been studied as a method to improve the binding capacity. There are also some cases where entrapment was carried out because the particles were too small to handle in conventional separation and the composite strategy was preferred. Table 2 lists some examples where composite cryogels have been used for bioseparation. Besides an increase in

Primary cryogel filled with the
new reaction mixture for the
secondary cryogel

Chemical reaction
in frozen state

Cryogel with double-continuous
macroporous structure and
gradient porosity

Freezing

Thawing

Pore wall in primary cryogel

Solution of gel precursors

Ice crystals

Initially forming polymer

Pore wall in secondary cryogel
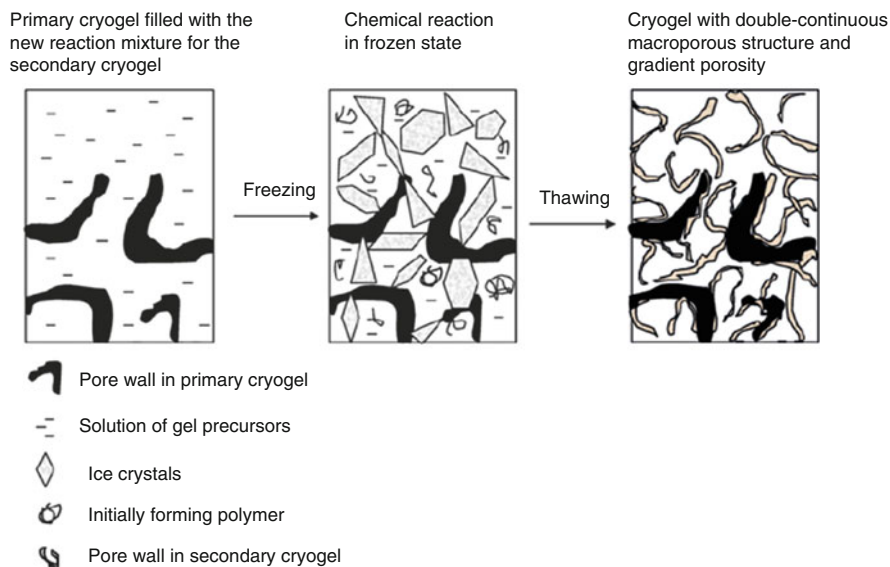
Fig. 14 Preparation of cryogels with double-continuous macroporous networks and gradient porosity

binding capacity, it has also been reported that the formation of composites can lead to improved mechanical stability of the gel.

From Table 2, it can be seen that a range of different materials have been used to create composite cryogels. An extreme case is the entrapment of microemulsions, which led to a preparation with one solid and one liquid phase with very different properties [79].

With the development of nanosized adsorbents, it may become more important to "pack" these nanoparticles such that they can be used conveniently. Cryogels offer an interesting alternative for this. Molecular imprinted polymers will be discussed later in Sect. 11.

8.3 Double Polymer Networks

Cryogels with unique double-continuous macroporous networks have been prepared by a sequential process. First, one cryogel is prepared according to regular procedures. After thawing, the porous volume of the gel is filled with a new solution of monomers and catalysts before the gel is frozen once more. After this second polymerization and subsequent thawing, a gel is obtained with two interlacing polymer networks (Fig. 14). The procedure can be repeated more times. The effect

Table 3 Proteins isolated using cryogels

Protein isolated	Cryogel affinity	Capacity	Comment	References
Lactoferrin	Phage display	Low	Whole phages	[61]
Yeast alcohol dehydrogenase	IDA-Zn	10 mg/g gel	–	[82]
Lysozyme	Hydrophobic	47 mg/g dry gel	–	[83]
Human serum albumin	Dye-affinity	74 mg/g dry gel	–	[84]
IgG	Protein A	88 mg/g dry gel	–	[85]
IgG	Thiophilic gel	Up to 68 mg/g dry gel	–	[86]
Cytochrome c	Metal affinity	21 mg/g dry gel	–	[87]
Fibronectin	Gelatin	38 mg/mL gel	–	[88]
Papain	Reactive Green 5	68 mg/g polymer	–	[89]
Horseradish peroxidase	Concanavalin A	–	–	[75]
His$_6$-lactate dehydrogenase	Metal chelate	–	–	[90]
Milk proteins (lactoferrin, lactoperoxidase)	Ion exchange	2.1 mg/mL gel	–	[91]
Plasmids	Polycation grafted cryogel	–	–	[71]
Endotoxins	Immobilized polyethylene imine, lysozyme, or polymyxin B	–	–	[92]
Bacteriocins	Phenyl ligands on cryogel	–	–	[93]

of working with double polymer networks is that the capacity for binding target molecules increases and the mechanical stability is also improved. This latter might be important for tissue engineering applications. By using two different polymer systems, it is possible to study the final preparation using confocal microscopy and then clearly see the interconnected networks. The flow-rate through the gel is reduced by the procedure. When dealing with gels that are mechanically weak, it might be possible to combine such a material with a stronger network, like a skeleton, to stabilize the structure (see SEM photos in Fig. 1) [81].

9 Separation of Proteins

As has already been stated, cryogels are not especially suitable for isolation or separation of proteins because of their relatively low capacity. The gels offer, however, the possibility to operate with non-clarified solutions such as cell homogenates, blood containing blood cells, suspensions of microbial cells, and milk. What can be separated using conventional chromatographic media can also be separated

using cryogels. There are many examples of such separations and, taking into consideration the means to improve capacity while still keeping the tolerance to operate at high flow-rates, it is realistic to think that sometime in the future there will be technology that makes it possible to use cryogels as viable alternatives to conventional chromatographic media for separation of proteins.

Table 3 lists some of the published examples where cryogels have been used for separation of proteins and a few other biomolecules. The list is not complete, but it covers different types of separations.

Cryogels are mainly used for separation of proteins on the basis of ion exchange, hydrophobic interactions, and affinity. The large pores and the relatively few meso- or nanopores make cryogels less suitable for gel permeation chromatography.

As stated above, it is easy to scale-up column chromatography using cryogels. Normally, there are no problems with pressure drop over the column unless very viscose media are used. Cell homogenates, fermentation broth, and plasma are examples of media that have been processed successfully.

9.1 High Through-Put Screening

The elasticity of cryogels has been mentioned earlier in this paper. Due to its elasticity, it is possible to squeeze a cryogel into a somewhat smaller column such that the gel will tighten towards the walls of the column. This property was utilized when placing small cryogel monoliths into microtiter plates with no bottom. The gels held the buffer due to capillary forces. When a volume of liquid was added, an equal volume was displaced. This leads to the use of cryogels in microtiter format for screening of cell homogenates for certain target proteins [94].

The same technology is very suitable for evaluating the conditions for binding of cells to adsorbents, and the elution conditions. This was demonstrated by Dainiak et al. [95, 96].

9.2 Environmental Pollutants

Cryogels have been used in environmental technology applications, both as matrices for immobilizing cells and/or enzymes for treatment of pollutants, and as adsorbents for enriching pollutants. Some of the applications of microbial cells and enzymes for remediation are listed in Table 1. The advantage of using cryogels in treatment of pollutants is the high porosity that facilitates exchange of media components. In some cases, improved stability of the immobilized cells has also been reported. Furthermore, when cells are entrapped in cryogels and start to grow, some cells are released to the surrounding medium. The cryogel then functions as a seeding unit from where cells are continuously released.

Fig. 15 Selective filters are produced within the plastic housings by polymerizing the monomers in the semifrozen state. Several different adsorbents are shown, e.g., the *light blue* is a chelating gel loaded with copper and the *dark blue* is a gel derivatized with textile dye. Some housings are without filling
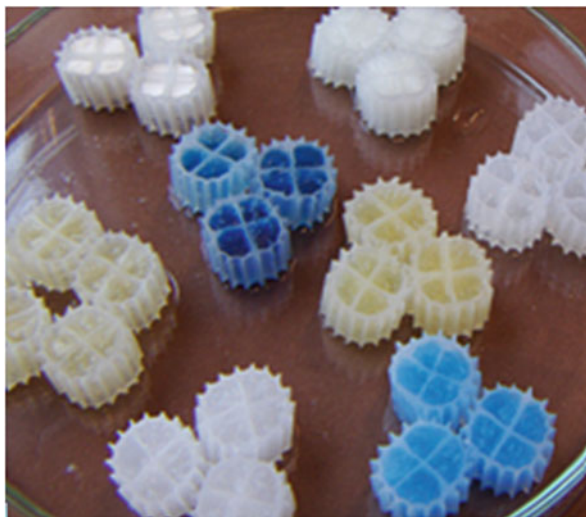
It is important when open systems are treated in environmental applications that the polymer systems used are not easily degraded by organisms present in the environment. Up to now, PVA seems to be the most popular polymer for this type of application.

Chromatography is to a large extent focused on adsorption/desorption processes. The main emphasis has been on separation of various cell components, especially proteins. The introduction of selective affinity ligands has meant a dramatic simplification and increased efficiency of the separation processes. It is also possible to enrich compounds present at very low concentrations in an efficient way using chromatography. It is tempting to apply this technology in environmental science where many of the emerging pollutants are present at submicromolar concentrations in a complex medium with varying composition over time.

The low concentrations mean that the capacity of the adsorbent is of less importance than factors such as robustness, ability to function in the presence of particulate matter, risk of fouling, etc. Cryogels seem to have suitable properties for addressing these challenges.

10   Cryogels in Housings

Adsorbents are normally used in columns, where they are exposed to a relatively well-controlled feed stream from which some substances are adsorbed. However, it would be useful to be able to use adsorbents under harsher conditions, e.g., processes with vigorous stirring or in media that are complex and with a composition that varies over time. An example of the latter is the use of adsorbents in environmental technology to capture, e.g., environmental pollutants.

Cryogels have properties making them attractive for adsorbing substances in the presence of particulate matter, e.g., microbial cells, and therefore cryogels seem to have a field of application in environmental separation. However, the gels are relatively soft and may be degraded by mechanical attrition. Therefore, cryogels were produced within plastic housings of a form that has earlier been used for microorganisms in wastewater treatment plants. The housings allow the microorganisms to grow and form biofilms and thereby stay in the reactor without being washed out [97]. A photo of such a plastic housing is shown in Fig. 15. The housings are open structures that allow free passage of liquid in and out, which is a prerequisite for a system that houses biofilms. Similar demands are valid for the adsorbents.

The missing link in this construction was access to stable, selective, and efficient affinity adsorbents. Protein-based binders are not suitable because microbes will hydrolyze them, so synthetic materials are preferable, in this case molecularly imprinted polymers (MIPs).

11 Molecularly Imprinted Polymers

Molecularly imprinted polymers (MIPs) are synthetic materials that are tailor-made to offer high molecular recognition, sometimes as good as that of antibodies [98]. MIPs can be synthesized from simple monomer building blocks using template-directed radical polymerization. The target molecule itself is used as a molecular template to form the molecular imprints. First, the "print molecule" is mixed with some functional monomers and, after some time, crosslinkers and other monomers may be added before radical polymerization is initiated. After polymerization, it is important to remove the print molecule, which is often a cumbersome process. Extraction with organic solvents may be used. After the target molecule is removed, specific cavities are formed that correspond to the space that the print molecules occupied during polymerization.

Why bother about MIPs when dealing with cryogels? The answer is simple, MIPs represent a very interesting group of affinity binders that are robust, not degradable by microorganisms, and can have high selectivity. They are therefore of great interest in the area of environmental separation. The procedure for preparation of MIPs is schematically presented in review by Mosbach [99].

MIPs can be used for capturing organic molecules that appear as pollutants in water. An early example dealt with endocrine disruptors. A problem with, e.g., estrogen, is that many different molecules bind to the estrogen receptors, and therefore one needs to have an affinity binder that will capture as many as possible of these molecules. A problem with MIPs is that they are composed of tight polymer material with very small pores. Therefore, MIPs are used as small particles so that many binding sites are exposed to the surface. On the other hand, it becomes problematic to handle these small structures and, when packed in columns, massive back-pressures are built up. Thus, a composite with the MIP particles immobilized

Table 4 MIPs used as composite components in cryogels

Target	Type of MIP	comments	Capacity	Regeneration	References
HSA	Surface imprinted	–	98 mg/g, 683 mg/g from serum	>10 times, 97 % recovered	[100]
Bilirubin	–	–	36 mg/g	>10 times, 90 % recovered	[101]
Bilirubin	Block copolymer, mechanical break, <100 μm diameter	–	10.3 mg/g	>10 times, >90 % recovered	[102]
Lysozyme	Imprint in cryogel	–	23 mg/g	>10 times	[103]
Fe^{3+}	Composite MIP	–	2.23 mg/g	>20 times, approx 90 %	[104]
Cytochrome c	Imprint in cryogel	–	126 mg/g	5 times, lost 5 %	[105]
Pb^{2+}, Cd^{2+}, Zn^{2+}, Cu^{2+}	Imprint in cryogel	Competition between different ions	mg quantities	10 times, >90 % recovered	[106]
β-blockers	–	High selectivity for the print molecule	–	>5 times	[107]

in a cryogel offers an attractive arrangement because good accessibility is offered by the cryogel and low back-pressure is maintained. Applications in environmental biotechnology are obvious, but also other areas of utilization seem realistic (Table 4).

Surface imprinting is an attractive approach for designing synthetic affinity adsorbents for proteins. One needs a large surface area because it is only the surface that is utilized. This leads to use of nanoparticles because of their advantageous relation between surface area and volume. However, nanoparticles are difficult to handle, so embedding them in the polymer network of a cryogel is attractive. The gel offers large pores with convective flow and thus good mass transfer conditions, and the nano-MIPs represent the affinity binders. When characterizing such preparations, one has to study selectivity, capacity, and ability to regenerate. In theory, use of surface imprinting for macromolecules facilitates the dissociation step when releasing bound molecules as compared to imprinting in a three-dimensional polymer network where some of the print molecules are completely entrapped. A recent paper by the group of Denizli presents a composite cryogel with embedded beads of poly(hydroxyethylmethacrylate)-based MIP [100]. The MIPs were prepared by surface imprinting using mini-emulsion polymerization [108]. The beads

were, after proper washing to remove the template, mixed with 2-hydroxyethyl methacrylate and polyethylene glycol diacrylate, which was then polymerized at low temperature.

Binding of human serum albumin (HSA) to the composite cryogel showed a clear pH-dependence, which could be correlated to the charges on the HSA molecule. The MIP was 28 times more efficient at binding HSA than was the NIP (non-imprinted polymer; the same composition and the same treatment, except for no exposure to HSA). Adsorption studies revealed that the binding of HSA to the cryogel followed the Langmuir isotherm. When placing the gel plug in a column and feeding a solution of HSA continuously, a capacity of 98 mg/g of dry polymer was reported. This was calculated to be close to the theoretical value for the MIPs used, 103 mg/g. These values are really astonishing because one might expect steric hindrance when the MIPs are partially entrapped in a tight polymer network. It was furthermore reported that when HSA from serum was captured, a maximum capacity of 683 mg/g of dry gel was obtained. To fully understand the mechanism behind these very high values, further studies will be needed. Values of capacities in this range are now matching what is reported for conventional adsorbents.

Composites involving MIPs have been extensively studied and Table 4 lists some of these systems.

11.1 Applications of MIP-Cryogels in Environmental Biotechnology

11.1.1 Heavy Metal Ions

Heavy metal ions (HMs) constitute a severe environmental problem. High concentrations in leachates from mining activities are usually treated by precipitation. However, lower concentrations of HMs can also cause severe problems. This is seen when water is used for irrigation or when water is consumed. Therefore, it is attractive to remove HMs almost completely from water. So far, this has not been possible, even if low levels are reported.

Use of chelating gels for capturing HMs turns out to be efficient [109]. MIPs also offer interesting alternatives. Chelating groups are not selective; they capture all heavy metals ions, but with somewhat different efficiencies. It is obvious that there is competitive binding between different heavy metal ions and the chelating groups.

11.1.2 Endocrine Disruptors

An emerging environmental problem is the presence of physiologically active compounds in very low concentrations (micrograms per liter or lower). Such compounds are difficult to degrade in the biological steps in wastewater treatment
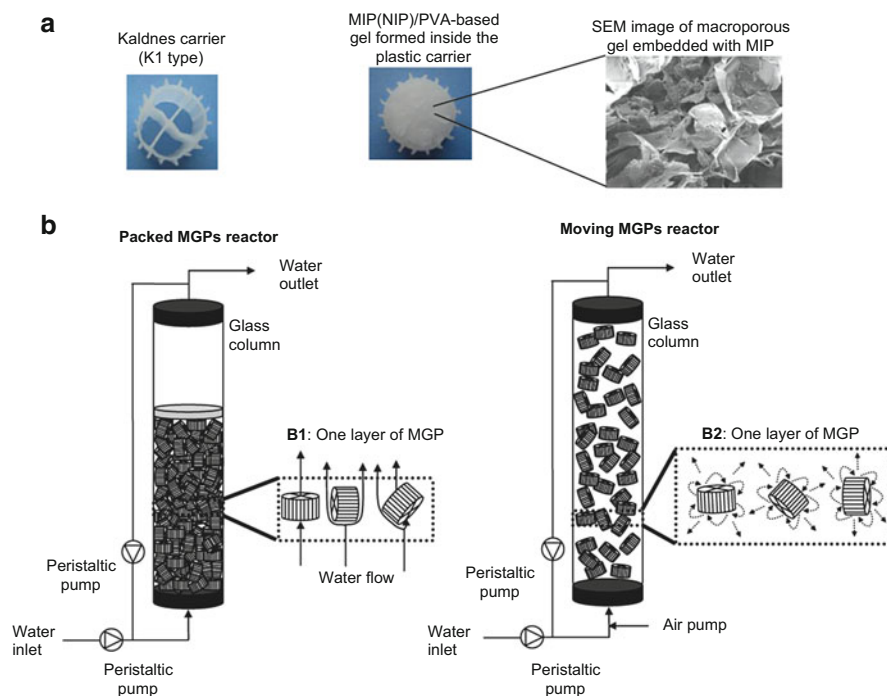
Fig. 16 (**a**) Appearance of an empty Kaldnes carrier (*left*) and an MGP, i.e., MIP/PVA-MG (*MG* macroporous gel) formed inside a plastic carrier (*center*). SEM image ofthe MIP/PVA-MG (*right*). (**b**) Packed MGP reactor (*left*) and a moving MGP reactor (*right*). *B1*: One layer of MGPs in a packed MGP reactor. The *arrows* show the water flow routes in the column. *B2*: One layer of MGPs in a moving MGP reactor. The *arrows* show the perpetual motion of the MGPs in the column. (From [111] with permission)

plants; they pass unaffected through the bio-bed and out in the recipient. If one just considers estrogen-active compounds, there are more than 100 different compounds with hormonal activity, i.e., they interact with the hormone receptor and thereby cause a physiological response. Because microorganisms are not efficient in removing such compounds, other methods have to be used. Advanced oxidation processes would be one alternative, but they are regarded as too expensive. Therefore, adsorption methods could offer an alternative, provided they are efficient enough and robust enough to withstand the conditions in a wastewater plant. Natural protein-based affinity binders (receptors or antibodies) will not survive in the environment because proteases from microorganisms will degrade them. An attractive alternative is then use of MIPs. These can be made selective, have good binding properties, are inert in the sense that they can be autoclaved, and are not degraded by microbes. MIPs can be introduced into cryogels (as described above) and it is possible to contain cryogels in plastic housings (see Sect. 10). The result of combining these three (the MIP, the cryogel, and the plastic housing) is a tool for
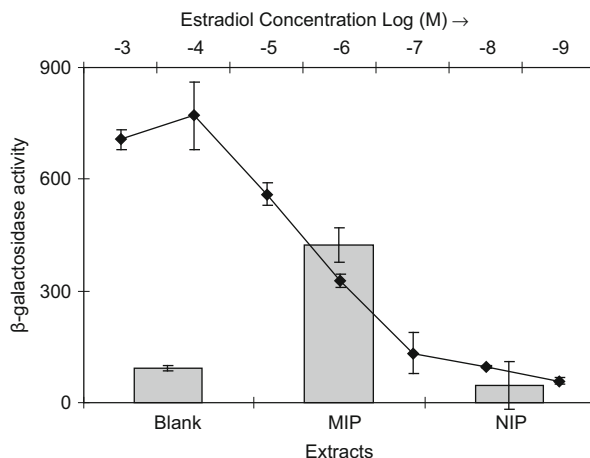
Fig. 17 β-galactosidase activity in transformed *Saccharomyces cerevisiae* cultures exposed to estradiol concentrations of 1×10^{-3} to 1×10^{-9} M in methanol/acetic acid (4:1 v/v) (MeOH:Aa) (*symbols*) compared to clean MeOH:Aa (*bar, Blank*) or extracts from solid-phase extraction (SPE) columns packed with 100 mg MIP or NIP and percolated with 100 mL of a wastewater sample (*bars, MIP* and *NIP*, respectively). The results from the different adsorbents are presented as bars in the figure. The polymers were extracted with 4 mL of MeOH:Aa and the values shown represent the average yeast activity (normalized to 100 mL of wastewater) $\pm$ standard deviation. No activity was found in the extracts (4 mL MeOH:Aa) from SPE columns packed with clean MIP and NIP (100 mg). β-Galactosidase activity is calculated as $1000 \times OD_{420}/(t \times V \times OD_{660})$, where OD_{420} is the final absorbance at 420 nm, t is the time of reaction of the mixture (41 min), V is the volume of culture used in the assay, and OD_{660} is the absorbance of the diluted yeast inoculum. (Reproduced from [111] with permission)

addressing the challenge. These combined units are often named MGPs (macroporous gel particles).

MIPs were synthesized with 17β-estradiol as template in the presence of some acrylic monomers and crosslinkers. The polymerization gave a block polymer that was mechanically disrupted; the particles were sieved and two fractions were saved, 25–38 μm and 38–106 μm. The MIPs were extensively washed with methanol in order to remove the print molecule. After drying, the smaller fraction was added to the monomer solution that was going to be polymerized to a cryogel. The polymerization took place in a glass tube filled with plastic housings of AnoxKaldnes type. After polymerization, the housings with their content (the MGPs) were separated from surplus cryogel and then washed properly before use. More details can be found in the literature [110–112].

The MGPs were placed in a fluidized bed through which the water to be treated was passed. Fluidization was used in order to get some mixing in the bed. A schematic presentation of the set-up is shown in Fig. 16 [112]. When running buffer solutions spiked with estradiol, it was shown that 100 % (within the experimental error) was removed. No estrogen could be detected afterwards. Estradiol is very hydrophobic, and therefore hydrophobic monomers had been used to create the cryogel. Whereas the MIPs gave efficient removal of all estradiol from the water

solution, the non-imprinted polymers (NIPs) gave between 49 and 74 %, depending on their composition. Captured material was eluted and the recovery could be calculated. Estradiol was recovered almost quantitatively.

When dealing with wastewater (water that had gone through the conventional wastewater treatment process and was to be released to the recipient), the adsorbent could also capture material via its artificial estradiol receptors. However, in this case, there is a broad spectrum of compounds, not just one compound. Therefore, the estradiol activity of the eluate was monitored, rather than identifying and quantifying each and every compound. Because the compounds interacting with the receptor have different "estradiol activities" this type of assay is more relevant. A transformed strain of *Saccharomyces cerevisiae* was used with an estradiol receptor cloned and expressed in such a way that production of β-galactosidase started when the receptor was stimulated. The activity of this enzyme could then be correlated to the amount of estradiol activity present [113]. Figure 17 shows the β-galactosidase activity expressed at different estradiol activities, and also the result of eluate analysis after polishing treated wastewater from the wastewater treatment plant in Lund municipality, Sweden [111].

11.1.3 Pharmaceuticals and Pesticides

Pharmaceuticals and pesticides also represent emerging pollutants present at low concentration, but with potentially strong effects on living organisms. Such compounds can be treated in a similar way to that described for the hormone active compounds [107].

12 Concluding Remarks

Cryogels in biotechnology represents something new–supermacroporous adsorbents in monolithic shape. These new gels do not fill all the demands that gels have traditionally satisfied, but cryogels can offer some new possibilities. As time goes by, improvements in capacity will be seen and then cryogels may also find use in certain separation processes where capacity versus cycle time can be balanced such that productivity governs the choice of gel.

It is furthermore clear that cryogels have certain advantages when particulate matters are involved in the separation, and also when it comes to applications in environmental technology.

That particles can be separated using cryogels has also opened a window for separation of cells and other particulate matters. When cells are adsorbed to the pore walls of a cryogel, then multipoint interaction takes place that may lead to difficulties in releasing the captured cells. The chemo-mechanical approach, i.e., combining elution conditions with a mechanical deformation of the gel structure

such that the cells are released, has shown promising results, including in handling of mammalian cells.

References

1. Varfolomeyev SD, Rainina EI, Lozinsky VI, Kalyuzhny SV, Sinitsyn AP, Makhlis TA, Bachurina GP, Bokova IG, Sklyankina OA, Agafonov EB (1990) Application of polyvinyl alcohol cryogels for immobilization of mesophilic and thermophilic microorganisms. In: De Bont JAM, Visser J, Mattiasson B, Tramper J (eds) Physiology of immobilized cells. Elsevier, Amsterdam, pp 325–330
2. Lozinsky VI, Galaev IY, Plieva FM, Savina IN, Jungvid H, Mattiasson B (2003) Polymeric cryogels as promising materials of biotechnological interest. Trends Biotechnol 21:445–451
3. Plieva FM, De Seta E, Galaev IY, Mattiasson B (2009) Macroporous elastic polyacrylamide monolith columns: processing under compression and scale up. Sep Purif Technol 65: 110–116
4. Hassan CM, Peppas NA (2000) Structure and morphology of freeze/thawed PVA hydrogels. Macromolecules 33:2472–2479
5. Gough S, Barron N, Zubov AL, Lozinsky VI, McHale AP (1998) Production of ethanol from molasses at 45 °C using *Kluyveromyces marxianus* IMB3 immobilized in calcium alginate gels and poly(vinyl alcohol) cryogel. Bioproc Eng 19:87–90
6. Efremenko EN, Nikolskaya AB, Lyagin IV, Senko OV, Makhlis TA, Stepanov NA, Maslova OV, Mamedova F, Varfolomeev SD (2012) Production of biofuels from pretreated microalgae biomass by anaerobic fermentation with immobilized *Clostridium acetobutylicum* cells. Bioresour Technol 114:342–348
7. Velizarov SG, Rainina EI, Sinitsyn AP, Varfolomeyev SD (1992) Production of L-lysine by free and PVA-cryogel immobilized *Corynebacterium glutamicum* cells. Biotechnol Lett 14:291–296
8. Efremenko E, Spiricheva O, Varfolomeyev S, Lozinsky V (2006) *Rhizopus oryzae* fungus cells producing L (+)-lactic acid: Kinetic and metabolic parameters of free and PVA-cryogel-entrapped mycelium. Appl Microbiol Biotechnol 72:480–485
9. Efremenko E, Spiricheva OV, Veremeenko DV, Baibak AV, Lozinsky VI (2006) L(+)-acid acid production using poly(vinyl alcohol)-cryogel-entrapped *Rhizopus oryzae* fungal cells. J Chem Technol Biotechn 81:519–522
10. Alekseiva P, Petricheva E, Konstantiov H (1998) Enhancement of acid proteinase production by the fungus *Humicaola lutea* 120-5 immobilized in crosslinked poly(vinyl alcohol) mixed with poly(ethylene glycol). Proc Biochem 33:725–728
11. Long ZE, Huang Y, Cai Z, Cong W, Ouyang F (2003) Biooxidation of ferrous iron by immobilized *Acidithiobacillus ferrooxidans* in poly(vinyl alcohol) cryogel carriers. Biotechnol Lett 25:245–249
12. Martins RF, Plieva FM, Santos A, Hatti-Kaul R (2005) Integrated immobilized cell reactor-adsorption system for β-cyclodextrin production: A model study using PVA-cryogel entrapped *Bacillus agaradharens*. Biotechnol Lett 25:1537–1543
13. Lusta KA, Chung IK, Sul IW, Park HS, Shin DI (2000) Immobilization of fungus *Aspergillus* sp. by a novel cryogel technique for production of extracellular hydrolytic enzymes. Proc Biochem 35:1177–1182
14. El-Hadi AA (2003) Factors affecting the production of prednisolone by immobilization of *Bacillus pumilus* E601 cells in poly(vinyl alcohol) cryogels produced by radiation polymerization. Proc Biochem 38:1659–1664

15. Szczesna-Antczak M, Antczak T, Bielecki S (2004) Stability of extracellular proteinases productivity by *Bacillus subtilis* cells immobilized in PVA-cryogel. Enzyme Microb Technol 34:168–176

16. Bezbradica D, Obradovic B, Leskosek-Cukalovic I, Bugarksi B, Nedovic V (2007) Immobilization of yeast cells in PVA particles for beer fermentation. Proc Biochem 42:1348–1351

17. Kim J-W, Rainina EI, Mulbry WW, Engler CR, Wild JR (2002) Enhanced-rate biodegradation of organophosphate neurotoxins by immobilized non-growing bacteria. Biotechnol Prog 18: 429–436

18. Fokina V, Suzina N, Arinbasarova A, Zubov A, Loziinsky V, Koshcheyenko K (1996) Immobilization of *Arthrobacter globiformis* 193 cells in PVA cryogel. Dehydrogenation of steroid substrates. In: Wijffels RH, Buitelaar RM, Bucke C, Tramper J (eds) Immobilized cells: basics and applications. Elsevier, Amsterdam, pp 90–97

19. Manolov RJ (1992) Batch and continuous ribonuclease production by immobilized *Aspergillus clavatus* cells in a bubble-column bioreactor. Appl Microbiol Biotechnol 37:32–36

20. Martynenko NN, Gracheva IM, Sarishvili NG, Zubov AL, El-Regisatan GI, Lozinsky VI (2004) Immobilization of champagne yeasts by inclusion into cryogels of polyvinyl alcohol: means of preventing cell release from the carrier matrix. Appl Biochem Microbiol 40: 158–164 (translated from Russian)

21. Stanescu MD, Fogorasi M, Shaskolskiy BL, Gavrilas S, Lozinsky VL (2010) New potential biocatalysts by laccase immobilization in PVA cryogel type carrier. Appl Biochem Biotechnol 160:1947–1954

22. Hedström M, Plieva FM, Galaev IY, Mattiasson B (2008) Monolithic macroporous albumin/chitosan gel: a new matrix for enzyme immobilization. Anal Bioanal Chem 390:907–912

23. Busto MD, Meza V, Ortega N, Perez-Mateos M (2007) Immobilization of naringinase from *Aspergillus niger* CECT 2088 in poly (vinyl alcohol) cryogels for the debittering of juices. Food Chem 104:1177–1182

24. Doretti L, Ferrara D, Lora S, Schiavon F, Veronese FM (2000) Acetyl choline biosensor involving entrapment of acetylcholine esterase and poly (ethylene glycol)-modified choline oxidase in a poly (vinyl alcohol) cryogel membrane. Enzyme Microb Technol 27:279–285

25. Belokon YN, Kochetkov KA, Plieva FM, Ikonnikov NS, Maleev VI, Parmar VS, Kumar R, Lozinsky VI (2000) Enantioselective hydrolysis of a Shiff's based of DL-phenylalanine ethyl ester in water-poor media via the reaction catalyzed with a-chymotrypsin immobilized on hydrophilic macroporous gel support. Appl Biochem Biotechnol 84:97–106

26. Doretti L, Ferrara D, Gattolin P, Lora S, Schiavon F, Veronese FM (1998) PEG-modified glucose oxidase immobilized on PVA cryogel membrane for amperometric biosensor applications. Talanta 45:891–898

27. Plieva FM, Kochetkov KA, Singh I, Parmar VS, Belkon YN, Lozinsky VI (2000) Immobilization of hog pancrease lipase in macroporous poly (vinyl alcohol)-cryogel carrier for the biocatalysis in water-poor media. Biotechnol Lett 22:551–554

28. Szczesna-Antczak M, Antczak T, Rzyska M, Bielecki S (2002) Catalytic properties of membrane-bound *Mucor* lipase immobilized in a hydrophilic carrier. J Mol Catal B-Enzym 19–20:261–268

29. Kuyukina MS, Ivshina IB, Serebrennikova MK, Krivorutchko AB, Podorozhko EA, Ivanov RV, Lozinsky VI (2009) Petroleum-contaminated water treatment in a fluidized-bed bioreactor with immobilized *Rhodococcus* cells. Int Biodeter Biodegr 63:427–432

30. Efremenko E, Senko O, Zubaerova D, Podorozhko E, Lozinsky VI (2008) New biocatalyst with multiple enzymatic activities for treatment of complex wastewater. Food Technol Biotech 46:208–212

31. Kuyukina MS, Rubtsova EV, Ivshina IB, Ivanov RV, Lozinsky VI (2009) Selective adsorption of hydrocarbon-oxidizing *Rhodococcus* cells in a column with hydrophobized poly (acrylamide) cryogel. J Microbiol Meth 79:76–81

32. Kuyukina MS, Ivshina IB, Kamenskikh TN, Bulicheva AV, Stukova GI (2013) Survival of cryogel-immobilized *Rhodococcus* strains in crude oil-contaminated soil and their impact on biodegradation efficiency. Int Biodeter Biodegr 84:118–125

33. Cunningham CJ, Ivshina IB, Lozinsky VI, Kuyukina MS, Philp JC (2004) Bioremediation of diesel-contaminated soil by microorganisms immobilized in polyvinyl alcohol. Int Biodeter Biodegr 54:167–174

34. Siripattanakul S, Wirojanagud W, McEvoy J, Khan E (2008) Effect of cell-to-matrix ratio in polyvinyl alcohol immobilized pure and mixed cultures on atrazine degradation. Water Air Soil Pollut 8:257–266

35. Rainina EI, Badalian IE, Ignatov OV, Fedorov AY, Simonian AL, Varfolomeyev SD (1996) Cell biosensor for detection of phenol in aqueous solutions. Appl Biochem Biotechnol 56:117–127

36. Simonian AL, Rainina EI, Lozinsky VI, Badalian IE, Khachatrian GE, Tatikian SS, Makhlis TA, Vorfolomeyev SD (1992) A biosensor for L-proline determination by use of immobilized microbial cells. Appl Biochem Biotechnol 36:199–210

37. Rainina EI, Efremenco EN, Varfolomeyev SD (1996) The development of a new biosensor based on recombinant *E. coli* for the direct detection of organophosphorus neurotoxins. Biosens Bioelectron 11:991–1000

38. Philp JC, Balmand S, Hajto E, Bailey MJ, Wiöes S, Whiteley AS, Lilley AK, Hajto J, Dunbar SA (2003) Whole cell immobilized biosensors for toxicity assessment of a wastewater treatment plant treating phenolics-containing waste. Anal Chim Acta 487:61–74

39. Häggström L, Enfors SO (1982) Continuous production of butanol with immobilized cells of *Clostridium acetobutylicum*. Appl Biochem Biotechnol 7:35–37

40. Senthuran A, Senthuran V, Hatti-Kaul R, Mattiasson B (1999) Lactic acid production by immobilized *Lactobacillus casei* in recycle batch reactor: a step towards optimization. J Biotechnol 73:61–70

41. Plieva FM, Oknianska A, Degerman E, Mattiasson B (2008) Macroporous gel particles as robust macroporous matrices for cell immobilization. Biotechnol J 3:410–417

42. Plieva FM, Galaev IY, Mattiasson B (2007) Macroporous gels prepared at subzero temperatures as novel materials for chromatography of particulate containing fluids and cell culture applications. J Sep Sci 30:1657–1671

43. Nilsang S, Nehru V, Plieva FM, Nandakumar KS, Rakshit SK, Holmdahl R, Mattiasson B, Kumar A (2008) Three-dimensional culture for monoclonal antibody production by hybridoma cells immobilized in macroporous gel particles. Biotechnol Prog 24:1122–1131

44. Kumar A, Rodrigues-Caballero A, Plieva FM, Galaev IY, Nandakumar KS, Kamihira M, Holmdal R, Orfao A, Mattiasson B (2005) Affinity binding of cells to cryogel adsorbents with immobilized specific ligands: effect of ligand coupling and matrix architexture. J Mol Recognit 18:84–93

45. Kirsebom H, Mattiasson B, Galaev IY (2009) Building macroporous material from microgels and microbes via one-step cryogelation. Langmuir 25:8462–8465

46. Kirsebom H, Mattiasson B (2011) Cryostructuration as a tool for preparing highly porous polymer materials. Polym Chem 2:1059–1062

47. Zaushitsyna O, Berillo D, Kirsebom H, Mattiasson B (2014) Cryostructured and crosslinked viable cells forming monoliths suitable for bioreactor applications. Top Catal 57:339–348. doi:10.1007/s11244-013-0189-9

48. Aragao Börner R, Zaushitsyna O, Derillo D, Scaccia N, Mattiasson B, Kirsebom H (2013) Immobilization of *Clostridium acetobutylicum* DSM 792 as macroporous aggregates through cryogelation for butanol production. Proc Biochem 49:10–18

49. Elowsson L, Kirsebom H, Carmignac V, Mattiasson B, Durbeej M (2013) Evaluation of macroporous blood and plasma scaffolds for skeletal muscle tissue engineering. Biomater Sci 4:402–408

50. Yang ST, Luo J, Chen C (2004) A fibrous-bed bioreactor of continuous production of monoclonal antibody by hybridoma. Adv Biochem Eng Biotechnol 87:61–96

51. Hu X, Xiao C, Huang Z, Zhang Z, Li Z (2000) Pilot production of u-PA with porous microcarrier cell culture. Cytotechnology 33:13–19

52. Kumar A, Bansal V, Nandakumar KS, Galaev IY, Roychourhury PK, Holmdahl R, Mattiasson B (2006) Integrated bioprocess for the production and isolation of urokinase from animal cell culture using supermacroporous cryogel matrices. Biotechnol Bioeng 93:636–646

53. Nilsang S, Nandakumar KS, Galaev IY, Rakshit SK, Holmdahl R, Mattiasson B, Kumar A (2007) Monoclonal antibody production using a new supermacroporous cryogel bioreactor. Biotechnol Prog 23:932–939

54. Arvidsson P, Plieva FM, Savina IN, Lozinsky VI, Fexby S, Bülow L, Galaev IY, Mattiasson B (2002) Chromatography of microbial cells using continuous supermacroporous affinity and ion-exchange columns. J Chromatogr A 977:27–38

55. Daniak MB, Plieva FM, Galaev IY, Hatti-Kaul R, Mattiasson B (2005) Cell chromatography: separation of different microbial cells using IMAC supermacroporous monolithic columns. Biotechnol Progr 21:644–6649

56. Kumar A, Plieva FM, Galaev IY, Mattiasson B (2003) Affinity fractionation of lymphocytes using a monolithic cryogel. J Immunol Methods 283:185–194

57. Dainiak MB, Kumar A, Galaev IY, Mattiasson B (2006) Detachment of affinity-captured bioparticles by elastic deformation of a macroporous hydrogel. Proc Natl Acad Sci USA 103:849–854

58. Galaev IY, Dainiak MB, Plieva FM, Mattiasson B (2007) Effect of matrix elasticity on affinity binding and release of bioparticles. Elution of bound cells by temperature-induced shrinkage of the smart macroporous hydrogel. Langmuir 23:35–40

59. Tellum M, Hansson MJ, Dainiak MB, Månsson R, Surve S, Elmér E, Önnerfjord P, Mattiasson G (2006) Binding mitochondria to cryogel monoliths allows detection of proteins specially released following permeability transition. Anal Biochem 348:209–221

60. Ahlqvist J, Kumar A, Sundström H, Ledung E, Hörnsten EG, Enfors S-O, Mattiasson B (2006) Affinity binding of inclusion bodies on supermacroporous monolithic cryogels using labeling with specific antibodies. J Biotechnol 122:216–225

61. Noppe W, Plieva F, Galaev IY, Mattiasson B, Deckmyn H (2006) Immobilized peptide displaying phages as affinity ligands. Purification of lactoferrin from defatted milk. J Chromatogr 1101:79–85

62. Noppe W, Plieva F, Vanhoorelbeke K, Deckmyn H, Tuncel M, Tuncel A, Galaev IY, Mattiasson B (2007) Macroporous monolithic gels, cryogels, with immobilized phages from phage-display library as a new platform for fat development of affinity adsorbent capable of target capture from crude feeds. J Biotechnol 131:293–299

63. Noppe W, Plieva F, Galaev IY, Pottel H, Deckmyn H, Mattiasson B (2009) Chromato-panning: an efficient new mode of identifying suitable ligands from phage display libraries. BMC Biotechnol 9:21

64. Kovac K, Gutiérrez-AguirreI BM, PeterkaM P-PM, RavnikarM ZMJ, SchultzAC RP (2009) A novel method for concentrating hepatitis A virus and caliciviruses from bottled water. J VirolMethods 162:272–275

65. Plieva FM, Savina IN, Deraz S, Andersson J, Galaev IY, Mattiasson B (2004) Characterization of supermacroporous monolithic polyacrylamide based matrices designed for chromatography of bioparticles. J Chromatogr B 807:129–137

66. Savina IN, Galaev IY, Mattiasson B (2005) Anion-exchange supermacroporous monolithic matrices with grafted polymer brushes of N, N-dimethylaminoethylmethacrylate. J Chromatogr A 1092:199–205

67. Savina IN, Mattiasson B, Galaev IY (2005) Graft polymerization of acrylic acid onto macroporous polyacrylamide gel (cryogel) by potassium diperiodateocuprate. Polymer 46: 9596–9603

68. Savina IN, Mattiasson B, Galaev IY (2006) Graft polymerization of vinyl monomers inside macroporous polyacrylamide gel, cryogel, in aqueous and aqueous-organic media initiated by diperiodatocuproate(III) complexes. J Polym Sci Polym Chem 44:1952–1963
69. Savina IN, Galaev IY, Mattiasson B (2006) Ion-exchange macroporous hydrophilic gel monolith with grafted polymer brushes. J Mol Recognit 19:315–321
70. Yao K, Yun J, Shen S, Chen F (2007) In-situ graft-polymerization preparation of cation-exchange supermacroporus cryogel with sulfo groups in glass columns. J Chromatogr 1157:246–251
71. Hanora A, Savina IN, Plieva FM, Izumrudov VA, Mattiasson B, Galaev IY (2006) Direct capture of plasmid DNA from non-clarified bacterial lysate using polycation-grafted monoliths. J Biotechnol 123:343–355
72. Ünlü N, Ceylan S, Erzengin M, Odabasi M (2011) Investigation of protein adsorption performance of Ni^{2+}-attached diatomite particles embedded in composite monolithic cryogels. J Sept Sci 34:2173–2180
73. Erzengin M, Ünlü N, Odabasi M (2011) Novel adsorbent for protein chromatography: Supermacroporous monolithic cryogel embedded with Cu^{2+}-attached sporopollenin particles. J Chromatogr 1218:484–490
74. Xu P, Yao Y, Shen S, Yun J, Yao K (2010) Preparation of supermacroporous composite cryogel embedded with SiO2 nanoparticles. Biotechnol Bioeng Chin J Chem Eng 18:667–671
75. Hajizadeh S, Kirsebom H, Leistner A, Mattiasson B (2012) Composite cryogel with immobilized concanavalin A for affinity chromatography of glycoproteins. J Sept Sci 25:2978–2985
76. Savina IN, English CJ, Whitby RLD, Zheng Y, Leistner A, Mikhalosky SV, Cundy AB (2011) High efficiency removal of dissolved As(III) using iron nanoparticle-embedded macroporous polymer composites. J Hazard Mater 192:1002–1008
77. Sun S, Tang Y, Fu Q, Liu X, Guo L, Zhao Y, Chang C (2012) Monolithic cryogel made of agarose-chitosan composite and loaded with agarose beads for purification of immunoglobulin G. Int J Biol Macromol 50:1002–1007
78. Hajizadeh S, Kirsebom H, Mattiasson B (2010) Characterization of macroporous carbon-structured particle gel as adsorbent for small organic molecules. Soft Matter 6:5562–5569
79. Komarova GA, Starodubtsev SG, Lozinsky VI, Kalinina EV, Landfester K, Kokhlov AR (2008) Intelligent gels and cryogels with entrapped emulsions. Langmuir 24:4467–4469
80. Podorozhko EA, Korlyukov AA, Lozinsky VI (2010) Cryostructuring of polymer systems, XXX. Poly(vinyl alcohol)-based composite cryogels filled with small disperse oil droplets: a gel system capable of mechanically induced releasing of lipophilic constituents. J Appl Polym Sci 117:1332–1349
81. Plieva FM, Ekström P, Galaev IY, Mattiasson B (2008) Monolithic cryogels with open porous structure and unique double-continuous macroporous networks. Soft Matter 4:2418–2428
82. Akduman B, Uygun M, Uygun DA, Akgöl S, Denizli A (2013) Purification of yeast alcohol dehydrogenase by using immobilized metal affinity cryogels. Mat Sci Eng C 33:4842–4848
83. Yilmaz F, Bereli N, Yavuz H, Denizli A (2009) Supermacropoorous hydrophobic affinity cryogels for protein chromatography. Biochem Eng J 43:272–279
84. Demiryas N, Tüzmen N, Galaev IY, Piskin E, Denizli A (2007) Poly(acrylamide-allyl glycidyl ether) cryogel as a novel stationary phase in dye-affinity chromatography. J Appl Polym Sci 105:1808–1816
85. Alkan H, Bereli N, Baysal Z, Denizli A (2009) Antibody purification with protein A attached to supermacroporous poly(hydroxyethyl methacrylate) cryogel. Biochem Eng J 45:207–208
86. Bakhshpour M, Bereli N, Senel S (2014) Preparation and characterization of thiophilic cryogels with 2-mercapto ethanol as a ligand for IgG purification. Colloid Surface B 113:261–268

87. Duygu C, Denizli A (2012) Immobilized metal affinity monolithic cryogels for cytochrome c purification. Colloid Surf C 93:29–35

88. Percin I, Aksöz E, Denizli A (2013) Gelatin-immobilized poly(hydroxyethyl methacrylate) cryogel for affinity purification of fibronectin. Appl Biochem Biotechnol 171:352–365

89. Uygun DA, Akduman B, Uygun M, Akgöl S, Denizli A (2012) Purification of papain using reactive green 5 attached supermacroporous monolithic cryogel. Appl Biochem Biotechnol 167:552–563

90. Arvidsson P, Plieva FM, Lozinsky VI, Galaev IY, Mattiasson B (2003) Direct chromatographic capture of enzyme from crude homogenate using immobilized metal affinity chromatography on a continuous supermacroporous adsorbent. J Chromatogr A 986:275–290

91. Billacanti JM, Fee CJ (2009) Characterization of cryogel monoliths for extraction of minor proteins from milk by cation exchange. Biotechnol Bioeng 103:1155–1163

92. Hanora A, Plieva FM, Hedström M, Galaev IY, Mattiasson B (2005) Capture of bacterial endotoxins using a supermacroporous monolithic matrix with immobilized polyethyleneimine, lysozyme or polymyxin B. J Biotechnol 118:421–433

93. Deraz S, Plieva FM, Galaev IY, Karlsson EN, Mattiasson B (2007) Capture of bacteriocins directly from non-clarified fermentation broth using macroporous monolithic cryogels with phenyl ligands. Enzyme Microb Technol 40:786–793

94. Galaev IY, Dainiak MB, Plieva FM, Hatti-Kaul R, Mattiasson B (2005) High throughput processing of particulate-containing samples using supermacroporous elastic monoliths in microtitre (multiwall) plate format. J Chromatogr A 1065:169–175

95. Dainiak MB, Galaev IY, Mattiasson B (2006) Affinity cryogel monoliths for screening for optimal separation conditions and chromatographic separation of cells. J Chromatogr A 1123:145–150

96. Dainiak MB, Galaev IY, Mattiasson B (2007) Macroporous monolithic hydrogels in a 96-minicolumn plate format for cell surface analysis and integrated binding/quantification of cells. Enzyme Microb Technol 40:688–695

97. Plieva FM, Mattiasson B (2008) Macroporous gel particles as novel sorbent materials: rational design. Ind Eng Chem Res 47:4131–4141

98. Vlatakis G, Andersson LI, Muller R, Mosbach K (1993) Drug assay using antibody mimics made by molecular imprinting. Nature 361:645–647

99. Mosbach K (1994) Molecular imprinting. Trends Biochem Sci 19:9–14

100. Andac M, Baydemir G, Yavuz H, Denizli A (2012) Molecularly imprinted composite cryogel for albumin depletion from human serum. J Mol Recognit 25:555–563

101. Baydemir G, Bereli N, Andac M, Say R, Galaev IY, Denizli A (2009) Supermacroporous poly(hydroxyethyl methacrylate) based cryogel with embedded bilirubin imprinted particles. React Funct Polym 69:36–42

102. Baydemir G, Bereli N, Andac M, Say R, Galaev IY, Denizli A (2009) Bilirubin recognition via molecularly imprinted supermacroporous cryogels. Colloid Surf 68:33–38

103. Bereli N, Andac M, Baydemir G, Say R, Galaev IY, Denizli A (2008) Protein recognition via ion-coordinated molecularly imprinted supermacroporous cryogels. J Chromatogr A 1190:18–26

104. Ergün B, Daydemir G, Andac M, Yavuz H, Denizli A (2012) Ion imprinted beads embedded cryogels for in vitro removal of iron from β-thalassemic human plasma. J Appl Polym Sci 125:254–262

105. Tamahkar E, Bereli N, Say R, Denizli A (2011) Molecularly imprinted supermacroporous cryogels for cytochrome c recognition. J Sept Sci 34:3433–3440

106. Tekin K, Uzun L, Sahin CA, Bektas S, Denizli A (2011) Preparation and characterization of composite cryogels containing imidazole group and use in heavy metal removal. React Funct Polym 71:985–993

107. Hajizadeh S, Changgang X, Kirsebom H, Ye L, Mattiasson B (2013) Cryogelation of molecularly imprinted nanoparticles: A macroporous structure as affinity chromatography column for removal of β-blockers from complex samples. J Chromatogr A 1272:6–12

108. Tan CJ, Chua HG, Ker KH, Tong YW (2008) Preparation of bovine serum albumin surface-imprinted submicrometer particles with magnetic susceptibility through core-shell mini-emulsion polymerization. Anal Chem 80:683–692
109. Önnby L, Georgi C, Plieva FM, Mattiasson B (2010) Removal of heavy metals from water effluents using supermacroporous metal chelating cryogels. Biotechnol Prog 26:1295–1302
110. Le Noir M, Plieva FM, Hey T, Guieysse B, Mattiasson B (2007) Macroporous molecularly imprinted polymer/cryogel composite systems for the removal of endocrine disrupting trace contaminants. J Chromatogr A 1154:158–164
111. Le Noir M, Lepeuple A-S, Guieysse B, Mattiasson B (2007) Selective removal of 17 β-estradiol at trace concentrations using a molecularly imprinted polymer. Water Res 41: 2825–2831
112. Le Noir M, Plieva FM, Mattiasson B (2009) Removal of endocrine disrupting compounds from water using macroporous molecular imprinted cryogels in a moving bed reactor. J Sept Sci 32:1471–1479
113. Gaido KW, Leonard LS, Lovell S, Gold JC, Babal D, Protier CJ, McDonnell DP (1997) Evaluation of chemicals with endocrine modulating activity in a yeast-based steroid hormone receptor gene transcription assay. Toxicol Appl Pharmacol 143:205–212

Poly(Vinyl Alcohol) Cryogels for Biomedical Applications

Wankei Wan, A. Dawn Bannerman, Lifang Yang, and Helium Mak

Contents

Abstract Poly(vinyl alcohol) (PVA) is a hydrophilic and biocompatible polymer that can be crosslinked to form a hydrogel. When physically crosslinked using a freeze–thaw cycling process, the product hydrogel or cryogel (PVA-C) possesses

W. Wan (✉)

Graduate Program in Biomedical Engineering, University of Western Ontario, London, ON, Canada N6A5B9

Department of Chemical and Biochemical Engineering, University of Western Ontario, London, ON, Canada N6A5B9
e-mail: wkwan@uwo.ca

A.D. Bannerman • L. Yang • H. Mak
Graduate Program in Biomedical Engineering, University of Western Ontario, London, ON, Canada N6A5B9

unique mechanical properties that can be tuned to closely match those of soft tissues, thus making it an attractive candidate for biomedical and especially medical device applications. We review the freeze–thaw cycling process and processing parameters that impact on the properties of PVA-C and its nanocomposite products. Both the mechanical properties and diffusion properties relevant to biomedical application are discussed. Applications to orthopedic and cardiovascular devices are summarized and discussed. The concept of biomaterial–tissue hybrids that can impart the necessary hemocompatibility to PVA-C for cardiovascular device is introduced and demonstrated.

Keywords Poly(vinyl alcohol) • Physical crosslinking • Cryogel • Medical device • Controlled release

List of Abbreviations

BC	Bacterial cellulose
BSA	Bovine serum albumin
DMSO	Dimethyl sulfoxide
DP	Degree of polymerization
E'	Young's modulus
FITC	Fluorescein isothiocyanate
FT	Freeze–thaw
FTC	Freeze–thaw cycle
WIC	Water insoluble chitosan
IVD	Intervertebral disc
Nano-HA	Nanohydroxyapatite
NP	Nucleus pulposus
PAAm	Poly(acrylamide)
PEG	Poly(ethylene glycol)
PVA	Poly(vinyl alcohol)
PVA-C	Poly(vinyl alcohol) cryogel
PVA-BC	Poly(vinyl alcohol) bacterial cellulose composite
PVP	Polyvinyl pyrrolidone
RGD	Arginyl-glycyl-aspartic acid
SANS	Small-angle neutron scattering
TEM	Transmission electron microscopy
UHMWPE	Ultrahigh molecular weight polyethylene
ULMP	Unfrozen liquid microphase
WSC	Water-soluble chitosan

1 Introduction

Polyvinyl alcohol (PVA) is a hydrogel with desirable properties for biomedical applications [1, 2]. Ivalon™, a highly porous PVA sponge crosslinked with formaldehyde, was probably one of the first medical products marketed [3]. It was used extensively in duct replacement, articular cartilage replacement [4], as a pharmaceutical release agent [1], and in reconstructive (vocal cord) surgery [5]. In addition to the use of chemical crosslinking agents such as formaldehyde and glutaraldehyde, PVA can also be crosslinked using several other methods, such as the use of electron beam,γ-irradiation, and physical crosslinking. For biomedical applications, physical crosslinking has the advantage of not leaving residual amounts of toxic crosslinking agents, as well as providing higher and more tunable mechanical strength than the PVA gels crosslinked by either chemical or irradiative techniques [6]. The physical crosslinking methods have generated the most interest because no new chemicals are introduced that could complicate their use in the biomedical environment.

Physical crosslinking can be accomplished using a freeze–thaw (FT) cycling method in which a solution of PVA is allowed to undergo repeated freezing and thawing cycles. For obvious reasons, the product hydrogel is popularly called a PVA cryogel (PVA-C). Using this approach, and by carefully controlling the process parameters used in the hydrogel preparation procedure, material properties, including mechanical and diffusion properties, can be tailored. Moreover, with the incorporation of nanomaterials into the PVA solution, nanocomposites of interesting mechanical properties (tensile and compressive) relevant to a range of medical device applications can be created. We will focus on the preparation and properties of PVA-C and its composites by the freeze–thaw method. Biomedical applications in the areas of medical device and drug delivery will be used to illustrate the range of biomedical applications possible for this class of hydrogel material.

2 Processing Parameters for PVA-C Preparation

PVA-C is today one of the most commonly investigated cryogels for biomedical applications. PVA, which is synthesized through hydrolysis of polyvinyl acetate synthesized via free radical polymerization of vinyl acetate [6], consists of a secondary alcohol group attached to a linear carbon chain. The alcohol group allows for hydrogen bonding and, therefore, PVA dissolved in an aqueous solution is able to produce a hydrogel with high water content. Subsequent thermal cycling leads to physical crosslinking via formation of structured crystalline domains of the polymer chains through phase separation. Several phases occur during the thermal cycling process. First, the gel is brought down to a temperature of between -5 and $-20\,^{\circ}\text{C}$ [7], during which time the water phase freezes. This creates regions of high polymer concentration, where crystallites are formed, as well as regions of low

polymer concentration resulting in pores [8–10]. The solution is then thawed back to room temperature leading to the formation of a solid gel—PVA-C. The micro-/nanostructure of PVA-C has been examined through several techniques including transmission electron microscopy (TEM) [9], small angle X-ray scattering (SAX) [9] and small angle and ultrasmall angle neutron scattering (SANS and USANS) [10, 11]. Observations conclude that the first freeze–thaw cycle (FTC) produces polymer-rich regions due to the formation of ice crystals in the amorphous regions [10, 12]. Subsequent FTCs further modify the structure of the polymer matrix.

Formation of the PVA-C takes place during the thawing stages [13]. Crystallization and phase separation are two important mechanisms that contribute to the structure of PVA-C, with crystallization occurring in the first three FTCs and phase separation through at least six cycles. Phase separation has a very important impact on the mechanical properties of PVA, even apart from crystallization [14].

A range of parameters in the processing procedures for PVA cryogels can be modified to alter the structure and properties of PVA-C and therefore its application. Polymer molecular weight and PVA solution concentration both have significant effects on structure [7, 12, 15–17]. The conditions of the FTCs, such as freezing and thawing rate, number of FTCs, and upper and lower temperature limits, all contribute to the determination of polymer matrix structure [7]. This wide range of processing parameters provides alternatives for tuning the properties of PVA cryogels. This is extremely beneficial because it makes the material useful for a large number of applications, and precise adjustments can be made to tailor the material for a specific application.

Significant work has been reported on how the Young's modulus of PVA cryogel is affected by processing parameters [7]. Work by Pazos et al. studied the nonlinear elastic response of PVA cryogel under uniaxial tension. The authors found that varying the number of cycles and the thawing rate could have similar effects on the elastic modulus, but changing the thawing rate gave finer control. Gels processed under specific conditions were found to mimic the uniaxial elastic response of healthy porcine coronary arteries [18]. Studies by our group using SANS were able to show that anisotropic mechanical properties can be achieved for PVA cryogels through processing the gel under controlled applied stress. This is extremely beneficial for biomedical devices such as coronary bypass grafts, where the tissue being replaced possesses orientational-dependent mechanical properties [10].

2.1 Molecular Weight

Molecular weight has a significant effect on PVA-C formation [19]. As molecular weight increases, the number and size of the crystalline regions increases due to the increase in length of the polymer chain. However, this effect is limited by the decrease in free volume and mobility of the high molecular weight polymers. Hassan and Peppas found that during swelling there was more instability in crystal

uniformity and degree of crystallinity in the higher molecular weight PVA due to an increase in chain length. This contributes to additional crystallization during swelling and increased mobility because of less physical crosslinking, as indicated by higher overall volume swelling ratio.

Lozinsky et al. found that gels produced with a lower molecular weight were more rigid than those of a higher molecular weight, up to a maximum. The unfrozen liquid microphase (ULMP), specific to cryotropic gelation, is important in explaining this phenomenon. The viscosity of the ULMP is highest in the system with the highest molecular weight polymer because the polymers have the longest chain length. This decreased mobility reduces intermolecular interactions. Therefore, although the rigidity normally increases as polymer molecular weight increases, a build-up in ULMP viscosity limits this increase [20].

The ability to change the degree of crystallinity by adjusting molecular weight is an important factor for biomedical applications. Degree of crystallinity has an effect on the mechanical properties and diffusion properties. For example, PVA-C can be tuned in this way to achieve mechanical properties that mimic tissue ranging from cardiovascular tissue to skin [7].

2.2 Solution Concentration

Initial PVA solution concentration was studied as one of the first processing parameters that can be altered to affect the structure and properties of PVA-C. Trieu and Qutubuddin showed that many processing parameters have an effect on the structure and mechanical properties of PVA cryogels, including initial PVA concentration. They found that a higher initial PVA concentration produces a structure with less porosity. This, in turn, lowers the equilibrium swelling, resulting in an inverse relationship between equilibrium swelling and porosity [21].

Hassan and Peppas varied the PVA solution concentration and noted that the higher concentration solutions resulted in more stable gels that have higher degrees of crystallinity and lower secondary crystallization. Lower degrees of swelling in higher concentration solutions indicate that more crosslinking occurs in higher concentration solutions [19].

Lozinsky et al. demonstrated that an increase in PVA concentration results in an increase in cryogel rigidity. This is due to the increased concentration of hydroxyl groups present, creating an increase in intermolecular hydrogen bonding. This factor was also determined to be more effective in controlling the properties than the effect of ULMP viscosity previously described. Furthermore, as polymer concentration is increased, porosity decreases and a more ordered structure results [20].

An increase in the concentration of PVA has been shown to produce more crystalline structures with greater stability. This, in turn, causes an increase in the tensile strength and tear resistance [22]. Wan et al. found that an increase in the PVA concentration caused the stiffness of PVA-C to increase significantly. With an

increase in PVA concentration from 10 % to either 15 or 20 %, the tangent elastic modulus increased by 69 and 137 %, respectively, and the secant elastic modulus increased by 83 and 180 %, respectively, at a strain of 0.25 [23].

2.3 Solvent

The use of different solvents in the processing of PVA can dramatically alter the PVA-C properties. Hassan and Peppas have reviewed this area well [6]. Hyon and Ikada showed that the use of organic solvents such as dimethyl sulfoxide (DMSO), glycerin, ethylene glycol, propylene glycol, and ethyl alcohol provides excellent light transmittance, along with good tensile strength and high water content, making a gel material with good potential for contact lens applications [24]. The addition of DMSO has been studied extensively because it imparts transparency to the PVA-C. Ohkura et al. showed that DMSO/water solutions with PVA exhibit transparency, high elasticity and higher gelation rates because gelation occurs without phase separation at temperatures below $-20\,^\circ$C [25]. Murase et al. showed that crystallinity increased over time due to the interaction between water and DMSO in the PVA-C [6].

Additives are sometimes put into the PVA solution. Lozinsky et al. showed that by adding triethylene glycols and its higher oligomers, the strength and thermal stability of the PVA cryogels increased and the gelation process was altered [26, 27].

For biomedical applications, the presence of salts or other solutes in the environment while producing PVA-C can be beneficial because the biomaterial will eventually be used in an electrolyte-containing physiological environment. Due to freezing point depression as a result of increased solute concentration, the freezing point of PVA solution decreases with the addition of salts. Gordon showed that the freezing point of PVA in water was $-18.7\,^\circ$C [28], whereas Shaheen et al. demonstrated a decrease of freezing point to $-30\,^\circ$C when PVA, theophylline, and 11 % NaCl was used [29]. The intermolecular and intramolecular hydrogen bonds that are so important to the formation of crystallites in PVA-C are disrupted by the presence of salts [30]. The crystallinity of PVA-C was shown to decrease and the cryogel became weaker when prepared in the presence of NaCl (0.0125–0.0625 M) compared to when distilled water was used [31].

2.4 Freeze–Thaw Cycling

As described above, the freeze–thaw cycling process allows the formation of amorphous and crystalline regions to form a physically crosslinked matrix of PVA. The number of FTCs, rate of freezing and thawing, and the time for which the gel is held frozen (freezing holding time) all have direct impact on the structure

of the resulting cryogel. For example, with an increase in the number of FTCs, there is a decrease in pore size within the polymer matrix [8, 32], an increase in mechanical properties [7] and a decrease in diffusion rates (see Sect. 3.2). An increase in freezing rate has been shown to decrease the size and density of crystallites. The freeze–thaw process is reviewed here in terms of its effect on PVA-C for applications in biomedicine.

2.4.1 Rate of Freeze–Thaw Cycles

The rate of the thermal cycles has been shown to affect the mechanical properties of the PVA hydrogel. A stiffer material is produced by using a slower thawing rate because of the increased amount of time for the reorganization of polymer chains and squeezing out of water molecules. Hatakeyama et al. showed that the rate of freezing affects the size of the crystals and, therefore, the number of crystals formed [33]. Slower thawing increases the period in which the specimen is at temperatures optimal for gel network formation [13].

Lozinsky et al. found that the more time that the solution spends at temperatures below 0 °C, the more time is available for movement of polymer chains. This allows for more time for entanglements to occur and increases the crystallinity by increasing both the number and size of crystallites [34]. This produces PVA-C with increased tensile strength. The rate of freezing has less of an effect on the properties, but has been shown to affect the formation of ice crystals [33]. Thawing rates, on the other hand, affect the formation of the PVA-C and its mechanical properties [7, 18, 35, 36].

It is important to keep thawing rates below 10 °C/min, as higher rates are not acceptable for producing hydrogels [35]. In many studies, precise control of freezing and thawing rates are not maintained because samples are simply placed in a freezer for freezing and then removed to room temperature for thawing [37–39]. This will still result in cryogel formation, but the structure, and therefore the properties, of the PVA-C will not be reproducible.

2.4.2 Number of Freeze–Thaw Cycles

In work by Hassan et al., the amount of dissolution of PVA cryogels was shown to decrease as the number of FTCs was increased [40]. This is consistent with the results that each FTC after the second causes a significant increase in the degree of crystallinity [37, 41].

It has been shown that the number of FTCs has an effect on mechanical properties. A maximum number of FTCs, after which the structure and properties of the cryogel no longer changes, has been demonstrated [8], and several studies have found this maximum number to be six [39, 42]. The increase in PVA-C stiffness with increasing number of FTCs has been attributed to the crystallite formation mechanism and liquid–liquid phase separation [7]. An alternative

explanation is the reinforcement of additional existing crystals within the structure with each additional FTC, up to a maximum level [19, 34].

2.4.3 Freeze Holding Time

The freezing holding time has a significant effect, with samples frozen up to 10 days at $-10\,°C$ giving the most mechanically strong PVA hydrogels [34]. On the other hand, holding the sample at a lower temperature for varying amounts of time did not seem to have an effect on the mechanical properties. Wan et al. showed that holding times of 1 or 6 h at $-20\,°C$ did not cause any change in the tensile properties of the PVA hydrogel [7]. Nevertheless the lower temperature limit, at which the hydrogel freezes, has an effect on the phase equilibrium of PVA, with storage of frozen solutions at higher negative temperatures resulting in PVA-C that is to some extent more rigid [21].

3 Properties of PVA and PVA Composites

3.1 Mechanical Properties

PVA cryogel (PVA-C) has caught the interest of researchers in the biomedical field since its creation in the early 1980s [43]. Apart from its long-term biocompatibility and nontoxicity [44], its mechanical properties, which can be tailored to mimic a wide range of soft tissues [7, 45], are the main reason why PVA-C is an attractive candidate material for many prosthetic devices such as heart valves, blood vessels, and articular cartilages.

In terms of mechanical strength (compressive or tensile), PVA-C can be isotropic or anisotropic [10]. Its Young's modulus is nonlinear and dependent on strain, strain rate, and temperature [46]. It is viscoelastic and strongly hydrophilic. Its strength is a function of concentration of the PVA solution, the mean molecular weight of the polymer material, the number of FTCs it has gone through during its formation, post-hydration processing, the type of buffer solution, and the solution temperature.

To understand the mechanical properties of PVA-C, one has to understand the microstructure of the cryogel, which is a direct result of its formation process. Although the gelation mechanism is still under discussion, it is thought to be a combination of mechanisms involving hydrogen bonding [47], crystallite formation, and liquid–liquid phase separation through spinodal decomposition [48].

Willcox et al. proposed a gelation scheme in support of the above hypothesis. When a PVA solution is subjected to a number of FTCs, during the first freezing cycle, ice crystallizations cause the remaining polymer solution to concentrate, bringing the molecular chains closer together. This promotes PVA crystallite

formation between the ice crystals. Inter- and intramolecular hydrogen bonds are also formed that connect the crystallites together and create an amorphous polymer network. Thawing of the ice crystals leaves behind regions of low polymer concentration solutions. Subsequent FTCs will repeat the process, reinforcing the PVA crystallites and tying up an increasing amount of the PVA molecules in the solution. At the end of the process, the final thawing of the ice crystals leaves behind micropores in the hydrogel body that are filled with the original solvent, typically water [9].

The structure of PVA hydrogels by repeated freezing and thawing cycles has been studied by several groups and the consensus is that they consists of a polymer-rich region and a polymer-poor region, which is consistent with Willcox's model [8, 10, 12, 15, 49, 50].

Based on micro-/nanodimension characterization, several structural models have been proposed [8, 9, 32]. One of the most recent and up-to-date studies used SANS. It was determined that the PVA-C structure consists of polymer crystallites of ~3 nm in size dispersed in the polymer-rich region with a spacing of ~19 nm between them [10]. During thawing, melting ice crystals create water-filled micrometer-sized macropores that make up the polymer-poor regions. The structural evolution during the FT process is illustrated in Fig. 1a.

Interestingly, the FT process can be altered by adding one additional step to the freeze–thaw procedure to create anisotropic PVA-C with orientation-dependent mechanical properties. Since most natural tissues are anisotropic in structure and properties, it is beneficial to be able to achieve this with polymer materials for tissue replacement applications. Millon et al. produced the first PVA-C flat sheet and conduit displaying anisotropic mechanical behavior similar to that of the porcine aorta. Structural anisotropy was created by applying an orientational-specific strain to the PVA sample after the initial FTC, and performing further thermal cycling on it. It was suggested that the applied strain forces the polymer mesh and polymer-poor phase to elongate in the direction of the strain. Subsequent FTCs then produce ice crystals that freeze and thaw in the strained pores that are already present, reinforcing the structure in the direction the strain is applied. The pores semi-oriented in the direction of strain can increase in size with the additional cycling. Additional crosslinking can also occur [10]. Figure 1b shows a model constructed on the basis of the SANS data.

The unique poro-viscoelastic mechanical property of PVA-C when subjected to external forces has been modeled using the finite element method. It has been shown to be a direct result of the part-solid and part-liquid biphasic structure [51]. This result is consistent with the model shown in Fig. 1b.

As the number of FTCs increases, the network mesh becomes denser and, hence, the strength of the PVA-C increases with the number of FTCs. However, after seven cycles, all available PVA materials in the initial solution are tied up in the mesh and the mechanical strength of PVA-C levels off [45].

As the initial concentration of the PVA solution increases, more polymers are available for network formation. The crystallinity increases and the polymer mesh becomes denser, but the pore size becomes smaller [23]. The denser polymer mesh
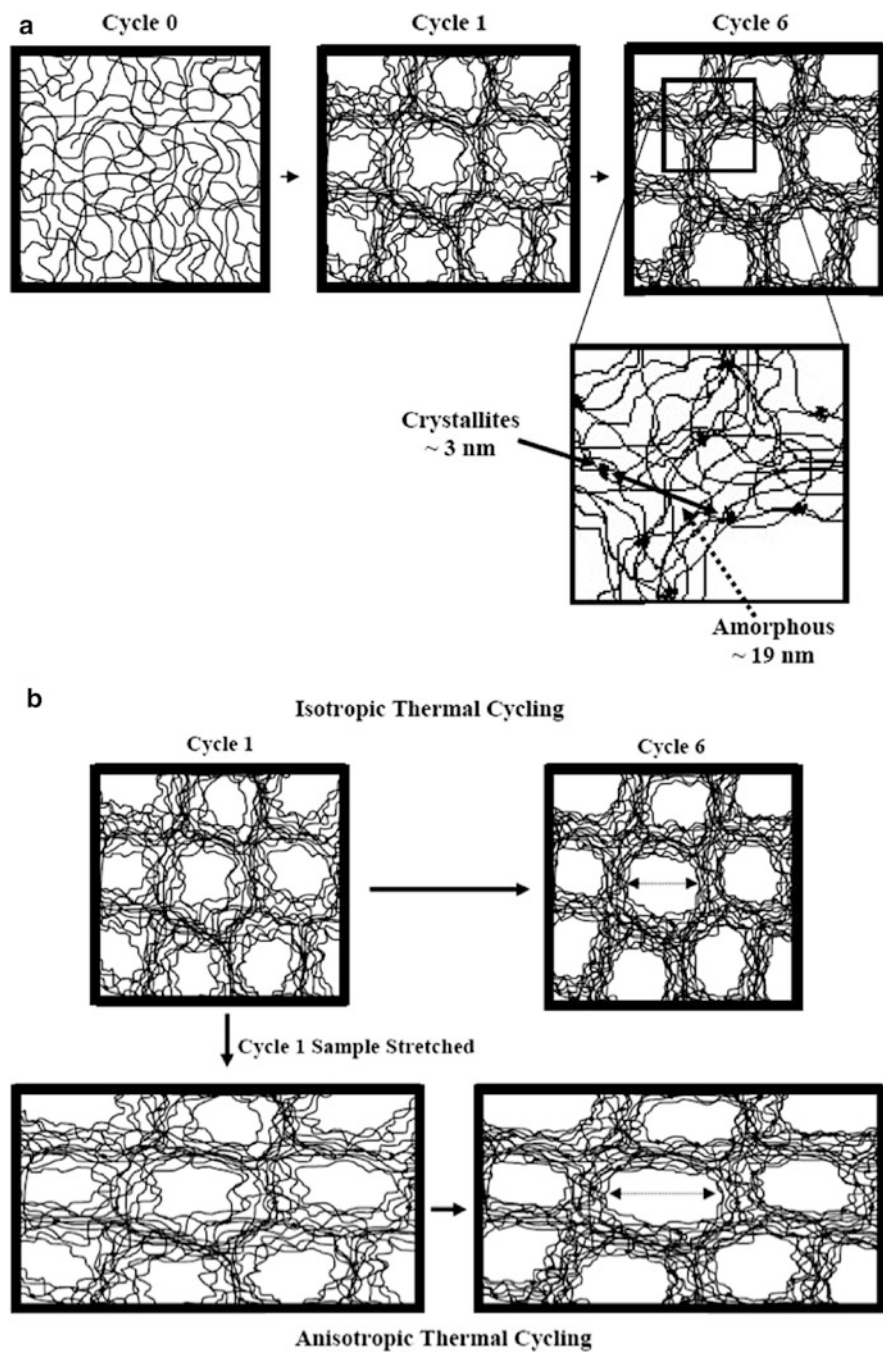
Fig. 1 (**a**) Effect of freeze–thaw cycles on the microstructure of PVA. (**b**) Effect of initial strain and freeze–thaw cycles in production of anisotropic PVA-C. Reprinted from [10] with permission. Copyright (2007) American Chemical Society
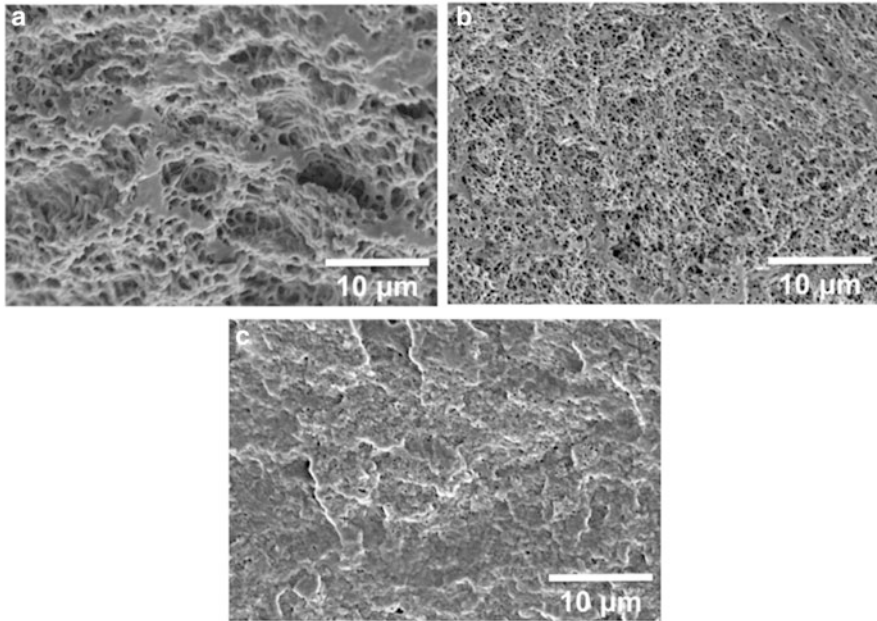
Fig. 2 SEM images of fractured cross-sections of critical point dried PVA-C of different initial concentrations: (**a**) 10 %, (**b**) 15 %, and (**c**) 20 %. Reprinted from [23]

increases the strength of the PVA-C. Figure 2 shows the effect of increasing initial PVA concentrations on the pore size of the PVA-C [23]. Willcox et al. used cryo-TEM to measure the pore size of 19 wt% PVA-C after 12 FTCs to be ~30 nm [9]. Nakaoki and Yamashita used thermodynamic equations to derive the pore size of 10 wt% PVA-C to be 30.2 nm [52].

Medical devices, depending on the physiological environment surrounding them, can be subjected to either compressive or tensile stress. Typical characterizations of the mechanical properties of a polymer material involve the measurements of its stress–strain curves, stress relaxation curves, and creep curves.

3.1.1 Compressive

The muscloskeletal system is a compressive stress environment. Any medical device in this system will operate under a state of compression. Compressive mechanical properties can be experimentally measured in either confined or unconfined conditions. Due to the porous nature of tissue, most experiments are carried out under unconfined conditions, in which the sample is compressed using nonporous platens and is allowed to expand at the circumferential direction without restrictions.
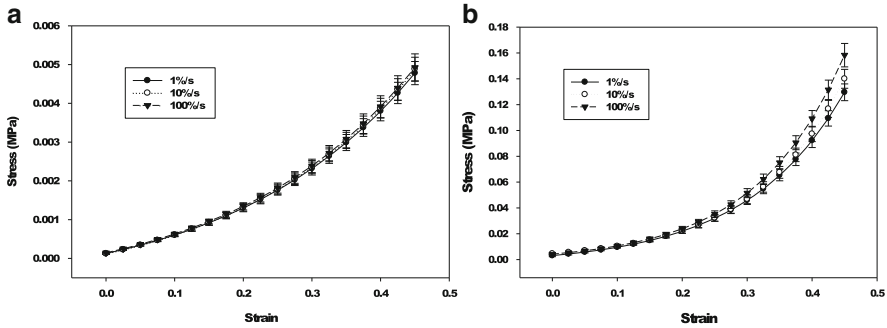
Fig. 3 Effect of strain rate on 10 % PVA of (**a**) one and (**b**) six FTCs. Reprinted from [45] with permission. Copyright © 2009 Wiley Periodicals

Stammen et al. performed unconfined compression on samples made from two formulations of Salubria, which is a commercial cryogel of PVA and 0.9% saline (but the number of FTCs were not specified in the paper), containing 80 wt% water (~20 wt% PVA) and 75 wt% water (~25 wt% PVA). They measured the Young's modulus and the compressive failure of the samples in 37 °C deionized water using a compressive ramp to 65 % at a strain rate of 100 %/min (1.67 %/s) and 1,000 %/min (16.67 %/s). Their objective was to mimic the physiological conditions of articular cartilage. The authors found that the compressive mechanical properties of Salubria were significantly affected by strain and strain rate, exhibiting nonlinear viscoelastic behavior [53]. At strains less than 40 %, the Young's modulus of the 25 wt% was consistently higher than the 20 wt% samples, irrespective of material strain rate; however, the trend reversed above 60 % strain. At 30 % strain, a strain rate increase from 100 to 1,000 %/min had a strong effect on the 25 % samples but not on the 20 % samples. The compressive Young's modulus for the 20 % and 25 % samples were 0.7–6.8 MPa (at a strain rate of 100 %/min) and 1.1–18.4 MPa (at strain rate of 1,000 %/min), respectively. The compressive failure for the 20 % and the 25 % samples were found to be around 45 % strain at 1.4 MPa stress and 60 % strain at 2.1 MPa stress, respectively [53].

Millon et al. performed unconfined compressive tests on 10 wt% PVA-C samples through 1, 3, and 6 FTCs. The samples were tested using strain-rates of 1, 10, and 100 %/s at 0–45 % strain at 37 °C to mimic the physiological conditions of cartilage. Figure 3 shows the strain-rate dependency of 10 % PVA at 1 and 6 FTCs. The authors concluded that PVA-C exhibits the same exponential characteristic in stress–strain behavior as cartilage. However, it has weak strain-rate dependency. Only the six-cycle samples showed a statistically significant difference between the strain rates tested. The elastic modulus measured was 1.18 MPa at 45 % strain and at 100 %/s strain rate [45].

Wang and Campbell performed unconfined compressive tests on 3, 5, 15, 25, 35, and 40 % (all wt%) PVA-C samples through 1, 3, and 6 FTCs using a strain rate of 2 mm/min (~0.28 %/s) with strain up to 25 % and temperature of 37 °C to mimic the physiological conditions of intervertebral discs in the lumbar section. The

Young's moduli were measured at 5 and 20 % strain. They found that the Young's modulus increased with an increase in strain, PVA-C concentration, and number of FTCs. The Young's modulus measured was between 0.001 and 2.117 MPa at all combinations of concentration, FTCs, and strain level [54].

Duboeuf et al. reported unconfined compression tests on 10 % PVA-C samples through 2–5 FTCs using a strain rate of 5 mm/min (~0.45 %/s) with strain up to 8 % at room temperature (22 ± 2 °C). They found that the stress–strain curves were linear and that the Young's modulus increased with the number of FTCs. The Young's modulus, measured between 3 and 8 % strain, was found to range from 0.065 to 0.167 MPa from two to five cycles. The authors also measured the stability of the Young's modulus over a 7-month period. For cycles 2 and 4, the authors found that the Young's modulus did not change significantly. However for cycles 3 and 5, there was a slight increase [55].

Nishinari, Watase, and coworkers studied the effect of degree of polymerization (DP) on the strength of PVA-C. They performed dynamic mechanical analysis on PVA-C samples of seven DPs (ranging from 470 to 17,900 of cycle 1) and of different PVA concentrations. The storage Young's modulus E' and the mechanical loss of the samples were measured using a 2-Hz excitation strain and at a temperature range of 2–85 °C at a rate of 2 °C/min. The authors found that the storage Young's modulus E' increased with concentration, and the same E' value could be obtained at lower concentration by increasing the DP [56]. In addition to the results outlined above, there were several other related studies that reported similar results [20, 57].

Based on the findings of the above papers, all concluded that the unconfined compressive Young's modulus of PVA-C is dependent on the strain, strain rate, DP of PVA, concentration of PVA solution, and the number of FTCs. The Young's modulus reported falls in the range 2–20 MPa, depending on the chosen composition, processing parameters, and the testing conditions used.

The compressive strength of PVA-C can be greatly enhanced by pre- and postgelation processes such as solvent dehydration and thermal annealing; however, these treatments will significantly reduce the water content of the PVA-C and its lubricating properties, which is undesirable for cartilage and other orthopedic applications. Bodugoz-Senturk et al. introduced a method to counteract this effect by adding poly(ethylene glycol) (PEG) and poly(acrylamide) (PAAm) to PVA, creating PVA-PEG theta gels and PVA-AAm hydrogels [58]. Unfortunately, instead of reporting improvements in compressive strength, they reported improvements in creep resistance.

3.1.2 Stress Relaxation and Creep

Stress relaxation characterizes how viscoelastic materials relieve stresses over time under a constant strain. Creep characterizes how viscoelastic materials deform slowly over time under constant stress. Both stress relaxation and creep are typically measured using the normalized value (stress or strain) versus time curve after stress or strain is applied at time zero.

Stammen et al. measured the stress relaxation curves for 20 and 25 % PVA-C by applying a 20 % constant strain and monitoring the stress relaxation for 24 h. They did not report the normalized stress-relaxation curves, instead they plotted the stress (in MPa) variation over time [53].

Millon et al. studied the stress relaxation properties of 10 % PVA-C after 6 FTCs by applying a 45 % constant strain and measuring the normalized stress relaxation for 1 h. They observed that the stress remaining after 1 h did not completely level off [45].

Wang and Campbell studied the stress relaxation curves for their samples by applying a 25 % constant strain and measuring the normalized stress relaxation for 30 s. They also performed creep measurement. The initial load was applied by compressing the samples at 4 mm/s (~33 %/s) up to 25 % strain or when it reached 223 N and holding the force for 30 s [54].

Wong performed creep measurements on 10, 15, and 20 % PVA-C of cycle 6 by applying a constant stress of 0.05 MPa over 1 h The test was done in phosphate-buffered saline. She found that the samples did not relax completely after 1 h and that increasing the PVA concentration decreased the amount of creep [23].

Due to the biphasic nature and microporous structure of PVA-C, when it is under compression, fluid will flow out of the PVA-C structure gradually until the hydro-static pressure reaches equilibrium with the external load. This explains the observed results that, as the concentration of PVA increases, the available water content decreases and the stress relaxation and creep effect decrease [23, 51, 53]. For the rate of stress relaxation, both Millon et al. [45] and Wong [23] found that after 1 h the PVA-C had relaxed to 45 % of its initial value but the relaxation still continued. Stammen et al. reported that the relaxation had attained equilibrium after 24 h [53].

3.1.3 Tensile

In many biomedical applications in the soft tissue environment or as soft tissue replacement, such as the cardiovascular system, the material will experience stress in tension. Knowledge of the tensile properties of PVA-C is therefore essential for its consideration for use in such physiological environments. The tensile properties of PVA-C have been measured by numerous research groups in the past. Typically, the properties are measured using a material testing system. The test is performed in deionized water or a buffer solution at room temperature or 37 °C. Tensile prop-erties are found to be affected by the average molecular weight or degree of polymerization and concentration of the PVA used, the number of FTCs the samples have undergone, the strain and strain rate employed, the post-hydration period, and the temperature and solution the samples are tested in. The resulting stress–strain curves have a typical "J" shape, are nonlinear, and very similar to those of soft-tissues.

Wan et al. researched into using PVA-C to mimic the tensile properties of the porcine aortic root and evaluated the feasibility of fabricating a stent prototype for
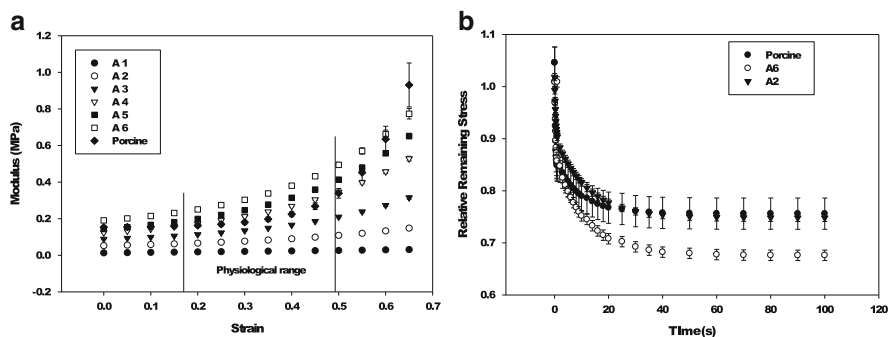
Fig. 4 (**a**) Tensile stress–strain curves of 15 % PVA-C through 1–6 FTCs (series *A*) in comparison with porcine aortic root. (**b**) Comparison of stress-relaxation properties of 15 % PVA-C of cycles 2 (*A2*) and 6 (*A6*) with porcine aortic root. Processing conditions of PVA-C: freezing rate 0.2 °C/min; thawing rate 0.2 °C/min; holding time at +20 °C 6 h; holding time at −20 °C 6 h. Reprinted from [7] with permission. Copyright © 2002 Wiley Periodicals

the bioprosthetic heart valve [7]. They subjected PVA solution with 15 wt% to 1–6 FTCs with a hold time of 6 h at −20 °C and thawing rate of 0.2 °C/min. The samples were tested under a constant strain rate of 40 mm/s (~200 %/s) to a maximum of 80 % strain at 37 °C. In addition, the samples were also subjected to stress-relaxation tests at 80 % strain held constant for 100 s. Figure 4a shows one of the results obtained from their tensile test experiments. It shows the typical J-shaped curves of the stress–strain characteristics of PVA-C in comparison with those of porcine aortic roots. Figure 4b shows the stress-relaxation results. The authors concluded that the variations in holding time at −20 °C had no significant effect on the tensile properties of PVA-C and that the slower thawing rate improved the tensile properties but did not affect the relaxation properties. The authors also determined that the stress–strain curves of 15 wt% PVA-C at cycle 4 best matched those of the porcine aortic root at 17–49 % strain. The typical Young's modulus was about 350 kPa at 120 mmHg pressure.

Millon et al. developed techniques to fabricate anisotropic PVA-C by applying an initial strain to the PVA samples in a given direction after they had undergone one FTC. The strain was held during subsequent FTCs. This resulted in an increase in the stiffness (Young's modulus) of the sample in the direction (longitudinal) of the applied strain. In the orthogonal (perpendicular) direction, stiffness remained comparable to the isotropic control sample. The direction in which an initial strain was applied resulted in a higher tensile strength than in the perpendicular direction. As soft tissues are typically anisotropic, the PVA-C fabricated using this technique provides a better matching of soft tissue properties than typical isotropic PVA-C. Figure 5a shows the effects on the stress–strain curves in the longitudinal and perpendicular directions of such PVA-C fabricated with an initial 25 % strain applied in the longitudinal direction, in comparison with a sample with no initial strain applied during the FTC. Figure 5b shows the effects on the Young's modulus of the resulting PVA-C with different initial strains applied during the FTCs [59].
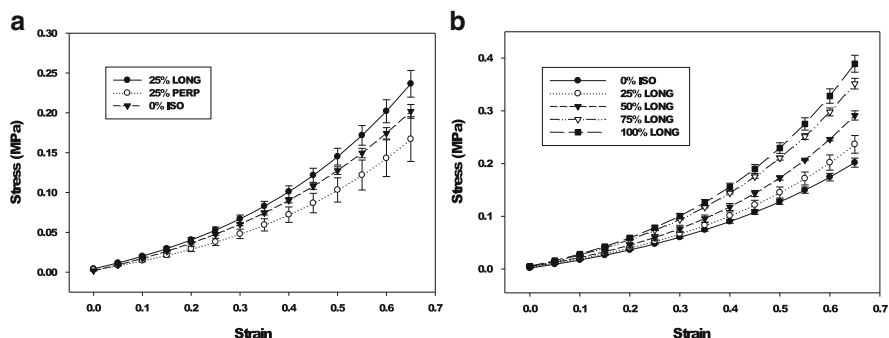
Fig. 5 (**a**) Stress–strain curves at the longitudinal and perpendicular direction of an anisotropic 10 % PVA-C of cycle 6 with an initial 25 % strain applied in the longitudinal direction during the FTCs. (**b**) Effects of variation of initial strains applied to PVA-C during the FTCs. Reprinted from [59] with permission. Copyright © 2006 Wiley Periodicals

Typically, tensile properties are measured using material testing machines, but Fromageau et al. developed a method to measure the tensile properties of PVA-C using four ultrasound elastography techniques. The authors measured the Young's moduli of 10 wt% PVA-C samples that had gone through 1–10 FTCs using this technique and compared the results with those obtained from tensile testing machines. Good correlations were obtained for samples from cycle 1 to cycle 6 [60].

3.2 Diffusion Characteristics

The porous structure of PVA-C, comprised of crystalline regions (~3 nm) and amorphous regions (~19 nm) [10], allows for diffusion of molecules from the cryogel matrix. Work reported by Stauffer and Peppas showed that the water diffusion coefficient decreased as the number of FTCs increased [37], with a diffusion coefficient decrease of 62 % occurring between the second and fifth FTC.

Hickey and Peppas showed that diffusion of solutes from a PVA cryogel membrane is related to the mesh size, which is roughly related to the percentage crystallinity. Also, there is a size exclusion phenomenon present as a result of the presence of the crystallite network. The solute diffusion coefficient for theophylline and FITC-dextran was determined to be dependent on the mesh size [61].

Release of protein (bovine serum albumin, BSA) molecules from PVA cryogel nanoparticles was studied by Li et al. [62]. The authors found that the release was diffusion controlled and that approximately 95 % of the total incorporated protein was released within 30 h. Furthermore, BSA remained stable during the preparation process. It was shown that diffusion increased as temperature increased, and decreased as the number of FTCs increased from one to three. These observations
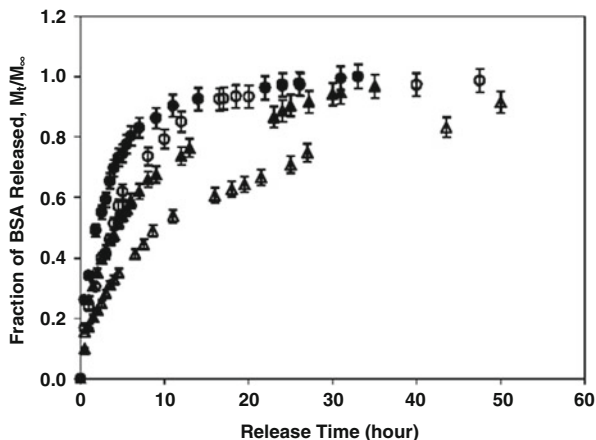
Fig. 6 Release profiles of BSA from PVA hydrogels subjected to 1 (*filled circle*), 2 (*open circle*), 3 (*filled triangle*), and 6 (*open triangle*) FTCs. These hydrogels were composed of 10 % (w/w) PVA, 0.10 % (w/w) BSA. The freezing and thawing rates were both at 0.50 °C/min
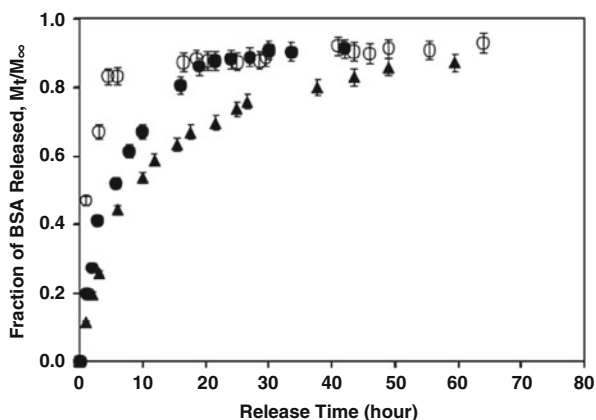
Fig. 7 Effect of thawing rate on the release of BSA from the PVA hydrogels subjected to two FTCs. These hydrogels were prepared using a fixed freezing rate of 0.10 °C/min and varying thawing rate of 1.00 (*open circle*), 0.25 (*filled circle*), and 0.10 °C/min (*filled triangle*). These hydrogels contained 10 % (w/w) PVA and 0.10 % (w/w) BSA

are consistent with what is known about the PVA matrix structure and the effects of changing the processing parameters [62]. Building on these results, a comprehensive and systematic study was undertaken by our group to provide a global view of the effect of processing (number of FTCs, freezing rate, thawing rate) and composition (PVA concentration) parameters on protein release. PVA-C films prepared by freeze–thaw cycling were used as model drug delivery vehicles with BSA as the model protein. The results are summarized in Figs. 6, 7, and 8. Consistent with the

Fig. 8 Release profiles of
BSA from PVA hydrogels
composed of varying
concentrations of PVA at
8 (*open circle*), 10 (*filled
triangle*), and 15 % (w/w)
(*filled circle*). The
hydrogels contained 0.50 %
(w/w) BSA and were
subjected to two FTCs at a
constant freezing and
thawing rate of 0.10 °C/min
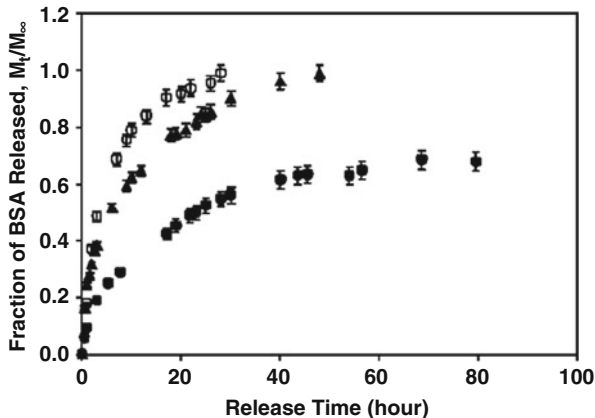
earlier study, it was found that BSA release was mainly by means of a diffusion
mechanism. The diffusion coefficients of BSA could be controlled over a 20-fold
range by adjusting the processing parameters, including the number of FTCs, PVA
concentration, and freezing and thawing rates.

Increasing the number of thermal cycles decreases the release rate (Fig. 6).
Every thermal cycle after the first FTC resulted in an increase in the local PVA
concentration in the polymer-rich regions concomitant with an increase in the
volume fraction of the crystalline regions [61]. This leads to an increase in the
time required for the movement of BSA through the amorphous zones of the
polymer-rich region, resulting in the observed decrease in the release rate.

Decreasing the freezing rate also decreases the release rate at constant thawing
rate. The effect of changing thawing rate is similar to that of changing freezing rate
(Fig. 7). A decrease in the freezing or thawing rate allows more time for the
polymer chains to reorganize themselves into ordered domains, resulting in an
increase in the volume fraction of crystalline PVA and/or increase in the size of
the crystalline domains. This leads to a decrease in BSA mobility in the PVA matrix
and thus to a decrease in its release rate.

Increasing the PVA concentration in the PVA-C preparation solution decreases
the rate of BSA release (Fig. 8). An increase in PVA solution concentration results
in a higher polymer concentration in the polymer-rich region after a fixed number of
thermal cycles. This decreases the mobility of BSA, leading to an inverse relation-
ship between PVA solution concentration and release rate.

The BSA release rate can be contrasted to that reported for the mechanical
properties of PVA-C prepared under similar conditions. The trend in the BSA release
rate as a function of PVA solution concentration and number of thermal cycles is
analogous to that reported for the mechanical properties of PVA-C. It is interesting to
note that, although freezing and thawing rates have an effect on BSA release rate, the
thawing rate has a greater effect than that of the freezing rate. In addition, the effects
of these two parameters on the PVA-C mechanical properties are quite different.
Decreasing the thawing rate leads to significant increases in the mechanical proper-
ties, whereas changing the freezing rate had little or no effect [7, 63, 64].
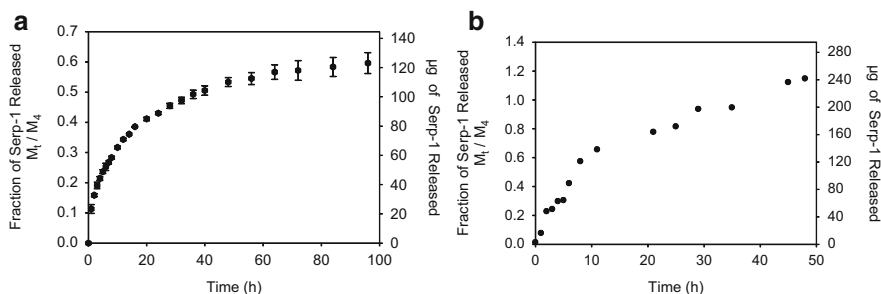
Fig. 9 (**a**) Release profile of Serp-1 from PVA-C in a buffer medium. PVA-C samples were prepared using 10 % PVA solution, 0.1 °C/min freezing and thawing rate, two FTCs, and 200 μg Serp-1. (**b**) Release profile of Serp-1 from PVA-C in human whole blood medium. PVA-C samples were prepared using 10 % PVA solution, 0.1 °C/min freezing and thawing rate, two FTCs, and 200 μg Serp-1. Reprinted from [65] with permission

Although the close parallel between the effects of processing parameters on diffusion and the mechanical properties of PVA-C can be clearly seen, the structural characteristics leading to these observations are quite different. For mechanical properties, the changing stiffness as a function of processing condition is a result of the changing volume fraction of crystalline regions of the material. On the other hand, the diffusion properties are more a function of the properties of the amorphous zone of the polymer-rich regions, largely affected by PVA concentration. Indirectly, the crystalline regions affect the amorphous zone by dictating how tightly the polymer chains are packed, thus making the number of FTCs, freezing rate, and thawing rate contributing parameters to the diffusive properties. Irrespective of the origin of these two observed properties, they could be used to create medical devices with integrated controlled release function, such as the drug-eluting coronary stent, by tuning the mechanical and diffusion properties of the PVA hydrogel simultaneously.

A recent study reports the release profile of the Serp-1 proteinase from PVA-C [65]. Serp-1 is a serine proteinase inhibitor (serpin) secreted by the myxoma virus and is a potential new therapeutic for cardiovascular diseases. It has exhibited anti-inflammatory activity through the modulation of immune cell responses [66]. The release profile of this protein in a buffer medium is typical of that of a diffusion controlled process. However, it is interesting to know that the release rate of Serp-1 and its final release level attained differ in human blood and in buffer. The release rate is twice as fast and in half of the time in blood than in buffer. The final release level is complete in blood and appears to level off at around 50% in buffer. It was suggested that there may be a difference in behavior between the two release media, which is important to consider because human whole blood represents a more realistic setting of the physiological environment in arteries. It is also possible that interaction between PVA-C and blood components play a role in determining the ultimate release rate (Fig. 9a, b) [65].

4   PVA Composite Cryogels

PVA-C composites are prepared by the addition of fillers into the PVA solution before the freeze–thaw process. The main purposes of filler addition are for improving mechanical properties and for controlled release and delivery. A wide variety of filler materials that vary in dimensions from micro- to nanometers have been reported, but here we focus on two widely studied filler materials for their relevance in biomedical applications: bacterial cellulose and chitosan.

4.1   Cellulose-PVA Composites

Bacterial cellulose (BC), a biocompatible natural polymer, has been studied significantly for the production of composite materials for biomedical applications. Its polyfunctionality, hydrophilicity, and biocompatibility [67] make it a desirable material for many different biomedical applications. It is a nanomaterial of roughly 50 nm diameter [68]. Cellulose produced by bacteria has high crystallinity, mechanical strength, the capacity to absorb water, and a large aspect ratio [69, 70]. The use of BC as a composite material for PVA that has been crosslinked using freeze–thaw cycling has so far been limited. The fabrication and use of this composite material with its advantageous properties for biomedical applications will be discussed here.

Wan et al. found that the addition of BC nanofibers to a PVA solution that was then thermally cycled resulted in a PVA-BC composite cryogel that could be tuned to possess the mechanical properties of cardiovascular tissue. BC and PVA-C mimic the role of collagen and elastin, respectively, in soft tissues, making PVA-BC a good candidate material for possible use as a cardiovascular tissue replacement [42]. With the addition of 0.6 wt% BC, the nanocomposite material had higher strength (for FTCs 1–3) and also possessed a broader range of mechanical property control. Because the BC has a very large surface area per unit mass, there is opportunity for significant hydrogen bonding with the PVA matrix, both BC and PVA being hydrophilic polymers. This bonding results in the high strength of the nanocomposite material. The material can be tuned easily by changing processing parameters. Particular compositions of this material were able to show excellent matching with the stress–strain properties of porcine aorta as well as porcine heart valve. Additionally, the material showed faster relaxation and a lower residual stress, which are desirable characteristics for cardiovascular soft tissue replacement applications [42].

The PVA-BC nanocomposite is able to provide a wide range of mechanical properties, depending on the processing parameters chosen for the material's application. As discussed in Sect. 3.1.2, the addition of an initial strain following the first FTC can produce a cryogel with anisotropic mechanical properties. Cardiovascular tissue is composed of the structural proteins collagen and elastin, and is

Fig. 10 Effect of addition of bacterial cellulose (BC) on the compression elastic modulus of the PVA-BC nanocomposite as a function of the number of FTCs at 45 % strain and 100 %/s strain rate. Reprinted from [45] with permission. Copyright © 2009 Wiley Periodicals
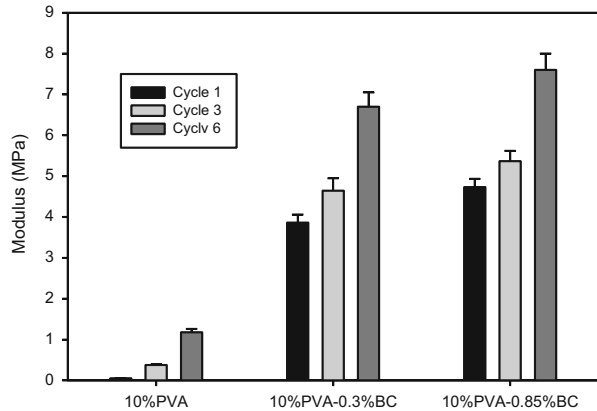
anisotropic with a higher stiffness in the circumferential direction compared to the axial direction [71–73]. For replacement of tissue such as this, or other soft tissue, a composite material that possesses anisotropic properties could be extremely beneficial. Millon et al. prepared PVA-BC samples and found that, compared to the plain PVA system [59], the addition of BC resulted in an almost doubled anisotropic effect, with the overall mechanical properties of the composite material dominated by changes in the longitudinal direction. This is probably due to the fact that the BC crystallites act as nucleation sites during freeze–thaw cycling and therefore promote formation of PVA crystallites around the BC fibers when strain is applied. Stiffness in both directions was found to increase with an increase in the number of FTCs. The anisotropic PVA-BC demonstrated stiffness and relaxation properties very similar to those of the porcine aorta, proving to be an excellent material for potential applications [59].

Following this work, Wan et al. conducted studies on the PVA-BC composite cryogel material for potential use in total joint replacement. In this application, the mechanical properties must be tuned to replicate the properties of the articular cartilage, with its composition of collagen fibrils and proteoglycans. Through compression testing, it was determined that as the number of FTCs increases, the stiffness of the composite material increases. This was consistent with previous results and knowledge. Additionally, stiffness increases with increasing amounts of BC in the PVA matrix. A small increase in weight percent of BC (from 0 to 0.3 %) results in a significant increase in the composite material's compressive properties. This is shown in Fig. 10. Stress relaxation tests show that the remaining relative stress decreases with an increase in BC concentration. These results are accounted for by the fact that addition of a highly crystalline, hydrophilic BC as a reinforcing biomaterial causes a strong interfacial interaction with the PVA matrix, resulting in significant hydrogen bonding and, thus, creating a stronger material. This could have potential for several biomedical applications [45].

A study conducted by Wang et al. employed the use of PVA-BC produced by freeze–thawing as a composite material for use as an artificial cornea replacement.

The work showed that this composite material is able to achieve similar mechanical properties as the natural cornea and better than pure PVA-C. The composite containing 12 wt% BC had a tensile strength of 3.9 MPa, which is very close to the human cornea tensile strength of about 3.8 MPa [74–76]. Furthermore, the water content of the PVA-BC composites decreases as BC concentration increases. However, composite water content was close to that of the human cornea (78 % [77]) at 67–73 %. Of utmost importance for this application is light transmittance of the material. PVA-BC composite was found to have a high visible light transmittance. Some of the tested compositions actually had a higher transmittance of visible light than pure PVA, due to the nano-effect of the BC nanofibrils. In addition, PVA-BC has good UV absorbance, which is important in preventing damage to internal eye tissue. Overall, this composite material is promising for use as an artificial cornea material [78].

4.2 Chitosan-PVA Composites

Another material that has been added to PVA to produce a composite cryogel is chitosan. Chitosan is obtained from chitin by alkaline deacetylation. It is a cationic polysaccharide, and has been proposed as a good material for addition to the PVA matrix for cryogel composite production in order to enhance protein absorption [79]. Due to the hydrophilicity of PVA, cell adhesion proteins are not able to absorb, preventing cell adhesion [79]. Because of this, work to create a more favorable environment for cell growth while still maintaining the beneficial mechanical properties of the PVA cryogel structure is important for certain applications.

PVA cryogels used for vascular tissue engineering scaffolds were modified to improve cell attachment [80]. In this work, chitosan was added to PVA because of its ability to improve vascular smooth muscle and endothelial cell attachment. The blend was subjected to FTCs, immersed in a KOH/Na$_2$SO$_4$ coagulation bath, and the surface modified with collagen type I. The structures were then seeded with bovine aortic vascular smooth muscle and endothelial cells. The presence of chitosan resulted in cell attachment to the surface in patches, which suggests that the regions of high cell density are chitosan-rich and that the other areas are chitosan-poor. Cell attachment and proliferation were shown to increase with an increase in FTCs. Since the coagulation bath treatment essentially eliminates the mechanical difference between samples of different numbers of FTCs, the surface topography is suspected to be responsible for this difference [80].

In another study that focused on the mechanical and morphological properties of PVA-chitosan cryogels, water-soluble chitosan with a deacetylation degree of 85 % (WSC), and water-insoluble chitosan (WIC) were added to PVA separately to produce two different chitosan-PVA cryogel materials, as well as a control plain PVA cryogel. After freeze–thaw cycling, the samples were submerged in a coagulation bath to crosslink the chitosan, because it would not be crosslinked by

thermal cycling, as well as to neutralize the low pH due to the presence of acetic acid. It was found that, again, the number of FTCs has an impact on the mechanical properties. Both WSC and WIC samples demonstrated similar elastic behavior, and the PVA-chitosan samples provided a fairly good replication of the stress–strain behavior of porcine aortic tissue. The macroporous structure was shown to change with the addition of chitosan. For plain PVA, the structure changed visually as the number of FTCs increased, but the change in pore size was not statistically significant after one, two, and four FTCs. When either WSC or WIC was added, the internal structure changed significantly as a function of the number of FTCs. After the second FTC, the pore size increased, and it increased again after the fourth FTC. This study was effective in showing that, although the addition of chitosan may be beneficial for cell adhesion, we cannot ignore the effects that it has on the PVA-C macrostructure and mechanical properties [81].

A system comprised of PVA and chitosan was produced for use as a drug delivery vehicle for the antibiotic sparfloxacin, as well as for use in an antibacterial wound healing device. The addition of chitosan for drug delivery systems can be done to help sustain the release of water-soluble drugs or enhance the availability of water-insoluble drugs. Chitosan also has an intrinsic antimicrobial activity. Different compositions of PVA and chitosan were made and processed through freeze–thaw cycling. Results showed that swelling percentage and gel fraction percentage increased with an increase in chitosan concentration and decreased with an increase in PVA concentration and the number of FTCs. The amount of polymer degraded over a fixed time increased with an increase in chitosan content or a decrease in FTC number. Antimicrobial activity for a variety of Gram-positive and Gram-negative bacteria was tested and it was found that no antimicrobial activity was present at low chitosan percentages but increased as chitosan content increased. Sparfloxacin was added to the chitosan/PVA blend solution before freeze–thaw cycling and its release was determined to be affected by the thickness of the membrane, pH, and temperature of the medium. The total amount of drug released was decreased with an increase in pH due to the presence of NH_2 within the hydrogel structure that can be ionized at low pH to allow for release. The drug release increased with an increase in thickness and media temperature. This system shows how the addition of chitosan to the PVA cryogel can impart important antimicrobial activity, as well as provide a temperature- and pH-responsive system for drug release [82].

A comparison of composite materials using chitosan, gelatin, and starch added to PVA was reported [79]. A sample for each different component added to PVA was prepared and treated with freeze–thaw cycling and coagulation techniques for application as artificial blood vessels. The resulting mechanical properties were found to be controlled by the PVA rather than by the other components. Each PVA composite sample was found to have similar stiffness behavior to arteries. Increasing the number of FTCs as well as coagulation bath treatment (7.5 % KOH and 1 M Na_2SO_4) increased the modulus of the hydrogels. Coagulation bath treatment was also shown to increase the resistance of the hydrogel to degradation. Cell adhesion and proliferation studies showed that the addition of a composite material was

beneficial for both cell adhesion and proliferation relative to plain PVA-C. The addition of gelatin was most effective in improving these factors compared to addition of chitosan or starch [79].

5   Biomedical Applications

The properties of PVA-C summarized and reviewed thus far demonstrate many of the desirable properties that make it the material of choice for a broad range of biomedical applications. Using the freeze–thaw cycling procedure, PVA-C can be prepared with both tunable mechanical properties and diffusion properties. With the addition of biocompatible nanofillers such as bacterial cellulose and chitosan, the range of these properties can be further broadened. The diffusion properties and some applications of PVA-C for controlled release and delivery have already been covered (see Sect. 3.2). The focus of this section will be on the use of PVA-C as a material for medical devices.

5.1   Medical Devices

With tunable properties and the ability to create anisotropic orientation-dependent mechanical properties, PVA-C and its composites are suitable candidate materials for medical device application. In this section, we will focus on the use of PVA-C in cardiovascular devices, including vascular grafts and heart valves, and in orthopedic devices, including cartilage and intervertebral discs.

5.1.1   Orthopedic Devices

Orthopedic devices are used for repair and/or replacement in the musculoskeletal system, which is under varying amounts of compressive stress. In considering the use of PVA-C in orthopedic applications, its compressive mechanical properties (discussed in the section on mechanical properties, Sect. 3.1.1.) are the most important parameters to be taken into account.

5.1.2   Intervertebral Discs

Intervertebral discs (IVD) maintain the space between vertebrae. This gap serves as a passageway for spinal nerve bundles to pass through to various parts of the body from the spinal cord. It also allows for motion in the spine, distributes and transfers load to the vertebrae, and provides shock absorption [83]. As humans age, the IVDs degenerate. As a result, some may lose their original thickness or mechanical

integrity. Diseases of the IVD are among the causes of neck and back pain [84, 85] that lead to work absenteeism [86], disability claims [87, 88], and a decrease in the quality of life [89]. IVDs are cartilaginous, composed mainly of collagen and proteoglycans, and have a high water content [84, 90, 91]. They also have low cell numbers and little to no vascularity [84]. Therefore, IVDs have limited ability to heal and regenerate to regain function. The main surgical treatment is to fuse adjacent vertebrae together. However, this approach limits the movement of the patient and effectively shifts the stress to the adjacent vertebrae, developing problems down the road. In recent years, total disc replacement is gaining popularity. The FDA had approved several IVD prosthetic devices. These are mainly made from metal and are typically designed for supporting the bodily load and movements, but with questionable shock-absorbing capabilities. PVA-C prosthesis for IVD total replacement has potential because of its shock absorption capability and biocompatibility.

Wang and Campbell measured the characteristics of PVA-Cs made with varying PVA solution concentrations (3–40 %) and FTCs (1–6) in an attempt to match the mechanical behavior of IVDs based on the Young's modulus, stress relaxation, and creep characteristics under simulated physiological conditions. The authors were only able to match the stress-relaxation and creep characteristic of the IVDs [54].

Instead of total disc replacement, another approach is the replacement or reinforcement of the nucleus pulposus (NP) at the center of the disc with a material that can re-inflate the disc to restore disc height and function. Materials tested include stainless steel ball bearings, polymethylmethacrylate, and silicon, all without much success. More recently, NP implants have been made from cycle-6 cryogels fabricated from a mixture of PVA and polyvinyl pyrrolidone (PVP) with a ratio varying from 1 to 5 % by weight. The implants have been tested and found to better match the physical properties of the NP [92].

Future research efforts in IVD arthroplasty should focus on either partial or full disc functional restoration. This may include NP implants and/or reinforcement or total disc replacement. PVA-C, as a hydrogel, has many interesting properties, such as its long-term biocompatibility and nontoxicity. It is also strongly hydrophilic and viscoelastic with nonlinear stress–strain characteristics similar to the IVD. It has a very low coefficient of friction and has good wear resistance [23]. However, its strength is still too low to serve as a practical functional replacement of the annulus fibrosus. PVA-BC may further increase the strength of the PVA-C to make it a viable candidate material for IVD fabrication.

5.1.3 Cartilage

Damaged cartilage can occur from sports or accident-related injuries, as well being a result of degenerative joint disease, which is very common. Total joint replacement is one of the main approaches for treating cartilage degeneration. There is need for a synthetic biomaterial that can mimic the natural cartilage tissue for this purpose. Commonly, ultrahigh molecular weight polyethylene (UHMWPE) is used

as the articular cartilage component, but is not a good match for the mechanical properties. The shock absorption, lubrication, and deformation are inadequate and cause high levels of wear [45]. PVA-C has been studied as a candidate for use as artificial cartilage tissue due to its high water content, viscoelastic properties, and porous structure, all contributing to the resemblance to natural articular cartilage tissue. Furthermore, the natural articular cartilage has been described as possessing biphasic lubrication qualities, which allow movement of fluid away from the contact site over a period of loading. This lubrication, which is intrinsic to natural join tissue, should be mimicked by artificial replacements [93]. According to Oka et al., the requirements for a good artificial articular cartilage material include good lubrication, sufficient shock-absorbing ability, good biocompatibility, firm attachment to the bones underneath, and high resistance to wear [94].

It was been shown that under both tension and compression, PVA-C displays nonlinear mechanical properties and viscoelastic behavior [95]. Additionally, PVA-C has been observed to have better wear resistance and friction coefficient than UHMWPE [96, 97].

Oka et al. used PVA dissolved in a mixture of water and DMSO to prepare PVA-C and study its properties as artificial articular cartilage. They found that the PVA-C sample allowed a fluid-filled gap, very similar in thickness to the joint space present in natural articular cartilage, to be maintained between the sample and the counter-surface under loading. This is beneficial in maintaining proper fluid film lubrication and weight bearing. In addition, PVA-C displayed a good damping effect by having a lower peak stress value and maintained it for a longer period of time under loading [94].

Articular joints are exposed to compressive forces that are applied very quickly, as well as to very large shear forces. Stammen et al. [53] recognized PVA-C as a viable option for total joint replacement but only if the load-bearing properties could be matched with those of natural tissue. Studies of the compressive tangent modulus and shear tangent modulus were undertaken for the PVA-C product, and a limited strain-rate dependence under unconfined compression was displayed.

Kobayashi et al. were able to use PVA cryogels as an artificial meniscus in animal models. The mechanical properties and viscoelastic characteristics as well as biocompatibility of the material are beneficial for this application. PVA was processed in a DMSO/water solvent, vacuum dried, and heated for annealing. It was then left in water, cut and processed into meniscus form, and used as a prosthesis in rabbits. The samples remained intact for up to 2 years and no fracture or degradation of its mechanical properties occurred. Biocompatibility was also found to be satisfactory [98].

Swieszkowski et al. studied the use of PVA-C as cartilage replacement for the shoulder joint. PVA-C was used as the articular layer of the glenoid component. The mechanical effects of using this material in the glenoid component were evaluated and a model of the cryogel as a hyperelastic material was developed to allow design modifications to limit contact stress [96].

To overcome the issues of limited durability and poor adhesion to tissue, Pan et al. incorporated nano-hydroxyapatite (nano-HA) into the PVA-C matrix

[99]. Nano-HA has been used as a biomaterial for bone repair because it provides bioactive properties and increases adhesion between the natural tissue and composite biomaterial. The nano-HA improves osteoblast adhesion to the biomaterial surface, providing a bioactive bonding interface. The composite material displayed typical viscoelastic properties, with the elastic properties being contributed by the crystalline regions of the PVA and the nano-HA particles, and the viscous characteristics coming from the amorphous PVA regions and incorporated free water. The addition of nano-HA changed the tensile properties of the material by increasing the strength with an increase in HA weight percent, until 4.5 wt%, at which point the strength begins to decrease with an increase in HA content. These trends were accounted for by the increase in interfacial bonding strength between nano-HA particles and polymer matrix, until a certain point at which agglomeration of nano-HA particles reduces the composite strength. The tensile modulus was shown to increase initially with an increase in nano-HA content and then decrease and stabilize due to improved rigidity and decreased degree of crystallinity occurring simultaneously as nano-HA content increased. The effect of elongation and freeze–thaw cycle times on the tensile modulus was studied and it was found that the tensile modulus increased linearly as elongation ratio increased and also increased as FTC time increased. The relationship of tensile modulus and elongation is similar in the composite material and in natural articular cartilage because good deformation ability occurs under low stress conditions. The biomaterial can better withstand high stress conditions due to its higher tensile modulus. These properties are beneficial for a material that must withstand both low and high stress activities, uniformly distribute stress across the tissue, and resist large compressive forces to prevent tissue damage [99].

Another composite material, PVA-BC (described in Sect. 4.1), was studied by Millon et al. as a potential material for cartilage tissue replacement. Bacterial cellulose added to PVA to form a nanocomposite cryogel showed improved strain-rate dependence and good viscoelastic properties for mimicking natural cartilage tissue [45].

Research efforts so far indicate that PVA-C and its composites are promising artificial cartilage replacement materials. Future research efforts should focus on increasing the strength and stiffness of PVA-C. This could be achieved by better-designed nanocomposites. Another challenge is the incorporation of strain-rate dependence properties into the PVA-C material, which are essential for it to withstand high rates of stress changes and function like natural cartilage tissue.

5.1.4 Cardiovascular Devices

Due to the necessity of maintaining blood flow in the cardiovascular system, a positive pressure is always maintained within the system. As a result, tissues making up the system are always under pulsatile tensile stress. In considering the use of PVA-C in cardiovascular applications, its response to pulsatile tensile stress must be taken into consideration. Mechanical property parameters of relevance
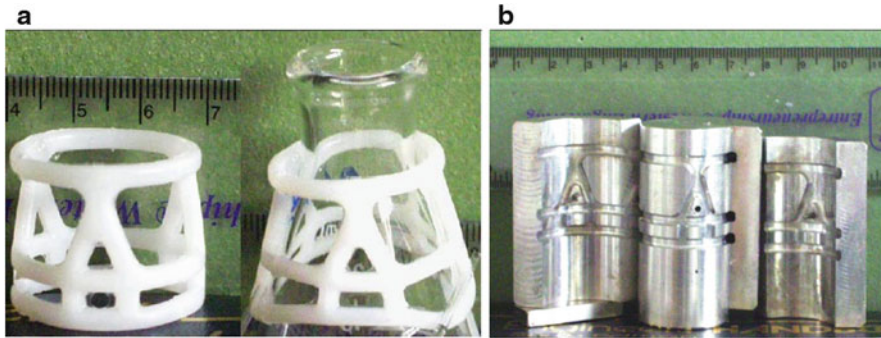
Fig. 11 (**a**) PVA-C heart valve stent in natural state and deformed state. (**b**) Four-part injection mold for the PVA-C heart valve stent. Reprinted from [7] with permission. Copyright © 2002 Wiley Periodicals

include Young's modulus and stress relaxation properties. These parameters have been discussed in the section on mechanical properties (Sect. 3.1).

The aortic heart valve, which controls the flow of oxygenated blood from the left ventricle into the ascending aorta for distribution to the whole body, is prone to failure. The most common types of artificial replacement are the mechanical and the bioprosthetic heart valves, but they both have shortcomings. One of the early attempts to use PVA-C to alleviate the mechanical problems that can lead to tissue tearing, calcification, and eventual failure of the bioprosthetic heart valve addressed the lack of expansibility of the mounting stent [7]. The PVA solution composition and freeze–thaw cycling processing conditions for the preparation of PVA-C that best mimics the mechanical properties of the porcine aortic root were determined. A prototype heart valve stent was designed and produced using selected PVA-C processing conditions. This study showed that PVA-C can be prepared with tensile and relaxation properties that span a fairly broad range, thus opening the possibility of their use in soft tissue replacement applications (see Fig. 11a, b).

A subsequent study explored the use of PVA-C to produce a one-piece trileaflet heart valve. In this case, a separate heart valve stent is not necessary [100]. A prototype valve was designed and produced using PVA-C (shown in Fig. 12). Using a cyclic flow tester, opening and closing of the PVA-C heart valve prototype was successfully demonstrated. A beneficial property of this design and the choice of PVA-C as the valve material is that the heart valve can be compressed temporarily into a small size so that it can be inserted into the chest cavity through a keyhole incision, thus alleviating the need for open heart surgery [100].

Because natural tissues have anisotropic mechanical properties, in order to better replicate the properties of soft tissue, specifically cardiovascular tissues such as heart valve leaflet and vascular conduits, these anisotropic mechanical properties should be incorporated into the design of PVA-C. PVA-C prepared by the standard freeze–thaw cycling process is isotropic, with mechanical properties independent of sample orientation. Millon et al. [59] produced anisotropic PVA-C by subjecting the hydrogel to an initial controlled unidirectional strain after the PVA solution

Fig. 12 PVA-C heart valve prototype constructed using the arc subtending two straight lines geometry that integrates into a single part the three leaflets, stent, and sewing ring. Reprinted from [100] with permission. Copyright (2004) Elsevier
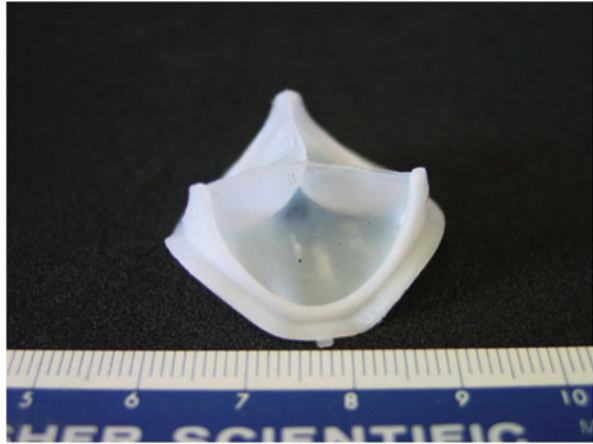
underwent the first thermal cycle of the freeze–thaw cycling process [59]. This changed the microstructure of the PVA-C, causing the crystallites to orient in the direction of the stress. Details of the nanostructure of the anisotropic PVA-C have been studied using SANS and USANS [11]. Differences for tensile properties between the longitudinal and perpendicular directions increased as the initial strain applied after the first cycle was increased. The porcine aorta has a higher strength in the circumferential direction than in the axial direction by a factor of 1.75 at a strain of 65 % [42]. These properties are closely matched by the anisotropic PVA-C prepared using three FTCs at an initial strain of 75 %. Finally, stress relaxation tests show that the anisotropic PVA relaxes as fast as porcine aortic tissue and to a lower residual stress, making it a promising material for aortic tissue replacement applications, including heart valves and vascular grafts. Preparation of prototype vascular grafts using the anisotropic PVA-C has been demonstrated [10].

In the process of expanding the mechanical properties range of PVA-C by the creation of the PVA-BC nanocomposite [42], an anisotropic PVA-BC nanocomposite was also prepared using a procedure similar to that for the anisotropic PVA-C [59]. This anisotropic PVA-BC nanocomposite proved to be a material that possesses mechanical properties that closely match those of the porcine aorta, thus making it an attractive material for replacement vascular graft preparation and other cardiovascular applications. The material properties of the anisotropic PVA-BC have been incorporated into the design of a one-piece trileaflet heart valve using a nonlinear finite element modeling method [101].

5.2 PVA-C Tissue Hybrid

For medical device application of PVA-C, it is certainly important that its mechanical properties closely match the tissue it is replacing and are compatible with the tissue environment it is implanted into. However, for cardiovascular devices, which
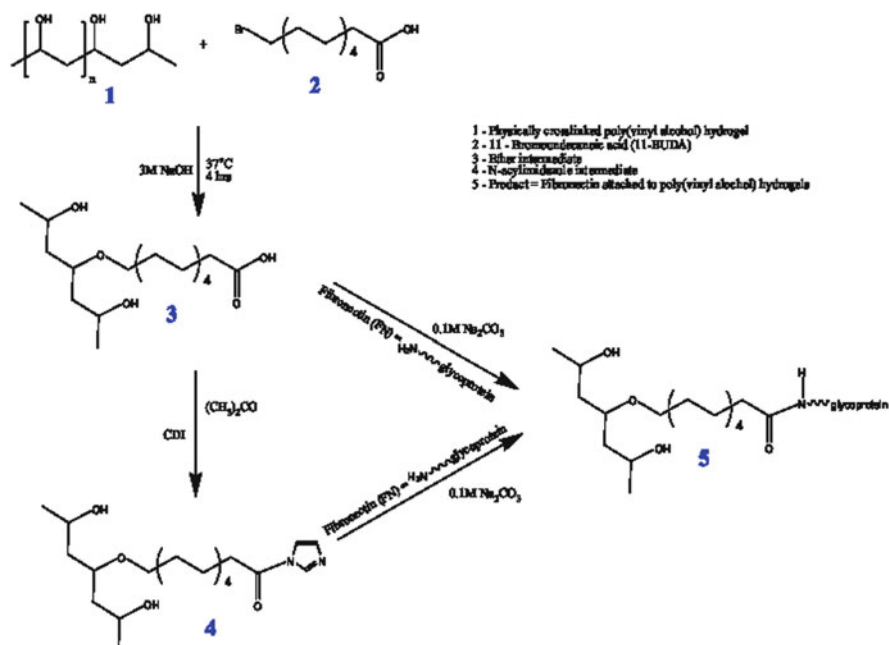
Fig. 13 Schematic of PVA hydrogels functionalized via fibronectin by two pathways: a simpler route (path 1) works well for PVA-C ($1 + 2 \rightarrow 3 \rightarrow 5$). For chemically crosslinked PVA hydrogels, the route necessary (path 2) requires an additional step involving the reagent carbonyl diimidazole (*CDI*) ($1 + 2 \rightarrow 3 \rightarrow 4 \rightarrow 5$). Reprinted from [110] with permission. Copyright (2011) Elsevier

have direct blood contact, PVA-C would also have to be hemocompatible. Unfortunately, as with most synthetic materials, PVA is not hemocompatible [102]. One way to overcome this is to create a hemocompatible surface for PVA-C. In vascular tissue, hemocompatability is provided by a monolayer of vascular endothelial cell on the tissue surface. PVA, being a very hydrophilic polymer, is not conducive to cell adhesion [103]. Many approaches have been tried to promote cell adhesion to the PVA surface with varying degrees of success [79, 104–109]. We have recently reported two approaches that successfully functionalized the PVA-C surface for cell adhesion, including the vascular endothelial cells that are required for hemocompatibility. The resulting material consists of mechanically tuned PVA-C and a living interface of vascular endothelial cells. It can be regarded as belonging to a novel class of "biomaterial–tissue" hybrid materials and, in the present combination of materials, we called it a "PVA-C tissue hybrid".

In one study [110, 111], the cell adhesion peptide RGD was chemically attached to the PVA-C surface using a more simplified functionalization reaction route than that reported for glutaraldehyde-crosslinked PVA (Fig. 13) and endothelization was demonstrated on the functionalized surface (Fig. 14). It is interesting that the chemical reactions required for RGD bonding are simpler than those used for

Radial Artery Cell Seeding
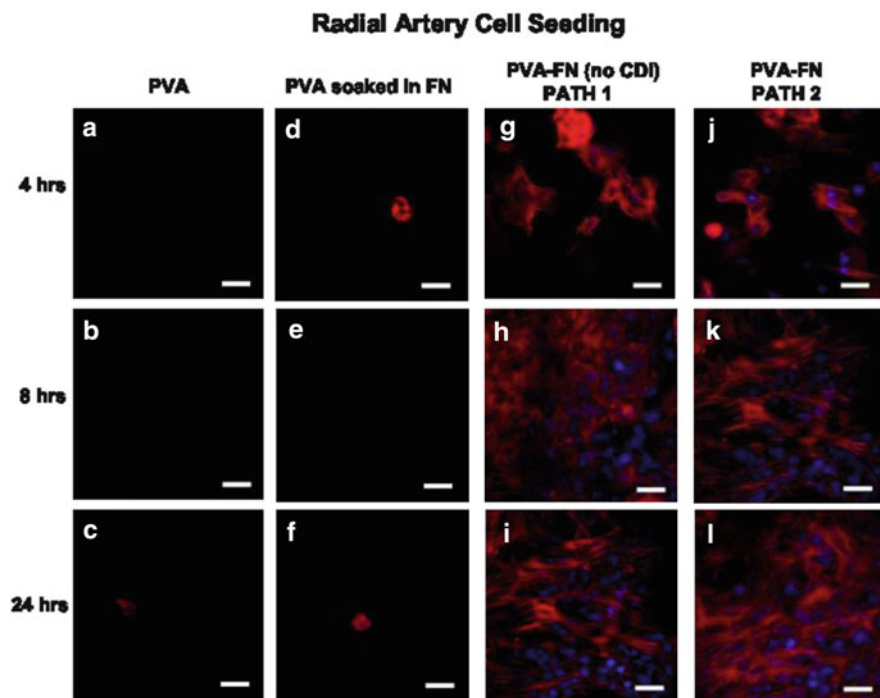
Fig. 14 Confocal micrographs of radial artery cells seeded onto samples of PVA-C control, PVA-C soaked in fibronectin (FN), PVA-C–FN (FN-functionalized PVA-C) prepared without CDI, and PVA-C–FN prepared with CDI. Cytoskeleton (*red*) was labeled with anti-smooth muscle α-actin–Cy3-conjugated IgG2a primary. Cell nuclei (*blue*) were labeled with Hoechst 33342. *Scale bars*: 50 μm. For further experimental details, refer to [110]. Reprinted from [110] with permission. Copyright (2011) Elsevier

glutaraldehyde-crosslinked PVA hydrogel. The difference clearly shows the advantage of PVA-C and is attributed to the availability of all the –OH groups for functionalization in PVA-C. In the case of glutaraldehyde-crosslinked PVA, an appreciable fraction of these –OH groups are used for crosslinking and are thus not available for functionalization [110].

Another study aiming to impart cell adhesion properties to PVA-C made use of a recently synthesized novel poly(amic acid) (PAA) polymer that has been shown to be cell compatible to form a PAA-grafted/crosslinked-PVA hydrogel (PAA-*g/c*-PVA). Functionalization of the PVA-C surface was accomplished by grafting of the PAA onto it to provide sites for cell attachment (Fig. 15). Successful endothelization with vascular endothelial cells was demonstrated (Fig. 16) [111].

Both of these approaches are important steps towards the creation of PVA-C tissue hybrids for cardiovascular applications and specifically for heart valves and vascular grafts.
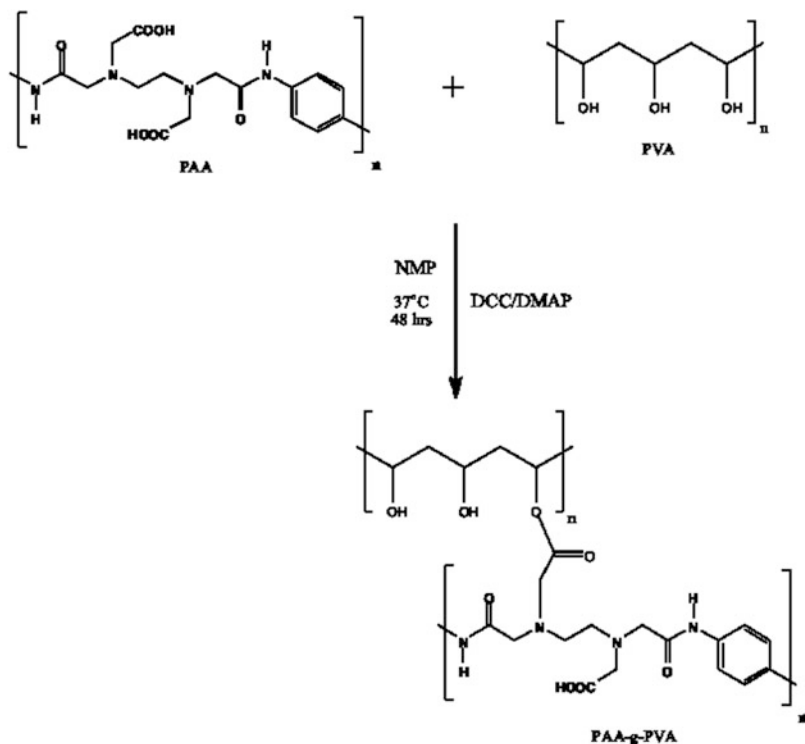
Fig. 15 PAA-g/c-PVA cryogel synthesis. The reaction requires the use of equimolar amounts of PAA, PVA, and 4-dimethyl aminopyridine (*DMAP*) and an excess of 1,3-dicyclohexyl carbodiimide (*DCC*). Reprinted from [111] with permission. Copyright © 2011 Wiley Periodicals

6 Future Perspectives

PVA is a well-known biocompatible material that can be chemically crosslinked into a hydrogel with many demonstrated biomedical applications. When it is physically crosslinked into PVA-C using the freeze–thaw cycling process, the resulting hydrogel (cryogel) possesses additional characteristics such as nontoxicity and tunable mechanical properties. The anisotropic PVA-C has mechanical properties that closely match those of the natural soft tissue, including orientation. These additional characteristics make it an especially attractive candidate material for medical device applications.

For orthopedic devices such as the IVD, the key is to be able to increase the stiffness and strength of the PVA-C. This could be accomplished via PVA-C nanocomposites. In both IVD and cartilage applications, a strain-rate dependent mechanical response is essential. This again may be possible by formulating PVA-C composites with a specially designed filler that can mimic the properties of elastin and protoglycans in the tissue.
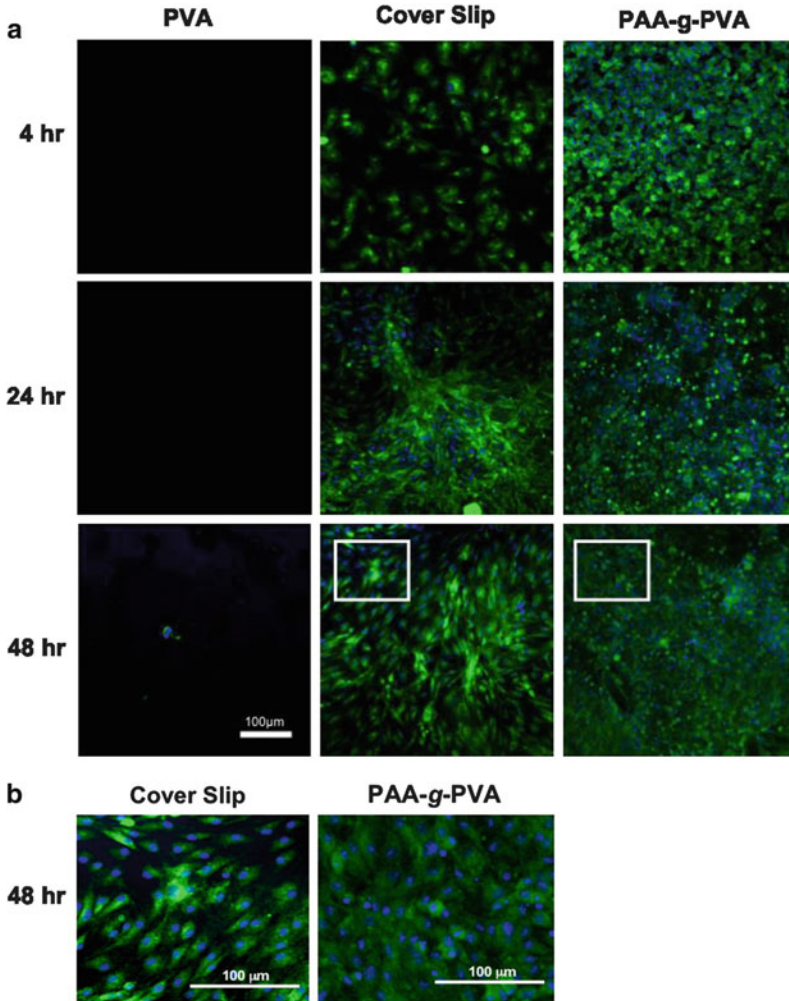
Fig. 16 (**a**) Confocal images of endothelial cells at 4, 24 and 48 h on PVA-C hydrogel, on an uncoated (control) coverslip, and on PAA-*g/c*-PVA. (**b**) Confocal images of endothelial cells at 48 h on glass coverslips and on PAA-*g/c*-PVA, focusing on the *boxed areas* in (**a**). Cell nuclei (*blue*) are labeled with Hoechst 33342. Cytoplasmic protein is stained *green* with the anti-von Willebrand factor. For further experimental details, refer to [111]. Reprinted from [111] with permission. Copyright © 2011 Wiley Periodicals

In cardiovascular devices, it is essential to impart hemocompatibility to PVA-C. The concept of a biomaterial–tissue hybrid in the form of endothelized PVA-C has been demonstrated. Much work still needs to be done to firmly established this approach and translate the results into the geometry of a vascular conduit.

Moving ahead, there are certainly challenges facing the use of PVA-C in biomedical applications, but the future looks promising.

References

1. Peppas NA (1996) Hydrogels. In: Ratner BD, Hoffman AS, Shoen FJ, Lemons JE (eds) Biomaterials science: an introduction to materials in medicine, 1st edn. Academic, Toronto, ON, Elsevier Academic Press pp 60–64
2. Ratner BD, Hoffman AS (1976) Synthetic hydrogels for biomedical applications. In: Andrade JD (ed) Hydrogels for medical and related applications, vol 31, ACS symposium series. American Chemical Society, Washington, DC, pp 1–36
3. Tadavarthy S, Moller J, Amplatz K (1975) Polyvinyl-alcohol (ivalon)—new embolic material. Am J Roentgenol 125:609–616
4. Bray JC, Merrill EW (1973) Poly(vinyl alcohol) hydrogels for synthetic articular cartilage material. J Biomed Mater Res 7:431–443
5. Peppas N, Benner R (1980) Proposed method of intracordal injection and gelation of poly (vinyl alcohol) solution in vocal cords—polymer considerations. Biomaterials 1:158–162
6. Hassan C, Peppas N (2000) Structure and applications of poly(vinyl alcohol) hydrogels produced by conventional crosslinking or by freezing/thawing methods. Adv Polym Sci 153:37–65
7. Wan W, Campbell G, Zhang Z, Hui A, Boughner D (2002) Optimizing the tensile properties of polyvinyl alcohol hydrogel for the construction of a bioprosthetic heart valve stent. J Biomed Mater Res 63:854–861
8. Yokoyama F, Masada I, Shimamura K, Ikawa T, Monobe K (1986) Morphology and structure of highly elastic poly (vinyl alcohol) hydrogel prepared by repeated freezing-and-melting. Colloid Polym Sci 264:595–601
9. Willcox PJ, Howie DW, SchmidtRohr K, Hoagland DA, Gido SP, Pudjijanto S, Kleiner LW, Venkatraman S (1999) Microstructure of poly (vinyl alcohol) hydrogels produced by freeze/thaw cycling. J Polym Sci Polym Phys 37:3438–3454
10. Millon LE, Nieh M, Hutter JL, Wan W (2007) SANS characterization of an anisotropic poly (vinyl alcohol) hydrogel with vascular applications. Macromolecules 40:3655–3662
11. Hudson SD, Hutter JL, Nieh M, Pencer J, Millon LE, Wan W (2009) Characterization of anisotropic poly(vinyl alcohol) hydrogel by small- and ultra-small-angle neutron scattering. J Chem Phys 130:034903
12. Kanaya T, Ohkura M, Kaji K, Furusaka M, Misawa M (1994) Structure of poly(vinyl alcohol) gels studied by wide-angle and small-angle neutron-scattering. Macromolecules 27:5609–5615
13. Lozinsky V (2002) Cryogels on the basis of natural and synthetic polymers: preparation, properties and application. Usp Khim 71:559–585
14. Holloway JL, Lowman AM, Palmese GR (2013) The role of crystallization and phase separation in the formation of physically cross-linked PVA hydrogels. Soft Matter 9:826–833
15. Kanaya T, Ohkura M, Takeshita H, Kaji K, Furusaka M, Yamaoka H, Wignall G (1995) Gelation process of poly(vinyl alcohol) as studied by small-angle neutron and light-scattering. Macromolecules 28:3168–3174
16. Ficek BJ, Peppas NA (1993) Novel preparation of poly(vinyl alcohol) microparticles without cross-linking agent for controlled drug-delivery of proteins. J Control Release 27:259–264

17. Peppas NA, Scott JE (1992) Controlled release from poly(vinyl alcohol) gels prepared by freezing-thawing processes. J Control Release 18:95–100
18. Pazos V, Mongrain R, Tardif J (2009) Polyvinyl alcohol cryogel: optimizing the parameters of cryogenic treatment using hyperelastic models. J Mech Behav Biomed Mater 2:542–549
19. Hassan C, Peppas N (2000) Structure and morphology of freeze/thawed PVA hydrogels. Macromolecules 33:2472–2479
20. Lozinsky V, Damshkaln L, Shaskol'skii B, Babushkina T, Kurochkin I, Kurochkin I (2007) Study of cryostructuring of polymer systems: 27. Physicochemical properties of poly (vinyl alcohol) cryogels and specific features of their macroporous morphology. Colloid J 69:747–764
21. Trieu H, Qutubuddin S (1995) Poly (vinyl alcohol) hydrogels: 2. Effects of processing parameters on structure and properties. Polymer 36:2531–2539
22. Millon LE (2006) Isotropic and anisotropic polyvinyl alcohol based hydrogels for biomedical applications. Dissertation, The University of Western Ontario, Canada
23. Wong EYL (2012) Poly(vinyl alcohol) nanocomposite hydrogels for intervertebral disc prostheses. Dissertation, The University of Western Ontario, Canada
24. Hyon SH, Ikada Y (1987) Porous and transparent poly(vinyl alcohol) gel and method of manufacturing the same. US Patent 4,663,358A
25. Ohkura M, Kanaya T, Keisuka K (1992) Gels of poly(vinyl alcohol) from dimethyl sulphoxide/water solutions. Polymer 33:3686–3690
26. Lozinsky V, Solodova E, Zubov A, Simenel I (1995) Study of cryostructuration of polymer systems. 11. The formation of PVA cryogels by freezing-thawing the polymer aqueous-solutions containing additives of some polyols. J Appl Polym Sci 58:171–177
27. Lozinsky V, Domotenko L, Zubov A, Simenel I (1996) Study of cryostructuration of polymer systems. 12. Poly(vinyl alcohol) cryogels: influence of low-molecular electrolytes. J Appl Polym Sci 61:1991–1998
28. Gordon M (1999) Controlling the mechanical properties of PVA hydrogels for biomedical applications. Dissertation, The University of Western Ontario, Canada
29. Shaheen S, Yamaura K (2002) Preparation of theophylline hydrogels of atactic poly(vinyl alcohol)/NaCl/H_2O system for drug delivery system. J Control Release 81:367–377
30. Briscoe B, Luckham P, Zhu S (2000) The effects of hydrogen bonding upon the viscosity of aqueous poly(vinyl alcohol) solutions. Polymer 41:3851–3860
31. Nugent M, Hanley A, Tomkins P, Higginbotham C (2005) Investigation of a novel freeze-thaw process for the production of drug delivery hydrogels. J Mater Sci Mater Med 16:1149–1158
32. Peppas N, Stauffer S (1991) Reinforced uncrosslinked poly (vinyl alcohol) gels produced by cyclic freezing-thawing processes—a short review. J Control Release 16:305–310
33. Hatakeyama T, Yamauchi A, Hatakeyama H (1987) Effect of thermal hysteresis on structural-change of water restrained in poly(vinyl-alcohol) pseudo-gel. Eur Polym J 23:361–365
34. Lozinsky V, Plieva F (1998) Poly (vinyl alcohol) cryogels employed as matrices for cell immobilization. 3. Overview of recent research and developments. Enzyme Microb Technol 23:227–242
35. Lozinsky VI, Zubov AL, Savina IN, Plieva FM (2000) Study of cryostructuration of polymer systems. XIV. Poly (vinyl alcohol) cryogels: apparent yield of the freeze–thaw-induced gelation of concentrated aqueous solutions of the polymer. J Appl Polym Sci 77:1822–1831
36. Lozinsky V, Damshkaln L (2000) Study of cryostructuration of polymer systems. XVII. Poly (vinyl alcohol) cryogels: dynamics of the cryotropic gel formation. J Appl Polym Sci 77:2017–2023
37. Stauffer SR, Peppas NA (1992) Poly(vinyl alcohol) hydrogels prepared by freezing-thawing cyclic processing. Polymer 33:3932–3936
38. Ricciardi R, D'Errico G, Auriemma F, Ducouret G, Tedeschi A, De Rosa C, Laupretre F, Lafuma F (2005) Short time dynamics of solvent molecules and supramolecular organization

of poly(vinyl alcohol) hydrogels obtained by freeze/thaw techniques. Macromolecules 38:6629–6639

39. Holloway JL, Spiller KL, Lowman AM, Palmese GR (2011) Analysis of the in vitro swelling behavior of poly(vinyl alcohol) hydrogels in osmotic pressure solution for soft tissue replacement. Acta Biomater 7:2477–2482

40. Hassan C, Stewart J, Peppas N (2000) Diffusional characteristics of freeze/thawed poly(vinyl alcohol) hydrogels: applications to protein controlled release from multilaminate devices. Eur J Pharm Biopharm 49:161–165

41. Cha WI, Hyon SH, Ikada Y (1993) Microstructure of poly(vinyl alcohol) hydrogels investigated with differential scanning calorimetry. Macromol Chem Phys 194:2433–2441

42. Millon LE, Wan WK (2006) The polyvinyl alcohol-bacterial cellulose system as a new nanocomposite for biomedical applications. J Biomed Mater Res B 79B:245–253

43. Watase M, Nishinari K, Nambu M (1983) Anomalous increase of the elastic-modulus of frozen poly (vinyl alcohol) gels. Cryo-Letters 4:197–200

44. National Toxicology Program (1998) NTP toxicology and carcinogenesis studies of polyvinyl alcohol (CAS no.9002-89-5) in female B6C3F1 mice (intravaginal studies). Natl Toxicol Program Tech Rep Ser 474:1–110

45. Millon LE, Oates CJ, Wan W (2009) Compression properties of polyvinyl alcohol—bacterial cellulose nanocomposite. J Biomed Mater Res B 90B:922–929

46. Watase M, Nambu M, Nishinari K (1983) Rheological properties of an anomalous poly (vinyl alcohol) gel. Polym Commun 24:52–54

47. Fink JK (2011) Handbook of engineering and specialty thermoplastics, water soluble polymers. Wiley, Hoboken, NJ

48. van Aartsen J (1970) Theoretical observations on spinodal decomposition of polymer solutions. Eur Polym J 6:919–924

49. Fergg F, Keil F, Quader H (2001) Investigations of the microscopic structure of poly(vinyl alcohol) hydrogels by confocal laser scanning microscopy. Colloid Polym Sci 279:61–67

50. Ricciardi R, Auriemma F, De Rosa C, Laupretre F (2004) X-ray diffraction analysis of poly (vinyl alcohol) hydrogels, obtained by freezing and thawing techniques. Macromolecules 37:1921–1927

51. Liu K, Ovaert TC (2011) Poro-viscoelastic constitutive modeling of unconfined creep of hydrogels using finite element analysis with integrated optimization method. J Mech Behav Biomed Mater 4:440–450

52. Nakaoki T, Yamashita H (2008) Bound states of water in poly(vinyl alcohol) hydrogel prepared by repeated freezing and melting method. J Mol Struct 875:282–287

53. Stammen JA, Williams S, Ku DN, Guldberg RE (2001) Mechanical properties of a novel PVA hydrogel in shear and unconfined compression. Biomaterials 22:799–806

54. Wang BH, Campbell G (2009) Formulations of polyvinyl alcohol cryogel that mimic the biomechanical properties of soft tissues in the natural lumbar intervertebral disc. Spine 34:2745–2753

55. Duboeuf F, Basarab A, Liebgott H, Brusseau E, Delachartre P, Vray D (2009) Investigation of PVA cryogel Young's modulus stability with time, controlled by a simple reliable technique. Med Phys 36:656–661

56. Nishinari K, Watase M, Tanaka F (1996) Structure of junction zones in poly (vinyl alcohol) gels by rheological and thermal studies. J Chim Phys Physicochim Biol 93:880–886

57. Urushizaki F, Yamaguchi H, Nakamura K, Numajiri S, Sugibayashi K, Morimoto Y (1990) Swelling and mechanical-properties of poly(vinyl alcohol) hydrogels. Int J Pharm 58:135–142

58. Bodugoz-Senturk H, Macias CE, Kung JH, Muratoglu OK (2009) Poly(vinyl alcohol)-acrylamide hydrogels as load-bearing cartilage substitute. Biomaterials 30:589–596

59. Millon LE, Mohammadi H, Wan WK (2006) Anisotropic polyvinyl alcohol hydrogel for cardiovascular applications. J Biomed Mater Res B 79B:305–311

60. Fromageau J, Gennisson J, Schmitt C, Maurice RL, Mongrain R, Cloutier G (2007) Estimation of polyvinyl alcohol cryogel mechanical properties with four ultrasound elastography methods and comparison with gold standard testings. IEEE Trans Ultrason Ferroelectr Freq Control 54:498–509

61. Hickey AS, Peppas NA (1995) Mesh size and diffusive characteristics of semicrystalline poly (vinyl alcohol) membranes prepared by freezing/thawing techniques. J Membr Sci 107:229–237

62. Li JK, Wang N, Wu XS (1998) Poly(vinyl alcohol) nanoparticles prepared by freezing-thawing process for protein/peptide drug delivery. J Control Release 56:117–126

63. Gusev D, Lozinsky V, Vainerman E, Bakhmutov V (1990) Study of the frozen water poly (vinyl alcohol) system by H-2 and C-13 nmr-spectroscopy. Magn Reson Chem 28:651–655

64. Lozinsky VI, Damshkaln LG, Kurochkin IN, Kurochkin II (2012) Study of cryostructuring of polymer systems. 33. Effect of rate of chilling aqueous poly(vinyl alcohol) solutions during their freezing on physicochemical properties and porous structure of resulting cryogels. Colloid J 74:319–327

65. Kennedy KL, Lucas AR, Wan W (2011) Local delivery of therapeutics for percutaneous coronary intervention. Curr Drug Deliv 8:534–556

66. Richardson J, Viswanathan K, Lucas A (2006) Serpins, the vasculature, and viral therapeutics. Front Biosci 11:1042–1056

67. Eichhorn S, Baillie C, Zafeiropoulos N, Mwaikambo L, Ansell M, Dufresne A, Entwistle K, Herrera-Franco P, Escamilla G, Groom L et al (2001) Review: current international research into cellulosic fibres and composites. J Mater Sci 36:2107–2131

68. Guhados G, Wan W, Hutter J (2005) Measurement of the elastic modulus of single bacterial cellulose fibers using atomic force microscopy. Langmuir 21:6642–6646

69. Klemm D, Schumann D, Udhardt U, Marsch S (2001) Bacterial synthesized cellulose—artificial blood vessels for microsurgery. Prog Polym Sci 26:1561–1603

70. Berglund L (2005) Cellulose-based nanocomposites. In: Mohanty AK, Misra M, Drzal LT (eds) Natural fibers, biopolymers, and biocomposites. CRC, Boca Raton, FL, pp 819–842

71. Schoen F, Levy R (1999) Tissue heart valves: current challenges and future research perspectives. J Biomed Mater Res 47:439–465

72. Fung YC (1993) Biomechanics: mechanical properties of living tissues, 2nd edn. Springer, New York

73. Abé H, Hayashi K, Sato M (1996) Data book on mechanical properties of living cells, tissues, and organs. Springer, Tokyo

74. Liu W, Merrett K, Griffith M, Fagerholm P, Dravida S, Heyne B, Scaiano JC, Watsky MA, Shinozaki N, Lagali N et al (2008) Recombinant human collagen for tissue engineered corneal substitutes. Biomaterials 29:1147–1158

75. Zeng Y, Yang J, Huang K, Lee Z, Lee X (2001) A comparison of biomechanical properties between human and porcine cornea. J Biomech 34:533–537

76. Dravida S, Gaddipati S, Griffith M, Merrett K, Madhira SL, Sangwan VS, Vemuganti GK (2008) A biomimetic scaffold for culturing limbal stem cells: a promising alternative for clinical transplantation. J Tissue Eng Regen Med 2:263–271

77. Chirila T, Hicks C, Dalton P, Vijayasekaran S, Lou X, Hong Y, Clayton A, Ziegelaar B, Fitton J, Platten S et al (1998) Artificial cornea. Prog Polym Sci 23:447–473

78. Wang J, Gao C, Zhang Y, Wan Y (2010) Preparation and in vitro characterization of BC/PVA hydrogel composite for its potential use as artificial cornea biomaterial. Mater Sci Eng C Mater Biol Appl 30:214–218

79. Liu Y, Vrana NE, Cahill PA, McGuinness GB (2009) Physically crosslinked composite hydrogels of PVA with natural macromolecules: structure, mechanical properties, and endothelial cell compatibility. J Biomed Mater Res B Appl Biomater 90B:492–502

80. Vrana NE, Liu Y, McGuinness GB, Cahill PA (2008) Characterization of poly(vinyl alcohol)/chitosan hydrogels as vascular tissue engineering scaffolds. Macromol Symp 269:106–110

81. Mathews DT, Birney YA, Cahill PA, McGuinness GB (2008) Mechanical and morphological characteristics of poly(vinyl alcohol)/chitosan hydrogels. J Appl Polym Sci 109:1129–1137

82. Abdel-Mohsen AM, Aly AS, Hrdina R, Montaser AS, Hebeish A (2011) Eco-synthesis of PVA/chitosan hydrogels for biomedical application. J Polym Environ 19:1005–1012

83. Causa F, Manto L, Borzacchiello A, De Santis R, Netti P, Ambrosio L, Nicolais L (2002) Spatial and structural dependence of mechanical properties of porcine intervertebral disc. J Mater Sci Mater Med 13:1277–1280

84. Adams MA, Roughley PJ (2006) What is intervertebral disc degeneration, and what causes it? Spine 31:2151–2161

85. Smith LJ, Nerurkar NL, Choi K, Harfe BD, Elliott DM (2011) Degeneration and regeneration of the intervertebral disc: lessons from development. Dis Model Mech 4:31–41

86. Cote P, van der Velde G, Cassidy JD, Carroll LJ, Hogg-Johnson S, Holm LW, Carragee EJ, Haldeman S, Nordin M, Hurwitz EL et al (2008) The burden and determinants of neck pain in workers—results of the bone and joint decade 2000-2010 task force on neck pain and its associated disorders. Eur Spine J 17:S60–S74

87. Cote P, Kristman V, Vidmar M, Van Eerd D, Hogg-Johnson S, Beaton D, Smith PM (2008) The prevalence and incidence of work absenteeism involving neck pain—a cohort of Ontario lost-time claimants. Spine 33:S192–S198

88. Hoy D, March L, Brooks P, Woolf A, Blyth F, Vos T, Buchbinder R (2010) Measuring the global burden of low back pain. Best Pract Res Clin Rheumatol 24:155–165

89. Kovacs F, Abraira V, Zamora J, del Real M, Llobera J, Fernandez C, Kovacs-Atencion Primaria Group (2004) Correlation between pain, disability, and quality of life in patients with common low back pain. Spine 29:206–210

90. Cassidy JJ, Hiltner A, Baer E (1990) The response of the hierarchical structure of the intervertebral-disk to uniaxial compression. J Mater Sci Mater Med 1:69–80

91. Perie D, MacLean J, Owen J, Iatridis J (2006) Correlating material properties with tissue composition in enzymatically digested bovine annulus fibrosus and nucleus pulposus tissue. Ann Biomed Eng 34:769–777

92. Joshi A, Fussell G, Thomas J, Hsuan A, Lowman A, Karduna A, Vresilovic E, Marcolongo M (2006) Functional compressive mechanics of a PVA/PVP nucleus pulposus replacement. Biomaterials 27:176–184

93. Northwood E, Fisher J (2007) A multi-directional in vitro investigation into friction, damage and wear of innovative chondroplasty materials against articular cartilage. Clin Biomech 22:834–842

94. Oka M, Ushio K, Kumar P, Ikeuchi K, Hyon S, Nakamura T, Fujita H (2000) Development of artificial articular cartilage. Proc Inst Mech Eng H 214:59–68

95. Gu Z, Xiao J, Zhang X (1998) The development of artificial articular cartilage-PVA-hydrogel. Biomed Mater Eng 8:75–81

96. Swieszkowski W, Ku D, Bersee H, Kurzydlowski K (2006) An elastic material for cartilage replacement in an arthritic shoulder joint. Biomaterials 27:1534–1541

97. Pan Y, Xiong D, Ma R (2007) A study on the friction properties of poly(vinyl alcohol) hydrogel as articular cartilage against titanium alloy. Wear 262:1021–1025

98. Kobayashi M, Chang Y, Oka M (2005) A two year in vivo study of polyvinyl alcohol-hydrogel (PVA-H) artificial meniscus. Biomaterials 26:3243–3248

99. Pan Y, Xiong D, Chen X (2007) Mechanical properties of nanohydroxyapatite reinforced poly(vinyl alcohol) gel composites as biomaterial. J Mater Sci 42:5129–5134

100. Jiang H, Campbell G, Boughner D, Wan W, Quantz M (2004) Design and manufacture of a polyvinyl alcohol (PVA) cryogel tri-leaflet heart valve prosthesis. Med Eng Phys 26:269–277

101. Mohammadi H, Boughner D, Millon LE, Wan WK (2009) Design and simulation of a poly (vinyl alcohol)-bacterial cellulose nanocomposite mechanical aortic heart valve prosthesis. Proc Inst Mech Eng H 223:697–711

102. Hui AJ (1998) Hydrogel-based artificial heart valve stent material. Dissertation, The University of Western Ontario, Canada

103. Nuttelman C, Mortisen D, Henry S, Anseth K (2001) Attachment of fibronectin to poly(vinyl alcohol) hydrogels promotes NIH3T3 cell adhesion, proliferation, and migration. J Biomed Mater Res 57:217–223
104. Sailaja GS, Sreenivasan K, Yokogawa Y, Kumary TV, Varma HK (2009) Bioinspired mineralization and cell adhesion on surface functionalized poly(vinyl alcohol) films. Acta Biomater 5:1647–1655
105. Zajaczkowski M, Cukierman E, Galbraith C, Yamada K (2003) Cell-matrix adhesions on poly(vinyl alcohol) hydrogels. Tissue Eng 9:525–533
106. Sugawara T, Matsuda T (1995) Photochemical surface derivatization of a peptide-containing Arg-Gly-Asp (RGD). J Biomed Mater Res 29:1047–1052
107. Mansur HS, Costa ES Jr, Mansur AAP, Barbosa-Stancioli EF (2009) Cytocompatibility evaluation in cell-culture systems of chemically crosslinked chitosan/PVA hydrogels. Mat Sci Eng C 29:1574–1583
108. Mathews DT, Birney YA, Cahill PA, McGuinness GB (2008) Vascular cell viability on polyvinyl alcohol hydrogels modified with water-soluble and -insoluble chitosan. J Biomed Mater Res B 84B:531–540
109. Jiang T, Wang G, Qiu J, Luo L, Zhang G (2009) Heparinized poly(vinyl alcohol)-small intestinal submucosa composite membrane for coronary covered stents. Biomed Mater 4:025012
110. Millon LE, Padavan DT, Hamilton AM, Boughner DR, Wan W (2012) Exploring cell compatibility of a fibronectin-functionalized physically crosslinked poly(vinyl alcohol) hydrogel. J Biomed Mater Res B 100B:1–10
111. Padavan DT, Hamilton AM, Millon LE, Boughner DR, Wan W (2011) Synthesis, characterization and in vitro cell compatibility study of a poly(amic acid) graft/cross-linked poly(vinyl alcohol) hydrogel. Acta Biomater 7:258–267

Index